Exposing hidden dangers in dietary supplements *p. 780*

Limiting the dark side *pp. 786, 849, & 851*

Diverse opinions on bioweapons *p. 792*

Science

$10
21 AUGUST 2015
sciencemag.org

AAAS

SPECIAL ISSUE

FOREST HEALTH

THREATS AND RESILIENCE

CONTENTS

21 AUGUST 2015 • VOLUME 349 • ISSUE 6250

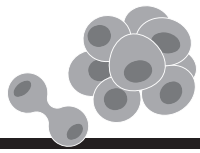

789 & 873
Membrane voltage changes cell proliferation

SPECIAL SECTION
FOREST HEALTH

ON THE COVER

Ecologist Roman Dial goes to great lengths to perform an ecological survey of mountain ash trees (*Eucalyptus regnans*) in an Australian forest. Researchers making similar efforts globally help us understand and monitor the health of forests as they face increasing challenges in our changing world. See page 800. *Photo: Bill Hatcher/National Geographic Creative*

SEE ALSO ▸ EDITORIAL P. 771 ▸ PERSPECTIVE P. 794 ▸ VIDEO ▸ SLIDESHOW

NEWS

IN BRIEF

IN DEPTH

FEATURE

INSIGHTS

PERSPECTIVES

Published by AAAS

784 & 858
Who's the predator now?

788 & 860
Sculpting the root microbiome

RESEARCH

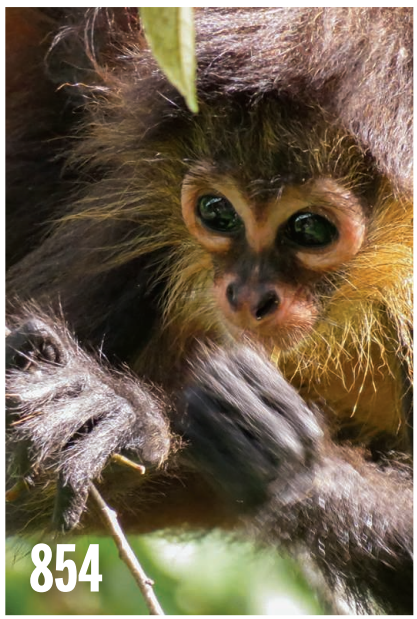

PHOTO: (RIGHT) KEVIN LAFFERTY/U.S. GEOLOGICAL SURVEY

SCIENCE (ISSN 0036-8075) is published weekly on Friday, except the last week in December, by the American Association for the Advancement of Science, 1200 New York Avenue, NW, Washington, DC 20005. Periodicals mail postage (publication No. 484460) paid at Washington, DC, and additional mailing offices. Domestic individual membership and subscription (51 issues): $153 ($74 allocated to subscription). Domestic institutional subscription (51 issues): $1282; Foreign postage extra: Mexico, Caribbean (surface mail) $55; other countries (air assist delivery) $85. First class, airmail, student, and emeritus rates on request. Canadian rates with GST available upon request, GST #1254 88122. Publications Mail Agreement Number 1069624. **Printed in the U.S.A.**
Change of address: Allow 4 weeks, giving old and new addresses and 8-digit account number. **Postmaster:** Send change of address to AAAS, P.O. Box 96178, Washington, DC 20090–6178. **Single-copy sales:** $10.00 current issue, $15.00 back issue prepaid includes surface postage; bulk rates on request.

Published by AAAS

Science
AAAS
1200 New York Avenue, NW, Washington, DC 20005
Bateman House, 82-88 Hills Road, Cambridge, UK CB2 1LQ

SUBSCRIPTION SERVICES For change of address, missing issues, new orders and renewals, and payment questions: 866-434-AAAS (2227) or 202-326-6417, FAX 202-842-1065. Mailing addresses: AAAS, P.O. Box 96178, Washington, DC 20090-6178 or AAAS Member Services, 1200 New York Avenue, NW, Washington, DC 20005

INSTITUTIONAL SITE LICENSES 202-326-6755 **REPRINTS:** Author Inquiries 800-635-7181 **COMMERCIAL INQUIRIES** 803-359-4578 **PERMISSIONS** 202-326-6765, permissions@aaas.org **AAAS Member Services** 202-326-6417 or http://membercentral.aaas.org/discounts

INFORMATION FOR AUTHORS See pages 678 and 679 of the 6 February 2015 issue or access www.sciencemag.org/about/authors

Published by AAAS

EDITORIAL

Forestry in the Anthropocene

Human activity has had enormous effects on the species composition of floras and faunas, creating new ecological biomes worldwide. A principal challenge in forestry research and conservation is how to deal with these novel ecosystems. Most attention to this phenomenon is centered on the negative effects of species introductions and the need to stem the tide of species invasion. However, we need to scientifically understand new ecosystems and learn to recognize adaptive species combinations that will function sustainably in changing environmental conditions.

In 1965, George E. Hutchinson famously published *The Ecological Theater and the Evolutionary Play*, helping to launch influential discussion about the feedback between ecology and evolution. The idea is that ecology governs evolution by "tailoring" organisms to fit niches. But human activity has become both theater manager and stage agent in this framework, spurring the movement of species across historical biogeographical boundaries into new situations and ecosystems. Human activity is also changing environmental conditions—including climate, biogeochemistry, and geomorphology—on a planetary scale. In short, human activity is tweaking the theater and plot of Hutchinson's play, thereby changing the speed of evolution.

"Human activity is tweaking the theater and plot of Hutchinson's play...changing the speed of evolution."

In particular, the global forestry situation has changed dramatically over the the last several decades. The role of forests in mitigating climate change is foremost in the minds of most conservationists and for scientists responsible for global ecosystem models. Forests are now valued as much for their diverse ecological services as they are for their wood production. As such, efforts have been increasing to sustain the world's forests. In the tropics, which contain over half of the world's forests and a disproportionate amount of global biodiversity, over half of the forest area is now "secondary" regenerating forest, replacing trees that have been lost to agricultural activities. The amount of global land covered by cultivated plantation forests is now at a historical high—roughly 200 million ha. And urban forests are now recognized for their role in supporting the quality of life in cities where over half of the world's population lives.

These changes in the forest landscape, coupled with the accelerated movement of species across biogeographical barriers, are creating novel ecosystems that we don't fully understand. What are our options? Because the planet and its biota are already responding naturally to Anthropocene conditions, should we accept the change passively, revert natural processes to historical conditions, or intervene when conditions and opportunity for success appear favorable?

Research is the most effective tool for finding the answers. For forests, the major questions include how they respond to Anthropocene conditions and how they mitigate anthropogenic disturbances. Without abandoning current research, priorities include focusing on novel forests, urban environments, and anthropogenic biomes. Good examples of forward-thinking research can be found in tropical islands such as the Seychelles and Puerto Rico, where conservation of native and novel forests is being tackled through tight coupling of science and conservation. So far, research has identified areas within these insular landscapes where native forests function with little human modification, and where new combinations of species, including introduced ones, function sustainably in spite of anthropogenic disturbances. Thus, while keeping an eye on troublesome invasive species, we must also understand their ecological roles, ecological services, and legitimate place in the natural landscape.

Professional foresters and ecologists must share the responsibility of forest research and conservation with other professions from the natural and social sciences through new combinations of science such as eco-hydrology and social-ecological sciences. Because of the uncertainty of Anthropocene conditions, research that looks at new sustainable ecosystem dynamics and conservation actions must come together as never before.

– Ariel E. Lugo

Ariel E. Lugo is director of the International Institute of Tropical Forestry of the United States Department of Agriculture Forest Service, Río Piedras, Puerto Rico. E-mail: alugo@fs.fed.us

10.1126/science.aad2208

PHOTOS: (TOP RIGHT) UNITED STATES DEPARTMENT OF AGRICULTURE FOREST SERVICE; (INSET) NICOLAS RAYMOND/FLICKR

NEWS

16% Amount by which existing estimates overstate China's 2013 greenhouse emissions due to fossil fuel burning, according to a study in *Nature*.

IN BRIEF

How the gas giants got so big

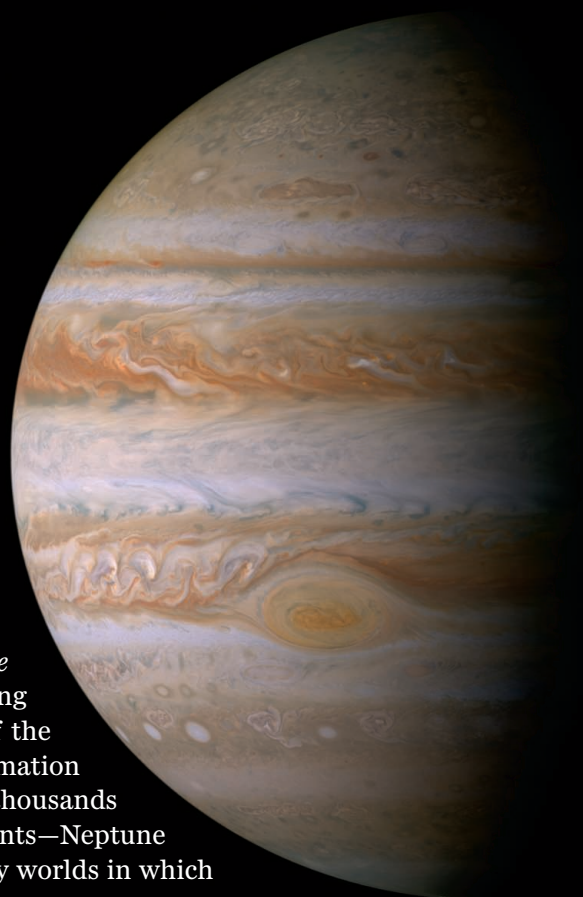

To get their giant girths, Jupiter (shown) and Saturn had to form quickly from the sun's disk of gas and dust—within a few million years. Most theorists believe that they grew from rocky cores, about 10 times the mass of Earth, which then gravitationally sucked up the remaining gas in the disk. Models have successfully shown pebbles of dust clumping together into planetesimals that gobble up the rest of the pebbles and form rocky cores, but they also generated hundreds of cores, not just a few. Now, a new solar system model published on 19 August in *Nature* solves this problem, by slowing down the pebble-eating process so that all but a few cores are kicked out of the plane of the solar system. The model predicts the formation of one to four giant planets within just hundreds of thousands of years. As a byproduct, it also generates a few ice giants—Neptune and Uranus—and a Kuiper belt, the region of small icy worlds in which Pluto resides. http://scim.ag/gasgiants

PHOTO: NASA/JPL/SPACE SCIENCE INSTITUTE

AROUND THE WORLD

Crowdsourcing animal research

COLUMBUS | The Beagle Freedom Project (BFP), an animal advocacy group, is crowdsourcing hundreds of public records requests to target cat and dog research across the United States. Supporters visit the group's "Identity Campaign" website, "adopt" a dog or cat at one of 17 public research universities, and learn how to file a Freedom of Information Act request with the school to get information on the animal. More than 1000 people have participated, resulting in about 100 public records, says Identity Campaign coordinator Jeremy Beckham. Some of the records, BFP claims, suggest that an Ohio State University lab violated National Institutes of Health rules concerning the use of dogs in biomedical research. The university denies those charges—and provided *Science* with evidence to the contrary. But BFP's effort could cause headaches for animal researchers, says Michael Halpern of the Union of Concerned Scientists in Washington, D.C. http://scim.ag/ICanirights

Severe weather threatens crops

LONDON | Weather-related crop disasters will become more likely with climate change, as drought, flooding, and heat waves strike fields more often, warns a report released 14 August by the Global Food Security (GFS) program, a network of public research funding agencies in the United Kingdom. Dozens of scientists, policy wonks, and industry experts examined the global food system and its vulnerabilities to severe weather. They used existing models of how crops respond to temperature, precipitation, and other factors to determine that by 2040, severe crop failures—previously estimated to occur once a century—are likely to happen every 3 decades. If a "plausible" worst-case scenario of drought simultaneously hitting four key staples—wheat, rice, corn, and soybeans—were to occur next year, it would likely triple the price of grain, the researchers suggest. http://scim.ag/foodweather

Published by AAAS

Push for chronic fatigue research

WASHINGTON, D.C. | Patient advocates and scientists joined forces this week to boost research funding for the mysterious and debilitating disease chronic fatigue syndrome (CFS), also known as myalgic encephalomyelitis (ME). In an open letter to U.S. senators, the group, #MEAction, noted that ME/CFS affects an estimated 836,000 to 2.5 million people in the United States, and stated that research into treatments should be "proportional to and commensurate with other diseases with similar patient populations." Through changes to an authorizing bill for the National Institutes of Health (NIH), the group aims to increase research funds available for ME/CFS from $5.4 million to levels similar to diseases that cause comparable disability, such as multiple sclerosis. It also wants to transfer responsibility for the disease from an isolated office within the U.S. Department of Health and Human Services to the National Institute for Neurological Disorders, a part of NIH. http://scim.ag/_MEAction

A hillside in southern California failed in March 1998 due to El Niño–related storms.

'Godzilla El Niño' is coming

Conditions are pointing to a strong El Niño event for the winter of 2015 to 2016, and possibly one of the strongest on record, according to climatologists with the National Oceanic and Atmospheric Administration (NOAA). The forecasted event is strong enough to earn comparisons to both martial arts star Bruce Lee (at NOAA's ENSO blog) and Godzilla (by NOAA climatologist Bill Patzert, to CBS News). El Niño events occur every 2 to 7 years, when trade winds over the equatorial Pacific Ocean weaken and sea-surface temperatures increase, which can, in turn, dramatically alter weather patterns around the globe. Last week, NOAA scientists noted that sea-surface temperatures have been near or exceeding 2°C above normal since July. The most recent powerful El Niño event was in 1997 to 1998, which pushed global temperatures to new highs and triggered extreme events around the world, including widespread drought and flooding.

FINDINGS

Support for 'exercise hormone'

New evidence lends support to the existence of irisin, a hormone secreted from muscles and believed to mediate the effects of exercise on metabolism, in humans. First described in 2012 by a team led by researchers at Harvard Medical School, irisin appears to circulate in blood and prompt energy-storing white fat cells to behave like energy-burning brown fat cells. But other groups have suggested that humans produce only negligible quantities of the protein due to a genetic mutation, and that common tests for irisin are inaccurate (*Science*, 20 March, p. 1299). Last week in *Cell Metabolism*, the Harvard group used mass spectrometry to sort human blood protein fragments by mass. They found evidence of the hormone at levels similar to insulin and suggest the approach could validate other tests. http://scim.ag/irisin

Humans do produce the hormone irisin during exercise, researchers say.

Gut bacteria linked to eye disease

Some microbes that naturally dwell in our intestines might be bad for our eyes, triggering autoimmune uveitis, one of the leading causes of blindness. In this disease, T cells that target ocular proteins invade the eye and spur damaging inflammation. Although these cells occur even in the blood of healthy people, they won't enter the eye unless they first encounter their target proteins—so the mystery is how the invading T cells happened upon proteins that are still locked up in the eye. Now, a new mouse study in *Immunity* suggests an answer to the conundrum: Still-unidentified bacteria in the intestines produce proteins that closely resemble the eye proteins. Some T cells, after encountering the microbial proteins in the gut, may attack similar molecules elsewhere, such as the eyes. Identifying these molecular mimics of the eye proteins and the bacteria that spawn them could help researchers develop new treatments for autoimmune uveitis. http://scim.ag/eyeproteins

The spectacular Pueblo Bonito ruins were part of a vast Chacoan landscape.

ENERGY DEVELOPMENT

Big Archaeology fights Big Oil to preserve ancient landscape

Researchers say fracking threatens hundreds of early Pueblo sites and endangers future excavations

By **Michael Balter**, *in Chaco Canyon, New Mexico*

When Larry Turk was appointed superintendent of Chaco Culture National Historical Park in 2013, he took charge of a silent and ghostly desert landscape with crystalline skies and deep roots in Native American history. Between about 850 C.E. and 1250 C.E., Chaco Canyon here in northwestern New Mexico's San Juan Basin was at the center of a vast and sophisticated Pueblo culture that covered more than 10,000 square kilometers. Centuries later, dramatic stone and adobe ruins stand silent witness to a vanished civilization.

But today, this park is at the center of an oil and gas boom that archaeologists, environmentalists, and Native American activists say threatens a broader landscape filled with hundreds of Chacoan sites, many yet to be discovered or studied. "If you go out to Chaco Canyon today," Turk says, "the whole landscape has changed. There are new wells going in all the time. At night you see the flaring of the oil and gas rigs against the once-dark skies, and the oil and gas trucks are creating huge potholes" on the dirt roads leading to the park. In New Mexico, still reeling from the recent recession, some welcome the boom. But Chaco's defenders argue that the drilling—much of which involves hydraulic fracturing, or "fracking"—is bad not only for the visitor experience, but also for archaeological research.

Earlier this month, at a major archaeology meeting just outside of Mancos, Colorado, Chaco experts presented a plan to slow down the granting of drilling leases in the San Juan Basin. They are urging that a current temporary 16-kilometer buffer around the national park be made permanent and that no new leases be granted in the basin until aerial surveys of the entire Chaco landscape can be completed. With a $105,000 grant from the National Park Service (NPS), the archaeologists are also preparing a white paper arguing that the widest possible region around Chaco Canyon should be protected from drilling. And in a separate effort, environmental and Native American groups have filed suit against the U.S. Department of the Interior and the Bureau of Land Management (BLM) to block 239 pending drilling permits in the Chaco area. Although a federal court denied their request for an immediate injunction late last week, the case is expected to continue to trial.

For the archaeologists, the fight to protect the remnants of Chacoan culture is rooted in the relatively new field of landscape archaeology, which looks beyond individual sites to their larger context. Chaco's 50,000 visitors a year are drawn to dramatic features such as the 600-room Great House of Pueblo Bonito, the sunken circular "kiva" at Chetro Ketl, and the Petroglyph Trail, where Chacoans carved images of birds, mountain lions, and mysterious spirals into a towering cliff. But across thousands of square kilometers of surrounding desert, archaeologists have identified more than 200 great houses, as far north as Colorado and possibly as far south as Mexico, according to Chaco expert Stephen Lekson of the University of Colorado, Boulder, who negotiated the grant with NPS. Hundreds more Chacaoan sites may remain to be discovered in the San Juan Basin alone.

In the NPS white paper, the archaeologists will argue that failing to protect the entire Chacoan landscape will hamper efforts to understand the culture. For example, they point to a number of still poorly understood "Chacoan roads," 5 to 10 meters wide, that run from the center of the national park to points far beyond the proposed 16-km buffer. The most famous of these, the Great North Road (see map, p. 775), is bounded by land parcels already

leased for oil and gas exploration.

"We will never understand Chaco Canyon until we understand the entire Chaco world," says team member Ruth Van Dyke, an archaeologist at the State University of New York at Binghamton. "Ideally I would like to just draw a big circle around the San Juan Basin and say, 'Oil and gas off limits, stay away!' But we know that's not going to fly." Paul Reed, an archaeologist with the Tucson, Arizona–based organization Archaeology Southwest, which has played a leading role in the fight to protect the Chaco landscape, agrees that any protection scheme should take into account the need for economic growth in the region. "We have to engage with all parties and work out a balanced negotiated settlement here."

But to the energy companies operating in the region, which include such major players as WPX Energy, ConocoPhillips Co., and the Canadian company Encana Corporation, Chaco advocates are asking too much. "We think it's completely unreasonable," says Wally Drangmeister, vice president of the Santa Fe–based New Mexico Oil & Gas Association. "The protections they want would encompass the entire San Juan Basin." Drangmeister says that the 16-km buffer that BLM has imposed around the park is sufficient protection for the Chaco landscape.

BLM alone can't stop all new drilling within the buffer zone, however. The agency is only responsible for about 19% of the total lease parcels within the 16-km radius, according to Victoria Barr, BLM's district manager for northwest New Mexico. The rest are controlled by the state of New Mexico or held by Native American tribal trusts or individual Native American allottees, mostly members of the Navajo tribe.

"Oil and gas companies are offering Navajo allottees thousands of dollars to access their lands," Reed says. Ora Marek-Martinez, manager of the Navajo Nation's Historic Preservation Department, notes that poverty and high unemployment lead many landholders to accept. "The socioeconomic situation is that many of our people had pretty much nothing, no electricity or running water." She and others say the tribe is divided over the drilling, because Native Americans also have a strong interest in protecting the Chaco world. "Everything here is sacred; our spirituality is tied to the landscape," she says. "More and more of our communities are saying they are against the drilling."

For the archaeologists, such emotional ties to the land are a key part of understanding this far-flung ancient civilization. "What was important about living in this place?" Van Dyke asked the Mancos meeting. "Was it the mountain peaks all around you, was it who your neighbors were, was it the night sky, the raven flying overhead, the silence?" ■

Too close for comfort?

An energy boom in New Mexico's northwest has brought oil and gas drilling to the archaeological landscape of ancient roads and ruins that surrounds Chaco Canyon.

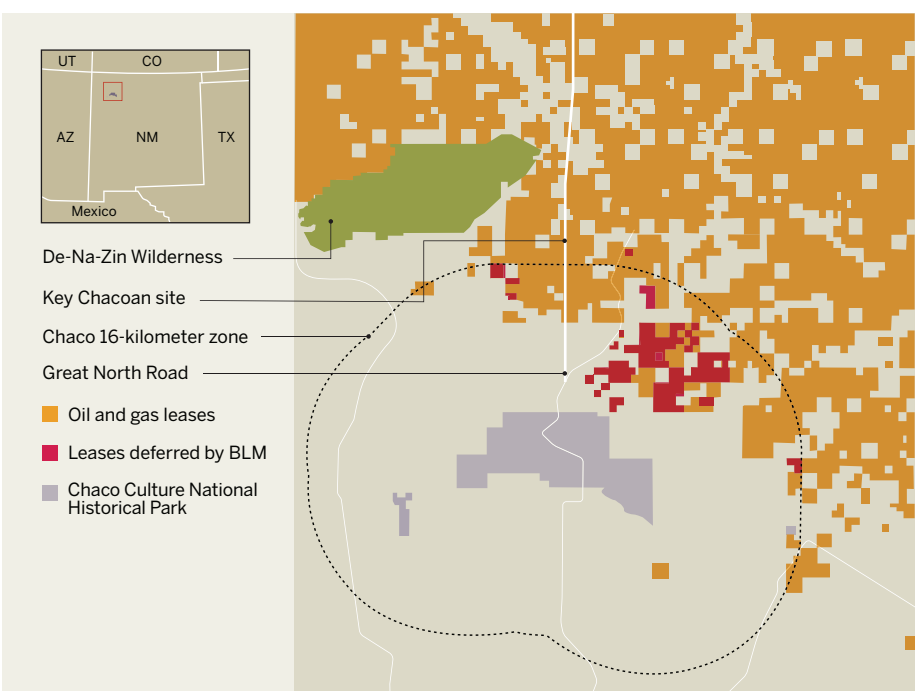

DATA: ADAPTED FROM THE WILDERNESS SOCIETY

POLAR SCIENCE

War over Belgian polar station

Science at risk in ownership quarrel over Antarctic base

By **Tania Rabesandratana**

The Belgian government and a private foundation are battling for control of the country's research station in Antarctica—and science is stuck in the middle. The government says it has ended its agreement with the International Polar Foundation (IPF), which built the station and has managed it since its 2009 inauguration but has since been accused of misusing public funds. The government vows to continue operations at the center with the help of the Belgian army.

But IPF, led by Alain Hubert, a charismatic explorer with several polar exploits under his belt, is fighting back. The foundation claims it remains in charge of the base, the Princess Elisabeth Antarctica.

The fight is creating uncertainty for scientists who are preparing for the 2015 to 2016 Antarctic research season, says Reinhard Drews of the Université Libre de Bruxelles (ULB). "We are scheduled to leave in November and not much time is left to figure out all the details," says Drews, who studies mass changes in Antarctica's coastal ice sheet.

Located about 220 kilometers from the coast at an altitude of 1382 meters, the sleekly designed €21 million station can accommodate up to 40 people. It was built by IPF, with the state chipping in about €9 million and the remainder coming from private funders. After its completion, IPF transferred 99.9% of the ownership to the Belgian government; the foundation held on to a symbolic 0.1% share. IPF was tasked with handling logistics and day-to-day operations, while Belgium's science policy office (BELSPO) manages and implements the science programs through its Polar Secretariat.

Relations soured 2 years ago after Philippe Mettens, then the president of BELSPO, filed a complaint with Brussels's public prosecutor against Hubert, who is president of IPF's board and, until last week, was a member of the Polar Secretariat's strategic council.

Mettens alleged that Hubert had channeled public money through the foundation and several private companies set up in his own name or that of his wife, IPF vice president Nighat Amin. The prosecutor's investigation is still ongoing.

Hubert did not respond to an email from *Science*, but Amin writes that IPF rescinded its donation agreement in 2013 because the government did not fulfill its part of the deal. "The station now belongs 100% to the Polar Foundation, and will continue to support international collaborative research," Amin says. "Since we made the gesture of giving the station to the Belgian people in March 2010 … our lives have been turned into a living hell by the public servants."

IPF planned to hold a press conference on 20 August, after *Science* went to press, but a statement issued on 17 July says that its books are clean and that IPF's "affiliated companies" are "historical partners" that "have been remunerated for their services at fair market value."

In a Royal Decree signed on 10 August, the government announced it would change the Polar Secretariat's rules to remove six private sector members, including Hubert, from the 12-member strategic council. The government said that the presence of IPF representatives on the council was a conflict of interest, because the foundation is the main beneficiary of funds managed by the secretariat.

IPF says it will run future science expeditions to the station on its own. "The Princess Elisabeth Antarctica has now become an international research station and will no longer be associated with any one country," the foundation wrote in an 8 August email, seen by *Science,* which invited researchers to travel to the station in the upcoming season. The government struck back 5 days later in an email to the same researchers that called the invitation "legally null and void." IPF "is no longer the official operator of the Belgian State," the government said, adding that the secretariat will run the upcoming science campaign itself, with help from the Ministry of Defense.

The fight puts researchers in a delicate position. Jan Lenaerts of Utrecht University in the Netherlands, who studies the melting ice shelves of East Antarctica, relies on private grants that have so far been managed by IPF. "This dispute makes my project's financial situation uncertain," says Lenaerts, who's hoping for a quick solution. "My only interest is science, and this science is endangered in this uncertain situation."

> ***"Our lives have been turned into a living hell by the public servants."***
>
> **Nighat Amin**, International Polar Foundation

Some scientists say that they will work with the government instead of IPF for this year's expedition. "We have several instruments running in Antarctica that need to be checked and revised," says Frank Pattyn, a glaciologist at ULB. "Any failure in getting there means the loss of months [or] years of data and investment." But glaciologist Konrad Steffen of the Swiss Federal Institute of Technology in Zurich says he'd rather abandon his research than accept what he sees as a government takeover. "I cannot understand how a government can nullify a contract with a foundation that has raised the money and organized the building of a research station," Steffen says.

One open question is whether the Belgian government can even run the station this year without IPF's involvement. The Princess Elisabeth is a "complex machine" that needs specialized technicians to maintain power, heating, and data servers, says one scientist who asked to remain anonymous, and researchers need experienced mountain guides. "Failure to get adequate support will for sure end in injury or loss of life," the scientist says. But Pattyn doesn't expect problems. "We can count on people from the Belgian army that were also involved in the construction project of the station," he says.

Mettens says he always opposed the complex deal between the government and IPF and is glad to see it end. "Alain Hubert's strength was his skill and experience," he says. "This is an interesting turning point that will push the Belgian state to acquire those skills." ■

The €21 million Princess Elisabeth Antarctica hosts studies of ice shelves and other research during the southern summer.

PHOTO: © INTERNATIONAL POLAR FOUNDATION - RENÉ ROBERT

ANIMAL WELFARE

New rules may end U.S. chimpanzee research

As of 14 September, no U.S. labs will be conducting invasive studies on chimps

By **David Grimm**

Zero. That's the number of labs that have applied for a permit to conduct invasive research on chimpanzees in the United States, as required by a new U.S. Fish and Wildlife Service (FWS) rule. The number suggests that all biomedical research on chimps in the United States has stopped—or is about to stop—and it's unclear whether the work will ever start again.

"This is the beginning of the end of invasive chimpanzee research," says Stephen Ross, director of the Lester E. Fisher Center for the Study and Conservation of Apes at the Lincoln Park Zoo in Chicago, Illinois, who pushed for the FWS rule. "Scientists have seen the writing on the wall."

Biomedical research on chimpanzees has been waning since 2013, when the National Institutes of Health (NIH) announced that it would phase out most government-funded chimp research and retire the majority of its research chimps to sanctuaries. The most recent blow came in June, when FWS stated that all chimpanzees in the United States—including the more than 700 chimps used in research—would be classified as endangered under the Endangered Species Act (ESA). Any labs that wished to continue invasive work on these animals would need to apply for an ESA permit, and the agency would grant permits only for work that enhances the survival of the species and benefits chimpanzees in the wild.

The agency's move was certain to have "a chilling impact" on biomedical research, warned John VandeBerg, the former director of the Southwest National Primate Research Center (SNPRC) in San Antonio, Texas, at the time. And so it has. According to FWS, by 17 August not a single lab had applied for an ESA permit. And because the agency needs 90 days or more to review permit requests, no labs will have one by the time the rule goes into effect on 14 September. That means any ongoing projects must stop on that date.

Robert Lanford, the current director of SNPRC, says no research is being done with any of the center's 129 chimpanzees, and that his organization is not applying for permits at this time. The most recent project—a test of antiviral drugs against hepatitis B—was ended early to avoid running into the 14 September deadline, he says. "If we weren't required to go through all of these processes, we'd still have several ongoing projects." He notes that in the past the center has made its animals available to scientists who study everything from AIDS to cutting-edge antibody research. "There were still critical experiments being done."

All chimpanzees in the United States are now classified as endangered, so invasive research requires a federal permit.

PHOTO: AP PHOTO/GERALD HERBERT

Lanford says he's not surprised that other labs haven't applied for permits. Any request is likely to attract opposition from animal advocates, he says, and it's not clear whether FWS would grant the permit. "Nobody wants to be the first test case."

The FWS ruling also may affect labs that conduct only behavioral research on chimpanzees. Typically, behavioral research doesn't require a permit, says FWS spokeswoman Vanessa Kauffman. But the requirement could kick in if the research involves activities that constitute a "take," which means actions that harm, stress, harass, or noticeably change the animal's behavior. Even snipping hair and drawing blood could be considered a take in some circumstances. To be safe, any researcher working on a chimpanzee should consult with FWS before continuing their project, Kauffman says. (The Yerkes National Primate Research Center in Atlanta, which houses 57 chimpanzees for behavioral research, says it is still figuring out whether it needs permits.)

NIH says it is not currently funding any biomedical or behavioral research involving chimpanzees. If it resumes such funding, NIH says it will ask researchers to consult with FWS.

Even though chimpanzee research is winding down in the United States, Lanford believes it will continue in some capacity. "We will eventually negotiate a path to getting permits for highly innovative projects where there is no other animal model," he predicts. "The chimpanzee is still an extraordinarily important model for medical research."

In the meantime, researchers are pondering where the animals should live out their days. Lanford says SNPRC's 129 chimpanzees are in the best place possible. With its extensive staff and medical capabilities, he says, "we believe that our facility provides the greatest quality of care these animals will get anywhere." He also notes that NIH has said it plans to maintain a colony of 50 chimps to meet future research needs, and that his center could meet that need. "I don't foresee a situation where we would send these animals to a sanctuary."

That's a shame, says Ross of the Lincoln Park Zoo, who believes sanctuaries are not only better for these animals—but better for noninvasive research. He studies chimp cognition at the zoo using a touch screen that the animals can use whenever they like, and he says similar experiments could be conducted in sanctuaries. "They would be in a place where the primary consideration is their care, and we could work with them in a much more open environment," he says. "We still have a lot to learn from them." ■

Shell is hoping the drilling rig *Polar Pioneer* can strike oil in the Chukchi Sea off Alaska.

PHOTO: MARK MEYER

ENERGY

As Arctic drilling starts, Shell-funded researchers keep watch

Critics uneasy at industry role in environmental monitoring

By **Eli Kintisch**, *in Barrow, Alaska*

Some 100 kilometers west of this small Arctic community—the northernmost settlement in the United States—a massive drilling rig this week began a controversial search for oil beneath the Chukchi Sea. Petroleum giant Royal Dutch Shell is hoping that an exploratory well drilled by the *Polar Pioneer* will help identify lucrative new oil fields and show the company can work safely in frigid Arctic seas. But many environmentalists fiercely oppose drilling here, the company's first foray into Arctic waters since an earlier effort faltered in 2012. They argue it threatens sensitive ecosystems and are watching the operations closely.

So are scientists involved with two little-known research programs here that are operated by a pair of Native Alaskan municipalities—and funded by Shell. These "Shell Baseline" programs have quietly funneled more than $15 million to studies of existing and potential drilling impacts and have collected elusive data on wildlife populations, ocean currents, and ice movements. Some researchers and local officials say the information will be key to safeguarding the region if drilling in nearby seas ever takes off—and they give Shell credit for giving local communities the power to help shape the research.

Others, however, criticize the arrangement as too close for comfort, and worry that Shell's influence will skew the science. "What's needed here," says Rick Steiner, an independent marine scientist and advocate in Anchorage, is "a truly independent ecological baseline research program."

Shell's interest in the Arctic stretches back decades, but it entered a new phase in 2008, when the company began purchasing federal offshore leases in the Chukchi Sea off the north coast of Alaska. Edward Itta, then the mayor of the North Slope Borough, headquartered here, subsequently approached the company about creating a research program. Itta says he saw the need for detailed baseline data that could be used to document any drilling impacts, such as changes in the behavior of seals and whales hunted by local residents. He also hoped the program could fill gaps in ongoing research efforts by federal regulators, whom he did not trust to effectively oversee drilling. They are "too close to industry," he says.

Itta made sure that the final deal, inked in 2010, gives Native Alaskans a major voice in selecting projects. In other Arctic research, "the local people are often in an advisory capacity," says Henry Huntington, an independent researcher from Eagle River who serves on the advisory board of the second Shell-funded program, begun 2 years ago by the Northwest Arctic Borough. But "in this case you have local people on the committees deciding what research gets done." In the North Slope program, an 18-member board including Shell staff, outside scientists, and native Inupiat representatives oversees an effort that will spend more than $1 million this year, its sixth. (The Northwest borough's program will spend roughly the same amount.)

The sister programs have supported a range of research projects. Several have installed undersea acoustic monitors to track whale movements, and to understand how the noise created by Shell ships and platforms might be affecting seals in Goodhope Bay off Kotzebue. "Before Shell started using the bay, it was pretty pristine—rarely even an outboard [boat] engine," says Alex Whiting, a Kotzebue government wildlife official.

Other projects are using drifting buoys and other sensors to track the movement of ice floes and currents. Such data could be crucial "if we ever have an oil spill," says subsistence hunter Lee Kayotuk of Kaktovik, one of many local residents who have been sharing their extensive knowledge of coastal waters with researchers. More than 30 Inupiat hunters and elders, for instance, participated in a 2013 workshop co-organized by the University of Alaska, Fairbanks (UAF), which focused on issues such as oil spill preparedness. Among other things, the Inupiat helped identify four key currents that could influence ice movements during a spill, and areas where slushy ice or other factors are likely to hamper response crews. Such results, says Tom Weingartner, a UAF oceanographer and adviser to the North Slope program, have "made me understand the value of traditional knowledge in my work."

The programs have produced several peer-reviewed papers. Shell declined to discuss the programs with *Science*, but it has included data from the research in recent filings to federal regulators, who on 17 August approved full-scale exploratory drilling.

It could be years before Shell knows whether the area is worth developing. In the meantime, some Inupiat officials oppose accepting the company's money for research. The previous mayor of the Northwest Arctic Borough, for example, declined Shell funding before current officials accepted it. And some researchers would prefer that Shell funnel its support through fully independent "citizen advisory councils," like those created in southern Alaska with Exxon funding after the 1989 *Exxon Valdez* oil spill. But "Shell has opposed that," Steiner says.

Whiting, of Kotzebue, is more sanguine. Regardless of Shell's aims, he says, the onus is on locals to use the funds for good. "You can argue Shell should be funding this research," he says, "since they're the ones potentially causing the damage to the ecosystem." ■

DATA CHECK

BEHIND THE NUMBERS

Rethinking the time 'lost' to red tape

By **Jeffrey Mervis**

When university lobbyists complain about excessive U.S. government regulation, they often use this statistic to bolster their argument: Administrative tasks take up 42% of the time that faculty members devote to their federal research grant. In other words, only 35 minutes of every hour paid for by U.S. taxpayers are devoted to research.

The statistic comes from a 2005 survey sponsored by a consortium of government agencies and research institutions called the Federal Demonstration Partnership. It was repeated in 2012 with the same result, fueling a meme that academic scientists are being strangled by red tape. A committee at the U.S. National Academies of Sciences, Engineering, and Medicine is currently looking into the problem, which another blue-ribbon advisory panel has blamed on "a culture of overregulation" that has led to "wasted federal research dollars."

But a closer look at the findings challenges that conventional wisdom. The survey also asked faculty members how much of their grant time would be devoted to administrative duties if they could set the rules. The answer—an average of 31%—may surprise you. In fact, nearly one-third of the researchers said that a significant easing of existing regulations would free up no more than 2 additional hours a week to spend doing science. (A similar fraction, it should be noted, said they would gain as many as 9 hours.)

If the paperwork on a federal grant is so crippling, why wouldn't reforms make more of a difference? The answer lies in the survey's definition of administrative tasks, which includes every function besides the conduct of "active research."

It turns out that many of those tasks are things that most scientists don't consider to be a burden, such as applying for a grant, training graduate students and postdocs, reporting to a federal agency on how its money was spent, and sharing the results of the research with colleagues and the public. "Writing grants and papers and managing your lab is just part of a scientist's job," says Robert Decker, who helped design the survey.

42

percent

Amount of time U.S. faculty say they spend on nonresearch activities as part of a federal grant

One such task is preparing for the next project. Faculty reported that fully 36% of the "administrative" slice of their research time—some 15.4% of their total effort—goes to preparing research proposals. That's not just writing time. Before sending in a proposal, scientists must review the literature. And in most fields they are also expected to have preliminary data to bolster their hypothesis.

Researchers do have reasons to complain, says Decker, who retired in 2009 after a career as a cardiology researcher, first at Northwestern University in Evanston, Illinois, and later at the University of Texas Southwestern Medical Center in Dallas. Low success rates may make the time devoted to grant writing seem more burdensome. A ceiling on what universities can charge the federal government for the cost of administering a grant has also added to researchers' loads.

Before the cap, Decker says, most faculty members could hire an assistant to handle purchases and keep the books. The ceiling, which Congress imposed in 1991 in response to improper accounting practices at several universities, meant that the government no longer reimbursed institutions for all of the administrative costs needed to comply with federal regulations, Decker says. "So the university administrators punted to the departments," he says, "and that left it up to the faculty. To be fair," he adds, "the sponsored research offices were woefully understaffed, and faculty are ultimately responsible under the law for managing their grants."

The 2005 survey prompted the federal government "to change some of the worst rules," Decker says. The current National Academies panel is expected to propose several additional changes, some of which could be inserted into pending legislation.

Even so, Decker warns scientists not to get hung up on the 42% number. "You need to figure out how to eliminate the stuff that is so time-consuming that you lose your focus as a researcher," Decker says. "The rest is probably a reasonable burden." ■

Published by AAAS

Internist and amateur detective Pieter Cohen is outraged that some of the supplements on the market are unsafe.

THE SUPPLEMENT SLEUTH

Some dietary supplements are spiked with drugs. Pieter Cohen is out to expose the hazards

By **Jennifer Couzin-Frankel**

Pieter Cohen's brush with death came at a most inconvenient time: just as he was about to nail another menacing ingredient in a dietary supplement.

Hiking last August in New Hampshire with his wife and three children, Cohen, an internist at Cambridge Health Alliance in Massachusetts, stumbled and fell. A rock punctured his left calf. "It was a little cut, but deep," recalls his wife, Lauren Budding. By the next day, bacteria were coursing through Cohen's bloodstream. The leg turned red and swelled. His blood pressure dropped precipitously. Cohen was rushed to a community hospital and soon after by ambulance to a trauma unit in Boston.

Doctors worked feverishly to stabilize him and stop the spread of infection. Over the next few days, the threat of death ebbed, though the risk that he would never walk normally remained. Cohen, meanwhile, fretted about the same matters he usually did: consumers, including his patients, who might be swallowing dietary supplements spiked with drugs. Bedbound and in searing pain, he asked for his computer. His wife refused.

"I'm like, 'I'm sorry, this person needs to sleep,'" she told the hospital staff. So Cohen had his mother smuggle in the laptop, along with data sets concealed inside *The Boston Globe*. "I could work on the manuscript when Lauren wasn't looking," he reasoned.

Eleven days after the accident, and after the fourth of what would be five surgeries, Cohen and two collaborators submitted their paper to *Drug Testing and Analysis*. The report was unnerving: At least a dozen supplements sold in the United States for weight loss, enhanced brain function, and improved athletic performance contained a synthetic stimulant. The compound, which Cohen and his co-authors named DMBA, resembled methamphetamine in its chemical structure. It had never been tested in people, only in two animal studies from the 1940s. "Its efficacy and safety are entirely unknown," they wrote.

By now ensconced in a hospital bed in his living room and waiting for skin grafts to heal, Cohen appealed to the journal: "I can't walk, I'm totally available. Can you guys crank this review?" The paper was published online a month later, last October. In April of this year, the U.S. Food and Drug Administration (FDA) issued warning letters to 14 companies selling products containing DMBA. "The FDA considers these dietary supplements to be adulterated," it wrote. And boom, Cohen was on to his next project.

Since 2005, when he found his patients were being sickened by a Brazilian weight loss supplement containing antidepressants and thyroid hormones, Cohen has become something of a mix of Indiana Jones and Sherlock Holmes in the supplement world. With chemist colleagues in the United States, Brazil, and Europe, he hunts for drugs illegally buried in supplements. Then he goes public. His unorthodox public relations strategy is to publish research fast in low-profile, specialty journals, reach out to a network of hand-picked journalists, and, he hopes, ultimately inspire new regulations. He has virtually no funding, nor does he aspire to secure any. "I have total freedom," he says. So far, he and his collaborators have identified three hidden stimulant drugs in supplements.

Cohen's discoveries highlight a broader problem, he and others contend: a dysfunctional system for policing dietary supplements. "It comes to this," says Paul Offit, director of the Vaccine Education Center at the Children's Hospital of Philadelphia, who published a book called *Do You Believe in Magic?* about alternative medicine. "Essentially a private citizen [is] doing the testing to make sure what's on the label is in the bottle. … It's absurd."

But that private citizen is having an impact. FDA actions have cited Cohen's work or followed his publications, as the DMBA warnings did. He has also caught the attention of supplement companies, including in a lawsuit filed against him in April seeking $200 million in damages. "Everything I write gets such scrutiny" that it creates tremendous pressure, he says. "I want our science to be bulletproof."

Tainted supplements

Prescription and illegal drugs are routinely found in supplements. Here's a sampling of more than 50 culprits from 2015.

PRODUCT NAME	CATEGORY	HIDDEN INGREDIENT
Smart Lipo	Weight loss	Sibutramine (a withdrawn weight loss drug); phenolphthalein (unapproved laxative ingredient)
Xcel	Weight loss	Fluoxetine (brand name Prozac)
Extreme Diamond 3000	Sexual enhancement	Desmethyl carbodenafil (unapproved, structurally similar to Viagra's active ingredient)
King of Romance	Sexual enhancement	Sildenafil (brand name Viagra)
Asihuri Plus Forte	Joint and nerve pain	Dexamethasone a (corticosteroid); phenylbutazone (discontinued NSAID)

THE MODERN SUPPLEMENT ERA began in 1994, when Congress passed the Dietary Supplement and Health Education Act, or DSHEA (pronounced duh-shay-uh). In the decades before, the supplements industry was overwhelmingly focused on vitamins and minerals. Much of the regulation centered on recommended daily allowances of products like vitamin C, iron, or calcium.

DSHEA established the first broad framework for regulating supplements. It also gave supplements a legal definition: as substances intended to "supplement the diet," containing "dietary ingredients" such as herbs, botanicals, or vitamins.

At the same time, the law sharply curtailed FDA's power. Companies were not required to notify FDA provided the dietary ingredi-

CREDITS: (PHOTO) DOMINICK REUTER; (DATA SOURCE) FDA

ent had a history of use before the law was passed. For the first time, DSHEA allowed them to make claims on the label suggesting supplements affected the structure or function of the body—for example, by boosting the immune system or protecting prostate health. And DSHEA codified a loose arrangement: Under the law, as FDA notes on its website, "unlike drug products that must be proven safe and effective for their intended use before marketing, there are no provisions in the law for FDA to 'approve' dietary supplements … before they reach the consumer." The agency can act only after a supplement is on the market and evidence shows it's unsafe.

Whereas the industry and many consumers celebrated DSHEA for expanding access to supplements, the act was skewered by physicians, journalists, and consumer protection groups. In an editorial shortly before DSHEA passed, *The New York Times* called it the "snake oil protection act," suggesting that it was "about the right of unscrupulous companies and individuals to maximize profits by making fraudulent claims." Meanwhile, the industry grew exponentially: Since 1994, the number of dietary supplements marketed in the United States has swelled from about 4000 to more than 75,000. About $36 billion worth were sold last year.

The ink had barely dried on DSHEA when trouble began. Within 2 years, a Chinese herb called ma huang or ephedra, which companies promoted as a legal alternative to ecstasy, was under scrutiny. Although a natural product, the herb contains the chemical ephedrine, which stimulates the nervous system and constricts blood vessels. By early 1996, it had been linked to at least 15 deaths. Meanwhile, FDA was regularly issuing warnings about liver, kidney, and other health risks tied to supplements.

"There are authentic dietary supplements—multivitamins, calcium, iron—which do supplement the diet" and can help many people, says rheumatologist and immunologist Donald Marcus of Baylor College of Medicine in Houston, Texas, an early critic of the supplement industry. But other supplements, like "St. John's wort, echinacea … are used as medicine," he points out. In part because "botanicals are complex mixtures of chemicals," supplements in this category present "a serious and growing public health problem," Marcus and a colleague, pharmacologist Arthur Grollman of the State University of New York at Stony Brook, wrote in *The New England Journal of Medicine* in 2002. Just how big a problem was unclear, however, because FDA hears about only a tiny fraction of adverse events from the companies, they noted.

Meanwhile, concerns about ephedra continued to mount. Army commissaries stopped selling it after it was implicated in the deaths of soldiers; after a 16-year-old taking the supplement died in Illinois, that state halted ephedra sales, too. FDA banned ephedra in 2004, after a 23-year-old Major League Baseball pitcher collapsed and died during practice and was found to be taking the herb.

53%
of U.S. adults report taking at least one dietary supplement.

34%
of U.S. adults report taking both a dietary supplement and a prescription medication.

18%
of U.S. adults report taking at least one natural product (not including vitamins and minerals).

$36 billion
The amount that Americans spend a year on dietary supplements

Cohen's initiation into supplements came on the job. After finishing at the Yale School of Medicine, he began his residency and then went to work at Cambridge Health Alliance, a network of neighborhood clinics and community hospitals. Many of Cohen's patients were Brazilian immigrants who had settled nearby.

Before long, the clinic's patients developed mysterious symptoms. One woman came in "with palpitations, sweating, anxiety, but also feeling very tired," remembers Daniel McCormick, a primary care internist in the same practice, who mentored Cohen in residency and shares a small office with him. Another wound up in the emergency room with kidney failure. One man lost his job after his urine tested positive for amphetamines.

Cohen made the connection: The patients were all taking weight loss pills known as rainbow diet pills, imported in bulk from Brazil. He sent the capsules off to a private lab for testing. The results shocked the doctors. The tests revealed amphetamines, thyroid hormones, diuretics, benzodiazepines, and antidepressants such as fluoxetine. "It was a pharmacopeia in one pill," McCormick says. "It became clear to a lot of us that you could explain the symptoms from the diet pills."

McCormick, Cohen, and three other colleagues conducted a survey of 307 Brazilian patients in their clinic and two nearby churches. They found that 18% in the clinic and 9% in the churches reported taking the pills, and two-thirds reported side effects. The paper was published online in 2007 in the obscure *Journal of Immigrant and Minority Health*.

"Less than 10 people are going to read that," Cohen admitted to himself, because the journal is so specialized. "I knew that if I wanted more … I needed to do some outreach." He contacted a local NPR reporter who had recently run a story on Latino bodegas selling antibiotics without a prescription, thinking he might be interested. The reporter invited him in for a studio interview. *Folha de S.Paulo*, a major Brazilian newspaper, contacted Cohen and ran a front-page story. Several years later, rainbow diet pills were banned in Brazil, though Cohen doesn't know whether his work had anything to do with that.

Cohen thought the spiked supplements were an anomaly confined to the Brazilian neighborhoods. But then he got a call from an official in the drug division at FDA. "What you found in those diet pills shipped up from Brazil," the official told him, "actually are found in weight loss supplements in the United States, and it's a major problem."

"WE HAVE BEEN WORRIED about contaminated dietary supplements for ages," says Amy Eichner of the U.S. Anti-Doping Agency in Colorado Springs, Colorado. In 2003 and 2008, two elite swimmers lost the chance to compete in the Olympics after testing positive for performance-enhancing drugs they said they didn't know were in their supplements. A similar fate befell two top cyclists. "That's our nightmare scenario," Eichner says.

Another with longstanding concerns is Patricia Deuster at the Uniformed Services University of the Health Sciences in Bethesda, Maryland, who estimates that between 15% and 20% of military members are swallowing the supplements she and others fret about most: products marketed for bodybuilding, weight loss, and athletic performance. Another worrying category includes sexual enhancement products.

So in 2013, she and Eichner began systematically parsing supplement ingredients. Preliminary results, still unpublished, show that of the 169 high-risk products tested so far, 107 "contained at least one substance prohibited in sports," Eichner says, and often that substance wasn't listed clearly on the label. In many cases, she says, the ingredients are "either Schedule III substances on the Controlled Substances Act—that's pretty major—or they have been specifically declared illegal by the FDA."

DATA SOURCES: (TOP TO BOTTOM) CDC; *JOURNAL OF THE ACADEMY OF NUTRITION AND DIETETICS*; CDC; NIH

At around that time, Cohen had an electrifying phone conversation. A lab scientist who tests supplements for companies confided in Cohen that he was deeply disturbed by the prevalence of an ephedra substitute, a stimulant called dimethylamylamine or DMAA, which kept appearing in products despite mounting concerns about its safety. That conversation was "the catalyst that opened this whole new world to me," Cohen says.

With rainbow diet pills, he'd been focused on prescription drugs. Although DMAA had appeared in nasal sprays many decades ago before being removed from the market, it was now more like a "research chemical," Cohen says, which some companies argued came from plants but which Cohen and many others disputed. He began searching for dangerous additives in supplements. FDA declared supplements containing DMAA illegal soon after, in 2013, but as Cohen quickly learned, there was no shortage of other targets.

"It's a Sherlock Holmes situation," he says with relish. "There's a crime scene, there's hints of struggle, people are dying after taking supplements. … What is actually going on?"

He found a perfect partner more than 5000 kilometers away near Utrecht, the Netherlands: Bastiaan Venhuis, a medicinal chemist who was also analyzing supplement ingredients. One of their first joint publications, in collaboration with NSF International, which tests food, supplements, and other consumer products, appeared online in the fall of 2013 in *Drug Testing and Analysis*. It examined a popular workout supplement called Craze. When Venhuis diluted the powder and ran it through his analyzer, telltale peaks indicated DEPEA, a methamphetamine analog.

To garner publicity, Cohen expanded the strategy he had followed with the Brazilian supplements. He sought a final manuscript from the journal about a week in advance and sent personal emails to upward of three dozen journalists, carefully selected for their prior coverage or relationships he had nurtured with them.

Cohen's office buddy McCormick acknowledges that such media outreach, which he's done himself, can feel awkward. It's often regarded "as self-promotional," McCormick says. "In the beginning I felt that way intensely and it was very uncomfortable. But … the vast number of hours that go into thinking about a research project, writing it, is just wasted" if it stops there, especially when it might have an impact on health policy.

Cohen has caught the attention not only of myriad journalists but of the supplement industry, too. In late April, a company called Hi-Tech Pharmaceuticals filed a $200 million claim for damages against Cohen and two colleagues, after the researchers published a paper suggesting Hi-Tech and other companies were marketing supplements that contained an amphetaminelike stimulant, BMPEA, which they mislabeled as *Acacia rigidula*, a shrub that grows in Texas and south into Mexico.

The company vigorously disputes that BMPEA is not part of the plant. "A real scientist concerned with objectivity would have taken steps to ensure that they weren't disparaging products before they did this to the public," says Edmund Novotny, an attorney in Atlanta who represents Hi-Tech.

Cohen wasn't alone in singling out BMPEA: His study came about 18 months after FDA scientists reported detecting BMPEA in supplements, too, noting that nowhere could they find evidence that BMPEA was a natural component of plants. Soon after Cohen's publication, FDA sent warning letters to five companies selling BMPEA-laced supplements, including Hi-Tech.

Like others, Cohen agrees that FDA's supplement policing powers are too limited. But that doesn't mean the agency has no muscle. "There's so many things FDA could be doing that they're not doing," he says—for example, removing supplements from store shelves when companies don't fully pass FDA inspections. The agency, Cohen believes, is overwhelmed by the sheer volume of supplements and discouraged by political forces from acting aggressively. When it comes to pulling a supplement ingredient, FDA's attitude is "show us the dead bodies," he says.

FDA officials wouldn't put it that way, but they don't entirely disagree. "Under current law, the FDA faces a high burden before it can take enforcement action on a dietary supplement," wrote spokeswoman Lyndsay Meyer in an email message. The agency has its own frustrations. "The supply chain … is extremely fragmented," Meyer wrote. "The individuals and businesses selling these products may operate out of residential homes, and distribute via internet, small stores, and mail … We recognize that more can and should be done."

Nearly a year after his harrowing ordeal while hiking, Cohen has regained full function of his leg, though he still wears a black compression stocking. Sitting in his office in June, surrounded by photos of his three children and a jumble of supplement bottles patients have handed over to him for testing, Cohen shows little of the fatalism of others who have battled supplements for years. The reform movement "definitely has momentum," he says. "I think we're going to look back 50 years from now, and say 'How could supplements have been regulated like this?'"

In anticipation of that day, Cohen is working now to nail two more drugs that show up in supplements. He's also been studying yohimbine, a prescription drug that can be extracted from the bark of a species of West African evergreen tree and sometimes appears in bodybuilding capsules. Like ephedrine, yohimbine "comes from a plant but is pharmaceutically active," he says, blurring the line between drug and supplement.

His dream is an informed populace, with companies required to fork over the recipes and the risks of their products. "Whenever possible, we should have the freedom of being able to purchase whatever we want to put in our body," Cohen says. "People should be able to purchase echinacea. It's just, when they purchase echinacea, they should know what they're getting." ■

Top swimmer Jessica Hardy tested positive for a banned substance she said she didn't know was in a supplement she was taking. "That's our nightmare scenario," says a U.S. antidoping official.

PHOTO: MARK SAVAGE/CORBIS

INSIGHTS

Limits on dark matter and energy *p. 786*

A roadmap for economic equality *p. 797* ▸

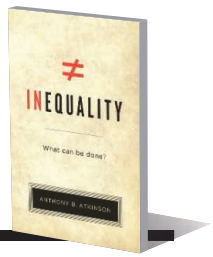

PERSPECTIVES

Unnatural selection. Human hunters and fishers (such as Ernest Hemingway, pictured with a marlin) specialize in adult prey and often target large, healthy individuals.

ECOLOGY

A most unusual (super)predator

Effects of human hunting and fishing differ fundamentally from those of other predators

By **Boris Worm**

Modern humans evolved as cooperative hunter-gatherers whose cultural and technological evolution enabled them to slay prey much larger than themselves, across many species groups. One might think that those hunting skills have faded since the advent of agriculture and animal husbandry almost 10,000 years ago. Yet, as Darimont *et al.* show in a global analysis on page 858 of this issue (*1*), we are still the unique superpredator that we evolved to be. Analyzing an extensive database of 2135 exploited wild animal populations, the authors find that humans take up to 14 times as much adult prey biomass as do other predators. Our trophic dominance is most pronounced outside our own habitat, in the oceans (see the chart).

Several recent studies have tracked the impacts of people on past (*2*, *3*) and contemporary (*4*) wildlife populations, as well as their knock-on effects across many ecosystems (*5*). Darimont *et al.* go beyond this previous work to compare land and sea animals across various trophic levels. They show that on land, hunters put much greater pressure on top carnivores than on herbivores. In contrast, fishing pressure appears similarly

Biology Department, Dalhousie University, Halifax, Nova Scotia, Canada, B3H4R2. E-mail: bworm@dal.ca

PHOTO: CORBIS

high across different trophic groups (see the chart), a pattern that has been dubbed "fishing through marine food webs" (*6*). Consistent with this hypothesis, the rate of population collapse in small fish low in the food chain, such as herring or anchovies, matches or exceeds that of higher trophic level predators such as sharks and tuna (*7*). One reason for this imbalance between land and sea is likely that fishing is now mainly a mechanized industry, much like agriculture (but unlike hunting) on land. Total marine fish catch (including unreported catch and discards) likely exceeds 100 million tons (Mt) per year (*8*), whereas the terrestrial take is estimated to be less than 5 Mt per year (*9*). Historical shifts from hunting to fishing can locally reverse where fisheries are depleted: Coastal overfishing off West Africa, for example, has caused food scarcity that intensified again the hunt for wild meat on land (*10*).

Why do human hunters and fishers focus so heavily on adults rather than juveniles, the preferred prey for most nonhuman predators? Probably this relates again to our technological means, which, for example, allow killing from a safe distance, and specific culture, for example, hunting for trophy and status (see the photos). This unique preference, however, has implications for the sustainability of exploitation and even the course of evolution. Adult individuals provide the "reproductive capital" of a population, akin to the financial capital in a bank account or retirement fund. The interest that is generated by annual growth is represented by the juveniles produced every year, as well as the physical growth of individuals. Depleting the capital is risky, particularly in long-lived, late-maturing organisms. Trophy hunters and fishers, in particular, often target the largest, healthiest, and fittest organisms (see the photos). This produces a strong selection pressure away from certain traits, such as the ability to grow rapidly to large size. As a consequence, the gene pool of many exploited populations changes in ways that could compromise their potential to recover from previous depletion (*11*).

Two potential biases are associated with research into human effects on contemporary wildlife. First, there is survivorship bias: We only measure what is left. Many vulnerable wildlife species on land have already disappeared during the past 40,000 years in successive waves of extinction on continents and islands that were colonized by people (*3*). Related to that is observer bias: The data-rich populations that are scientifically observed and monitored likely also experience some form of management, which may motivate data collection in the first place. Both biases render the results of Darimont *et al.* conservative. More worrying are populations that are hunted or fished essentially unobserved; at least in the oceans, there is clear evidence (*12*) that these are worse off than the assessed stocks represented in the chart below.

What does this general body of work (*1*–*5*) tell us then, about our own species? There are three key insights. First, the hunting of large prey is deeply embedded in our identity and remains a powerful ecological and evolutionary force. Second, the ability to target mostly adult individuals across marine and terrestrial prey groups makes us unique among all other predators. And third, we have the unusual ability to analyze and consciously adjust our behavior to minimize deleterious consequences. This final point, I believe, will prove critical for our continued coexistence with viable wildlife population on land and in the sea. ■

Trophy hunt. On land as well as on sea, humans exploit their ability to hunt from a safe distance and hunt for trophies or status.

PHOTO: PAULA FRENCH/SHUTTERSTOCK; ILLUSTRATION: ADAPTED BY P. HUEY/*SCIENCE*

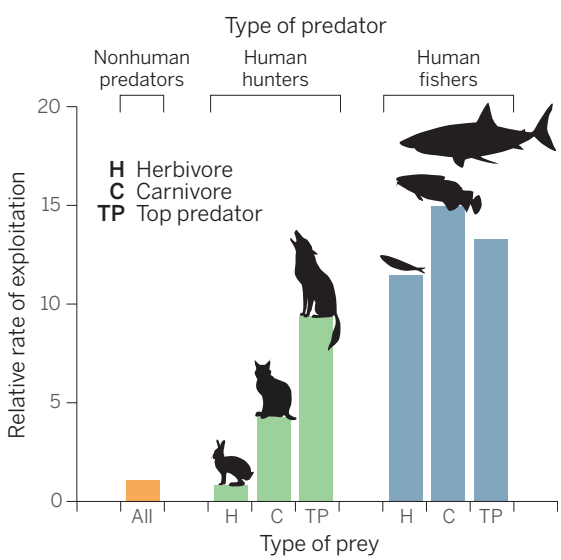

Wildlife under pressure. Darimont *et al.* show that the rates at which humans exploit adult land mammals and marine fish vastly exceeds the impacts of other predators (*1*). Marine fish experience "fishing through marine food webs," with different trophic groups similarly affected. In contrast, land predators are exploited at much higher rates than herbivores.

REFERENCES

1. C. T. Darimont, C. H. Fox, H. M. Bryan, T. E. Reimchen, *Science* **349**, 858 (2015).
2. H. K. Lotze, B. Worm, *Trends Ecol. Evol.* **24**, 254 (2009).
3. P. S. Martin, D. W. Steadman, in *Extinctions in Near Time*, R. D. E. MacPhee, Ed. (Kluwer Academic/Plenum, New York, 1999), pp. 17–56.
4. R. Dirzo *et al.*, *Science* **345**, 401 (2014).
5. J. A. Estes *et al.*, *Science* **333**, 301 (2011).
6. T. E. Essington, A. H. Beaudreau, J. Wiedenmann, *Proc. Natl. Acad. Sci. U.S.A.* **103**, 3171 (2006).
7. M. L. Pinsky, O. P. Jensen, D. Ricard, S. R. Palumbi, *Proc. Natl. Acad. Sci. U.S.A.* **108**, 8317 (2011).
8. B. Worm, T. A. Branch, *Trends Ecol. Evol.* **27**, 594 (2012).
9. E. J. Milner-Gulland, E. L. Bennett, S. A. M. W. M. Group, *Trends Ecol. Evol.* **18**, 351 (2003).
10. J. S. Brashares *et al.*, *Science* **306**, 1180 (2004).
11. J. A. Hutchings, S. H. Butchart, B. Collen, M. K. Schwartz, R. S. Waples, *Trends Ecol. Evol.* **27**, 542 (2012).
12. C. Costello *et al.*, *Science* **338**, 517 (2012).

10.1126/science.aac8697

Scientists working on the heart of the XENON100 dark matter detector.

ASTROPHYSICS

Probing the dark side

Fundamental questions about dark matter and dark energy are probed in laboratory experiments

By **Jörg Schmiedmayer** *and* **Hartmut Abele**

In the past 17 years, a new picture of our cosmos has emerged based mainly on the energy-matter budget of the universe, as determined by the percent level by observation (*1*). A striking consequence is that regular matter built from the known particles of the standard model (e.g., quarks, leptons, neutrinos, and photons) accounts for only 4.9% of the total energy-matter density. Most of our universe consists of two components of unknown origin that are colloquially called dark matter (26.8%) and dark energy (68.3%). Two reports in this issue describe experimental efforts in the search for the proposed constituents. On page 849, Hamilton *et al.* (*2*) search for chameleon fields, one of the most prominent dark energy candidates, and on page 851, the XENON Collaboration (*3*) reports on their search for dark matter.

Dark matter is conjectured to be responsible for the excess of gravitational interaction observed in the universe down to the scales of galaxy clusters and individual galaxies. Besides indirect observations through its gravitational effects on visible matter and radiation, it has evaded more conventional observation, which indicates very weak electromagnetic coupling, hence the name. Although there have been a large number of theoretical proposals about the nature of dark matter, consistency with our detailed and precise knowledge of physical processes forming our universe favors proposals based on new particles like axions or WIMPs (weakly interacting massive particles).

The goal of experiments that test these proposals is to look for effects of dark matter other than gravity, mostly through interactions with the particles of the standard model (*4*). For example, WIMPs interacting with regular matter may create recoiling charged particles that can be seen in detectors. To be consistent with both cosmology and the present standard model, the interactions need to be very weak, so events will be very rare. The detectors must have very large mass and extremely low background signals.

The latest dark matter experiment of XENON100 (*5*) uses a detector located in the Gran Sasso underground laboratory in central Italy (see the first figure). The detector material is liquid xenon, which has superb ionization and scintillation properties and can be made exceptionally pure to minimize background signals. The liquid xenon volume is used as a position-sensitive time projection chamber for measuring trajectories of charged particles. The xenon liquid is also viewed by arrays of photomultiplier tubes to detect the predicted WIMP signal—a primary prompt scintillation in connection with a delayed ionization signal from the recoil (see the second figure for additional background reduction).

The simultaneous measurement of charge and light and a three-dimensional position-vertex reconstruction allows unprecedented rejection of background events. A dark matter particle in the form of a WIMP is expected to induce nuclear recoils in a terrestrial detector target with an annually modulated rate determined by the motion of the Earth around the Sun. The DAMA/LIBRA collaboration, using a sodium iodine target, found such a modulation signal, and a dark matter–induced electronic recoil was proposed as an explanation for the observed modulation (*6*). However, the XENON100 detector, being orders of magnitude more sensitive, explicitly rules out this possibility for three different representative dark matter models (*3*).

The true nature of dark energy, which is needed to explain the observed accelerated expansion of the universe, is an even bigger mystery. The two most prominent candidates for dark energy are Einstein's cosmo-

Vienna Center for Quantum Science and Technology Atominstitut, TU-Wien Stadionallee 2 1020 Vienna, Austria. E-mail: schmiedmayer@atomchip.org; abele@ati.ac.at

PHOTO: XENON100 COLLABORATION

logical constant (*7*), resulting in a smooth component with an effective negative pressure, and quintessence theories (*8*, *9*), where the vacuum energy is associated with a field (the cosmon), which is assumed to be a fundamental scalar that changes over time. Both might be connected—it is conjectured that the cosmological constant can be seen as the "mean field" of the cosmon.

The main problem in observing a scalar field of a quintessence theory is that if the cosmon couples to matter, it should have been seen in measurements of the equivalence principle. To fix this problem, Khoury and Weltman proposed in 2004 (*10*) a mechanism that would make the effect of the cosmon interacting with matter nearly vanish at laboratory scale, and simultaneously keep it effective at cosmological scale. The basic idea is that the scalar field acquires a mass that depends on the local matter density. On Earth, where the density is high, the interaction range of the field is sufficiently short to satisfy all existing tests of gravity. In interstellar space, where the density is tiny, the field causes the observed cosmic acceleration, which fixes the magnitude of the vacuum energy of the field. Because its physical properties depend sensitively on the environment (the density of matter), such a scalar field was dubbed a chameleon (see the third figure).

Cosmological observations and precision gravity and equivalence principle experiments leave a large parameter range available for these chameleon theories because in standard experiments, both the source and the "sensor" are macroscopic pieces of matter, and for both objects, heavy screening reduces any signal. The use of a single atom or neutron as a sensor dramatically avoids the screening effect for the sensor over a wide range of possible parameters.

Until recently, not much was known about hypothetical chameleon fields and their coupling parameter β to matter. The best constraints came from atomic physics but still allowed for a coupling (in units of the inverse Planck mass) as large as $\beta = 10^{14}$. A huge step forward (by seven orders of magnitude) was made by analyzing precision measurements of gravitational quantum states of neutrons bouncing above a flat surface (*11*) and by analyzing neutron interferometer experiments (*12*), as suggested by (*13*, *14*). The use of neutrons as test particles bypasses the electromagnetic background induced by van der Waals and Casimir forces and allows probing at very short distances.

Recently, Burrage, Copeland, and Hinds (*15*) have proposed using atom interferometers to search for chameleons. An ultrahigh-vacuum chamber containing atomic test particles simulates the low-density conditions of empty space, liberating the chameleon field so that it becomes long-ranged and measurable at a distance from the surface. Hamilton *et al.* now implement this idea by using a light-pulse atom interferometer to look for minute changes in the accelerations of cesium atoms near a spherical mass as a source for the chameleon fields. They conclude that any residual acceleration has to be smaller than 5.5 $\mu m/s^2$ at the 95% confidence level. These values exclude all chameleon theories that could account for dark energy with a coupling constant $\beta > 4.3 \times 10^4$.

The approximations entering the calculations of (*14*) were recently addressed by numeric integration of the full field equations (*16*). Based on this additional information, the limits may even be better.

The interferometer experiments of Hamilton *et al.* are currently limited by systematic shifts. Pushing to the standard sensitivity limit of such atom interferometers will push the limits of the coupling constant β to $\beta < 1$, and thereby completely exclude a large class of chameleon theories. It is remarkable that such a laboratory-scale precision experiment has the potential to probe the physics of dark-energy chameleon fields at the Planck scale and beyond.

A swan song for chameleon fields? One candidate for dark energy is a chameleon field, which modifies the wave functions of matter (here depicted as the strings of a lyre). The experiments of Hamilton *et al.*, which use a small atomic test mass, greatly constrain these theories.

Both of these experiments (*2*, *3*) illustrate how fundamental questions of cosmology can be addressed by measurable effects in laboratory-scale experiments with ultimate sensitivity and precision, rather than looking for predicted particles directly in a high-energy collision. The study by Hamilton *et al.* is in the spirit of a series of ultraprecision experiments probing the most fundamental questions of nature. Other examples are the tests of equivalence principle probing new physics related to gravity, or measurements of electric dipole moments of neutrons, electrons, or atoms, which can search for physics beyond the standard model up to very high energy scales. Pushing the sensitivity of these types of experiments might very well be our best chance to probe energy ranges that cannot be reached in present-day accelerator experiments. One remarkable side effect is that many of these experiments are performed at a university research group scale. The essential input is a deep understanding of very broad aspects of physics covering many disciplines and new ingenious ideas. ■

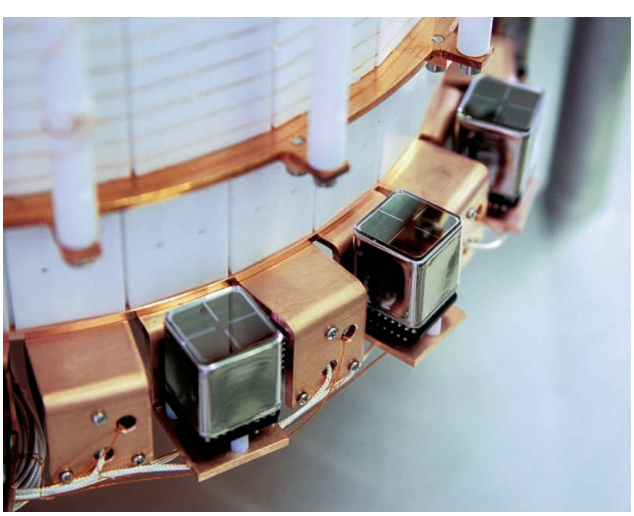

Xenon detection. Veto photomultiplier tubes (PMTs) are shown in detail together on a white Teflon cylinder, which acts as an effective reflector for xenon scintillation light. A coincidence signal in the veto PMTs indicates a double-scatter event, which is not compatible with a dark matter signal.

ILLUSTRATION: LEON FILTER & QBOUNCE COLLABORATION; PHOTO: XENON100 COLLABORATION

REFERENCES

1. Planck Collaboration, http://arxiv.org/abs/1502.01589v2 (2015).
2. P. Hamilton *et al.*, *Science* **349**, 849 (2015).
3. The XENON Collaboration, *Science* **349**, 851 (2015).
4. L. Baudis *et al.*, *Phys. Dark Universe* **1**, 94 (2012).
5. E. Aprile *et al.*, *Astropart. Phys.* **35**, 573 (2012).
6. R. Bernabei *et al.*, *Eur. Phys. J. C* **73**, 2648 (2013).
7. A. Einstein, *K. Preuss Akad. Wiss. Sitzungsberichte (Berlin)* **142** (1917).
8. C. Wetterich, *Nucl. Phys. B* **302**, 668 (1988).
9. B. Ratra, P. J. E. Peebles, *Phys. Rev. D Part. Fields* **37**, 3406 (1988).
10. J. Khoury, A. Weltman, *Phys. Rev. D Part. Fields Gravit. Cosmol.* **69**, 044026 (2004).
11. T. Jenke *et al.*, *Phys. Rev. Lett.* **112**, 151105 (2014).
12. H. Lemmel *et al.*, *Phys. Lett. B* **743**, 310 (2015).
13. P. Brax, G. Pignol, *Phys. Rev. Lett.* **107**, 111301 (2011).
14. P. Brax, G. Pignol, D. Roulier, *Phys. Rev. D Part. Fields Gravit. Cosmol.* **88**, 083004 (2013).
15. C. Burrage, E. J. Copeland, E. A. Hinds, *J. Cosmol. Astropart. Phys.* **3**, 42 (2015).
16. S. Schlögel, S. Clesse, A. Füzfa, http://arxiv.org/abs/1507.03081v1 (2015).

10.1126/science.aac9828

MICROBIOME

Plant microbiome blueprints

A plant defense hormone shapes the root microbiome

By **Cara H. Haney**[1,2]
and **Frederick M. Ausubel**[1,2]

Just as the number of petals in a flower or the number of limbs on an animal follow predictable rules, host-associated microbial communities ("microbiomes") have predictable compositions. At the level of bacterial phylum, the structure of the host-associated microbiome is conserved across individuals of a species (*1*, *2*). The consistency and predictability of host-associated microbiomes—like many of the phenotypes of a particular multicellular organism—suggest that they too may, in part, be under the regulation of a genetic blueprint. Indeed, evidence in animals shows that through production of broad-spectrum antimicrobials, the innate immune system shapes the composition of the gut microbiome (*3*, *4*). On page 860 of this issue, Lebeis *et al.* (*5*) reveal a critical role of the plant hormone salicylic acid in determining the higher-order organization of the root-associated microbiome of the reference plant *Arabidopsis thaliana*.

The plant root system, where nutrients are taken up by the host and exposure to environmental microbes occurs, is functionally analogous to the animal gut. As such, the associated microbial communities perform analogous functions, including aiding with nutrient uptake and protecting the host from pathogens. Correspondingly, the plant innate immune system must simultaneously allow beneficial microbes to survive while limiting the growth of potential pathogens.

The plant hormones salicylic acid, jasmonic acid, and ethylene are key regulators of innate immunity in plant leaves (*6*). Mutants impaired in salicylic acid synthesis and signaling are hypersusceptible to a number of biotrophic pathogens (microbes that colonize the host plant, rather than kill host tissue, to obtain nutrients), whereas mutants impaired in jasmonic acid and ethylene synthesis and signaling are hypersusceptible to herbivorous insects and necrotrophic pathogens (microbes that kill host cells and extract nutrients). Most studies that demonstrate these features of plant hormones have been carried out in leaves with a single or limited number of pathogens. However, the challenge of modulating a community of diverse microbes in plant roots is distinct from that of clearing a relatively limited number of pathogens from inside a plant leaf. Consequently, it is not clear that the same immune mechanisms that control foliar microbes will be effective in regulating root microbiome composition.

Using 16*S* ribosomal RNA sequencing, Lebeis *et al.* profiled the root microbiomes of a panel of *Arabidopsis* hormone mutants impaired in synthesis or signaling of individual or combinations of plant hormones. Specifically, the authors looked at the microbial community in the rhizosphere (the soil adjacent to the root) and in the endophytic compartment of roots (see the figure). The latter refers to bacteria living within plant root tissue as endosymbionts. They found that when salicylic acid signaling was constitutive [in an *Arabidopsis* strain (*cpr5* mutant) that displays hyperimmunity] or disrupted [in a hypoimmune *Arabidopsis* strain (*pad4* mutant)], a reproducible shift in the relative abundance of bacterial phyla in the endophytic compartment occurred. These changes were consistent across many families within the affected phyla, indicating that salicylic acid signaling does not simply modulate the growth of particular bacterial taxa, but may be a key component of the blueprint that determines microbiome community structure.

To complicate matters, the classical plant defense hormones also function in plant growth, metabolism, and responses to abi-

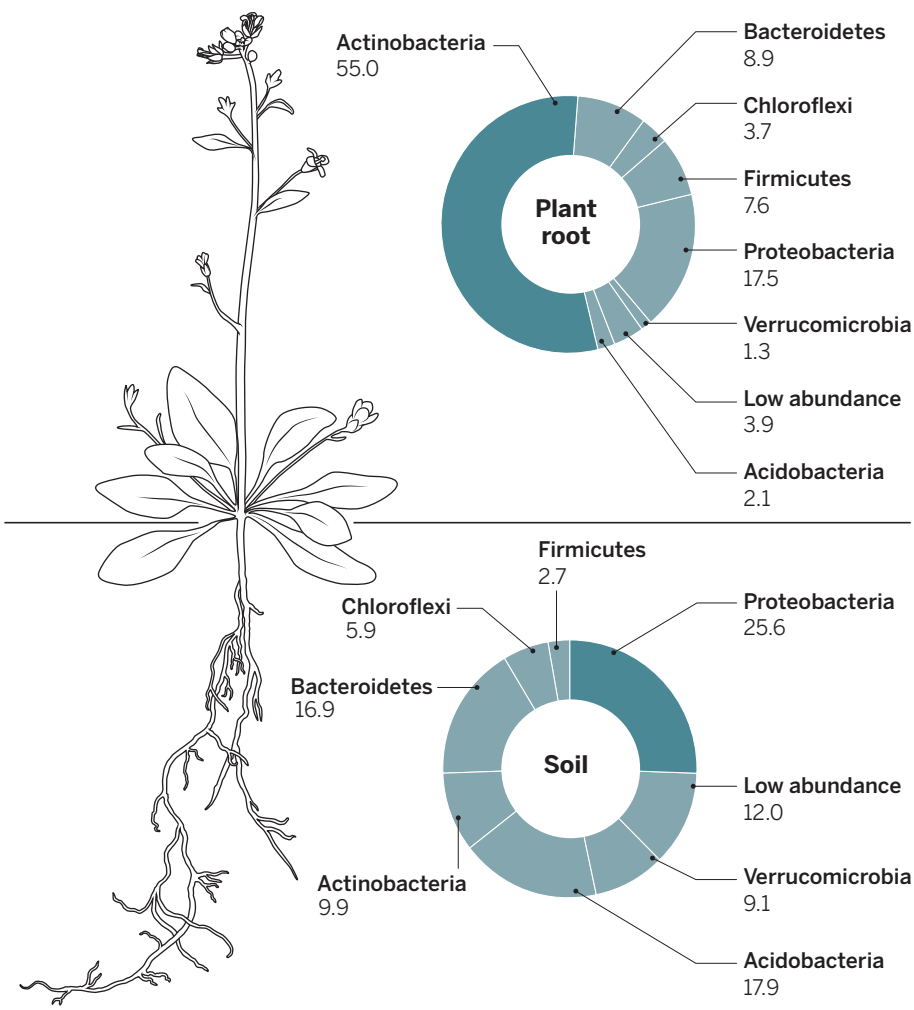

Bacterial profiles. Plant roots consistently enrich for and deplete certain bacterial phyla relative to their abundance in bulk soil. This process depends on salicylic acid synthesis and signaling, indicating that plant hormones regulate the root microbiome composition. Shown are the relative abundance of bacterial taxa in the plant root (endophytic compartment) of *Arabidopsis thaliana* and bulk soil (*5*).

ILLUSTRATION: ADAPTED BY P. HUEY/*SCIENCE*

[1]*Department of Genetics, Harvard Medical School, Boston, MA 02114, USA.* [2]*Department of Molecular Biology, Massachusetts General Hospital, Boston, MA 02114, USA.*
E-mail: haney@molbio.mgh.harvard.edu

otic stresses, obfuscating the precise mechanism by which salicylic acid regulates the root microbiome. By constructing a synthetic microbial community in an artificial soil, Lebeis *et al.* found that salicylic acid produced by the plant had either a direct negative or direct positive effect on the growth of a subset of bacteria in the root microbiome. In one case, salicylic acid directly inhibited the growth of some microbes, whereas in two other cases, the hormone served as a metabolite for bacteria. This finding is consistent with previous work showing that direct application of plant hormones to soil can affect microbial community composition (*7*). Thus, by using a synthetic microbial community, Lebeis *et al.* reveal that the role of salicylic acid in structuring the plant root microbiome might be intertwined with its function in plant physiology and as a microbial catabolite. Future work using similar reductionist approaches will hopefully elucidate the basic mechanisms that shape the rhizosphere and endophytic microbiome. Indeed, defined synthetic microbial communities have helped reveal mechanisms that shape the animal gut microbiome (*8*, *9*).

During plant domestication, humans have selected for traits related to plant improvement for food, fiber, and fuel. However, we have not consciously selected for plant associations with a beneficial microbiome. Lebeis *et al.* have shown that both hyper- and hypoimmune plants have altered root microbiome communities, indicating that selecting for plant disease resistance traits (or the accidental loss of resistance traits through inbreeding) might change the plant microbiome blueprint. The importance of microbial community structure on host health is largely unknown. However, even minor changes in abundance of certain bacteria can have a major effect on plant defenses and physiology, with only minimal effects on the overall structure of the microbiome (*10*, *11*). Understanding the factors that contribute to a healthful microbial community may allow for conscious selection of microbiomes for improvement of crop yields and increased crop resilience in the face of biotic and abiotic stresses. ■

ILLUSTRATION: V. ALTOUNIAN/*SCIENCE*

REFERENCES

1. D. S. Lundberg *et al.*, *Nature* **488**, 86 (2012).
2. D. Bulgarelli *et al.*, *Nature* **488**, 91 (2012).
3. N. H. Salzman *et al.*, *Nat. Immunol.* **11**, 76 (2010).
4. S. Mukherjee *et al.*, *Nature* **505**, 103 (2014).
5. S. L. Lebeis *et al.*, *Science* **349**, 860 (2015).
6. A. Robert-Seilaniantz, M. Grant, J. D. Jones, *Annu. Rev. Phytopathol.* **49**, 317 (2011).
7. L. C. Carvalhais *et al.*, *Appl. Soil Ecol.* **84**, 1 (2014).
8. J. J. Faith *et al.*, *Science* **333**, 101 (2011).
9. P. D. Newell, A. E. Douglas, *Appl. Environ. Microbiol.* **80**, 788 (2014).
10. C. M. Pieterse *et al.*, *Annu. Rev. Phytopathol.* **52**, 347 (2014).
11. C. H. Haney *et al.*, *Nat. Plants* **1**, 1 (2015).

10.1126/science.aad0092

CELL SIGNALING

Lipids link ion channels and cancer

Membrane voltage connects lipid organization to cell proliferation

By **Alessio Accardi**

How does membrane voltage control cellular proliferation? This is a key but poorly understood step in understanding how dysregulation of the electrical balance in a cell can lead to uncontrolled proliferation and, eventually, to tumor development. Although the phenomenon is well established (*1*–*3*), the underlying mechanisms have been unclear. On page 873 of this issue, Zhou *et al.* (*4*) show that persistent changes in the resting membrane potential (the voltage across the membrane of a cell), caused by the uncontrolled expression of ion channels, can cause negatively charged lipid in the inner membrane leaflet to cluster and attract the signaling protein K-Ras, enhancing its ability to promote cell proliferation.

Ion channels control the rapid movement of ions across cellular membranes (*5*). They are best known as the gatekeepers of excitatory cellular processes such as neuronal firing, muscle contraction, and heartbeat. They also control ion homeostasis and set the membrane potential of all resting or non-excitable cells. Less well understood is their role in regulating cell division (mitosis). It has been known for nearly 40 years that cells undergoing mitosis are more depolarized—less negatively charged on the inside—than their quiescent counterparts (*6*–*8*) and that, as cells transition through the different states of the cell division cycle, their membrane voltage changes (*9*) in concert with the expression of many different ion channels (*3*). Furthermore, overexpression of K^+, Na^+, Ca^{2+}, and Cl^- channels has been observed in numerous tumors (*2*), and their pharmacological inhibition can restore normal proliferative behavior (*2*, *10*).

In addition to their role in tumorigenesis, ion channels are also involved in other aspects of cancer biology such as cell adhesion, cell volume regulation, programmed cell death (apoptosis), and angiogenesis (*1*, *8*). It is therefore not surprising that ion channels are viewed as highly promising targets for cancer treatment, especially given the great variety of readily available compounds that specifically target various channel types and can serve as scaffolds for the development of anticancer drugs (*10*). However, efforts in these directions have been stymied by a poor understanding of the cellular signaling pathways that are affected by channel overexpression and by the ensuing alterations in the resting membrane potential.

Zhou *et al.* investigated whether changes in membrane potential might alter the lateral spatiotemporal distribution of charged lipids in the membrane, which in turn might affect the distribution of membrane-bound signaling proteins, such as the Ras family of guanosine triphosphatases (GTPases). The human genes encoding H-, N-, and K-Ras are among the most commonly occurring mutated oncogenes. Mutations that constitutively activate K-Ras are found in nearly 25% of all human tumors (*11*). Positively charged residues in the C termini of Ras proteins interact with negatively charged lipids that sequester these proteins into spatially localized assemblies called nanoclusters. Such aggregation is essential for K-Ras–induced activation of the RAF–mitogen-activated protein kinase (MAPK) cascade (*12*).

> ***"The study provides...a breakthrough that should pave the way for developing strategies that silence oncogenic pathways."***

Using an elegant combination of electron microscopy, electrophysiological recordings, and fluorescence imaging, Zhou *et al.* show that membrane depolarization specifically and reversibly promotes clustering of two types of negatively charged lipids, phosphatidylserine and phosphatidylinositol 4,5-bisphosphate (PIP_2). Upon depolarization, nanoclustering of phosphatidylserine and K-Ras increased with closely matching

Departments of Anesthesiology, Biochemistry, and Physiology and Biophysics, Weill Cornell Medical College, New York, NY 10065, USA. E-mail: ala2022@med.cornell.edu

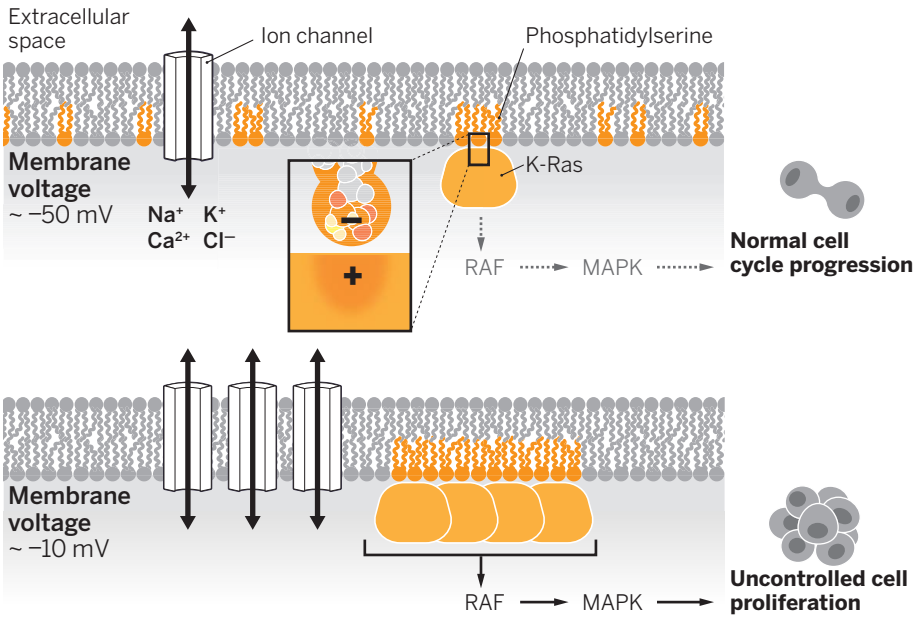

Potential and proliferation. In a normal, nonproliferating cell, the resting membrane potential (V_m ≈ –50 mV) is set by ion channel activity. Phosphatidylserine lipids are in small clusters that localize with K-Ras, which leads to low activation of the RAF-MAPK pathway. Channel overexpression depolarizes the cell (V_m ≈ –10 mV), increasing the clustering of phosphatidylserine and K-Ras. This promotes RAF-MAPK signaling uncontrolled cell proliferation.

spatiotemporal and voltage dependencies. This activated the RAF-MAPK cascade, thereby promoting cell proliferation (see the figure). By contrast, hyperpolarizing potentials had the opposite effect of reducing phosphatidylserine and K-Ras clustering and decreasing RAF-MAPK signaling.

The study provides a long-awaited mechanism by which membrane voltage directly affects the cell division cycle, a breakthrough that should pave the way for developing strategies that silence oncogenic pathways. It also, perhaps, offers an accessible tuning knob—in the form of ion channel activity—that can be manipulated to influence cell signaling. Interestingly, the observed effects are highly specific in that only the distribution of phosphatidylserine and PIP_2 is affected by membrane voltage, whereas that of other anionic lipids, such as phosphatidic acid or phosphatidylinositol 3,4,5-trisphosphate (PIP_3), are unaffected. Similarly, K-Ras, unlike H- or N-Ras, responds to changes in phosphatidylserine distribution. The high selectivity of these effects among different Ras isoforms and similarly charged lipids could allow for the development of specifically targeted therapies. However, the molecular bases underlying the specificity of these effects remain unclear, and other unidentified proteins might be involved in these processes.

The results of Zhou *et al.* also raise the question of how the depolarization-induced lipid rearrangements affect signaling in excitable cells (neurons) that undergo repeated depolarization. It is possible that the millisecond time scale of an action potential is too fast to induce substantial lateral rearrangement of anionic lipids; the fastest rearrangement detected by Zhou *et al.* (using electron microscopy) in nonexcitable cells is 30 s, nearly four orders of magnitude slower than observed in excitable "firing" cells (those exhibiting bursts of repetitive and rapid changes in electrical potential). However, it may be that under particular conditions, such as during firing, there may not be enough time for lipids to reorganize back to a state that restores membrane potential to its baseline level. Over time, these small increments in clustering could accumulate, leading to a progressive activation of the MAPK pathway. If this were the case, it could represent a novel mechanism by which long-lasting effects of repeated firing could occur in excitable cells. ■

REFERENCES

1. L. A. Pardo, W. Stühmer, *Nat. Rev. Cancer* **14**, 39 (2014).
2. V. R. Rao *et al.*, *Cancers* **7**, 849 (2015).
3. A. Litan, S. A. Langhans, *Front. Cell. Neurosci.* 10.3389/fncel.2015.00086 (2015).
4. Y. Zhou *et al.*, *Science* **349**, 873 (2015).
5. B. Hille, *Ion Channels of Excitable Membranes* (Sinauer, Sunderland, MA, ed. 3, 2001).
6. C. D. J. Cone Jr., *Ann. N. Y. Acad. Sci.* **238**, 420 (1974).
7. D. J. Blackiston *et al.*, *Cell Cycle* **8**, 3527 (2009).
8. D. Urrego, A. P. Tomczak, F. Zahed, W. Stuhmer, L. A. Pardo, *Philos. Trans. R. Soc. B* **369**, 20130094 (2014).
9. E. F. Stillwell *et al.*, *Nat. New Biol.* **246**, 110 (1973).
10. H. Wulff *et al.*, *Nat. Rev. Drug Discov.* **8**, 982 (2009).
11. J. Downward, *Nat. Rev. Cancer* **3**, 11 (2003).
12. T. Tian *et al.*, *Nat. Cell Biol.* **9**, 905 (2007).

10.1126/science.aad0874

MEDICINE

Global control of hepatitis C virus

A comprehensive strategy to control HCV infection must include a vaccine

By **Andrea L. Cox**

Hepatitis C virus (HCV) infection is a blood-borne disease that infects ~185 million people (~3% of the world's population) worldwide (*1*). It can result in severe liver disease and is the leading cause of liver cancer in many countries. Although directly acting antivirals (DAAs) that target the viral life cycle have created enormous optimism about controlling HCV infection, achieving that goal remains a substantial challenge. Both acute and chronic infections are largely asymptomatic, infection incidence is rising in the United States (*2*), and comprehensive screening programs are rare in the most highly endemic regions of the world. As a result, less than 5% of the world's HCV-infected population, and only 50% of the United States' HCV-infected population, are aware that they are infected (*3*, *4*) (see the figure). Most of these individuals will not receive treatment and will remain at risk for transmitting the infection to others. Successful control of HCV infection will most likely require a combination of mass global screening to identify those with infection, treatment, and prevention. Prophylactic HCV vaccination would also go a long way to reducing harm for uninfected people who are at risk.

Even if everyone with HCV infection were identified and rising infection incidence reversed, treatment as the primary means to eradicate HCV disease still would be challenging. One reason is the prohibitive cost of DAAs for most countries with moderate to high HCV prevalence. HCV transmission occurs through receipt of contaminated blood and poor needle hygiene in many parts of the world. Nations lacking the financial resources and health care infrastructure to ensure safety of the blood supply or medical supplies likely can-

Johns Hopkins University, Baltimore, MD, USA.
E-mail: acox@jhmi.edu

ILLUSTRATION: V. ALTOUNIAN/*SCIENCE*

not afford treatment. Even in high-income countries, treating all infected individuals would create financial burden. Access to HCV is also limited in high-income nations because those most at risk for HCV infection include people who inject drugs, many of whom do not routinely access the health care system.

Preexposure protection with DAAs is difficult to imagine given the cost and unproven long-term safety. These antivirals also do not protect against reinfection (following successful therapy) of those at ongoing risk of infection (*5*). In addition, DAAs can select for HCV resistance–associated variants that limit treatment efficacy. Such variants currently arise rarely on treatment, but can persist for years after ineffective therapy is discontinued and be transmitted from person to person (*6*–*8*).

Adding to the difficulty of controlling HCV disease is that successful treatment does not fully reverse severe liver damage. Liver disease usually stabilizes or improves after cure, but further disease progression can occur, necessitating ongoing monitoring for liver failure and cancer after successful therapy (*9*). Given the challenges of identifying infected people before severe liver disease occurs, the possibility of repeated infection, the cost of and potential resistance to therapy, and the inability to heal the most severely damaged livers, maximal reduction of HCV-associated morbidity may require prevention of chronic HCV in the first place.

A vaccine to prevent chronic HCV could prevent liver damage associated with infection, limit the importance of resistance-associated variants, and reduce the need for engaging at-risk populations at the time of greatest risk (such as during active drug use). However, this approach is not without substantial barriers as well. These include the genetic diversity of HCV, the lack of immunologically competent and convenient model systems to test a vaccine (limitations on chimpanzee models), the numerous mechanisms through which HCV evades the immune response, and the infeasibility of using live attenuated and inactivated whole virus as HCV vaccines due to limited culture capacity and risk of reversion to virulence. However, there is evidence that protective immunity against HCV exists in people. Spontaneous clearance of HCV infection occurs in about 25% of acutely infected individuals. Although people who spontaneously control an initial HCV infection can develop recurrent HCV viremia after additional HCV exposures, clearance of secondary HCV infections occurs commonly—about 80% rather than 25% of the time (*10*–*12*). This response to HCV reinfection is characterized by more rapid and effective control of viral replication compared to initial exposure and is associated with broadened cellular immune responses and the presence of broadly cross-reactive neutralizing antibodies (*10*). This suggests that adaptive immunity can be induced to protect against chronic HCV infection in people who are repeatedly exposed to the virus. Several strategies to induce immune responses to HCV have been tested in nonhuman primates (*13*), and a much smaller subset of vaccine candidates (such as a recombinant viral envelope glycoprotein-based vaccine and adjuvanted HCV core protein) have moved to clinical trials of healthy people who are not at risk for infection. To date, only one candidate vaccine has moved to trials in an at-risk human population (*13*).

Adenovirus strains that infect chimpanzees (ChAd) and that are not commonly neutralized by human sera have been used to create replication-defective vaccine vectors that induce potent immune responses. Of these, treatment with a ChAd3 vector expressing the nonstructural (NS) region of HCV, followed by boosting with modified vaccinia virus expressing NS, induced long-lasting HCV-specific T cell responses in healthy volunteers not at risk for HCV infection (*14*). This vaccine is currently being evaluated in a phase I/II study to prevent HCV persistence in people who inject drugs who are at high risk for infection, with results expected in 2016 (*15*). If unsuccessful, further advances in our understanding of virus-host interactions and the correlates of protective immunity against diverse HCV infections will be critical next steps to developing a successful preventive vaccine.

A multifaceted approach to global control of HCV infection is needed. Current limitations include lack of knowledge of an individual's HCV status, partial treatment uptake and success, reinfection or continued liver disease progression after cure in some, and limited ability to access those at the highest risk and intervene. Vaccination could be given before individuals are at risk—this would translate into a much larger window in which to prevent infection. ■

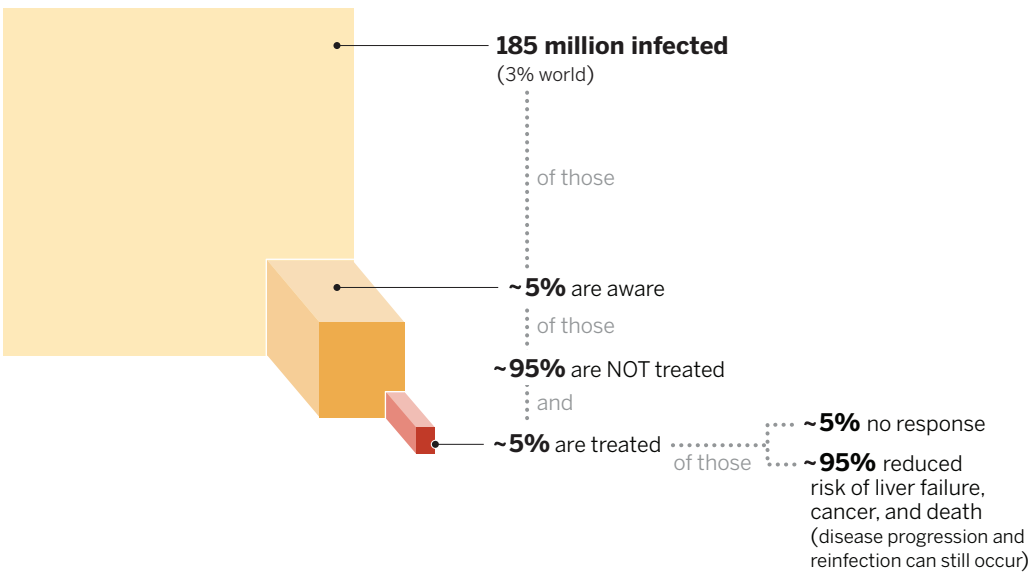

The global reach of HCV infection. The approximations show that a minority of HCV infected persons are treated. Treatment doesn't prevent reinfection in those at ongoing risk of infection and disease progression continues in a minority of patients treated.

REFERENCES

1. K. Mohd Hanafiah, J. Groeger, A. D. Flaxman, S. T. Wiersma, *Hepatology* **57**, 1333 (2013).
2. A. G. Suryaprasad *et al.*, *Clin. Infect. Dis.* **59**, 1411 (2014).
3. L. Gravitz, *Nature* **474**, S2 (2011).
4. S. D. Holmberg, P. R. Spradling, A. C. Moorman, M. M. Denniston, *N. Engl. J. Med.* **368**, 1859 (2013).
5. M. S. Sulkowski *et al.*, *N. Engl. J. Med.* **370**, 211 (2014).
6. S. Franco *et al.*, *Gastroenterology* **147**, 599 (2014).
7. P. Krishnan *et al.*, 50th Annual Meeting of the European Association for the Study of the Liver, Vienna, Austria, 22 to 26 April 2015, abstr. 0057.
8. D. Wyles *et al.*, 50th Annual Meeting of the European Association for the Study of the Liver, Vienna, Austria, 22 to 26 April 2015, abstr. 0059.
9. B. J. Veldt *et al.*, *Ann. Intern. Med.* **147**, 677 (2007).
10. W. O. Osburn *et al.*, *Gastroenterology* **138**, 315 (2010).
11. S. H. Mehta *et al.*, *Lancet* **359**, 1478 (2002).
12. K. Page *et al.*, *J. Infect. Dis.* **200**, 1216 (2009).
13. J. R. Honegger, Y. Zhou, C. M. Walker, *Semin. Liver Dis.* **34**, 79 (2014).
14. L. Swadling *et al.*, *Sci. Transl. Med.* **6**, 261ra153 (2014).
15. https://clinicaltrials.gov/ (NCT01436357).

10.1126/science.aad1302

BIOSECURITY

Assessing the bioweapons threat

Is there a foundation of agreement among experts about risk?

By **Crystal Boddie,[1] Matthew Watson,[1] Gary Ackerman,[2] Gigi Kwik Gronvall[1]***

The U.S. government (USG) has taken steps intended to diminish the likelihood of misuse of research—in one recent action, declaring a funding moratorium on gain-of-function studies on influenza until a risk-benefit analysis can be conducted (*1*). The analysis is expected to examine biosafety concerns, the potential for such research to produce a biological weapons agent, and the possibility that publication may lower barriers to bioweapons development (*1*). To analyze the security risks of biological research, however, it is first necessary to determine the likelihood that bioweapons will threaten national security and to what degree legitimate research is at risk of misuse. This type of assessment is fraught with uncertainty.

POLICY

Empirical data for threat assessment is sparse: Thankfully, there have been only a handful of historical examples of bioterrorism or biowarfare (use by a nation state), although multiple nations and terrorist organizations have developed the capability to varying degrees. Intelligence about bioweapons programs and intent to use them has been difficult to acquire; miscalculations include type 1 errors (Iraq was thought to have a biological weapons program during the lead up to the Second Gulf War, at which time it did not) and type 2 errors (the former Soviet Union was not thought to have a biological weapons program but, in fact, employed tens of thousands of weapons scientists). Given the paucity of other data, judgments about the bioweapons threat rest largely on expert opinions. Understanding how experts in national security, biosecurity, and biosafety perceive the bioweapons threat is therefore important for assessing the threat, as well as the potential for misuse of legitimate research.

ASSESSING COLLECTIVE JUDGMENTS. We used a Delphi method study to elicit, combine, and analyze the collective judgments of multiple experts. Focused on obtaining collective expert opinion, but avoiding "groupthink," the Delphi method's salient features are preserving the anonymity of participant inputs, iterated response and feedback, and statistical aggregation of expert judgments (*2*). Individuals were invited to participate in this study if they held responsibility for shaping public policy at the nexus of life science and national security or on the basis of their expertise and knowledge in the field or the recommendations of other participants (using a snowball sampling methodology). Participant affiliations included USG and former USG; academia; and nongovernmental, private sector, and industry organizations. The participants had responsibility for shaping public policy from ~3 to more than 45 years. Participant training and background included biological and nonbiological science, medicine, public health, national security, political science, foreign policy and international affairs, economics, history, and law. Of the 63 experts originally approached to participate, 62 completed the first round of the survey, and 59 completed the second round.

Participants were asked to respond anonymously to questions about biological threats, review each other's answers, and either amend or maintain their answers after reflecting on others' opinions. They were asked to supply rationales for their responses (*3*). The process was terminated when the mean response did not change more than one standard deviation across all questions, which occurred after two rounds (*4*). Results were analyzed with STATA statistical package 11.2 and Wilcoxon-Mann-Whitney nonparametric tests (significance level $P \leq 0.05$).

LIKELIHOOD OF A BIOWEAPONS ATTACK. We asked participants to estimate the percentage likelihood of a large-scale biological weapons attack occurring within the next 10 years in any country (see the first chart). We defined a large-scale attack conservatively, as resulting in more than 100 ill people. There was a wide diversity of opinions. Participants' answers ranged from 1 to 100% likelihood, with a mean of 57.5%, [95% confidence interval (CI) 49.4 to 65.7]. In general, those trained as biological scientists perceived a lower likelihood of bioweapons use than other participants ($z = 2.9$, $P = 0.0035$), although that was certainly not true in every case. Also, participants classified as members of the Baby Boomers and/or Silent Generation (50 years of age or older) believed the likelihood of attack was greater than did Generation X and/or Millennials (21 to 49 years of age); with mean responses of 64.6% and 46.0%, respectively ($z = -2.1$, $P = 0.035$).

Likelihood of attack. What do you estimate to be the likelihood of a large-scale biological weapons attack occurring within the next 10 years?

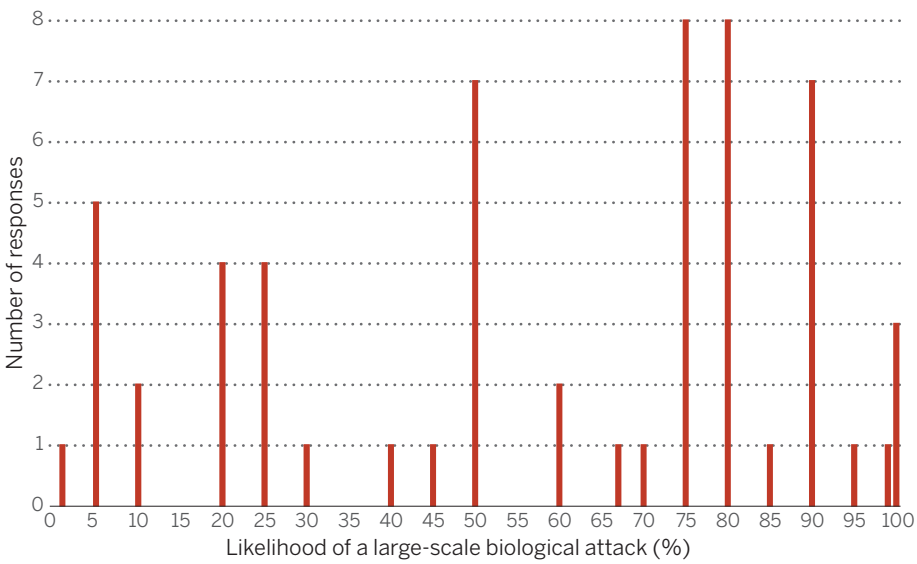

THE MOST LIKELY ACTOR AND AGENT. Participants were also asked about the likelihood of different types of state and nonstate actors to be the perpetrator of a biological weapons attack within the next 10 years. Although participants held a wide range of

[1]UPMC Center for Health Security, University of Pittsburgh Medical Center, Baltimore, MD, USA. [2]Unconventional Weapons and Technology Division, National Consortium for the Study of Terrorism and Response to Terrorism (START), University of Maryland, College Park, MD, USA.
*Corresponding author. E-mail: ggronvall@upmc.edu

opinions, overt state bioweapons use was considered to be less likely than covert use by a state or use by a nonstate group. An overt attack by a state actor was rated significantly less likely than even the next lowest rated actor: criminal groups ($z = -3.9$, $P < 0.001$). Religious extremists were judged to be the most likely group to perpetrate an attack—significantly more likely than a covert attack by a state actor ($z = -3.6$, $P < 0.001$) or any other attack by a state but not significantly more likely than a right-wing violent nonstate actor or a disgruntled or mentally ill individual. Participants who were especially concerned about terrorist use cited rapid technological advances in the biosciences, ease of acquiring pathogens, democratization of bioscience knowledge, information about a nonstate actors' intent, and the demonstration of the chaos surrounding the Ebola epidemic in West Africa in 2014 as support for their views. Those more concerned about the nation-state threat cited the technological complexities of developing a bioweapon, the difficulty in obtaining pathogens, and ethical and/or cultural barriers to using biological weapons. Pathogen access and the technical complexity required to produce a biological weapon were cited as support for opposite conclusions about potential actors.

We also asked about types of biological agents likely to be used as weapons within the next 10 years. Participants felt that the likelihood of use was highest for biological toxins. This was followed by spore-forming bacteria, non–spore-forming bacteria, and viruses. Participants generally did not think that fungi and prions were likely to be weaponized and felt that the likelihood of a synthetic pathogen being used as a weapon in the next 10 years was fairly low (*4*).

Since 2001, a point of emphasis for the U.S. intelligence community (IC) has been the prevention of the use of a weapon of mass destruction. Despite IC efforts, however, most participants believed that intelligence agencies are unlikely to provide actionable information or warnings before a biological attack (see the second chart). Of 59 participants, 53 considered there to be a 50% or lower probability that a warning would be forthcoming in advance of an attack.

Although a few participants felt that the IC had improved their level of access and detection capabilities, many cited the difficulties inherent in detecting and tracking biological weapons capabilities owing to biology's dual-use nature; the ease of concealing preparations for a biological attack; limitations in expertise and investment in biological threats by the IC; and past experiences of the challenges associated with intelligence collection against biological threats. The realities of classification of information make a fully informed analysis of IC capabilities vis-à-vis the biological threat impossible—a fact that several participants acknowledged.

Likelihood of actionable warning. If a biological attack were being planned today, what is the probability that intelligence information will provide actionable indications and warning preceding the attack?

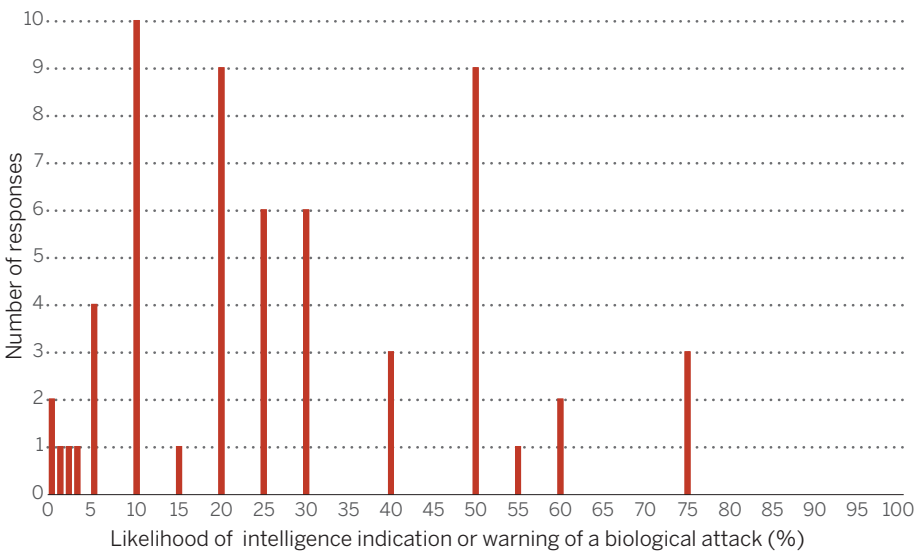

RED LINE FOR RESEARCH. Our study also obtained participants' judgments about acceptable limits for U.S. biodefense, particularly "threat characterization" laboratory studies (usually classified) that are performed to gain knowledge about potential bioweapons for purposes of defense (i.e., is there a "red line" that should not be crossed?). Most said yes (51), but there was a wide variety of opinions of what types of research would cross that line.

Three participants felt that the only "red line" for biodefense is human subjects research and that all other defensive research that furthers national security should be allowed. A majority of participants said that research that violates the Biological and Toxin Weapons Convention crosses a red line and should not be pursued. Two participants felt that threat-characterization research should not be conducted at all because of the inherent risks. Of the participants, 27 mentioned gain-of-function experiments as a situation where a red line could be drawn. Even under the secure conditions of threat-characterization research, there was a lack of consensus among experts about where the "red line" should be drawn and whether that line is gain-of-function research.

RISK OF MISUSE OF RESEARCH. The potential for devastating consequences if biological weapons were used is enough to spur planning. Yet, given the scantiness of the historical record, it is not surprising that experts reached different conclusions about the likelihood of a biological weapons attack. Highly classified intelligence, if available, may have reduced the degree of variation; given the importance of a shared, informed perception of the threat in order to prepare, investments should be made to acquire intelligence on biosecurity threats and share with relevant parties.

The diversity of views, even in this experienced group of participants, means that it will be more challenging to assess the risks that research would be misused and to develop a regulatory system for legitimate dual-use research. Risks and benefits should still be examined and recommendations made about the conduct of this or other research. However, a red line for what is allowable and what is forbidden in the name of security may not be clearly defined, and the way forward will be nuanced and complicated, possibly requiring a case-by-case evaluation with guidelines agreed upon by the scientific and policy communities. ■

REFERENCES AND NOTES

1. White House Office of Science and Technology (S&T) Policy, "Doing diligence to assess the risks and benefits of life sciences gain-of-function research" (White House, Washington, DC, 2014).
2. G. Rowe, G. Wright, *Int. J. Forecast.* **15**, 353–375 (1999).
3. G. Rowe, G. Wright, in *Principles of Forecasting*, J. S. Armstrong, Ed. (Springer, New York, 2001), pp. 125–144.
4. See the supplementary materials for further details.

ACKNOWLEDGMENTS

We thank the participants in the Delphi study, as well as the S&T Directorate, U.S. Department of Homeland Security, for funding and support.

SUPPLEMENTARY MATERIALS

www.sciencemag.org/content/349/6250/792/suppl/DC1

10.1126/science.aab0713

Traces of the emerald ash borer on the trunk of a dead ash tree in Michigan, USA. This non-native invasive insect from Asia threatens to kill most North American ash trees.

BIOTECHNOLOGY

Genetically engineered trees: Paralysis from good intentions

Forest crises demand regulation and certification reform

By **Steven H. Strauss[1]*, Adam Costanza[2], Armand Séguin[3]**

Intensive genetic modification is a long-standing practice in agriculture, and, for some species, in woody plant horticulture and forestry (*1*). Current regulatory systems for genetically engineered crops, in which recombinant DNA is used to asexually insert or modify DNA, were created decades ago with good intentions for caution and forethought. Likewise, forest certification systems were created to promote responsible forest management and sustainable practices. However, both systems are at odds with the need for rapid and innovative biotechnologies to help forests cope with growing pest epidemics and mounting abiotic stresses as a result of global travel and climate change. As the U.S. government recently initiated an update of the Coordinated Framework for the Regulation of Biotechnology (*2*), now is an opportune time to consider foundational changes.

POLICY

Difficulties of conventional tree breeding make genetic engineering (GE) methods relatively more advantageous for forest trees than for annual crops (*3*). Obstacles include multiyear delays until onset of flowering, intolerance of inbreeding, and, as a consequence, introgression of genes from other species or populations is usually not possible in an acceptable time frame. GE methods improve on conventional breeding by enabling rapid modifications without shuffling the genotype during meiosis and without the maladaptation of early hybrids from wide crosses. GE could help in refining wood characteristics for specific products, responding to emerging pest problems (see the photo), adding high-value coproduct traits, improving growth, or accelerating adaptation to changing climates. It can also provide a means for strong containment of tree species when spread beyond plantations is problematic (*4*).

Although only a few forest tree species might be subject to GE in the foreseeable future, regulatory and market obstacles prevent most of these from even being subjects of translational laboratory research. There is also little commercial activity: Only two types of pest-resistant poplars are authorized for commercial use in small areas in China and two types of eucalypts, one approved in Brazil and another under lengthy review in the USA (*5*).

METHOD-FOCUSED AND MISGUIDED. Many high-level science reports state that the GE method is no more risky than conventional breeding, but regulations around the world essentially presume that GE is hazardous and requires strict containment during research and breeding (*6*). Regulatory systems in the EU and most other countries are focused almost exclusively on GE as a method. In the United States and Canada, regulations try to focus on trait novelty or use existing trait-associated authorities. In practice, however, the regulatory triggers have become predominantly method-based and have drifted far from the intent of their authorizing statutes. The U.S. Environmental Protection Agency (EPA) regulates pest-resistant genetically engineered plants as pesticide-producers even if they produce no novel or broadly toxic pesticides (and may regulate genetically engineered plants with genes that are simply growth regulators) (*7*). The U.S. Department of Agriculture uses plant pest sequences that, on their own, are of no conse-

[1]*Oregon State University, Corvallis, OR 97331, USA.* [2]*Institute of Forest Biosciences, Cary, NC 27513 USA* [3]*Natural Resources Canada, Québec, Quebec G1V 4C7, CANADA.*
E-mail: Steve.Strauss@OregonState.edu

quence to plant pest risk or that use a former plant pathogen as a vector (now disarmed), as triggers for regulation. No GE regulatory system adequately accounts for the costs of not using a genetically engineered technology or product.

Most genetically engineered trees are scrutinized as any other genetically engineered crop would be by the regulatory system, and subject to strict, zero-tolerance isolation requirements: Regardless of genomic familiarity, trees are placed very far from wild, feral, or planted populations of interfertile species; a large area nearby is monitored for possible spread (e.g., many km^2); and trial trees generally must be cut down before flowering. To develop trees that can actually be used, long-term trials are needed in a variety of environments and genotypes (*7*), where trees will be grown normally—beyond onset of flowering and to a size that will make absolute containment of experimental populations infeasible.

GE can modify complex abiotic stress-tolerance traits in crops—in some cases, where conventional breeding has shown limited success (*8*). This is likely to require multiple gene modifications and extensive phenotypic screening for high levels of resistance without unacceptable pleiotropy—for which the regulatory focus on single insertion events, mostly studied in artificial, contained environments, is a barrier. Many gene combinations and events will need to be studied and tested in conjunction with conventional breeding, so that adding genetically engineered modifications does not unacceptably slow breeding progress. Containment of every event and gene combination over many years during breeding, followed by years of regulatory review before approval of every event of interest, is restrictive, costly, and opens developers to legal liabilities (*7*).

FAST-TRACK AND REGISTER. A better regulatory approach would give agencies legal authority to fast-track or exempt field research with a genetically modified product intended to provide options for existing or emerging forest health problems, or that have high genomic familiarity. Agencies could rapidly (e.g., in 60 days) perform a categorical assessment when a species, or its ecological function, may be threatened by a spreading pest. This should be a presumptive, categorical exemption when intragenic, homologous, gene-edited, or otherwise functionally familiar genes are used, whose benefits and risks are similar to those of conventional breeding.

In the United States, EPA might take the regulatory lead, with the possible benefit of embedding decisions based on the National Environmental Policy Act in the overall risk assessment of the product rather than having a separate environmental impact statement. This would create stronger authority for future mitigation because of the ongoing registration and renewal process already in place for such products. In contrast to current EPA timing and demands for data, it would need to be more rapid and nimble, with most data generated along the way in an adaptive management framework and opportunities for legal challenges greatly narrowed, especially at the research stage. EPA should categorically exempt plant-incorporated protectants that do not produce broadly toxic pesticides, e.g., genetically engineered plants with genes that induce RNA interference or the various R-genes that trigger natural response pathways.

Environmental risk assessments of forest trees also need reconsideration, given the time required and the constraints to doing ecologically relevant field studies (i.e., complete containment). Such studies often become irrelevant as soon as they are produced owing to ongoing "no-analog" changes to ecosystem structure as a result of climate change (*9*) or introduced insects or diseases. Major changes in the rules and, possibly, new legislation are required.

"No GE regulatory system adequately accounts for the costs of not using a genetically engineered technology or product."

We are not suggesting separate regulations for genetically engineered trees. Fundamental regulatory reforms for all crops, discussed for years (*6*, *10*), are needed. In addition to the reforms discussed above, changes should focus on the novelty of functional traits compared with conventional breeding rather than on GE methods. A more realistic and responsive approach would include (i) best management practices rather than strict legal limits for dispersal from most types of research trials; (ii) globally recognized and workable tolerances for adventitious presence during research and commercial use (to avoid costly trade problems due to biologically trivial levels of adventitious presence); and (iii) exemptions for familiar markers and genetic modifications, which are usually more precise and less disruptive than conventional breeding.

A revised system might also require organisms modified using any GE method to be registered before use in the environment—to facilitate detection for trade or market certification and to ensure that they are not missed by regulatory agencies should they pose unanticipated hazards. Registration, however, should not preclude exemptions or accelerated review pathways based on trait and/or genomic familiarity or urgency.

MARKET REFORM. Regulatory processes are not the only obstacles to GE tree research and breeding. All major "sustainable certification" systems prevalent in forestry and forest products preclude use of genetically engineered trees in certified forests (*11*). Although the reason given is often a lack of data, legally authorized research is also not allowed on certified land (*12*). This signals to forest companies that investments in GE are risky and GE field research more difficult and costly. A cautious approach was perhaps warranted when GE tree research was nascent. But the Forest Stewardship Council first put in place genetically engineered tree preclusion in 1999; there have since been hundreds of scientific studies, many of them field tests, and none has shown categorical risks once feared (*13*). A product-not-process approach seems appropriate.

Despite confidence from the majority of scientists, there is public concern over genetically engineered crops and their safety. However, public attitudes vary widely among GE applications (*14*); views toward forest health and genomically familiar applications are likely to be received most favorably. Nonetheless, stakeholder dialogue use will be required for change.

It would be prudent and precautionary to ensure that GE tools are available to address urgent forest health and productivity problems. Regulatory agencies and certification systems should reconsider the foundations for their policies, refocusing on trait novelty and need, not method. ■

REFERENCES AND NOTES

1. R. Burdon, W. Libby, *Genetically Modified Forests: From Stone Age to Modern Biotechnology* (Forest History Society, Durham, NC, 2006).
2. Office of Science and Technology Policy, "Memorandum to agencies on modernizing the regulatory system for biotechnology products" (White House, Washington, DC, 2015); http://1.usa.gov/1lQGGfR.
3. A. Harfouche *et al.*, *Trends Plant Sci.* **17**, 64 (2012).
4. A. M. Brunner *et al.*, *Tree Genet. Genomes* **3**, 75 (2007).
5. H. Ledford, *Nature* **512**, 357 (2014).
6. S. H. Strauss, *Science* **300**, 61 (2003).
7. S. H. Strauss *et al.*, *Bioscience* **60**, 729 (2010).
8. E. Waltz, *Nat. Biotechnol.* **32**, 610 (2014).
9. J. W. Williams, S. T. Jackson, *Front. Ecol. Environ* **5**, 475 (2007).
10. K. J. Bradford, A. Van Deynze, N. Gutterson, W. Parrott, S. H. Strauss, *Nat. Biotechnol.* **23**, 439 (2005).
11. A. Costanza, S. McCord, *Regulation, Certification, and Use of Biotech Trees* (Institute of Forest Biosciences, 2013); http://forestbio.org/publications/biotech_tree_use/
12. S. H. Strauss *et al.*, *J. For.* **99**, 4 (2001).
13. C. Walter, M. Fladung, W. Boerjan, *Nat. Biotechnol.* **28**, 656 (2010).
14. S. H. Priest, *Nat. Biotechnol.* **18**, 939 (2000).

10.1126/science.aab0493

A California sea lion swims off the coast of La Paz, Baja California Sur Mexico.

MARINE ECOLOGY

Hosting nature's "Super Bowl"

Conservation scientist M. Sanjayan prepares to anchor PBS's first live nature program

By **Valerie Thompson**

Touted as a large-scale conservation success story, the Monterey Bay National Marine Sanctuary off California's central coast was once ravaged by overfishing, pollution, and other stresses. Today, the "Serengeti of the Sea" plays host to a panoply of charismatic creatures—from humpback whales to great white sharks—drawn by seasonal infusions of nutrient-laden waters that transform the region into a rich feeding ground.

On 31 August 2015, PBS will offer viewers a glimpse into the area's remarkable recovery, airing the first episode of a three-part series anchored in real time from the sanctuary's shores and seas. M. Sanjayan, a senior scientist at Conservation International, will cohost the program, which will also feature short, prefilmed segments that will augment and expand the live coverage.

This interview has been edited for clarity and brevity.

Q: How was the project pitched to you?
A: Today, the only things that are live are sporting events, critical debates, and late night TV. This was like the Super Bowl for nature was going to happen right in a place that I love and know, and myself and other colleagues were going to get a chance to be sportscasters for a natural history event. [They asked], "Do you want to be involved?" and I was like, "Yeah!"

Q: Why do a live program?
A: Take a sporting event. It's one of the rare things a lot of people watch live. Because it's an event that becomes rooted in space, they can form a community around it. That's the same thing we're trying to do here. As presenters, we see these amazing natural history moments, and then we bring it [to the audience] in a very edited, very stylized form—sometimes years later. You can watch entire scenes from *Planet Earth* and not even recognize it as actually being planet Earth. There's no geography to it, and there certainly is no time to it. It doesn't engage audiences in the immediacy of what's going on.

I think that's the real advantage of this show. We can bring people along for the ride, and it's a gripping ride because we don't know what's going to happen next.

Q: As someone who has traveled on assignment to the far corners of the earth, what stands out about the Monterey Bay National Marine Sanctuary?
A: There are two things that really stand out to me. One is that it's probably the greatest predictable gathering of marine animals anywhere on earth. It's astonishing. You've got everything from anchovies, to sardines, to tuna, to the blue whale. The second is that it's an incredible story of recovery, of the resilience of nature, and of redemption—not just for nature, but for people who put their lives into bringing back the bay. Most places you go, you think, "God, I wish I was here 50 years ago. It would have been amazing to have seen this and that." This is a place that's actually better today than it was 50 or 100 years ago. Tell me that isn't an amazing story.

Q: What can a science-savvy audience look forward to seeing on the program?
A: When I was out there this week, I filmed two sequences: one with humpback whales and another with sea otters. So, all the stuff I did with sea otters—it's all the big science themes you want to hit: trophic cascades, mesopredator release, community ecology. We can talk about genetics, we can talk about recovery, and then we can talk about the massive impact that the sea otters had when they made it back into Monterey Bay. We can also talk about physiology: about why sea otters have dense fur instead of blubber, their diving capabilities, why they have to eat a third of their body weight every day. Honestly, there isn't a show that I've been part of that has had so much real science.

Q: What do you hope viewers will take away from the experience?
A: First of all, I want viewers to be entertained, and thrilled, and amazed. I want them to go "Holy Cow! I didn't know this actually was going on right off our coast." The second thing is I want viewers to understand how powerful and complex the natural world really is, and that with a little bit of help, much of it can still come back, and come back in a way that really benefits humans.

Big Blue Live
Airing on PBS at 8:00 pm ET and 8:00 pm PT;
31 August, 1 September, and 2 September 2015.
www.pbs.org/bigbluelive

10.1126/science.aad0946

ECONOMICS

Achieving equality

Economist Anthony Atkinson proposes ambitious policies for combating inequality

By **Marc Fleurbaey**

Inequality
What Can Be Done?
Anthony B. Atkinson
Harvard University Press, 2015. 398 pp.

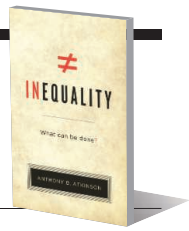

Anthony Atkinson is one of the founders of inequality studies, having made seminal contributions to the theory of the measurement of inequality, to the analysis of public policies, and, more recently, to the development of empirical measures of top incomes across the world. While making such academic contributions, he has also been constantly active in advising policymakers. Therefore, when he publishes a book, one should pay attention: Atkinson is the best expert on the topic of inequality, mastering the theory and the empirics as well as the relevant politics.

Inequality: What Can Be Done? is intended for a general audience, avoiding jargon and equations, and is thus very pleasant to read. The main thread of the book is that there is no iron law of inequalities because many things can be done to reverse the recent trend of growing divergence between the top and the bottom of the distribution of wealth and income. The book starts by diagnosing the problem, recalling that inequalities have fluctuated considerably in the past century through a combination of economic factors (e.g., the Great Depression), social trends (e.g., increased female participation in the labor market), and policies (in particular, tax breaks for high incomes in recent dec-ades). Then, looking forward in the direction of policy action, it contains no less than 15 concrete reform proposals and 5 ideas that could, with more development, lead to further proposals. All the proposals involve governmental action, but, most interestingly for the reader worried about the constraints imposed by globalization, many of them could be enacted at the national level, and essentially all of them could be enacted at the regional level.

In *Inequality*, Anthony Atkinson debunks common arguments against interventions designed to restore economic equality.

Some of the proposals are familiar and already in place in various countries (e.g., a national pay policy, national savings bonds with guaranteed interest, or the creation of a social and economic council), but some are much less debated, let alone implemented. One such idea is that the direction of technological innovation should be a topic of public deliberation, so that societies might examine potential consequences of new technologies on jobs and social relations—for example, in the service industry (automated servers cannot replace the human interaction that many users value). Another idea that Atkinson discusses, which unfortunately is not often debated today, is John Stuart Mill's 19th-century proposal to replace inheritance taxes (that bear on the total amount left as a bequest by the deceased) with taxes paid by the recipients of gifts and bequests, as a function of how much each of them receives over the course of his life. This is a very natural idea, given that there is nothing wrong with bequeathing one's wealth at the end of one's life. The true problem is that some receive immensely more than others. Such a tax would be used to fund a capital endowment that every individual would receive at the onset of adulthood, helping many secure housing, fund education, and create new businesses.

The reader will enjoy the passages in which Atkinson takes sides on classical debates about basic income (arguing that countries that choose to provide a regular, minimum sum of money to every citizen should require some contribution to society in return), the targeting of social aid (arguing that it is largely a mistake and that we should institute universal social insurance instead), and development aid (arguing that it is effective and should be increased). Written by an economist, this book focuses on income and wealth more than other aspects of inequality, but it does mention the key question of the balance of power among stakeholders, and indeed one of the 15 proposals centers around the idea of empowering consumers and workers.

Atkinson spends the last part of the book debunking the standard objections to action against inequalities. No, fighting inequalities does not necessarily kill growth and economic incentives. In fact, he maintains that providing opportunities to all is a recipe for a healthier economy. No, globalization does not prevent national action for the less advantaged, as proved by the diversity of redistributive policies pursued in countries facing similar economic conditions, even if a globalized economy does impose some constraints and requires international coordination. Yes, the policies proposed can have a real effect on inequalities without jeopardizing public finances. He even proposes a concrete estimate of the financial and social effect his proposals could have in the United Kingdom.

This is a book that all concerned with growing inequalities and interested in policy ideas should read. Its general philosophy is that it is not easy to delineate the contours of a "just society" and perhaps illusory to set out to achieve it, but that it is definitely possible to determine a direction of improvement and to find levers that can realistically move us in the right direction. It aims at stimulating and enriching the policy debate, and there is no doubt that it will.

The reviewer is at the Woodrow Wilson School of Public and International Affairs, Princeton University, Princeton, NJ 08544, USA. E-mail: mfleurba@princeton.edu

10.1126/science.aac8272

LETTERS

Edited by **Jennifer Sills**

Isolated tribes: Contact misguided

IN THEIR EDITORIAL "Protecting isolated tribes" (5 June, p. 1061), in addition to proposing the implausible notion of a flawlessly engineered "controlled contact" with isolated indigenous peoples in which events go according to plan and nobody dies, R. S. Walker and K. R. Hill ask us to ignore the likelihood that such processes would be co-opted by powerful vested interests. Oil companies, loggers, and governments are desperate to promote contact and access the precious natural resources in these peoples' territories.

Walker and Hill are right, however, that "unless protection efforts…are drastically increased, the chances that these tribes will survive are slim." They cite Peru's "leave them alone" policy, but the reality is very different. In the case of the Yora people cited by Hill and Walker, roughly a third of the protected area established for them has been opened up for gas exploitation (*1*). If these rights are so trampled even in countries with "leave them alone" policies, what would happen if "controlled contact" were actively promoted? Walker and Hill should be demanding that these standards are upheld rather than weakened.

However well intentioned the proposal of "controlled contact," it is not the place of others, be they academics or governments, to determine the future of peoples who, for their own reasons, are holding the rest of the world at arm's length. It is up to the people themselves to assume this weighty responsibility and to decide if, when, and how contact should occur. This is called self-determination. It is the job of wider society to safeguard this right by declaring their lands illegal for logging or mining, guarding these areas to prevent illegal activities, improving public health in surrounding areas, and enabling emergency medical assistance if and when contact is initiated. In this way, we can provide them with the space and time to decide their own future.

Conrad Feather

Forest Peoples Programme, Moreton in Marsh, Gloucestershire GL56 9NQ, UK.
E-mail: conrad@forestpeoples.org

REFERENCE

1. C. Feather, "Violating rights and threatening lives: The Camisea gas project and indigenous peoples in voluntary isolation" (Forest Peoples Programme, UK, 2014); www.forestpeoples.org/sites/fpp/files/publication/2014/01/camisea-englishlowres_0.pdf.

Isolated tribes: Human rights first

I APPLAUD THE coverage of isolated tribes in the 5 June issue and agree that government protection efforts need to be well organized and funded ("Protecting isolated tribes," Editorial, R. S. Walker and K. R. Hill, p. 1061; "Making contact," A. Lawler, News Feature, p. 1072; "In peril," H. Pringle, News Feature, p. 1080). However, the section provides an incomplete view of a complex policy debate that has pitted "realists" against "idealists" since the 19th century over the survival of independent indigenous peoples (*1*, *2*). The issue is more about human rights to cultural survival than it is about "isolation."

Policy realists have consistently maintained that tribal peoples could not survive autonomously. Only recently has this debate been idealistically framed as how to defend the tribal peoples' basic human rights to cultural autonomy. In 2005, the UN General Assembly called for a "global mechanism" to support tribal peoples living in voluntary isolation (*3*); in 2007, it adopted the Declaration on the Rights of Indigenous Peoples (*4*). In 2012, the UN High Commissioner for Human Rights issued guidelines for the protection of isolated peoples in South America (*5*); the office added specific recommendations for Peru in 2014 (*6*).

The situation has improved substantially since I first visited the Peruvian Amazon in 1964. At that time, there were no indigenous political organizations, and most of their territories were still officially viewed as "uninhabited" and open for development (*7*). Indigenous activists began organizing in Peru to press for land rights and cultural autonomy in the 1980s, and by 2012, 1270 indigenous communities held titles to 106,585 km^2 of territory as communal reserves. This was nearly 14% of the Peruvian Amazon, and another 67,889 km^2 was in proposed or designated territorial reserves (*8*). Isolated tribes have been legally protected in Peru since 2006 (*9*). This idealist policy is supported by indigenous organizations [such as the Interethnic Association for the Development of the Peruvian Rainforest (AIDESEP)] and international nongovernmental organizations (such as International Work Group for Indigenous Affairs and Survival International). Surely Walker and Hill did not mean to characterize these human rights advances as a conceptually flawed "leave them alone" policy. Rights-based protection policies are not yet being adequately implemented, but their existence is crucial, and they are not flawed in principle. The long-term viability of isolated tribes is an open question, as is the viability of the commercial world. Likewise, no one knows whether "contact" would ultimately be a good choice, especially when it could mean joining the ranks of the global poor. Rejecting idealist policies would constitute a return to the flawed "realist" policies that accept as inevitable the politics that are degrading Amazonia in the name of development, which then forces some isolated tribes to forage outside their reserves to survive.

John H. Bodley

Allowing villagers in the remote Peruvian Amazon to determine their own future is a matter of human rights.

PHOTO: JASON HOUSTON

Department of Anthropology, Washington State University College of Arts and Sciences, Pullman, WA 99164-2630, USA. E-mail: bodleyj@wsu.edu

REFERENCES

1. J. H. Bodley, in *Western Expansion and Indigenous Peoples*, E. Sevilla-Casas, Ed. (Mouton, The Hague, Netherlands, 1977), pp. 31–50.
2. J. H. Bodley, *Victims of Progress* (Rowman & Littlefield, Lanham, MD, ed. 6, 2015).
3. United Nations, General Assembly, "Draft programme of action for the second international decade of the world's indigenous people" (Report of the Secretary-General, A/60/270, 2005), paragraphs 45 and 51; www.iom.int/jahia/webdav/shared/shared/mainsite/policy_and_research/un/60/A_60_270_en.pdf.
4. United Nations, "United Nations declaration on the rights of indigenous peoples" (United Nations, New York, 2007); www.un.org/esa/socdev/unpfii/documents/DRIPS_en.pdf.
5. United Nations, Office of the High Commissioner for Human Rights, "Directrices de protección para los pueblos indígenas en aislamiento y en contacto inicial de la Región Amazónica, el Gran Chaco y la Región Oriental de Paraguay" (United Nations, Geneva, 2012); http://acnudh.org/wp-content/uploads/2012/03/Directrices-de-Protección-para-los-Pueblos-Indígenas-en-Aislamiento-y-en-Contacto-Inicial.pdf.
6. J. Anaya, "Report of the Special Rapporteur on the rights of indigenous peoples, Addendum: The situation of indigenous peoples' rights in Peru with regard to the extractive industries" (UN Human Rights Council, A/HRC/27/52/Add. 3, 2014); www.refworld.org/docid/53eb3c774.html.
7. J. H. Bodley, "Tribal survival in the Amazon: The Campa case" (International Work Group for Indigenous Affairs, Document No. 5, Copenhagen, 1972).
8. RAISG, "Amazon 2012 Protected Areas Indigenous Territories" (2012); www.ibcperu.org/public/directorio_com_nativas_2012.pdf.
9. Ley No. 28736, "Ley para la protección de pue los indigenas u originarios en situaciön de aislamiento y en situaciön de contacto inicial, El Peruano" (2006); http://faolex.fao.org/docs/pdf/per64175.pdf.

Drought threatens California's levees

CALIFORNIA HAS MORE THAN 21,000 km (*1*) of earthen embankments (referred to as levees) that protect dryland from floods and also function as water storage and management systems. The resilience of these levees under the record drought conditions California faces is an emerging issue that requires attention.

Prolonged droughts undermine the stability of levee systems by increasing water seepage through soil, soil cracking, soil strength reduction, soil organic carbon (SOC) decomposition, and land subsidence and erosion (*2*). The sand-clay mixtures, which form the body of the levees and consequently the entire structure, can lose a substantial amount of strength under dry conditions. Furthermore, levees in California are built on peaty soils, and the extreme drought leads to greater SOC decomposition in these soils. A large amount of the global carbon stock is found in peaty soils, and ~25% of this estimated stock is predicted to diminish under extremely dry conditions (*3*). Oxidation of

Broken levee under repair in the Sacramento River delta.

PHOTO: MICHAEL NEVINS/U.S. ARMY CORPS OF ENGINEERS DIGITAL VISUAL LIBRARY

SOC under a prolonged drought can also accelerate land subsidence. In fact, 75% of the land subsidence across California is accredited to oxidation of SOC (*3*). Land subsidence can increase the risk of water rising over the top of the levees.

Australia's Millennium Drought (1997–2009) is often considered the type of event for which California should prepare (*4*). At the peak of the drought (i.e., 2008 to 2009), Australia experienced disastrous failures of alluvial river banks along the Murray River (*5*). Similar failures occurred in other parts of the world during extreme drought conditions, such as the 2003 Wilnis Levee failure in the Netherlands (*6*).

California's drought is yet another stress that poses a great risk to an already endangered levee system. At this time, 55% of California's levee systems are rated as "high hazard," meaning that they are in danger of failing if a flood event or an earthquake occurs (*1*). This indicates that California's levee systems have a high failure risk without even considering an extreme event such as a prolonged drought. If the drought ends with heavy rainfall-induced flooding, as seen in 2010 in Australia (*5*) and 2015 in Texas and Oklahoma (*7*), the levees could be at even greater risk. Drought risk and potential changes in the future climate were not considered in the engineering design of these levee systems and are still not considered in maintenance guidelines today. There is an urgent need to invest in research on (i) effects of the rate and variability of drought on the short- and long-term behavior of levees; (ii) constraints in existing levee design, maintenance, and monitoring guidelines for extreme droughts; (iii) adaptation and mitigation strategies for reducing drought impacts on the performance of levee systems; (iv) socioeconomic consequences of levee failures; and (v) multi-hazard disaster risk science to assess the impacts of compound and consecutive extreme events on levees. Community engagement, public risk education, and close collaboration with stakeholders are key to enhancing societal resilience of levees to extreme droughts.

Farshid Vahedifard,[1]* Amir AghaKouchak,[2] Joe D. Robinson[1]

[1]Department of Civil and Environmental Engineering, Mississippi State University, Mississippi State, MS 39762, USA. [2]Department of Civil and Environmental Engineering, University of California, Irvine, CA 92697, USA.

*Corresponding author. E-mail: farshid@cee.msstate.edu

REFERENCES

1. California Department of Water Resources, *Flood Control System Status Report* [Central Valley Flood Management Planning (CVFMP) Program, California, 2011];www.water.ca.gov/cvfmp/docs/FCSSRDec2011_FullDocument.pdf.
2. P. Vardon, *Env. Geotechnics* **2**, 166 (2014).
3. B. A. Brooks *et al*., *San Francisco Estuary Watershed Sci.* **10**(1) (2012); http://escholarship.org/uc/item/15g1b9tm.
4. A. Aghakouchak *et al*., *Science* **343**, 1430 (2014).
5. E. V. De Carli, T. C. T. Hubble, in *Proceedings of the 7th Australian Stream Management Conference*, G. Vietz, I. D. Rutherfurd, R. Hughes, Eds. (Townsville, Queensland, Australia, 2014), pp. 255–261.
6. S. Van Baars, *Géotechnique* **55**, 319 (2005).
7. A. Freedman, A. Li, "Texas and Oklahoma hit by severe flooding, killing 2" (2015); http://mashable.com/2015/05/24/texas-oklahoma-flash-flooding/.

TECHNICAL COMMENT ABSTRACTS

Comment on "Tectonic control of Yarlung Tsangpo Gorge revealed by a buried canyon in Southern Tibet"

Peter K. Zeitler, Peter O. Koons, Bernard Hallet, Anne S. Meltzer

Wang *et al.* (Reports, 21 November 2014, p. 978) describe a buried canyon upstream of the Yarlung Tsangpo Gorge and argue that rapid erosion of the gorge was merely a passive response to rapid uplift at ~2.5 million years ago (Ma). We view these data as an expected consequence emerging from feedbacks between erosion and crustal rheology active well before 2.5 Ma.

Full text at http://dx.doi.org/10.1126/science.aaa9380

Response to Comment on "Tectonic control of Yarlung Tsangpo Gorge revealed by a buried canyon in Southern Tibet"

Ping Wang, Dirk Scherler, Jing Liu-Zeng, Jürgen Mey, Jean-Philippe Avouac, Yunda Zhang, Dingguo Shi

In their Comment, Zeitler *et al.* do not challenge our results or interpretation. Our study does not disprove coupling between tectonic uplift and erosion but suggests that this coupling cannot be the sole explanation of rapid uplift in the Himalayan syntaxes.

Full text at http://dx.doi.org/10.1126/science.aaa9636

TECHNICAL COMMENT

GEOMORPHOLOGY

Comment on "Tectonic control of Yarlung Tsangpo Gorge revealed by a buried canyon in Southern Tibet"

Peter K. Zeitler,[1]* Peter O. Koons,[2] Bernard Hallet,[3] Anne S. Meltzer[1]

Wang *et al*. (Reports, 21 November, 2014, p. 978) describe a buried canyon upstream of the Yarlung Tsangpo Gorge and argue that rapid erosion of the gorge was merely a passive response to rapid uplift at ~2.5 million years ago (Ma). We view these data as an expected consequence emerging from feedbacks between erosion and crustal rheology active well before 2.5 Ma.

Wang *et al*. (*1*) address the debate over the roles of tectonic versus surface forcing in orogenesis (*2*), concluding that "our results suggest that rapid incision within the Tsangpo Gorge is the result rather than the cause of rock uplift." We offer an alternate viewpoint in which the important data reported by Wang *et al*. (*1*) match predictions (*3*) made using the aneurysm model and provide support for the idea that feedbacks between tectonic, rheological, thermal, and surface phenomena will inevitably and spontaneously develop in regions where sufficiently rapid tectonic uplift and focused erosion are superimposed.

As Wang *et al*. note, the reported 2 to 2.5 million years ago (Ma) age for the initiation of sediment accumulation upstream of the Namche Barwa knickpoint is a minimum, due to the complex infilling patterns in time and space expected after tectonic impoundment of a large sediment-laden river having major tributaries. Moreover, given the location of the dated core (well 3; 567 m in a basin of >1000 m total depth) and assuming a constant sedimentation rate, sediment at the base of the projected ~1000 m of deepest fill could be 3 to 4 Ma in age.

In interpreting their data, Wang *et al*. assume that a singular impoundment occurred behind a sharply defined structure that became abruptly active at 2 to 2.5 Ma, but neither of these conditions applies to the Namche Barwa antiform and the Namche Barwa–Gyala Peri metamorphic massif. The current massif is terminated along its western, northern, and northeastern margins by active structures marked by sharp cooling-age discontinuities and abundant seismicity (Fig. 1A) (*4*). In contrast, to the southwest where sediments have accumulated, the cooling-age transition from the massif to the Namche Barwa antiform is gradual across the Nam La thrust zone that defines the southern boundary of the massif (Fig. 1B). The extreme rates and magnitude of rock uplift and exhumation are focused within the massif and decline progressively toward the antiform without any discontinuities across structural boundaries.

Available evidence also argues strongly against abrupt initiation of activity at 2.5 Ma. Thermochronologic and other data document a longer history of systematic focusing of exhumation and strain in southeastern Tibet, as predicted by the aneurysm model (*3*, *5*–*7*). In the southeastern Lhasa block and Namche Barwa antiform, rapid exhumational cooling occurred from ~10 Ma to ~5 Ma, and within the massif itself, petrologic and age data suggest 10s of km of exhumation over the same interval (*3*, *4*), a conclusion also supported by detrital dating (*8*). Rapid exhumation ceased in the Lhasa Block by 6 to 7 Ma and then in the antiform by ~4 Ma, but within the metamorphic massif, rapid cooling has continued and possibly accelerated (*4*). This progressive cessation of rapid cooling everywhere but the massif can be explained by focusing of deformation first into the antiform and then further localization into the massif, where acceleration of rock uplift could have slowed upstream exhumation rates by establishing a new local base level for the Yarlung Tsangpo at the stabilized knickpoint. Evolution of this coupled system would have taken place over an interval of time, starting as early as 10 Ma, with a focused zone of rapid uplift and erosion becoming a distinct emergent phenomenon by 5 Ma.

The observed distribution of structures and their evolution over several million years are consistent with upstream sediment accumulation beginning at 2.5 Ma or earlier. As regional rock uplift focused into the massif, uplift and erosion rates became locally sufficient to permit feedbacks to develop between coupled tectonic

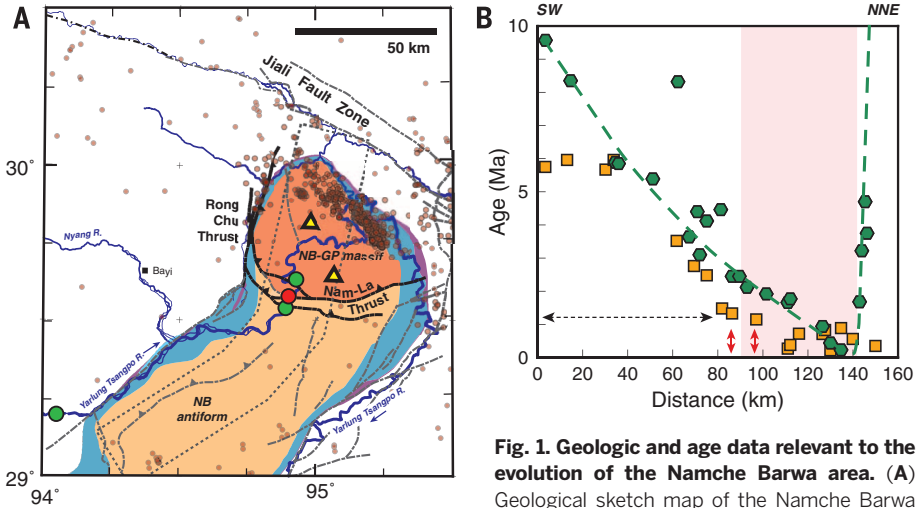

Fig. 1. Geologic and age data relevant to the evolution of the Namche Barwa area. (**A**) Geological sketch map of the Namche Barwa knickpoint, showing its seismically active structural boundaries [modified from (*4*)]. Orange and brown regions show, respectively, the Namche Barwa–Gyala Peri metamorphic massif and the Namche Barwa antiform. The region in blue shows Tethyan metasedimentary cover, and rocks of the Yarlung-Tsangpo Suture Zone are shown in purple. Yellow triangles, Gyala Peri and Namche Barwa peaks; green circles, from left, wells 3, 4, and 5 (*1*); red circle, approximate location of top of knickzone. Small circles show epicenters of local earthquakes [16 months of data (*4*)]. The dashed polygon shows the swath across which ages were projected for the profile shown in (B). (**B**) Cooling-age profile across the core of the metamorphic massif and the axis of antiform, showing a sharp discontinuity in the north but only a gradual rise toward the southwest, ruling out a large-magnitude structural offset at the top of the Yarlung Tsangpo Gorge over the past few million years [data from (*4*)]. The pink region shows the extent of the metamorphic massif. Green hexagons, $^{40}Ar/^{39}Ar$ biotite cooling ages; orange squares, U-Th/He zircon cooling ages. Small red arrows give projected location of wells 4 and 5 of (*1*), and the black arrow highlights U-Th/He zircon cooling ages of bedrock at those sites.

[1]Department of Earth and Environmental Sciences, Lehigh University, Bethlehem, PA 18015, USA. [2]Department of Earth and Climate Sciences, University of Maine, Orono, ME 04469, USA. [3]Department of Earth and Space Sciences, University of Washington, Seattle, WA 98195, USA.
*Corresponding author. E-mail: peter.zeitler@lehigh.edu

and surface processes. These feedbacks led to development of a stabilized knickpoint with an upstream reduction in river gradient sufficient to permit sediment aggradation and, ultimately, accumulation. Patterns of sedimentation and sediment preservation behind such a developing bedrock uplift are likely to be complicated and dynamic. Given high rates of rock uplift, sediment supply by the Yarlung Tsangpo and its tributaries, and incision downstream of the knickpoint, such factors as perturbations to the sediment supply (e.g., a Quaternary increase), temporary glacial or landslide damming (*9*), and localized changes in the tectonic strain field would affect sediment distribution, accumulation, and preservation upstream of the knickpoint. Repeated episodes of sediment accumulation and evacuation could occur, as is suggested by the coarse basal sediments in well 5. In contrast to the 2.5 Ma age of basal sediments at well 3, at well 5 these sediments must be considerably younger than nearby bedrock having a U-Th/He zircon cooling age of 1.2 Ma (*4*).

We conclude with a comment about misunderstanding of the tectonic aneurysm model that emerges in Wang *et al.* (*1*) and elsewhere [e.g., (*2*)]. As we proposed (*3*, *5*–*7*), this model operates at local scales and is foremost about tectonic processes. It is not about surface processes "triggering" rock uplift, at any rate. The tectonic aneurysm develops in response to exhumation-driven thermal thinning of the upper, high-strength portion of the crust in actively deforming regions that have the potential for rapid erosional flushing. The model produces characteristic observable signatures that include an elevated viscous-frictional transition as seen in hypocentral locations (*10*), active high-temperature hydrothermal systems (*11*, *12*), and decompression anatexis and metamorphic *PT* paths (*13*, *14*). In the context of the aneurysm model, when we have used the word "triggering," it has referred to the emergence of feedbacks among several sets of coupled phenomenon, and not, as Wang *et al.* as well as others suggest (*1*, *2*), instigation of rock uplift by erosion. Several elements are needed for these feedbacks to emerge: strong erosive power coupled to a vigorous transport system sufficient to remove enough material to perturb the thermal field; a nonlinear temperature-dependent rheology; and, above all, a crust, near failure, that is undergoing active deformation collocated with the strong erosion. Once feedbacks come into play, chicken-versus-egg arguments about tectonic versus erosional "control," and cause-and-effect become irrelevant. Rather than challenging the concept of feedbacks between tectonics and erosion, we think that the results of Wang *et al.* provide striking confirmation.

REFERENCES

1. P. Wang *et al.*, *Science* **346**, 978–981 (2014).
2. K. X. Whipple, *Science* **346**, 918–919 (2014).
3. P. O. Koons, P. K. Zeitler, B. Hallet, in *Treatise on Geomorphology*, J. F. Shroder, Ed. (Academic Press, San Diego, CA, 2013), pp. 318–349.
4. P. K. Zeitler *et al.*, in *Toward an Improved Understanding of Uplift Mechanisms and the Elevation History of the Tibetan Plateau*, J. Nie, B. K. Horton, G. D. Hoke, Eds. (Geological Society of America Special Paper 507, 2014), pp. 23–58.
5. P. Zeitler *et al.*, *GSA Today* **11**, 4–8 (2001).
6. P. O. Koons, P. K. Zeitler, C. P. Chamberlain, D. Craw, A. S. Meltzer, *Am. J. Sci.* **302**, 749–773 (2002).
7. P. K. Zeitler *et al.*, *Tectonics* **20**, 712–728 (2001).
8. K. Lang, K. Huntington, R. Burmester, B. Housen, River antecedence and the onset of rapid exhumation in the Eastern Himalayan Syntaxis. Abstract EP21A-3519 presented at the American Geophysical Union Fall Meeting, San Francisco, 16 December 2014.
9. O. Korup, D. R. Montgomery, *Nature* **455**, 786–789 (2008).
10. A. S. Meltzer, G. L. Sarker, B. Beaudoin, L. Seeber, J. Armbruster, *Geology* **29**, 651–654 (2001).
11. C. P. Chamberlain *et al.*, *Am. J. Sci.* **302**, 726–748 (2002).
12. D. Craw, P. O. Koons, P. K. Zeitler, W. F. S. Kidd, *J. Metamorph. Geol.* **23**, 829–845 (2005).
13. A. G. Whittington, N. B. W. Harris, R. W. H. Butler, *Spec. Pap. Geol. Soc. Am.* **328**, 129–144 (1999).
14. A. L. Booth, C. P. Chamberlain, W. S. F. Kidd, P. K. Zeitler, *Geol. Soc. Am. Bull.* **121**, 385–407 (2009).

18 February 2015; accepted 21 July 2015
10.1126/science.aaa9380

TECHNICAL RESPONSE

GEOMORPHOLOGY

Response to Comment on "Tectonic control of Yarlung Tsangpo Gorge revealed by a buried canyon in Southern Tibet"

Ping Wang,[1] Dirk Scherler,[2]*† Jing Liu-Zeng,[1] Jürgen Mey,[3] Jean-Philippe Avouac,[2]‡ Yunda Zhang,[4] Dingguo Shi[4]

In their Comment, Zeitler *et al*. do not challenge our results or interpretation. Our study does not disprove coupling between tectonic uplift and erosion but suggests that this coupling cannot be the sole explanation of rapid uplift in the Himalayan syntaxes.

In their Comment on our study (*1*), Zeitler *et al.* (*2*) imply that we interpreted our findings to question the possible existence of feedbacks between surface and tectonic processes, which is not the case. We therefore appreciate the opportunity to clarify potential misunderstandings.

Zeitler *et al.* (*2*) suggest that the oldest sediments at the base of the valley fill could be 3 to 4 million years ago (Ma) in age. We have no objection to this assessment. As noted previously (*1*), our burial age stems from a drill hole located ~150 km upstream of the gorge and therefore represents a minimum age for the onset of deposition. We note, however, that discussing the exact timing of the onset of sediment accumulation was not the main focus of our study.

Zeitler *et al.* furthermore argue, "Wang *et al.* assume that a singular impoundment occurred behind a sharply defined structure that became abruptly active at 2 to 2.5 Ma." This sentence is not correct. First, as mentioned above, we inferred that uplift commenced earlier than the burial age that we obtained from the base of drill core 3, and therefore we did not assume that a certain structure became "abruptly active at 2 to 2.5 Ma." Consequently, we have no objections regarding the following paragraph, in which Zeitler *et al.* cite published evidence for regional exhumation before 2.5 Ma, many of which we have cited in our study (*1*) already. Second, we did not make any inferences about which structures are responsible for the uplift. From the pattern of bedrock cooling ages that we summarized in figure 2C in (*1*), we would not infer a sharply defined structure, and we did not do so in the original Report. We also did not comment on whether one or more impoundments occurred, but, in the absence of evidence for a more complicated scenario, our preferred model is that uplift of the Namche Barwa–Gyala Peri massif was a one-directional process with time. Nevertheless, it is conceivable that impounding and upstream sediment accumulation did not occur continuously at a steady rate. For example, if climatic fluctuations during the Quaternary resulted in changing river transport capacities and/or occasional glacial damming and catastrophic flooding (*3*), the net long-term deposition, which is evident in the valley fill, could have been superimposed with short periods of reincision. Although the details of the valley-filling episode could provide interesting insights into the Quaternary landscape evolution of this region, our observations do not bring any constraints, and therefore, we refrained from commenting on these aspects.

It is clear that we do not question the potential existence of feedbacks between erosion and uplift when we wrote, "Even if positive feedbacks between erosion and uplift nowadays help to maintain these gorges in their current location, our results suggest that rapid incision within the Tsangpo Gorge is the result rather than the cause of rock uplift." The actual question raised by our observations regards the initiation of these feedbacks. Why do we see exceptionally rapidly uplifting, young metamorphic massifs in the syntaxes regions, where the Yarlung Tsangpo and Indus Rivers traverse the Himalaya, but nowhere else in the Himalaya? Is it because of large-magnitude river incision, as was suggested by Zeitler and colleagues earlier (*4*), or is it because of the unique tectonic setting in these corner regions of the Himalaya? This, in our view, important question remains unanswered and avoided by Zeitler *et al.*

In fact, we find comments by Zeitler *et al.* contradictory when they write, "As regional rock uplift focused into the massif, uplift and erosion rates became locally sufficient to permit feedbacks to develop between coupled tectonic and surface processes," which suggests to us that focusing of rock uplift into the massif occurred before initiation of feedbacks, seemingly irrespective of surface erosion. Later, Zeitler *et al.* write, "The tectonic aneurysm develops in response to exhumation-driven thermal thinning of the upper, high-strength portion of the crust in actively deforming regions that have the potential for rapid erosional flushing." In this case, the "potential for rapid erosional flushing" appears to be a necessary condition. Perhaps we misunderstood Zeitler *et al.*'s (*4*) previous use of the word "triggering," but we still think that it is important to understand under which conditions coupled rapid uplift and exhumation with positive feedbacks between surface processes and tectonics can develop, and if it can initiate solely from below (i.e., by focused uplift) or from above (i.e., by surface erosion). The observation that the Tsangpo-Brahmaputra River was able to carve a deep canyon into southern Tibet and develop a graded profile with no knickpoint before rapid uplift of the Namche Barwa and Gyala Peri massifs suggests the former.

To conclude, we agree with Zeitler *et al.* that feedbacks between tectonic uplift and erosion play an important role in the development of orogens and that they are at play in the evolution of the Himalayan syntaxes. However, our study makes it unlikely that these feedbacks are the primary cause for the exceptionally rapid uplift that is observed in these regions.

[1]State Key Laboratory of Earthquake Dynamics, Institute of Geology, China Earthquake Administration, Beijing 100029, P. R. China. [2]Division of Geological and Planetary Sciences, California Institute of Technology, Pasadena, CA 91125, USA. [3]Institute of Earth and Environmental Sciences, University of Potsdam, 14476 Potsdam, Germany. [4]Chengdu Engineering Corporation, Chengdu 610072, P. R. China.
***Corresponding author. E-mail: scherler@gfz-potsdam.de**
†Present address: German Research Centre for Geosciences (GFZ), Section 3.4, Telegrafenberg, D-14473 Potsdam, Germany.
‡Present address: Department of Earth Sciences, University of Cambridge, Cambridge, UK.

REFERENCES

1. P. Wang *et al.*, *Science* **346**, 978–981 (2014).
2. P. K. Zeitler, P. O. Koons, B. Hallet, A. S. Meltzer, *Science* **349**, 799 (2015).
3. D. R. Montgomery *et al.*, *Quat. Res.* **62**, 201–207 (2004).
4. P. Zeitler *et al.*, *GSA Today* **11**, 4–9 (2001).

4 March 2015; accepted 21 July 2015
10.1126/science.aaa9636

FOREST HEALTH IN A CHANGING WORLD

By **Andrew Sugden, Julia Fahrenkamp-Uppenbrink, David Malakoff,** *and* **Sacha Vignieri**

Forests and woodlands cover about 20% of Earth's land surface, spanning all but the highest latitudes. In the millennia since humans dispersed across all forested continents, we have transformed large areas of natural forest. Historically, our greatest impacts were made in temperate regions, but they now extend to forests in the tropics and the boreal zone. Only a fraction of the forests present centuries ago have escaped human influence; in many regions the forest is gone, has regrown as secondary forest, or consists of managed and plantation forests. Humans have also introduced new species, including pests and pathogens of trees. Other influences—such as climate warming that causes tree species to shift geographically and anthropogenic drought that causes forest dieback—take effect more slowly and may occur far from their source.

Even though modern forests are generally much altered from their natural state, their "health" still matters. It will dictate whether forests persist and function into the future, sustaining wildlife, producing timber, sequestering carbon, and performing other services.

Yet forest health is difficult to define. Forests experience plenty of natural disturbances: fire, weather variations, competition between plant species, and attacks by insect pests and pathogens. They also experience longer-term successional change. When we speak of threats to forest health, we tend to imply the impacts of humans. However, it may not always be obvious whether human activity or a forest's natural dynamics are at play in, for example, the dieback of a stand or the outbreak of an insect herbivore.

Recognizing the signs of ill forest health and teasing apart the causes are important both for sustaining the services that humans rely on and for the effective conservation of forest biomes. Understanding how we influence forest health and function is a key challenge for the future, as we increasingly realize the importance of forests to the maintenance of a healthy planet.

INSIDE

RELATED ITEMS
- ▸ EDITORIAL P. 771
- ▸ PERSPECTIVE P. 794
- ▸ VIDEO http://scim.ag/6250_ForestVid
- ▸ SLIDESHOW http://scim.ag/6250_ForestSlide

Mountain pine beetle infections are becoming more intense as weather warms in coniferous forests, like this one in central British Columbia. Infected trees die slowly, resulting in a forest full of various levels of colorful dieback.

PHOTO: TOM NEVESELY/ALL CANADA PHOTOS/CORBIS

BATTLING A GIANT KILLER

The iconic eastern hemlock is under siege from a tiny invasive insect

By **Gabriel Popkin** *in Highlands, North Carolina; photography by* **Katherine Taylor**

On a frigid morning this past March, arborist Will Blozan snuck behind a small church here and headed down into a gorge thick with rhododendron. He crashed through the shrubs until he spotted the gorge's treasure: the world's largest known living eastern hemlock tree, known as the Cheoah.

In 2006, Blozan had climbed the nearly 50-meter-tall giant and calculated that it contained 44.29 cubic meters of wood—then a record. Blozan would later discover two even larger hemlocks in the nearby Great Smoky Mountains National Park. Both of those champions, however, are now dead.

So are millions of other hemlocks across eastern North America. They've been reduced to leafless gray skeletons by the hemlock woolly adelgid (*Adelges tsugae*), a tiny sap-sucking insect about the size of a pinhead. Originally from Japan, the adelgid has spread from Georgia to Maine in recent decades, entering new hemlock stands every year. Left unchecked, it kills nearly every tree it attacks. Paradoxically, large, seemingly vigorous trees like the Cheoah often go fastest.

For years, forest managers have been in a fierce fight against the adelgid, and the battle has recently expanded to new fronts. The Cheoah and hundreds of thousands of other hemlocks are still alive because they have been treated with insecticides. But that's an expensive and labor-intensive tactic, so scientists are trying out more sustainable strategies. They're rearing and releasing predatory insects that eat the adelgid, and even looking for rare hemlock genes that might help them breed resistant trees. Eastern hemlocks, warns forester Jesse Webster of the Great Smoky Mountains park, "are in intensive care." Like the family of a gravely ill patient, ecologists are also preparing for the possibility that these efforts will fail, and the eastern forest will lose one of its defining species.

Near death, a barren hemlock in the Harvard Forest in Massachusetts displays the telltale effects of an attack by hemlock woolly adelgids.

TSUGA CANADENSIS is one of eastern North America's largest native conifers. It has been called the "redwood of the east" and the "queen of the conifers." A healthy tree resembles an evergreen waterfall; overlapping layers of short, downy needles cascade from the crown almost to the ground.

Biologists believe the species diverged from its Asian cousins some 23 million to 40 million years ago. When Europeans arrived nearly 500 years ago, hemlocks dominated valleys in the 3000-kilometer Appalachian corridor and grew as far north as present-day Canada and as far west as Minnesota. Loggers once targeted the tree, but typically not for its wood, which is brittle. Instead, they prized its coffee-colored bark, which is rich in the tannins traditionally used to tan leather.

Distinctive tufts help protect adult hemlock woolly adelgids. The insects stay put once they start feeding on hemlock needles.

Hemlocks nurture an ecosystem that has evolved nowhere else. Their defining characteristic is deep shade; unlike many pines, hemlocks keep needles on their lower branches, creating a thick canopy that blocks up to 99% of sunlight. Few plants grow in the gloom, but a hemlock seedling can bide its time for decades or more, waiting for a sunlit opening. Hundreds of species of insects, mites, and spiders appear to live primarily or exclusively in hemlock forests, and some aquatic invertebrates eat the hemlock needles that fall into mountain streams. Many migratory birds seek out the trees.

The oldest known specimen was 555 years old when dendrochronologist Edward Cook measured it in 1991; just four other eastern tree species are known to live longer. "There's no tree, certainly in the east, that has anything like that kind of complete control" over its environment, says David Foster, an ecologist and director of the Harvard Forest in Petersham, Massachusetts.

THE HEMLOCK'S MIGHTY GRIP is now being loosened by the diminutive *A. tsugae*. Hemlock woolly adelgids "are bizarre little things," says entomologist Lynne Rieske-Kinney of the University of Kentucky in Lexington. An adult is about a millimeter long, with a threadlike proboscis that can be three times as long as its body. They can easily catch a ride to new trees on the wind or on birds and mammals. Once an adelgid pierces the base of a hemlock needle and starts sucking out starch, starving the tree, it stays put and envelops itself in a distinctive white fluff—hence the "woolly"—to protect itself and its eggs. The adelgid reproduces asexually in North America, rapidly spawning genetically identical offspring. All you need to get an outbreak, Rieske-Kinney explains, is "a susceptible host and one insect."

Nobody knows for sure how the Asian species got to North America, but all evidence points to ornamental hemlocks that were imported from Japan. The invader was first documented near Richmond in 1951. It went essentially unnoticed until 1986,

when Mark McClure, then a scientist with the Connecticut Agricultural Experiment Station in New Haven, warned that it was killing trees in his state. Two years later, researchers found adelgids in Virginia's Shenandoah National Park, and by 1994 most of the park's hallmark hemlocks were dead or dying. "That was a big wake-up call," says entomologist Rusty Rhea of the U.S. Forest Service's Southern Research Station in Asheville, North Carolina.

Alarmed, federal biologists moved to stop the invasion. But there was one problem, recalls recently retired Forest Service entomologist Brad Onken: They knew nothing about the adelgid. "We had to really start from scratch."

The hemlock woolly adelgid's spread prompted ecologist David Orwig of the Harvard Forest in Massachusetts to launch an unusual study of forest death.

AS THE TREES KEPT DYING, researchers scrambled to locate and inventory important stands. Blozan and his colleagues, for instance, used aerial photos and ground surveys to locate 75 hemlocks that were taller than the previously known record of 48.8 meters. All stood within a 100-kilometer-wide area that includes parts of North Carolina, Tennessee, Georgia, and South Carolina; most were within the Great Smoky Mountains park. Blozan and colleagues measured the trees and found that, contrary to theory, hemlocks reached their largest sizes at the southern edge of their range, not the geographical center.

Unfortunately, the large southern trees also proved among the most vulnerable to the adelgid, because the region's relatively mild winters didn't keep the insect in check. To fight infestations, some researchers tried soaps and oil-based insecticides, with only modest success. One problem is that the adelgid attacks hemlock needles from below, where aerial spraying doesn't reach. In 2003, however, the chemical company Bayer gained the necessary approvals to sell neonicotinoid insecticides—primarily used in agriculture—for use in forests. Unlike soaps and oils, neonicotinoids are systemic; trees pull the chemicals into their tissues and can become toxic to insects for 5 years or more. The compounds gave forest managers a powerful new weapon, but they came too late for the 75 "superlative" hemlocks, Blozan says. The insects, aided by a major drought, weakened them beyond saving.

Other trees have been luckier. On a rainy spring morning earlier this year, Great Smoky's Webster bounded up a streamside trail in the Low Gap conservation area near Cosby, Tennessee, to show off the results of an aggressive chemical campaign against the adelgid. Massive hemlocks towered overhead. Most had lower branches killed by the insects, but the upper branches were lush, thanks to workers who have injected insecticides into—or drenched the soil around—more than 200,000 trees since 2002.

The effort has saved some of eastern North America's last remaining old-growth temperate rainforest, Webster says. But the chemicals have downsides. They can harm invertebrates, so their use is limited, especially near streams. (Neonicotinoids have been implicated in harming bee populations, but bees do not pollinate hemlocks and so are unlikely to be affected.) They also aren't cheap; costs are declining, but treating a single 30-centimeter-diameter tree requires $1.20 worth of chemicals plus labor, and projects often involve thousands of trees. And, in the end, insecticides do not permanently eliminate adelgids; they only reduce the numbers. "Chemical treatments are just a Band-Aid," Rhea says.

THE LONG-TERM CURE, Webster believes, is down the road at a facility called an insectary. Here, personnel from the park, the Forest Service, and the University of Tennessee, Knoxville, are cultivating four species of adelgid-eating beetles—part of a larger effort to develop biocontrol methods.

Hammering some wet hemlock branches with a stick, Webster manages to collect one of the attack insects—a torpid 3-millimeter-long black *Laricobius nigrinus* beetle—on a white canvas "beat sheet." Thousands of its cousins, whose ancestors lived in the Pacific Northwest, have been released at 120 sites in the park, and at hundreds of other places in the 20 states now infested with the adelgid. The goal is to establish permanent populations of beetles that do nothing but hunt adelgids.

It took decades to get this far. The adelgids exploded in eastern North America partly because few native insects eat them. So scientists looked abroad for predators, in the adelgid's home range. The first promising candidate was a tiny ladybird beetle that McClure and a Japanese scientist found in 1992, munching adelgids on a local hemlock species. After testing to ensure that the beetle wouldn't harm North American ecosystems, forest managers began releasing it by the millions in the United States. "There was a lot of optimism," recalls Scott Salom, an entomologist at the Virginia Polytechnic Institute and State University in Blacksburg, who has led much of the biocontrol research. But hope faded as the introduced insects disappeared without making a dent in adelgid numbers.

Other candidates show greater promise. A few biocontrol insects, including the beetle Webster found at the insectary, have established stable, but small, wild populations. But rearing the insects has been challenging. Salom's technicians spend days trying to coax finicky beetles to reproduce in rooms cooled to 18°C or below. Recent cold winters have complicated matters by killing the adelgids that, ironically, researchers now need to feed their beetles. That's one reason scientists are exploring other biocontrol options, including a silver fly native to the Pacific Northwest and a fungus that may kill adelgids. A discouraging precedent tempers hopes. In the 1900s, scientists introduced more than 30 different insects to the eastern United States and Canada to try to control the balsam woolly adelgid (*Adelges piceae*), a related insect that devastates native fir trees. Each introduction failed, and the balsam adelgid is still a serious pest. "There are dozens of reasons why biocontrol programs don't work quite as planned," Rieske-Kinney says. "Biological control is not for the faint of heart."

A FEW SCIENTISTS think the hemlock's future rests not with finicky beetles, but with special genes. As early as

the mid-2000s, scientists noticed that a few hemlocks appeared to resist adelgid infestations longer than their neighbors. Now, the hunt is on for genes that might be responsible. Ecologists Richard Casagrande and Evan Preisser of the University of Rhode Island, Kingston, have collected cuttings from what some call "putatively resistant" hemlocks found at isolated sites in New Jersey, Connecticut, and elsewhere, and they are now growing seedlings in Rhode Island and North Carolina. Some do seem to be less susceptible to the adelgid, Preisser says. That may be because the trees contain unusually high levels of terpenes, chemicals that can provide resistance to insects, says ecologist Joseph Elkinton of the University of Massachusetts, Amherst.

Others are skeptical about the effort. "In my estimation, there's not much hope that we're going to find genetic resistance to this insect," the Forest Service's Rhea says. He and others note that the hemlock has relatively little genetic variation through its range, making resistant outliers unlikely.

The Forest Service is trying another approach: figuring out how to protect hemlocks from other stresses, so they are more likely to resist the beetle. Biologists from the service and North Carolina State University (NC State) in Raleigh are studying how well hemlocks grow under different conditions, including sunlit or shaded, and with and without deer fences, weeding, and fertilizers. They are also evaluating combinations of chemical and beetle treatments. As Bud Mayfield, a U.S. Forest Service entomologist at the Southern Research Station in Asheville, explains, "maybe one thing won't let you grow hemlocks, but four things will."

The service is also preparing for the worst-case scenario: the extinction of eastern hemlock in the wild. It is funding Camcore, a tree breeding and conservation group housed at NC State, to collect seeds and genetic material from eastern hemlocks and the related, but rarer, Carolina hemlock. The group has planted trees in places likely to remain adelgid-free, including Chile and Brazil, in case they are needed to help seed reintroductions. "If everything else fails," says NC State biologist Robert Jetton, "we're the hemlock insurance policy."

ONE GROUP OF ECOLOGISTS reacted to the adelgid not by trying to save the hemlock, but by trying to learn from its death. In 1995, when ecologist David Orwig started his first research position at the Harvard Forest, the adelgid was working its way north toward the 1500-hectare research preserve, which holds extensive hemlock stands. Rather than invest in insecticides or beetles, Orwig and his colleagues decided to take the rare opportunity to study what happens when an ecologically important tree disappears. "At this site, I think you could learn more, unfortunately, by watching the demise of hemlocks than by trying to save them," Orwig says.

The adelgid's arrival also represented an experimental ecologist's dream, says Foster, Orwig's colleague. It's "the gentlest way that you can alter the abundance of something," he says. "You're not directly disturbing anything else; you're just selectively affecting the one species."

Because Harvard Forest is part of the National Science Foundation's Long Term Ecological Research Network, the researchers were already collecting preinfestation baseline data. The floor of Prospect Hill, the forest's main hemlock study site, sprouts a garden of instrumentation, including moisture sensors and baskets for capturing leaf litter. Metal bands called dendrometers record the growth of almost a thousand trees. A 34-meter tower rises above the canopy to measure gases emanating from the forest. As a result, Prospect Hill now hosts one of the world's most comprehensive studies of forest death.

During a recent visit to the site, Orwig noted that some trees have survived longer than expected. But from the tower, he pointed out the yellowish needles that are the hallmark of a dying hemlock. "This should be a sea of bright green right now," he lamented. "This is just kind of sick."

The Harvard researchers haven't just watched their hemlocks decline in real time; they've also accelerated the process. In 2003, they girdled or felled some healthy trees, then watched what happened. As the trees decayed, wood and nutrients entered streams and the trunks began releasing carbon. In newly sunlit clearings, black birch, white pine, and other saplings shot up.

In a 2014 book that summarizes their findings, Orwig and his colleagues predict that dying hemlock forests will store less carbon for a decade or two, but that fast-growing young trees will eventually reverse the trend and soak up carbon even faster than the absent hemlocks. Stream flows might decline, because deciduous trees use more water. But local forest biodiversity is likely to increase, because deciduous forests typically support more species. At a broader scale, however, the researchers believe the New England landscape will become more homogeneous as hardwoods replace hemlocks. In short, they say, the forest will live on, changed but still functional.

THANKS TO REPEATED chemical treatments, the Cheoah hemlock is still standing. But Blozan says that in big trees like this one, with complicated branching structures, water and chemicals—including insecticides—can be slow to reach some branches. Indeed, one of the Cheoah's four forks has lost most of its needles. But on the whole, the tree looks healthy. "It's the last of its kind," Blozan says wistfully.

He takes some photographs and records health data for the Eastern Native Tree Society, a group that he helped found. At worst, the documentation will help memorialize a remarkable life. But Blozan and others hope it will ultimately enable them to look back on the time when they began to turn the tide against the adelgid. "They'll come back," he predicts. "It's just going to take a long time. Tree time." ■

Gabriel Popkin is a freelance writer in Mount Rainier, Maryland.

A creeping conflict

The hemlock woolly adelgid now infests about half of the eastern hemlock's range, and has been spreading by about 15 kilometers per year.

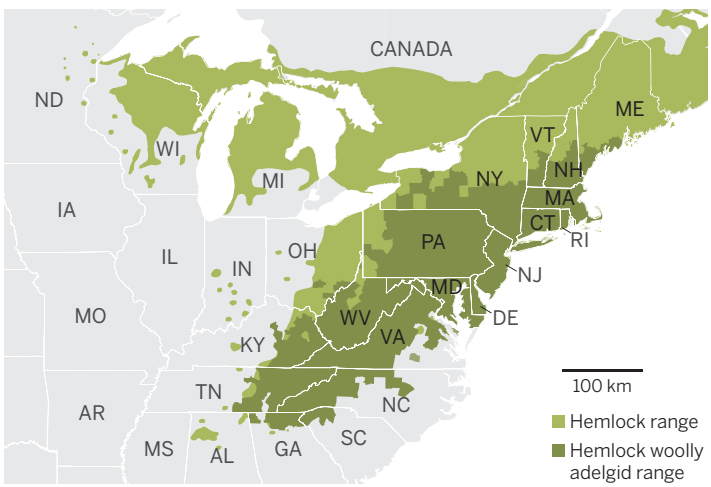

CREDITS: (GRAPHIC) M. ATAROD; (DATA SOURCE WOOLLY ADELGID RANGE) LITTLE, E.L., JR., *ATLAS OF UNITED STATES TREES*, P. 9 , 1971; (HEMLOCK RANGE) USDA FOREST SERVICE STATE AND PRIVATE FORESTRY, FOREST HEALTH PROTECTION

THE NEW NORTH

Stoked by climate change, fire and insects are remaking the planet's vast boreal forest

By **Tim Appenzeller**

For 7 weeks last year, Yellowknife was besieged by smoke. In the vast evergreen forests encircling this small city in Canada's Northwest Territories, years of drought had set the scene for a historic fire year. Across the territories, 3.4 million hectares burned—an area equal to the state of Maryland, and seven times the annual average. The smoke darkened the sky, stung eyes, and filled Yellowknife residents with "a sense of panic," says Frank Lepine, who manages wildfire response for the Northwest Territories government.

When the snow fell and the fires died, Lepine's army of firefighters—about 1000 strong at one point—could stand down. But for scientists the work is just beginning. The fires, they say, were an extreme example of the forces transforming the boreal forest, a stronghold of spruce, pine, and other conifers that rings the top of the planet, spanning northern Canada, Alaska, Russia, and Scandinavia. With its millions of square kilometers of pristine timber, thick carpet of moss and needles, and organic-rich frozen soil, the boreal forest stores more carbon than any other land ecosystem. And more than any other forest, it is bearing the brunt of climate change, warming roughly twice as fast as the rest of the planet. The effects on its cold-adapted trees are already evident. "We are on the cusp of a transformation," says ecologist Michelle Mack of Northern Arizona University in Flagstaff.

The early signs can be seen from space,

PHOTO: KYLE THOMAS

Corrected 24 August 2015; see full text.

Published by AAAS

Megafires such as this one in Canada's Northwest Territories last year are transforming the boreal forest.

where orbiting sensors that monitor photosynthesis show that much of the boreal belt is "browning": not literally turning brown but losing its vigor. They can be seen on the ground, in tree-ring studies that show trees are struggling to grow during the increasingly hot summers. They can be seen in insect outbreaks that are killing trees hundreds of kilometers farther north than they did 20 years ago. Most dramatically, the transformation can be seen in forest fires so fierce and voracious that they kick the forest into a new state, with a different mix of species and untold impacts on wildlife and climate.

"Fire is a catalyst for change," says Mike Flannigan, a fire specialist at the University of Alberta in Edmonton, Canada. Across the boreal, fires are burning as never before, favored by heat and drought that dry out the forest floor and spawn thunderstorms that bring lightning but little rain. In Canada, the total average area burned each year has more than doubled since the 1970s, Flannigan says—and that's in spite of more effective firefighting. In Alaska and Siberia, too, fire is on the rise. But it is a change in the nature of the fires, as much as their extent, that is transforming the forest.

The trees of the boreal, after all, are used to fire. The dominant species in Alaska and much of Canada, black spruce, maintains an aerial storehouse of seeds, locked in cones that form a distinctive tuft at the treetop. When a fire singes the cones and melts their resin, they spring open, releasing years of seeds all at once—an adaptation known as fire-mediated serotiny. Normally, this seed rain ensures that black spruce comes back strong after a fire, outcompeting other species. But the most severe fires can break this stranglehold and open the way to a new kind of forest.

When ecologist Jill Johnstone was a graduate student at the University of Alaska, Fairbanks, she set out to study how the boreal forest regenerates after fires of differing severities. A convenient laboratory was at hand: burned areas near Fairbanks left by recent fires. The severity of the fires had been low; they had spared much of the organic layer of moss and duff that carpets the floor of black spruce stands. Johnstone decided to simulate a more severe fire by taking a propane torch and burning off the organic layer to various depths, in some cases all the way to the bare, silty soil beneath. Then she sowed the seeds of spruce, aspen, and other trees, mimicking what happens after a natural fire.

Where the organic layer remained, she found that black spruce held the advantage. The charred duff "is a really bad seedbed" for most tree species, she says. "It's black, it dries out, and it heats up in the sun to 40°C. To regenerate trees you need to have a lot of seeds"—exactly what black spruce provides after a fire. But the spruce's advantage disappeared in plots where she burned off the organic layer. On the exposed soil, cooler and moister than the duff, aspen germinated in greater numbers.

Boreal fires increasingly resemble Johnstone's propane torch, searing the forest

Corrected 24 August 2015; see full text.

floor to bare soil. These days, "people talk about megafires," she says. "The fire weather is shifting." Fires are also recurring more frequently, in some cases sweeping across areas that burned as little as a decade before, consuming any organic material left on the forest floor. Today, Johnstone says, late-summer fires "burn and burn until the snow falls. They'll burn pretty much everything in their path—they'll blow right through old fire scars."

As her small-scale experiments suggested, black spruce is losing out. The clinching evidence came after Alaska experienced its biggest fire year in modern history in 2004. Some of the more than 700 fires just singed the forest floor, others blowtorched it away, giving Johnstone, Mack, and their colleagues a chance to compare how the forest recovered over large areas. Four years after the fires, they surveyed 90 burned sites and found that whereas those with an intact organic layer were thick with baby black spruce, sites where the fires had left bare soil were typically covered with seedlings of trembling aspen and paper birch. At those sites, Johnstone, Mack, and their colleagues wrote in 2010, the "legacy lock" of black spruce was broken.

To a satellite looking down on the forest, aspen and birch appear brighter than black spruce, says Scott Goetz, a remote-sensing expert at the Woods Hole Research Center in Falmouth, Massachusetts. By matching up a record of Alaska's most severe fires over the past 50 years with satellite measurements of forest brightness, he and colleagues including Mack confirmed the pattern seen on the ground: The most severe fires led to the most extensive regrowth of deciduous trees. Other researchers predict that deciduous stands, which accounted for less than half of interior Alaska's forests in 2001, will expand to cover two-thirds of the forested area by 2020.

Once established, researchers say, the broad-leaved trees are unlikely to be dislodged, as they grow faster and are less prone to burning than the conifers they replaced. For black spruce, the shift spells the end of a long reign, Johnstone says. "Black spruce have been pretty stable on the landscape for about 5000 years—we can tell from pollen records."

Not every year brings a forest-transforming megafire. But warming temperatures are applying their own, steadier pressure to the forest. Again, the effects are apparent from space, in data from sensors that monitor specific wavelengths of light absorbed by chlorophyll. The resulting false-color maps show much of the boreal belt in green, indicating vigorous photosynthesis. But at its heart, especially in North America, are regions where photosynthesis—the vital function of a forest—has slowed over the past 30 years. They are depicted as patches of brown.

When Goetz and his colleagues reported the browning in 2005, he says, "it certainly got people's attention." Modelers had expected the warming of the north, together with a fertilizing effect from rising carbon dioxide, to trigger a surge of forest growth. Instead, wide swaths—roughly a quarter of Alaska's forest, Goetz estimates—are languishing.

The browning isn't always obvious at ground level, but land-based measurements corroborate the remote sensing. Collaborators of Goetz's took core samples from black and white spruce, another common tree in the boreal, across much of Alaska, then analyzed tree rings to track the trees' growth history. In nearly every sample from the interior of the state, they reported in 2011, the rings had narrowed over the past 30 years, and the density of the annual increments of wood had risen. Those are signs that the increasingly hot summers are causing the trees to run short of water. To stem water loss, they are narrowing tiny pores, or stomata, on their needles—choking off their intake of carbon dioxide and slowing photosynthesis.

If the trend continues, the trees will begin to die, says Glenn Juday, a forestry expert at the University of Alaska, Fairbanks, who collaborated with Goetz on the 2011 study. In a new tree-ring study, Juday and his colleagues studied growth trends in white spruce at sites across Alaska. They found that trees in the interior of the state, where summers are hotter and drier than near the coast, are struggling to keep pace with climate warming. (Annual average temperatures at Fairbanks are up 1.5°C over the past 50 years.) Conditions are now nearing the trees' physiological limits, they fear. "Coming generations won't see the same large, old conifers," Juday predicts.

Besides stressing trees directly, warming is favoring their enemies: the insect pests that are exploding across the boreal forest. Warming is enabling them to expand their ranges by accelerating their life cycles, helping them survive the winter, and weakening host trees. One of the most dramatic cases involves the mountain pine beetle. Until the late 1990s, the scourge was confined to lodgepole pine in British Columbia, west of the Canadian Rockies. Scientists had hoped that two barriers would restrain its spread: the Rockies and a vegetation boundary just to the east of the mountains, where the beetle's favored lodgepole pine gives way to a related species, jack pine.

Those hopes were dashed, says insect specialist Barry Cooke of the Canadian Forest Service in Edmonton. In the mid-2000s, the beetle staged "a mass exodus," spilling eastward into Alberta and attacking jack

After fires, clusters of cones in the tops of black spruce release a rain of seeds that ensures a new generation of spruce. But the most severe fires allow other species to take over.

PHOTO: MOMATIUK - EASTCOTT/CORBIS

Corrected 24 August 2015; see full text.

Published by AAAS

pine. So far its range has extended 300 kilometers to the east and more than 1000 kilometers to the north, Cooke estimates. "The mountain pine beetle is poised to go all the way to Newfoundland" on Canada's eastern seaboard, he says.

The beetle joins a host of other boreal pests on the march: the spruce beetle, western spruce budworm, Douglas-fir tussock moth, hemlock looper, and willow leaf blotch miner, to name a few. And like severe fires, Cooke says the worst insect outbreaks may drive long-lasting ecological change, as the denuded forests regrow in a different form, better adapted to the new normal. "We will see irreversible changes. Whereas insects used to play a temporary role, they will become agents of permanent change."

Researchers have varying visions of what the future boreal forest will look like. "I think there will be shrublands, even grass," Flannigan says. "My gut instinct is that the forest may be gone in some places."

"I think we're going to see some interesting changes regionally," says Carissa Brown, a former student of Johnstone's who is now at Memorial University of Newfoundland in St. John's. But she's cautiously optimistic: "The boreal forest is a very resilient system."

Juday suggests it may respond by migrating. Although his recent study showed that trees in the center of Alaska are suffering, it revealed a surge of growth near the Bering Sea coast, where summers are cooler and wetter and the forest gives way to tundra. The productive heart of the forest is shifting, Juday says. "An early stage of biome shift is underway."

Whatever the new shape of the forest, the change will ripple through wildlife communities. Caribou, for instance, like evergreen black spruce stands, which are carpeted with lichen, an important forage. But in stands of deciduous aspen and birch, the lichen never gain a foothold among the fallen leaves. "That takes from the caribou their source of winter forage," Brown says. Moose, on the other hand, are fond of aspen shoots and may thrive as the broadleaf forest expands.

The transformation will also affect climate, for better and worse. Fires, for example, turn wood and needles into climate-warming carbon dioxide—a positive feedback. But Mack, who has studied carbon flows in the changing forest, says that forest regrowth ultimately takes up the lost carbon—especially when aspen, which grows fast and quickly locks away carbon in wood, takes over. The spread of aspen could even restrain climate change through a pair of negative feedbacks: The aspen canopy reflects more sunlight than spruce, and broadleaf forests are less flammable.

Feeling the heat

Satellite data show that photosynthesis has declined (brown) over the last 30 years in much of North America's boreal forest belt while increasing (light green) in parts of Russia and Scandinavia, where forests have responded differently to warming temperatures. Warming is also driving an increase in massive forest fires, in both Alaska and Canada (bottom).

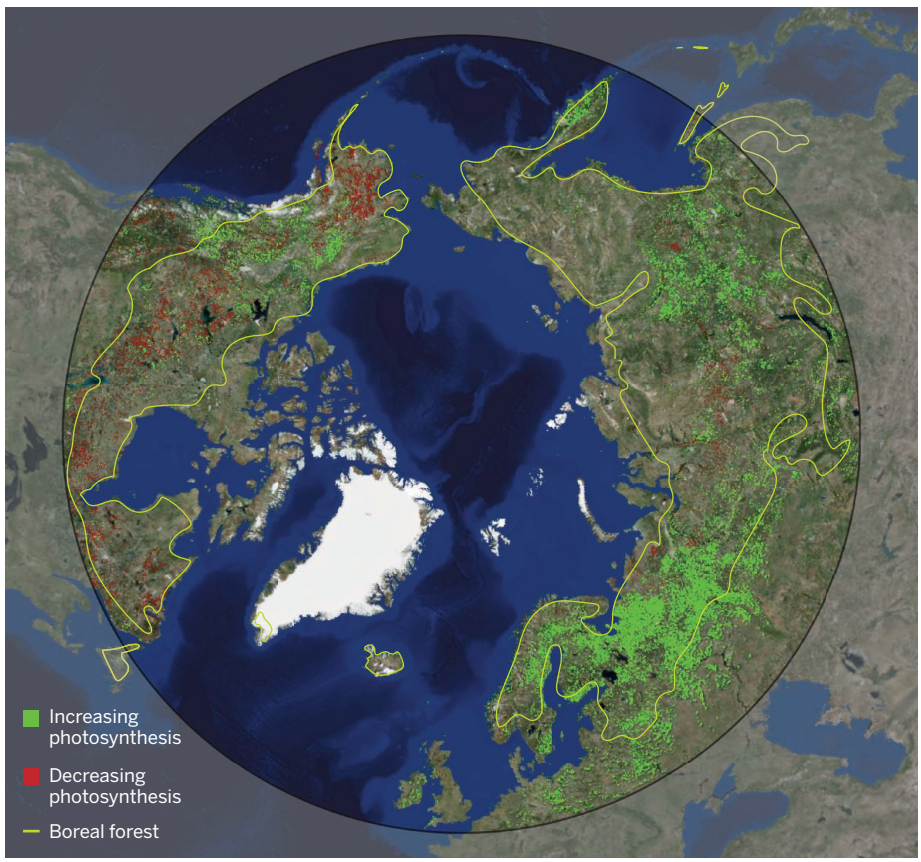

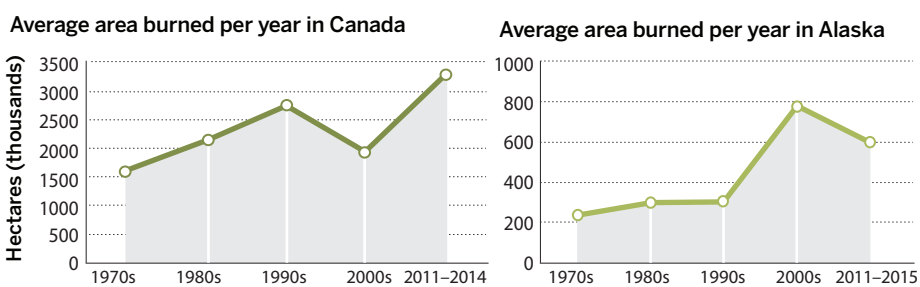

Bad news, however, may be unfolding below the forest floor. Underlying much of the boreal forest is permafrost, deep-frozen soil filled with thousands of years of organic matter—a massive reserve of carbon. The duff layer beneath a spruce forest, up to a meter thick, insulates the permafrost from summer warmth. But when a fire burns off the duff, the permafrost can start to thaw and release carbon dioxide or methane, another potent warming gas. After a severe fire in the Yukon, Brown recalls, "we even had a hillside fall away" as the frozen soil softened. "You could actually smell all that carbon being released."

Nature is providing plenty of opportunities for further study. The scars of last year's fires in the Northwest Territories are now a field site for Johnstone, Mack, and other researchers. And this year's fire season promises a generous new crop of natural experiments. In the Northwest Territories, the burning season it got an early start thanks to a phenomenon that used to be rare: a dozen "holdover fires" that started last year and then smoldered beneath snowbanks through the long winter. With the spring thaw, the flames rekindled, and the transformation of the boreal forest began anew. ■

CREDITS: (BOREAL) BRENDAN ROGERS, WOODS HOLE RESEARCH CENTER; DATA SOURCE: (ALASKA FIRES) ALASKA INTERAGENCY COORDINATION CENTER; (CANADA FIRES) MIKE FLANNIGAN, UNIVERSITY OF ALBERTA

Corrected 24 August 2015; see full text.

SECOND ACT

Forest ecologist Robin Chazdon is helping show that regenerating tropical forests aren't wastelands

By **Elizabeth Pennisi**

When ecologist Robin Chazdon began studying tropical forests in the 1990s, she took the road less traveled. Whereas many researchers were scrambling to study undisturbed forests before they disappeared, she focused on what grew back once the trees were burned or logged. Rather than working in the forest's shaded understory, an ecosystem celebrated in Hollywood films, she labored in scraggly deforested plots in the broiling sun, covered head to toe to keep prickly bushes and biting chiggers at bay.

For decades, Chazdon worked in relative obscurity, barely scraping together funding for long-term studies of these so-called secondary forests. Her findings challenged some prevailing views: that tropical forests wouldn't regenerate, and that second growth was a biological wasteland. And over time, Chazdon and like-minded colleagues began building a case that, although protecting intact tropical forest was essential, second growth couldn't be ignored in efforts to protect the environment and human livelihoods. Secondary forests are "very dynamic places where nature is reasserting itself," Chazdon says. "It's an elegant thing to behold."

The rest of the world is beginning to see her point. Chazdon has "done a huge amount to elevate the visibility of secondary forests," says tropical community ecologist Stephen Hubbell of Princeton University. Now that humanity has cleared or damaged at least three-quarters of the world's primary forests, governments and conserva-

PHOTO: JOANNA B. PINNEO

Robin Chazdon made a career of studying tropical secondary forests, but she feels just at home in this regenerating forest on her family ranch in Colorado.

tion organizations are increasingly turning their attention to the "junk" that regrows. Thanks in part to Chazdon's work, many now see secondary forests as key to restoring biodiversity and performing important ecosystems services, such as providing clean water and sequestering carbon. And last year, nations attending a United Nations climate conference set a goal of reforesting 350 million hectares of degraded land—an area larger than India—by 2030.

Reaching that goal, however, will require resolving some thorny issues. Some advocates insist "reforestation" should mean recreating, as closely as possible, the original forest. But others think planting rows of oil palms or timber trees should qualify. There are also disagreements over which areas should be targeted for reforestation, and whether people can and should accelerate the process with costly tree-planting programs. Some worry that efforts to promote second growth could undermine efforts to preserve intact forest.

For Chazdon, 58, the rising interest in secondary forests has prompted a second act of her own. After 27 years as an academic at the University of Connecticut (UConn), Storrs, she's taken a leave of absence, moved to Colorado, and shifted much of her attention from collecting and analyzing data to influencing policy—most notably in Brazil, which has made tropical reforestation a centerpiece of its efforts to combat climate change. "She has the drive, the personality to be a major player" in policy, says Peter Raven, president emeritus of the Missouri Botanical Garden in St. Louis.

But Chazdon is aware of the risks. She worries that policymakers might think she's been in the ivy tower too long, whereas scientists might look askance at her entanglement in policy. She'd like to make policy work her full-time job, but has no offers yet. "I'm facing a very uncertain next few years," she admits. "And that's weighing heavily."

STROLLING THROUGH A WOODED GLEN on the family ranch 2 hours southwest of Denver, Chazdon examines the new growth on a chest-high lodgepole pine. She impulsively gives the young tree a hug, telling it that despite the risk of drought and disease, it may one day be a giant. She identifies with a forest, she says: "When I just stand in there, I can feel the photosynthesis flowing."

That affinity developed early. Despite growing up in Chicago in the late 1960s, family camping trips and summer camps turned her into an environmentalist. She fell in love with the tropics after a field course in Costa Rica in 1976, her sophomore year of college. "I felt like it was a second home," she recalls. "That was very empowering."

As a graduate student at Cornell University, she returned to Costa Rica and did her dissertation research at La Selva, a field station run by the Organization for Tropical Studies. Trying to understand how understory palm trees could grow in the deep shade of a mature rainforest canopy, she spent days using a homemade sensor to measure the light that filtered through the leaves. She discovered that flecks of sunlight were the secret to palm success: Eighty percent of the plants' productivity was fueled by these temporary patches of light.

Her studies of photosynthesis continued for years, but each time she returned to Costa Rica, more forest had disappeared, cleared by loggers, farmers, and developers. So once she moved to UConn in 1989, she decided to shift gears. Chazdon and Julie Denslow, an ecologist who studied forest dynamics and is now with the U.S. Forest Service's Pacific Southwest Research Station in Hilo, Hawaii, began to track how shrubs and trees were returning to plots on abandoned pastures purchased by La Selva and on nearby farms. The work would ultimately lead to a landmark 25-year project.

At the time, many ecologists doubted a tropical rainforest would ever grow back—they thought the soils were too fragile and would erode away before new roots could take hold, or too nutrient-poor to sustain regrowth. In La Selva, however, Chazdon and her colleagues found that tropical forests can make a comeback. They documented that, gradually, biodiversity returns, with a mix of plants reestablishing the understory and canopy layers that support key ecosystem services. Even species with commercial potential can regain a foothold.

A site's "ecological memory" helps shape what returns. Residual seeds that survive in the soil, waiting for a chance to sprout, are part of this biological memory bank, as are trees that remain standing nearby. Visits by bats, birds, and other seed dispersers also play a role in determining which plants reemerge, as does the site's history of use.

After a forest is cleared, a few remaining trees, such as those in this Costa Rican pasture (left), can help promote the return of a relatively diverse forest (right) once the pasture is abandoned.

At the time, few paid much mind to these findings: Tropical plant succession wasn't a sexy topic. So attracting funding was a challenge. "We don't do secondary forests," one funder told Chazdon as she scrambled to find money after a grant from an early backer, the Andrew W. Mellon Foundation, expired. They were "too messy," said another. "That was the low point," Chazdon recalls. Still, she persevered, often with her husband, the recently retired ecologist Rob Colwell, and their two children in tow.

In 2007, just when she thought she had finally exhausted her funding opportunities, she enlisted Brazilian and Mexican researchers in a successful bid for a National Science Foundation (NSF) grant. In part, it aimed to use what had been learned over decades in La Selva to examine the validity of a common, less time-consuming approach to studying forest regrowth, known as "chronosequence" studies. Unlike long-term projects that track changes at a single site for

PHOTOS: (LEFT TO RIGHT) BRYAN FINEGAN; ROBIN CHAZDON

decades, chronosequence studies—which have become a backbone of regeneration science—take a simultaneous snapshot of a set of plots in the same area, each at a different stage of regrowth. The goal is to get a quick read on how local forests might regenerate—without waiting years for the answer. "The assumption is that what's happening in the younger forest [plots] is what happened in the older forest [plots]," says forest ecologist Jess Zimmerman of the University of Puerto Rico, Río Piedras, another pioneer of studying tropical secondary forests. The long-term studies indicated that young forest plots did not necessarily reflect what older forest plots were like in their past. So researchers need to be careful about the conclusions they draw from chronosequence studies, the researchers concluded in June in a paper published online in the *Proceedings of the National Academy of Sciences*.

Chazdon says the work underscores perhaps the most important message to emerge from La Selva and related studies: that each regenerating site "tends to have its own path," even when they share similar soils and climate. That's because chance plays a big role in what regenerates in the forests both short- and long-term. The research shows "you can reforest," says Stefan Schnitzer, an ecologist at Marquette University in Milwaukee, Wisconsin, "but you still don't know what you will get."

As policymakers come to grips with that ecological uncertainty, they are finding Chazdon's recent book, *Second Growth: The Promise of Tropical Forest Regeneration in an Age of Deforestation* (University of Chicago Press), all the more valuable. Five years in the writing and published last year, the tome is a kind of guide to restoration, synthesizing decades of research and explaining how tropical forests can come back on their own—and what to do if they don't. "It's an opus; it covers all you would want to know and could imagine you want to know about secondary forests," says Thomas Rudel, a rural sociologist at Rutgers University, New Brunswick, in New Jersey. "There's nothing quite like [it]."

THE BOOK, *SECOND GROWTH*, ARRIVED at a timely moment, just as large-scale forest restoration was gaining momentum. In 2010, nations that had signed the United Nations' Convention on Biological Diversity set a goal of restoring 15% of the world's ecosystems by 2020. The following year, ministers from many countries issued the Bonn Challenge, which called for widespread reforestation. Then at last year's U.N. meeting, they upped the ante in a statement known as the New York Declaration on Forests, setting the 350-million-hectare goal. "I was

For decades, researchers have periodically measured the trees in this regenerating Costa Rican forest to learn how forests grow back. The data could now prove useful for global reforestation efforts.

PHOTO: ROBIN CHAZDON

thrilled—the international dialogue is not just about deforestation anymore," Chazdon says. "It changes the vision."

But the new vision is still blurry—and Chazdon thinks she can help achieve clarity. The Food and Agriculture Organization of the United Nations' official definition of reforestation is "very imprecise," she notes. By its criteria, replacing a natural forest with plantations of introduced trees to make fuel and wood, or soak up carbon, could qualify as reforestation.

Not surprisingly, many conservationists oppose that idea, arguing that monocultures provide fewer of the ecological benefits of less homogenized forests. "Such projects have a long history of failure and they do nothing to restore 'health' to forests," Hubbell argues. Some advocates say projects should count in official tallies only if they aim to restore a forest to some original state—typically a long and difficult task.

Chazdon isn't a big fan of monoculture plantations, but believes that to reforest "is not just to create a forest like before." There are now too many people in need on the planet to allow for the return of unmanaged forests in very many places, she says. And she notes that the discovery of ancient pottery shards and earthworks in tropical forests once considered pristine shows that people have long played a role in shaping landscapes. "I used to be a little bit more idealistic," she says. "But it's not realistic to have it all natural forest."

Reforesters face another pressing question: to plant or not to plant. There's a long history of planting trees to speed the process along, Chazdon notes. But her work has shown that, if left alone, some forests come back on their own—with less effort and cost. And although active managers often replace mixed forests with a single species, or introduce exotic species, she notes that more passive strategies can restore something closer to the original species mix.

Chazdon concedes that natural regeneration can be a long process. It "isn't just a Band-Aid for a photo shoot after 2 years," she says. And she notes that it may make sense in some places to plant some native species, particularly commercially valuable ones, to kick-start regeneration—in part to give local people a greater financial incentive to protect nascent forests. "We must meet the needs of the people or we are not going to be able to protect the landscape," she argues.

Chazdon's approach has attracted particular attention in Brazil, where Environment Ministry officials have pledged to reforest some 12 million hectares of land as part of the nation's climate commitments. With official support, she'll be spending at least 3 months a year in Brazil, helping researchers and policymakers figure out how best to harness passive reforestation approaches. "Before we spend a lot of money on active restoration, let's first take advantage of the free help of nature," says ecologist Pedro Brancalion of the University of São Paulo, who is involved in the effort.

DECIDING EXACTLY WHERE to grow new forests is another source of friction. Since 2009, the World Resources Institute (WRI), an influential think tank based in Washington, D.C., together with researchers at the International Union for Conservation of Nature and the University of Maryland, have been developing global and regional maps that highlight more than 2 billion hectares of land that could be reforested. When Chazdon borrowed the maps and displayed them at a workshop last year, however, some researchers were stunned—and infuriated. That's because the maps identify some endangered grassland ecosystems, including portions of Africa's savannas, as having "high reforestation potential." (That's because they, too, have climates suitable for trees.)

The maps "provided a clear illustration of the fact that grassy biomes are undervalued and misunderstood as 'degraded' ecosystems," says one critic of the effort, ecologist Joseph Veldman of Iowa State University in Ames. Earlier this year, he, University of Cape Town vegetation ecologist William Bond, and others criticized the map in a letter to *Science* (30 January, p. 484), and they have another critique in press at *BioScience*.

Chazdon would like to see the maps reworked and has been corresponding with both sides toward that goal. In the meantime, she's busy trying to catalyze discussion and consensus elsewhere. She and two colleagues have founded People and Reforestation in the Tropics, an NSF-funded networking effort aimed at getting policymakers, landowners, and scientists talking about what reforestation means, how to implement it on a large scale, and how to monitor the impact on local people.

It's a potentially contentious conversation, but colleagues believe she's got the people skills to hold her own—and produce results. "She has the rare ability to bring disparate communities together around a common cause," says Toby Gardner of the Stockholm Environment Institute. "She's standing with two feet in science, but she communicates it in a way that policy people like me can use," says Lars Laestadius, a senior associate at WRI.

For Chazdon, the dive into policy is a chance to put decades of science to practical use—and to try to make sure that reforestation is done right. And it is rooted in her belief that once-ignored secondary forests can play a phoenixlike role in restoring global forest health. "Things are dying and things are coming back to life at the same time," she says. "It fills me with a lot of hope." ■

Where new forests can grow—but should they?

More than 2 billion hectares of land have potential for reforestation, according to a map compiled by the World Resources Institute and other groups. But some scientists worry the map could promote the replacement of grasslands and other ecosystems with trees.

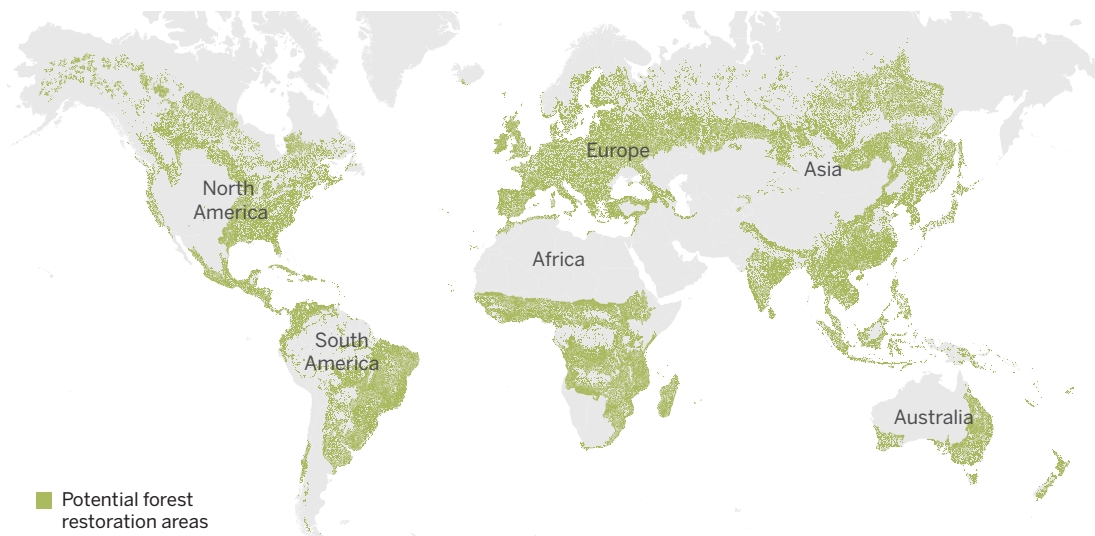

CREDITS: ADAPTED BY M. ATAROD/*SCIENCE*; (DATA SOURCE) WORLD RESOURCES INSTITUTE. 2011. GLOBAL MAP OF FOREST LANDSCAPE RESTORATION OPPORTUNITIES. ONLINE AT WWW.WRI.ORG/FOREST-RESTORATION-ATLAS

REVIEW

Forest health and global change

S. Trumbore,[1,2]* P. Brando,[3,4] H. Hartmann[1]

Humans rely on healthy forests to supply energy, building materials, and food and to provide services such as storing carbon, hosting biodiversity, and regulating climate. Defining forest health integrates utilitarian and ecosystem measures of forest condition and function, implemented across a range of spatial scales. Although native forests are adapted to some level of disturbance, all forests now face novel stresses in the form of climate change, air pollution, and invasive pests. Detecting how intensification of these stresses will affect the trajectory of forests is a major scientific challenge that requires developing systems to assess the health of global forests. It is particularly critical to identify thresholds for rapid forest decline, because it can take many decades for forests to restore the services that they provide.

Forests have evolved while experiencing disturbances such as drought, windthrow (when trees are uprooted or overthrown by wind), insect and disease outbreaks, and fire. However, forests worldwide increasingly must also cope with human-related intensification of stressors that affect forest condition, either directly through logging and clearing or indirectly through climate change, air pollution, and invasive species. These novel disturbances alter forest communities and environmental conditions outside the ranges in which current forests evolved and occur too fast for evolutionary adaptation processes to keep pace. Thus, the future of global forests will be determined by the trajectory of complex forest system responses to multiple stressors that span local to global scales.

The papers in this special section describe ongoing changes in tropical (*1*), temperate (*2*), boreal (*3*), and managed (*4*) forests as they respond to shifts in land use, climate, biodiversity, the frequency and intensity of extreme events, and disturbance regimes. These papers document how humans have fundamentally altered forests across the globe and warn of potential broad-scale future declines in forest health, given increased demand for land and forest products combined with rapid climate change. This review focuses on overarching questions common to all forests: How do we define forest health and detect when it is declining? How can we attribute observed broad-scale declines to interactions among the varied stresses that affect forests today? What are the time scales and trajectories of recovery for unhealthy forests, and can we identify dangerous levels of change in global forest health?

We argue that approaches to monitoring global forest health need to combine detection of changes in forest condition with observations that enable the attribution of observed changes to combinations of human, climatic, and biotic drivers. Further, mechanistic understanding based on experiments and long-term observations is required to identify trajectories leading to recovery or to rapid decline of forest functions. Such approaches need to be undertaken at scales that span current gaps and link remote sensing and plot-level data.

How do we measure forest condition and assess forest health?

Health as a concept applied to forests shares common problems with its application to human populations. At the scale of an individual, health can be defined as the absence of disease (Fig. 1). However, as the unit of scale of monitoring shifts from trees to entire forest stands or biomes, indicators of forest health become more difficult to assess. In forestry, for example, one common measure of forest condition at the stand level is productivity. Although this is a good proxy for timber production, it neglects important attributes of forest ecosystems such as species assemblage, vegetation structure, biomass, and nutrient cycling. This shortcoming necessitates the definition of more holistic but often less easily quantified measures, and for decades researchers have struggled with operational definitions of ecosystem health (*5*).

Existing measures of forest health range from strictly utilitarian and related to local human needs, to more ecological definitions related to the persistence of forests or stands within a given landscape (Fig. 1) (*6*). The Food and Agriculture Organization of the United Nations (FAO) combines these perspectives by defining "forest health and vitality" based on the combined presence of abiotic (e.g., drought, heat, and pollution) and biotic (e.g., disease and pests) stresses and how they affect tree growth and survival; the yield and quality of wood and nonwood forest products; wildlife habitat; and recreation, scenic, or cultural value. Edmonds *et al.* (*7*) enumerate eight conditions of a healthy forest: (i) an ecosystem in which abiotic and biotic factors do not threaten current and future management objectives; (ii) a fully functional community of plants and animals and their physical environment; and (iii) an ecosystem in balance that (iv) sustains its complexity while providing for human needs, (v) is resilient to change and (vi) is able to recover from natural and human stressors while (vii) maintaining and sustaining functions and processes, and (viii) is free of "distress" symptoms such as reduced primary productivity, loss of nutrient capital, loss of biodiversity, or widespread incidence of disease or potentially tree-killing insects.

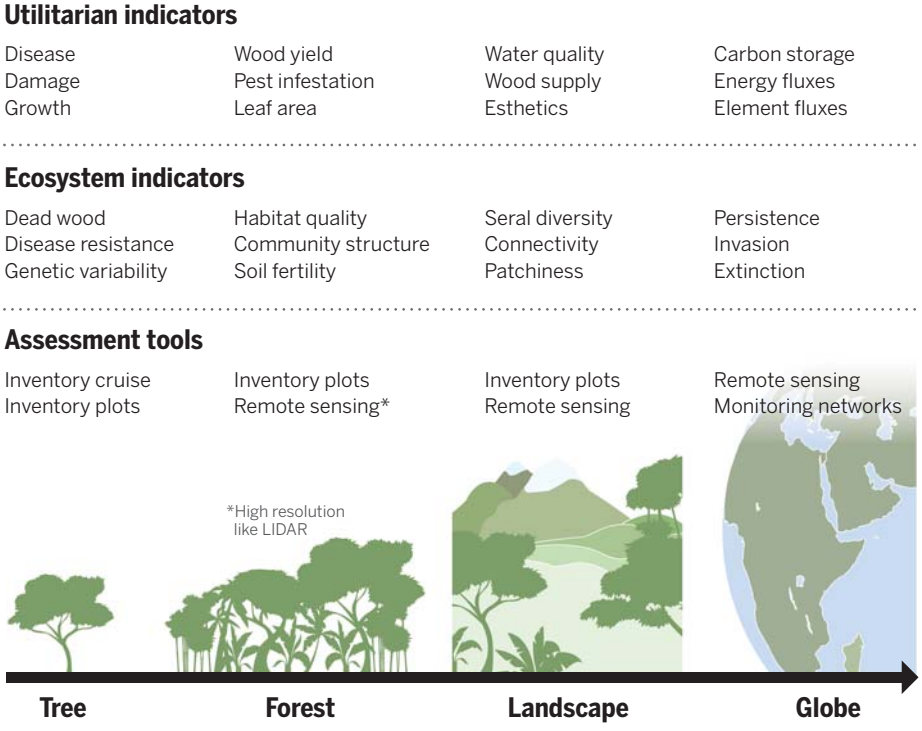

Fig. 1. Examples of forest-health indicators for utilitarian and ecosystem-centered perspectives. The common criteria spanning all of the spatial scales shown are (utilitarian) continued supply of forest products and services and (ecosystem) resistance and resilience to stress and disturbance. Some indicators cannot be directly measured or occur on spatial or temporal scales beyond human perception.

[1]Max Planck Institute for Biogeochemistry, 07745 Jena, Germany. [2]University of California–Irvine, Irvine, CA 92697, USA. [3]Instituto de Pesquisa Ambiental da Amazônia, Belém, Pará 66035-170, Brazil. [4]Woods Hole Research Center, Falmouth, MA 02450, USA.
*Corresponding author. E-mail: trumbore@bgc-jena.mpg.de

However, even such a detailed set of attributes cannot completely capture forest health if spatial and temporal scales of forest ecosystems are not considered. Forests contain trees subjected to periodic stresses (e.g., drought stress) that affect the resilience of individuals and, if very intense or often repeated, can lead to mortality. We distinguish such stresses from disturbances that can kill healthy as well as unhealthy trees (e.g., windthrow, fire, and logging). Both can produce a dying patch of forest that might be considered in itself unhealthy but can facilitate a whole suite of essential ecological process such as regeneration, nutrient cycling, or habitat creation at broader spatial scales. Thus, a healthy forest is one that encompasses a mosaic of successional patches representing all stages of the natural range of disturbance and recovery (*7*, *8*). Such forests promote a diversity of nutrient dynamics, cover types, and stand structures, and they create a range of habitat niches for endemic fauna (*9*). The challenge is determining when the frequency, spatial extent, and strength of stresses and disturbances exceed the natural range of variability and affect the trajectory of vegetation recovery at the landscape to regional scale.

What is the legacy of declines in forest health?

One of the key attributes of a healthy forest system is its ability to recover from disturbance. The accompanying papers in this issue provide accounts of specific instances where declines in forest health have been documented. These declines differ in each forest type and are driven by increased physiological stress [e.g., hot droughts (*2*)], susceptibility to pathogens (*3*, *4*), increased disturbance-related mortality from fire (*3*), and tropical forest degradation by processes such as defaunation and selective logging (*1*). Most of these examples rely on observations of increased tree mortality, which is perhaps the most obvious symptom of an unhealthy forest.

Trees are long-lived organisms, and although an individual tree can die quickly, it can take decades to centuries to be replaced. Thus, the legacy of increased tree mortality can persist for a long time, which lends urgency to identifying and detecting potentially dangerous thresholds of forest-health decline. Even if the affected forests eventually recover, more information is needed about how long the legacy of broad-scale forest dieback will affect important forest services and functions.

The various functions associated with forests recover over different time scales after major disturbances (Fig. 2). For example, even in severely damaged forests, new leaf cover can obscure open canopy areas in as little as a few months (*10*). As leaf area recovers, so do rates of photosynthesis and transpiration (*11*), key forest climate and water regulation services. These fluxes can approach predisturbance levels within years to a decade in selectively logged tropical forests (*12*) or forests recovering from fire. However, many other forest functions take much longer to regain predisturbance levels. Biomass and the associated carbon storage functions of forests recover more slowly than fluxes, taking decades to centuries to replace losses (*13*, *14*).

Other forest functions, such as biodiversity, can take even longer to recover, because they depend on the presence of individual species (Fig. 2). Although gap formation in forests can sustain biodiversity at the landscape or regional level (*15*), very broad-scale disturbances such as deforestation and firestorms dramatically reduce diversity. In such cases, the recovery of biodiversity requires replacement of the full range of tree species as well as of the fauna they host. For example, dead wood is an important carbon store and provides habitat for specific fauna; if the dead-wood pool is destroyed by harvesting or burning, it can take centuries to recover (*14*). Soil-derived nutrients are resupplied slowly by atmospheric dust or mineral weathering. Thus, nutrient depletion associated with disturbance may ultimately limit the rate and degree of recovery of other functions. The difficulty is to determine which of these functions are required to recover a healthy forest condition.

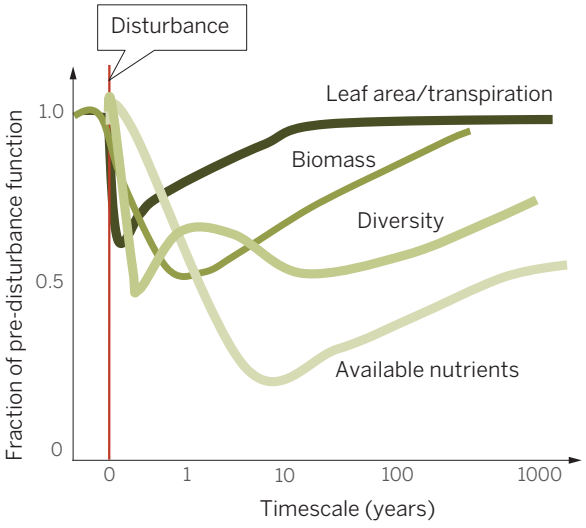

Fig. 2. Time scales of recovery for different forest functions after a disturbance. Disturbances, such as deforestation or fire, are followed by erosion and forest regrowth. Whereas functions associated with leaf area, such as photosynthesis and transpiration, recover within a decade, biomass (and therefore carbon storage) recovers more slowly, with mineral nutrients recovering most slowly of all.

Although we have concentrated on ecosystem properties, the definition of forest recovery also has implications for the utilitarian perspective. Forests that do not fully achieve predisturbance levels of diversity or nutrient status can almost fully regain wood production or carbon storage services, given sufficient time. A single large event such as a drought may remove the most susceptible species and leave behind more drought-resistant trees (*16*), potentially reducing tree mortality in successive droughts. However, if selective mortality occurs over a large enough area, the carbon storage and diversity services that were offered by the drought-sensitive species will take decades to centuries to recover. Thus, broad-scale and persistent degradation of forests will have lasting consequences, even if the forests themselves eventually recover. Given how long we may live with the consequent loss of function, it is important to develop methods to evaluate the risks of broad-scale forest decline, especially given the novel combinations of stresses and disturbances expected to affect forests in the coming century.

How much disturbance or stress is too much?

Healthy forests maintain their overall services over areas large enough to encompass the spatial scale of natural disturbance and recovery. Levels of disturbance that fall within the range of "background" variability to which forests are adapted (green area in Fig. 3) tend to produce a healthy mix of forest patches and to maintain water balance, biomass, and diversity at landscape scales. At very high levels of stress or disturbance and low levels of forest health (red area in Fig. 3), risks such as net loss of soil nutrients through erosion or loss of seed bank or seed dispersal vectors mean that the forest has lost many of its intrinsic characteristics, which may delay or prevent recovery. In such extreme cases, a shift to a new vegetation state is possible. The real concern is how to define where the transition between "normal" and "too much" stress takes place (orange area in Fig. 3) and how to determine whether this transition is an abrupt threshold or a linear decline.

Whereas deforestation fundamentally changes the ability of forests to perform basic functions, changes in forest structure and diversity linked to other forms of disturbance are less obvious and harder to quantify. Increased disturbance intensity, disturbance frequency, or even the introduction of new kinds of disturbances can trigger abrupt nonlinear declines in the ability of forests to perform intrinsic functions (*17*–*19*). Increasingly, forests are subjected to climatic or biotic stresses and to stochastic disturbances, some of which fall outside the range of normal background levels (Fig. 4) (*20*–*22*). Of particular concern is the coupling of direct, local, human-related disturbances with ongoing, more diffuse changes in climate and atmospheric composition. Although not all global changes are likely to cause declines in forest health [e.g., increased atmospheric CO_2 may stimulate productivity (*23*)], overall levels of tree stress and forest disturbances are mostly expected to increase individually beyond their historic values in the next century (Fig. 4) (*24*).

Disturbances and stresses also do not act independently. For example, the interactions among extreme weather events, logging, and human-ignited forest fires have caused widespread tree mortality and degradation in tropical forest ecosystems (*25*). Broad-scale deforestation reinforces

such processes by expanding areas of forest edges, thereby increasing vulnerability to further disturbances (*26*). A second example is the relationship between warmer temperatures and accelerated insect life cycles, which allows pest species to cause greater damage during the growing season (*27*). Interactions with climate stressors such as drought can further increase mortality rates in weakened or insect-damaged trees (*28*). Although both of these examples probably cause mortality in excess of background conditions, the larger question is whether they are novel and severe enough to change the trajectory and rate of subsequent forest recovery (Fig. 3). In both examples, deciphering the causes of increased mortality required intensive studies at the plot scale, as well as controlled experiments to understand how individual and combined factors lead to tree mortality.

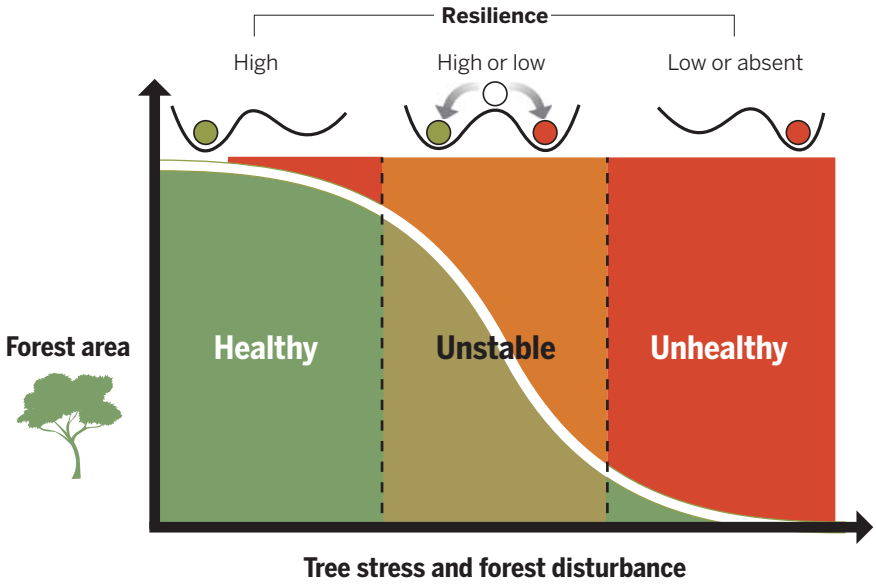

Fig. 3. Schematic representation of changes in forest health as a function of tree stress and forest disturbances. Resilience (top) is indicated by the tendency of a system to stay in its current vegetation state (high resilience) or to switch to another state (low resilience); states are indicated by "wells," with the system more likely to move to the deeper well once some threshold has been crossed. The green area indicates forests experiencing background levels of stress and disturbance that are relatively weak, affect mostly small areas, and cause no fundamental changes in forest functioning. Such forests tend to be resilient at a broad range of spatial scales (i.e., they tend to stay in their current state, as indicated by the circle in the deeper well above). This background level of tree stress and disturbance is difficult to measure using current remote sensing techniques; it is usually estimated using plot-based inventories. As unprecedented levels of tree stress and disturbances are reached, the area experiencing complete breakdown of basic functions and resilience is expected to substantially increase, creating positive feedbacks with climate that could cross a threshold and lead to a novel (nonforest) ecosystem. This shift in forest condition is detectable from space using high-resolution images. Our main questions have to do with the orange area: How can we determine whether the transition from healthy to unhealthy is an abrupt threshold, and (if so) how can we detect early signs that an abrupt threshold is about to be crossed?

How can we monitor declines in forest condition at global scales?

The tools currently applied to measure forest condition leave large gaps in coverage and cannot supply all the information needed to systematically assess changes in global forest health. Although remote sensing techniques provide some useful proxies for forest condition globally (e.g., canopy cover, photosynthesis, and phenology) (*29*), it remains unclear how trends detected from space correspond to other aspects such as tree mortality, diversity, and function (*30*). Other measures, such the fraction of trees in a stand infested by insects, are highly informative but require repeated measurements of individual trees in forest plots. Thus, most assessments of forest health at the continental-to-global scale rely on more easily measured indicators of selected processes or key attributes (e.g., tree cover), but they may miss other indicators of declines in health, such as increased mortality or the loss of key fauna that serve as pollinators or seed vectors.

The only systematic global assessment of forest health is the FAO Global Forest Resource Assessment (*31*, *32*). This report evaluates "forest health and vitality" based on individual countries' reporting of areas of forest affected by various stresses (fire, insects, disease, physical damage by animals, weather extremes, and invasive species). Although the FAO assessment represents an ecosystem approach and is therefore less affected by stakeholder interests than are utilitarian assessments, the reporting framework relies on submissions by individual countries, complemented by remote sensing data on changes in forest distribution and land use. Because there are no standard protocols for data collection, methods are highly variable, and information on insect pests and diseases, fires, and biotic and abiotic disturbances is sparse, sporadic, or even unavailable for many countries. In particular, spatial and temporal patterns of stressor occurrence may be difficult to identify without a more standardized approach. Nonetheless, the FAO assessment currently provides the best-available information on areas of forest subjected to different kinds of disturbances.

Another initiative that would benefit from better quantification of changes in forest conditions is the United Nations program for Reducing Emissions from Deforestation and forest Degradation (REDD; www.un-redd.org). This is an economic instrument for rewarding tropical nations that avoid carbon emissions to the atmosphere or that regain carbon by reforestation. To be successful, REDD requires spatial and temporal monitoring of changes in carbon stocks due to deforestation and forest degradation, the latter of which usually results from selective logging, forest fragmentation, and surface fires. Although efforts are being made to make processes across nations more comparable (*33*), REDD is being implemented largely at the country and sub-country level.

Given the global importance of forests, the projections of increased future disturbances, and the need to inform conservation mechanisms, it is vital to design an approach that can identify the transition from healthy to unhealthy forests as well as characterize the underlying causes. This includes developing a strong enough understanding of the background levels of forest disturbance to identify events that could alter recovery trajectories. Systematic identification and attribution of individual tree-mortality events based on field plots have proven effective in this respect, but they are too costly to be performed at global scales. Progress has also been made toward mapping broad-scale forest degradation caused by selective logging (*34*), mortality events associated with hurricanes (*35*) or strong winds (*36*, *37*), and disturbances including fires (*38*–*41*). Over the decades for which they are available, Landsat data can be used to help define background levels of disturbance. However, the spatial resolution (one pixel, usually about 30 × 30 m) of these multidecadal records is not sufficient to document smaller-scale mortality (e.g., a few trees or less within a pixel). Lack of information at this scale limits our ability to track changes in forest condition globally, because it is the scale at which the most tree mortality can occur (*36*, *42*).

We currently have no way to assess the importance of observed occurrences of drought- and heat-induced tree mortality and associated declines in global forest health. Allen *et al.* (*43*) indicate the need for establishing a global network for monitoring broad-scale tree mortality and its ecological consequences (*44*). Global trends in mortality rates might be one of the most robust indicators of global forest health; monitoring these trends would also yield valuable information

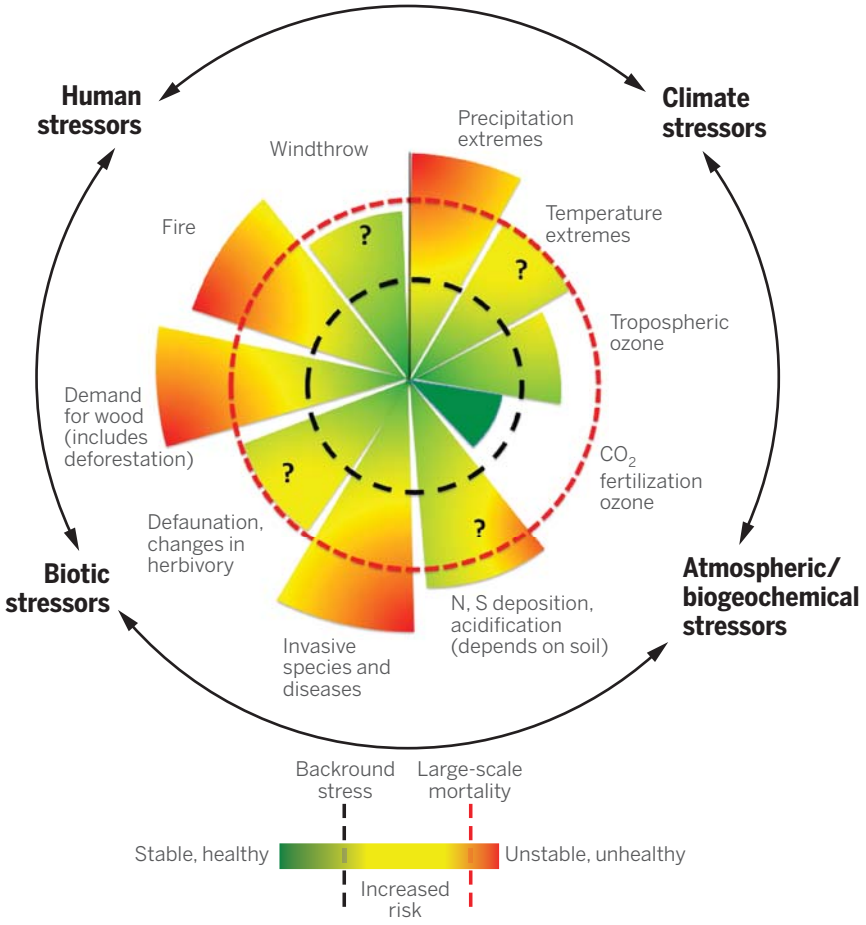

Fig. 4. Examples of different stresses and disturbances affecting forests and how they are expected to change in the future, compared with preindustrial background levels. We have adopted the approach and style used for planetary boundaries (*50*). Stressors can be broadly placed in categories such as "climate," "biotic," and "human," but there are many connections among them. For example, fires, even those set by humans, are more severe and more likely to cause mortality during extreme drought and humidity events. Similarly, a tree stressed by drought may have fewer reserves and succumb more easily to insect or disease outbreak. Although some global changes are probably making forests more resilient (e.g., elevated CO_2 or possibly increased deposition of limiting nutrients from pollution or dust), many others that may negatively affect forests have increased in severity and/or frequency over the past decades and are predicted to increase further in the future. Question marks signify processes for which uncertainties are large, either in terms of how current levels exceed background conditions or how effects may increase or decrease resilience (e.g., nutrient deposition).

about the role of forest disturbance and recovery in the global carbon cycle (*14*, *38*, *42*) and provide test models and remote sensing products that could be used to scale up results from plots. Understanding the trajectory of complex forest-system responses to multiple stressors from local to global scales requires three steps: (i) detection of acute and long-term changes in forest condition and attribution of the causes, (ii) identification of mechanistic relationships between forest-health decline and multiple stressors, and (iii) long-term monitoring of forest recovery after decline and of the natural range of variability in forest condition.

Monitoring allows rapid identification of where and when unusual forest decline is occurring. Monitoring deforestation and severe forest degradation, as well as broad-scale climate-induced vegetation disturbance, is possible at the global level using remote sensing products with high spatial and temporal resolution (*42*, *39*, *45*). However, it is more difficult to use these tools to attribute observed changes to specific causes, especially when the causes are combinations of human, biotic, and climatic stresses. For example, a large stand-killing fire may have a human ignition source, but its intensity could reflect drought conditions and fuel-load buildup from previous disturbance or management decisions.

Forest inventory assessments often measure indicators of tree and forest health (e.g., crown condition and disease occurrence) to evaluate forest condition in plots, which then must be aggregated to provide information at regional or national scales. Data at this intermediate scale that are needed for linking plots with remote sensing observations are largely missing for many regions [with some exceptions (*12*)], as they depend on an understanding of disturbance intensity and frequency across large areas. Protocols for forestry inventory plots need to be as similar as possible, at least for assessments of key parameters such as pest infestation level and crown dieback. Only then can forest condition data can be compared across different legislative regions.

Information at the scales needed to link plot data to remote sensing pixels constitutes a major gap, especially with respect to detecting and attributing altered rates of tree mortality. Repeated aircraft surveys to detect changes in biomass over large regions using lidar and radar techniques can be useful at this intermediate scale (*10*, *12*, *46*). Efforts to evaluate tropical forest degradation (e.g., loss of biomass and diversity) using a combination of satellites have proven effective in identifying areas of future deforestation, but they may underestimate the area of degradation created by selective logging, fire, or windthrow (*34*). A recently approved European Space Agency satellite mission (Biomass) will, for the first time, enable repeated global surveys of forest structure and change (*47*).

Mechanistic relationships between the multiple and interacting stresses and disturbances and forest decline (orange area in Fig. 3) are not well characterized. Most ecological experiments are designed to test the effects of a single factor such as drought, elevated CO_2, or changes in ozone (*48*), and those that attempt to test more than two factors quickly grow to an unmanageable size. New theoretical and experimental approaches, combined with long-term observations, are needed to link forest performance parameters to climatic, biogeochemical, and biotic stressors at multiple scales and to allow identification of stress thresholds. In particular, mortality functions in global dynamic vegetation models should be responsive to multiple stressors.

The dynamics of long-term forest recovery, and especially the time scales required to restore different utilitarian or ecosystem functions, are poorly understood for many ecosystems. Long-term monitoring of forest plots combined with chronosequences of disturbance and recovery (*14*, *15*, *49*) in multiple forest types are required. Understanding factors such as the role of plant (tree) diversity or herbivore abundance in the trajectory of recovery will be critical for supporting increased resilience of forests to more frequent, intense, or novel disturbances in the future.

A successful strategy for global monitoring of forest health, for attributing the causes of decline, and for developing a mechanistic understanding of the underlying processes should thus comprise (Fig. 5): (i) observations of naturally occurring forest conditions, especially improvements in detecting tree and forest mortality; (ii) in situ manipulations of the hypothesized causes of decline in vulnerable ecosystems to verify their attribution and to determine the parameters of mechanistic relationships; (iii) focused research on the underlying processes under controlled environmental conditions in lab facilities and greenhouses; and (iv) the integration of understanding with models that can span spatial and temporal scales. Such a structured approach will

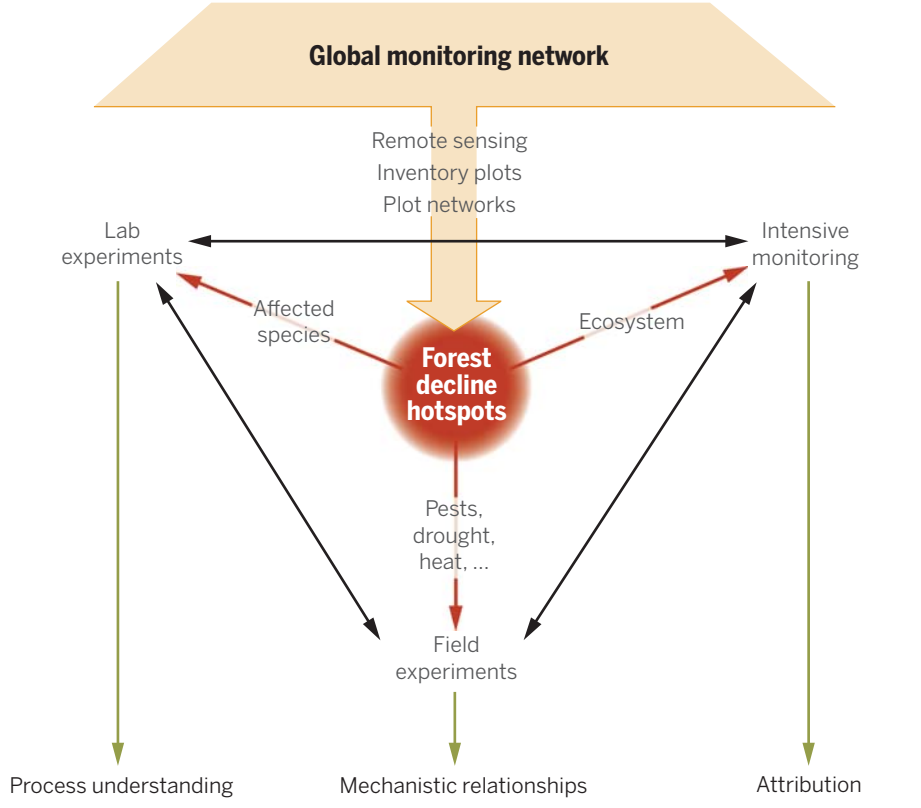

Fig. 5. Proposed design for global assessment of forest health and prediction of future forest conditions. A network of inventory and research plots combined with remote sensing information allows detection of hotspots of forest decline. In these locations, intensive monitoring and manipulations of environmental drivers allow attribution of the causes of decline and clarify mechanistic relationships between drivers and responses; in addition, investigations under controlled conditions (e.g., greenhouse studies) of physiological responses to environmental cues yield understanding of the underlying processes. Taken together, these approaches allow assessments of current forest health and provide the understanding of process-based mechanisms required for modeling future forest health.

generate understanding of the processes involved and provide the scientific mechanisms required for modeling future forest condition in a rapidly changing environment (Fig. 5).

Are we facing a future without healthy forests?

This key question is not yet possible to answer, and no existing observing system can track ongoing changes in a way that enables confident attribution of causes, predictions of recovery trajectories versus further decline, or understanding of the consequences for the maintenance or loss of forest services. Given that many of the trees alive today will experience temperatures and CO_2 levels outside the range to which they are adapted, it is critical to improve efforts to monitor forests and especially tree mortality.

Forests have existed for far longer than humans and have already survived a wide range of past changes in climate conditions. Over the long term, forests will probably prove resilient to rapid anthropogenic changes in climate and environment, whether in their current form or in novel community assemblages. Human concerns about forest health mostly reflect our dependence on the continued availability of the products and services that forests provide. Our vulnerability to even temporary disruptions in their supply underlines our urgent need to detect, understand, and predict potential declines in global forest health.

REFERENCES AND NOTES

1. S. L. Lewis, D. P. Edwards, D. Galbraith, *Science* **349**, 827–832 (2015).
2. C. I. Millar, N. L. Stephenson, *Science* **349**, 823–826 (2015).
3. S. Gauthier, P. Bernier, T. Kuuluvainen, A. Z. Shvidenko, A. D. Schepaschenko, *Science* **349**, 819–822 (2015).
4. M. J. Wingfield, E. G. Brockerhoff, B. D. Wingfield, B. Slippers, *Science* **349**, 832–836 (2015).
5. R. Costanza, B. Norton, B. Haskell, in *Ecosystem Health: New Goals for Environmental Management*, R. Costanza, Ed. (Island Press, Washington, DC, 1992), pp. 239–256.
6. T. E. Kolb, M. R. Wagner, W. W. Covington, *J. For.* **92**, 10–15 (1994).
7. R. L. Edmonds, J. K. Agee, R. I. Gara, *Forest Health and Protection* (McGraw-Hill, New York, 2000).
8. K. F. Raffa *et al.*, *J. For.* **5**, 276–277 (2009).
9. T. Kolb, M. R. Wagner, W. W. Covington, in *Forest Health Through Silviculture: Proceedings of the 1995 National Silviculture Workshop*, L. G. Eskew, Ed. (General Technical Report RM-GTR-267, U.S. Forest Service, Fort Collins, CO, 1995), pp. 5–13.
10. G. P. Asner, M. Keller, J. N. M. Silva, *Glob. Change Biol.* **10**, 765–783 (2004).
11. S. D. Miller *et al.*, *Proc. Natl. Acad. Sci. U.S.A.* **108**, 19431–19435 (2011).
12. G. P. Asner *et al.*, *Proc. Natl. Acad. Sci. U.S.A.* **107**, 16738–16742 (2010).
13. J. Q. Chambers *et al.*, *Oecologia* **141**, 596–611 (2004).
14. J. E. Janisch, M. E. Harmon, *Tree Physiol.* **22**, 77–89 (2002).
15. D. M. Marra *et al.*, *PLOS ONE* **9**, e103711 (2014).
16. P. Meir *et al.*, in *Amazonia and Global Change*, M. Keller, M. Bustamante, J. Gash, P. Silva Dias, Eds. (AGU Geophysical Monograph Series vol. 186, American Geophysical Union, Washington, DC, 2009), pp. 429–449.
17. C. A. Nobre, L. Borma, *Curr. Opin. Environ. Sustain.* **1**, 28–36 (2009).
18. C. D. Allen *et al.*, *For. Ecol. Manage.* **259**, 660–684 (2010).
19. P. M. Brando *et al.*, *Proc. Natl. Acad. Sci. U.S.A.* **111**, 6347–6352 (2014).
20. J. A. Marengo, J. Tomasella, W. R. Soares, L. M. Alves, C. A. Nobre, *Theor. Appl. Climatol.* **107**, 73–85 (2012).
21. N. Diffenbach, M. Ashfach, *Geophys. Res. Lett.* **37**, 1–5 (2010).
22. E. Litchman, K. F. Edwards, C. A. Klausmeier, *Front. Microbiol.* **6**, 254 (2015).
23. R. J. Norby *et al.*, *Proc. Natl. Acad. Sci. U.S.A.* **102**, 18052–18056 (2005).
24. Intergovernmental Panel on Climate Change, *Managing the Risks of Extreme Events and Disasters to Advance Climate Change Adaptation. A Special Report of Working Groups I and II of the Intergovernmental Panel on Climate Change*, C. B. Field *et al.*, Eds. (Cambridge Univ. Press, Cambridge, 2012).
25. M. A. Cochrane *et al.*, *Science* **284**, 1832–1835 (1999).
26. K. A. Harper *et al.*, *Conserv. Biol.* **19**, 768–782 (2005).
27. J. A. Hicke *et al.*, *Glob. Change Biol.* **18**, 7–34 (2012).
28. K. F. Raffa *et al.*, *Bioscience* **58**, 501–517 (2008).
29. M. C. Hansen *et al.*, *Science* **342**, 850–853 (2013).
30. S. J. Goetz, A. G. Bunn, G. J. Fiske, R. A. Houghton, *Proc. Natl. Acad. Sci. U.S.A.* **102**, 13521–13525 (2005).
31. FAO, *Global Forest Resources Assessment 2005* (FAO Forestry Paper 147, FAO, Rome, 2005).
32. FAO, *Global Forest Resources Assessment 2010* (FAO Forestry Paper 163, FAO, Rome, 2010).
33. UN Reducing Emissions from Deforestation and forest Degradation (UN-REDD+) Programme, *Emerging Approaches to Forest Reference Emission Levels and/or Forest Reference Levels for REDD+* (FAO, Rome, 2014).
34. G. P. Asner *et al.*, *Science* **310**, 480–482 (2005).
35. R. Negrón Juárez, D. B. Baker, H. Zeng, T. K. Henkel, J. Q. Chambers, *J. Geophys. Res. D Atmos.* **115**, G04030 (2010).
36. J. Q. Chambers *et al.*, *Proc. Natl. Acad. Sci. U.S.A.* **110**, 3949–3954 (2013).
37. F. D. B. Espírito-Santo *et al.*, *Nat. Commun.* **5**, 3434 (2014).
38. D. J. Mildrexler, M. Zhao, F. A. Heinsch, S. W. Running, *Ecol. Appl.* **17**, 235–250 (2007).
39. D. J. Mildrexler, M. Zhao, S. W. Running, *Remote Sens. Environ.* **113**, 2103–2117 (2009).
40. M. Flannigan, B. Stocks, M. Turetsky, M. Wotton, *Glob. Change Biol.* **15**, 549–560 (2009).
41. A. A. C. Alencar, P. M. Brando, G. P. Asner, F. E. Putz, *Ecol. Appl.* (2015).
42. N. G. McDowell *et al.*, *Trends Plant Sci.* **20**, 114–123 (2015).
43. C. D. Allen, D. D. Breshears, N. G. McDowell, *Ecosphere* (2015); www.esajournals.org/doi/full/10.1890/ES15-00203.1.
44. H. Hartmann, H. D. Adams, W. R. L. Anderegg, S. Jansen, M. J. B. Zeppel, *New Phytol.* **205**, 965–969 (2015).
45. M. C. Hansen, S. V. Stehman, P. V. Potapov, *Proc. Natl. Acad. Sci. U.S.A.* **107**, 8650–8655 (2010).
46. S. R. Levick, G. P. Asner, *Biol. Conserv.* **157**, 121–127 (2013).
47. K. Scipal *et al.*, in *Geoscience and Remote Sensing Symposium (IGARSS), 2010 IEEE International* (Institute of Electrical and Electronics Engineers, Piscataway, NJ, 2010), pp. 52–55.
48. Z. E. Kayler *et al.*, *Front. Ecol. Environ.* **13**, 219–225 (2015).
49. M. L. Goulden *et al.*, *Glob. Change Biol.* **12**, 2146–2162 (2006).
50. W. Steffen *et al.*, *Science* **347**, 1259855–1259855 (2015).

ACKNOWLEDGMENTS

P.B. received funding from NSF (DEB-1146206) and the Brazilian National Council for Scientific and Technological Development (Bolsa de Produtividade number 307084/2013-2). S.T. and H.H. thank C. Allen for sharing an early draft of his paper and the participants of the International Interdisciplinary Workshop on Tree Mortality, held in October 2014 in Jena, Germany.

10.1126/science.aac6759

REVIEW

Boreal forest health and global change

S. Gauthier,[1]* P. Bernier,[1] T. Kuuluvainen,[2] A. Z. Shvidenko,[3] D. G. Schepaschenko[3]

The boreal forest, one of the largest biomes on Earth, provides ecosystem services that benefit society at levels ranging from local to global. Currently, about two-thirds of the area covered by this biome is under some form of management, mostly for wood production. Services such as climate regulation are also provided by both the unmanaged and managed boreal forests. Although most of the boreal forests have retained the resilience to cope with current disturbances, projected environmental changes of unprecedented speed and amplitude pose a substantial threat to their health. Management options to reduce these threats are available and could be implemented, but economic incentives and a greater focus on the boreal biome in international fora are needed to support further adaptation and mitigation actions.

The boreal forest encompasses ~30% of the global forest area (*1*), contains more surface freshwater than any other biome (*2*), and has large tracts of unmanaged forests, mostly in lower-productivity, high-latitude regions of Canada, Russia, and Alaska (*3*) (Fig. 1, A and B). Spread across only a few countries, the biome is characterized by a very low population density and generally low human impacts, although extraction of natural resources is also taking place regionally (Fig. 1C).

Boreal forests provide critical services to local, regional, and global populations. Communities, including those of indigenous people, benefit from ecosystem services provided by the forest for fishing, hunting, leisure, spiritual activities, and economic opportunities (*2*). Countries such as Canada, Finland, Sweden, and Russia (*2*) extract wood from boreal regions for their forest industries. More than 33% of the lumber and 25% of the paper on the export market originate from boreal regions (*2*). Globally, boreal forests help regulate climate through the exchange of energy and water (*4*). They are also a large reservoir of biogenic carbon—on a level comparable to, if not greater than, that of tropical forests—with a likely underestimated 32% of global terrestrial carbon (C) stocks mostly in climate-sensitive peat, soils, and permafrost deposits (*5*, *6*). The boreal forest is estimated to sequester ~20% of the total C sink generated by the world's forests (*5*). Because of these multiple roles, the fate of boreal forests should be a global concern (*4*, *7*).

Global change, which is the combination of climate change and other changes linked to human activities, is rapidly altering the boreal forest environment (*4*, *8*). The rate of these alterations and their cumulative impacts will determine the future health of this biome, including its potential to shift to new undesirable equilibrium states (*9*). In this Review, we evaluate the current status of boreal forest health and discuss the increasing threats these forests face under global change. Based on (*1*), we define forest health as the capacity of forest ecosystems to adjust to changing environmental conditions and to maintain the generation of a wide range of goods and services for society. We assess forest health as a function of two related ecosystem properties: (i) biodiversity at scales from genes to landscapes and (ii) resilience, or the ability to recover from disturbances. We focus our assessment on services linked to wood production and climate regulation, and on forest dynamics and productivity. Finally, we provide examples of the potential impacts of global change and propose options for the long-term maintenance of boreal forest health.

The character of boreal forests

Boreal forests are defined as forests growing in high-latitude environments where freezing temperatures occur for 6 to 8 months (*2*) and in which trees are capable of reaching a minimum height of 5 m and a canopy cover of 10% (*10*). Boreal forest ecosystems have evolved under the constraints imposed by a short growing season and severe winters during which snow cover may last for several months (*2*, *11*). About one-third of their extent is underlain by permafrost (Fig. 1A) (*12*, *13*). Boreal forests have a low diversity of tree species, of which gymnosperms such as *Abies*, *Larix*, *Pinus*, and *Picea* species usually dominate, with varying proportions of angiosperm *Populus*, *Betula*, and *Alnus* species (*2*, *11*, *14*) in stands that may nevertheless support thousands of species of living organisms (*15*).

Different types of disturbances (fire, insects, wind, etc.) have been an essential part of the dynamics of boreal forest landscapes, with events that affect several square meters to millions of hectares (*14*, *16*). Severe stand-replacing crown fires have historically been common in North America and parts of Russia, whereas nonlethal surface fires have been prevalent in Eurasia (*11*, *14*, *17*). Insect outbreaks have also been recurrent in North America and eastern Russia, but windstorms may have been a more important disturbance type in Fennoscandia and western Russia (*14*). Despite these regional differences, the combination of large- and small-scale disturbances over millennia has shaped the biodiversity of all boreal forests through the maintenance of a high landscape-level diversity of stands varying in size, age, structure, and composition, whose proximity creates a large array of habitats for native species (*15*, *18*).

Because of the recurrent nature of disturbances, boreal plant species are generally less affected by fragmentation than tropical forest species (*19*), although specialized species from other groups can be sensitive to fragmentation or change in habitat representation (*15*, *18*). Boreal tree species in particular have evolved mechanisms to survive or recover from disturbances, although the recovery process can be slow (*20*). They also have a generally high adaptive capacity expressed through large environmental tolerance ranges, large population sizes, and high population-level genetic diversity (*21*, *22*). The resilience of these systems is well illustrated in the boreal forest of eastern North America, where the regional tree species pool has remained mostly unchanged over the past 8000 years despite large fluctuations in climate and regional disturbance regimes (*23*).

Is boreal forest health compromised by forest management?

Nearly two-thirds of boreal forests are considered to be managed (*24*), largely for industrial wood production [35 to 40% in Canada (*2*, *25*), 58% in Russia (*26*), and 90% in Fennoscandia (*2*)]. Management intensity ranges from low-input extensive in Canada and Russia to high-input intensive in Fennoscandian forests that represent ~5% of the global boreal forest (*2*). It is estimated that more than 60% of the stands within the managed forest have been harvested at least once (*25*, *27*), although this percentage varies regionally.

Managed forests in Sweden and Finland have been heavily homogenized as a result of long-term use and increasingly intensive silviculture for timber production (*15*, *27*), together with fire suppression (Fig. 1D). Forest productivity and growing stock is increasing, and the aim is to further augment timber extraction (*28*). Lower-yielding managed boreal forests in Canada have retained higher stand and landscape-level diversities through the presence of natural regeneration in postharvest stands and the occurrence of natural disturbances across landscapes (*25*) (Fig. 1D). In boreal Russia, harvest levels, along with investments in forest protection and management, have dropped substantially since the collapse of the Soviet Union (*8*, *29*). Additionally, in spite of existing laws and regulations, up to 20% of current logging is carried out illegally (*8*), with practices that include overharvesting of high-value stems or tree species in the most productive or accessible stands (*30*).

[1]Natural Resources Canada, Canadian Forest Service, Laurentian Forestry Centre, Québec, Quebec G1V 4C7, Canada. [2]Department of Forest Sciences, University of Helsinki, P.O. Box 27, 00014 Helsinki, Finland. [3]Ecosystems Services and Management Program, International Institute for Applied Systems Analysis, Schlossplatz 1, A-2361 Laxenburg, Austria.
*Corresponding author. E-mail: sylvie.gauthier@rncan.gc.ca

Harvesting has decreased the extent of older forests as compared with natural conditions in all regions with forest management (*14*, *16*). The resulting decline in structural attributes such as large trees for cavity shelters and coarse woody debris associated with older forests has negatively affected biodiversity (*31*). Harvesting has also increased the proportion of early-successional, regenerating stands, but these retain less biological and structural diversity than those originating from natural disturbances in which rapidly changing habitats and high species turnover enhance the adaptation potential to new environmental conditions (*25*). Postharvest stands may be further homogenized through tree plantation with varying degrees of genetic selection and through the control of forest structure and competing vegetation, thereby further reducing their potential for adaptation to a changing environment (*25*). Recently, demand for biomass as a renewable energy feedstock has increased, especially in Nordic countries, with a risk of removing nutrients needed for tree growth (*28*). However, negative effects of harvest residue removal on site fertility have been demonstrated only for specific site types (*32*, *33*).

Although past management practices have been shown to decrease species and landscape diversity, it appears that most boreal forest landscapes have at least partially retained their resilience to disturbance (*25*). However, current evidence suggests that the intensification of forest management to enhance wood production has reduced forest biodiversity and resilience (*15*). With intensified forest management, the maintenance of a productive forest increasingly shifts from a natural process to one whose costs and risks must be borne by the forest sector (*34*). For example, in the Swedish province of Götaland, the 2005 windstorm felled 75 Mm^3 of intensively managed wind-prone conifer stands, increasing unit wood costs by 21% that year for the recovery and storage of the wind-felled trees and the replanting of damaged areas (*35*).

Finally, in addition to forest management, the exploration, development, and extraction of other resources (mining, oil and gas, flooding for hydroelectric projects, etc.) have been taking place in regions spread across both the managed and unmanaged portions of the boreal forest (*1*, *2*, *36*) (Fig. 1C). Cumulatively, these activities across northern territories in recent decades have had negative impacts on the health of forest ecosystems through air pollution, soil and water contamination, changes in hydrological regimes, and the physical alteration and fragmentation of forested landscapes (*1*, *37*)—notably in the permafrost forest ecosystems of Siberia (*36*, *37*).

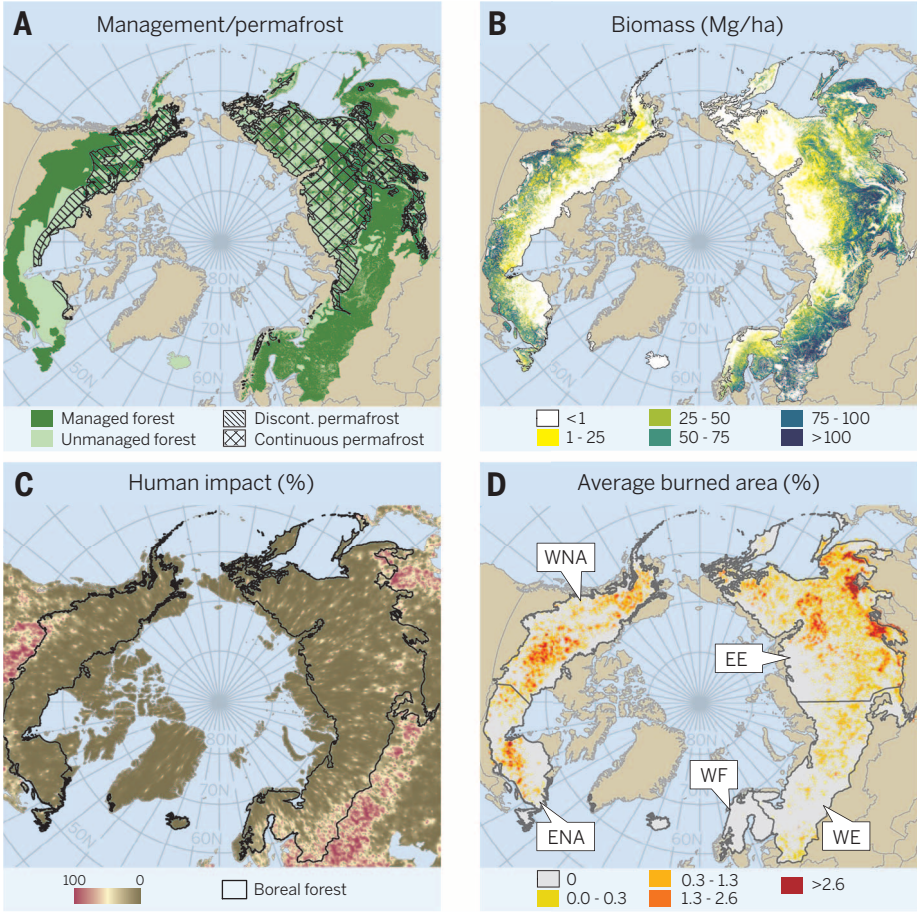

Fig. 1. Characteristics of the circumboreal forest. (**A**) The extent of the managed and unmanaged boreal forests is shown on the map. Forest growing on permafrost covers a large region. (**B**) The current biomass distribution shows the strong south-to-north decrease in forest productivity and the east-to-west increase in the latitude of productive forests across continents. (**C**) The human impact index reflects the overall low but locally important impact due to harvesting, agriculture, human settlements, natural resource exploration and exploitation, mining, or roads, as well as their cumulative importance. (**D**) The mean annual fraction burned (1997–2014) ranges from very low to more than 5% in the drier areas of Eurasian forests. Boreal regions delineated on the map correspond to those considered in Fig. 2B. WNA, western North America; ENA, eastern North America; WF, western Fennoscandia; WE, western Eurasia; EE, eastern Eurasia. See (*70*) for details on data sources.

What risks to boreal forest health are posed by global change?

Over the course of the 21st century, the boreal biome is expected to experience the largest increase in temperatures of all forest biomes (*38*, *39*). In the meantime, the development and extraction of natural resources will likely impose more pressure on boreal forest health (*37*). The expected and unprecedented rate of changes, particularly those of climate and related disturbances, may overwhelm the resilience of species and ecosystems, possibly leading to important biome-level changes (*9*).

Mean annual temperature increases of 1.5°C or more have recently been documented over much of the boreal forest (*38*). Under a globally averaged projection of a warming of 4°C by the end of this century, boreal regions could experience temperature increases from 4° to 11°C, accompanied by a far more modest expected increase in precipitation (*40*) (Fig. 2). In such an extreme scenario, large regions of the boreal forests could, by the end of the century, shift to the drier climate space normally occupied by the woodland/shrubland biome (Fig. 2) (*41*).

Given these changes in climate, biotic and abiotic disturbances are generally predicted to increase in extent, frequency, or severity over the same time frame, although uncertainties in the projections remain (*22*, *39*, *42*–*44*). Fire occurrence, area, and severity are projected to increase considerably, notably for parts of Russia where the share of stand-replacing fires is forecast to increase substantially (*43*–*45*). Warmer temperatures would also lift the climate barriers to population growth or range expansion of native or invasive forest pests, resulting in severe outbreaks similar to those recently experienced in Canada with the mountain pine beetle (*46*) and in Siberia with the Siberian silk moth (*36*). Moreover, the intensification of global trade provides an ever-more efficient vector for the propagation of invasive pests and pathogens to boreal forests (*47*).

Limited evidence suggests a slow northward migration of temperate deciduous tree species

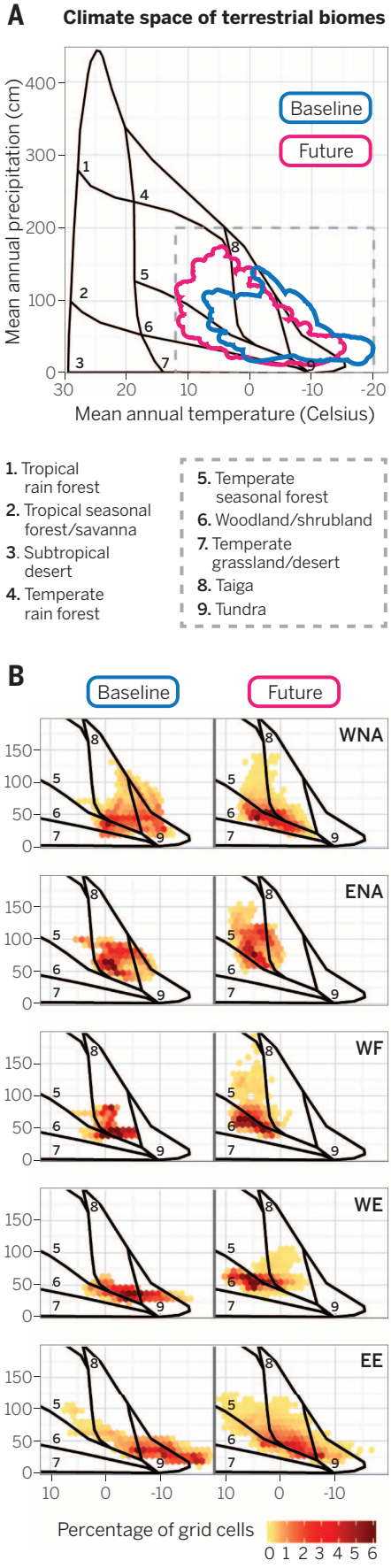

into the boreal zone of eastern North America (*48*) and an expansion of evergreen coniferous species into the current habitat of the deciduous larch in Siberia (*49*). However, climate zones are shifting northward at speeds one order of magnitude faster than the trees' ability to migrate (*36*, *50*). Therefore, forests will be affected directly by the changes in their local climatic conditions and indirectly by changes in the local disturbance regimes. Drought-induced mortality has been reported in several boreal regions (*42*) and is predicted to increase regionally (*8*, *39*). Forest productivity has been on the rise in Fennoscandia, in the northern reaches of the North American boreal forest (*51*, *52*), and over major parts of Russia (*53*), partially in response to increased temperature and growing-season length. Additionally, productivity is projected to increase until 2030 in most of Russia's boreal forests (*8*). By contrast, productivity has been shown or predicted to decrease in response to regional drier conditions in parts of the North American boreal forest (*54*, *55*).

The shift to a drier climate and increasingly frequent disturbances may lead to extensive forest cover thinning or loss, as suggested by the projected climate space for large regions of the boreal forest (Fig. 2) (*43*, *56*). Such a change could be accelerated by the documented ability of successive disturbances to rapidly transform closed forests into low-productivity open woodlands (*41*, *56*, *57*). The projected changes from surface to crown fires in Russian forest ecosystems dominated by tree species not adapted to regenerate after stand-replacing fires could also impair regeneration and the return to closed-canopy stands (*43*). The thawing of the permafrost in dry continental Siberia may lead to widespread drought-induced mortality in both the dark coniferous forests (*8*) and in the larch forests that cover 20% of the global boreal forest (*13*).

Projections of forest dynamics under a range of climate scenarios suggest a greater probability that boreal C stocks will decrease rather than increase or stay unchanged (*8*, *58*). Globally, the boreal forest may have started transitioning from a C sink to a C source (*6*), and certain regions [e.g., western Canada (*46*) and Siberia (*59*)] may already be emitting more C than they capture. The characterization and understanding of C stock dynamics vary considerably among different regions of the boreal forest (*58*, *60*), but this biome's numerous peatlands and deep organic deposits encased in permafrost may become highly vulnerable to global warming (*58*). In Russia alone, the release of C from the thawing permafrost by the end of the century could potentially be several times larger than that of current tropical deforestation (*8*). Regionally, such impacts may be exacerbated by industrial development (*36*, *37*). The full consequences of these changes—including long-term geophysical effects on global climate (*61*) and on systems integrity (*4*)—remain to be understood and evaluated.

Fig. 2. Mean annual temperature and precipitation in the circumboreal forest represented on the climate space of terrestrial biomes. (**A**) Potential impacts of a changing climate on boreal forests are illustrated by overlaying the climatic envelope of global circumboreal forests on the climate space of terrestrial biomes. Baseline (1975) climate conditions of boreal forests correspond closely to the taiga and tundra climate space. Projections of future climate conditions (2090) under an extreme CO_2 emission scenario (AR4 A2) would also overlap the climate space of the woodland/shrubland (6) and temperate seasonal forest (5) biomes. (**B**) Panels display the frequency of baseline (left) and future (right) climate conditions within a 10-min gridded representation of each region (see Fig. 1D for location). Eastern North America (ENA) is the only region projected to remain within the climate space of forested biomes [either taiga (8) or temperate seasonal forest (5)]. In all other regions, projected precipitation changes appear to be insufficient to fully compensate for the increased evaporative demand generated by warmer temperatures. Large areas of these regions would shift into the climate space of the woodland/shrubland biome. See (*70*) for details on data sources and methods.

A way forward

The maintenance of ecosystem services from boreal forests depends on the preservation of forest health, which is threatened by the speed and amplitude of changes in climate projected for these northern latitudes. Considering the importance of the potential impacts these changes may have and the extent over which they may take place, it is imperative that actions be taken to maintain the health of the boreal forest or to enhance its contribution to climate change mitigation. Forest management and economic and global policy considerations represent important avenues to achieve such goals.

Forest management actions to mitigate the effects of climate change can be undertaken (*58*, *62*); these include afforestation and practices to maintain in situ C stocks or to enhance on-site and off-site sequestration (*6*, *62*). Afforestation in the boreal forests should be pursued where possible, but the potential gains are generally small because of low rates of boreal deforestation (*58*, *62*), with a yearly rate of deforestation close to 0.02% (*58*). A notable exception may be the abandonment of 45 Mha of agricultural land in boreal Russia (*63*), of which 18 Mha is already undergoing natural regeneration (*64*). Reforestation could also be used to speed the postdisturbance recovery of forests in the unmanaged boreal region (*8*), across areas that may cover millions of hectares in Russia alone (*36*). In addition, sequestration of C in harvested wood products, the substitution of wood for more energy-intensive building material, and the use of wood as energy feedstock can all be enhanced to provide additional mitigation benefits. However, economic incentives to specifically support afforestation or other carbon-related management actions, such as substitution of energy-intensive building materials, are limited in boreal forests (*7*, *62*).

Forest management strategies such as continuous-cover silviculture and the enhancement of tree species diversity and of landscape heterogeneity may aid in the maintenance of forest cover, the conservation of C stocks, and biodiversity (*8*, *65*). Implementation of new management approaches based on the closer emulation of natural processes or on an adaptive systems perspective (*18*) may also alleviate some of the ecological problems associated with past forest management practices while providing economically viable alternatives (*31*, *66*). Large, well-distributed conservation areas, where natural processes are occurring, remain important for the maintenance of biodiversity and the resilience of boreal forest landscapes (*67*). However, considerations for their establishment must now include the changing climate (*67*).

Better control of natural disturbances is often suggested as a means to conserve boreal C stocks (*6*), but achieving this goal—particularly in remote areas—may be economically impossible, especially given future climate conditions. Rather, the incorporation of disturbance risks in timber supply planning can be used to set sustainable management objectives within a changing climate environment (*68*). Managing for multiple objectives may be challenging, but integrated approaches can support the development of strategies that maximize positive outcomes and find trade-offs between possible contradictory objectives such as management for wood production, climate change mitigation, and biodiversity conservation (*6*, *62*).

Monitoring is essential to continuously assess the state of the boreal forests and to improve our understanding of interactions and feedback among processes. The postdisturbance regeneration phase deserves particular attention (*34*), as it may provide early warnings of forest health degradation, such as species invasion, and allow the rapid implementation of remedial actions to prevent, for instance, the loss of forest cover (*36*). Forests on permafrost and in remote areas are also critically linked to climate and should be monitored closely to detect or predict impending signals of permanent shifts from C sinks to C sources (*60*) or from closed to open forest status (*8*). Coupled with modeling, such change-tracking can be used to project the future of this important biome. However, the current models need improvement, as they may not account for regional specificities such as permafrost (*36*) and often fail to converge on similar outcomes [e.g., (*56*, *69*) for central Siberia].

The health of the immense and seemingly timeless boreal forest is presently under threat, together with the vitality of many forest-based communities and economies. On the larger scale, the long-term provisioning of vital ecosystem services such as global climate regulation is at risk. Our vast knowledge of boreal forests can inform solution development, but current international agreements and regional market mechanisms fail to provide incentives or opportunities to fully implement the existing options (*7*, *8*). To support critical and timely action across the boreal forest, global discussions on sustainable development, biodiversity conservation, and climate change mitigation need to place a greater focus on this vast biome.

REFERENCES AND NOTES

1. J. P. Brandt, M. D. Flannigan, D. G. Maynard, I. D. Thompson, W. J. A. Volney, *Environ. Rev.* **21**, 207–226 (2013).
2. P. J. Burton *et al.*, in *Forests and Society – Responding to Global Drivers of Change*, G. Mery *et al.*, Eds. (International Union of Forest Research Organizations, Vienna, Austria, 2010), pp. 249–282.
3. P. Potapov *et al.*, *Ecol. Soc.* **13**, 51 (2008).
4. W. Steffen *et al.*, *Science* **347**, 1259855 (2015).
5. Y. Pan *et al.*, *Science* **333**, 988–993 (2011).
6. C. J. A. Bradshaw, I. G. Warkentin, *Global Planet. Change* **128**, 24–30 (2015).
7. J. Moen *et al.*, *Conserv. Lett.* **7**, 408–418 (2014).
8. Food and Agriculture Organization of the United Nations (FAO), "The Russian Federation forest sector. Outlook study to 2030" (FAO, Rome, 2012); www.fao.org/docrep/016/i3020e/i3020e00.pdf
9. C. P. O. Reyer *et al.*, *J. Ecol.* **103**, 5–15 (2015).
10. FAO, "Global forest resources assessment 2010. Terms and definitions," Working paper 144/E, FAO, Rome, 2010; www.fao.org/docrep/014/am665e/am665e00.pdf.
11. D. Kneeshaw, Y. Bergeron, T. Kuuluvainen, in *The Sage Handbook of Biogeography*, A. Millington, M. Blumler, U. Schickhoff, Eds. (Sage, London, 2011), pp. 261–278.
12. S. A. Zimov, E. A. G. Schuur, F. S. Chapin III, *Science* **312**, 1612–1613 (2006).
13. A. Osawa, Y. Matsuura, T. Kajimoto, in *Permafrost Ecosystems. Siberian Larch Forests*, A. Osawa, O. A. Zyryanova, Y. Matsuura, T. Kajimoto, R. W. Wein, Eds. (Springer, Netherlands, 2010), pp. 459–481.
14. E. Shorohova, D. Kneeshaw, T. Kuuluvainen, S. Gauthier, *Silva Fenn.* **45**, 785–806 (2011).
15. T. Kuuluvainen, J. Siitonen, in *Managing Forests as Complex Adaptive Systems - Building Resilience to the Challenge of Global Change*, C. Messier, K. J. Puettmaan, K. D. Coates, Eds. (Routledge, New York, 2013), pp. 244–268.
16. T. Kuuluvainen, T. Aakala, *Silva Fenn.* **45**, 823–839 (2011).
17. B. M. Rogers, A. J. Soja, M. L. Goulden, J. T. Randerson, *Nat. Geosci.* **8**, 228–234 (2015).
18. P. J. Burton, in *Managing Forests as Complex Adaptive Systems - Building Resilience to the Challenge of Global Change*, C. Messier, K. J. Puettmaan, K. D. Coates, Eds. (Routledge, New York, 2013), pp. 79–108.
19. K. A. Harper *et al.*, *J. Ecol.* **103**, 550–562 (2015).
20. D. K. Bolton, N. C. Coops, M. A. Wulder, *Remote Sens. Environ.* **163**, 48–60 (2015).
21. S. N. Aitken, S. Yeaman, J. A. Holliday, T. Wang, S. Curtis-McLane, *Evol. Appl.* **1**, 95–111 (2008).
22. M. Lindner *et al.*, *For. Ecol. Manage.* **259**, 698–709 (2010).
23. O. Blarquez, C. Carcaillet, T. Frejaville, Y. Bergeron, *Front. Ecol. Evol.* **2**, 1–8 (2014).
24. A forest is considered to be managed when it is included within a forest management plan for purposes such as conservation, fire protection, or wood production. A managed forest may not be accessible or may not yet have been subjected to active management activities.
25. L. A. Venier *et al.*, *Environ. Rev.* **22**, 457–490 (2014).
26. Federal Agency of Forest Service, *Forest Fund of the Russian Federation (state by 1 January 2009)* (Federal Agency of Forest Service, Moscow, 2009) [in Russian].
27. P. J. Burton *et al.*, in *Towards Sustainable Management of the Boreal Forest*, P. J. Burton, C. Messier, D. W. Smith, W. L. Adamowicz, Eds. (NRC Research Press, Ottawa, Canada, 2003), pp. 1–40.
28. H.-S. Helmisaari, L. Kaarakka, B. A. Olsson, *Scand. J. For. Res.* **29**, 312–322 (2014).
29. State Program of the Russian Federation, *Development of Forest Management for 2013-2020* [in Russian]; www.mnr.gov.ru/upload/iblock/e82/GP_2013-2020.pdf.
30. J. P. Newell, J. Simeone, *Eurasian Geogr. Econ.* **55**, 37–70 (2014).
31. T. Kuuluvainen, O. Tahvonen, T. Aakala, *Ambio* **41**, 720–737 (2012).
32. D. G. Maynard *et al.*, *Environ. Rev.* **22**, 161–178 (2014).
33. E. Thiffault *et al.*, *Environ. Rev.* **19**, 278–309 (2011).
34. S. Gauthier *et al.*, *Environ. Rev.* **22**, 256–285 (2014).
35. Skogsstyrelsen, Swedish Forest Agency, www.skogsstyrelsen.se/en/AUTHORITY/Statistics/Subject-Areas/Economy/Tables-and-figures/.
36. A. Z. Shvidenko *et al.*, in *Regional Environmental Changes in Siberia and Their Global Consequences*, P. Y. Groisman, G. Gutman, Eds. (Springer, New York, 2013), pp. 171–249.
37. A. A. Baklanov *et al.*, in *Regional Environmental Changes in Siberia and Their Global Consequences*, P. Y. Groisman, G. Gutman, Eds. (Springer, New York, 2013), pp. 303–346.
38. Intergovernmental Panel on Climate Change (IPCC), *Climate Change 2013: The Physical Science Basis. Contribution of Working Group I to the Fifth Assessment Report of the Intergovernmental Panel on Climate Change*, T. F. Stocker *et al.*, Eds. (Cambridge Univ. Press, Cambridge, 2013).
39. D. T. Price *et al.*, *Environ. Rev.* **21**, 322–365 (2013).
40. World Bank, "Turn down the heat: Confronting the new climate normal" (World Bank, Washington, DC, 2014); https://openknowledge.worldbank.org/handle/10986/20595.
41. M. Scheffer, M. Hirota, M. Holmgren, E. H. Van Nes, F. S. Chapin III, *Proc. Natl. Acad. Sci. U.S.A.* **109**, 21384–21389 (2012).
42. C. D. Allen *et al.*, *For. Ecol. Manage.* **259**, 660–684 (2010).
43. A. Z. Shvidenko, D. G. Schepaschenko, *Contemp. Probl. Ecol.* **6**, 683–692 (2013).
44. Y. Boulanger, S. Gauthier, P. J. Burton, *Can. J. For. Res.* **44**, 365–376 (2014).
45. W. J. de Groot, M. D. Flannigan, A. S. Cantin, *For. Ecol. Manage.* **294**, 35–44 (2013).
46. W. A. Kurz *et al.*, *Nature* **452**, 987–990 (2008).
47. D. W. Langor *et al.*, *Environ. Rev.* **22**, 372–420 (2014).
48. L. Boisvert-Marsh, C. Périé, S. de Blois, *Ecosphere* **5**, 83 (2014).
49. V. Kharuk, K. J. Ranson, M. L. Dvinskaya, *Eurasian J. For. Res.* **10**, 163–171 (2007).
50. D. W. McKenney, J. H. Pedlar, K. Lawrence, K. Campbell, M. F. Hutchinson, *Bioscience* **57**, 939–948 (2007).
51. P. E. Kauppi, M. Posch, P. Pirinen, *PLOS ONE* **9**, e111340 (2014).
52. K. Zhang *et al.*, *J. Geophys. Res.* **113**, G03033 (2008).
53. A. Lapenis, A. Shvidenko, D. Shepaschenko, S. Nilsson, A. Aiyyer, *Glob. Change Biol.* **11**, 2090–2102 (2005).
54. P. S. A. Beck *et al.*, *Ecol. Lett.* **14**, 373–379 (2011).
55. M. P. Girardin, F. Raulier, P. Y. Bernier, J. C. Tardif, *Ecol. Model.* **213**, 209–228 (2008).
56. N. M. Tchebakova, E. I. Parfenova, A. J. Soja, *Reg. Environ. Change* **11**, 817–827 (2011).
57. J. P. P. Jasinski, S. Payette, *Ecol. Monogr.* **75**, 561–583 (2005).
58. W. A. Kurz *et al.*, *Environ. Rev.* **21**, 260–292 (2013).
59. A. J. Dolman *et al.*, *Biogeosciences* **9**, 5323–5340 (2012).
60. C. S. R. Neigh *et al.*, *Remote Sens. Environ.* **137**, 274–287 (2013).
61. G. B. Bonan, *Science* **320**, 1444–1449 (2008).
62. T. C. Lemprière *et al.*, *Environ. Rev.* **21**, 293–321 (2013).
63. I. Kurganova, V. Lopes de Gerenyu, J. Six, Y. Kuzyakov, *Global Change Biol.* **20**, 938–947 (2014).
64. A. Z. Shvidenko, D. G. Schepaschenko, *Siberian J. For. Sci.* **1**, 69–92 (2014) [in Russian].
65. T. Pukkala, E. Lähde, O. Laiho, *J. For. Res.* **25**, 627–636 (2014).
66. J. Rämö, O. Tahvonen, *Scand. J. For. Res.* **29**, 777–792 (2014).
67. M. E. Andrew, M. A. Wulder, J. A. Cardille, *Environ. Rev.* **22**, 135–160 (2014).
68. S. Gauthier *et al.*, *Can. J. For. Res.* 10.1139/cjfr-2015-0079 (2015).
69. E. J. Gustafson, A. Z. Shvidenko, B. R. Sturtevant, R. M. Scheller, *Ecol. Appl.* **20**, 700–715 (2010).
70. Supplementary information on data sources and methods on the figures are available on *Science* Online.

ACKNOWLEDGMENTS

We thank D. Boucher, D. Gervais, and Y. Boulanger for help with the figures and V. Roy, Y. Boulanger, M. Lorente, R. van Bogaert, and M. Cusson for comments on an earlier version of the paper.

SUPPLEMENTARY MATERIALS

www.sciencemag.org/content/349/6250/819/suppl/DC1
Figs. S1 and S2
References (*71*–*82*)

10.1126/science.aaa9092

REVIEW

Temperate forest health in an era of emerging megadisturbance

Constance I. Millar[1]* and Nathan L. Stephenson[2]

Although disturbances such as fire and native insects can contribute to natural dynamics of forest health, exceptional droughts, directly and in combination with other disturbance factors, are pushing some temperate forests beyond thresholds of sustainability. Interactions from increasing temperatures, drought, native insects and pathogens, and uncharacteristically severe wildfire are resulting in forest mortality beyond the levels of 20th-century experience. Additional anthropogenic stressors, such as atmospheric pollution and invasive species, further weaken trees in some regions. Although continuing climate change will likely drive many areas of temperate forest toward large-scale transformations, management actions can help ease transitions and minimize losses of socially valued ecosystem services.

Forests not only are essential components of the natural environment but also offer profound spiritual and material benefits to humanity. After centuries of exploitation, there is much to celebrate in the resilience (ability to rebound after perturbation) of temperate forests. Broad swaths of forest that were cut in recent centuries continue to regrow vigorously, absorbing a substantial proportion of anthropogenic carbon-dioxide emissions (*1*). Despite deeply concerning declines of ancient trees in forests worldwide (*2*), large trees are increasingly abundant in areas of temperate forests that are regrowing after logging (*3*). In other regions, air-quality regulations have reduced acidic deposition and other air-pollution effects on forests, providing improved conditions for forest growth and sustainability (*4*).

Despite some encouraging trends, 21st-century forests still face grave threats. For millennia, the main threat to forests was overexploitation, but recent research has identified a range of emerging challenges to forest persistence and health. We focus on emerging "megadisturbances" that are capable of driving abrupt tree mortality of a spatial extent, severity, and frequency surpassing that recorded during recent human history. Where these occur, effects to ecosystems and society follow. Thus, while acknowledging the resilience of many forests, we highlight here the nature and consequences of changing environmental conditions that increasingly threaten widespread regions of temperate forest. In particular, we describe the rise of an especially potent threat to forest health that has only recently begun to receive broad attention, that is, persistent and recurring drought combined with high temperatures (see Fig. 1).

Forest health, thresholds, and megadisturbance

Concepts of temperate forest health have changed substantially over the past several decades (*5*, *6*). Early definitions (*7*) described healthy forests as those with trees growing at their optimal capacity, free from serious effects from insects, disease, or wildfire. Fires were suppressed, and insects and pathogens controlled. Through the mid to late 20th century, evolving understanding of ecological dynamics, as well as increasing focus on forests as including organisms beyond the trees, led to recognition that natural disturbances—including fires, insects, and diseases—were essential ingredients of ecosystem functioning (*8*). Combined opinion shifted to a recognition that disturbance was inherent to forest dynamics and contributes to healthy forest functioning and resilience.

Most recently, however, researchers are seeking to understand how much disturbance can be tolerated before forest health and persistence are threatened. This concern emerges from several trends: increasing frequency, extent, and severity of disturbances; growing recognition of the profound effects of anthropogenic climate change; presence of novel anthropogenic stressors; and a burgeoning global human population that imposes escalating demands on forests (*9*). The focus of forest health has shifted toward evaluating forest conditions relative to supporting human needs—that is, the capacity of forests to sustainably provide ecosystem services. These services include provisioning (e.g., water), regulating (e.g., carbon sequestration), supporting (e.g., biogeochemical cycling), and cultural (e.g., recreational) benefits (*10*). To the complexity of ecological dynamics affecting forest health are thereby added the many ways in which humans use and value forests (*9*).

Recent forest research has thus focused on the role of thresholds and ecological conversions (changes in ecological state) (*11*–*14*). Whereas in recent decades, promoting resilience has been a widespread goal of forest management, the increasing pressure of chronic and acute disturbances is pushing many temperate forests toward and over resilience thresholds. The consequences of heat waves, extreme droughts, massive wildfire, and widespread insect outbreaks demonstrate to the public and scientists alike that resilience can be exhausted and that major ecological transformations can result. Serious thresholds are crossed when forests convert to vegetation types without trees and, as a result, lose valued forest ecosystem services.

Forest health can be considered in the context of disturbance effects. Four patterns of 21st-century forest response to cumulative disturbance range from resilient (healthy) to collapse (unhealthy) states, as megadisturbances increase in frequency and extent (Fig. 2). Thresholds can

Fig. 1. Drought- and bark-beetle–induced mortality in high-elevation whitebark pine (*Pinus albicaulis*) forests, northern Warner Mountains (Drake Peak), Oregon. [Photo by C. I. Millar]

[1]U.S. Department of Agriculture Forest Service, Pacific Southwest Research Station, Albany, CA 94710, USA. [2]U.S. Geological Survey, Western Ecological Research Center, Three Rivers, CA 93271, USA.
*Corresponding author. E-mail: cmillar@fs.fed.us

occur within and between classes; ecological functions of forests change; and capacities to deliver ecosystem services are altered. This framework helps to distinguish a healthy amount of disturbance from profound transformations that affect society in undesired ways.

Rise of the "hotter drought"

For millennia, drought has been a key disturbance agent in temperate forests. Over the past few decades, however, rising global temperatures have contributed to droughts of a severity that is unprecedented in the last century or more (*12*, *15*–*18*). These exceptional droughts have been variously called "global-change-type droughts" (*19*), "hot droughts" (*20*), or "hotter droughts" (*14*); we use the last term because it best contrasts these recent droughts with the generally cooler droughts of earlier in the last century. Hotter droughts have emerged as particularly powerful drivers of temperate forest mortality (*14*).

Hotter droughts affect forests both directly and indirectly (*14*). Directly, higher temperatures increase tree water stress by increasing the atmosphere's evaporative demand for water (*21*). Such temperature-induced increases in evaporative demand have transformed what would otherwise be typical droughts (in terms of low precipitation) into droughts of historically unprecedented severity (*15*, *17*, *18*). Additionally, with warming temperatures, precipitation that formerly fell as snow increasingly falls as rain (*22*, *23*). In historically snow-dominated forests, the diminished snowpacks melt earlier and are thus unable to replenish soil moisture during the driest parts of the year (*23*–*25*), further increasing water stress on trees. Finally, the direct effects of tree water stress can be exacerbated by detrimental physiological effects of high temperatures (*12*). Hotter droughts can also affect forests indirectly by making them more vulnerable to attacks by insects and pathogens (described in the next section). Both the direct and indirect effects of hotter drought can yield abrupt and threshold responses in forest condition and process (Fig. 2) (*14*).

The historically unprecedented severity of some recent hotter droughts has, in turn, driven unprecedented temperate forest mortality (*15*, *26*, *27*) (Fig. 3). Although the most severe examples come from semi-arid forests, as global temperatures continue to rise most temperate forests may experience elevated forest mortality during hotter droughts (*28*). Importantly, in addition to the acute effects of hotter drought, increasing temperatures can also result in long-term chronic increases in drought stress even when precipitation remains average or increases (*29*). Such chronic temperature-induced increases in drought stress in the absence of declining precipitation have been implicated in long-term increases in background (noncatastrophic) tree mortality rates, such as in western North America (*30*).

Compound stressors

Hotter droughts are emerging as novel drivers of forest megadisturbance, but they do not act in isolation, and their effects are often compounded

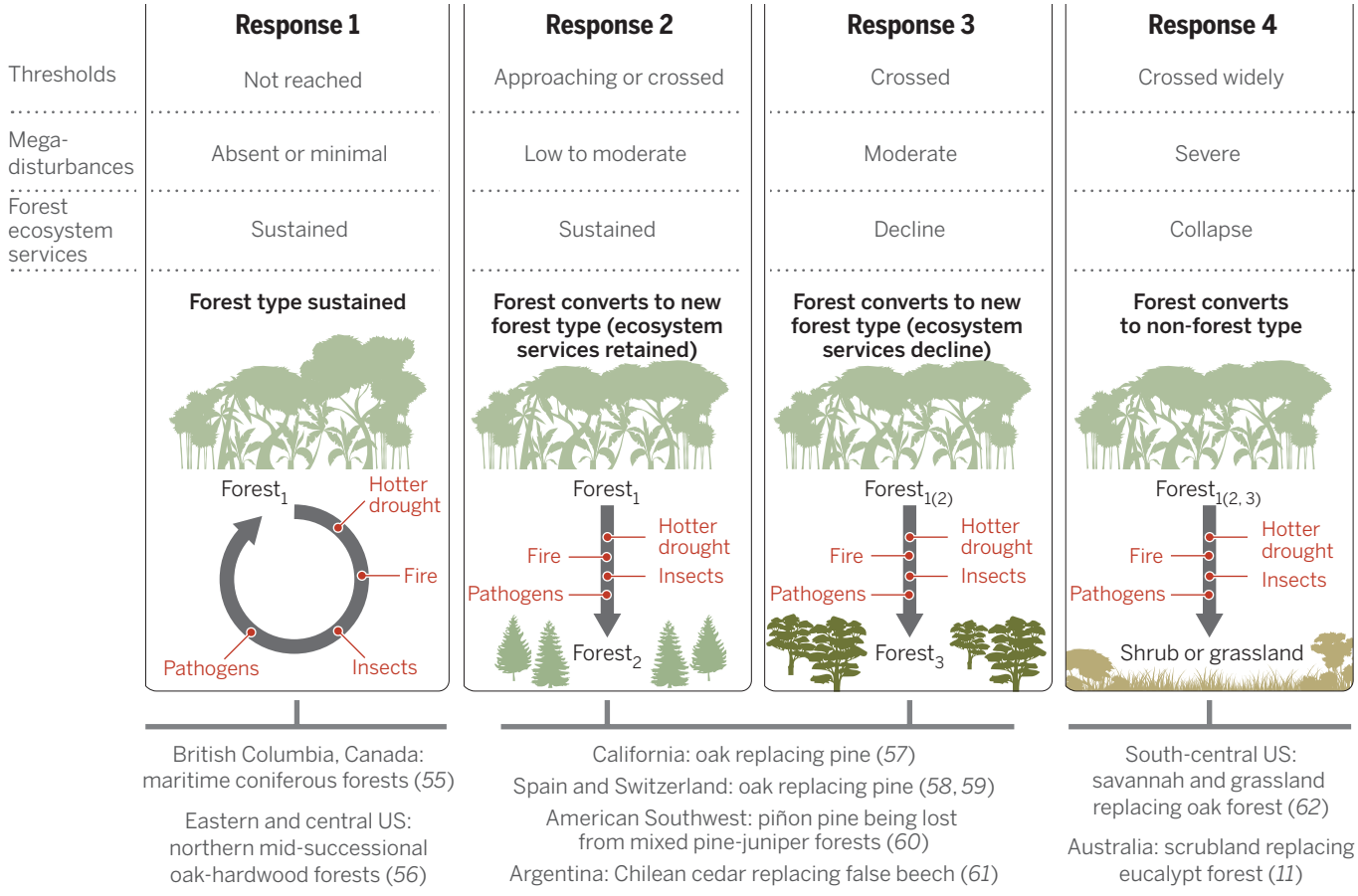

Fig. 2. Temperate forest responses to 21st-century disturbances. (**Response 1**) Existing forests are resilient and capable of sustaining structure, composition, function, and forest ecosystem services. (**Response 2**) As a result of disturbances that affect species composition, forests convert to new forest types but retain primary ecosystem functions and services. The transition results from changes in species abundances or the loss of one or more minor species. (**Response 3**) Existing forests convert to new forest types, and the changes are substantial enough that ecologic functions change and forest ecosystem services decline. Major structural changes may have occurred, or one or more dominant tree species are lost and may or may not be replaced by species not formerly present or present in minor amounts. (**Response 4**) Existing forests transform to nonforest types, such as shrublands or grasslands, losing forest structure, composition, and function; forest ecosystem services severely decline. Thresholds can occur both within classes and between classes. [Examples from (*55*–*62*)]

through interactions with other stressors. In recent decades, outbreaks of insects and pathogens have resulted in millions of hectares of forest defoliation, canopy dieback, declines in growth, and forest mortality in western North America and Europe (*31*–*34*). In many cases, climate was a direct or indirect trigger for these other agents of megadisturbance or influenced the severity and extent of outbreaks. In temperate forests, warming temperatures can trigger population increases in many insect species, which serve as catalysts for widespread outbreaks. Indirectly, drought can weaken trees to a point where insects and pathogens are able to overwhelm tree defenses, further catalyzing widespread outbreaks and epidemics. In some cases, insect outbreaks are not directly related to climatic events, and causes pertain instead to vagaries of regional context and forest type (*34*, *35*). Independently or in combination with other stressors, insect and pathogen disturbances can lead to changes in forest condition similar in magnitude to climate effects (*36*).

Hotter droughts interacting with other stressors are also catalyzing major changes in fire regimes (*37*, *38*), and the term "mega" is most often applied to fires (*11*, *39*). Of overriding concern is the increasing frequency of uncharacteristically severe and large fires and longer fire seasons in temperate forests globally (*37*, *38*). Megafires are more likely where conditions favor build-up of dry fuel, either standing or on the forest floor. Droughts directly affect fuel flammability and structure through lowering moisture contents and increasing tree mortality, and indirectly through cumulative effects from insect epidemics and diseases that alter forest conditions. As with insects and disease, megafires often occur in atypically dense forest stands (often the legacy of past management actions, including fire suppression), homogeneous forest structure, and where large fires occurred previously (*39*, *40*). To the extent that these large fires increase in the future, the potential for shifts to new forest types and nonforest vegetation will accelerate (Fig. 2).

Other anthropogenic environmental changes affect forest health, although not all detrimentally. In some cases, nitrogen and carbon dioxide as atmospheric pollutants can act as fertilizers, improving tree growth, although effects are highly varied and often transient (*4*, *41*, *42*). At chronically high concentrations, and in combination with climate-change effects, air pollutants can defoliate and weaken trees, reduce forest growth, and contribute to forest mortality (*4*, *43*, *44*). Similarly, many nonnative invasive species—including insects, pathogens, plants, and mammals—interact with heat and drought to impair forest health (*32*, *33*). In North America, for instance, alien pathogens widely transformed chestnut and elm forests and increasingly threaten high-elevation pine ecosystems (*32*, *33*). After wildfires in the Great Basin woodlands of western North America, invasion by nonnative cheatgrass (*Bromus tectorum*) can alter fire regimes to the extent that they favor persistence of invasive grassland and exclude restoration of native tree species (*45*).

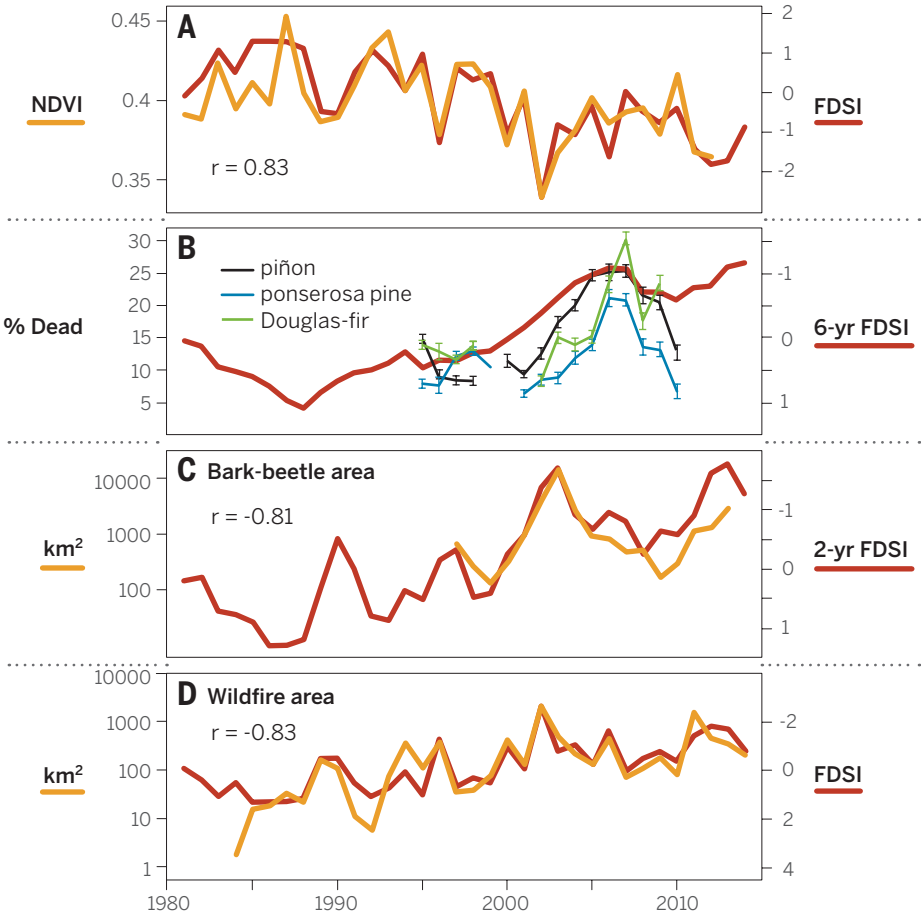

Fig. 3. Effects of hotter drought in the American Southwest. The forest drought-stress index (FDSI) integrates the effects of warm-season water deficit (controlled mostly by high temperature) and cold-season precipitation. Declining values of FDSI correspond to increasing drought. In the Southwest, increasing drought has been accompanied by (**A**) declining vegetation greenness [normalized difference vegetation index (NDVI)], a remotely sensed index of greenness; (**B**) increasing mortality of the three most common conifers; (**C**) increasing area affected by bark-beetle outbreaks; and (**D**) increasing area affected by wildfires. [Adapted by A. P. Williams (July 2015) with permission from Macmillan Publishers Ltd. (*15*)]

Effects on forest ecosystem services

The effects on ecosystem services resulting from hotter droughts and compounding stresses vary, based on how the ecological functions of forests are affected and on the regional demands and needs of society (*9*). Extensive forest mortality can impair water quantity and quality, forest products, cultural and spiritual values, and recreation, with concomitant effects on rural and urban economies (*33*, *46*). Forest fires, in particular, have profound effects on human life, property, and economies. While megafires represent a small fraction of total wildfires, they account for a disproportionately large percentage of suppression costs, private property losses, natural resource damages, and fatalities, representing some of the worst civil disasters on record (*11*, *39*, *47*).

Forests play a particularly critical role in the global carbon cycle, mediating climatic changes by providing feedback to atmospheric carbon dioxide concentrations. Over at least the past several decades, temperate forests have provided a valuable ecosystem service by acting as a net sink of atmospheric carbon dioxide (*1*), partly offsetting anthropogenic emissions. As megadisturbances increase in frequency, extent, and severity, this service is likely to diminish. At the extreme, temperate forests could become net sources rather than sinks of atmospheric carbon dioxide (*9*, *48*).

Forests of the future: Easing transitions

What do these changes portend for temperate forests through the 21st century? In the short term, some forests will likely continue to absorb or rebound from disturbances, sustain a diversity of ecological functions, and deliver ecosystem services similar to those of past decades (Fig. 2). Over the longer term, however, most temperate forests are likely to change in condition (*49*), with megadisturbances frequently catalyzing these effects (*14*). The changes could range from minor shifts in forest structure (e.g., tree density and ages) and species compositions to major transformation of vegetation types, some resulting in novel ecosystems relative to recent centuries. In many cases,

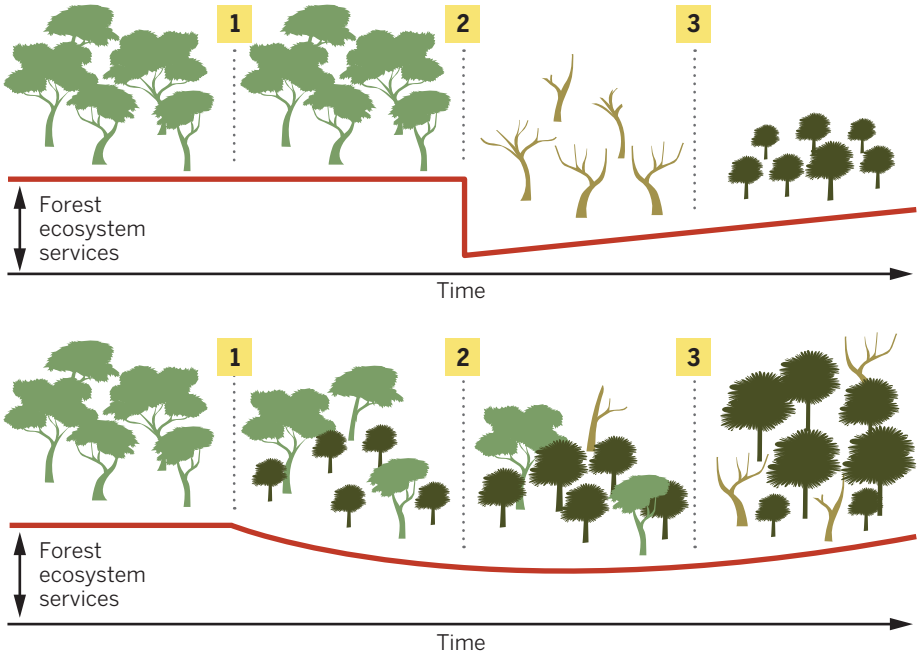

Fig. 4. Management practices can influence the nature of transitions between forest types. Numbers represent forest transitions through time. (**Top**) (**1**) Despite rapid directional environmental changes, managers strive to maintain forests within historical ranges of conditions and may initially succeed. (**2**) The forest may be inherently unstable in the new environment and, once a threshold is exceeded, substantial mortality occurs, with an abrupt loss of most forest ecosystem services. (**3**) After the die-back, recovery of forest ecosystem services is slow. (**Bottom**) (**1**) Managers anticipate an impending forest transition and facilitate it by reducing the probability of sudden die-back (e.g., by thinning the forest to reduce competition for water) and by assisting establishment of species better adapted to future conditions. (**2**) The transition is gradual rather than abrupt, and ecosystem services are maintained at a higher (although reduced) level. (**3**) Forest ecosystem services more rapidly approach their original levels. Although some forest ecosystem services are eventually lost in both cases, active management might facilitate a gradual rather than abrupt transition.

drought-hardy species, species with physiological plasticity capable of coping with compound stresses, and species with shorter statures might outcompete current species (*50*, *51*). Native insects and pathogens may effectively act as invasive exotics as they move beyond their historic ranges (*52*).

Minimizing the effects to society from these transitions is emerging as a primary goal for forest management today (Fig. 4). A challenge to research will be to develop tools to assess the sensitivity of forests to thresholds from cumulative disturbances and evaluate their vulnerability to transformation. If we can identify in advance the most vulnerable forests, in some cases management intervention might be able to ease the transition to new and better-adapted forest states, minimizing losses of ecosystem services. Because the scope of the challenge is vast, triage exercises will almost certainly be necessary to identify the highest-priority forests and those where management action might have the greatest effect.

Success will depend on far more integrated and coordinated efforts by institutions, agencies, and governments than presently exists (*53*). Distributed monitoring systems that observe changes on multiple scales of forest health are essential; these will become increasingly reliant on remote methods. Climate adaptation will likely move from compartmentalized to comprehensive strategies, with attention to proactive methods (*54*). Although thresholds are likely to be approached in the future, and changes are inevitable, the actions we take now in temperate forests can ease and guide transitions, diminishing effects to forest ecosystems and human societies.

REFERENCES AND NOTES

1. Y. Pan *et al.*, *Science* **333**, 988–993 (2011).
2. D. B. Lindenmayer, W. F. Laurance, J. F. Franklin, *Science* **338**, 1305–1306 (2012).
3. P. E. Kauppi *et al.*, *Biogeosciences* **12**, 855–862 (2015).
4. W. deVries, M. H. Dobbertin, S. Solberg, H. F. van Dubben, M. Schaub, *Plant Soil* **380**, 1–45 (2014).
5. W. A. Warren, *Soc. Nat. Resour.* **20**, 99–117 (2007).
6. A. Sulak, L. Huntsinger, *J. For.* **110**, 312–317 (2012).
7. T. E. Kolb, M. R. Wagner, W. W. Covington, *J. For.* **92**, 10–15 (1994).
8. K. F. Raffa *et al.*, *J. For.* **107**, 276–277 (2009).
9. D. Thom, R. Seidl, *Biol. Rev. Camb. Philos. Soc.* 10.1111/brv.12193 (2015).
10. Millennium Ecosystem Assessment, *Ecosystems and Human Well-Being: Synthesis* (Island Press, Washington, DC, 2005).
11. M. A. Adams, *For. Ecol. Manage.* **294**, 250–261 (2013).
12. R. Teskey *et al.*, *Plant Cell Environ.* **38**, 1699–1712 (2015).
13. C. P. O. Reyer *et al.*, *J. Ecol.* **103**, 5–15 (2015).
14. C. D. Allen, D. D. Breshears, N. G. McDowell, *Ecosphere* **6**, 129 (2015).
15. A. Park Williams *et al.*, *Nat. Clim. Change* **3**, 292–297 (2013).
16. M. Lindner *et al.*, *J. Environ. Manage.* **146**, 69–83 (2014).
17. S. M. Vicente-Serrano *et al.*, *Environ. Res. Lett.* **9**, 044001 (2014).
18. N. S. Diffenbaugh, D. L. Swain, D. Touma, *Proc. Natl. Acad. Sci. U.S.A.* **112**, 3931–3936 (2015).
19. D. D. Breshears *et al.*, *Proc. Natl. Acad. Sci. U.S.A.* **102**, 15144–15148 (2005).
20. J. Overpeck, B. Udall, *Science* **328**, 1642–1643 (2010).
21. D. D. Breshears *et al.*, *Front. Plant Sci.* **4**, 266 (2013).
22. G. J. McCabe, D. M. Wolock, *Clim. Change* **99**, 141–153 (2010).
23. T. P. Barnett, J. C. Adam, D. P. Lettenmaier, *Nature* **438**, 303–309 (2005).
24. P. W. Mote, A. F. Hamlet, M. P. Clark, D. P. Lettenmaier, *Bull. Am. Meteorol. Soc.* **86**, 39–49 (2005).
25. I. T. Stewart, D. R. Cayan, M. D. Dettinger, *J. Clim.* **18**, 1136–1155 (2005).
26. J. Carnicer *et al.*, *Proc. Natl. Acad. Sci. U.S.A.* **108**, 1474–1478 (2011).
27. G. Matusick, K. X. Ruthrof, N. C. Brouwers, B. Dell, G. S. J. Hardy, *Eur. J. For. Res.* **132**, 497–510 (2013).
28. B. Choat *et al.*, *Nature* **491**, 752–755 (2012).
29. G. J. McCabe, D. M. Wolock, *Clim. Change* **2015**, 1–13 (2015).
30. P. J. van Mantgem *et al.*, *Science* **323**, 521–524 (2009).
31. B. J. Bentz *et al.*, *Bioscience* **60**, 602–613 (2010).
32. R. N. Sturrock *et al.*, *Plant Pathol.* **60**, 133–149 (2011).
33. A. S. Weed, M. P. Ayres, J. A. Hicke, *Ecol. Monogr.* **83**, 441–470 (2013).
34. A. Sallé, L.-M. Nageleisen, F. Lieutier, *For. Ecol. Manage.* **328**, 79–93 (2014).
35. W. R. Anderegg *et al.*, *New Phytol.* 10.1111/nph.13477 (2015).
36. C. E. Flower, M. A. Gonzalez-Meler, *Annu. Rev. Plant Biol.* **66**, 547–569 (2015).
37. M. Flannigan *et al.*, *For. Ecol. Manage.* **294**, 54–61 (2013).
38. W. M. Jolly *et al.*, *Nat. Commun.* **6**, 7537 (2015).
39. S. L. Stephens *et al.*, *Front. Ecol. Environ* **12**, 115–122 (2014).
40. M. J. Jenkins, J. B. Runyon, C. J. Fettig, W. G. Page, B. J. Bentz, *For. Sci.* **60**, 489–501 (2014).
41. M. E. Fenn *et al.*, *Bioscience* **53**, 404–420 (2003).
42. S. Piao *et al.*, *Glob. Change Biol.* **21**, 1601–1609 (2015).
43. M. Lorenz *et al.*, in *Forest and Society: Responding to Global Drivers of Change*, G. Mery *et al.*, Eds. (IUFRO World Series, Vienna, International Union of Forest Research Organizations, 2010), pp. 55–74.
44. Y. Hoshika *et al.*, *Sci. Rep.* **5**, 9871 (2015).
45. W. D. Billings, in *The Earth in Transition: Patterns and Processes of Biotic Impoverishment*, G. M. Woodell, Ed. (Cambridge Univ. Press, Cambridge, 1990), pp. 301–322.
46. I. L. Boyd, P. H. Freer-Smith, C. A. Gilligan, H. C. J. Godfray, *Science* **342**, 1235773 (2013).
47. J. Williams, *For. Ecol. Manage.* **294**, 4–10 (2013).
48. J. A. Hicke, A. J. H. Meddens, C. D. Allen, C. A. Kolden, *Environ. Res. Ltrs.* **8**, 035032 (2013).
49. P. Gonzalez, R. P. Neilson, J. M. Lenihan, R. J. Drapek, *Glob. Ecol. Biogeogr.* **19**, 755–768 (2010).
50. X. Jiang *et al.*, *J. Clim.* **26**, 3671–3687 (2013).
51. N. G. McDowell, C. D. Allen, *Nat. Clim. Change* **5**, 669–672 (2015).
52. A. J. Woods, *J. For. Sci.* **60**, 484–486 (2014).
53. B. E. Law, *Glob. Change Biol.* **20**, 3595–3599 (2014).
54. C. I. Millar, C. W. Swanston, D. L. Peterson, in *Climate Change and United States Forests*, D. L. Peterson, J. M. Vose, T. Patel-Weynand, Eds. (Springer, Berlin, 2014), pp. 183–222.
55. R. A. Hember *et al.*, *Glob. Change Biol.* **18**, 2026–2040 (2012).
56. M. C. Dietze, P. R. Moorcroft, *Glob. Change Biol.* **17**, 3312–3326 (2011).
57. P. J. McIntyre *et al.*, *Proc. Natl. Acad. Sci. U.S.A.* **112**, 1458–1463 (2015).
58. A. Rigling *et al.*, *Glob. Change Biol.* **19**, 229–240 (2013).
59. J. Carnicer *et al.*, *Glob. Ecol. Biogeogr.* **23**, 371–384 (2014).
60. D. D. Breshears, L. López-Hoffman, L. J. Graumlich, *Ambio* **40**, 256–263 (2011).
61. M. Suarez, T. Kitzberger, *Can. J. For. Res.* **38**, 3002–3010 (2008).
62. D. P. Bendixsen, S. W. Hallgren, A. E. Frazier, *For. Ecol. Manage.* **347**, 40–48 (2015).

ACKNOWLEDGMENTS

We thank M. Dettinger (U.S. Geological Survey), C. J. Fettig (U.S. Forest Service), J. Hicke (University of Idaho), S. Stephens (University of California, Berkeley), and A. P. Williams (Lamont-Doherty Earth Observatory) for reviewing the draft manuscript; A. P. Williams for providing an update of FDSI trends for Fig. 3; and D. Delany (U.S. Forest Service) for help with figures. C.I.M. and N.L.S. are supported by the U.S. Forest Service and U.S. Geological Survey, respectively.

10.1126/science.aaa9933

REVIEW

Increasing human dominance of tropical forests

Simon L. Lewis,[1,2]* David P. Edwards,[3] David Galbraith[2]

Tropical forests house over half of Earth's biodiversity and are an important influence on the climate system. These forests are experiencing escalating human influence, altering their health and the provision of important ecosystem functions and services. Impacts started with hunting and millennia-old megafaunal extinctions (phase I), continuing via low-intensity shifting cultivation (phase II), to today's global integration, dominated by intensive permanent agriculture, industrial logging, and attendant fires and fragmentation (phase III). Such ongoing pressures, together with an intensification of global environmental change, may severely degrade forests in the future (phase IV, global simplification) unless new "development without destruction" pathways are established alongside climate change–resilient landscape designs.

The functioning of Earth is dominated by the redistribution of incoming solar radiation through fluxes of both energy and matter, within which life plays a pivotal role. Tropical forests are critical to this functioning as a major regulator of global climate, via water transpiration, cloud formation, and atmospheric circulation (*1*–*3*). Overall, they exchange more water and carbon with the atmosphere than any other biome: Changes in the balance of photosynthesis and respiration in tropical vegetation dominate interannual variability in Earth's atmospheric CO_2 concentration (*4*). Furthermore, over half of Earth's 5 to 20 million species reside in tropical forests (*5*, *6*).

Some 1.2 to 1.5 billion people directly rely on tropical forests for food, timber, medicines, and other ecosystem services (*7*), including both closed-canopy and more open seasonal systems (Fig. 1). This multiplicity of forest functions and services are underpinned by their diverse resident species, such that diverse forests are healthy forests (*8*). Here we consider threats to tropical forests and their impacts on forest health and the ecosystem services they supply in three parts: first, historical changes since humans began living in the tropical forest biome, because impacts can last millennia; second, the much greater changes over recent decades; and third, the future of tropical forests, given the twin pressures of further agricultural expansion and rapid global environmental change.

Historical human impacts on forest health

There are five major biogeographic regions in the moist tropics—Neo- (tropical America), Afro-, Indo-Malayan, and Australasian (largely New Guinea) tropics, plus Madagascar—each an evolutionary descendant following the breakup of Pangea ~200 million years ago (Fig. 1). Rainforest area contractions during glacial periods have left Africa depauperate in tree species (*9*), while Indo-Malayan forests are often dominated by one family of trees, the Dipterocarpaceae (*10*, *11*). Differences in structure occur: Closed-canopy African forests have fewer trees per hectare (mean, 426 stems >10-cm diameter ha^{-1}) than forests in Amazonia or Borneo (both mean, ~600 stems ha^{-1}) (*12*), while Amazonian forests have shorter trees for a given diameter (*10*) and, on average, contain one-third lower aboveground biomass (AGB) than African or Bornean forests (*12*). Thus, a priori it is expected that different regions may respond differently to environmental changes.

> ***"Beyond national networks of well-protected forested landscapes and formal collective tenure of forest lands, large-scale landscape planning will be required to maintain forest health."***

Humans began living in African tropical forests ~60,000 years before the present (yr B.P.) and have since colonized all tropical forests (since ~50,000 yr B.P. in Indo-Malayan and Australasian tropics, ~10,000 yr B.P. in Neotropics, and ~2000 yr B.P. in Madagascar). The first impact was hunting, with greater fractions of the megafauna becoming extinct in more recently colonized biogeographic regions. Thus, whereas only 18% of African megafauna were lost, some 83% disappeared in South America (*13*). Regardless of the exact contributions of hunting relative to glacial-to-interglacial climate change, these extinctions likely altered plant and animal species composition, nutrient cycling, and forest structure (*12*, *14*, *15*). The lower AGB of Amazonia may reflect long-term cascading impacts of megafauna loss (*12*).

Tropical agriculture began ~6000 yr B.P., with the area affected slowly increasing over millennia (*16*). There is debate around the extent to which farming and enrichment planting of tree crops led to tropical forests being "cultural parklands" and thus whether current "primary" forests are actually very old secondary forest and forest gardens (*17*). Archaeological remains indicate some intensively cultivated areas, including anthropogenic soil creation in Africa and Amazonia (*18*), as well as extensively cultivated areas associated with ancient empires (Maya, Khmer), forest kingdoms (West Africa), concentrated resources [Southern Amazonia near rivers (*17*)], and technological innovation [western Congo basin, 2500 to 1400 yr B.P. (*19*)]. These were always a small fraction of total forest area. Even when farming collapsed after the 1492 arrival of Europeans in the Americas, when ~90% of indigenous Americans died, pre-Colombian cultivated land likely represented <10% of Neotropical forest extent (*13*). Additionally, the tendency to compare contemporary changes only to the recent past, known as shifting baselines, gives pervasive underestimates of wildlife abundance before European arrival in the tropics. For example, 24 million Amazonian turtle eggs were harvested in 1719 alone, producing 100,000 liters of lighting oil (*20*). Overall, although pre-Colonial human activity altered parts of the tropical forest landscape, low population densities and shifting cultivation systems maintained forest health.

Recent changes in forest function and health

Three major trends dominate tropical forest function and health in the recent past: conversion to nonforest, mostly for farmland (*21*, *22*) and mining (*23*); degradation of remaining forest, via hunting (*24*), selective logging (*11*), fire (*25*), and fragmentation and associated edge effects (*26*); and regeneration of secondary forest (*8*). Logging is a frequent gateway to degradation and conversion, although other routes occur (Fig. 2A). These trends are driven by socioeconomic factors that scale from local use to international markets and that occur legally and illegally, making their management and mitigation complex.

The extent of these changes is large: ~100 million ha of tropical forest were converted to farmland between 1980 and 2012, a rate of ~0.4% $year^{-1}$, commonly for soybean or oil palm production (*21*, *22*). Selective logging affected ~20% of tropical forests between 2000 and 2005 (*27*). Only a minority remain as Intact Forest Landscapes: i.e., areas >500 km^2 and >10 km wide with no settlements or industrial logging (Fig. 1) (*28*). Across the world's extant tropical forests a recent estimate suggests, 24% are intact, 46% fragmented, and 30% otherwise degraded (*29*). Because even structurally intact forests are hunted, including in protected areas (*30*), threats are global.

Global carbon and water cycle impacts

Changes in forest extent alter biogeochemical cycles and the biophysical properties of Earth's surface. Net tropical land carbon flux estimates have high uncertainty, with studies giving net zero exchange or a modest source over recent decades (*31*, *32*). Net values mask large and uncertain opposing gross fluxes: to the atmosphere

[1]Department of Geography, University College London, London, UK. [2]School of Geography, University of Leeds, Leeds, UK. [3]Department of Animal and Plant Sciences, University of Sheffield, Sheffield, UK.
*Corresponding author. E-mail: s.l.lewis@leeds.ac.uk

from deforestation and degradation (2.0 to 2.8 Pg C year^{-1}); and from the atmosphere in intact (0.5 to 1.0 Pg C year^{-1}) and regenerating forest [1.4 to 1.7 Pg C year^{-1}; the three pairs of figures are central estimates, the first from (*33*) and the second from (*34*), over the early 2000s]. Thus, intact forest provides a valuable service, avoidable emissions from deforestation and degradation are globally significant, and substantial carbon sequestration via permanent forest restoration is possible (compared to 7.8 Pg C year^{-1} emitted from fossil fuels over 2000 to 2010).

Deforestation and degradation also cause biophysical changes, including albedo, surface roughness, and evapotranspiration. Deforestation leads to warming: Simulations of complete tropical deforestation lead to a 0.9°C global temperature increase, due to both carbon cycle and biophysical changes (*35*). Conversely, tropical forest restoration cools Earth, unlike in boreal zones where albedo effects dominate, because albedo changes are small in tropical forests while evaporative cooling and carbon sequestration are high (*35*). The impacts of land-cover change on rainfall are highly scale dependent: Local deforestation has little effect, but at the mesoscale rainfall increases, whereas very large-scale forest loss likely reduces it (*1*–*3*).

Subtracting and adding species

Hunting for local consumption is likely sustainable if population density is about one person km^{-2} and smaller, higher-fecundity species are targeted (*24*). Higher densities of forest-dwelling communities and commercial hunting to supply larger towns or the international wildlife trade (e.g., tiger bone; rhinoceros horn; elephant tusk) drive the "empty forest syndrome" where expansive forests contain few to no large-bodied vertebrates (*20*). Increasing rarity raises prices and makes it economically viable to seek out even the last individuals of a species (*36*). For example, the last Javan rhino (*Rhinoceros sondaicus annamiticus*) in mainland Southeast Asia was shot in 2010 for its horn, commanding a higher price than gold (Fig. 2B) (*37*).

Large-bodied vertebrates, which disperse large-seeded trees, are vital to healthy tropical forests. In their absence, seed dispersal becomes more clustered and seedling survival is reduced, as documented in Borneo (*38*), Congo (*14*), and Amazonia (*39*). Altered tree seedling communities suggest longer-term impacts on tree species composition and carbon stocks because larger-seeded trees tend to have higher wood density than wind-dispersed species (*40*). Given increasing hunting pressure, with 62% of Africa's forest elephants killed in the decade to 2011 (*41*), such changes may become the norm for Africa and Amazonia. By contrast, defaunation may not reduce AGB in areas of Asia where wind-dispersed dipterocarps dominate (*38*).

Human activity has not only selectively removed species from forests but added them, too. A suite of invasive species and diseases have been introduced to tropical forests, particularly on oceanic islands, driving species extinctions that have degraded pollination, dispersal, and predation functions that underpin forest health. Hunting, introduced predators, and avian malaria have decimated birds in the Pacific, where some 2000 endemic species were lost (*42*). Cascades of extinction often unfold: Over a century, the loss of Hawaiian endemic birds drove 31 plant species that they pollinated to extinction (*43*). On Guam, the introduction of brown tree snakes (*Boiga irregularis*) led to the extinction of all forest bird and bat frugivores, stopping seed dispersal services, including to secondary forest areas dominated by an invasive tree species, thereby arresting its carbon stock recovery (*44*). Away from islands, an invasive fungus has contributed to the extinction of several mainland Neotropical amphibian species (*45*).

Directly degrading tropical forest health

Over 400 million ha of tropical forest are within the permanent timber estate (*46*). Logging in tropical forests usually selectively removes only valuable trees (Fig. 2, C and D). Logging intensity varies regionally (1 to 2 trees ha^{-1} in Amazon and Congo, >10 in Southeast Asia) and locally with topography and variation in timber stocks (*11*, *47*). Such forests retain 76% (range, 47 to 97%) of carbon stocks shortly after logging (*47*) and maintain large-scale hydrological processes (*11*). Though logging is less extensive than hunting, it has greater consequences for forest health. Critically, logging provides road access to hunters, increasing the number of empty forests (Fig. 2D).

Studied logged forests, averaging across logging intensities, retain similar species richness (*11*, *47*) but have altered community composition (*11*). Reductions in biodiversity are lower at lower logging intensities (*48*), under reduced-impact logging (*49*), and when areas of primary forest are spared within concessions (*11*). The contribution of invertebrates to litter decomposition, seed predation and removal, and invertebrate predation is reduced by up to one-half on Borneo, but increases in the abundance of small mammals, amphibians, and insectivorous birds compensate to retain these ecosystem processes

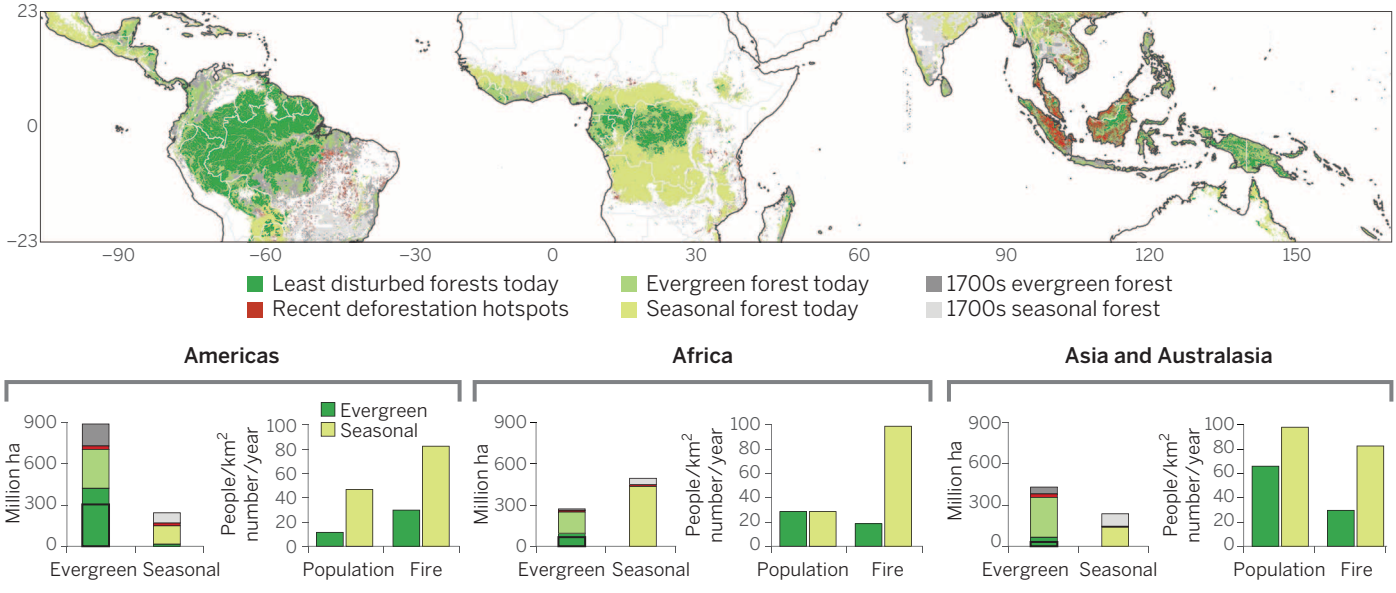

Fig. 1. Map of current and historical evergreen and seasonal tropical forest extent. The figure is adapted from (*88*). Gray shading represents the extent of forest before the Industrial Revolution [~1700; based on (*89*)]. Green indicates current extent. Darkest green represents Intact Forest Landscapes, 95% of which are evergreen forests (*28*). Red represents recent intense land-cover change [2000 to 2012, ≥10% deforestation per 10 km^2 (*22*)]. Below, for each continent, a pair of bar plots summarize forest area data (left) and human population density plus fire numbers within forested areas (right); dark boxes denote a more conservative definition of least disturbed forests: a 5-km buffer from any high-intensity human influence.

at primary forest levels (*50*). Forest health is therefore maintained, but only if the forest is not further degraded or deforested [Fig. 2A, (*11*)].

The conversion of logged or intact forest, mainly to agriculture (*21*, *22*), drives fragmentation of remaining forests into smaller, isolated patches. With the exception of the vast Congo and Amazon regions (only 25% within 1 km of an edge), the majority of tropical forests are now edge affected; for example, 91% of Brazilian Atlantic forest is within 1 km of an edge (*51*). Fragmentation has two key impacts on forest health. First, landscape connectivity is reduced, disrupting metapopulation dynamics and driving species losses, particularly in the smallest fragments (*52*). Species-poor communities have reduced ecosystem function and services: for example, decreased seed dispersal mutualism in Africa (*53*) and dominance of low–wood density tree species in Amazonia (*26*). Second, fragments suffer edge effects that penetrate into the forest, such as winds and woody vines, that increase tree mortality and alter species composition (*26*). Thus, carbon stocks are reduced in fragments (*54*), particularly at their edges (*26*, *51*, *55*). Nevertheless, even after a century or more of isolation, fragments can retain appreciable biodiversity, carbon, and multiple functions (*54*, *55*), especially in hotspots of extinction risk where contiguous forest cover has been widely disrupted, such as the Brazilian Atlantic, East and West Africa, the Tropical Andes, and the Himalayas.

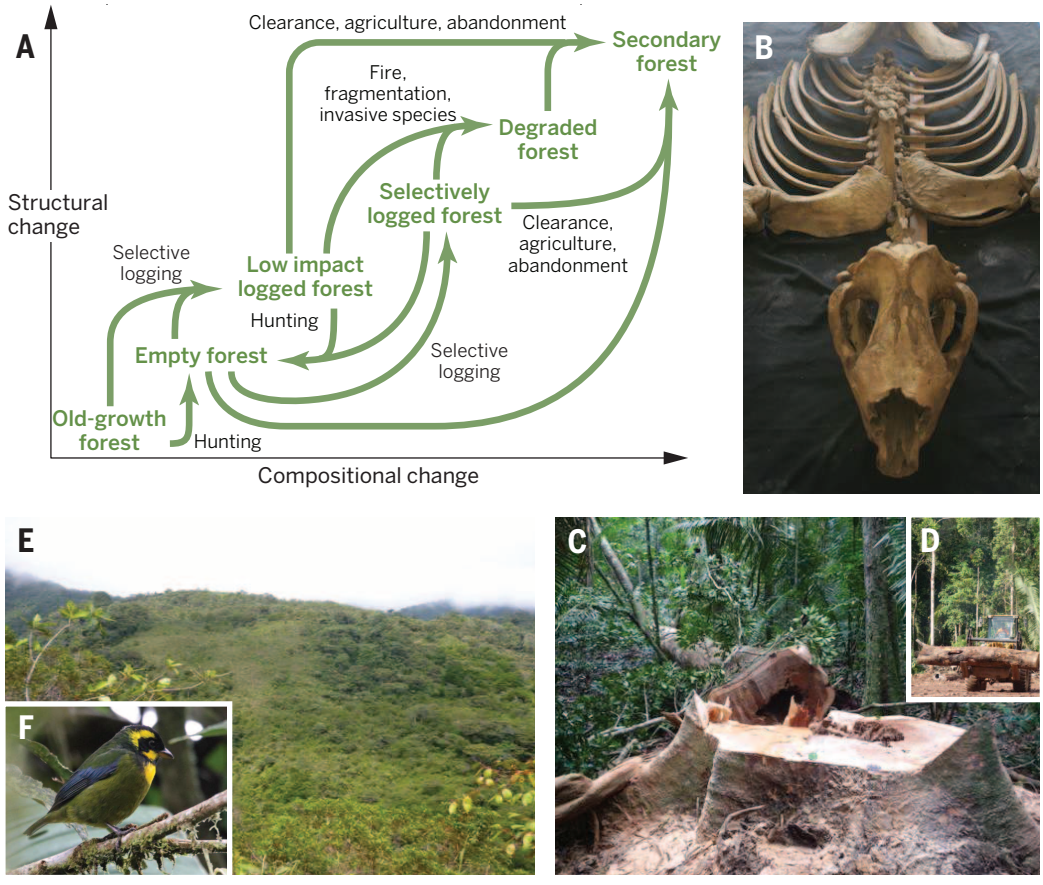

Fig. 2. Examples of direct human impacts on tropical forests. (**A**) Schematic of common land-use changes that alter forest structure and species composition; all are classified as "forest" (*8*). (**B**) Skeleton of the last Javan rhino from mainland Southeast Asia, shot in 2010 for its horn, which has been removed by hunters; an example of hunting pressure that drives the "empty forest syndrome." (**C**) A logged canopy emergent in Brazilian Amazonia. If protected from further impacts, selectively logged forest retains most biodiversity and much carbon. (**D**) Logging road in the Brazilian Amazon. By 2050, >25 million km of roads are predicted to be built across the tropics (*70*), driving further forest degradation from fragmentation and encroachment by fire and hunters. (**E**) Secondary forest in the Colombian Andes. Across the tropics, areas of marginal farmland are being abandoned followed by regeneration, providing multiple ecosystem services from carbon sequestration to reduced landslides. (**F**) The endangered gold-ringed tanager that has recolonized secondary forests in the Tropical Andes (*59*), showing their increasingly important role in tropical forest conservation. [Photo credits: (B) Sarah Brook/WWF; (C to E) David Edwards; (F) James Gilroy].

Natural fires are extremely rare in moist tropical forest, but anthropogenic fires are common today (Fig. 1). Following logging and fragmentation, fuel loads (woody debris, ongoing tree mortality), conditions (drier, warmer in canopy openings), and ignition sources (people) all promote fires (*25*). Fires have major impacts on forest health: Experiments in Amazonia show 226 to 464% increases in tree mortality, 23 to 31% decline in canopy cover, and 12 to 20% decline in AGB (*56*), plus almost all primary forest birds are replaced by secondary and nonforest species (*57*). Furthermore, the risk of repeat burning increases, eventually leading to a deflected successional community of savanna or shrubby vegetation, losing most species and many functions (*58*). Severe large-scale impacts can result from drought–fire interactions: During the last major El Niño, in 1997 to 1998, ~20 million ha of tropical forest burned (*25*), contributing to a corresponding record increase in atmospheric CO_2 concentration (*31*).

Forest recovery

New extensive areas of logged and secondary forest provide enormous scope to improve forest health and ecosystem services (Fig. 2, C and E) (*59*). If fire and conversion are avoided, logged tropical forests naturally recover structure and carbon stocks over time, and if overhunting is avoided, species composition will also likely be maintained (*11*). Following conventional logging, recovery of AGB may take several decades (*60*), but stocks returned to primary levels only 16 years after reduced-impact logging in the southern Amazon (*11*). Silvicultural techniques can enhance the rate of forest recovery; nontimber tree thinning and vine cutting nearly doubled the rate of AGB recovery in Africa (*60*), and vine cutting had minimal impacts on birds and wider forest health in Borneo (*37*).

Secondary forest regrows when economically marginal farmland is abandoned, often because it is too dry, steep, or high altitude for modern agriculture, including in the Tropical Andes, Caribbean, southern Mexico, and Philippines (Fig. 2E) (*27*). With protection from fire, forest recovery is fast (*59*, *61*) and carbon sequestration high (*34*), with soil erosion, landslides, and flood risk all reduced (*62*). In the Tropical Andes, carbon stocks reached half of primary forest levels after 30 years (*59*). Biodiversity began recovering, including the return of 33 of 40 threatened bird species (Fig. 2F) (*59*). Enrichment planting can boost early forest recovery in terms of carbon uptake and biodiversity (*61*). Regrowing areas can be large: In Latin America and the Caribbean, over 35 million ha of woody vegetation began recovery between 2001 and 2010 (*63*). Restoration can therefore provide many benefits, but such forests are not, in many respects, equivalent to faunally intact old-growth forests.

Future health of tropical forests

The 21st century will see large increases in demand for products from tropical lands. Thus,

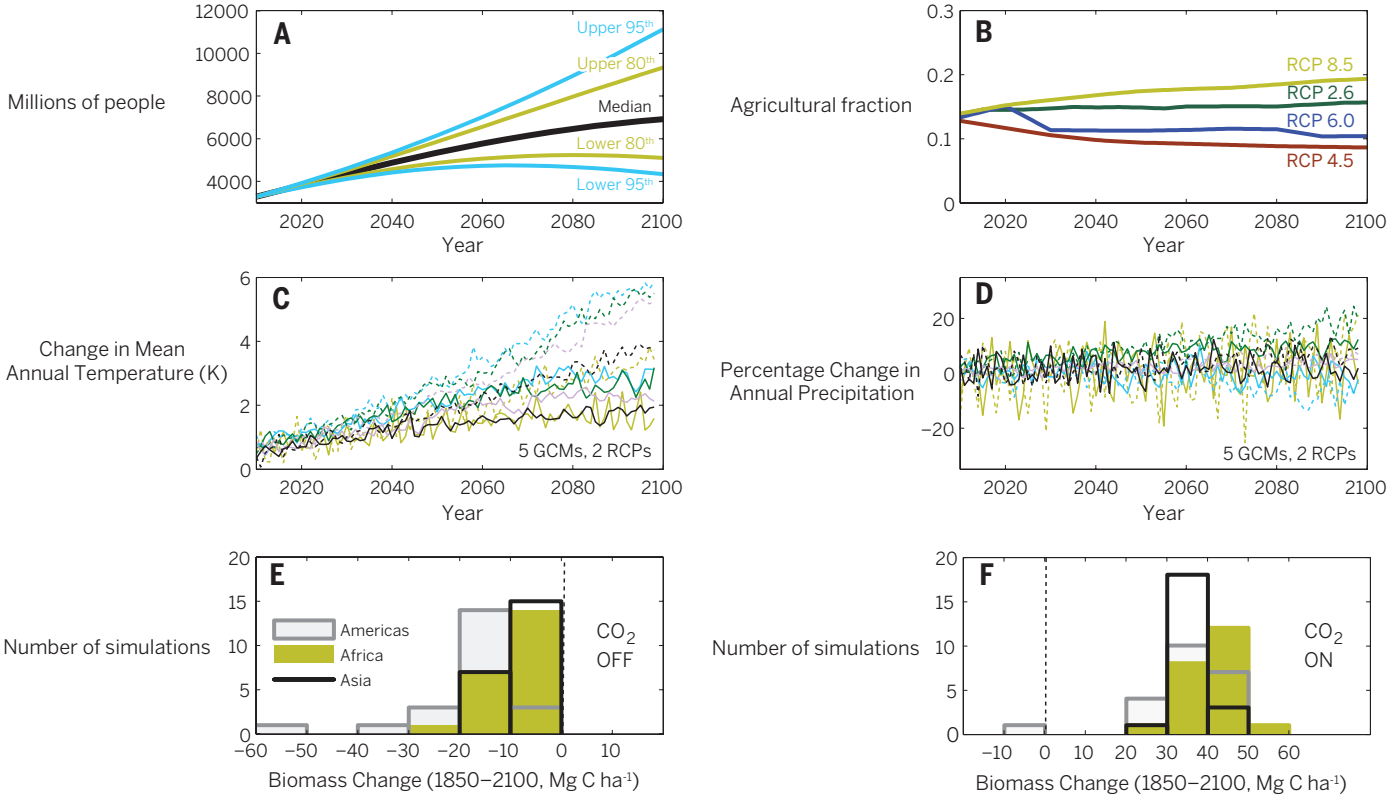

Fig. 3. Projected 21st-century trends for tropical forest regions: human population, agricultural extent, annual surface air temperature, annual precipitation, and changes in forest biomass. (**A**) Human population projections for tropical forest–containing countries (*64*). Median, black line; 80% probability interval, olive lines; 95% probability intervals, blue lines. (**B**) Mean agricultural-cropland and pasture fraction of land points in tropical-forest–containing regions, for four IPCC Representative Concentration Pathway (RCP) scenarios (*82*). Each land-use scenario uses a different integrated assessment model: IMAGE, green line (RCP2.6); MiniCAM, brown line (RCP4.5); AIM, navy line (RCP6.0); and MESSAGE, olive line (RCP8.5). Data from http://luh.umd.edu/data.php. (**C**) Change in mean annual temperature of land points in tropical-forest–containing regions, relative to the 1960 to 2005 mean, for RCP4.5 (solid lines), and RCP8.5 (dashed lines), each from five CMIP5 general circulation models (GCMs): GFDL-ESM2M, olive line; HadGEM2-ES, blue line; IPSL-CM5A-LR, green line; MIROC-ESM-CHEM, lilac line; and NORESM1-M, black line (*82*). Data from http://pcmdi9.llnl.gov. (**D**) Identical to (C), but reporting percentage change in mean annual precipitation. (**E**) Histograms of biomass change between 1850 and 2100 for tropical moist forest areas of the Americas, Africa, and Asia (Indo-Malayan and Australasian tropics combined) simulated by the MOSES-TRIFFID land-surface model, run with climate data outputs from 22 different CMIP3 general circulation models under an A2 emissions scenario (relatively high emissions), excluding the impacts of CO_2 fertilization on plants (*74*). (**F**) Identical to (E) except that plants also respond to CO_2 increases. The impacts of climate change are generally projected to be negative, and CO_2 positive, on tropical forest biomass. Panels (A) to (D) include areas of evergreen and seasonal forests (see Fig. 1), (E) and (F) evergreen only.

the greatest threats will likely continue to be conversion and degradation but will be increasingly combined with the impacts of rapid climatic changes (Fig. 3). The outcomes for forests will depend on their natural resilience plus management interventions that increase or decrease their vulnerability to multiple environmental changes. Here we synthesize model results and suggest alternative policy responses to maintain forest health.

Continued forest conversion

Predicting the future of land-use change in the tropics is challenging, given complex interactions among biophysical, economic, policy, and behavioral factors. Six billion people are projected to live in the tropics by 2100, rising from 40 to 55% of global population, with growth centered on Africa (Fig. 3A) (*64*). Gross domestic product (GDP) is projected to increase three- to sixfold by 2050 in rapidly industrializing nations, including Brazil, China, and India (*65*). These trends imply increased demand for commodities from tropical lands. For individual countries, Forest Transition Theory shows a slowing and reversal of net forest cover loss as country GDP increases and marginal farmlands are abandoned, thereby reverting back to forest (*66*). However, a global forest transition is unlikely because agricultural and forestry products are then obtained from other countries, leaking deforestation and degradation elsewhere (*67*).

Global land-use scenarios are included within the latest Intergovernmental Panel on Climate Change (IPCC) scenarios of greenhouse gas concentrations, termed "Representative Concentration Pathways" (RCPs). However, each of the four RCP scenarios utilizes a different Integrated Assessment Model driven by different assumptions. Thus, land-use projections within RCPs appear idiosyncratic and include both increases and decreases in agricultural area in 2100 (Fig. 3B). Uncertainty is also seen in the Agricultural Model Inter-comparison Project (AMIP), showing an average 200 million ha increase in cropland by area 2050, primarily in the tropics, yet 7 of the 10 economic models report a 10 to 25% increase in croplands, two a very modest increase, and one a decrease (*68*). Such uncertainty is unsurprising, as current models, both stochastic and deterministic, have largely failed to capture observed deforestation patterns, such as the large decline in deforestation rates in Brazilian Amazonia between 2004 and 2011 (*69*). The RCP and AMIP scenarios may grossly underestimate forest loss, as major new road infrastructure—some 25 million km by 2050 (*70*)—and highly lucrative mining and oil extraction look set to expand further (*23*). Despite the predictive challenges, there is agreement that land-use change is a much more important driver of tropical forest loss than climate, even under the most extreme emissions scenario (RCP8.5) (*71*).

Impacts of a changing climate

Climatic risks to tropical forests emerged from some early models that incorporated a dynamic

link between vegetation and the atmosphere and simulated severe drying and warming over Amazonia, with considerable loss ("dieback") of forests (*72*). By contrast, more recent ensemble-based approaches, in which vegetation models are forced with output from multiple climate models, project gains in tropical forest biomass and cover under most future scenarios across the tropics (*73*, *74*). These changes reflect a balance of carbon losses due to climate change—higher air temperature and in some regions less rainfall—and carbon gains from increasing atmospheric CO_2, with gains generally outweighing the losses (*74*) (Fig. 3, C to F). By contrast, climate envelope-type approaches show a decreasing "niche space" for tropical forests but do not include the direct influence of CO_2 on photosynthesis and water-use efficiency (*75*). Thus, forest responses to CO_2 are critical to understanding the resilience of tropical forests to global change (compare Fig. 3, E and F).

Indeed, the balance of sensitivities to increasing CO_2 and a changing climate may be overly optimistic in most vegetation models. First, observations from 321 intact long-term inventory plots across Amazonia report net gains in AGB, in line with CO_2 fertilization, but also show these gains declining over the past two decades (*76*). That is, sink strength is declining, whereas vegetation models show the opposite (*74*, *77*). Second, current vegetation models fail to capture the doubling of tropical land sensitivity to increased temperatures over the past five decades (*4*) or the observed reductions in biomass under extreme drought (*77*). Third, the models generally lack representations of the mechanisms expected to curtail CO_2-related biomass increases such as soil phosphorus availability, which limits productivity in many tropical forests.

Changes not captured by plant physiology–based models will also occur, such as the responses to the projected 2° to 9°C temperature increase over tropical lands by 2100, depending on the emissions scenario and model (*74*). Populations will adapt, move, or die. In the montane tropics, some species are moving upslope (*78*), but in extensive low-altitude areas, including the Amazon and Congo basins, species would have to travel 0.33 km $year^{-1}$ to maintain their temperature niche over the 21st century (A1B scenario, ~4°C increase over tropical lands by 2100) (*79*). This implies high levels of population extinction. However, some tolerance of higher air temperatures may exist, as some species are old enough to have encountered Pliocene temperatures that were warmer than that of today (*80*), while others may exploit cool microhabitats to survive extreme weather events (*81*).

In contrast to air temperature, tropical precipitation projections vary considerably across climate models (*82*) (compare Fig. 3, C and D). There is some regional agreement: Southern and eastern Amazonia see longer dry seasons and East African forests become wetter (*82*). Longer dry seasons may lead to shorter forests through disproportionate mortality of tall canopy trees (*83*) and rapidly altered species composition: A 40-year rainfall decline in West Africa was accompanied by a dramatic shift to dry-adapted and deciduous species (*84*). Both drought and higher temperatures increase fire risk, potentially overwhelming all other changes and increasing the risk of widespread "savannization" of once-moist forest regions (*25*, *56*).

A choice of futures

Human-induced changes to tropical forests can be synthesized in stages: phase I, hunting and megafauna extinctions; phase II, low-intensity shifting cultivation; and phase III, global integration. This latest phase is defined by permanent intensive agriculture, often driven by distant socioeconomics directing land-use change, frontier industrial logging for export, cross-continental species invasions, and the early impacts of global atmospheric and climatic changes, where even the most remote forests are affected (*76*, *34*). A phase IV may occur: global simplification, in which species are lost across landscapes through a combination of rapid changes in climate, population isolation in fragmented landscapes, competition from invasive species, and the impacts of increasing disturbances—notably, fires combining with logging. Such changes would adversely affect local communities and global ecosystem services.

Human activity will dictate the future of tropical forests (*13*). Therefore, management decisions will deliver benefits to some groups over others and strongly influence the future health of tropical forests. The central policy question is, who derives benefits, and who bears the costs? In the face of widespread poverty in tropical forest regions, a goal of "development without destruction" would allow prosperity without undermining current ecosystem services—that over a billion people rely on—or globally critical functions (*2*, *7*, *34*). From a human rights perspective, forest-dwelling communities should be the overwhelming recipients of benefits flowing from tropical forests (which has not been the case with industrial logging or export farming). From a policy perspective, avoiding deforestation is often best achieved by allocating forest-dwellers legal rights over their land. An analysis of 292 protected areas in Brazilian Amazonia found that indigenous reserves were the most effective at avoiding deforestation in locations with high deforestation pressure (*85*). Furthermore, a pan-tropical study of 80 forest commons in 10 countries showed that collective long-term use rights maintain forest cover and carbon stocks better than other management systems (*86*). Such human rights–conservation win-win scenarios are gaining traction (*87*).

Beyond national networks of well-protected forested landscapes and formal collective tenure of forest lands, large-scale landscape planning will be required to maintain forest health. This would include halting deforestation (*87*), improving yields on existing agricultural lands, implementing low-impact logging methods for timber production (*37*, *49*), carefully targeting new road construction (*70*), and effective fire management (*37*, *58*). Some forest restoration will be required as species are moving under a rapidly changing climate; therefore, unbroken forested corridors linking tropical forest landscapes with those ~4°C cooler will be necessary to reduce levels of extinction. Combining these measures with near–real-time satellite monitoring, and effective enforcement to curb illegal activity, would substantially benefit forest-dependent communities, increase the resilience of tropical forests, and maintain the flow of ecosystem services they provide. This would lessen the unwelcome shocks that living in the Anthropocene will bring this century.

REFERENCES AND NOTES

1. N. Devaraju, G. Bala, A. Modak, *Proc. Natl. Acad. Sci. U.S.A.* **112**, 3257–3262 (2015).
2. D. Lawrence, K. Vandecar, *Nat. Clim. Change* **5**, 27–36 (2015).
3. D. V. Spracklen, S. R. Arnold, C. M. Taylor, *Nature* **489**, 282–285 (2012).
4. X. Wang *et al.*, *Nature* **506**, 212–215 (2014).
5. B. Groombridge, M. D. Jenkins, *World Atlas of Biodiversity.* University of California Press, Berkeley, CA. (2003).
6. B. R. Scheffers, L. N. Joppa, S. L. Pimm, W. F. Laurance, *Trends Ecol. Evol.* **27**, 501–510 (2012).
7. B. Vira, C. Wildburger, S. Mansourian, *Forests, Trees and Landscapes for Food Security and Nutrition. A Global Assessment Report*. IUFRO, Vienna (2015).
8. FAO, Global Forest Resources Assessment 2010. *FAO Forestry Paper No. 163. Food and Agriculture Organization of the United Nations* (2010).
9. I. Parmentier *et al.*, *J. Ecol.* **95**, 1058–1071 (2007).
10. L. Banin *et al.*, *Glob. Ecol. Biogeogr.* **21**, 1179–1190 (2012).
11. D. P. Edwards, J. A. Tobias, D. Sheil, E. Meijaard, W. F. Laurance, *Trends Ecol. Evol.* **29**, 511–520 (2014).
12. S. L. Lewis *et al.*, *Philos. Trans. R. Soc. London B Biol. Sci.* **368**, 20120295 (2013).
13. S. L. Lewis, M. A. Maslin, *Nature* **519**, 171–180 (2015).
14. J. R. Poulsen, C. J. Clark, T. M. Palmer, *Biol. Conserv.* **163**, 122–130 (2013).
15. C. E. Doughty, *Annu. Rev. Environ. Resour.* **38**, 503–527 (2013).
16. E. C. Ellis *et al.*, *Proc. Natl. Acad. Sci. U.S.A.* **110**, 7978–7985 (2013).
17. J. Barlow, T. A. Gardner, A. C. Lees, L. Parry, C. A. Peres, *Biol. Conserv.* **151**, 45–49 (2012).
18. V. Frausin *et al.*, *Hum. Ecol.* **42**, 695–710 (2014).
19. R. Oslisly *et al.*, *Philos. Trans. R. Soc. London B Biol. Sci.* **368**, 20120304 (2013).
20. K. H. Redford, *Bioscience* **42**, 412–422 (1992).
21. H. K. Gibbs *et al.*, *Proc. Natl. Acad. Sci. U.S.A.* **107**, 16732–16737 (2010).
22. M. C. Hansen *et al.*, *Science* **342**, 850–853 (2013).
23. D. P. Edwards *et al.*, *Conserv. Lett.* **7**, 302–311 (2014).
24. J. G. Robinson, E. L. Bennett, *Hunting for Sustainability in Tropical Forests* (Columbia Univ. Press, New York, 2000).
25. M. A. Cochrane, *Nature* **421**, 913–919 (2003).
26. W. F. Laurance *et al.*, *Conserv. Biol.* **16**, 605–618 (2002).
27. G. P. Asner *et al.*, *Conserv. Biol.* **23**, 1386–1395 (2009).
28. P. Potapov *et al.*, *Ecol. Soc.* **13**, 51 (2008).
29. B. Mercer, *Tropical Forests: A Review* (International Sustainability Unit, London, 2015).
30. W. F. Laurance *et al.*, *Nature* **489**, 290–294 (2012).
31. P. Ciais *et al.*, in *Climate Change 2013: The Physical Science Basis. Contribution of Working Group I to the Fifth Assessment Report of the Intergovernmental Panel on Climate Change*, T. F. Stocker *et al.*, Eds. (Cambridge Univ. Press, Cambridge, 2013).
32. L. V. Gatti *et al.*, *Nature* **506**, 76–80 (2014).
33. J. Grace, E. Mitchard, E. Gloor, *Glob. Chang. Biol.* **20**, 3238–3255 (2014).
34. Y. Pan *et al.*, *Science* **333**, 988–993 (2011).
35. R. G. Anderson *et al.*, *Front. Ecol. Environ* **9**, 174–182 (2011).
36. F. Courchamp *et al.*, *PLOS Biol.* **4**, e415 (2006).
37. D. S. Wilcove, X. Giam, D. P. Edwards, B. Fisher, L. P. Koh, *Trends Ecol. Evol.* **28**, 531–540 (2013).
38. R. D. Harrison *et al.*, *Ecol. Lett.* **16**, 687–694 (2013).
39. J. Terborgh *et al.*, *Ecology* **89**, 1757–1768 (2008).
40. J. F. Brodie, H. K. Gibbs, *Science* **326**, 364–365 (2009).
41. F. Maisels *et al.*, *PLOS ONE* **8**, e59469 (2013).
42. D. W. Steadman, *Science* **267**, 1123–1131 (1995).
43. P. A. Cox, T. Elmqvist, *Conserv. Biol.* **14**, 1237–1239 (2000).
44. E. M. Caves, S. B. Jennings, J. Hillerislambers, J. J. Tewksbury, H. S. Rogers, *PLOS ONE* **8**, e65618 (2013).

45. T. L. Cheng, S. M. Rovito, D. B. Wake, V. T. Vredenburg, *Proc. Natl. Acad. Sci. U.S.A.* **108**, 9502–9507 (2011).
46. J. Blaser, A. Sarre, D. Poore, S. Johnson, *Status of Tropical Forest Management. ITTO Technical Series 38*. International Tropical Timber Organization, Yokohama, Japan (2011).
47. F. E. Putz *et al.*, *Conserv. Lett.* **5**, 296–303 (2012).
48. Z. Burivalova, C. H. Sekercioğlu, L. P. Koh, *Curr. Biol.* **24**, 1893–1898 (2014).
49. J. E. Bicknell, M. J. Struebig, D. P. Edwards, Z. G. Davies, *Curr. Biol.* **24**, R1119–R1120 (2014).
50. R. M. Ewers *et al.*, *Nat. Commun.* **6**, 6836 (2015).
51. N. M. Haddad *et al.*, *Sci. Adv.* **1**, e1500052 (2015).
52. G. Ferraz *et al.*, *Proc. Natl. Acad. Sci. U.S.A.* **100**, 14069–14073 (2003).
53. N. J. Cordeiro, H. F. Howe, *Proc. Natl. Acad. Sci. U.S.A.* **100**, 14052–14056 (2003).
54. E. Berenguer *et al.*, *Glob. Chang. Biol.* **20**, 3713–3726 (2014).
55. L. F. S. Magnago *et al.*, *J. Ecol.* **102**, 475–485 (2014).
56. P. M. Brando *et al.*, *Proc. Natl. Acad. Sci. U.S.A.* **111**, 6347–6352 (2014).
57. J. Barlow, C. A. Peres, *Ecol. Appl.* **14**, 1358–1373 (2004).
58. J. Barlow, C. A. Peres, *Philos. Trans. R. Soc. London B Biol. Sci.* **363**, 1787–1794 (2008).
59. J. J. Gilroy *et al.*, *Nat. Clim. Change* **4**, 503–507 (2014).
60. S. Gourlet-Fleury *et al.*, *Philos. Trans. R. Soc. London B Biol. Sci.* **368**, 20120302 (2013).
61. P. A. Omeja *et al.*, *For. Ecol. Manage.* **261**, 703–709 (2011).
62. R. L. Chazdon, *Second Growth* (Chicago Univ. Press, Chicago, 2014).
63. T. M. Aide *et al.*, *Biotropica* **45**, 262–271 (2013).
64. United Nations, *Probabilistic Population Projections Based on the World Population Prospects: The 2012 Revision* (U.N. Population Division, New York, 2014).
65. PriceWaterhouseCoopers, *The World in 2050: Will the Shift in Global Economic Power Continue?* www.pwc.com/gx/en/issues/the-economy/assets/world-in-2050-february-2015.pdf (2015).
66. T. K. Rudel, L. Schneider, M. Uriarte, *Land Use Policy* **27**, 95–97 (2010).
67. P. Meyfroidt, T. K. Rudel, E. F. Lambin, *Proc. Natl. Acad. Sci. U.S.A.* **107**, 20917–20922 (2010).
68. C. Schmitz *et al.*, *Agric. Econ.* **45**, 69–84 (2014).
69. I. M. D. Rosa, S. E. Ahmed, R. M. Ewers, *Glob. Change Biol.* **20**, 1707–1722 (2014).
70. W. F. Laurance *et al.*, *Nature* **513**, 229–232 (2014).
71. R. A. Betts *et al.*, *Biogeosciences* **12**, 1317–1338 (2015).
72. P. M. Cox, R. A. Betts, C. D. Jones, S. A. Spall, I. J. Totterdell, *Nature* **408**, 184–187 (2000).
73. A. Rammig *et al.*, *New Phytol.* **187**, 694–706 (2010).
74. C. Huntingford *et al.*, *Nat. Geosci.* **6**, 268–273 (2013).
75. Y. Malhi *et al.*, *Proc. Natl. Acad. Sci. U.S.A.* **106**, 20610–20615 (2009).
76. R. J. W. Brienen *et al.*, *Nature* **519**, 344–348 (2015).
77. D. Galbraith *et al.*, *New Phytol.* **187**, 647–665 (2010).
78. I. C. Chen *et al.*, *Proc. Natl. Acad. Sci. U.S.A.* **106**, 1479–1483 (2009).
79. S. R. Loarie *et al.*, *Nature* **462**, 1052–1055 (2009).
80. C. W. Dick, S. L. Lewis, M. Maslin, E. Bermingham, *Ecol. Evol.* **3**, 162–169 (2013).
81. B. R. Scheffers, D. P. Edwards, A. Diesmos, S. E. Williams, T. A. Evans, *Glob. Chang. Biol.* **20**, 495–503 (2014).
82. M. Collins *et al.*, in *Climate Change 2013: The Physical Science Basis. Contribution of Working Group I to the Fifth Assessment Report of the Intergovernmental Panel on Climate Change*, T. F. Stocker *et al.*, Eds. (Cambridge Univ. Press, Cambridge and New York, 2013).
83. O. L. Phillips *et al.*, *Science* **323**, 1344–1347 (2009).
84. S. Fauset *et al.*, *Ecol. Lett.* **15**, 1120–1129 (2012).
85. C. Nolte, A. Agrawal, K. M. Silvius, B. S. Soares-Filho, *Proc. Natl. Acad. Sci. U.S.A.* **110**, 4956–4961 (2013).
86. A. Chhatre, A. Agrawal, *Proc. Natl. Acad. Sci. U.S.A.* **106**, 17667–17670 (2009).
87. United Nations, *New York Declaration on Forests* (United Nations, New York, 2015).
88. Y. Malhi, T. A. Gardner, G. R. Goldsmith, M. R. Silman, P. Zelazowski, *Annu. Rev. Environ. Resour.* **39**, 125–159 (2014).
89. N. Ramankutty, J. A. Foley, *Global Biogeochem. Cycles* **13**, 997–1027 (1999).

ACKNOWLEDGMENTS

We thank the World Climate Research Programme's Working Group on Coupled Modelling, the U.S. Department of Energy's Program for Climate Model Diagnosis and Intercomparison, the Global Organization for Earth System Science Portals and climate modeling groups (see Fig. 3 legend for list) for CMIP and other model output; our three reviewers; and M. Irving and P. Zalazowski for assistance with the figures. S.L.L. is supported by the European Research Council (T-FORCES) and a Phillip Leverhulme Prize.

10.1126/science.aaa9932

REVIEW

Planted forest health: The need for a global strategy

M. J. Wingfield,[1]* E. G. Brockerhoff,[2] B. D. Wingfield,[1] B. Slippers[1]

Several key tree genera are used in planted forests worldwide, and these represent valuable global resources. Planted forests are increasingly threatened by insects and microbial pathogens, which are introduced accidentally and/or have adapted to new host trees. Globalization has hastened tree pest emergence, despite a growing awareness of the problem, improved understanding of the costs, and an increased focus on the importance of quarantine. To protect the value and potential of planted forests, innovative solutions and a better-coordinated global approach are needed. Mitigation strategies that are effective only in wealthy countries fail to contain invasions elsewhere in the world, ultimately leading to global impacts. Solutions to forest pest problems in the future should mainly focus on integrating management approaches globally, rather than single-country strategies. A global strategy to manage pest issues is vitally important and urgently needed.

Forests and woodland ecosystems are a hugely important natural resource, easily overlooked and often undervalued (*1*–*3*). Globally, one in six people is estimated to rely on forests for food (*3*), and many more depend on forests for other critical ecosystem services, such as climate regulation, carbon storage, human health, and the genetic resources that underpin important wood and wood products–based industries. However, the health of forests, both natural and managed, is more heavily threatened at present than ever before (*4*–*6*). The most rapidly changing of these threats arise from direct and indirect anthropogenic influences on fungal pathogens and insect pests (hereafter referred to as pests), especially their distribution and patterns of interactions.

Here we focus on the importance of pests of planted forests, which are particularly vulnerable to invasive organisms yet are of growing importance as an economic resource and for various ecosystem services. Planted forests are typically of a single species. In plantations in the tropics and Southern Hemisphere, they are usually of non-native species, such as species of *Pinus*, *Eucalyptus*, and *Acacia*. Northern Hemisphere plantations often comprise species of *Pinus*, *Picea*, *Populus*, *Eucalyptus*, and other genera, often in native areas or with closely related native species. These intensively managed tree farms cover huge areas [currently 7% and potentially 20% of global forests by the end of the century (*1*)], and they sustain major industries producing wood and pulp products. These tree genera have become natural resources of global importance, much like major agricultural crops, and are unlikely to be easily replaced.

Planted forests face various serious health threats from pests (Fig. 1). Non-native trees in plantations are in part successful because they have been separated from their natural enemies. However, when plantation trees are reunited with their coevolved pests, which may be introduced accidentally, or when they encounter novel pests to which they have no resistance, substantial damage or loss can ensue (*7*). The longer these non-native trees are planted in an area, the more threatened they become by native pests. Where the trees are of native species, they can be vulnerable to introduced pests. But the relative species uniformity of monoculture stands in intensively managed native plantation forests can make them especially susceptible to the many native pests occurring in the surrounding natural forests (*8*–*10*).

There are many opportunities to mitigate potential losses caused by pests in planted forests through exclusion (e.g., pre-export treatments and quarantine), eradication of newly established pests, and avoidance of disease through pest containment and management. Yet the lack of investment and capacity, especially in poorer countries, as well as the limited coordination of efforts at a global level, means that the impact of these tools to stem the global problem is limited. Unless this is addressed, pest problems will continue to grow and will threaten the long-term sustainability of forests and forestry worldwide. It should be recognized that the sustainable use of these tree "crops" will require the same global focus and investment to manage pest threat as that of agricultural crops.

Prevention is important but remains porous

Biological invasions of alien pests have been shown to be growing at constant or even increasing rates—and not only for those affecting trees (*4*–*6*, *11*). Few pests are ever eradicated or completely suppressed, leading to an ever-changing and increasing number of management programs to juggle. Phytosanitary measures are the major line of defense available to limit the global movement of pests, and various international policies seek to promote them [such as the International Standards For Phytosanitary Measures No. 15 (ISPM 15)

[1]Department of Genetics, Forestry and Agricultural Biotechnology Institute, University of Pretoria, Pretoria 0002, South Africa. [2]Scion (New Zealand Forest Research Institute), Post Office Box 23297, Christchurch 8540, New Zealand.
*Corresponding author. E-mail: mike.wingfield@fabi.up.ac.za

(*12*, *13*) that regulates the treatment of wood pallets to avoid bark beetle and wood borer invasions (*14*)].

There is evidence that strictly applied phytosanitary measures can reduce the rate of pest introductions into new environments (*12*, *14*), and this is the most cost-effective way to deal with the challenge. Some wealthy and biogeographically isolated countries in particular, such as New Zealand and Australia, have tackled this quite successfully (*15*). But there are limitations to what can be achieved realistically through phytosanitary measures at a global scale. For example, it is unlikely that poorer countries can afford to institute biosecurity actions to achieve effective exclusion to the same extent, and even where the best possible phytosanitary measures have been applied, serious new pest problems continue to occur. The accidental introduction of myrtle rust caused by *Puccinia psidii* into Australia, despite considerable knowledge of this pathogen and significant efforts to exclude it, is an apt example of the limitations of quarantine (*13*). This pathogen has now become established on many native Australian Myrtaceae, some of which are now threatened with extinction.

Traditionally, quarantine regulations have been underpinned by a listing process, in which pests threatening to a particularly country are listed after risk analyses. However, many of the most damaging forest pests introduced into new environments were unknown in their areas of origin before their introductions. For example, no listing process would have included *Phytophthora pinifolia*, which has devastated some *Pinus radiata* plantations in Chile (*16*), before its arrival. Its origin remains unknown. For this reason, contemporary thinking on phytosanitary measures has begun to focus on introduction pathways rather than on particular pests (e.g., the ISPM 15 measures discussed above) (*6*, *12*, *17*). In this regard, there is a growing realization that trade in live plants poses a particular threat that is inadequately regulated in most countries (*6*, *17*).

Quarantine can be only as effective as the proverbial weakest link in the chain. A large proportion of countries appear to have no effective quarantine in place for plants or plant products. Even where regulations are in place, the capacity to implement these effectively is often lacking. Therefore, invasive pest problems appear in these countries relatively frequently. Once a pest has become a successful invader in one region, it can serve as a source of new invasions elsewhere: a process that has been referred to as the bridgehead effect (*18*) (Fig. 2). A correlation is expected between the level of connectivity (e.g., the volume of trade) of a country and its vulnerability to invasion and potential to serve as a hub for the spread of invasive pests, but other factors also play a role in this regard (*5*–*7*).

Opportunities for mitigation

Despite the obstacles, there is reason to be optimistic about the power of established and emerging opportunities to mitigate the impact of pests. Intensive plantation forestry provides some vivid examples of how established pest problems can be confronted. To deal with the global scale and increasing intensity of the problem, however, greater global coordination and alignment of the use of the most effective tools are required.

Intensive management of forests increasingly involves planting tree species that have been selected for particular environments and traits, including resistance to certain pests. From a species base (taxa and provenance trails), it has been possible to breed and select for increasingly better properties.

One of the best examples of modern intensive tree farming is the global *Eucalyptus* forestry industry. Plantations of these trees now cover some 20 million ha, mostly in the tropics and Southern Hemisphere (*19*) (Fig. 1). *Eucalyptus* is mostly native to Australia, where more than 700 species are

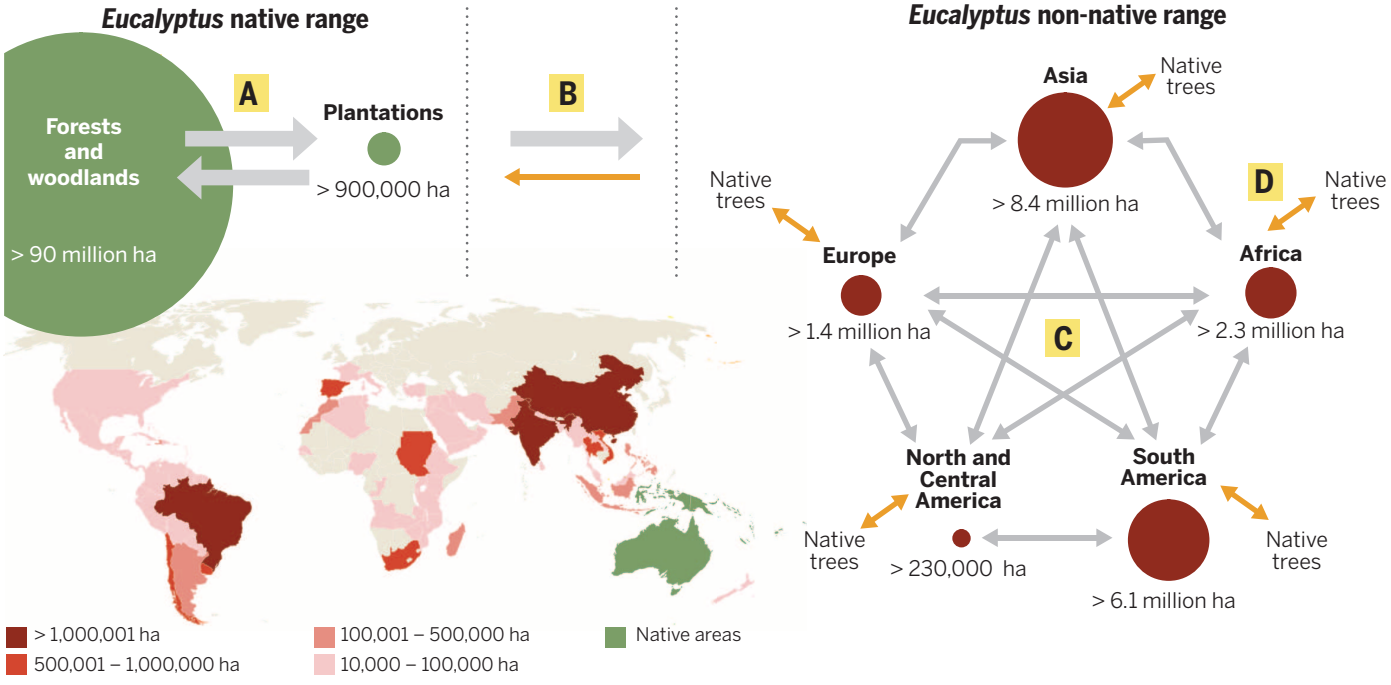

Fig. 1. *Eucalyptus* as a model to illustrate the origin and spread of planted forest pests. Plantations of *Eucalyptus* have increased from <1 million ha by 1950 to around 20 million ha today; the map shows the current distribution. These plantations experienced a steady increase of pest problems that has been accelerating during the past two decades. The origin of these pests can include the following: (**A**) Uninterrupted bidirectional spread of pests between natural and plantation areas of *Eucalyptus* in its native region. Increasing populations in plantations, and association with trade and human movement (e.g., from urban areas), increase changes in transport to other parts of the world. (**B**) Fairly large numbers of pests and pathogens spread from the native area to one or more non-native environments. Few pests spread via non-native plantations back to native *Eucalyptus* areas, but these can have devastating consequences [see, for example, the discussion on *Puccinia psidii* in the text (*13*)]. (**C**) As population numbers build up in some of the non-native environments, further movement around the world is enhanced through a bridgehead effect. The rate of this spread appears to be increasing because of the confluence of a number of processes linked to globalization (*18*, *22*) (Fig. 2). (**D**) Fairly large numbers of native pests and pathogens adapt to feed on or infect *Eucalyptus* in its non-native range. Some eventually spread to other areas of the world and can threaten *Eucalyptus* in its native range (B).

found in a wide range of environments, of which more than 10 and their hybrids are commonly planted commercially around the world today. This diversity of genetic background has provided opportunities to capture traits for fast growth in many different environments, favorable wood properties, and resistance to many different fungal and insect pests.

Vegetative propagation has underpinned the rapid growth of the *Eucalyptus* forestry industry—and similarly for poplars, pines, and acacias. Mastering vegetative propagation has made it possible to produce and intensively propagate hybrids between tree species, leading to a paradigm shift for the global forest plantation industry. It has also provided one of the most important opportunities to avoid pest problems.A classic example is the case of the stem disease known as Cryphonectria canker, now recognized to be caused by a suite of cryptic species in the fungal genus *Chrysoporthe* (*20*). In the early 1980s, Cryphonectria canker was a major threat to the sustainability of *Eucalyptus* propagation in Brazil and later South Africa. Yet the selection of clones and particularly clonal hybrids with resistance made it possible to avoid the disease to the point where it is hardly considered important today (*10*).

An approach that is increasingly contemplated is to promote resistance to pest threats by increasing diversity through mixed plantings of species rather than monocultures (*9*, *21*). From a managed forest perspective, this approach can be useful, but it is typically at odds with the needs of commercial forestry when done at a stand level. Nevertheless, introducing this form of resistance could be considered at a landscape level—for example, using clones in uniform but smaller blocks and including a diversity of genes rather than a diversity of species or even genotypes. Exploring the use of tree species and genera other than those currently used could offer further opportunities for mitigating the impact of pests and contribute to the resilience of the industry.

For introduced insect pests, biological control has provided superb solutions. Early examples of biological control in forestry date back to the early 1900s, using two introduced predators against the scale insect *Eriococcus coriaceus* on *Eucalyptus* in New Zealand and an egg parasitoid against the *Eucalyptus* snout beetle, known then as *Gonipterus scutellatus* (*22*). There have been many subsequent examples in planted forests, such as, for example, the widely applied *Sirex* woodwasp biological control using the parasitic nematode *Deladenus siricidicola* (*23*). Dealing with native insect pests is somewhat more complex, and in the absence of resistant planting stock, the application of biocides such as formulations of the insect pathogenic bacterium *Bacillus thuringiensis* and insect pathogens (e.g., *Beauvaria bassiana*) and behavior-altering semiochemical-based strategies provide opportunities (*24*, *25*). But there also remains a strong dependence on synthetic chemical insecticides that may be harmful to the environment and inconsistent with environmental certification (see http://pesticides.fsc.org).

Invest in research and innovation

Our capacity to deal with tree pest problems far outstrips the level of investment in exploring and applying these opportunities. At the outset of dealing with pest problems, we are challenged by our ability to accurately identify the pest in question. There are many examples where new pests appear that are misidentified or unknown elsewhere in the world. This is largely the result of poor or unequal levels of investment in global surveys and in our knowledge of global biodiversity. Hundreds of known pests and pathogens remain undetected, especially in poorer countries, and this problem is significantly more severe in forestry (*26*).

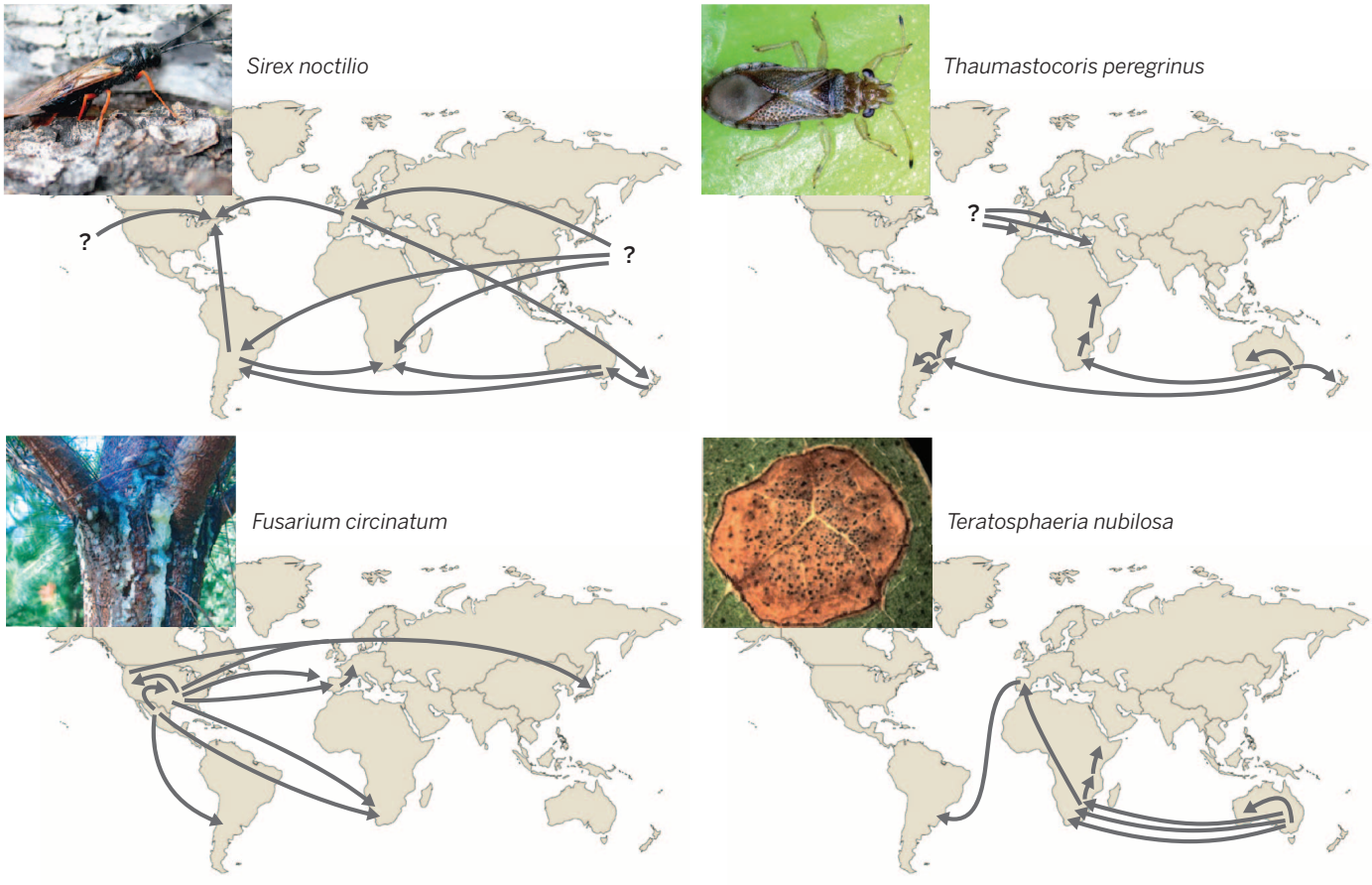

Fig. 2. Examples of invasion routes of pests of planted forests that illustrate an apparently common pattern of complex pathways of spread to new environments, including repeated introductions and with either native or invasive populations serving as source populations (*18*). Invasion routes of the pine pitch canker pathogen *Fusarium circinatum* (origin in Central America) (*39*), eucalypt leaf pathogen *Teratosphaeria nubilosa* (origin in southeast Australia) (*40*), the pine woodwasp *Sirex noctilio* (origin in Eurasia) (*23*), and the eucalypt bug *Thaumastocoris peregrinus* (origin in southeast Australia) (*41*) were determined through historical and genetic data. [Photo credits: (top left) Brett Hurley; (top right) Samantha Bush; (bottom left) Jolanda Roux; (bottom right) Guillermo Perez]

Table 1. The potential global use of various control strategies for forest pests in planted forests.

TOOLS FOR DEALING WITH FOREST PESTS	OPPORTUNITY FOR GLOBALIZATION*	POTENTIAL GLOBAL IMPACT*	CURRENT GLOBALIZATION*
Pest research tools			
Pest risk assessment			
Pest information database			
Pathway risk management			
National quarantine			
Surveillance tools			
Incursion response/eradication			
Biological control			
Genetic resources/breeding			
Genetic engineering			

*Yellow = low; Orange = medium; Red = high

Research on the identification and taxonomy of forest pests, and novel ways to speed up biodiversity discovery and description (*27*), should be promoted if we hope to deal with pest problems in the future. Ideally, such efforts will be integrated with the similar needs for agricultural pests, and even for human disease.

The application of DNA-based technologies to identify forest pests has shown that these organisms often represent cryptic species that are different from those originally thought to be present. For example, the Cryphonectria canker pathogen of *Eucalyptus* in South Africa was originally treated as being in the same genus as the fungus responsible for the devastating chestnut blight disease, *Cryphonectria parasitica*. DNA-based technologies, however, very clearly showed that the fungus on *Eucalyptus* is only distantly related to *C. parasitica*, and the disease is caused by at least four different species of *Chrysoporthe* (*20*). Their correct identification is essential for the selection of resistant *Eucalyptus* clones described earlier. We easily recognize that the accurate identification of pathogens is crucial to human health and well-being, and it is equally true for the health of forests and forestry. The barcoding and typing technologies that are already available allow for much greater levels of accuracy in disease diagnosis than is currently the case.

Research in molecular genetics, including the development of tools for accelerated breeding (including marker-aided selection and genetic engineering), is already well advanced, and the genomes of the most widely planted forest tree species either have been or are in the process of being sequenced (*28*, *29*). The recent approval of the release of a genetically engineered *Eucalyptus* is an important step toward this end (*30*). The application of this technology still faces significant regulatory and technical challenges but seems set to play a major role in the industry soon. In parallel, there are also growing numbers of genome sequences available or being determined for the most important pests of these trees (*31*). The availability of these genome sequences, as well as the rapid growth of associated phenotypic and other "-omics" data, will make it possible to better understand the biology and diversity of the pests, as well as their interactions with their host trees. The continuous emergence of previously unknown pests complicates these processes and highlights the need for identification of general mechanisms of resistance, as well as the continuing nature of this research.

Semiochemicals, which are naturally occurring chemicals that influence insect behavior, can be powerfully used for the surveillance and suppression of insect pests. This tool is underused in forestry in general, and in planted forests in particular (*25*), because of a lack of capacity to study the behaviorally active compounds of pest insects and a lack of investment in this promising field. Examining the genomics of forest pests could increase the speed of discovering promising alternatives through reverse chemical ecology (*32*).

There are many positive examples of biological control of invasive alien insect pests. However, many biological control programs for forest pests have been established on flimsy foundations. Although care is often taken today to avoid nontarget effects, biological control agents are often selected with little insight into possible ecological and evolutionary determinants of their success (*23*, *33*). They can also pose significant risks to native ecosystems through nontarget effects, a fact that is broadly recognized and typically tested for today. Admittedly, the tools to understand, for example, the genetic diversity of biological control agents were not previously readily available. But these and other tools are widely available today and should become standard practice for the development of biological control programs.

A category of pests that is emerging as important is that arising from adaptation after host shifts, symbiont shifts, or hybridization (*4*, *5*, *8*, *34*). Pathogens such as *Ceratocystis* spp. that have become adapted to infect forest trees, and the cossid moths *Coryphodema tristis* and *Chilicomadia valdiviana* that have emerged as serious pests of eucalypts in South Africa and Chile, are examples of emerging novel tree pests (*34*, *35*). Earlier we described the diseases caused by *P. psidii* and *Chrysophorthe* spp., which also resulted from host jumps from native plants to *Eucalyptus*. It is particularly important to understand the mechanisms and drivers of these changes, in light of the threat that these and other similar pests pose to native forests (Fig. 1).

Global versus local solutions

Forest pest problems, not only those relevant to planted forests, inevitably affect most or all areas where a particular tree species occurs. Yet these problems are typically being dealt with in an ad hoc and localized manner in response to local damage (Table 1). There are only a few examples where groups of forest scientists have been assembled to tackle particularly important problems at large scales. The European Union has launched a number of impressive programs in this regard, such as the COST Actions [www.cost.eu/COST_Actions/fps/Actions; see Santini *et al.* (*5*) for one of the outcomes related to invasive forest pathogens], to develop the networks necessary for a more coordinated approach to key problems.

The only means by which we can realistically deal with tree pests will be through the establishment of global networks of collaboration and to share locally available knowledge [see (*22*), on biological control). The structures for such networks exist in the International Union of Forest Research Organizations (www.iufro.org), for example, but funding instruments to enable a truly global approach are nonexistent for tree pests. Thus, the time is right to raise the issue of forest pest problems to the level of the United Nations—for instance, via the United Nations Forum on Forests (UNFF; www.un.org/esa/forests/)—and thus to seek intergovernmental support for a serious problem of global relevance.

Although most forest researchers would agree readily that global research collaborations hold the key to improving a clearly inadequate

capacity to deal with tree pest problems (not exclusive to managed and planted forests), answering the "who pays" question is much more challenging (*36*). Various models are in operation, but the answer most likely lies in collaborations between governments and the commercial sector. They would need to jointly take responsibility for preparedness and for the consequences of incursions, such as in the Government Industry Agreement for Biosecurity Readiness and Response in New Zealand (www.gia.org.nz/) or the Tree Protection Cooperative Program that has been jointly funded by the South African commercial sector, government, and university system for over 25 years. At present, however, it is clear that tree pest problems are made worse by the lack of clear global objectives, priorities, funding, and collaboration. This needs to be addressed, and externally supported where necessary, in developed and less-developed countries, because the overall goal will depend on a more uniform participation.

Outlook

The future of planted forests will be influenced by our ability to respond to damaging pests and the threat of biological invasions. The trends are clear, with at best a constant suite of emerging pests and sometimes a dramatically increasing rate of pest impacts. Increasing numbers of damaging hybrid genotypes and abiotic influences linked to global changes in the environment are further increasing the impact of these pests (*4*). It would be naïve to believe that local solutions such as quarantine at national borders can present a complete barrier to the global impact of pests on forests. For this reason, much greater focus will need to be placed on global strategies aimed at reducing pest movement and improving pest surveillance and incursion response, as well as optimizing the use of the most powerful tools to mitigate damage.

Genetics offers many outstanding opportunities to mitigate damage from pests, either alien invasive or native and that have undergone some form of adaptation. For managed forests and especially plantation forestry, traditional selection and breeding of species, provenances, clones, and clonal hybrids will increase in importance even further. Beyond this point, genetic engineering with genes conferring resistance to pests will be a valuable additional tool. Such genetic modification is already well advanced for *Eucalyptus* and poplar. They will also need to be managed with care, as has been true in agriculture, so as to avoid the development of resistance. The rapid decrease in the cost of generating relevant -omics data for nonmodel species, as well as inexpensive tools for gene editing such as CRISPR, will make these technologies available for more plant species sooner than previously anticipated (*37*). There are, however, valid concerns beyond the management of resistance that will require efficient platforms where the research community and various other societal interest groups can discuss the use of these technologies and collectively inform their regulation.

Pest problems in forests are well recognized and of considerable concern in many parts of the world, but this is not balanced with the investment that would be required to make a significant difference. This is a situation that should change, but funding and coordinated efforts from across a variety of disciplines and institutions would be needed to make this possible. For example, all the tools and much of the knowledge exist to develop an international database on the diversity of insects and fungi associated with trees used in plantations [there are various unlinked databases on pests and diseases, and with various levels of accessibility, that could be linked via a central database such as, for example, QBOL: Quarantine organisms Barcode Of Life (www.qbol.org)]. Such a database could be powerfully linked to metadata related to host use, natural enemies, climate, surveillance tools and information, and more.

It is not possible to predict which tree pest problems are likely to be most important and damaging in the future. The so-called unknown unknowns and black swan diseases will remain a challenge (*35*). The appearance of new pests can still surprise local industries and governments, and responses are often erratic and inadequate. Through a more coordinated global investment in relevant research, it should be possible to respond more rapidly and mitigate problems more effectively in the future. There are also increasing opportunities to capture the imagination and support of the public, to create awareness, and to expand the capacity for surveillance beyond the limited number of specialists, through the implementation of citizen science and crowdsourcing mechanisms.

Bill Gates recently called for new thinking about global systems to deal with human infectious disease problems in order to avoid a global health disaster (*38*). Although the situations for tree pests and human disease are not fully comparable, there are many similarities. Tree health specialists as well as funding agencies concerned with global tree health should learn from these. In particular, it should be recognized that although the impact of tree health disasters is experienced locally, the drivers of their emergence are global. This makes uncoordinated local efforts to slow the overall emergence all but futile. Our capacity to deal with serious tree pest problems will remain minimal unless we can find the support and vision to launch a more global and holistic approach to study these problems and to implement mitigation strategies.

A global strategy for dealing with pests in planted forests is urgently needed and should include:

- A clearly identified body with the mandate to coordinate and raise funds for global responses to key pests and to monitor compliance with regulations.
- A central database on pests and diseases of key forest plantation species.
- Shared information on tools for and information from the surveillance of pests and pathogens in planted forests.
- Identification of measures with potentially high global impact for pest mitigation, and support for the development and sharing of capacity.
- More-structured systems for facilitating biological control, including global sharing of knowledge, best practices, and the selection of agents (organisms).
- Protection of the genetic resources of the key forest plantation genera.

REFERENCES AND NOTES

1. E. G. Brockerhoff, H. Jactel, J. A. Parrotta, S. F. B. Ferraz, *For. Ecol. Manage.* **301**, 43–50 (2013).
2. K. N. Ninan, M. Inoue, *Ecol. Econ.* **93**, 137–149 (2013).
3. B. Vira, C. Wildburger, S. Mansourian, *IUFRO World Series* **33**, 1–172 (2015).
4. I. L. Boyd, P. H. Freer-Smith, C. A. Gilligan, H. C. J. Godfray, *Science* **342**, 1235773 (2013).
5. A. Santini *et al.*, *New Phytol.* **197**, 238–250 (2013).
6. B. A. Roy *et al.*, *Front. Ecol. Environ* **12**, 457–465 (2014).
7. M. J. Wingfield *et al.*, *Southern Forests* **70**, 139–144 (2008).
8. M. Branco, E. G. Brockerhoff, B. Castagneyrol, C. Orazio, H. Jactel, *J. Appl. Ecol.* **52**, 69–77 (2015).
9. H. Jactel, E. G. Brockerhoff, *Ecol. Lett.* **10**, 835–848 (2007).
10. M. J. Wingfield, *Australas. Plant Pathol.* **32**, 133–139 (2003).
11. M. C. Fisher *et al.*, *Nature* **484**, 186–194 (2012).
12. R. A. Haack *et al.*, *PLOS ONE* **9**, e96611 (2014).
13. L. Morin, R. Aveyard, J. R. Lidbetter, P. G. Wilson, *PLOS ONE* **7**, e35434 (2012).
14. E. G. Brockerhoff, M. Kimberley, A. M. Liebhold, R. A. Haack, J. F. Cavey, *Ecology* **95**, 594–601 (2014).
15. R. Eschen *et al.*, *Environ. Sci. Policy* **51**, 228–237 (2015).
16. A. Durán *et al.*, *Plant Pathol.* **57**, 715–727 (2008).
17. A. M. Liebhold, E. G. Brockerhoff, L. J. Garrett, J. L. Parke, K. O. Britton, *Front. Ecol. Environ* **10**, 135–143 (2012).
18. E. Lombaert *et al.*, *PLOS ONE* **5**, e9743 (2010).
19. Food and Agriculture Organization of the United Nations (FAO), *Global Forest Resource Assessment 2010* (FAO Forestry Paper 163, FAO, Rome, 2010).
20. M. Gryzenhout, H. Myburg, N. A. Van der Merwe, B. D. Wingfield, M. J. Wingfield, *Stud. Mycol.* **50**, 119–142 (2004).
21. R. A. Ennos, *Forestry* **88**, 41–52 (2015).
22. J. R. Garnas, B. P. Hurley, B. Slippers, M. J. Wingfield, *Int. J. Pest Manage.* **58**, 211–223 (2012).
23. B. Slippers, B. P. Hurley, M. J. Wingfield, *Annu. Rev. Entomol.* **60**, 601–619 (2015).
24. L. G. Copping, J. J. Menn, *Pest Manag. Sci.* **56**, 651–676 (2000).
25. R. L. Nadel, M. J. Wingfield, M. C. Scholes, S. A. Lawson, B. Slippers, *Ann. For. Sci.* **69**, 757–767 (2012).
26. D. P. Bebber, T. Holmes, D. Smith, S. J. Gurr, *New Phytol.* **202**, 901–910 (2014).
27. D. R. Maddison, R. Guralnick, A. Hill, A.-L. Reysenbach, L. A. McDade, *Trends Ecol. Evol.* **27**, 72–77 (2012).
28. A. A. Myburg *et al.*, *Nature* **510**, 356–362 (2014).
29. A. Zimin *et al.*, *Genetics* **196**, 875–890 (2014).
30. Anon., *Science* **348**, 264 (2015).
31. R. C. Hamelin, *Can. J. Plant Pathol.* **34**, 20–28 (2012).
32. K. P. Jayanthi *et al.*, *BMC Genomics* **15**, 209 (2014).
33. X. Fauvergue, E. Vercken, T. Malausa, R. A. Hufbauer, *Evol. Appl.* **5**, 424–443 (2012).
34. M. J. Wingfield, B. Slippers, B. D. Wingfield, *N. Z. J. For. Sci.* **40**, S95–S103 (2010).
35. R. C. Ploetz, J. Hulcr, M. J. Wingfield, Z. W. de Beer, *Plant Dis.* **97**, 856–872 (2013).
36. J. Hantula, M. M. Muller, J. Uusivuori, *Environ. Sci. Policy* **37**, 158–160 (2014).
37. H. Ledford, *Nature* **522**, 20–24 (2015).
38. B. Gates, *N. Engl. J. Med.* **372**, 1381–1384 (2015).
39. M. Berbegal, A. Pérez-Sierra, J. Armengol, N. J. Grünwald, *Phytopathology* **103**, 851–861 (2013).
40. G. C. Hunter, P. W. Crous, A. J. Carnegie, M. J. Wingfield, *Mol. Plant Pathol.* **10**, 1–14 (2009).
41. R. L. Nadel *et al.*, *Biol. Invasions* **12**, 1067–1077 (2010).

ACKNOWLEDGMENTS

We thank members of the Tree Protection Co-operative Programme (TPCP); the National Research Foundation (NRF); and the Departments of Trade and Industry (DTI), Water Affairs and Forestry (DAFF), and Science and Technology (DST) of South Africa for support. Contributions by E.G.B. were supported by Ministry of Business, Innovation, and Employment core funding to Scion. We also thank many colleagues for sharing their perspectives with us regarding the health of forests internationally. The views expressed in this paper are our own.

10.1126/science.aac6674

RESEARCH

Nuclear spins simulate complex materials

Alvarez et al., *p. 846*

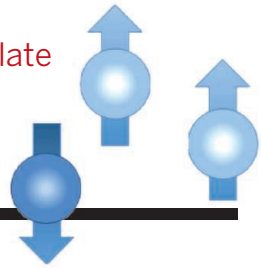

IN *SCIENCE* JOURNALS

Edited by **Nick Wigginton**

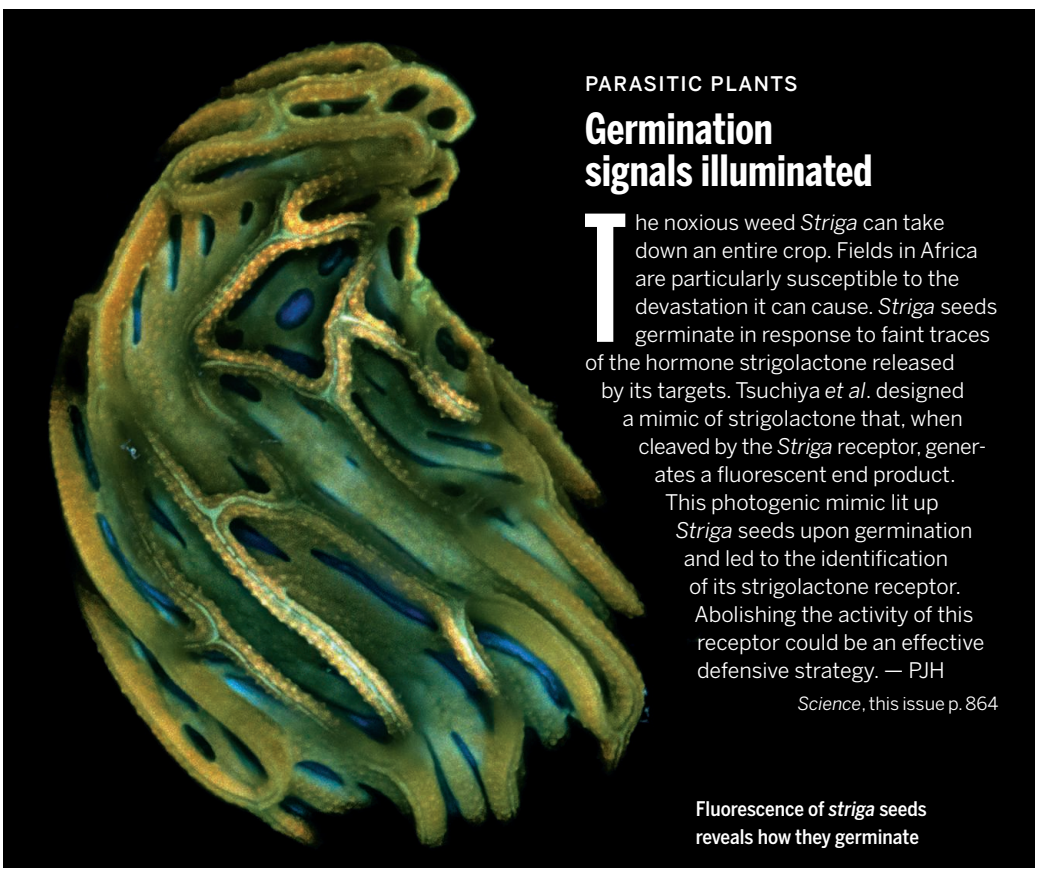

PARASITIC PLANTS

Germination signals illuminated

The noxious weed *Striga* can take down an entire crop. Fields in Africa are particularly susceptible to the devastation it can cause. *Striga* seeds germinate in response to faint traces of the hormone strigolactone released by its targets. Tsuchiya *et al*. designed a mimic of strigolactone that, when cleaved by the *Striga* receptor, generates a fluorescent end product. This photogenic mimic lit up *Striga* seeds upon germination and led to the identification of its strigolactone receptor. Abolishing the activity of this receptor could be an effective defensive strategy. — PJH

Science, this issue p. 864

Fluorescence of *striga* seeds reveals how they germinate

TRANSCRIPTION

Transcription factor shape-shifts DNA

Controlling when a gene is expressed or repressed is vital for cellular metabolism and development. In *Escherichia coli*, a copper-sensing transcription factor, CueR, can repress or activate expression when bound at exactly the same site in the gene promoter. Philips *et al.* used x-ray crystallography to show that CueR dramatically changes the topology of the DNA upon binding copper but does not affect protein-DNA contacts. The DNA shape change allows RNA polymerase to bind the promoter and transcribe the gene. — GR

Science, this issue p. 877

ASTROPHYSICS

Limiting unknowns in the dark side

Our knowledge of the inventory of stuff that makes up our universe amounts to a humbling 5%. The rest consists of either dark energy (~70%) or dark matter (~25%). Using atom interferometry, Hamilton *et al.* describe the results of experiments that controlled for dark energy screening mechanisms in individual atoms, not bulk matter. Aprile *et al.* report on an analysis of data taken with the XENON100 detectors aiming to identify dark matter particles directly by monitoring their rare interaction with ordinary matter. In this setup, a large underground tank of liquid xenon forms a target for weakly interacting m assive particles. These combined results set limits on several types of proposed dark matter and dark energy candidates (see the Perspective by Schmiedmayer and Abele). — ISO

Science, this issue p. 849, p. 851; see also p. 786

QUANTUM GASES

Making interacting atoms localize

Disorder can stop the transport of noninteracting particles in its tracks. This phenomenon, known as Anderson localization, occurs in disordered solids, as well as photonic and cold atom settings. Interactions tend to make localization less likely, but disorder, interactions, and localization may coexist in the so-called many-body localized state. Schreiber *et al*. detect many-body localization in a one-dimensional optical lattice initially filled with atoms occupying alternating sites. Externally induced disorder and interactions prevented the system from evolving quickly to a state with a single atom on each site. — JS

Science, this issue p. 842

HUMAN IMPACTS

An anomalous and unbalanced predator

In the past century, humans have become the dominant predator across many systems. The species that we target are thus far in considerable decline; however, predators in the wild generally achieve a balance with their prey populations such that both persist. Darimont *et al*. found several specific differences between how humans and other predatory species target prey populations (see the Perspective by Worm). In marine environments, for example, we regularly prey on other predator species. These differences may contribute to our much larger ecological

IMAGES: (TOP TO BOTTOM) ALVAREZ *ET AL.*; YOSHIKATSU SATO/LIVE IMAGING CENTER/INSTITUTE OF TRANSFORMATIVE BIO-MOLECULES

impact when compared with other predators. — SNV

Science, this issue p. 858; see also p. 784

SIGNAL TRANSDUCTION

Membrane potential regulates growth

Changes in electrical potential across the plasma membrane can affect cell growth. Zhou *et al*. discovered that membrane potential influenced the organization of phospholipids in the membrane of cultured mammalian cells and neurons in intact flies (see the Perspective by Accardi). This in turn regulated localization and activity of the small guanine nucleotide binding protein K-Ras, an important regulator of cell proliferation. The cell membrane may thus function analogously to a field-effect transistor by adjusting the strength of mitogenic signaling. — LBR

Science, this issue p. 873; see also p. 789

BIOCHEMICAL PROCESSES

Protonation by "Newton's cradle"

Imagine raising the ball on one end of a Newton's cradle. Upon release and the subsequent collision, the ball at the other end of the device flips up in response. Using high-resolution neutron diffraction, Nakamura *et al*. discovered an enzymatic proton relay chain that may operate in much the same fashion. In a glycoside hydrolase from the mushroom *Phanerocaete chrysosporium*, protons are relayed along a structure created by the enzyme from a distant asparagine to the catalytic asparagine through sequential tautomerizations. — PLY

Sci. Adv. 10.1126/sciadv.1500263 (2015)

PLANT MICRIOBIOME

Immune signals shape root communities

To thwart microbial pathogens aboveground, the plant *Arabidopsis* turns on defensive signaling using salicylic acid. In *Arabidopsis* plants with modified immune systems, Lebeis *et al*. show that bacterial communities change in response to salicylic acid signaling in the root zone as well (see the Perspective by Haney and Ausubel). Abundance of some root-colonizing bacterial families increased at the expense of others, partly as a function of whether salicylic acid was used as an immune signal or as a carbon source for microbial growth. — PJH

Science, this issue p. 860; see also p. 788

ASTHMA

A tale of two asthmas

Classifying diseases according to symptoms is rapidly becoming an outmoded practice. Targeted therapeutics have shown that sets of symptoms can be caused by different pathogenic mechanisms. Choy *et al*. demonstrate that asthma can be divided into three immunological clusters—T_H2-high, T_H17-high, and T_H2-T_H17-low. The T_H2-high and T_H17-high clusters inversely correlate in a mouse model of asthma, whereby neutralizing one signature promoted the other. Combination therapies targeting both pathways might better treat asthmatic individuals. — ACC

Sci. Transl. Med. **7**, 301ra129 (2015)

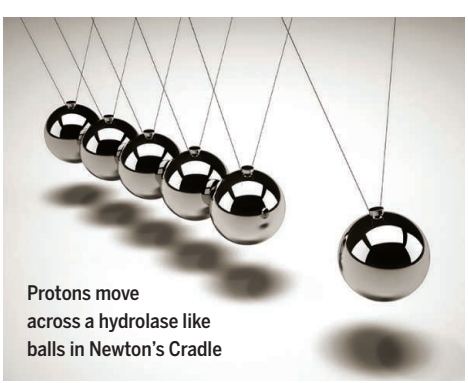

Protons move across a hydrolase like balls in Newton's Cradle

PHOTOS: (LEFT TO RIGHT) ORLA/ISTOCK; W.-K. LEE *ET AL*.

IN OTHER JOURNALS

Edited by **Kristen Mueller** *and* **Jesse Smith**

Hierarchical wrinkles made by three generations of sequential wrinkling

MATERIALS SCIENCE

When wrinkling is a good thing

A common feature of gecko feet, which show strong adhesion to many surfaces, and the lotus leaf, which can repel water, is a hierarchical, patterned surface that extends across many length scales with controlled regions of order and disorder. Textured surfaces can be synthetically mimicked, but can require complex lithographic methods to make. Lee *et al.* use a hierarchical wrinkling approach to achieve large-scale patterning, where both the wavelength and orientation of previous-generation wrinkles can be preserved and built upon. Reactive ion etching creates a skin layer on a polystyrene substrate, leading to wrinkling. By adjusting the etching time, they control the wavelength of the wrinkles, with the orientation tuned by prestretching the substrate in one or two directions. — MSL

Nano Lett. 10.1021/acs.nanolett.5b02394 (2015).

MEMBRANE PROTEINS

Probing the activity of two proteases

Presinilin (PS), the transmembrane catalytic subunit of the enzyme γ-secretase, is a drug target of high interest. This is because it cleaves both amyloid precursor protein, which is implicated in Alzheimer's disease, and Notch, a protein involved in several cancers. How potential therapeutics may affect related proteins, such as signal peptide peptidase (SPP), an enzyme that has an active site similar to that of PS, is unclear. To

investigate this, Gertsik *et al*. designed photolabeled molecular probes that targeted different parts of the catalytic subpockets of the enzymes. Comparing the labeling profiles of the probes revealed important similarities and differences between the two enzymes. Scientists should take into account such cross-talk as drug development proceeds. — VV

ACS Chem. Biol. 10.1021/acschembio.5b00321 (2015).

MICROBIAL COMMUNITIES

Abundant microbes hiding in plain sight

Natural microbial communities are frustratingly complex—even with the advent of powerful metagenomic tools. Overlooked abundant organisms often result in an incomplete view of the metabolic processes that affect major geochemical cycles. Hug *et al*. developed a subsampling metagenomic assembly technique which, when combined with metaproteomics, reveals a preponderance of highly abundant, novel microbial lineages in subsurface sediments at an old uranium mill tailings site. These organisms cycle carbon, nitrogen, and sulfur through unanticipated pathways. For example, despite low ammonium concentrations in the aquifer, the most abundant community member in the sediment is an ammonium-oxidizing archaeon that partially utilizes ammonium produced by nitrate-reducing bacteria. — NW

Environ. Microbiol. **17**, 10.1111/1462-2920.12930 (2015).

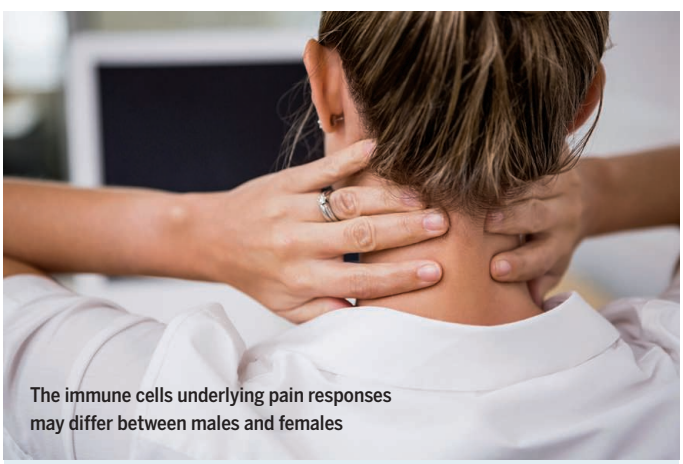

The immune cells underlying pain responses may differ between males and females

NEUROIMMUNOLOGY

For females, a different path to pain

Chronic pain affects more women than men. To better understand why, Sorge *et al*. compared the mechanisms that underlie neuropathic pain in male and female mice. Previous studies suggested that immune cells called microglia trigger pain sensitivity in response to nerve injury. Surprisingly, blocking microglia genetically or pharmacologically reduced pain in male but not in female mice. This sex-specific response depended on testosterone—blocking microglia alleviated pain in testosterone-treated females but not in castrated mice. Lymphocytes, rather than microglia, appeared to promote pain in female mice. These results suggest that scientists may need to examine sex-specific responses when testing new treatments for pain and other neurological diseases involving immune cells. — KLM

Nat. Neurosci. **18**, 1081 (2015).

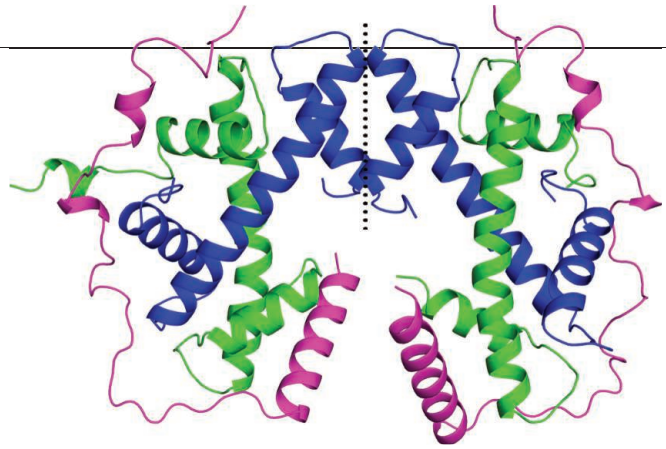

Structure of the MCM2 histone binding domain–histones H3–H4 tetramer complex

GENETICS

Copying chromatin to ensure identity

When cells divide, they must replicate both their DNA sequence and the chromatin state of their genome to maintain their identity. Huang *et al*. use structural and biochemical analyses to show how a central component of the human DNA replication machinery, the minichromsome maintenance (MCM) helicase, helps chaperone histones (proteins that package DNA into structures called nucleosomes) from old nucleosomes disassembled ahead of the replication fork to new ones formed behind the fork. The MCM2 subunit works with another histone chaperone, ASF1, to bind both old and new histones, together with variant histones, such as those from the centromeres. In this way, the cell likely ensures the accurate copying of chromatin as well as DNA. — GR

Nat. Struct. Mol. Biol. 10.1038/nsmb.3055 (2015).

GENETICS

How starving affects you and yours

Malnourished children are at higher risk for type 2 diabetes, cancer, and cardiovascular disease later in life. Some scientists hypothesize that this is because early-life experiences prime the body for such encounters later in life. Jobson *et al*. used the roundworm *Caenorhabditis elegans* to study this phenomenon. They observed that worms starved early in life were smaller and produced fewer offspring compared to normally fed worms. But the effects did not stop there: Progeny and grandprogeny of starved parents could better resist starvation, and resistance to heat stress persisted for three generations. These results suggest that at least in worms, early stress may be adaptive in an unpredictable environment. — LMZ

Genetics 10.1534/genetics.115.178699 (2015).

EDUCATION

What does one know and not know?

To demonstrate understanding, students need to answer questions correctly, as well as understand why those answers are correct. Lindsey and Nagel examine this metacognition, specifically students' ability to differentiate between questions for which they know the answer and questions that they cannot correctly answer. A knowledge survey mimicking a final exam was used to collect student data. Analysis at the level of students' overall scores showed that students in the lower third of the class misjudged their abilities, whereas students in the top third were better calibrated. However, at the level of individual questions, there was no difference between student level and the ability to identify questions they could answer correctly, suggesting that students at all levels could benefit from metacognitive awareness training. — MM

Phys. Rev. 10.1103/physrevstper.11.020103 (2015).

ALSO IN *SCIENCE* JOURNALS

Edited by **Nick Wigginton**

TRANSCRIPTION

Keeping gene transcription in check

Transcription of all genes is carried out by RNA polymerase (RNAP). The enzyme is thus a pivotal regulation point for many cell and developmental processes. In bacteria, sigma factors play a vital role in transcription regulation, with σ54 being critical for transcription of many stress response genes. Yang *et al.* determined the x-ray crystal structure of RNAP bound to σ54, as well as promoter DNA. In the initial inhibited state of the RNAP-σ54 complex, the σ54 blocks the template DNA from entering the RNAP active site and the downstream DNA channel. — GR

Science, this issue p. 882

POPULATION GENETICS

Genetic history of Native Americans

Several theories have been put forth as to the origin and timing of when Native American ancestors entered the Americas. To clarify this controversy, Raghavan *et al*. examined the genomic variation among ancient and modern individuals from Asia and the Americas. There is no evidence for multiple waves of entry or recurrent gene flow with Asians in northern populations. The earliest migrations occurred no earlier than 23,000 years ago from Siberian ancestors. Amerindians and Athabascans originated from a single population, splitting approximately 13,000 years ago. — LZ

Science, this issue p. 841

RNA SPLICING

Regulation of splicing regulators

The messenger RNAs of most eukaryotic genes are formed by splicing together a series of exons and removing the intervening introns. The identity and order of the exons can vary between mRNAs for the same gene. The alternatively spliced products can generate an increased diversity of protein products. Gueroussov *et al*. show that the alternative splicing of a mammalian splicing regulatory factor affects, in turn, the alternative splicing of a wide range of target RNAs. This regulation mechanism controls a brain-specific alternative splicing program. —GR

Science, this issue p. 868

ECOLOGICAL THEORY

A model for who eats and who is eaten

There are many types of interactions between those that eat and those that are eaten. A multitude of theoretical equations describe these dynamics, from predator and prey to parasite and host. Lafferty *et al*. show that all forms of these relationships come down to fundamental consumer-resource interactions. Derived from the myriad complex interactions, a simple model can accommodate any such interaction, simplifying past models into a general theory of eat and be eaten. — SNV

Science, this issue p. 854

QUANTUM SIMULATION

The dynamics of dipolar interactions

Well-controlled systems, such as cold atomic gases, can simulate more complicated materials. Applying this quantum simulation concept to the study of magnetism, Alvarez *et al*. add an interesting twist. Instead of cold atoms, a network of nuclear spins of hydrogen in polycrystalline adamantane serves as a simulator. Using nuclear magnetic resonance techniques, the authors could induce a transition from a state in which all spins coupled to each other to a state in which coherent spins grouped into clusters. — JS

Science, this issue p. 846

CANCER

Inhibiting two pathways is better than one

The ERK and JNK pathways are mitogen-activated protein kinase pathways that can be hijacked by cancer cells. Many melanoma patients have activating mutations in an upstream kinase in the ERK pathway, but its inhibitors produce only short-term improvement in these patients. Ramsdale *et al*. show that increased levels of a transcription factor activated by the JNK pathway were responsible for inhibitor resistance in the ERK pathway and contributed to metastatic potential. ERK kinase inhibitors were more effective at killing melanoma cells in culture and in mice if transcription cofactor levels or their activation by the JNK pathway also decreased. — LKF

Sci. Signal. **8**, ra82 (2015).

RESEARCH ARTICLE

POPULATION GENETICS

Genomic evidence for the Pleistocene and recent population history of Native Americans

Maanasa Raghavan,[1]* Matthias Steinrücken,[2,3,4]* Kelley Harris,[5]* Stephan Schiffels,[6]* Simon Rasmussen,[7]* Michael DeGiorgio,[8]* Anders Albrechtsen,[9]* Cristina Valdiosera,[1,10]* María C. Ávila-Arcos,[1,11]* Anna-Sapfo Malaspinas,[1]* Anders Eriksson,[12,13] Ida Moltke,[9] Mait Metspalu,[14,15] Julian R. Homburger,[11] Jeff Wall,[16] Omar E. Cornejo,[17] J. Víctor Moreno-Mayar,[1] Thorfinn S. Korneliussen,[1] Tracey Pierre,[1] Morten Rasmussen,[1,11] Paula F. Campos,[1,18] Peter de Barros Damgaard,[1] Morten E. Allentoft,[1] John Lindo,[19] Ene Metspalu,[14,15] Ricardo Rodríguez-Varela,[20] Josefina Mansilla,[21] Celeste Henrickson,[22] Andaine Seguin-Orlando,[1] Helena Malmström,[23] Thomas Stafford Jr.,[1,24] Suyash S. Shringarpure,[11] Andrés Moreno-Estrada,[11,25] Monika Karmin,[14,15] Kristiina Tambets,[14] Anders Bergström,[6] Yali Xue,[6] Vera Warmuth,[26,27] Andrew D. Friend,[28] Joy Singarayer,[29] Paul Valdes,[30] Francois Balloux,[26] Ilán Leboreiro,[21] Jose Luis Vera,[31] Hector Rangel-Villalobos,[32] Davide Pettener,[33] Donata Luiselli,[33] Loren G. Davis,[34] Evelyne Heyer,[35] Christoph P. E. Zollikofer,[36] Marcia S. Ponce de León,[36] Colin I. Smith,[10] Vaughan Grimes,[37,38] Kelly-Anne Pike,[37] Michael Deal,[37] Benjamin T. Fuller,[39] Bernardo Arriaza,[40] Vivien Standen,[41] Maria F. Luz,[42] Francois Ricaut,[43] Niede Guidon,[42] Ludmila Osipova,[44,45] Mikhail I. Voevoda,[44,46,47] Olga L. Posukh,[44,45] Oleg Balanovsky,[48,49] Maria Lavryashina,[50] Yuri Bogunov,[48] Elza Khusnutdinova,[51,52] Marina Gubina,[44] Elena Balanovska,[49] Sardana Fedorova,[53,54] Sergey Litvinov,[14,51] Boris Malyarchuk,[55] Miroslava Derenko,[55] M. J. Mosher,[56] David Archer,[57] Jerome Cybulski,[58,59,60] Barbara Petzelt,[61] Joycelynn Mitchell,[61] Rosita Worl,[62] Paul J. Norman,[63] Peter Parham,[63] Brian M. Kemp,[17,64] Toomas Kivisild,[14,65] Chris Tyler-Smith,[6] Manjinder S. Sandhu,[6, 66] Michael Crawford,[67] Richard Villems,[14,15] David Glenn Smith,[68] Michael R. Waters,[69,70,71] Ted Goebel,[69] John R. Johnson,[72] Ripan S. Malhi,[19,73] Mattias Jakobsson,[23] David J. Meltzer,[1,74] Andrea Manica,[12] Richard Durbin,[6] Carlos D. Bustamante,[11] Yun S. Song,[2,3,75]† Rasmus Nielsen,[75]† Eske Willerslev[1]†

How and when the Americas were populated remains contentious. Using ancient and modern genome-wide data, we found that the ancestors of all present-day Native Americans, including Athabascans and Amerindians, entered the Americas as a single migration wave from Siberia no earlier than 23 thousand years ago (ka) and after no more than an 8000-year isolation period in Beringia. After their arrival to the Americas, ancestral Native Americans diversified into two basal genetic branches around 13 ka, one that is now dispersed across North and South America and the other restricted to North America. Subsequent gene flow resulted in some Native Americans sharing ancestry with present-day East Asians (including Siberians) and, more distantly, Australo-Melanesians. Putative "Paleoamerican" relict populations, including the historical Mexican Pericúes and South American Fuego-Patagonians, are not directly related to modern Australo-Melanesians as suggested by the Paleoamerican Model.

It is generally agreed that ancestral Native Americans are descendants of Siberian peoples who traversed the Bering Land Bridge (Beringia) from northeast Asia in Late Pleistocene times, and although consensus has yet to be reached, it is mostly conceded that the Clovis archaeological complex, dating to ~13 thousands years ago (ka), does not represent the first migration as long supposed (*1*–*7*). Archaeological evidence accumulated over the past two decades indicates that people were south of the North American continental ice sheets more than a millennium earlier and had reached as far south as southern South America by at least ~14.6 ka (*1*–*3*). Interpretations differ, however, regarding the precise spatiotemporal dynamics of the peopling process, owing to archaeological claims for a substantially earlier human presence predating the Last Glacial Maximum (LGM) (~20 ka) (*8*–*10*) and conflicting interpretations of the number and timing of migrations from Beringia based on anatomical and genetic evidence (*11*–*16*). Much of the genetic evidence is from studies of mitochondrial DNA (mtDNA) and Y chromosome, which as single, uniparentally inherited loci are particularly subject to genetic drift and sex-biased demographic and cultural practices.

Among the principal issues still to be resolved regarding the Pleistocene and recent population history of Native Americans are (i) the timing of their divergence from their Eurasian ancestors; (ii) whether the peopling was in a single wave or multiple waves and, consequently, whether the genetic differences seen between major subgroups of Native Americans (such as Amerindian and Athabascan) result from different migrations or in situ diversification in the Americas (*5*, *6*, *17*, *18*); (iii) whether the migration involved ~15,000 years of isolation in the Bering Strait region, as proposed by the Beringian Incubation Model to explain the high frequency of distinct and widespread American mitogenomes and private genetic variants (*19*–*22*); and last, (iv) whether there was post-divergence gene flow from Eurasia and possibly even population replacement in the Americas, the latter suggested by the apparent differences in skull morphology between some early ("Paleoamerican") remains and those of more recent Native Americans (*23*–*27*). We address these issues using genomic data derived from modern populations, supplemented by ancient specimens that provide chronologically controlled snapshots of the genetics of the peopling process as it unfolded.

We sequenced 31 genomes from present-day individuals from the Americas, Siberia, and Oceania to an average depth of ~20×: Siberians—Altai (n = 2), Buryat (n = 2), Ket (n = 2), Koryak (n = 2), Sakha (n = 2), and Siberian Yupik (n = 2); North American Native Americans—Tsimshian (n = 1); southern North American and Central and South American Natives—Pima (n = 1), Huichol (n = 1), Aymara (n = 1), and Yukpa (n = 1); and Oceanians—Papuan (n = 14) (table S1) (*28*). All the genome-sequenced present-day individuals were previously genotyped by using single-nucleotide polymorphism (SNP) chips (*4*, *29*–*35*) except for the Aymara individual, which was SNP chip–genotyped in this study (tables S3 and S4). They were selected on the basis of their ancestry profiles obtained with ADMIXTURE (*36*) so as to best represent their respective populations and to minimize recent genetic admixture from populations of western Eurasian origin (*28*). For populations represented by more than one individual, we also verified from the genotype data that the sequenced individuals did not represent close relatives (*28*). We additionally sequenced 23 genomes from ancient individuals dating between ~0.2 and 6 ka from North and South America, with an average depth ranging between 0.003× and 1.7×, including specimens affiliated to putative relict Paleoamerican groups such as the Pericúes from Mexico and Fuego-Patagonians from the southernmost tip of South America (table S5) (*23*, *26*–*28*). Last, we generated SNP chip genotype data from 79 present-day individuals belonging to 28 populations from the Americas and Siberia (table S4) (*28*). All the

aforementioned data sets were analyzed together with previously published genomes and SNP chip genotype data (tables S1, S3, and S4), masking the data for recent European admixture in some present-day Native American populations (*28*).

The structure of Native American populations and the timing of their initial divergence

We explored the genetic structure of Native American populations in the context of worldwide populations using ADMIXTURE (*36*), using a reference panel consisting of 3053 individuals from 169 populations (table S3) (*28*). The panel included SNP chip genotype data from present-day individuals generated in this study and previously published studies, as well as the 4000-year-old Saqqaq individual from Greenland (*29*) and the 12,600-year-old Anzick-1 (Clovis culture) individual from Montana (table S3) (*5*). When assuming the number of ancestral populations (K) to be four ($K = 4$), we found a Native American–specific genetic component, indicating a shared genetic ancestry for all Native Americans, including Amerindians and Athabascans (fig. S4). Assuming $K = 15$, there is structure within the Native Americans. Athabascans and northern Amerindians (primarily from Canada) differ from the rest of the Native Americans in sharing their own genetic component (fig. S4). As reported previously, Anzick-1 falls within the genetic variation of southern Native Americans (*5*), whereas the Saqqaq individual shares genetic components with Siberian populations (fig. S4) (*29*).

To ascertain the population history of present-day Native American populations in relation to worldwide populations, we generated admixture graphs with TreeMix (*28*, *37*). All of the modern Siberian and Native American genomes sequenced in this study, except for the North American Tsimshian genome that showed evidence of recent western Eurasian admixture (*28*), were used for this analysis, together with previously published genomes from Africa (Yoruba) (*38*), Europe (Sardinian and French) (*38*), East Asia (Dai and Han) (*38*), Siberia (Nivkh) (*39*) and the Americas (Karitiana, Athabascan, and Greenlandic Inuit) (table S1) (*5*, *38*, *39*). The ancient individuals included in the analysis were Saqqaq, Anzick-1, and the 24,000-year-old Mal'ta child from south-central Siberia (*4*). By use of TreeMix, we affirmed that all Native Americans form a monophyletic group across all 10 migration parameter values, with further diversification into two branches, one representing Amerindians (represented in this analysis by Amerindians from southern North America and Central and South America) and the other representing Athabascans (Fig. 1B and fig. S5). Paleo-Eskimos and Inuit were supported as a separate clade relative to the Native Americans, as reported previously (Fig. 1B and fig. S5) (*29*, *39*). Our results show that the Siberian Yupik and Koryak are the closest Eurasian populations to the Americas, with the Yupik likely representing back-migration of the Inuit into Siberia (Fig. 1B and fig. S5).

To assess the pattern of the earliest human dispersal into the Americas, we estimated the timing of the divergence of ancestral Native Americans from East Asians (hereafter, including Siberians) using multiple methods. There is still some debate regarding mutation rates in the human genome (*40*), and this uncertainty could affect our estimates and results.

We applied diCal2.0 (method 1) (*28*), a new version of diCal (*41*) extended to handle complex demographic models involving multiple populations with migration (*42*), and an identity-by-state (IBS) tract method (method 2) (*43*) (supplementary materials, materials and methods 2) to the modern genomes data set (*28*). With these, we

[1]Centre for GeoGenetics, Natural History Museum of Denmark, University of Copenhagen, Øster Voldgade 5–7, 1350 Copenhagen, Denmark. [2]Computer Science Division, University of California, Berkeley, Berkeley, CA 94720, USA. [3]Department of Statistics, University of California, Berkeley, Berkeley, CA 94720, USA. [4]Department of Biostatistics and Epidemiology, University of Massachusetts, Amherst, MA 01003, USA. [5]Department of Mathematics, University of California, Berkeley, Berkeley, CA 94720, USA. [6]Wellcome Trust Sanger Institute, Wellcome Trust Genome Campus, Hinxton CB10 1SA, UK. [7]Center for Biological Sequence Analysis, Department of Systems Biology, Technical University of Denmark, Kemitorvet, Building 208, 2800 Kongens Lyngby, Denmark. [8]Departments of Biology and Statistics, Pennsylvania State University, 502 Wartik Laboratory, University Park, PA 16802, USA. [9]The Bioinformatics Centre, Department of Biology, University of Copenhagen, Ole Maaløes Vej 5, 2200 Copenhagen, Denmark. [10]Department of Archaeology and History, La Trobe University, Melbourne, Victoria 3086, Australia. [11]Department of Genetics, School of Medicine, Stanford University, 300 Pasteur Drive, Lane Building, Room L331, Stanford, CA 94305, USA. [12]Department of Zoology, University of Cambridge, Downing Street, Cambridge CB2 3EJ, UK. [13]Integrative Systems Biology Laboratory, King Abdullah University of Science and Technology (KAUST), Thuwal, 23955-6900, Kingdom of Saudi Arabia. [14]Estonian Biocentre, Evolutionary Biology Group, Tartu 51010, Estonia. [15]Department of Evolutionary Biology, University of Tartu, Tartu 51010, Estonia. [16]Institute for Human Genetics, University of California San Francisco, 513 Parnassus Avenue, San Francisco, CA 94143, USA. [17]School of Biological Sciences, Washington State University, Post Office Box 644236, Heald 429, Pullman, WA 99164, USA. [18]Centro de Investigación en Ciencias del Mar y Limnología/Centro Interdisciplinar de Investigação Marinha e Ambiental, Centro Interdisciplinar de Investigação Marinha e Ambiental, Universidade do Porto, Rua dos Bragas 289, 4050-123 Porto, Portugal. [19]Department of Anthropology, University of Illinois at Urbana-Champaign, 607 S. Mathews Avenue, Urbana, IL 61801, USA. [20]Centro Mixto, Universidad Complutense de Madrid–Instituto de Salud Carlos III de Evolución y Comportamiento Humano, Madrid, Spain. [21]Instituto Nacional de Antropología e Historia, Moneda 13, Centro, Cuauhtémoc, 06060 Mexico City, Mexico. [22]University of Utah, Department of Anthropology, 270 S 1400 E, Salt Lake City, UT 84112, USA. [23]Department of Evolutionary Biology and Science for Life Laboratory, Uppsala University, Norbyvägen 18D, SE-752 36 Uppsala, Sweden. [24]Acceleration Mass Spectrometry 14C Dating Centre, Department of Physics and Astronomy, Aarhus University, Ny Munkegade 120, 8000 Aarhus, Denmark. [25]Laboratorio Nacional de Genómica para la Biodiversidad (LANGEBIO), Centro de Investigación y de Estudios Avanzados, Irapuato, Guanajuato 36821, Mexico. [26]Genetics Institute, University College London, Gower Street, London WC1E 6BT, UK. [27]Evolutionsbiologiskt Centrum, Norbyvägen 18D, 75236 Uppsala, Sweden. [28]Department of Geography, University of Cambridge, Downing Place, Cambridge CB2 3EN, UK. [29]Centre for Past Climate Change and Department of Meteorology, University of Reading, Earley Gate, Post Office Box 243, Reading, UK. [30]School of Geographical Sciences, University Road, Clifton, Bristol BS8 1SS, UK. [31]Escuela Nacional de Antropología e Historia, Periférico Sur y Zapote s/n Colonia Isidro Fabela, Tlalpan, Isidro Fabela, 14030 Mexico City, Mexico. [32]Instituto de Investigación en Genética Molecular, Universidad de Guadalajara, Ocotlán, Mexico. [33]Dipartimento di Scienze Biologiche, Geologiche e Ambientali (BiGeA), Università di Bologna, Via Selmi 3, 40126 Bologna, Italy. [34]Department of Anthropology, Oregon State University, 238 Waldo Hall, Corvallis, OR 97331 USA. [35]Museum National d'Histoire Naturelle, CNRS, Université Paris 7 Diderot, Sorbonne Paris Cité, Sorbonne Universités, Unité Eco-Anthropologie et Ethnobiologie (UMR7206), Paris, France. [36]Anthropological Institute and Museum, University of Zürich, Winterthurerstrasse 190, 8057 Zürich, Switzerland. [37]Department of Archaeology, Memorial University, Queen's College, 210 Prince Philip Drive, St. John's, Newfoundland A1C 5S7, Canada. [38]Department of Human Evolution, Max Planck Institute for Evolutionary Anthropology, Deutscher Platz 6, Leipzig 04103, Germany. [39]Department of Earth System Science, University of California, Irvine, Keck Carbon Cycle Accelerator Mass Spectrometry Group, B321 Croul Hall, Irvine, CA 92697, USA. [40]Instituto de Alta Investigación, Universidad de Tarapacá, 18 de Septiembre 2222, Carsilla 6-D Arica, Chile. [41]Departamento de Antropologia, Universidad de Tarapacá, 18 de Septiembre 2222, Carsilla 6-D Arica, Chile. [42]Fundação Museu do Homem Americano, Centro Cultural Sérgio Motta, Campestre, 64770-000 Sao Raimundo Nonato, Brazil. [43]Laboratoire d'Anthropologie Moléculaire et Imagérie de Synthèse UMR-5288, CNRS, Université de Toulouse, 31073 Toulouse, France. [44]Institute of Cytology and Genetics, Siberian Branch of the Russian Academy of Sciences, Prospekt Lavrentyeva 10, 630090 Novosibirsk, Russia. [45]Novosibirsk State University, 2 Pirogova Street, 630090 Novosibirsk, Russia. [46]Institute of Internal Medicine, Siberian Branch of RAS, 175/1 ul. B. Bogatkova, Novosibirsk 630089, Russia. [47]Novosibirsk State University, Laboratory of Molecular Epidemiology and Bioinformatics, 630090 Novosibirsk, Russia. [48]Vavilov Institute of General Genetics, Gubkina 3, 119333 Moscow, Russia. [49]Research Centre for Medical Genetics, Moskvorechie 1, 115478 Moscow, Russia. [50]Kemerovo State University, Krasnaya 3, 650000 Kemerovo, Russia. [51]Institute of Biochemistry and Genetics, Ufa Scientific Center of Russian Academy of Sciences, Prospekt Oktyabrya 71, 450054 Ufa, Russia. [52]Department of Genetics and Fundamental Medicine, Bashkir State University, Zaki Validi 32, 450076 Ufa, Russia. [53]Department of Molecular Genetics, Yakut Scientific Centre of Complex Medical Problems, Sergelyahskoe Shosse 4, 677010 Yakutsk, Russia. [54]Laboratory of Molecular Biology, Institute of Natural Sciences, M. K. Ammosov North-Eastern Federal University, 677000 Yakutsk, Russia. [55]Institute of Biological Problems of the North, Russian Academy of Sciences, Portovaya Street 18, Magadan 685000, Russia. [56]Department of Anthropology, Western Washington University, Bellingham, WA 98225, USA. [57]Department of Anthropology, Northwest Community College, 353 Fifth Street, Prince Rupert, British Columbia V8J 3L6, Canada. [58]Canadian Museum of History, 100 Rue Laurier, Gatineau, Quebec K1A 0M8, Canada. [59]University of Western Ontario, London, Ontario N6A 3K7, Canada. [60]Simon Fraser University, Burnaby, British Columbia V5A 1S6, Canada. [61]Metlakatla Treaty Office, Post Office Box 224, Prince Rupert, BC V8J 3P6, Canada. [62]Sealaska Heritage Institute, 105 S. Seward Street, Juneau, AK 99801, USA. [63]Department of Structural Biology, Stanford University School of Medicine, D100 Fairchild Science Building, Stanford, CA 94305-5126, USA. [64]Department of Anthropology, Washington State University, Pullman, WA 99163, USA. [65]Division of Biological Anthropology, University of Cambridge, Henry Wellcome Building, Fitzwilliam Street, Cambridge CB2 1QH, UK. [66]Department of Medicine, University of Cambridge, Medical Research Council Laboratory of Molecular Biology, Francis Crick Avenue, Cambridge Biomedical Campus, Cambridge CB2 0QH, UK. [67]Laboratory of Biological Anthropology, University of Kansas, 1415 Jayhawk Boulevard, 622 Fraser Hall, Lawrence, KS 66045, USA. [68]Molecular Anthropology Laboratory, 209 Young Hall, Department of Anthropology, University of California, One Shields Avenue, Davis, CA 95616, USA. [69]Center for the Study of the First Americans, Texas A&M University, College Station, TX 77843-4352, USA. [70]Department of Anthropology, Texas A&M University, College Station, TX 77843-4352, USA. [71]Department of Geography, Texas A&M University, College Station, TX 77843-4352, USA. [72]Santa Barbara Museum of Natural History, 2559 Puesta del Sol, Santa Barbara, CA 93105, USA. [73]Carle R. Woese Institute for Genomic Biology, University of Illinois at Urbana-Champaign, Urbana, IL 61801, USA. [74]Department of Anthropology, Southern Methodist University, Dallas, TX 75275, USA. [75]Department of Integrative Biology, University of California, 3060 Valley Life Sciences Building 3140, Berkeley, CA 94720, USA.

*These authors contributed equally to this work. †Corresponding authors. E-mail: ewillerslev@snm.ku.dk (E.W.); rasmus_nielsen@berkeley.edu (R.N.); yss@berkeley.edu (Y.S.S.)

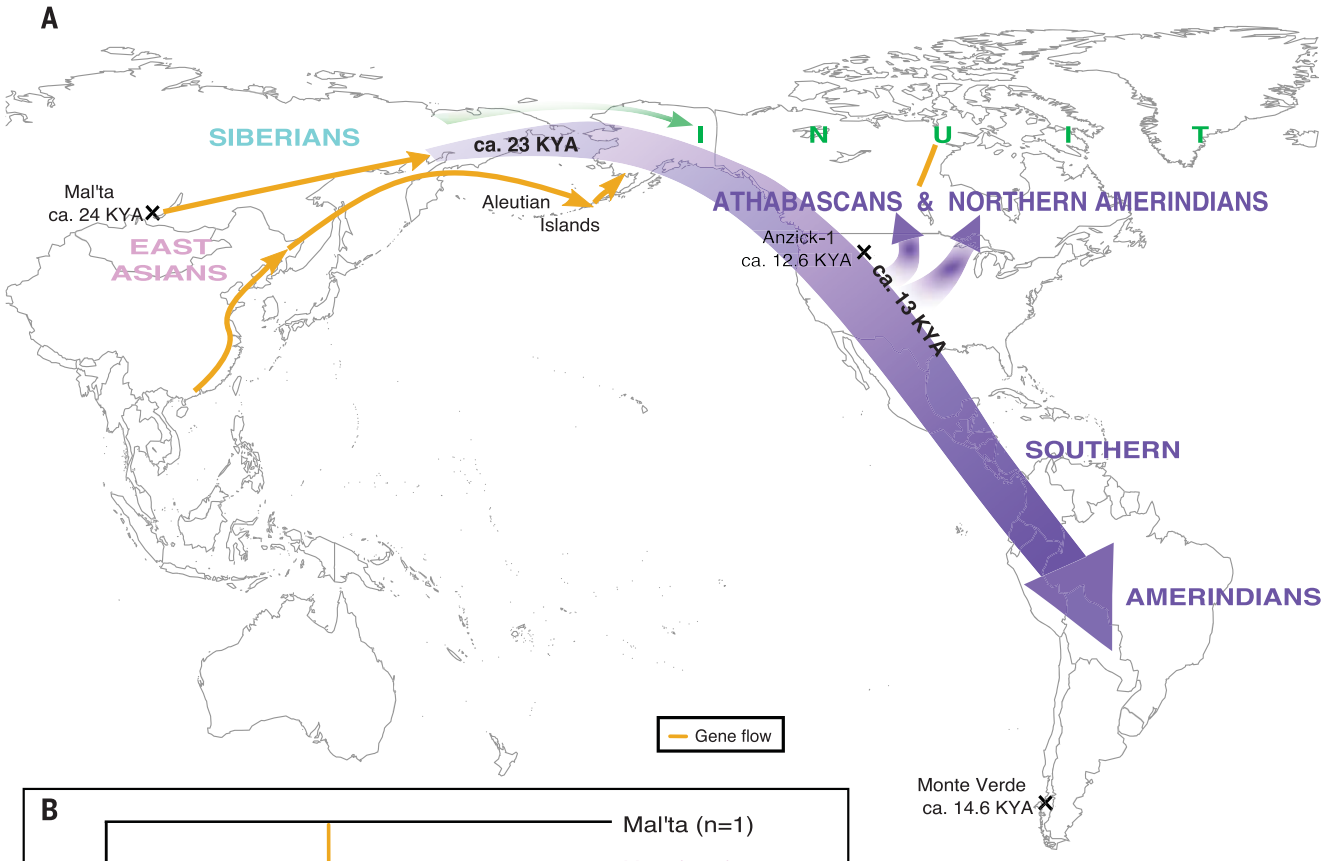

Fig. 1. Origins and population history of Native Americans. (**A**) Our results show that the ancestors of all present-day Native Americans, including Amerindians and Athabascans, derived from a single migration wave into the Americas (purple), separate from the Inuit (green). This migration from East Asia occurred no earlier than 23 ka and is in agreement with archaeological evidence from sites such as Monte Verde (*50*). A split between the northern and southern branches of Native Americans occurred ~13 ka, with the former comprising Athabascans and northern Amerindians and the latter consisting of Amerindians in southern North America and Central and South America, including the Anzick-1 individual (*5*). There is an admixture signal between Inuit and Athabascans as well as some northern Amerindians (yellow line); however, the gene flow direction is unresolved because of the complexity of the admixture events (*28*). Additionally, we see a weak signal related to Australo-Melanesians in some Native Americans, which may have been mediated through East Asians and Aleutian Islanders (yellow arrows). Also shown is the Mal'ta gene flow into Native American ancestors some 23 ka (yellow arrow) (*4*). It is currently not possible for us to ascertain the exact geographical locations of the depicted events; hence, the positioning of the arrows should not be considered a reflection of these. (**B**) Admixture plot created on the basis of TreeMix results (fig. S5) shows that all Native Americans form a clade, separate from the Inuit, with gene flow between some Native Americans and the North American Arctic. The number of genome-sequenced individuals included in the analysis is shown in brackets.

first estimated divergence times between Native Americans and the Koryak of Siberia, one of the genetically closest sampled East Asian populations to Native Americans (fig. S5), using demographic models that reflect a clean split between the populations (*28*). With both diCal2.0 and the IBS tract method, the split of Native Americans (including Amerindians and Athabascans) from the Koryak dates to ~20 ka (tables S11A and S12 and fig. S15) (*28*).

We further applied diCal2.0 to models with gene flow postdating the split between Native Americans and Koryak (Fig. 2A) and found that they provided a better fit to the data than did the models without gene flow (fig. S18) (*28*). Overall, simulated data based on the models inferred by using diCal2.0 and real data show very similar IBS tract length distributions (Fig. 2B) and relative cross coalescence rates (CCRs) between pairs of individuals estimated by using the Multiple Sequentially Markovian Coalescent (MSMC) method (method 3) (Fig. 2, C and D) (*28*, *44*). This serves as a confirmation for the model estimates from diCal2.0. We evaluated all three methods using simulations under complex demographic models and additionally investigated the effects of switch-errors in haplotype phasing on the estimates (*28*).

We then applied the diCal2.0 model that allows for gene flow between populations after

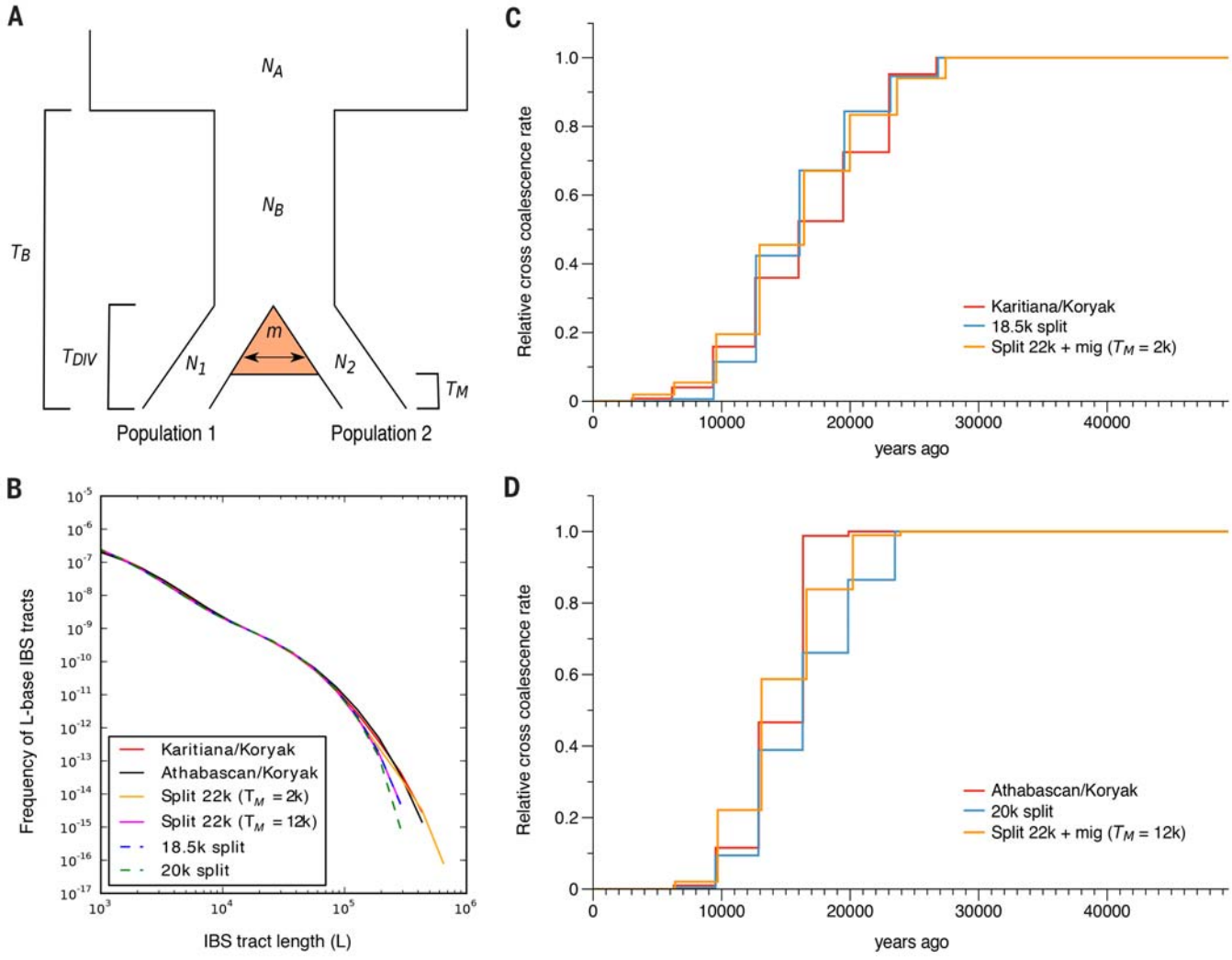

Fig. 2. Divergence estimates between Native Americans and Siberian Koryak. (**A**) The demographic model used allows for continuous gene flow between populations 1 and 2, starting from the time T_{DIV} of divergence and ending at T_M. The backward probability of migration per individual per generation is denoted by m. The bottleneck at T_B captures the out-of-Africa event. (**B**) The red and black solid curves depict empirical distributions of IBS tracts shared between Karitiana-Koryak and Athabascan-Koryak, respectively. The orange, pink, dashed blue, and dashed green curves depict IBS tracts shared between the two population pairs, simulated under two demographic models based on results from diCal2.0. Overall, for Karitiana-Koryak and Athabascan-Koryak, the migration scenarios (orange and pink, respectively) match the empirical curves (red and black, respectively) better than the clean split scenarios match (dashed blue and dashed green, respectively), with more long IBS tracts showing evidence of recent common ancestry between Koryaks and Native Americans. (**C** and **D**) Relative CCRs for the Karitiana-Koryak and Athabascan-Koryak divergence (red), respectively, including data simulated under the two demographic models in (B). In both cases, the model with gene flow (orange) fits the data (red) better than does the clean split model (blue). The migration model explains a broader CCR tail in the case of Karitiana-Koryak and the relatively late onset of the CCR decay for Athabascan-Koryak.

their split in order to estimate divergence times for Native Americans from more geographically and genetically distant East Asian groups, including the Siberian Nivkh and Han Chinese. As before, the divergence estimates for Amerindians and Athabascans were very similar to one another, ~23 ka (table S11B and figs. S18 and S21).

Hence, our results suggest that Amerindians and Athabascans were, by three different methods, consistently equidistant in time to populations that were sampled from different regions of East Asia, including some proximate to Beringia, and with varied population histories. This suggests that these two major Native American subgroups are descendants of the same source population that split off from ancestral East Asians during the LGM. It is conceivable that harsh climatic conditions during the LGM may have contributed to the isolation of ancestral Native Americans, ultimately leading to their genetic divergence from their East Asian ancestors.

We also modeled the peopling of the Americas using a climate-informed spatial genetic model (CISGeM), in which the genetic history and local demography is informed by paleoclimatic and paleovegetation reconstructions (*28*, *45*), and found the results to be in accordance with the conclusion of a single migration source for all Native Americans. Using present-day and ancient high-coverage genomes, we found that Athabascans and Anzick-1, but not Greenlandic Inuit and Saqqaq (*29*, *39*), belong to the same initial migration wave that also gave rise to present-day Amerindians from southern North America and Central and South America (Fig. 3) and that this migration likely followed a coastal route, given our current understanding of the glacial geological and paleoenvironmental parameters of the Late Pleistocene (fig. S31).

In all cases, the best fit of the demographic models to the IBS tract distribution and relative CCR by MSMC required gene flow between Siberian and Native American populations after their initial split (Fig. 2, B to D). We also found strong evidence for gene flow between Athabascans and

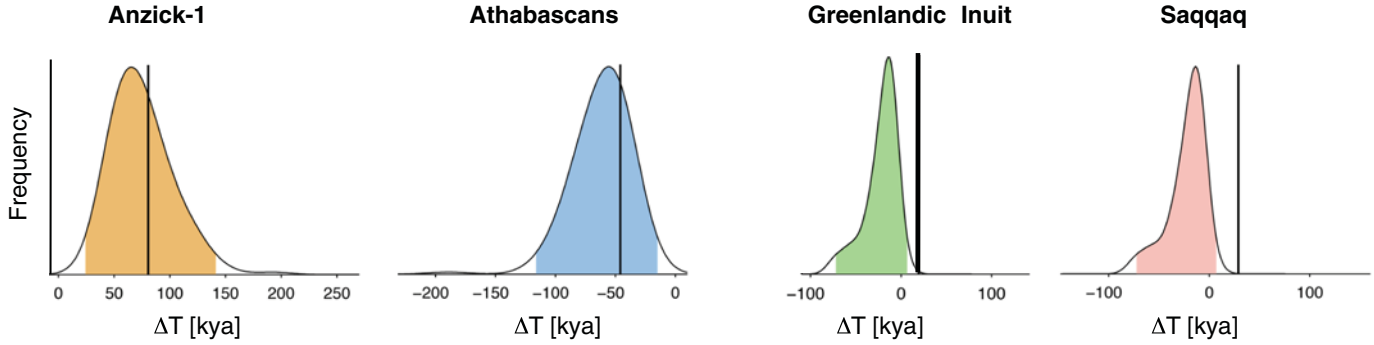

Fig. 3. Testing migrations into the Americas by using a climate-informed model. Estimates of difference in genetic divergence between Amerindians (from southern North America and Central and South America) or Koryak versus Athabascan and Greenlandic Inuit and the ancient Saqqaq and Anzick-1 genomes (black vertical lines), compared with posterior probability distribution predicted from a climate-informed spatial genetic model reconstructing a single wave into the Americas (curves, the colored part represents the 95% credibility interval). ΔT for population X is defined as $T(X, \text{Koryak}) - T(X, \text{Central and South Amerindians})$ (*28*). Both Anzick-1 and the Athabascans were part of the same wave into the Americas to which other Amerindian populations from southern North America and Central and South America belonged, whereas the Inuit and Saqqaq are the descendants of different waves (observed values outside the 95% credibility interval).

the Inuit (table S11B), supported by results from ADMIXTURE (fig. S4), TreeMix (fig. S5), *D*-statistics using both whole-genome and SNP chip genotype data (figs. S6 and S8A) (*28*, *46*, *47*), and outgroup f_3-statistics using whole-genome data (fig. S12) (*28*, *47*). We attempted to estimate the divergence times between Inuit and Siberians as well as Inuit and Native Americans (table S11 and figs. S19 and S25 to S27), but our analyses were complicated by gene flow between Inuit and Athabascans as well as complex admixture patterns among Arctic groups (fig. S5).

We tested the duration and magnitude of post-split gene flow between Native Americans and Siberians using diCal2.0 by introducing stopping time of gene flow as a free parameter (*28*). We still obtained the highest likelihood for a divergence time of 22 ka between Amerindians and Siberians as well as Athabascans and Siberians, although estimates for gene-flow rate and end of the gene flow differ (table S11C and fig. S22). Gene flow between Athabascans and Siberians seems to have stopped ~12 ka (table S11C), suggesting a link to the breaching of the Beringian Land Bridge by rising sea levels (*48*).

Overall, our results support a common Siberian origin for all Native Americans, contradicting claims for an early migration to the Americas from Europe (*49*), with their initial isolation and entrance into the Americas occurring no earlier than 23 ka, but with subsequent admixture with East Asian populations. This additionally suggests that the Mal'ta-related admixture into the early Americans (*4*), representing ancestors of both Amerindians and Athabascans (Fig. 1 and fig. S5), occurred sometime after 23 ka, after the Native American split from East Asians.

Subsequent in situ diversification of Native American groups

That Amerindian and Athabascan groups were part of the same migration implies that present-day genetic differences observed between them must have arisen later, after ~23 ka. Using the clean-split model in diCal2.0 on the modern genomes data set, we estimated that Athabascans and Karitiana diverged ~13 ka (95% confidence interval of ~11.5 to 14.5 ka, estimated from parametric bootstrap results) (table S11A and fig. S16), which is consistent with results from MSMC (fig. S27) (*28*).

Where the divergence between Karitiana and Athabascans occurred is not known. However, several independent lines of evidence suggest that it is more likely to have occurred in lower-latitude North America instead of eastern Beringia (Alaska). These include the equidistant split times of Amerindians and Athabascans to Asian populations, the relatively brief interval between their estimated divergence date range and the age of Anzick-1 (12.6 ka) (*5*), and last, the geographic location of Anzick-1 to the south of the North American ice sheets and its clear affiliation with the "southern branch" of Native Americans (taken broadly to include Amerindians from southern North America and Central and South America) (*5*), as determined with outgroup f_3-statistics by using SNP chip genotype data from present-day worldwide populations (Fig. 4 and figs. S13 and S14) (*47*). Divergence in North America would also be consistent with the known pre-Clovis age sites in the Americas, such as Monte Verde (14.6 ka) (*50*). The most parsimonious model would be that both Amerindians and Athabascans are descendants of the same ancestral Native American population that entered the Americas then subsequently diversified. However, we cannot discount alternative and more complex scenarios, which could be tested with additional ancient samples.

By the Clovis period (~12.6 ka), the ancestral Native American population had already diversified into "northern" and "southern" branches, with the former including ancestors of present-day Athabascans and northern Amerindian groups such as Chipewyan, Cree, and Ojibwa and the latter including Amerindians from southern North America and Central and South America (Fig. 4 and fig. S14). We tested whether later gene flow from East Asian sources, such as the Inuit, might explain the genetic differences between these two branches. Using *D*-statistics on SNP chip genotype data (*47*) masked for non-native ancestry, we observed a signal of gene flow between the Inuit and northwest Pacific Coast Amerindians such as Coastal Tsimshian and Nisga'a, residing in the same region as the northern Athabascans (fig. S8B) (*28*). However, this signal of admixture with the Inuit, also detected in Athabascans (figs. S6 and S8A), was not evident among northern Amerindian populations located further east, such as Cree, Ojibwa, and Chipewyan (fig. S8C) (*28*). This suggests that the observed difference between the northern and southern branches is not a consequence of post-split East Asian gene flow into the northern branch and also provides a possible explanation as to why the southern branch Amerindians such as Karitiana are genetically closer to the northern Amerindians located further east than to northwest coast Amerindians and Athabascans (fig. S9).

In contrast to Anzick-1, several of the Holocene individuals from the Americas—including those sequenced in this study, as well as the 8500-year-old Kennewick Man (*51*)—are closely related to present-day Native American populations from the same geographical regions (Fig. 4 and figs. S13 and S14). This implies genetic continuity of ancient and modern populations in some parts of the Americas over at least the past 8500 years, which is in agreement with recent results from Kennewick Man (*51*).

Evidence of more distant Old World gene flow into some Native Americans

When testing for gene flow between Athabascans and Inuit with masked SNP chip genotype data–based *D*-statistics (*47*) (fig. S8), we observed a weak tendency for the Inuit to be much closer to the Athabascans than to certain Amerindians such as the North American Algonquin and Cree, and the Yaqui and Arhuaco of Central and South America (respectively), as compared with other Amerindians such as the Palikur and Surui of Brazil (fig. S8).

To further investigate this trend, we tested for additional gene flow from Eurasian populations into the Americas with *D*-statistics using the

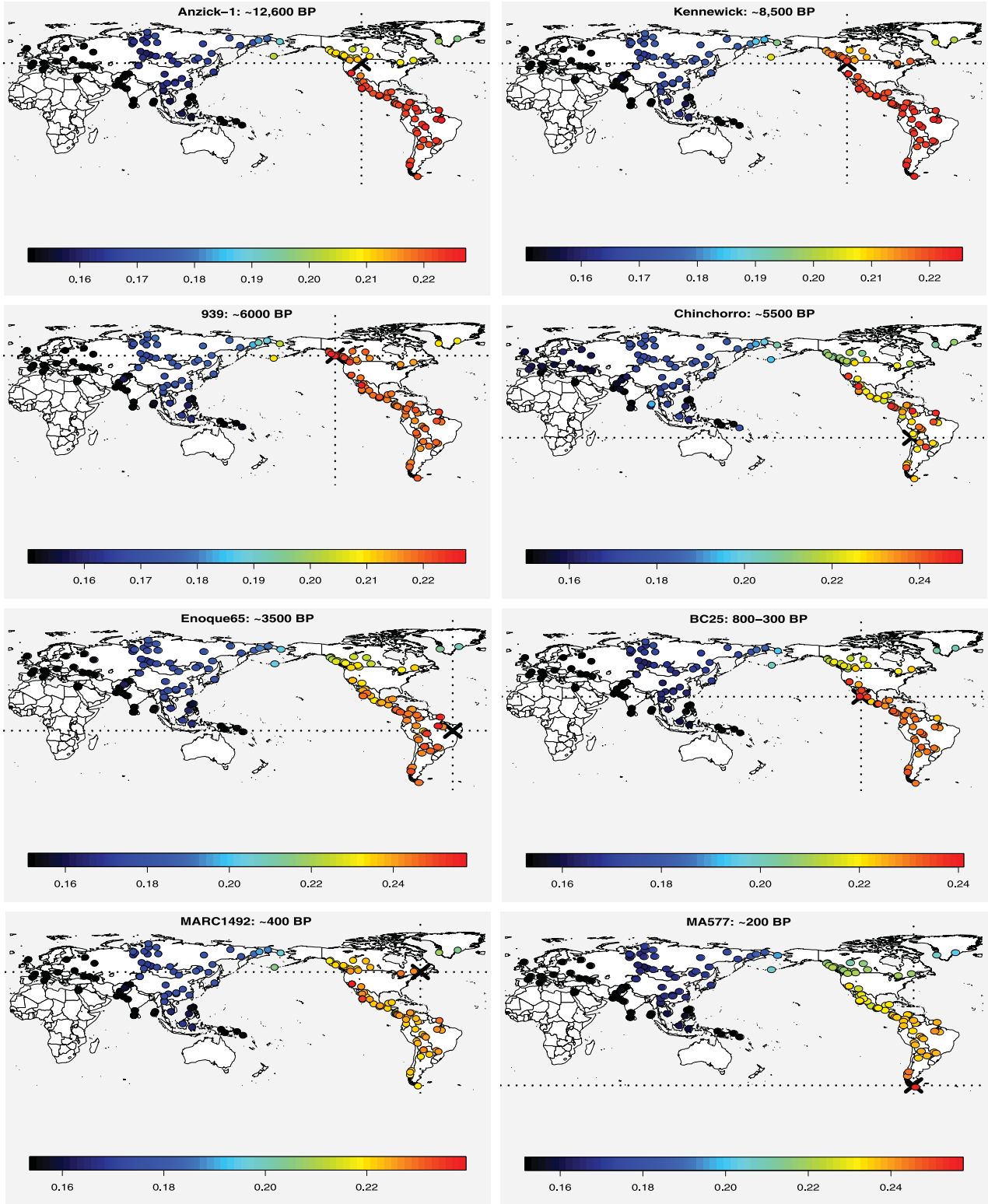

Fig. 4. Diversification within the Americas. SNP chip genotype data–based outgroup f_3-statistics (*47*) of the form $f_3(X, \text{Ancient}; \text{Yoruba})$ were used to estimate the shared ancestry between ancient samples from the Americas and a large panel of worldwide present-day populations (X), including Athabascan and Amerindian groups from North America (table S3), some of which were masked for non-native ancestry before the analysis (*28*). The outgroup f_3-statistics are depicted as heat maps, with the sampling location of the ancient sample marked by the dotted lines, and corresponding ranked plots with error bars are shown in fig. S14. "BP" refers to time before present. We find the Anzick-1 sample to share most ancestry with the southern branch of Native Americans when using multiple northern Native Americans sequenced in this study, which is consistent with (*5*). The seven Holocene age samples share most ancestry with Native Americans, with a general tendency to be genetically closer to present-day Native American populations from the same geographical region.

masked SNP chip genotype data set (47). We found that some American populations—including the Aleutian Islanders, Surui, and Athabascans—are closer to Australo-Melanesians as compared with other Native Americans, such as North American Ojibwa, Cree, and Algonquin and the South American Purepecha, Arhuaco, and Wayuu (fig. S10). The Surui are, in fact, one of closest Native American populations to East Asians and Australo-Melanesians, the latter including Papuans, non-Papuan Melanesians, Solomon Islanders, and South East Asian hunter-gatherers such as Aeta (fig. S10). We acknowledge that this observation is based on the analysis of a small fraction of the whole-genome and SNP chip genotype data sets—especially for the Aleutian Islander data, which is heavily masked owing to recent admixture with Europeans (28)—and that the trends in the data are weak.

Nonetheless, if it proves correct, these results suggest that there may be a distant Old World signal related to Australo-Melanesians and East Asians in some Native Americans. The widely scattered and differential affinity of Native Americans to the Australo-Melanesians, ranging from a strong signal in the Surui to a much weaker signal in northern Amerindians such as Ojibwa, points to this gene flow occurring after the initial peopling by Native American ancestors.

However, how this signal may have ultimately reached South America remains unclear. One possible means is along a northern route via the Aleutian Islanders, previously found to be closely related to the Inuit (39), who have a relatively greater affinity to East Asians, Oceanians, and Denisovan than Native Americans in both whole-genome and SNP chip genotype data–based *D* tests (table S10 and figs. S10 and S11). On the basis of archaeological evidence and mtDNA data from ancient and modern samples, the Aleutian Islands are hypothesized to have been peopled as early as ~9 ka by "Paleo-Aleuts" who were succeeded by the "Neo-Aleuts," with present-day Aleutian Islanders potentially resulting from admixture between these two populations (52, 53). Perhaps their complex genetic history included input from a population related to Australo-Melanesians through an East Asian continental route, and this genomic signal might have been subsequently transferred to parts of the Americas, including South America, through past gene flow events (Fig. 1). Evidence for this gene flow is supported with diCal2.0 and MSMC analyses showing a weak but recent gene flow into South Americans from populations related to present-day Northeast Asians (Koryak) (Fig. 2C and table S11C), who might be considered a proxy for the related Aleutian Islanders.

Testing the Paleoamerican model

The detection of an Australo-Melanesian genetic signal in the Americas, however subtle, returns the discussion to the Paleoamerican model, which hypothesizes, on the basis of cranial morphology, that two temporally and source-distinct populations colonized the Americas. The earlier population reportedly originated in Asia in the Late Pleistocene and gave rise to both Paleoamericans and present-day Australo-Melanesians, whose shared cranial morphological attributes are presumed to indicate their common ancestry (23). The Paleoamericans were, in turn, thought to have been largely replaced by ancestors of present-day Amerindians, whose crania resemble modern East Asians and who are argued to be descendants of later arriving Mongoloid populations (14, 23, 26, 54). The presence of Paleoamericans is inferred primarily from ancient archaeological specimens in North and South America and a few relict populations of more recent age, which include the extinct Pericúes and Fuego-Patagonians (24, 25, 55).

The Paleoamerican hypothesis predicts that these groups should be genetically closer to Australo-Melanesians than other Amerindians. Previous studies of mtDNA and Y chromosome data obtained from Fuego-Patagonian and Paleoamerican skeletons have identified haplogroups similar to those of modern Native Americans (55–57). Although these results indicate some shared maternal and paternal ancestry with contemporary Native Americans, uniparental markers can be misleading when drawing conclusions about the demographic history of populations. To conclusively identify the broader population of ancestors who may have contributed to the Paleoamerican gene pool, autosomal genomic data are required.

We therefore sequenced 17 ancient individuals affiliated to the now-extinct Pericúes from Mexico and Fuego-Patagonians from Chile and Argentina (28), who, on the basis of their distinctive skull morphologies, are claimed to be relicts of Paleoamericans (23, 27, 58, 59). Additionally, we sequenced two pre-Columbian mummies from northern Mexico (Sierra Tarahumara) to serve as morphological controls because they are expected to fall within the range of Native American morphological cranial variation (28). We found that the ancient samples cluster with other Native American groups and are outside the range of Oceanian genetic variation (Fig. 5 and figs. S32, S33, and S34) (28). Similarly, outgroup f_3-statistics (47) reveal low shared genetic ancestry between the ancient samples and Oceanians (figs. S36 and S37) (28), and genome-based and masked SNP chip genotype data–based *D*-statistics (46, 47) show no evidence for gene flow from Oceanians into the Pericúes or Fuego-Patagonians (fig. S39) (28).

Because the Paleoamerican model is based on cranial morphology (23, 27, 58, 59), we also measured craniometric data for the ancient samples and assessed their phenotypic affinities to supposed Paleoamericans, Amerindians, and worldwide populations (28). The results revealed that the analyzed Fuego-Patagonians showed closest craniometric affinity to Arctic populations and the Paleoamericans, whereas the analyzed female Pericúes showed closest craniometric affinities to populations from North America, the Arctic region, and Northern Japan (table S15). Our analyses demonstrated that the presumed ancestral ancient Paleoamerican reference sample from Lagoa Santa, Brazil (24) had closest affinities to Arctic and East Asian populations (table S15). Consequently, for the Fuego-Patagonians, the female Pericúes, and the Lagoa Santa Paleoamerican sample, we were not able to replicate previous results (24) that report close similarity of Paleoamerican and Australo-Melanesian cranial morphologies. Male Pericúes samples displayed more craniometric affinities with populations from Africa and Australia relative to the female individuals of their population (fig. S41). The results of analyses based on craniometric data thus are highly sensitive to sample structure and the statistical approach and data filtering used (51). Our morphometric analyses suggest that these ancient samples are not true relicts of a distinct migration as claimed and hence do not support the Paleoamerican model. Similarly, our genomic data also provide no support for an early migration of populations directly related to Australo-Melanesians into the Americas.

Discussion

That Native Americans diverged from their East Asian ancestors during the LGM and no earlier than 23 ka provides an upper bound, and perhaps the climatic and environmental context, for the initial isolation of their ancestral population and a maximum estimate for the entrance and subsequent spread into the Americas. This result is consistent with the model that people entered the Americas before the development of the Clovis complex and had reached as far as southern South America by 14.6 ka. Because archaeological evidence provides only a minimum age for human presence in the Americas, we can anticipate the possible discovery of sites that approach the time of the divergence of East Asians and Native Americans. However, our estimate for the initial divergence and entry of Native American ancestors does not support archaeological claims for an initial peopling substantially earlier than the LGM (8–10).

Although our data cannot provide the precise geographical context for the initial peopling process, it has allowed us to more accurately estimate its temporal dynamics. This, in turn, has enabled us to reassess the Beringian Incubation Model, which, based on mtDNA data and the timing and geographical distribution of archaeological sites, hypothesized a ~15,000-year-long period of isolation of ancestral Native Americans in Beringia during the LGM (19–21). Our results, along with recent findings of mtDNA haplogroup C1 in Iceland and ancient northwest Russia (60), do not fit with the proposed 15,000-year span of the Beringian Incubation Model (19–21). It is possible that a shorter period of isolation occurred (~8000 years), but whether it occurred in Siberia or Beringia will have to be determined from future ancient DNA and archaeological findings. Given the genetic continuity between Native Americans and some East Asian populations (figs. S4 and S5), other demographic factors, such as surfing during population expansions into unoccupied regions (61), may ultimately need to be taken into account to better understand the presence of a large number of high-frequency private variants in the indigenous populations of the Americas.

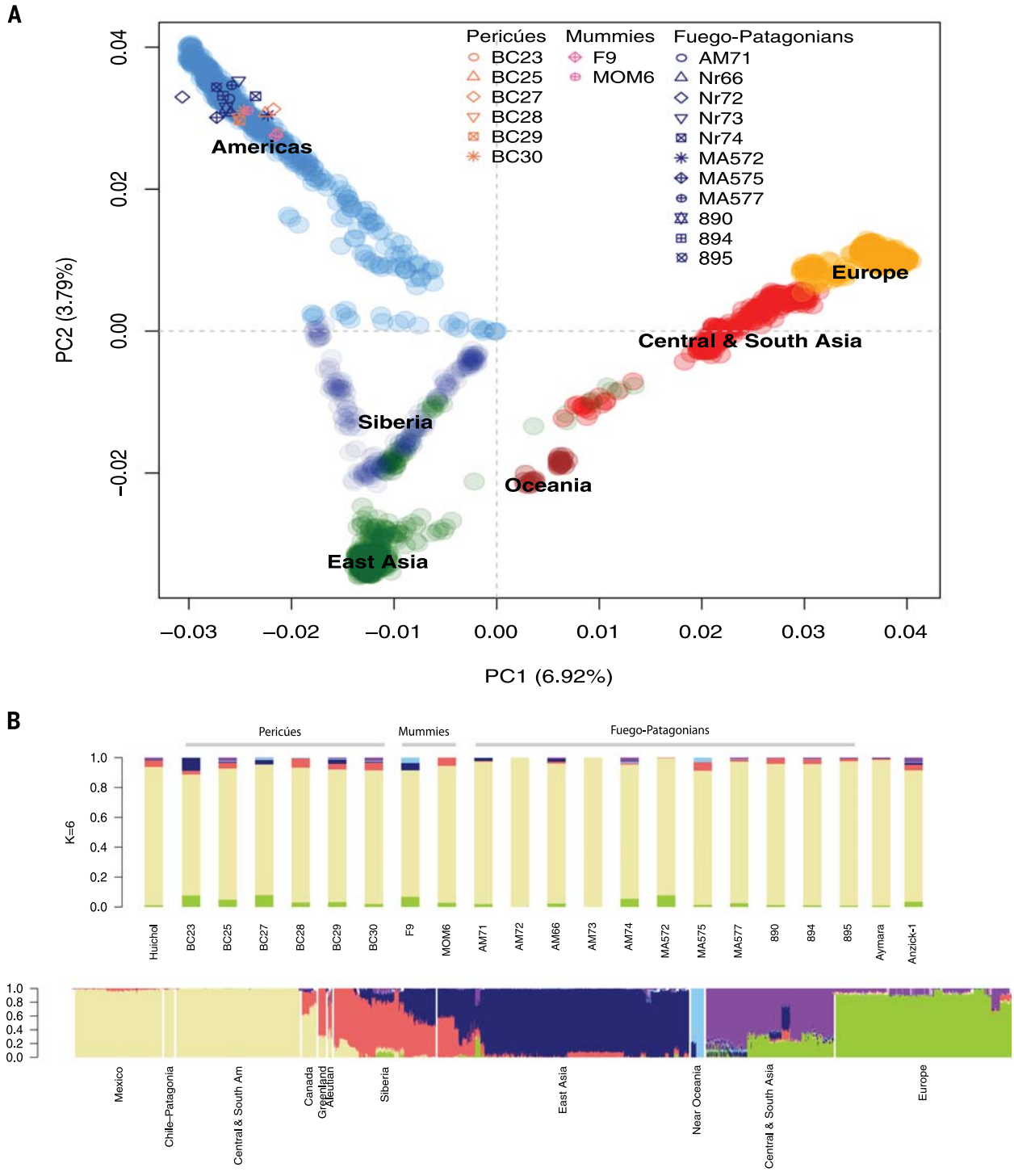

Fig. 5. The Paleoamerican model. (**A**) Principal component analysis plot of 19 ancient samples combined with a worldwide reference panel, including 1823 individuals from (6). Our samples plot exclusively with American samples. Plots with other reference panels consisting of Native American populations are provided in fig. S32. (**B**) Population structure in the ancient Pericú, Mexican mummy, and Fuego-Patagonian individuals from this study. Ancestry proportions are shown when assuming six ancestral populations ($K = 6$). The top bar shows the ancestry proportions of the 19 ancient individuals, Anzick-1 (5), and two present-day Native American genomes from this study (Huichol and Aymara). The plot at the bottom illustrates the ancestry proportions for 1823 individuals from (6). Our samples show primarily Native American (ivory, >92%) and Siberian (red, ~5%) ancestry. The plot with $K = 13$ is provided in fig. S33.

The data presented here are consistent with a single initial migration of all Native Americans and with later gene flow from sources related to East Asians and, more distantly, Australo-Melanesians. From that single migration, there was a diversification of ancestral Native Americans leading to the formation of northern and southern branches, which appears to have taken place ~13 ka within the Americas. This split is consistent with the patterns of uniparental genomic regions of mtDNA haplogroup X and some Y chromosome C haplotypes being present in

northern, but not southern, populations in the Americas (*18*, *62*). This diversification event coincides roughly with the opening of habitable routes along the coastal and the interior corridors into unglaciated North America some 16 and 14 ka, respectively (*63*, *64*), suggesting a possible role of one or both of these routes in the isolation and subsequent dispersal of Native Americans across the continent.

Methods

DNA was extracted from 31 present-day individuals from the Americas, Siberia, and Oceania and 23 ancient samples from the Americas and converted to Illumina libraries and shotgun sequenced (*28*). Three of the ancient samples were radiocarbon dated, of which two were corrected for marine reservoir offset (*28*). SNP chip genotype data was generated from 79 present-day Siberians and Native Americans affiliated to 28 populations (*28*). Raw data from SNP chip and shotgun sequencing were processed by using standard computational procedures (*28*). Error rate analysis, DNA damage analysis, contamination estimation, sex determination, mtDNA and Y chromosome haplogroup assignment, ADMIXTURE analysis, ancestry painting and admixture masking, principal component analysis using SNP chip genotype data, TreeMix analysis on genomic sequence data, *D*-statistic and outgroup f_3-statistic tests on SNP chip genotype and genomic sequence data, divergence time estimation by use of diCal2.0, an IBS tract method and MSMC, climate-informed spatial genetic model analysis, and craniometric analysis were performed as described (*28*).

REFERENCES AND NOTES

1. T. D. Dillehay, The late Pleistocene cultures of South America. *Evol. Anthropol.* **7**, 206–216 (1999). doi: 10.1002/(SICI)1520-6505(1999)7:6<206::AID-EVAN5>3.0.CO;2-G
2. D. L. Jenkins *et al.*, Clovis age Western Stemmed projectile points and human coprolites at the Paisley Caves. *Science* **337**, 223–228 (2012). pmid: 22798611
3. D. J. Meltzer, *First Peoples in a New World: Colonizing Ice Age America* (Univ. California Press, Berkeley, 2009).
4. M. Raghavan *et al.*, Upper Palaeolithic Siberian genome reveals dual ancestry of Native Americans. *Nature* **505**, 87–91 (2014). doi: 10.1038/nature12736; pmid: 24256729
5. M. Rasmussen *et al.*, The genome of a Late Pleistocene human from a Clovis burial site in western Montana. *Nature* **506**, 225–229 (2014). doi: 10.1038/nature13025; pmid: 24522598
6. D. Reich *et al.*, Reconstructing Native American population history. *Nature* **488**, 370–374 (2012). pmid: 22801491
7. M. R. Waters *et al.*, The Buttermilk Creek complex and the origins of Clovis at the Debra L. Friedkin site, Texas. *Science* **331**, 1599–1603 (2011). doi: 10.1126/science.1201855; pmid: 21436451
8. G. M. Santos *et al.*, A revised chronology of the lowest occupation layer of Pedra Furada Rock Shelter, Piauí, Brazil: The Pleistocene peopling of the Americas. *Quat. Sci. Rev.* **22**, 2303–2310 (2003). doi: 10.1016/S0277-3791(03)00205-1
9. S. R. Holen, K. Holen, K, in *Paleoamerican Odyssey*, K. E. Graf, C. V. Ketron, M. R. Waters, Eds. (Texas A&M Univ. Press, College Station, 2014), pp. 429–444.
10. E. Boëda *et al.*, A new late Pleistocene archaeological sequence in South America: The Vale da Pedra Furada (Piauí, Brazil). *Antiquity* **88**, 927–941 (2014). doi: 10.1017/S0003598X00050845
11. D. W. Owsley, R. L. Jantz, *Kennewick Man: The Scientific Investigation of an Ancient American Skeleton* (Texas A&M Univ. Press, College Station, 2014).
12. A. Achilli *et al.*, The phylogeny of the four pan-American MtDNA haplogroups: Implications for evolutionary and disease studies. *PLOS ONE* **3**, e1764 (2008). doi: 10.1371/journal.pone.0001764; pmid: 18335039
13. V. Battaglia *et al.*, The first peopling of South America: New evidence from Y-chromosome haplogroup Q. *PLOS ONE* **8**, e71390 (2013). doi: 10.1371/journal.pone.0071390; pmid: 23990949
14. C. L. Brace *et al.*, Old World sources of the first New World human inhabitants: A comparative craniofacial view. *Proc. Natl. Acad. Sci. U.S.A.* **98**, 10017–10022 (2001). doi: 10.1073/pnas.171305898; pmid: 11481450
15. U. A. Perego *et al.*, Distinctive Paleo-Indian migration routes from Beringia marked by two rare mtDNA haplogroups. *Curr. Biol.* **19**, 1–8 (2009). doi: 10.1016/j.cub.2008.11.058; pmid: 19135370
16. U. A. Perego *et al.*, The initial peopling of the Americas: A growing number of founding mitochondrial genomes from Beringia. *Genome Res.* **20**, 1174–1179 (2010). doi: 10.1101/gr.109231.110; pmid: 20587512
17. N. J. R. Fagundes, R. Kanitz, S. L. Bonatto, A reevaluation of the Native American mtDNA genome diversity and its bearing on the models of early colonization of Beringia. *PLOS ONE* **3**, e3157 (2008). doi: 10.1371/journal.pone.0003157; pmid: 18797501
18. S. L. Zegura, T. M. Karafet, L. A. Zhivotovsky, M. F. Hammer, High-resolution SNPs and microsatellite haplotypes point to a single, recent entry of Native American Y chromosomes into the Americas. *Mol. Biol. Evol.* **21**, 164–175 (2004). doi: 10.1093/molbev/msh009; pmid: 14595095
19. E. Tamm *et al.*, Beringian standstill and spread of Native American founders. *PLOS ONE* **2**, e829 (2007). doi: 10.1371/journal.pone.0000829; pmid: 17786201
20. A. Kitchen, M. M. Miyamoto, C. J. Mulligan, A three-stage colonization model for the peopling of the Americas. *PLOS ONE* **3**, e1596 (2008). doi: 10.1371/journal.pone.0001596; pmid: 18270583
21. C. J. Mulligan, A. Kitchen, M. M. Miyamoto, Updated three-stage model for the peopling of the Americas. *PLOS ONE* **3**, e3199 (2008). doi: 10.1371/journal.pone.0003199; pmid: 18797500
22. K. B. Schroeder *et al.*, A private allele ubiquitous in the Americas. *Biol. Lett.* **3**, 218–223 (2007). doi: 10.1098/rsbl.2006.0609; pmid: 17301009
23. R. González-José *et al.*, Craniometric evidence for Palaeoamerican survival in Baja California. *Nature* **425**, 62–65 (2003). doi: 10.1038/nature01816; pmid: 12955139
24. W. A. Neves, M. Hubbe, Cranial morphology of early Americans from Lagoa Santa, Brazil: Implications for the settlement of the New World. *Proc. Natl. Acad. Sci. U.S.A.* **102**, 18309–18314 (2005). doi: 10.1073/pnas.0507185102; pmid: 16344464
25. W. Neves *et al.*, in *Paleoamerican Odyssey*, K. E. Graf, C. V. Ketron, M. R. Waters, Eds. (Texas A&M Univ. Press, College Station, 2014), pp. 397–412.
26. R. González-José, M. C. Bortolini, F. R. Santos, S. L. Bonatto, The peopling of America: Craniofacial shape variation on a continental scale and its interpretation from an interdisciplinary view. *Am. J. Phys. Anthropol.* **137**, 175–187 (2008). doi: 10.1002/ajpa.20854; pmid: 18481303
27. M. M. Lahr, Patterns of modern human diversification: Implications for Amerindian origins. *Am. J. Phys. Anthropol.* **38** (S21), 163–198 (1995). doi: 10.1002/ajpa.1330380609
28. Materials and methods are available as supplementary materials on *Science* Online.
29. M. Rasmussen *et al.*, Ancient human genome sequence of an extinct Palaeo-Eskimo. *Nature* **463**, 757–762 (2010). doi: 10.1038/nature08835; pmid: 20148029
30. B. Yunusbayev *et al.*, The genetic legacy of the expansion of Turkic-speaking nomads across Eurasia. *PLOS Genet.* **11**, e1005068 (2015). doi: 10.1371/journal.pgen.1005068; pmid: 25898006
31. A. Cardona *et al.*, Genome-wide analysis of cold adaptation in indigenous Siberian populations. *PLOS ONE* **9**, e98076 (2014). pmid: 24847810
32. J. Z. Li *et al.*, Worldwide human relationships inferred from genome-wide patterns of variation. *Science* **319**, 1100–1104 (2008). doi: 10.1126/science.1153717; pmid: 18292342
33. A. Moreno-Estrada *et al.*, Reconstructing the population genetic history of the Caribbean. *PLOS Genet.* **9**, e1003925 (2013). doi: 10.1371/journal.pgen.1003925; pmid: 24244192
34. A. Moreno-Estrada *et al.*, The genetics of Mexico recapitulates Native American substructure and affects biomedical traits. *Science* **344**, 1280–1285 (2014). doi: 10.1126/science.1251688; pmid: 24926019
35. P. Verdu *et al.*, Patterns of admixture and population structure in native populations of Northwest North America. *PLOS Genet.* **10**, e1004530 (2014). doi: 10.1371/journal.pgen.1004530; pmid: 25122539
36. D. H. Alexander, J. Novembre, K. Lange, Fast model-based estimation of ancestry in unrelated individuals. *Genome Res.* **19**, 1655–1664 (2009). doi: 10.1101/gr.094052.109; pmid: 19648217
37. J. K. Pickrell, J. K. Pritchard, Inference of population splits and mixtures from genome-wide allele frequency data. *PLOS Genet.* **8**, e1002967 (2012). doi: 10.1371/journal.pgen.1002967; pmid: 23166502
38. M. Meyer *et al.*, A high-coverage genome sequence from an archaic Denisovan individual. *Science* **338**, 222–226 (2012). pmid: 22936568
39. M. Raghavan *et al.*, The genetic prehistory of the New World Arctic. *Science* **345**, 1255832–1255832 (2014). doi: 10.1126/science.1255832; pmid: 25170159
40. A. Scally, R. Durbin, Revising the human mutation rate: Implications for understanding human evolution. *Nat. Rev. Genet.* **13**, 745–753 (2012). doi: 10.1038/nrg3295; pmid: 22965354
41. S. Sheehan, K. Harris, Y. S. Song, Estimating variable effective population sizes from multiple genomes: A sequentially markov conditional sampling distribution approach. *Genetics* **194**, 647–662 (2013). doi: 10.1534/genetics.112.149096; pmid: 23608192
42. M. Steinrücken, J. S. Paul, Y. S. Song, A sequentially Markov conditional sampling distribution for structured populations with migration and recombination. *Theor. Popul. Biol.* **87**, 51–61 (2013). doi: 10.1016/j.tpb.2012.08.004; pmid: 23010245
43. K. Harris, R. Nielsen, Inferring demographic history from a spectrum of shared haplotype lengths. *PLOS Genet.* **9**, e1003521 (2013). doi: 10.1371/journal.pgen.1003521; pmid: 23754952
44. S. Schiffels, R. Durbin, Inferring human population size and separation history from multiple genome sequences. *Nat. Genet.* **46**, 919–925 (2014). doi: 10.1038/ng.3015; pmid: 24952747
45. A. Eriksson *et al.*, Late Pleistocene climate change and the global expansion of anatomically modern humans. *Proc. Natl. Acad. Sci. U.S.A.* **109**, 16089–16094 (2012). doi: 10.1073/pnas.1209494109; pmid: 22988099
46. R. E. Green *et al.*, A draft sequence of the Neandertal genome. *Science* **328**, 710–722 (2010). doi: 10.1126/science.1188021; pmid: 20448178
47. N. Patterson *et al.*, Ancient admixture in human history. *Genetics* **192**, 1065–1093 (2012). doi: 10.1534/genetics.112.145037; pmid: 22960212
48. J. F. Hoffecker, S. A. Elias, *Human Ecology of Beringia* (Columbia Univ. Press, New York, 2007).
49. S. Oppenheimer, B. Bradley, D. Stanford, Solutrean hypothesis: Genetics, the mammoth in the room. *World Archaeol.* **46**, 752–774 (2014). doi: 10.1080/00438243.2014.966273
50. T. D. Dillehay, Monte Verde, *A Late Pleistocene Settlement in Chile: The Archaeological Context and Interpretation* (Smithsonian Institution Press, Washington DC, 1997).
51. M. Rasmussen *et al.*, The ancestry and affiliations of Kennewick Man. *Nature* 10.1038/nature14625 (2015). doi: 10.1038/nature14625; pmid: 26087396
52. R. S. Davis, R. A. Knecht, Continuity and change in the eastern Aleutian archaeological sequence. *Hum. Biol.* **82**, 507–524 (2010). pmid: 21417882
53. M. H. Crawford, R. C. Rubicz, M. Zlojutro, Origins of Aleuts and the genetic structure of populations of the archipelago: Molecular and archaeological perspectives. *Hum. Biol.* **82**, 695–717 (2010). pmid: 21417890
54. M. Hubbe, W. A. Neves, K. Harvati, Testing evolutionary and dispersion scenarios for the settlement of the new world. *PLOS ONE* **5**, e11105 (2010). pmid: 20559441
55. J. C. Chatters *et al.*, Late Pleistocene human skeleton and mtDNA link Paleoamericans and modern Native Americans. *Science* **344**, 750–754 (2014). doi: 10.1126/science.1252619; pmid: 24833392
56. J. García-Bour *et al.*, Early population differentiation in extinct aborigines from Tierra del Fuego-Patagonia: Ancient mtDNA sequences and Y-chromosome STR characterization. *Am. J. Phys. Anthropol.* **123**, 361–370 (2004). doi: 10.1002/ajpa.10337; pmid: 15022364
57. S. I. Perez, V. Bernal, P. N. Gonzalez, M. Sardi, G. G. Politis, Discrepancy between cranial and DNA data of early Americans: Implications for American peopling. *PLOS ONE* **4**, e5746 (2009). doi: 10.1371/journal.pone.0005746; pmid: 19478947
58. M. Hernández, C. L. Fox, C. García-Moro, Fueguian cranial morphology: The adaptation to a cold, harsh environment.

Am. J. Phys. Anthropol. **103**, 103–117 (1997). doi: 10.1002/(SICI)1096-8644(199705)103:1<103::AID-AJPA7>3.0.CO;2-X; pmid: 9185954
59. R. González-José, S. L. Dahinten, M. A. Luis, M. Hernández, H. M. Pucciarelli, Craniometric variation and the settlement of the Americas: Testing hypotheses by means of R-matrix and matrix correlation analyses. *Am. J. Phys. Anthropol.* **116**, 154–165 (2001). doi: 10.1002/ajpa.1108; pmid: 11590587
60. C. Der Sarkissian *et al*., Mitochondrial genome sequencing in Mesolithic North East Europe Unearths a new sub-clade within the broadly distributed human haplogroup C1. *PLOS ONE* **9**, e87612 (2014). doi: 10.1371/journal.pone.0087612; pmid: 24503968
61. L. Excoffier, N. Ray, Surfing during population expansions promotes genetic revolutions and structuration. *Trends Ecol. Evol.* **23**, 347–351 (2008). doi: 10.1016/j.tree.2008.04.004; pmid: 18502536
62. A. Achilli *et al*., Reconciling migration models to the Americas with the variation of North American native mitogenomes. *Proc. Natl. Acad. Sci. U.S.A.* **110**, 14308–14313 (2013). pmid: 23940335
63. E. J. Dixon, Late Pleistocene colonization of North America from Northeast Asia: New insights from large-scale paleogeographic reconstructions. *Quat. Int.* **285**, 57–67 (2013). doi: 10.1016/j.quaint.2011.02.027
64. C. A. S. Mandryk, H. Josenhans, D. W. Fedje, R. W. Mathewes, Late Quaternary paleoenvironments of Northwestern North America: Implications for inland versus coastal migration routes. *Quat. Sci. Rev.* **20**, 301–314 (2001). doi: 10.1016/S0277-3791(00)00115-3

ACKNOWLEDGMENTS

We thank J. Valdés for providing craniometric measurements of the Pericúes at the National Museum of Anthropology in México; A. Monteverde from Centro Instituto Nacional de Antropología e Historia, Baja California Sur and V. Laborde at the Musée de l´Homme in Paris for providing documentation on Pericú and Fuego-Patagonian samples, respectively; T. Gilbert, M. McCoy, C. Sarkissian, M. Sikora, and L. Orlando for helpful discussions and input; D. Yao and C. Barbieri for helping with the collection of the Aymara population sample; B. Henn and J. Kidd for providing early access to the Mayan sequencing data; Canadian Museum of History; Metlakatla and Lax Kw'alaams First Nations; Listuguj Mi'gmaq Band Council; A. Pye of TERRA Facility, Core Research Equipment & Instrument Training (CREAIT) Network at Memorial University; the Danish National High-throughput DNA Sequencing Centre (Copenhagen) for help with sequencing; and Fondation Jean Dausset-Centre d'Etude du Polymorphism Humain (CEPH) for providing DNA for the Human Genome Diversity Project (HGDP) samples that were genome-sequenced in this study. This study was supported by several funding bodies: Lundbeck Foundation and the Danish National Research Foundation (Centre for GeoGenetics members); Wellcome Trust grant 098051 (S.S., A.B., Y.X., C.T.-S., M.S.S., and R.D.); Marie Curie Intra-European Fellowship-FP7-People-PIEF-GA-2009-255503 and the Transforming Human Societies Research Focus Areas Fellowship from La Trobe University (C.V.); George Rosenkranz Prize for Health Care Research in Developing Countries and National Science Foundation award DMS-1201234 (M.C.A.A); Swiss National Science Foundation (PBSKP3_143529) (A.-S.M.); Ministerio de Ciencia e Innovación (MICINN) Project CGL2009-12703-C03-03 and MICINN (BES-2010-030127) (R.R.-V.); Consejo Nacional de Ciencia y Tecnología (Mexico) (J.V.M.M.); Biotechnology and Biological Sciences Research Council BB/H005854/1 (V.W., F.B., and A.M.); European Research Council and Marie Curie Actions Grant 300554 (M.E.A.); Wenner-Gren Foundations and the Australian Research Council Future Fellowship FT0992258 (C.I.S.); European Research Council ERC-2011-AdG 295733 grant (Langelin) (D.P. and D.L.); Bernice Peltier Huber Charitable Trust (C.H. and L.G.D.); Russian Foundation for Basic Research grant 13-06-00670 (E.B.); Russian Foundation for Basic Research grant 14-0400725 (E.K.); European Union European Regional Development Fund through the Centre of Excellence in Genomics to Estonian Biocentre and Estonian Institutional Research grant IUT24-1 (E.M., K.T., M.M., M.K., and R.V.); Estonian Science Foundation grant 8973 (M.M.); Stanford Graduate Fellowship (J.R.H.); Washington State University (B.M.K.); French National Research Agency grant ANR-14-CE31-0013-01 (F-X.R); European Research Council grant 261213 (T.K.); National Science Foundation BCS-1025139 (R.S.M.); Social Science Research Council of Canada (K.-A.P. and V.G.); National Institutes of Health grants R01-GM094402 (M.S. and Y.S.S.), R01-AI17892 (P.J.N. and P.P.), and 2R01HG003229-09 (R.N. and C.D.B.); Packard Fellowship for Science and Engineering (Y.S.S.); Russian Science Fund grant 14-04-00827 and Presidium of Russian Academy of Sciences Molecular and Cell Biology Programme (O.B.); and Russian Foundation for Basic Research grant 14-06-00384 (Y.B.). Informed consent was obtained for the sequencing of the modern individuals, with ethical approval from the National Committee on Health Research Ethics, Denmark (H-3-2012-FSP21). SNP chip genotype data and whole-genome data for select present-day individuals are available only for demographic research under data access agreement with E.W. (a list of these samples is provided in tables S1 and S4). Raw reads from the ancient and the remainder of the present-day genomes are available for download through European Nucleotide Archive (ENA) accession no. PRJEB9733, and the corresponding alignment files are available at www.cbs.dtu.dk/suppl/NativeAmerican. The remainder of the SNP chip genotype data can be accessed through Gene Expression Omnibus (GEO) series accession no. GSE70987 and at www.ebc.ee/free_data. The authors declare no competing financial interests. C.D.B. is on the advisory board of Personalis, Identify Genomics, Etalon DX, and Ancestry.com.

SUPPLEMENTARY MATERIALS

www.sciencemag.org/content/349/6250/aab3884/suppl/DC1
Materials and Methods
Supplementary Text
Figs. S1 to S41
Tables S1 to S15
References (*65*–*205*)

4 May 2015; accepted 15 July 2015
Published online 23 July 2015
10.1126/science.aab3884

RESEARCH ARTICLE

QUANTUM GASES

Observation of many-body localization of interacting fermions in a quasirandom optical lattice

Michael Schreiber,[1,2] Sean S. Hodgman,[1,2] Pranjal Bordia,[1,2] Henrik P. Lüschen,[1,2] Mark H. Fischer,[3] Ronen Vosk,[3] Ehud Altman,[3] Ulrich Schneider,[1,2,4] Immanuel Bloch[1,2]*

Many-body localization (MBL), the disorder-induced localization of interacting particles, signals a breakdown of conventional thermodynamics because MBL systems do not thermalize and show nonergodic time evolution. We experimentally observed this nonergodic evolution for interacting fermions in a one-dimensional quasirandom optical lattice and identified the MBL transition through the relaxation dynamics of an initially prepared charge density wave. For sufficiently weak disorder, the time evolution appears ergodic and thermalizing, erasing all initial ordering, whereas above a critical disorder strength, a substantial portion of the initial ordering persists. The critical disorder value shows a distinctive dependence on the interaction strength, which is in agreement with numerical simulations. Our experiment paves the way to further detailed studies of MBL, such as in noncorrelated disorder or higher dimensions.

The ergodic hypothesis is one of the central principles of statistical physics. In ergodic time evolution of a quantum many-body system, local degrees of freedom become fully entangled with the rest of the system, leading to an effectively classical hydrodynamic evolution of the remaining slow observables (*1*). Hence, ergodicity is responsible for the demise of observable quantum correlations in the dynamics of large many-body systems and forms the basis for the emergence of local thermodynamic equilibrium in isolated quantum systems (*2*–*4*). It is therefore of fundamental interest to investigate how ergodicity breaks down and to understand the long-time stationary states that ensue in the absence of ergodicity.

One path to breaking ergodicity is provided by the study of integrable models, in which thermalization is prevented owing to the constraints imposed on the dynamics by an infinite set of conservation rules. Such models have been realized and studied in a number of experiments with ultracold atomic gases (*5*–*7*). However, integrable models represent very special and fine-tuned situations, making it difficult to extract general underlying principles.

Theoretical studies over the past decade point to many-body localization (MBL) in a disordered isolated quantum system as a more generic alternative to thermalization dynamics. In his original paper on single-particle localization, Anderson already speculated that interacting many-body systems subject to sufficiently strong disorder would also fail to thermalize (*8*). Only recently, however, have convincing theoretical arguments been put forward that Anderson localization remains stable under the addition of moderate interactions, even in highly excited many-body states (*9*–*11*). Further theoretical studies have established the many-body localized state as a distinct dynamical phase of matter that exhibits previously unknown universal behavior (*12*–*22*). In particular, the relaxation of local observables does not follow the conventional paradigm of thermalization and is expected to show explicit breaking of ergodicity (*23*).

Although Anderson localization of noninteracting particles has been experimentally observed in a variety of systems, including light scattering from semiconductor powders in three-dimensional (3D) (*24*), photonic lattices in 1D (*25*) and 2D (*26*), and cold atoms in 1D and 3D random (*27*–*29*) and quasirandom (*30*) disorder, the interacting case has proven more elusive. Initial experiments with interacting systems have focused on the superfluid- (*31*–*33*) or metal-to-insulator (*34*) transition in the ground state. Evidence for inhibited macroscopic mass transport was reported even at elevated temperatures (*34*) but is hard to distinguish from the exponentially slow motion expected from conventional activated transport or effects stemming from the inhomogeneity of the cloud. Possible precursors of MBL have also been reported in a transport experiment by using conventional thin-film electronic insulators (*35*).

Here, we report the experimental observation of ergodicity breaking because of MBL away from the ground state. Our experiments are performed in a 1D system of ultracold fermions in a bichromatic, quasirandomly disordered lattice potential. We identified the many-body localized phase by monitoring the time evolution of local observables following a quench of system parameters. Specifically, we prepared a high-energy initial state with a strong, artificially prepared charge density wave (CDW) order (Fig. 1A) and measured the relaxation of this CDW in the ensuing unitary evolution. Our main observable is the imbalance $\mathcal{I}$ between the respective atom numbers on even (N_e) and odd (N_o) sites

$$\mathcal{I} = \frac{N_e - N_o}{N_e + N_o} \quad (1)$$

which directly measures the CDW order. Although the initial CDW ($\mathcal{I} \sim 0.9$) will quickly relax to zero in the thermalizing case, this is not true in a localized system, in which ergodicity is broken and the system cannot act as its own heat bath (Fig. 1B) (*36*). Intuitively, if the system is strongly localized, all particles will stay close to their original positions during time evolution, thus only smearing out the CDW a little. A longer localization length ξ corresponds to more extended states and will lead to a lower steady-state value of the imbalance. The long-time stationary value of the imbalance thus effectively serves as an order parameter of the MBL phase and allows us to map the phase boundary between the ergodic and nonergodic phases in the parameter space of interaction versus disorder strength. In particular, close to the transition, the imbalance is expected to vanish asymptotically as a power law $\propto 1/\xi^{\alpha}$ with $\alpha > 0$ (*37*). In contrast to previous experiments, which studied the effect of disorder on the global expansion and transport dynamics (*27*, *30*, *31*, *33*, *34*), the CDW order parameter acts as a purely local probe, directly capturing the ergodicity breaking. Although ultimately facing a similar challenge, namely distinguishing very slow dynamics from no dynamics, the CDW is expected to undergo much faster dynamics, facilitating the detection of MBL.

Theoretical model

Our system can be described by the 1D fermionic Aubry-André model (*38*) with interactions (*36*), given by the Hamiltonian

$$\hat{H} = -J\sum_{i,\sigma}(\hat{c}^{\dagger}_{i,\sigma}\hat{c}_{i+1,\sigma} + \text{h.c.}) + \Delta\sum_{i,\sigma}\cos(2\pi\beta i + \phi)\hat{c}^{\dagger}_{i,\sigma}\hat{c}_{i,\sigma} + U\sum_{i}\hat{n}_{i,\uparrow}\hat{n}_{i,\downarrow} \quad (2)$$

Here, J is the tunneling matrix element between neighboring lattice sites, $\hat{c}^{\dagger}_{i,\sigma}$ denotes the creation operator, and $\hat{c}_{i,\sigma}$ denotes the annihilation operator for a fermion in spin state $\sigma \in \{\uparrow, \downarrow\}$ on site i. The second term describes the quasirandom disorder—the shift of the on-site energy due to an additional incommensurate lattice, characterized

[1]Fakultät für Physik, Ludwig-Maximilians-Universität München, Schellingstrasse 4, 80799 Munich, Germany. [2]Max-Planck-Institut für Quantenoptik, Hans-Kopfermann-Strasse 1, 85748 Garching, Germany. [3]Department of Condensed Matter Physics, Weizmann Institute of Science, Rehovot 7610001, Israel. [4]Cavendish Laboratory, University of Cambridge, J. J. Thomson Avenue, Cambridge CB3 0HE, UK.
*Corresponding author. E-mail: imb@mpq.mpg.de

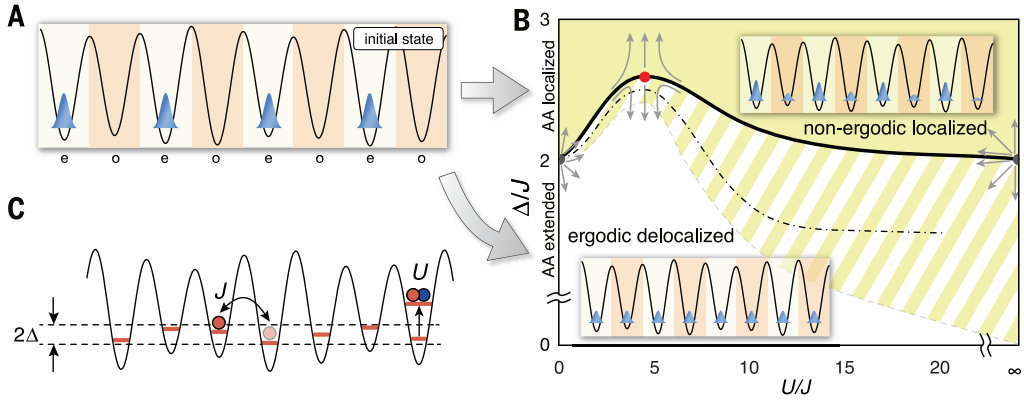

Fig. 1. Schematics of the many-body system, initial state, and phase diagram. (**A**) Initial state of our system consisting of a CDW, in which all atoms occupy even sites (e) only. For an interacting many-body system, the evolution of this state over time depends on whether the system is ergodic or not. (**B**) Schematic phase diagram for the system. In the ergodic, delocalized phase (white), the initial CDW quickly decays, whereas it persists for long times in the nonergodic, localized phase (yellow). The striped area indicates the dependence of the transition on the doublon fraction, with the black solid line indicating the case of no doublons. The black dash-dotted line represents the experimentally observed transition for a finite doublon fraction, extracted from the data in Fig. 4. The gray arrows depict the postulated pattern of renormalization group flows controlling the localization transition. For $U = 0$, as well as in the limit of infinite U with no doublons present (*37*), the transition is controlled by the noninteracting Aubry-André critical point, represented by the unstable gray fixed points. Generically, however, it is governed by the MBL critical point (*48*), shown in red. The $U = 0$ and $U = \infty$ as well as the $\Delta/J = 0$ limits represent special integrable cases that are not ergodic (*51*, *52*). (**C**) A schematic representation of the three terms in the Aubry-André Hamiltonian (Eq. 2).

by the ratio of lattice periodicities β, disorder strength Δ, and phase offset ϕ. Finally, U represents the on-site interaction energy, and $\hat{n}_{i,\sigma} = \hat{c}^{\dagger}_{i,\sigma}\hat{c}_{i,\sigma}$ is the local number operator (Fig. 1C).

This quasirandom model is special in that for almost all irrational β (*37*), all single-particle states become localized at the same critical disorder strength $\Delta/J = 2$ (*38*). For larger disorder strengths, the localization length decreases monotonically. Such a transition was indeed observed experimentally in a noninteracting bosonic gas (*30*). In contrast, truly random disorder will lead to single-particle localization in one dimension already for arbitrarily small disorder strengths. Previous numerical work indicates MBL in quasirandom systems to be similar to that obtained for a truly random potential (*36*).

Experiment

We experimentally realized the Aubry-André model by superimposing on the primary, short lattice ($\lambda_s = 532$ nm) a second, incommensurate disorder lattice with $\lambda_d = 738$ nm (thus, $\beta = \lambda_s/\lambda_d \approx 0.721$) and control J, Δ, and ϕ via lattice depths and relative phase between the two lattices (*37*). The interactions (U) between atoms in the two different spin states $|\uparrow\rangle$ and $|\downarrow\rangle$ are tuned via a magnetic Feshbach resonance (*37*). In total, this provides independent control of U, J, and Δ and enables us to continuously tune the system from an Anderson insulator in the noninteracting case to the MBL regime for interacting particles.

An additional long lattice ($\lambda_l = 1064$ nm $= 2\lambda_s$) forms a period-two superlattice (*39*, *40*) together with the short lattice and is used during the preparation of the initial CDW state and during detection (*37*). Deep lattices along the orthogonal directions [$\lambda_\perp = 738$ nm and $V_\perp = 36(1)E_R$] create an array of decoupled 1D tubes. Here, $E_R = h^2/(2m\lambda_{lat}^2)$ denotes the recoil energy, with h being Planck's constant, m the mass of the atoms, and λ_{lat} the respective wavelength of the lattice lasers.

We used a two-component degenerate Fermi gas of ^{40}K atoms, consisting of an equal mixture of 90×10^3 to 110×10^3 atoms in each of the two lowest hyperfine states $|F, m_F\rangle = |\frac{9}{2}, -\frac{9}{2}\rangle \equiv |\downarrow\rangle$ and $|\frac{9}{2}, -\frac{7}{2}\rangle \equiv |\uparrow\rangle$, at an initial temperature of $0.20(2)\,T_F$, where T_F is the Fermi temperature. The atoms were initially prepared in a finite temperature band insulating state (*41*), with up to 100 atoms per tube in the long and orthogonal lattices. We then split each lattice site by ramping up the short lattice in a tilted configuration (*37*) and subsequently ramped down the long lattice. This creates a CDW, in which there are no atoms on odd lattice sites but zero, one, or two atoms on each even site (*40*, *42*). This initial CDW is then allowed to evolve for a given time in the $8.0(2)E_R$ deep short lattice at a specific interaction strength U in the presence of disorder Δ. In a final step, we detected the number of atoms on even and odd lattice sites by using a band-mapping technique that maps them to different bands of the superlattice (*37*, *42*). This allows us to directly measure the imbalance $\mathcal{I}$, as defined in Eq. 1, in much larger systems than what is numerically feasible.

Results

We tracked the time evolution of the imbalance $\mathcal{I}$ for various interactions U and disorder strengths Δ (Fig. 2). At short times, the imbalance exhibits some dynamics consisting of a fast decay followed by a few damped oscillations. After a few tunneling times $\tau = h/(2\pi J)$, the imbalance approaches a stationary value. In a clean system ($\Delta/J = 0$), and for weak disorder, the stationary value of the imbalance approaches zero. For stronger disorder, however, this behavior changes dramatically, and the imbalance attains a nonvanishing stationary value that persists for all observation times. Because the imbalance must decay to zero on approaching thermal equilibrium at these high energies, the nonvanishing stationary value of $\mathcal{I}$ directly indicates nonergodic dynamics. Deep in the localized phase, in which unbiased numerical density-matrix renormalization group (DMRG) calculations are feasible because of the slow entanglement growth,

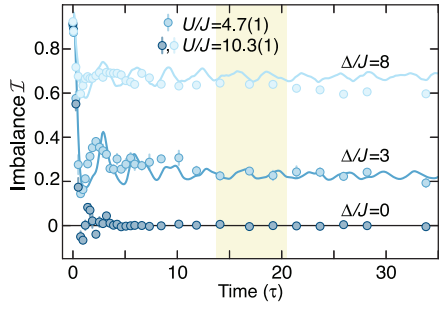

Fig. 2. Time evolution of an initial CDW. A CDW, consisting of fermionic atoms occupying only even sites, is allowed to evolve in a lattice with an additional quasirandom disorder potential. After variable times, the imbalance $\mathcal{I}$ between atoms on odd and even sites is measured. Experimental time traces (circles) and DMRG calculations for a single homogeneous tube (lines) (*37*) are shown for various disorder strengths Δ. Each experimental data point denotes the average of six different realizations of the disorder potential, and the error bars show the SD of the mean. The shaded region indicates the time window used to characterize the stationary imbalance in the rest of the analysis.

we found the stationary value obtained in the simulations to be in very good agreement with the experimental result. These simulations were performed for a single homogeneous tube without any trapping potentials (*37*). The stronger damping of oscillations observed in the experiment can be attributed to a dephasing caused by variations in J between different 1D tubes (*37*, *42*).

We experimentally observed an additional very slow decay of $\mathcal{I}$ on a time scale of several hundred tunneling times for all interaction strengths, which we attribute to the fact that our system is not perfectly closed owing to small background gas losses, technical heating, photon scattering, and coupling to neighboring

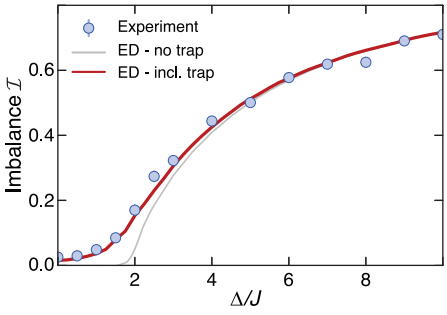

Fig. 3. Stationary values of the imbalance $\mathcal{I}$ as a function of disorder strength Δ for noninteracting atoms. The Aubry-André transition is at $\Delta/J = 2$. Circles show the experimental data, along with exact diagonalization (ED) calculations with (red line) and without (gray line) trap effects (*37*). Each experimental data point is the average of three different evolution times (13.7, 17.1, and 20.5 τ) and four different disorder phases ϕ, for a total of 12 individual measurements per point. To avoid any interaction effects, only a single spin component was used. The ED calculations are averaged over similar evolution times to the experiment and 12 different phase realizations. Error bars show the SD of the mean.

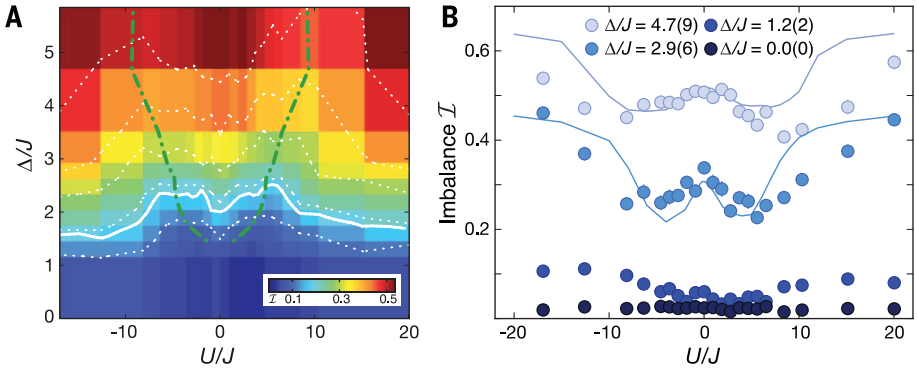

Fig. 4. Stationary imbalance for various interaction and disorder strengths. (**A**) Stationary imbalance $\mathcal{I}$ as a function of interactions U and disorder strength Δ. Moderate interactions reduce the degree of localization compared with the noninteracting or strongly interacting cases. The white dotted lines are contours of equal $\mathcal{I}$, and the solid white line is the contour of $\mathcal{I}$ matching the Aubry-André transition ($U = 0$ and $\Delta/J = 2$) extended to the interacting case. It indicates the MBL transition. The green dot-dashed line shows the fitted minima of $\mathcal{I}$ for each Δ (*37*). Each individual data point (vertices of the pseudo-color plot) is the average of the same 12 parameters as in Fig. 3. The color of each square represents the average imbalance of the four points on the corners. All data were taken with a doublon fraction of 34(2)%. (**B**) Cuts along four different disorder strengths. The effect of interactions on the localization gives rise to a characteristic "W" shape. Solid lines are the results of DMRG simulations for a single homogeneous tube. Error bars indicate the SD of the mean.

tubes (*37*, *43*). Another potential mechanism for delocalization at long times is related to the intrinsic SU(2) spin symmetry in our system (*44*). However, for the relevant observation times our numerical simulations do not indicate the presence of such a thermalization process.

To characterize the dependence of the localization transition on U and Δ, we focused on the stationary value of $\mathcal{I}$, plotted in Fig. 3 for noninteracting atoms and in Fig. 4 for interacting atoms. For noninteracting atoms (Fig. 3), the measured imbalance is compatible with extended states within the finite, trapped system for $\Delta/J \lesssim 2$. Above the critical point of the homogeneous Aubry-André model at $\Delta/J = 2$ (*38*), however, the measured imbalance strongly increases as the single-particle eigenstates become more and more localized. The observed transition agrees well with our theoretical modeling, including the harmonic trap (*37*).

The addition of moderate interactions slightly reduces the degree of localization compared with that of the noninteracting case; they decrease the imbalance $\mathcal{I}$ and hence increase the critical value of Δ necessary to cross the delocalization-localization transition (Fig. 4, A and B). We found that localization persists for all interaction strengths. For a given disorder, the imbalance $\mathcal{I}$ decreases up to a value of $U \sim 2\Delta$ before increasing again. For large $|U|$, the system even becomes more localized than in the noninteracting case. This can be understood qualitatively by considering an initial state consisting purely of empty sites and sites with two atoms (doublons): For sufficiently strong interactions, isolated doublons represent stable quasiparticles because the two atoms cannot separate and hence only tunnel with an effective second-order tunneling rate of $J_D = \frac{2J^2}{|U|} \ll J$ (*45*, *46*). This strongly increases the effective disorder $\propto \Delta/J_D \gg \Delta/J$ and promotes localization. In the experiment, the initial doublon fraction is well below one (*37*), and the density is finite, so that we observed a weaker effect. We found the localization dynamics and the resulting stationary values to be symmetric around $U = 0$, highlighting the dynamical $U \leftrightarrow -U$ symmetry of the Hubbard Hamiltonian for initially localized atoms (*47*). The effect of interactions can be seen in the contour lines (Fig. 4A, dotted white lines) as well as directly in the characteristic "W" shape of the imbalance at constant disorder (Fig. 4B), demonstrating the re-entrant behavior of the system (*22*). This behavior extends to our best estimate of the localization transition, which is shown in Fig. 4A as the solid white line.

We can gain additional insight into how localization changes with interaction strength by computing the growth of the entanglement entropy (*37*) between the two halves of the system during the dynamics (Fig. 5A). For long times, we observed a logarithmic growth of the entanglement entropy with time as $S(t) = S_{\text{offset}} + s_* \ln(t/\tau)$, which is characteristic of the MBL phase (*12*, *13*). The slope s_* is proportional to the bare localization length ξ_*, which in a weakly interacting system in the localized phase corresponds to the single-particle localization length. In general, ξ_* is the characteristic length over which the effective interactions between the conserved local densities decay (*17*, *18*) and connects to the many-body localization length ξ deep in the localized phase. In contrast to ξ, however, ξ_* is expected to remain finite at the transition (*48*). We found s_* to exhibit a broad maximum for intermediate interaction strengths (Fig. 5B), corresponding to a maximum in the thus inferred localization length. This maximum in turn leads to a minimum in the CDW value. Both the characteristic "W" shape in the imbalance and the maximum in the entanglement entropy slope are consequences of the maximum in localization length. Equivalent information on the localization properties as obtained from the entanglement entropy can be gained in experiments by monitoring the temporal decay of fluctuations around the stationary value of the CDW (*37*). Although we do not have sufficient sensitivity to measure these fluctuations in the current experiment, we expect them to be accessible to experiments with single-site resolution (*49*, *50*).

To systematically study the effect of the initial energy density on the MBL phase, we loaded the lattice using either attractive, vanishing, or repulsive interactions (Fig. 6), predominantly changing the number of doublons in the initial state (*37*). Because the initial state consists of fully localized particles only, the local energy density is directly given by the product of interaction strength U and doublon density. We found that for an interaction strength during the evolution of $|U/J| \leq 6$, the energy density does not substantially affect the localization properties, proving that MBL persists over a wide energy range. For $|U/J| > 8$, localization properties depend substantially on the doublon fraction because of the second emerging energy scale J_D, as discussed above. Thus, the localization transition can be tuned via changing the doublon fraction at large U. This constitutes a direct observation of a many-body mobility edge because the doublon density dominates the energy density.

For the case of repulsive loading, which results in a low fraction of doubly occupied sites, the imbalance for $U/J = 0$ and strong interactions match within error. Indeed, a rigorous mapping

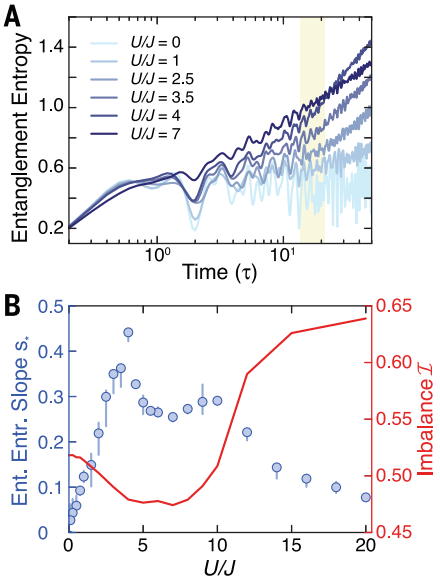

Fig. 5. Calculated growth of entanglement entropy and corresponding slope. (**A**) DMRG results of the entanglement entropy growth (*37*) for various interaction strengths and $\Delta/J = 5$. For long times, logarithmic growth characteristic of interacting MBL states is visible. The experimentally used evolution times indicated by the yellow shaded region are found to be in the region of logarithmic growth. (**B**) The slope of the logarithmic growth (circles), extracted by using linear fits up to the longest simulated time (50 τ) in (A), shows a nonmonotonic dependence on the interaction strength, which is correlated with the inverse of the steady-state value of the CDW order parameter (red line). Error bars reflect different initial starting times for the fit.

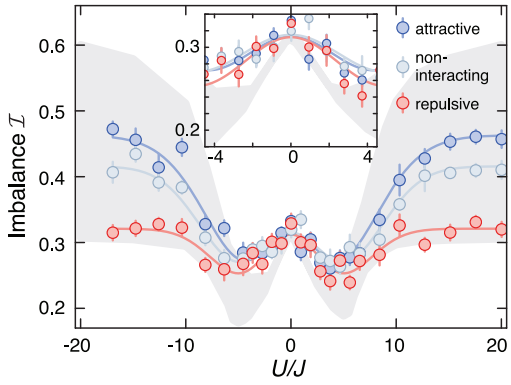

Fig. 6. Stationary imbalance $\mathcal{I}$ as a function of interaction strength during loading. Data were taken with disorder $\Delta/J = 3$. The loading interactions of $a_{load} = -89(2)\ a_0$ (attractive, where a_0 denotes Bohr's radius), $0(1)\ a_0$ (noninteracting), and $142(1)\ a_0$ (repulsive) correspond to initial doublon fractions of 51(1), 43(2), and 8(6)%, respectively (*39*). Each $\mathcal{I}$ value is the average of the same 12 parameters as in Fig. 3. Error bars show the SD of the mean. Solid lines are guides to the eye. The gray shaded area spans the limiting cases of 0 and 50% doublons, simulated by using DMRG for a single homogeneous tube.

can be made between the noninteracting system and the dynamics in the doublon-free subspace at strong interactions $|U/J| \to \infty$ (*37*). At very large interactions and high doublon fractions, the additional long time scales start to also compete with heating and loss processes, rendering the definition of stationary states challenging.

Conclusion

Our experimental demonstration of ergodicity breaking because of MBL paves the way for many further investigations. An interesting extension would be to use "true" random disorder created by, for example, an optical speckle pattern, as has been used to study Anderson localization (*27*). Another important next step is extending the present study to higher dimensions. Additional insight can also be gained by analyzing the full relaxation dynamics of local observables (*19*–*21*) in an experimental setup featuring single-site resolution (*49*, *50*). For instance, the decay of fluctuations of $\mathcal{I}$ with time could be directly measured, providing an even more direct connection to the entanglement entropy. Another important direction for future investigation is the effect of opening the system in a controlled way. This could be done, for example, by adding a near-resonant laser so as to deliberately enhance photon scattering or by using a Bose-Fermi mixture, in which excitations of the Bose-Einstein condensate form a well-controlled bath for the fermions. This will allow a systematic study of the critical dynamics associated with the MBL phase transition, in which the bath relaxation time now provides the only scale. Such a study would also allow the MBL phase to be clearly distinguished experimentally from classical glassy dynamics. The latter, unlike MBL, is insensitive to coupling of the system to an external bath.

REFERENCES AND NOTES

1. J. Lux, J. Müller, A. Mitra, A. Rosch, *Phys. Rev. A* **89**, 053608 (2014).
2. J. M. Deutsch, *Phys. Rev. A* **43**, 2046–2049 (1991).
3. M. Srednicki, *Phys. Rev. E Stat. Phys. Plasmas Fluids Relat. Interdiscip. Topics* **50**, 888–901 (1994).
4. M. Rigol, V. Dunjko, M. Olshanii, *Nature* **452**, 854–858 (2008).
5. B. Paredes *et al.*, *Nature* **429**, 277–281 (2004).
6. T. Kinoshita, T. Wenger, D. S. Weiss, *Nature* **440**, 900–903 (2006).
7. M. Gring *et al.*, *Science* **337**, 1318–1322 (2012).
8. P. W. Anderson, *Phys. Rev.* **109**, 1492–1505 (1958).
9. D. M. Basko, I. L. Aleiner, B. L. Altshuler, *Ann. Phys.* **321**, 1126–1205 (2006).
10. I. V. Gornyi, A. D. Mirlin, D. G. Polyakov, *Phys. Rev. Lett.* **95**, 206603 (2005).
11. J. Z. Imbrie, On many-body localization for quantum spin chains. http://arxiv.org/abs/1403.7837 (2014).
12. M. Žnidarič, T. Prosen, P. Prelovšek, *Phys. Rev. B* **77**, 064426 (2008).
13. J. H. Bardarson, F. Pollmann, J. E. Moore, *Phys. Rev. Lett.* **109**, 017202 (2012).
14. B. Bauer, C. Nayak, *J. Stat. Mech.* **09**, P09005 (2013).
15. R. Vosk, E. Altman, *Phys. Rev. Lett.* **110**, 067204 (2013).
16. M. Serbyn, Z. Papić, D. A. Abanin, *Phys. Rev. Lett.* **110**, 260601 (2013).
17. M. Serbyn, Z. Papić, D. A. Abanin, *Phys. Rev. Lett.* **111**, 127201 (2013).
18. D. A. Huse, R. Nandkishore, V. Oganesyan, *Phys. Rev. B* **90**, 174202 (2014).
19. F. Andraschko, T. Enss, J. Sirker, *Phys. Rev. Lett.* **113**, 217201 (2014).
20. R. Vasseur, S. A. Parameswaran, J. E. Moore, *Phys. Rev. B* **91**, 140202 (2015).
21. M. Serbyn, Z. Papić, D. A. Abanin, *Phys. Rev. B* **90**, 174302 (2014).
22. Y. Bar Lev, G. Cohen, D. R. Reichman, *Phys. Rev. Lett.* **114**, 100601 (2015).
23. A. Pal, D. A. Huse, *Phys. Rev. B* **82**, 174411 (2010).
24. D. S. Wiersma, P. Bartolini, A. Lagendijk, R. Righini, *Nature* **390**, 671–673 (1997).
25. Y. Lahini *et al.*, *Phys. Rev. Lett.* **100**, 013906 (2008).
26. T. Schwartz, G. Bartal, S. Fishman, M. Segev, *Nature* **446**, 52–55 (2007).
27. J. Billy *et al.*, *Nature* **453**, 891–894 (2008).
28. S. S. Kondov, W. R. McGehee, J. J. Zirbel, B. DeMarco, *Science* **334**, 66–68 (2011).
29. F. Jendrzejewski *et al.*, *Nat. Phys.* **8**, 398–403 (2012).
30. G. Roati *et al.*, *Nature* **453**, 895–898 (2008).
31. B. Deissler *et al.*, *Nat. Phys.* **6**, 354–358 (2010).
32. B. Gadway, D. Pertot, J. Reeves, M. Vogt, D. Schneble, *Phys. Rev. Lett.* **107**, 145306 (2011).
33. C. D'Errico *et al.*, *Phys. Rev. Lett.* **113**, 095301 (2014).
34. S. S. Kondov, W. R. McGehee, W. Xu, B. DeMarco, *Phys. Rev. Lett.* **114**, 083002 (2015).
35. M. Ovadia, D. Kalok, I. Tamir, S. Mitra, B. Sacepe, D. Shahar, Evidence for a finite temperature insulator. http://arxiv.org/abs/1406.7510 (2014).
36. S. Iyer, V. Oganesyan, G. Refael, D. A. Huse, *Phys. Rev. B* **87**, 134202 (2013).
37. Materials and methods are available as supplementary materials on *Science* Online.
38. S. Aubry, G. André, *Ann. Israel Phys. Soc.* **3**, 133 (1980).
39. J. Sebby-Strabley, M. Anderlini, P. S. Jessen, J. V. Porto, *Phys. Rev. A* **73**, 033605 (2006).
40. S. Fölling *et al.*, *Nature* **448**, 1029–1032 (2007).
41. U. Schneider *et al.*, *Science* **322**, 1520–1525 (2008).
42. S. Trotzky *et al.*, *Nat. Phys.* **8**, 325–330 (2012).
43. H. Pichler, A. J. Daley, P. Zoller, *Phys. Rev. A* **82**, 063605 (2010).
44. R. Vasseur, A. C. Potter, S. A. Parameswaran, *Phys. Rev. Lett.* **114**, 217201 (2015).
45. K. Winkler *et al.*, *Nature* **441**, 853–856 (2006).
46. S. Trotzky *et al.*, *Science* **319**, 295–299 (2008).
47. U. Schneider *et al.*, *Nat. Phys.* **8**, 213–218 (2012).
48. R. Vosk, D. A. Huse, E. Altman, Theory of the many-body localization transition in one dimensional systems. http://arxiv.org/abs/1412.3117 (2014).
49. W. S. Bakr, J. I. Gillen, A. Peng, S. Fölling, M. Greiner, *Nature* **462**, 74–77 (2009).
50. J. F. Sherson *et al.*, *Nature* **467**, 68–72 (2010).
51. F. Essler, H. Frahm, F. Göhmann, A. Klümper, V. Korepin, *The One-Dimensional Hubbard Model* (Cambridge Univ. Press, Cambridge, UK, 2005).
52. C. Gramsch, M. Rigol, *Phys. Rev. A* **86**, 053615 (2012).

ACKNOWLEDGMENTS

We acknowledge useful discussions with F. Essler and technical assistance by D. Garbe and F. Görg during the setup of the experiment. We acknowledge financial support by the Deutsche Forschungsgemeinschaft (FOR801, Deutsch-Israelisches Kooperationsprojekt Quantum phases of ultracold atoms in optical lattices), the European Commission (UQUAM and AQuS), the U.S. Defense Advanced Research Projects Agency (Quantum Emulations of New Materials Using Ultracold Atoms), the Minerva Foundation, ISF grant no. 1594/11, Nanosystems Initiative Munich (NIM), and the Swiss Society of Friends of the Weizmann Institute.

SUPPLEMENTARY MATERIALS

www.sciencemag.org/content/349/6250/842/suppl/DC1
Supplementary Text
Figs. S1 to S9
References (*53*–*62*)

22 January 2015; accepted 21 July 2015
Published online 30 July 2015
10.1126/science.aaa7432

REPORTS

QUANTUM SIMULATION

Localization-delocalization transition in the dynamics of dipolar-coupled nuclear spins

Gonzalo A. Álvarez,[1]* Dieter Suter,[2]* Robin Kaiser[3]*

Nonequilibrium dynamics of many-body systems are important in many scientific fields. Here, we report the experimental observation of a phase transition of the quantum coherent dynamics of a three-dimensional many-spin system with dipolar interactions. Using nuclear magnetic resonance (NMR) on a solid-state system of spins at room-temperature, we quench the interaction Hamiltonian to drive the evolution of the system. Depending on the quench strength, we then observe either localized or extended dynamics of the system coherence. We extract the critical exponents for the localized cluster size of correlated spins and diffusion coefficient around the phase transition separating the localized from the delocalized dynamical regime. These results show that NMR techniques are well suited to studying the nonequilibrium dynamics of complex many-body systems.

The complexity of many-body systems is a long-standing problem in physics (*1*–*4*). As an example, quantum states of many-body systems can be localized at well-defined positions in space or they can be delocalized, depending on parameters like disorder. In their localized regime, such systems may not reach a thermal state but retain information about their initial state on very long time scales (*5*–*10*). The role of the topology, dimension, long- and short-range interactions, and the presence of disorder is very important for the onset of these localization regimes. Much progress was achieved on the numerical and theoretical side, where these phenomena have been predicted under certain conditions. However, experimentally addressing three-dimensional (3D) many-body systems in a controlled manner poses severe experimental problems (*4*, *8*, *10*). The usual strategy to observe many-body phenomena is achieving very cold temperatures where sharp changes of the ground state as a function of a control parameter give evidence of quantum phase transitions (*11*–*13*). Alternatively, the nonequilibrium dynamics of many-body systems has been investigated to provide complementary information about a large variety of situations (*14*–*20*). This approach can even work at high or infinite temperatures; however, it is usually more challenging than monitoring static properties. The recent progress on the experimental control of cold atoms (*21*), trapped ions (*19*, *20*), Rydberg atoms (*22*), polar molecules (*23*), and nitrogen-vacancy centers in diamond (*24*) has led to promising new ways of studying the nonequilibrium dynamics and localization phenomena of many-body systems. In particular, a lot of effort is focused on studying many-spin systems with dipolar interactions of the Heisenberg type (*4*, *11*–*13*, *18*–*20*, *22*, *23*). Here, we use nuclear magnetic resonance (NMR), which provides a natural and versatile approach for coherently controlling large numbers of spins (up to ~7000) in solid-state systems, where dipolar interactions are present (*25*). NMR techniques allow to quantify the number of spins that are coherently correlated and allow control of the interaction types and strengths of the Hamiltonians (*25*–*27*).

Our experimental system consists of the ^{1}H nuclear spins of polycrystalline adamantane (Fig. 1A, inset). All experiments were performed on a home-built solid-state NMR spectrometer in a magnetic field of 7 Tesla. The interaction of the proton spins $I = 1/2$ with the static magnetic field results in a Zeeman splitting of $\omega_z = 300$ MHz (in frequency units), which is identical for all spins. The mutual dipole-dipole interactions between the spins corresponds to a 3D spin-coupling network (Fig. 1). The dipolar interaction scales with $1/r^3$ and leads to a resonance line width of 7.9 kHz of the NMR spectrum due to the homogeneous broadening [see (*27*) for details of the sample]. The spin system is initially left to reach thermal equilibrium at room temperature. In this high-temperature limit, the two spin states $\uparrow, \downarrow$ are almost equally populated, with the excess of the lower energy state on the order of $\hbar\omega_z/k_BT \sim 10^{-5}$. Its density operator can then be described as $\hat{\rho}_0 - \hat{1} \propto \hat{I}_z = \sum_i \hat{I}_z^i$ (*26*, *28*), considering that the Zeeman interaction is much stronger than the dipolar one ($\omega_z = 300$ MHz $\gg 7.9$ kHz). We omit the unity operator $\hat{1}$ since it does not evolve in time and does not contribute to the observable signal. Then $\hat{\rho}_0 \propto \hat{I}_z$ is the total spin operator component in the direction of the magnetic field and $\hat{I}_z^i$ that of the i^{th} spin.

The Hamiltonian of the system in the interaction picture—i.e., in a reference frame rotating at the Zeeman frequency around the z axis—is the spin-spin interaction

$$\hat{\mathcal{H}}_{dd} = \sum_{i<j} d_{ij}\left[2\hat{I}_z^i\hat{I}_z^j - (\hat{I}_x^i\hat{I}_x^j + \hat{I}_y^i\hat{I}_y^j)\right] \quad (1)$$

This is the part of the dipolar interaction that commutes with the much stronger Zeeman Hamiltonian, the so-called secular term in NMR. The noncommuting terms can be neglected due to $|d_{ij}/\omega_z| < 10^{-5}$ (*26*, *28*). The coupling constants are

$$d_{ij} = \frac{1}{2}\frac{\gamma^2\hbar^2}{r_{ij}^3}(1 - 3\cos^2\theta_{ij}) \quad (2)$$

with γ the gyromagnetic ratio, θ_{ij} the angle between the internuclear vector $\vec{r}_{ij}$ and the magnetic field direction. This Heisenberg-type Hamiltonian is of growing interest in the context of quantum information and simulation science (*4*, *11*, *18*–*20*, *22*, *23*).

The initial condition corresponds to a thermal equilibrium with uncorrelated spins, and the density operator $\hat{\rho}_0$ commutes with the system Hamiltonian $\hat{\mathcal{H}}_{dd}$ (Fig. 1A). To generate spin clusters of correlated spins, we quench the system by suddenly changing its Hamiltonian to

$$\hat{\mathcal{H}}_0 = -\sum_{i<j} d_{ij}\left[\hat{I}_x^i\hat{I}_x^j - \hat{I}_y^i\hat{I}_y^j\right] \quad (3)$$

which does not commute with the thermal equilibrium state (Fig. 1B). We use a method developed in (*29*, *30*) based on a sequence of $\pi/2$-pulses that act equally on all spins in such a way that the time-averaged effect on a time scale much shorter than $1/d_{ij}$ generates this effective Hamiltonian (*28*).

To study the effect of the quench and monitor the generation of clusters of correlated spins, we compare its evolution under a parametric set of Hamiltonians

$$\hat{\mathcal{H}} = (1-p)\hat{\mathcal{H}}_0 + p\hat{\mathcal{H}}_{dd} \quad (4)$$

These Hamiltonians are generated by concatenating short periods during which different Hamiltonians act on the system (*28*): the Hamiltonian $\hat{\mathcal{H}}_0$ for a duration τ_0 and $\hat{\mathcal{H}}_{dd}$ for a duration τ_{dd}, where $\tau_0, \tau_{dd} \ll 1/|d_{ij}|$. The total evolution operator is then equivalent to the evolution under an effective, time-independent Hamiltonian $\hat{\mathcal{H}}$ during a time $\tau_c = \tau_0 + \tau_{dd}$. This resulting cycle is then repeated N times, giving a total evolution time $t = N\tau_c$. The control parameter $p = \tau_{dd}/\tau_c$ defines a perturbation to the quench strength. If $p = 1$, there is no quench, and $1-p$ defines the strength of the quench. The two Hamiltonians $\hat{\mathcal{H}}_0$ and $\hat{\mathcal{H}}_{dd}$ have distinct symmetries with respect

[1]Department of Chemical Physics, Weizmann Institute of Science, 76100, Rehovot, Israel. [2]Fakultät Physik, Technische Universität Dortmund, D-44221, Dortmund, Germany. [3]Institut Non-Linéaire de Nice, CNRS, Université de Nice Sophia Antipolis, 06560, Valbonne, France.
*Corresponding author. E-mail: gonzalo.a.alvarez@weizmann.ac.il (G.A.A.); dieter.suter@tu-dortmund.de (D.S.); robin.kaiser@inln.cnrs.fr (R.K.)

to the total magnetic quantum number M_z, the eigenvalue of $\hat{I}_z$. Whereas the Hamiltonian $\hat{\mathcal{H}}_0$ simultaneously flips two spins and, accordingly, changes M_z by $\Delta M_z = \pm 2$ (green arrows in Fig. 1C), $\hat{\mathcal{H}}_{dd}$ mixes states that conserve M_z (red arrows in Fig. 1C).

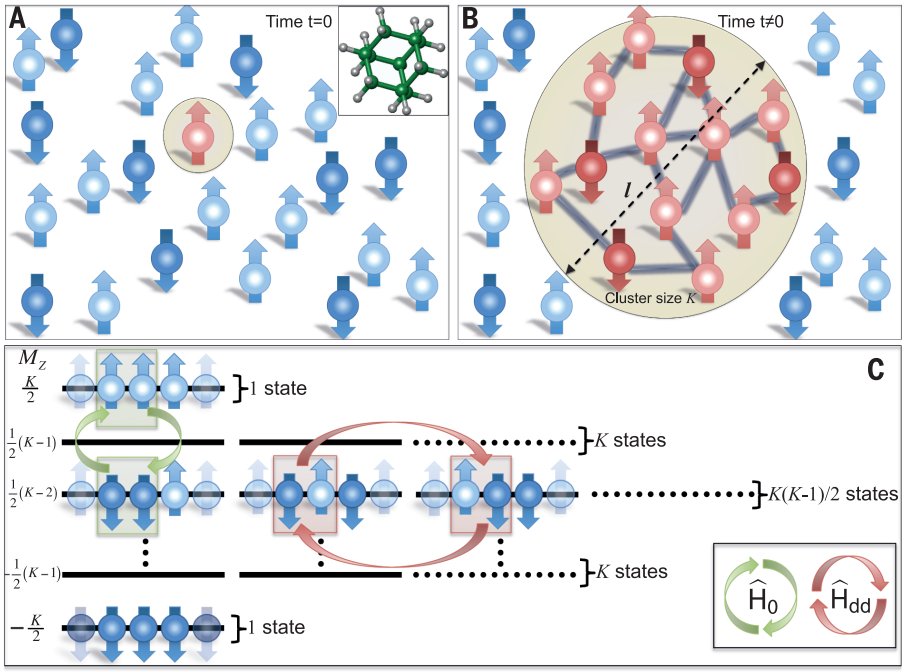

Fig. 1. Quantum evolutions and Hamiltonian characteristics. (**A**) Thermal equilibrium of the proton spins in the presence of a static magnetic field at time t = 0 just before the quench. The spins are uncorrelated, the density operator is $\hat{\rho}_0 \propto \hat{I}_z = \sum_i \hat{I}_z^i$, where $\hat{I}_z$ is the total spin magnetization operator and $\hat{I}_z^i$ the single spin operators. The red spin in the center represents an uncorrelated spin state $\hat{I}_z^i$ of the spin ensemble. It thus represents a cluster of correlated spins with size K = 1. (Inset) Adamantane molecule with 16 protons (small gray spheres). The large green spheres represent carbon atoms, consisting of 99% ^{12}C and 1% ^{13}C . (**B**) Cluster of correlated spins at time $t > 0$ after the quench with $\hat{\mathcal{H}}_0$ (red spins). The cluster consisting of K > 1 correlated spins occupies a volume l^3, where l is the effective coherence length. (**C**) Evolution of a system of K spins in the Zeeman product basis $|\alpha_1, \alpha_2, ..., \alpha_K\rangle$ ($\alpha_i = \uparrow, \downarrow$) (black solid lines), where $\hat{I}_z|\alpha_1, \alpha_2, ..., \alpha_K\rangle = M_z|\alpha_1, \alpha_2, ..., \alpha_K\rangle$. The green arrows represent the $\hat{\mathcal{H}}_0$ interactions, which simultaneously flip two spins, causing M_z to change by $\Delta M_z = \pm 2$. The red arrow represents the $\hat{\mathcal{H}}_{dd}$ interactions that conserve the quantum number M_z.

After the quench, the Hamiltonians (Eq. 4) generate correlations between the different spins. We measure the average number of correlated spins in the system (the cluster size) by decomposing the corresponding density operator according to its symmetry under rotations around the z axis, adapting a method from (*30*). The method is based on an interferometric detection of the overlap of the density operator with and without a rotation by an angle ϕ around the z axis. The resulting signal as a function of ϕ consists of the terms of the density operator with the additional phase $e^{i\phi\Delta M_z}$, where ΔM_z takes only even numbers. After a Fourier transform, one obtains the distribution of coherences generated by $\hat{\mathcal{H}}_0$ (nondiagonal terms in the eigenbasis of $\hat{I}_z$) of the density matrix as a function of the difference between quantum numbers ΔM_z. We determine the average number of correlated spins K in the generated clusters from the width of these distributions (*25*, *27*, *28*). We associate them to an effective volume l^3, with l the effective correlation length (Fig. 1B). Figure 2A shows the extracted cluster size K as a function of the evolution time $t = N\tau_c$ for different perturbation strengths on time scales much shorter than the time required for the system to thermalize with the lattice ($T_1 \approx 1$ sec). For the unperturbed evolution (black squares), the cluster size grows indefinitely within the time range measured before the experimental signal disappears due to decoherence processes (*25*, *27*, *28*). This changes qualitatively when the perturbation is turned on: The growth of the clusters generated by the perturbed Hamiltonian (colored symbols in Fig. 2A) does not continue indefinitely but saturates at a certain level, which we call the localization size. This localization size decreases with increasing perturbation strength p.

To quantitatively analyze the transition from the delocalized to the localized dynamical regimes, we exploit the powerful finite-time scaling

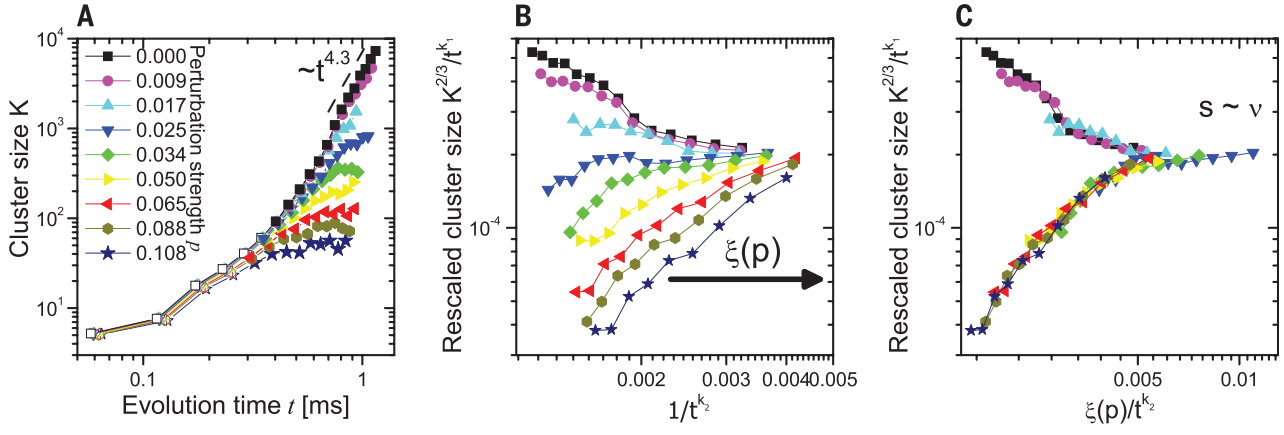

Fig. 2. Time evolution of the cluster size *K* for different perturbation strengths and finite-time scaling procedure. (**A**) Cluster-size K as a function of the time t after the quench. The unperturbed quenched evolution (black squares) shows a cluster-size K that grows as $\sim t^{4.3}$ at long times (dashed line is a guide to the eye). The solid symbols show the points used for the finite-time scaling analysis, while the empty symbols do not belong to the long time regime ($t < 0.3$ ms). For the largest perturbation strengths, localization effects are clearly visible by the saturation of the cluster size. (**B** and **C**) In these two panels, we present the finite-time scaling procedure. In (B), the rescaled and squared correlation length $l^2/t^{k_1^{exp}} = K^{2/3}(t)/t^{k_1^{exp}}$ as a function of the evolution time $1/t^{k_2^{exp}}$ is plotted, where $k_1^{exp} \approx 1.91$ and $k_2^{exp} \approx 0.96$ were determined using the experimentally measured $\alpha_{exp} \approx 2.87$ and the relations $k_1 = \frac{2\alpha}{3}$, $k_2 = \frac{\alpha}{3\nu}$ that hold when $s = \nu$ (*28*). In (C), the curves of (B) are rescaled horizontally by the factor $\xi(p)$ to obtain a universal scaling law.

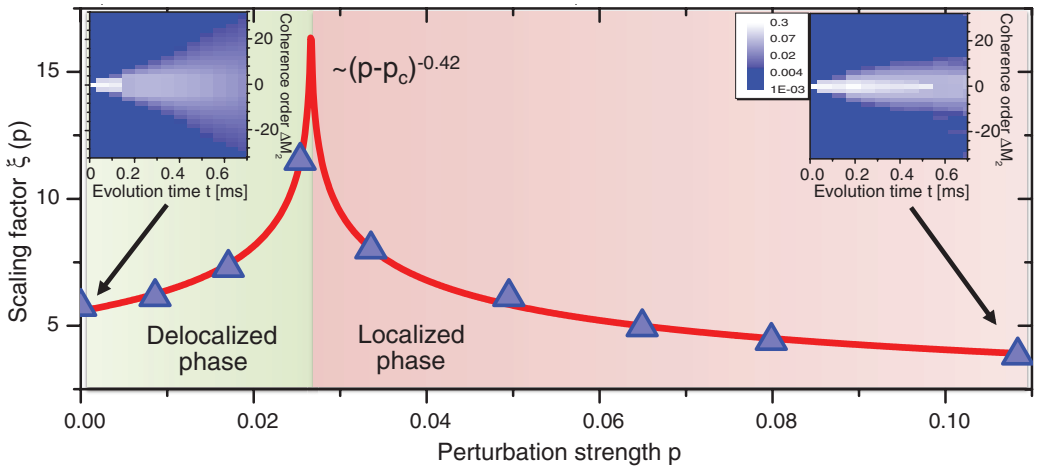

Fig. 3. Scaling factor and critical exponents. Normalized scaling factor $\xi(p)$ as a function of p (blue triangles). The normalization is based on equalizing $\xi(p = 0.108) = K_{loc}^{1/3} \approx (56.33)^{1/3}$ (*28*). The red solid line is a fit to the blue triangles with the expression $\xi(p) = (A|p - p_c|^{\nu} + B)^{-1}$, where $A = 0.58 \pm 0.08$, $B = 0.05 \pm 0.02$, the critical exponent $\nu = 0.42 \pm 0.07$, and the critical perturbation $p_c = 0.0266 \pm 0.0004$. From Fig. 2 we determined that $\nu \approx s$. The two insets show the distribution of coherence orders of the density matrix as a function of the evolution time t for the perturbation strengths $p = 0$ and $p = 0.108$, which correspond to the delocalized and localized regime, respectively. The corresponding scaling factors are indicated by the arrows.

technique (*31*, *32*). This procedure allows one to extract from finite-time experimental data the localization length l at $t \to \infty$. Without perturbation, the cluster size is expected to grow with a power law in agreement with several experimental observations in solid-state spin networks (*33*). In our system, this growth law is observed for times $t > 0.7$ ms and vanishing perturbation $p = 0$, where $K \propto t^{4.3}$ (*25*, *27*). Thus, $l^2 \sim K^{2/3} \sim Dt^{\alpha}$, where D is a generalized diffusion coefficient and α is the exponent of the "diffusion" process (*33*, *34*). This time evolution behaves in a qualitatively different way if the system remains localized. In our case, the system undergoes a phase transition to a localized evolution if the perturbation strength exceeds the critical value p_c. One expects then that the cluster-size evolution will depend on $p - p_c$ (*31*, *32*, *34*). We use the single-parameter Ansatz for the scaling behavior at long times

$$K^{2/3} \sim t^{k_1} F\left[(p_c - p)t^{k_2}\right] \qquad (5)$$

where $F(x)$ is an arbitrary function and k_1 and k_2 are constant parameters. We assume that $D(p) \propto (p_c - p)^{s}$, such that the diffusion coefficient vanishes, $D = 0$, at the onset of the localized regime for $p = p_c$, with s as a critical exponent of the delocalized phase.

In the localized regime, we found experimentally that the localization cluster size is a power-law function of the perturbation strength p (*25*, *27*). Therefore, we assume that at long times $K^{2/3} \sim (p - p_c)^{-2\nu}$ for $p > p_c$, as is typically assumed for localization phenomena; ν is the critical exponent for the localized phase (*31*, *32*, *34*). We performed the finite-time scaling analysis for different relations between the two critical exponents—i.e., varying β in the relation $s = \beta\nu$—and found the universal scaling for $s \approx \nu$ shown in Fig. 2, B and C, and in fig. S4 (*28*).

The scaling factor $\xi(p)$ that leads to the universal scaling behavior $f(\xi(p)t^{-k_2\nu}) = K^{2/3}t^{-k_1}$, with $f(x)$ an arbitrary function, is shown in Fig. 3 as the blue triangles. The solid red line is a fit with the expression $\xi(p) = (A|p - p_c|^{\nu} + B)^{-1}$, where B accounts for decoherence processes that smooth out the critical transition (*31*, *32*). We thus obtain a critical perturbation strength of $p_c = 0.0266 \pm 0.0004$ and the critical exponents $\nu = s = 0.42 \pm 0.07$. This result is consistent with the scaling law Ansatz of Eq. 5. The insets in Fig. 3 show the probability distribution of coherences (nondiagonal terms in the eigenbasis of $\hat{I}_z$) in the density matrix (*28*) as a function of the coherence order ΔM_z and the evolution time in both regimes. Although for a perturbation strength $p < p_c$, the coherence distribution spreads indefinitely (delocalized regime), for $p > p_c$ the coherence distribution becomes localized after a given time.

From the power-law coefficient $\alpha_{exp} \approx 2.86$, experimentally determined in the unperturbed free diffusion regime, our analysis shows a critical behavior on the transition from the localized to the delocalized dynamical regime with critical exponents $s \approx \nu$. This is consistent with Wegner's scaling law $s = (d - 2)\nu$ for a 3D system ($d = 3$) (*35*), in agreement with the assumption that the cluster-size K determines an effective volume occupied by the correlated spins and its respective effective correlation length, $l^3 \propto K$. Although a microscopic theory should be developed to confirm our findings, the present results represent strong evidence for a critical transition of the dynamic behavior of the coherence length of our system after the quench. This critical behavior is induced by competing dipole-dipole interactions in the many-body dynamics of the cluster of correlated spins.

REFERENCES AND NOTES

1. I. Bloch, J. Dalibard, W. Zwerger, *Rev. Mod. Phys.* **80**, 885–964 (2008).
2. L. Amico, R. Fazio, A. Osterloh, V. Vedral, *Rev. Mod. Phys.* **80**, 517–576 (2008).
3. T. Lahaye, C. Menotti, L. Santos, M. Lewenstein, T. Pfau, *Rep. Prog. Phys.* **72**, 126401 (2009).
4. I. Georgescu, S. Ashhab, F. Nori, *Rev. Mod. Phys.* **86**, 153–185 (2014).
5. P. W. Anderson, *Rev. Mod. Phys.* **50**, 191 (1978);
6. D. Basko, I. Aleiner, B. Altshuler, *Ann. Phys.* **321**, 1126–1205 (2006).
7. V. Oganesyan, D. A. Huse, *Phys. Rev. B* **75**, 155111 (2007).
8. F. Jendrzejewski *et al.*, *Nat. Phys.* **8**, 398–403 (2012).
9. R. Vosk, E. Altman, *Phys. Rev. Lett.* **110**, 067204 (2013).
10. G. Semeghini *et al.*, *Nat. Phys.* **11**, 554–559 (2015).
11. H. M. Rønnow *et al.*, *Science* **308**, 389–392 (2005).
12. E. Burzurí *et al.*, *Phys. Rev. Lett.* **107**, 097203 (2011).
13. C. Kraemer *et al.*, *Science* **336**, 1416–1419 (2012).
14. S. Hofferberth, I. Lesanovsky, B. Fischer, T. Schumm, J. Schmiedmayer, *Nature* **449**, 324–327 (2007).
15. M. Rigol, V. Dunjko, M. Olshanii, *Nature* **452**, 854–858 (2008).
16. S. Trotzky *et al.*, *Nat. Phys.* **8**, 325–330 (2012).
17. M. Cheneau *et al.*, *Nature* **481**, 484–487 (2012).
18. J. Schachenmayer, B. P. Lanyon, C. F. Roos, A. J. Daley, *Phys. Rev. X* **3**, 031015 (2013); http://dx.doi.org/10.1103/PhysRevX.3.031015.
19. P. Jurcevic *et al.*, *Nature* **511**, 202–205 (2014).
20. P. Richerme *et al.*, *Nature* **511**, 198–201 (2014).
21. W. S. Bakr, J. I. Gillen, A. Peng, S. Fölling, M. Greiner, *Nature* **462**, 74–77 (2009).
22. M. Saffman, T. G. Walker, K. Molmer, *Rev. Mod. Phys.* **82**, 2313–2363 (2010).
23. B. Yan *et al.*, *Nature* **501**, 521–525 (2013).
24. G. Waldherr *et al.*, *Nature* **506**, 204–207 (2014).
25. G. A. Álvarez, D. Suter, *Phys. Rev. Lett.* **104**, 230403 (2010).
26. C. Slichter, *Principles of Magnetic Resonance* (Springer, Berlin, 1996).
27. G. A. Álvarez, R. Kaiser, D. Suter, *Ann. Phys. (Berlin)* **525**, 833–844 (2013).
28. Supplementary materials are available on *Science* Online.
29. W. Warren, S. Sinton, D. Weitekamp, A. Pines, *Phys. Rev. Lett.* **43**, 1791–1794 (1979).
30. J. Baum, M. Munowitz, A. N. Garroway, A. Pines, *J. Chem. Phys.* **83**, 2015 (1985).
31. J. Chabé *et al.*, *Phys. Rev. Lett.* **101**, 255702 (2008).
32. G. Lemarié *et al.*, *Phys. Rev. A* **80**, 043626 (2009).
33. S. Lacelle, *Adv. Magn. Opt. Reson.* **16**, 173–263 (1991).
34. R. Metzler, J. Klafter, *Phys. Rep.* **339**, 1–77 (2000).
35. F. J. Wegner, *Z. Physik B* **25**, 327–337 (1976).

ACKNOWLEDGMENTS

We thank J. Chabé, F. Hebert, and E. Altman for fruitful discussions. This work was supported by the Deutsche Forschungsgemeinschaft through Su 192/24-1. G.A.A. acknowledges the support of the Alexander von Humboldt Foundation and of the European Commission under the Marie Curie Intra-European Fellowship for Career Development grant PIEF-GA-2012-328605.

SUPPLEMENTARY MATERIALS

www.sciencemag.org/content/349/6250/846/suppl/DC1
Materials and Methods
Supplementary Text
Figs. S1 to S4

12 September 2014; accepted 21 July 2015
10.1126/science.1261160

ASTROPHYSICS

Atom-interferometry constraints on dark energy

P. Hamilton,[1]* M. Jaffe,[1] P. Haslinger,[1] Q. Simmons,[1] H. Müller,[1,2]† J. Khoury[3]

If dark energy, which drives the accelerated expansion of the universe, consists of a light scalar field, it might be detectable as a "fifth force" between normal-matter objects, in potential conflict with precision tests of gravity. Chameleon fields and other theories with screening mechanisms, however, can evade these tests by suppressing the forces in regions of high density, such as the laboratory. Using a cesium matter-wave interferometer near a spherical mass in an ultrahigh-vacuum chamber, we reduced the screening mechanism by probing the field with individual atoms rather than with bulk matter. We thereby constrained a wide class of dark energy theories, including a range of chameleon and other theories that reproduce the observed cosmic acceleration.

Cosmological observations have firmly established that the universe is expanding at an accelerating pace, which can be explained by dark energy permeating all of space and accounting for ~70% of the energy density of the universe (*1*). What constitutes dark energy, and why it has its particular density, remain as some of the most pressing open questions in physics. What is clear is that dark energy presents us with a new energy scale, on the order of milli–electron volts. It is reasonable to speculate that new (usually scalar) fields might be associated with this scale and that these may make up all or part of the dark energy density (*2*, *3*). String theory with "compactified" extra dimensions, for instance, features a plethora of scalar fields, which typically couple directly to matter fields unless protected by a shift symmetry, as for axions (*4*, *5*). If the fields are light, this coupling would be observable as a "fifth force," in potential conflict with precision tests of gravity (*6*).

Theories with so-called screening mechanisms, on the other hand, have features that suppress their effects in regions of high density, so that they may couple to matter but nonetheless evade experimental constraints (*7*). One prominent example is the chameleon field, the mass of which depends on the ambient matter density (*8*, *9*). It is light and mediates a long-range force in sparse environments, such as the cosmos, but it becomes massive and thus short-ranged in a high-density environment, such as the laboratory (fig. S1). This makes it difficult to detect with fifth-force experiments.

Burrage and co-workers (*10*) recently proposed using atom interferometers (*11*, *12*) to search for chameleons. An ultrahigh-vacuum chamber containing atomic test particles simulates the low-density conditions of empty space, liberating the chameleon field to become long-ranged and thus measurable. In this study, we used a cavity-based atom interferometer (*13*, *14*), measuring the force between cesium-133 atoms and an aluminum sphere to search for a range of screened dark energy theories that can reproduce the estimated cosmological dark energy density (Fig. 1, A and B).

The chameleon dark energy field ϕ in equilibrium is determined by minimizing a potential density $V(\phi) + V_{\rm int}$, which is the sum of a self-interaction term $V(\phi)$ and a term $V_{\rm int}$ describing the interaction with ordinary matter. The simplest chameleon theories are characterized by two parameters that have the dimension of mass. The first one, Λ, enters the self-interaction potential term (*15*, *16*)

$$V(\phi) = \Lambda^4 e^{\Lambda^n/\phi^n} \simeq \Lambda^4 + \frac{\Lambda^{4+n}}{\phi^n} + \ldots \quad (1)$$

The term proportional to $1/\phi^n$, where n is a real exponent often taken to be 1, leads to screening, whereas the constant term is responsible for the chameleon's energy density in otherwise empty space. It can drive the cosmic acceleration observed today if $\Lambda = \Lambda_0 \approx 2.4$ meV, given by the current dark energy density of 7×10^{-27} kg/m^3, which is roughly the mass of four hydrogen atoms per cubic meter. The second parameter, M, enters the term for interaction with ordinary matter of density ρ (again using natural units)

$$V_{\rm int} = \frac{\phi\rho}{M} \quad (2)$$

The parameter M is essentially unconstrained but plausibly below the reduced Planck mass $M_{\rm Pl} = (\hbar c/8\pi G)^{1/2} \approx 2.4\times10^{18}$ GeV/c^2. A lower bound, $M > 10^4$ GeV/c^2, was derived from hydrogen spectroscopy (*17*).

Existing experimental bounds for $M < M_{\rm Pl}$ come from oscillations of rubidium atoms in a harmonic trap (*18*) and from ultracold neutrons (*19*, *20*). Limits from astrophysical observations (*7*) and torsion balances (*6*, *21*) are available for $M \approx M_{\rm Pl}$, where the chameleon is unscreened. Experiments such as the Chameleon Afterglow Search [CHASE (*22*)], the Axion Dark Matter Experiment [ADMX (*23*)], and the CERN Axion Solar Telescope [CAST (*24*)] place bounds, given an additional coupling of the chameleon to the photon. Our limits do not depend on such extra couplings.

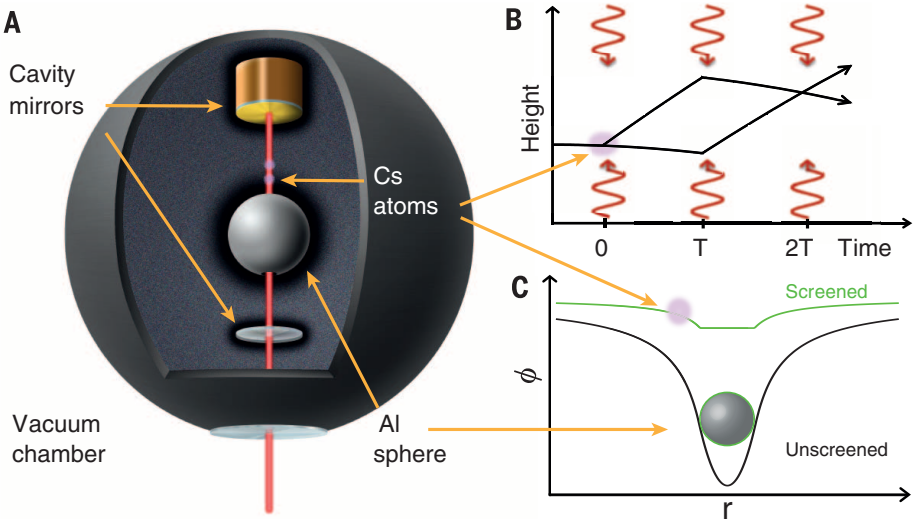

Fig. 1. Screened fields in our experiment. (**A**) The vacuum chamber (radius, 5 cm; pressure, ~6 × 10^{-10} Torr; mostly hydrogen) holds a pair of mirrors forming a Fabry-Perot cavity and the aluminum source sphere. Laser beams pass through a 1.5-mm-radius hole in the sphere (radius of the sphere, 9.5 mm). A Mach-Zehnder interferometer is formed using cold cesium atoms from a magneto-optical trap at an effective distance of 8.8 mm from the sphere surface (not shown). (**B**) Photons in three flashes of laser radiation that are resonant in the cavity impart momentum to the atoms, directing each atomic matter wave onto two paths. (**C**) The potential generated by a macroscopic sphere as a function of distance from the sphere's center.

[1]Department of Physics, 366 Le Conte Hall MS 7300, University of California–Berkeley, Berkeley, CA 94720, USA. [2]Lawrence Berkeley National Laboratory, One Cyclotron Road, Berkeley, CA 94720, USA. [3]Center for Particle Cosmology, Department of Physics and Astronomy, University of Pennsylvania, Philadelphia, PA 19104, USA. *Present address: Department of Physics and Astronomy, 475 Portola Plaza, University of California–Los Angeles, CA 90095, USA. †Corresponding author. E-mail: hm@berkeley.edu

The acceleration of an atom at a radius r from the center of the sphere (Fig. 1A), caused by the sphere via the chameleon interaction and gravity, is given by

$$a \approx \frac{Gm_s}{r^2}\left[1 + 2\lambda_a\lambda_s\left(\frac{M_{Pl}}{M}\right)^2\right] \quad (3)$$

where G is the gravitational constant, and m_s is the mass of the sphere (*10*). The screening factors λ_a and λ_s for the atom and the sphere, respectively, are functions of the object's mass and radius as well as of the parameters Λ, M, and n (eq. S1). They approach 1 for small and light particles. For macroscopic objects, however, only a thin outermost layer will interact with the chameleon field (Fig. 1C), leading to a screening factor much smaller than 1. Macroscopic fifth-force experiments are faced with two small screening factors, but atom interferometers avoid this double suppression.

The operation of the atom interferometer is based on the matter-wave concept of quantum mechanics. When the atom absorbs or emits a photon, it recoils with the momentum $\hbar k$ (where $\hbar$ is the reduced Planck constant, and k is the wavenumber of the photon). We use a two-photon Raman transition between the two hyperfine levels of the ground state of cesium, which are labeled by their total angular momentum quantum numbers of $F = 3$ and 4, respectively. The transition is driven by two vertical, counter-propagating laser beams (Fig. 1A). The atom absorbs a photon from the first beam and is stimulated by the second beam to emit a photon in the opposite direction. The net effect on the atom is a change of the internal quantum state from $F = 3$ to $F = 4$ and an impulse of $\hbar k_{eff}$, where the effective wavenumber k_{eff} is the sum of the wavenumbers of the two beams. The duration and intensity of the laser pulses can be tuned so that the transfer happens with 50 or nearly 100% probability, forming beam splitters and mirrors, respectively, for matter waves.

Our Mach-Zehnder interferometer (Fig. 1B) uses a sequence of three light pulses separated by equal time intervals T. The first pulse splits the matter-wave packet describing each atom into two partial ones that separate with a recoil velocity of about 7 mm/s. The second pulse acts as a mirror that reverses the direction of the relative motion, and the third pulse is a beam splitter that overlaps the partial wave packets. Interference of the partial matter waves determines the probability P that the atoms will arrive in each of the two interferometer outputs

$$P = \cos^2(\Delta\phi/2) \quad (4)$$

where the phase difference accumulated between the partial wave packets (*11*)

$$\Delta\phi = k_{eff}\, a_{tot}\, T^2 \quad (5)$$

is a function of the total acceleration ($a_{tot} = a + g$) of the atoms, the sum of the acceleration due to chameleon-mediated interactions with the sphere (Eq. 3), and the far larger acceleration g due to Earth's gravity (and small systematic effects).

The most sensitive atom interferometers use pulse separation times $T \approx 1$ s, over which the atoms fall up to ~10 m in tall atomic fountains (*25*–*27*). We, however, had to keep the atoms within a few millimeters of the sphere to sample the highest chameleon field gradient, and we were thus constrained to $T \approx 10$ ms, resulting in a 10,000-fold signal reduction. Our cavity-based atom interferometer (*12*, *28*), however, reached relatively high resolution under these constraints.

A full experimental run takes 1.7 s. We prepared about 10 million cesium atoms at a temperature

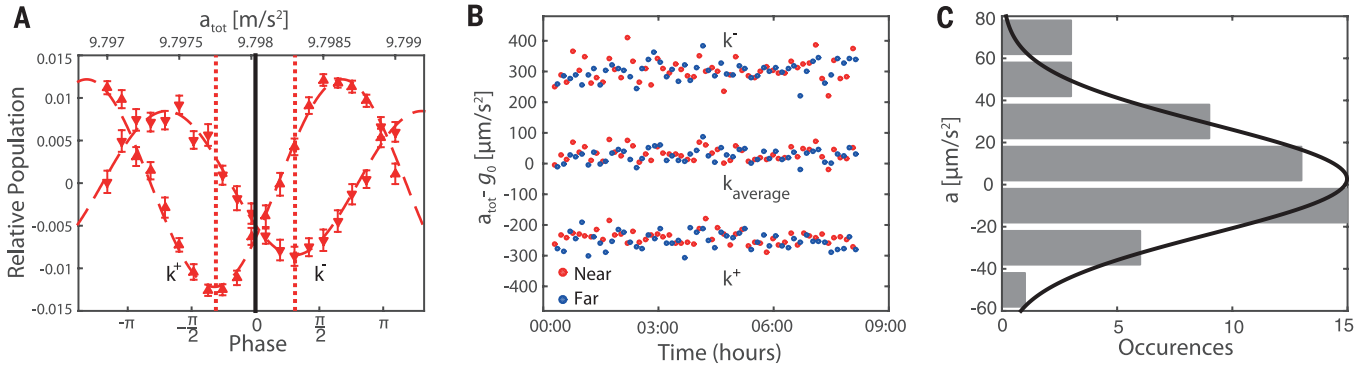

Fig. 2. Data. (**A**) Two interference fringes, measured with the wavevector normal (up, k^+) and inverted (k^-). (**B**) Acceleration $a_{tot} - g_0$, where $g_0 = 9.798$ m/s^2, measured with the wavevector normal and inverted and with the sphere in near (red) and far (blue) positions. The plotted data are from a total of 16,800 runs. Taking the average ($k_{average}$) suppresses systematic effects. Data recorded during the night, before about 6:30 AM, show the lowest noise, suggesting that sensitivity is limited by vibrations. (**C**) Histogram of differences between subsequent measurements with the sphere in the near and far positions.

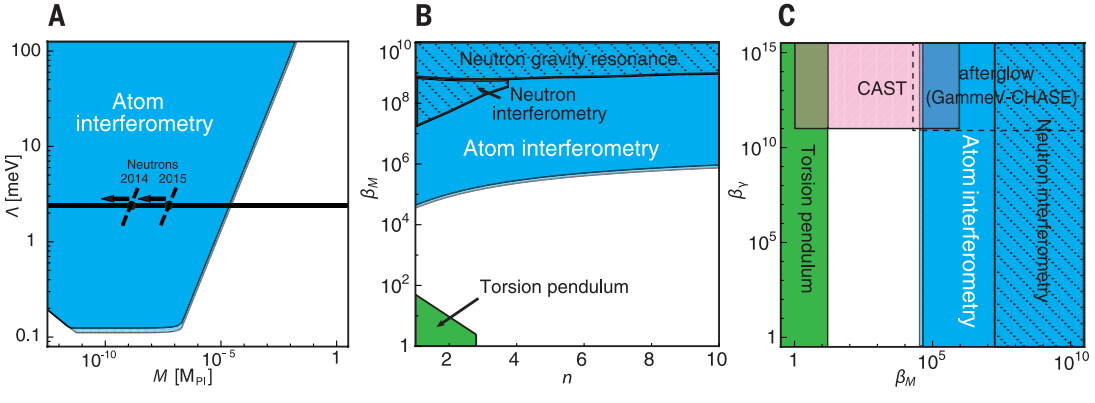

Fig. 3. Regions of exclusion. Blue areas are ruled out by our experiment. The narrow light blue stripes at their borders show the influence of the variation of $0.55 \le \xi \le 0.68$, which arises from different models for the boundary of the vacuum chamber (*14*), demonstrating the robustness of our limits. (**A**) The region excluded at the 95% confidence level in the M-Λ plane for $n = 1$ in Eq. 1. The horizontal line marks the range around $\Lambda_0 = 2.4$ meV, where the chameleon field would reproduce the current cosmic acceleration. Also indicated are the highest values of M excluded by neutron experiments (*19*, *20*); the regions to the left (indicated by arrows) are excluded. (**B**) Comparison of our atom-interferometry results with neutron gravity resonance (*19*) and neutron interferometry (*20*) results in the n-β_M plane, where $\beta_M = M_{Pl}/M$, assuming $\Lambda = \Lambda_0$. Our results are significantly lower for all values of the exponent n and β_M. Torsion pendulum experiments (*6*, *21*) limit chameleons from the other (low-β_M) end of the plane. (**C**) Comparison with CHASE (*22*) and CAST (*24*) experiments that assume photon coupling, assuming $n = 1$ and $\Lambda = \Lambda_0$. Atom interferometers as well as neutron and torsion pendulum experiments give bounds that are independent of the photon coupling parameter β_γ.

of 5 μK in the $F = 3$ state, using a two-dimensional magneto-optical trap (2D-MOT) to load a 3D-MOT through a differential pumping stage. We ran the interferometer with a pulse separation time of $T = 15.5$ ms and identified the two outputs separately via fluorescence detection with a camera (*14*).

Figure 2A shows an interference fringe obtained by measuring the atom number at the two interferometer outputs while varying the phase $\Delta\phi$ (*13*, *14*). Fitting the fringe with a sine wave determines the total acceleration of the atoms. To take out systematic effects, we applied wavevector reversal (i.e., we changed the direction of the photon impulse). This inverts the signal produced by accelerations, but many systematic effects remain unchanged and can be taken out (*29*). To measure the acceleration a originating from atom-sphere interactions (our signal for chameleons) separately from Earth's gravitational acceleration g, we compared the total acceleration $a_{tot} = a + g$ with the sphere located in the "near" position with g measured with the sphere in the "far" position. "Near" means an effective vertical distance of 8.8 mm from the surface of the sphere, and "far" means about 3 cm to the side.

One measurement consists of four interference fringes: two with the wavevector normal (one each with the sphere near and far) and two with the wavevector inverted (as above). Fifty such measurements with their statistical error bars are shown in Fig. 2B. For each, we averaged the acceleration as measured with normal and inverted wavevectors to eliminate systematic effects, and we compared the acceleration thus measured between the near and far positions of the sphere. Figure 2C shows a histogram of these acceleration differences. Fitting a Gaussian distribution to the histogram resulted in an estimate of $a = 2.7 \pm 3.3$ μm/s^2. We added corrections for systematic ac Stark shifts, magnetic fields, and electrostatic fields (*13*) (table S1) and arrived at $a = -0.7 \pm 3.7$ μm/s^2. The negative sign indicates acceleration away from the sphere. The 2σ (95%) confidence interval for these data is -8.2 μm/s^2 $< a <$ 6.8 μm/s^2.

A chameleon has a spin of 0 and can therefore only produce attractive forces (assuming universal coupling to matter). A one-tailed test shows $a <$ 5.5 μm/s^2 at the 95% confidence level. Comparison to the expected acceleration (Eqs. S8 to S11) yields the excluded range of parameters Λ and M, shown in Fig. 3A. Our experiments excluded chameleons at the scale of the cosmological constant $\Lambda = \Lambda_0 =$ 2.4 meV for $M < 2.3 \times 10^{-5}\ M_{Pl}$, making the most conservative assumption of $\xi = 0.55$ for a parameter ξ entering Eqs. S9 and S10 that describes the influence of the vacuum chamber walls (*14*). This result rules out chameleons that would reproduce the observed acceleration of the cosmos. To place our result in the context of previous experiments, we assumed that $\Lambda = \Lambda_0$. Figure 3B shows the excluded region for different values of the exponent n, and Fig. 3C shows the excluded region compared with experiments that assume photon-chameleon coupling (our results do not rely on such a coupling). In short, the only chameleon theories that are still viable are the white areas in Fig. 3, A to C, all of which we have narrowed by several orders of magnitude by using atom interferometry.

Our analysis can be generalized to constrain other scalar field theories, such as symmetron, varying-dilaton, and $f(R)$ theories. These theories belong to the same universality class as the chameleon theories, in that their screening effect is triggered by the local scalar field value, as opposed to its spatial derivatives. As a result, their phenomenology is similar to that of the chameleon (*7*).

REFERENCES AND NOTES

1. Planck Collaboration, http://xxx.lanl.gov/abs/1502.01589 (2015).
2. C. Wetterich, *Nucl. Phys. B* **302**, 668–696 (1988).
3. P. J. E. Peebles, B. Ratra, *Astrophys. J.* **325**, L17 (1988).
4. J. A. Frieman, C. T. Hill, A. Stebbins, I. Waga, *Phys. Rev. Lett.* **75**, 2077–2080 (1995).
5. L. J. Hall, Y. Nomura, S. J. Oliver, *Phys. Rev. Lett.* **95**, 141302 (2005).
6. D. J. Kapner *et al.*, *Phys. Rev. Lett.* **98**, 021101 (2007).
7. A. Joyce, B. Jain, J. Khoury, M. Trodden, *Phys. Rep.* **568**, 1–98 (2015).
8. J. Khoury, A. Weltman, *Phys. Rev. Lett.* **93**, 171104 (2004).
9. D. F. Mota, D. J. Shaw, *Phys. Rev. Lett.* **97**, 151102 (2006).
10. C. Burrage, E. J. Copeland, E. A. Hinds, *J. Cosmol. Astropart. Phys.* **2015**, 042 (2015).
11. M. Kasevich, S. Chu, *Phys. Rev. Lett.* **67**, 181–184 (1991).
12. A. D. Cronin, J. Schmiedmayer, D. E. Pritchard, *Rev. Mod. Phys.* **81**, 1051–1129 (2009).
13. P. Hamilton *et al.*, *Phys. Rev. Lett.* **114**, 100405 (2015).
14. See the supplementary materials on *Science* Online.
15. P. Brax, C. van de Bruck, A. C. Davis, J. Khoury, A. Weltman, *Phys. Rev. D Part. Fields Gravit. Cosmol.* **70**, 123518 (2004).
16. I. Zlatev, L. M. Wang, P. J. Steinhardt, *Phys. Rev. Lett.* **82**, 896–899 (1999).
17. P. Brax, C. Burrage, *Phys. Rev. D Part. Fields Gravit. Cosmol.* **83**, 035020 (2011).
18. D. M. Harber, J. M. Obrecht, J. M. McGuirk, E. A. Cornell, *Phys. Rev. A* **72**, 033610 (2005).
19. T. Jenke *et al.*, *Phys. Rev. Lett.* **112**, 151105 (2014).
20. H. Lemmel *et al.*, *Phys. Lett.* **743**, 310–314 (2015).
21. A. Upadhye, *Phys. Rev. D Part. Fields Gravit. Cosmol.* **86**, 102003 (2012).
22. J. H. Steffen *et al.*, *Phys. Rev. Lett.* **105**, 261803 (2010).
23. G. Rybka *et al.*, *Phys. Rev. Lett.* **105**, 051801 (2010).
24. V. Anastassopoulosa *et al.*, *Phys. Lett. B* 10.1016/j.physletb.2015.07.049 (2015); www.sciencedirect.com/science/article/pii/S0370269315005596.
25. G. Rosi, F. Sorrentino, L. Cacciapuoti, M. Prevedelli, G. M. Tino, *Nature* **510**, 518–521 (2014).
26. A. Sugarbaker, S. M. Dickerson, J. M. Hogan, D. M. S. Johnson, M. A. Kasevich, *Phys. Rev. Lett.* **111**, 113002 (2013).
27. G. M. Tino, M. A. Kasevich, Eds., *Atom Interferometry* (Proceedings of the International School of Physics "Enrico Fermi," vol. 188, IOS Press, Amsterdam, 2014).
28. M. A. Hohensee, B. Estey, P. Hamilton, A. Zeilinger, H. Müller, *Phys. Rev. Lett.* **108**, 230404 (2012).
29. J. M. McGuirk, G. T. Foster, J. B. Fixler, M. J. Snadden, M. A. Kasevich, *Phys. Rev. A* **65**, 033608 (2002).

ACKNOWLEDGMENTS

We acknowledge important discussions with D. Budker, C. Burrage, A. Charman, Y. Nomura, S. Perlmutter, S. Rajendran, and P. Steinhardt. This work was supported by the David and Lucile Packard Foundation; a Defense Advanced Research Projects Agency Young Faculty Award (no. N66001-12-1-4232); NSF grant PHY-1404566; and NASA grants NNH13ZTT002N, NNH13ZTT002N, and NNH11ZTT001N. P.Has. thanks the Austrian Science Fund (grant J3680). The work of J.K. is supported by the NSF Faculty Early Career Development Program (award PHY-1145525) and the NASA Astrophysics Theory Program (grant NNX11AI95G).

SUPPLEMENTARY MATERIALS

www.sciencemag.org/content/349/6250/849/suppl/DC1
Supplementary Text
Figs. S1 to S4
Tables S1 to S4
Equations S1 to S11
Reference (*30*)

12 February 2015; accepted 25 June 2015
10.1126/science.aaa8883

ASTROPHYSICS

Exclusion of leptophilic dark matter models using XENON100 electronic recoil data

The XENON Collaboration*†

Laboratory experiments searching for galactic dark matter particles scattering off nuclei have so far not been able to establish a discovery. We use data from the XENON100 experiment to search for dark matter interacting with electrons. With no evidence for a signal above the low background of our experiment, we exclude a variety of representative dark matter models that would induce electronic recoils. For axial-vector couplings to electrons, we exclude cross sections above 6×10^{-35} cm^2 for particle masses of $m_\chi = 2$ GeV/c^2. Independent of the dark matter halo, we exclude leptophilic models as an explanation for the long-standing DAMA/LIBRA signal, such as couplings to electrons through axial-vector interactions at a 4.4σ confidence level, mirror dark matter at 3.6σ, and luminous dark matter at 4.6σ.

Dark matter in the form of weakly interacting massive particles (WIMPs) is typically expected to induce nuclear recoils in a terrestrial detector target (*1*) with an annually modulated rate due to the motion of the Earth around the Sun (*2*, *3*). Although such a modulation has been observed by the DAMA/LIBRA collaboration using sodium iodine (*4*), it is difficult to interpret it as a dark matter signal, given the null results from other experiments (*5*).

*The XENON Collaboration authors and affiliations are listed in the supplementary materials.
†Corresponding authors: M. Cervantes and R. F. Lang; e-mail: mcervant@purdue.edu, rafael@purdue.edu

Indeed, dark matter–induced nuclear recoils are excluded by these results unless one invokes models that are fine-tuned to create a signal only in DAMA/LIBRA but not in other experiments (*6*–*8*). In contrast, dark matter–induced electronic recoils appear as a viable explanation for the observed modulation because exclusions of other experiments do not apply directly in this case (*9*, *10*). We use data from the XENON100 detector to rule out this possibility for three different, representative dark matter models.

We interpret data from the XENON100 detector that were acquired between 28 February 2011 and 31 March 2012 for a total exposure of 224.6 live days and 34-kg fiducial mass. We have previously searched this data set for spin-independent (*11*) and spin-dependent (*12*) WIMP-induced nuclear recoils, as well as for axion-induced electronic recoils (*13*). XENON100, located in the Gran Sasso underground laboratory, consists of a liquid xenon target that is operated as a low-background time projection chamber (*14*). Each particle interaction results in two signals: The prompt scintillation signal (S1) is used here for energy estimation, and the delayed ionization signal (S2) allows for three-dimensional vertex reconstruction. Data reduction is performed in order to select single-scatter low-energy (<10 keV) recoils in the fiducial volume, while retaining maximal detector efficiency (*13*, *15*). At low energies, the remaining background of XENON100 is dominated by forward-scattered Compton events, resulting in a flat spectrum with a rate of 5.3 events/(keV·tonne·day) in the fiducial volume (*16*) (data file A1). This rate is more than two orders of magnitude lower than the average background rate of about 1019 events/(keV·tonne·day) reported by DAMA/LIBRA in the same energy interval (*17*, *18*), and even smaller than their reported annual modulation amplitude of (11.2 ± 1.2) events/(keV·tonne·day) (*4*). Because the DAMA/LIBRA collaboration has not published the composition of their background at low energies, we test the minimum dark matter signal that would be required to cause the observed modulation. In this scenario, the constant spectrum is fully attributed to background, and only the modulated part itself is attributed to a 100% modulated dark matter signal (Fig. 1). We ignore the practical difficulties of realizing such a highly modulated signal (*3*, *19*) but conservatively consider it as the case that is most challenging to exclude. The dark matter–induced rate would then be zero on 2 December and twice the measured modulation amplitude on 2 June. It follows that there is an optimized time interval to consider for best sensitivity. To find this interval, the signal expected in XENON100 was simulated for different time intervals centered around 2 June. We take into account uncertainties from counting statistics in XENON100 and DAMA/LIBRA, as well as the systematic uncertainty from the conversion of kilo–electron volt (keV) energy into S1 (*13*). The optimum time interval is found to be 70 live days around 2 June, roughly corresponding to April 2011 to August 2011 (Fig. 1). Our expected sensitivity varies by less than 0.1σ with changes of this interval of ±40 live days.

A relativistic treatment of dark matter–electron scattering shows that keV-scale electronic recoils can only be induced by dark matter particles with masses $m_\chi \gtrsim 1\ \mathrm{GeV}/c^2$ scattering inelastically off electrons with momenta on the order of MeV/c (*9*, *20*). As shown in (*9*), even if the dark matter has tree-level (first-order) interactions only with leptons, loop-induced dark matter–hadron interactions dominate the experimental signatures and make the usual exclusions based on nuclear recoil analyses applicable. Thus, we consider here axial-vector $\vec{A}\otimes\vec{A}$ couplings between dark matter and leptons, since in this case, loop contributions vanish, whereas the WIMP–electron coupling is not suppressed by additional small factors of velocity v or mass ratio m_e/m_χ.

We use Eq. 30 in (*9*), with an additional factor of 2 to account for electron occupancy from spin, to calculate the differential rate for WIMP-electron scattering (data file A2). The expected rate includes a sum over the atomic shells of the target, and for each shell, integrates the momentum wave function of the electrons to get the contribution at a given recoil energy. Given the requirement that the energy deposited in the detector must be more than the binding energy of the electron, the largest contribution to the rate in a sodium iodide target comes from the 3s shell of iodine. The contributions from sodium are two orders of magnitude smaller. The momentum-space wave functions for xenon atoms and iodine anions are nearly identical as a result of their similar electron structure. This has the important consequence that a comparison between sodium iodide and xenon is independent of the dark matter halo. The ratio of the calculated differential rates in xenon and sodium iodide are shown in Fig. 2 as a function of deposited energy, considering the full shell structure. This ratio has negligible dependence on the WIMP mass.

We contrast the DAMA/LIBRA signal, interpreted as WIMPs coupling to electrons through axial-vector interactions, with XENON100 data. The energy spectrum of the modulation amplitude

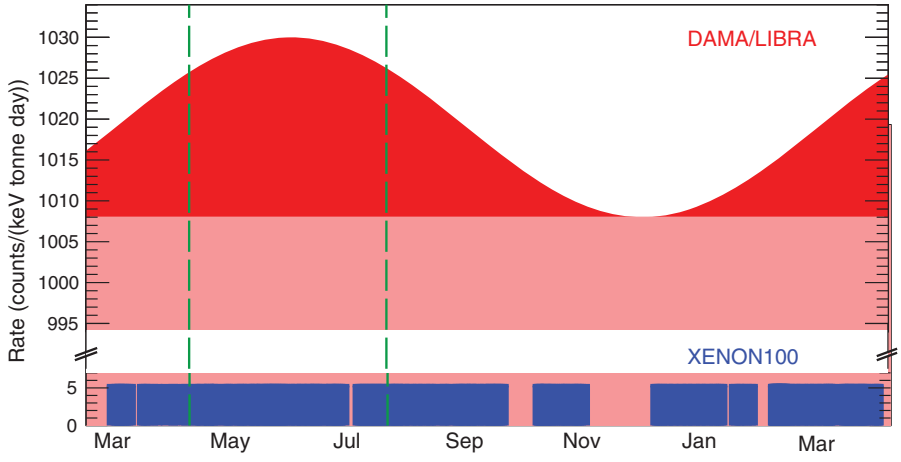

Fig. 1. Conceptual illustration of the analysis. Shown is the DAMA/LIBRA rate (red) (*17*) with the modulated rate in (2 to 6) keV from the fit parameters in (*4*) (dark red). The distribution of the XENON100 live time (blue) is indicated with its average background rate of 5.3 events/(keV·tonne·day), which shows dents due to maintenance or calibration campaigns. The region between the dashed lines (green) indicates the 70 summer live days in which the modulated signal is expected to be largest.

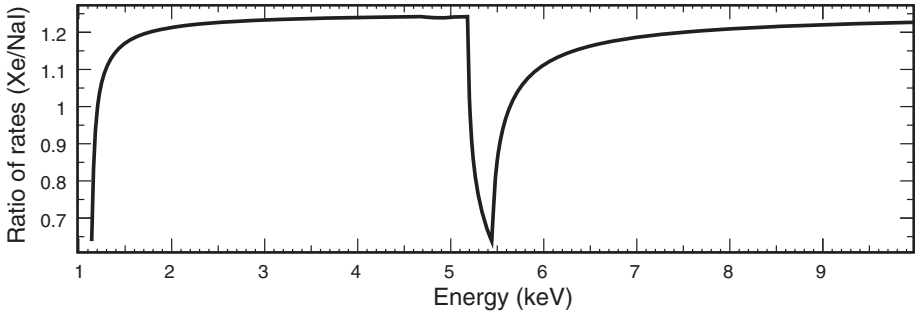

Fig. 2. Calculated ratio of the differential rates in xenon and sodium iodide for inelastic WIMP-electron scattering through axial-vector coupling. The structures around 1 and 5 keV are owing to the small difference in the binding energies of the 3s and 2s shells in xenon and iodine.

(*4*) is multiplied by the energy-dependent ratio from Fig. 2 and by a constant factor of 1.88, which accounts for the time integral of the modulated signal that is expected in our 70 summer live days (Fig. 1). The deposited electronic recoil energy in XENON100 is estimated from the S1 signal, measured in photoelectrons (PE), using the NESTv0.98 model (*21*), which consistently fits the available data (*22*–*25*). The energy scale, shown in (*13*), includes a systematic uncertainty that decreases from 20 to 7% from 1 to 10 keV, reflecting the spread and uncertainties in the measurements. The S1 generation is modeled as a Poisson process and the photomultiplier tube resolution is taken into account in order to obtain the predicted XENON100 S1 spectrum from the scaled energy spectrum (*15*). Our resolution is a factor of 2 worse than that of DAMA/LIBRA; the feature at 5.2 keV in Fig. 2 is lost in this process.

The converted DAMA/LIBRA and measured XENON100 energy spectra are shown in Fig. 3. Part of the DAMA/LIBRA signal is expected to be seen below 2 keV owing to the finite energy resolution of XENON100. The uncertainty in the converted signal includes both the statistical uncertainty in the original DAMA/LIBRA energy spectrum (*4*) and the uncertainties from our energy conversion. The electronic recoil cut acceptance, shown in (*13*), was applied to the converted DAMA/LIBRA spectrum. The uncertainty shown in the XENON100 data is statistical.

The energy region to determine the level of exclusion was chosen starting at the threshold of 3 PE (*11*) to the point where the DAMA/LIBRA signal falls below the expected average XENON100 rate (cyan in Fig. 3, calculated using a flat spectrum background model and scaled for the live time of the data set), which is at 14 PE, corresponding to (2.0 to 5.9) keV. Taking systematic uncertainties into account, a simple comparison of the integral counts in this energy interval excludes the DAMA/LIBRA signal as axial-vector coupling between WIMPs and electrons at 4.4σ significance level, even considering all events from the well-understood XENON100 background (*16*) as signal candidates. To be consistent with previous analyses (*13*), the same data selection cuts were applied. The exclusion remains unchanged if we only impose a minimum set of requirements; namely, that events have a single scatter in the fiducial volume with a prompt S1 and delayed S2 signal in the correct energy range. Furthermore, the exclusion stays above 3σ confidence level even if we consider a 4.5σ downward deviation in the measured data points (*22*–*24*) that are used to set the energy scale, or if we set the light yield in xenon to zero below 2.9 keV, in contradiction with direct measurement (*23*, *24*).

A profile likelihood analysis (*26*) was performed to constrain the cross section $\sigma^0_{\chi e} \equiv G^2 m_e^2/\pi$ for WIMPs coupling to electrons through axial-vector interactions. To this end, we drop the assumption of a 100% modulated rate and use the entire 224.6 live days data set. Fully analogous to (*13*), we use the same energy range and background likelihood function, derived from calibration data. We do not consider energy depositions below 1 keV, the lowest directly measured data point in (*23*). The resulting XENON100 exclusion limit (90% confidence level) is shown (Fig. 4) along with the 1σ/2σ-sensitivity bands based on the background-only hypothesis. It excludes cross sections above 6×10^{-35} cm^2 for WIMPs with a mass of m_χ = 2 GeV/c^2. This is more than five orders of magnitude stronger than the one derived in (*9*) based on data from the XENON10 detector, completely excludes the DAMA/LIBRA signal, and sets the strongest direct limit to date on the cross section

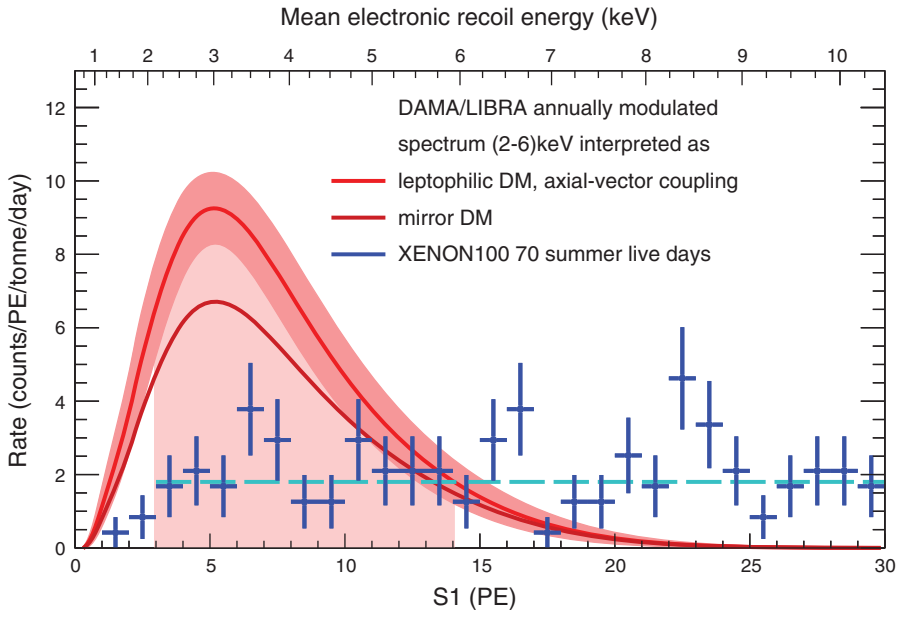

Fig. 3. Contrasting XENON100 data with DAMA/LIBRA. The DAMA/LIBRA modulated spectrum (red), interpreted as WIMPs scattering through axial-vector interactions, as it would be seen in the XENON100 detector. The 1σ band includes statistical and systematic uncertainties. The DAMA/LIBRA modulated spectrum interpreted as luminous dark matter is very similar, whereas the interpretation as mirror dark matter is indicated separately (dark red). The (blue) data points are XENON100 data from the 70 summer live days with their statistical uncertainty. The expected average XENON100 rate is also shown (dashed cyan). The shaded region from (3 to 14) PE was used to quantify the confidence level of exclusion. DM, dark matter.

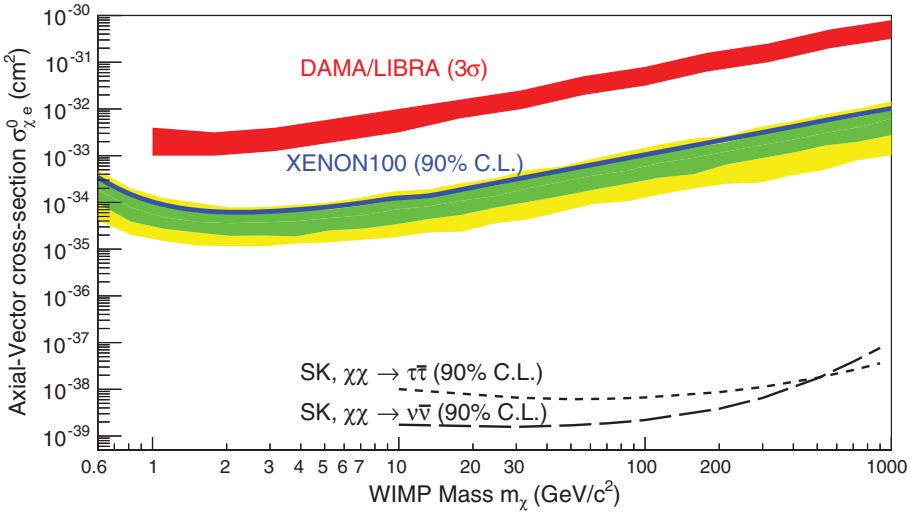

Fig. 4. Parameter space for WIMPs coupling to electrons through axial-vector interactions. The XENON100 upper limit (90% confidence level, C.L.) is indicated by the blue line, along with the green and yellow bands indicating the 1σ and 2σ sensitivity, respectively. For comparison, we also show the DAMA/LIBRA allowed region (red) and the constraint from Super-Kamiokande (SK) using neutrinos from the Sun, by assuming dark matter annihilation into ττ̄ or νν̄, both calculated in (*9*).

of WIMPs coupling to electrons through axial-vector interactions.

It has been suggested that multicomponent models with light dark matter particles of ~MeV/c^2 mass might explain the DAMA/LIBRA modulation (*27*). A specific example of such a model, kinematically mixed mirror dark matter (*28*), was shown to broadly have the right properties to explain the DAMA/LIBRA signal via dark matter–electron scattering. In this model, dark matter halos are composed of a multicomponent plasma of mirror particles, each with the same mass as their standard model partners. The mirror sector is connected to the normal sector by kinetic mixing of photons and mirror photons at the level of ~10^{-9}. Whereas mirror hadrons would not induce nuclear recoils above threshold, mirror electrons ($m_{e'} = 511\,\mathrm{keV}/c^2$) would have a velocity dispersion large enough to induce ~keV electronic recoils.

The differential scattering rate of mirror electrons is proportional to $gNn_{e'}$, where g is the number of loosely bound electrons, assumed to be those with binding energy <1 keV (*28*); N is the number of target atoms; and $n_{e'}$ is the mirror electron density. To compare DAMA/LIBRA directly with XENON100, we apply a constant scaling of $g_{Xe}/g_{NaI} \cdot N_{xe}/N_{NaI} = 0.89$ to the DAMA/LIBRA spectrum and use the same procedure as in the case of axial-vector coupling: We again consider only the DAMA/LIBRA modulation signal, use the 70 summer live days, model scintillation in liquid xenon as described previously, and simply compare integral counts up to the point where the DAMA/LIBRA signal falls below the expected average XENON100 background data rate (at 13 PE), without background subtraction. This excludes the DAMA/LIBRA signal as kinematically mixed mirror dark matter at 3.6σ confidence level.

The third model we consider is luminous dark matter (*29*), featuring a dark matter particle with a ~keV mass splitting between states connected by a magnetic dipole moment operator. The dark matter particle upscatters in the Earth and later de-excites, possibly within a detector, with the emission of a real photon. The experimental signature of this model is a mono-energetic line from the de-excitation photon. A mass splitting $\delta = 3.3$ keV provides a good fit to the DAMA/LIBRA signal (*29*), which would be explained as scattering of a real photon from the de-excitation of a ~GeV/c^2 dark matter particle that is heavy enough to undergo upscattering, but light enough to evade detection in other direct searches.

This signature is independent of the target material; only the sensitive volume affects the induced event rate. As rates are typically given per unit detector mass, scaling to volume is inversely proportional to target density. We thus apply a constant scaling factor to the differential rate in DAMA/LIBRA, which is the ratio of the target densities $\rho_{NaI}/\rho_{Xe} = 1.29$, in order to compare it to XENON100. Proceeding as in the previous two cases, we exclude the DAMA/LIBRA signal as luminous dark matter at 4.6σ confidence level. Together with the other two exclusions presented above, this robustly rules out leptophilic dark matter interactions as a cause for the DAMA/LIBRA signal.

REFERENCES AND NOTES

1. L. Bergström, *Annalen Phys.* **524**, 479–496 (2012).
2. A. K. Drukier, K. Freese, D. N. Spergel, *Phys. Rev. D Part. Fields* **33**, 3495–3508 (1986).
3. K. Freese, M. Lisanti, C. Savage, *Rev. Mod. Phys.* **85**, 1561 (2013).
4. R. Bernabei *et al.*, *Eur. Phys. J. C* **73**, 2648 (2013).
5. C. Savage, G. Gelmini, P. Gondolo, K. Freese, *J. Cosmol. Astropart. Phys.* **0904**, 010 (2009).
6. Y. Bai, P. J. Fox, Resonant dark matter. *J. High Energy Phys.* **0911**, 052 (2009). .
7. S. Chang, N. Weiner, I. Yavin, *Phys. Rev. D Part. Fields Gravit. Cosmol.* **82**, 125011 (2010).
8. S. Chang, R. F. Lang, N. Weiner, *Phys. Rev. Lett.* **106**, 011301 (2011).
9. J. Kopp, V. Niro, T. Schwetz, J. Zupan, *Phys. Rev. D Part. Fields Gravit. Cosmol.* **80**, 083502 (2009).
10. N. F. Bell, Y. Cai, R. K. Leane, A. D. Medina, *Phys. Rev. D Part. Fields Gravit. Cosmol.* **90**, 035027 (2014).
11. E. Aprile *et al.*, *Phys. Rev. Lett.* **109**, 181301 (2012).
12. E. Aprile *et al.*, *Phys. Rev. Lett.* **111**, 021301 (2013).
13. E. Aprile *et al.*, *Phys. Rev. D Part. Fields Gravit. Cosmol.* **90**, 062009 (2014).
14. E. Aprile *et al.*, *Astropart. Phys.* **35**, 573–590 (2012).
15. E. Aprile *et al.*, *Astropart. Phys.* **54**, 11 (2014).
16. E. Aprile *et al.*, *Phys. Rev. D Part. Fields Gravit. Cosmol.* **83**, 082001 (2011).
17. R. Bernabei *et al.*, *Eur. Phys. J. C* **56**, 333–355 (2008).
18. V. Kudryavtsev, M. Robinson, N. Spooner, *Astropart. Phys.* **33**, 91–96 (2010).
19. J. Herrero-Garcia, T. Schwetz, J. Zupan, *J. Cosmol. Astropart. Phys.* **1203**, 005 (2012).
20. R. Bernabei *et al.*, *Phys. Rev. D Part. Fields Gravit. Cosmol.* **77**, 023506 (2008).
21. M. Szydagis *et al. J. Instrum.* **6**, P10002 (2011).
22. A. Manalaysay *et al.*, *Rev. Sci. Instrum.* **81**, 073303 (2010).
23. E. Aprile *et al.*, *Phys. Rev. D Part. Fields Gravit. Cosmol.* **86**, 112004 (2012).
24. L. Baudis *et al.*, *Phys. Rev. D Part. Fields Gravit. Cosmol.* **87**, 115015 (2013).
25. M. Szydagis, A. Fyhrie, D. Thorngren, M. Tripathi, *Instrum.* **8**, C10003 (2013).
26. E. Aprile *et al.*, *Phys. Rev. D Part. Fields Gravit. Cosmol.* **84**, 052003 (2011).
27. R. Foot, H. Lew, R. Volkas, *Phys. Lett. B* **272**, 67–70 (1991).
28. R. Foot, *Int. J. Mod. Phys. A* **29**, 1430013 (2014).
29. B. Feldstein, P. W. Graham, S. Rajendran, *Phys. Rev. D Part. Fields Gravit. Cosmol.* **82**, 075019 (2010).

ACKNOWLEDGMENTS

We thank J. Kopp for providing the calculated wave functions and for useful discussions. We gratefully acknowledge support from the National Science Fundation, Department of Energy, Swiss National Science Foundation, Volkswagen Foundation, Bundesministerium fur Bildung und Forschung, Max Planck Gesellschaft, Research Center Elementary Forces and Mathematical Foundations, Foundation for Fundamental Research on Matter, Weizmann Institute of Science, Initial Training Network Invisibles, Fundacao para a Ciencia e a Tecnologia, Region des Pays de la Loire, Science and Technology Commission of Shanghai Municipality, National Natural Science Foundation of China, and Istituto Nazionale di Fisica Nucleare. We are grateful to Laboratori Nazionali del Gran Sasso for hosting and supporting the XENON project. XENON data are archived at the Laboratori Nazionali del Gran Sasso.

SUPPLEMENTARY MATERIALS

www.sciencemag.org/content/349/6250/851/suppl/DC1
The XENON Collaboration Author List
Data Files A1 and A2

28 March 2015; accepted 25 June 2015
10.1126/science.aab2069

ECOLOGICAL THEORY

A general consumer-resource population model

Kevin D. Lafferty,[1]* Giulio DeLeo,[3] Cheryl J. Briggs,[2] Andrew P. Dobson,[4,5] Thilo Gross,[6] Armand M. Kuris[2]

Food-web dynamics arise from predator-prey, parasite-host, and herbivore-plant interactions. Models for such interactions include up to three consumer activity states (questing, attacking, consuming) and up to four resource response states (susceptible, exposed, ingested, resistant). Articulating these states into a general model allows for dissecting, comparing, and deriving consumer-resource models. We specify this general model for 11 generic consumer strategies that group mathematically into predators, parasites, and micropredators and then derive conditions for consumer success, including a universal saturating functional response. We further show how to use this framework to create simple models with a common mathematical lineage and transparent assumptions. Underlying assumptions, missing elements, and composite parameters are revealed when classic consumer-resource models are derived from the general model.

Malthus (*1*) first postulated that resource availability constrains consumer population growth in 1798. Since then, there have been about 1000 host-parasitoid, 3000 parasite-host, and 5000 predator-prey modeling studies, all describing interactions between consumers and their resources [summarized in (*2*, *3*)]. Here, we show how the seven state variables and associated transitions used in classic models can comprise a general consumer-resource model that underlies the structure of all ecological food webs (*4*). The general model describes population rates of change for searching, or questing, (Q); handling, or attacking, (A); and feeding or consuming (C) activity states of consumers and the

of WIMPs coupling to electrons through axial-vector interactions.

It has been suggested that multicomponent models with light dark matter particles of ~MeV/c^2 mass might explain the DAMA/LIBRA modulation (*27*). A specific example of such a model, kinematically mixed mirror dark matter (*28*), was shown to broadly have the right properties to explain the DAMA/LIBRA signal via dark matter–electron scattering. In this model, dark matter halos are composed of a multicomponent plasma of mirror particles, each with the same mass as their standard model partners. The mirror sector is connected to the normal sector by kinetic mixing of photons and mirror photons at the level of ~10^{-9}. Whereas mirror hadrons would not induce nuclear recoils above threshold, mirror electrons ($m_{e'} = 511\,\mathrm{keV}/c^2$) would have a velocity dispersion large enough to induce ~keV electronic recoils.

The differential scattering rate of mirror electrons is proportional to $gNn_{e'}$, where g is the number of loosely bound electrons, assumed to be those with binding energy <1 keV (*28*); N is the number of target atoms; and $n_{e'}$ is the mirror electron density. To compare DAMA/LIBRA directly with XENON100, we apply a constant scaling of $g_{\mathrm{Xe}}/g_{\mathrm{NaI}} \cdot N_{\mathrm{xe}}/N_{\mathrm{NaI}} = 0.89$ to the DAMA/LIBRA spectrum and use the same procedure as in the case of axial-vector coupling: We again consider only the DAMA/LIBRA modulation signal, use the 70 summer live days, model scintillation in liquid xenon as described previously, and simply compare integral counts up to the point where the DAMA/LIBRA signal falls below the expected average XENON100 background data rate (at 13 PE), without background subtraction. This excludes the DAMA/LIBRA signal as kinematically mixed mirror dark matter at 3.6σ confidence level.

The third model we consider is luminous dark matter (*29*), featuring a dark matter particle with a ~keV mass splitting between states connected by a magnetic dipole moment operator. The dark matter particle upscatters in the Earth and later de-excites, possibly within a detector, with the emission of a real photon. The experimental signature of this model is a mono-energetic line from the de-excitation photon. A mass splitting δ = 3.3 keV provides a good fit to the DAMA/LIBRA signal (*29*), which would be explained as scattering of a real photon from the de-excitation of a ~GeV/c^2 dark matter particle that is heavy enough to undergo upscattering, but light enough to evade detection in other direct searches.

This signature is independent of the target material; only the sensitive volume affects the induced event rate. As rates are typically given per unit detector mass, scaling to volume is inversely proportional to target density. We thus apply a constant scaling factor to the differential rate in DAMA/LIBRA, which is the ratio of the target densities $\rho_{\mathrm{NaI}}/\rho_{\mathrm{Xe}} = 1.29$, in order to compare it to XENON100. Proceeding as in the previous two cases, we exclude the DAMA/LIBRA signal as luminous dark matter at 4.6σ confidence level. Together with the other two exclusions presented above, this robustly rules out leptophilic dark matter interactions as a cause for the DAMA/LIBRA signal.

REFERENCES AND NOTES

1. L. Bergström, *Annalen Phys.* **524**, 479–496 (2012).
2. A. K. Drukier, K. Freese, D. N. Spergel, *Phys. Rev. D Part. Fields* **33**, 3495–3508 (1986).
3. K. Freese, M. Lisanti, C. Savage, *Rev. Mod. Phys.* **85**, 1561 (2013).
4. R. Bernabei *et al.*, *Eur. Phys. J. C* **73**, 2648 (2013).
5. C. Savage, G. Gelmini, P. Gondolo, K. Freese, *J. Cosmol. Astropart. Phys.* **0904**, 010 (2009).
6. Y. Bai, P. J. Fox, Resonant dark matter. *J. High Energy Phys.* **0911**, 052 (2009). .
7. S. Chang, N. Weiner, I. Yavin, *Phys. Rev. D Part. Fields Gravit. Cosmol.* **82**, 125011 (2010).
8. S. Chang, R. F. Lang, N. Weiner, *Phys. Rev. Lett.* **106**, 011301 (2011).
9. J. Kopp, V. Niro, T. Schwetz, J. Zupan, *Phys. Rev. D Part. Fields Gravit. Cosmol.* **80**, 083502 (2009).
10. N. F. Bell, Y. Cai, R. K. Leane, A. D. Medina, *Phys. Rev. D Part. Fields Gravit. Cosmol.* **90**, 035027 (2014).
11. E. Aprile *et al.*, *Phys. Rev. Lett.* **109**, 181301 (2012).
12. E. Aprile *et al.*, *Phys. Rev. Lett.* **111**, 021301 (2013).
13. E. Aprile *et al.*, *Phys. Rev. D Part. Fields Gravit. Cosmol.* **90**, 062009 (2014).
14. E. Aprile *et al.*, *Astropart. Phys.* **35**, 573–590 (2012).
15. E. Aprile *et al.*, *Astropart. Phys.* **54**, 11 (2014).
16. E. Aprile *et al.*, *Phys. Rev. D Part. Fields Gravit. Cosmol.* **83**, 082001 (2011).
17. R. Bernabei *et al.*, *Eur. Phys. J. C* **56**, 333–355 (2008).
18. V. Kudryavtsev, M. Robinson, N. Spooner, *Astropart. Phys.* **33**, 91–96 (2010).
19. J. Herrero-Garcia, T. Schwetz, J. Zupan, *J. Cosmol. Astropart. Phys.* **1203**, 005 (2012).
20. R. Bernabei *et al.*, *Phys. Rev. D Part. Fields Gravit. Cosmol.* **77**, 023506 (2008).
21. M. Szydagis *et al. J. Instrum.* **6**, P10002 (2011).
22. A. Manalaysay *et al.*, *Rev. Sci. Instrum.* **81**, 073303 (2010).
23. E. Aprile *et al.*, *Phys. Rev. D Part. Fields Gravit. Cosmol.* **86**, 112004 (2012).
24. L. Baudis *et al.*, *Phys. Rev. D Part. Fields Gravit. Cosmol.* **87**, 115015 (2013).
25. M. Szydagis, A. Fyhrie, D. Thorngren, M. Tripathi, *Instrum.* **8**, C10003 (2013).
26. E. Aprile *et al.*, *Phys. Rev. D Part. Fields Gravit. Cosmol.* **84**, 052003 (2011).
27. R. Foot, H. Lew, R. Volkas, *Phys. Lett. B* **272**, 67–70 (1991).
28. R. Foot, *Int. J. Mod. Phys. A* **29**, 1430013 (2014).
29. B. Feldstein, P. W. Graham, S. Rajendran, *Phys. Rev. D Part. Fields Gravit. Cosmol.* **82**, 075019 (2010).

ACKNOWLEDGMENTS

We thank J. Kopp for providing the calculated wave functions and for useful discussions. We gratefully acknowledge support from the National Science Fundation, Department of Energy, Swiss National Science Foundation, Volkswagen Foundation, Bundesministerium fur Bildung und Forschung, Max Planck Gesellschaft, Research Center Elementary Forces and Mathematical Foundations, Foundation for Fundamental Research on Matter, Weizmann Institute of Science, Initial Training Network Invisibles, Fundacao para a Ciencia e a Tecnologia, Region des Pays de la Loire, Science and Technology Commission of Shanghai Municipality, National Natural Science Foundation of China, and Istituto Nazionale di Fisica Nucleare. We are grateful to Laboratori Nazionali del Gran Sasso for hosting and supporting the XENON project. XENON data are archived at the Laboratori Nazionali del Gran Sasso.

SUPPLEMENTARY MATERIALS

www.sciencemag.org/content/349/6250/851/suppl/DC1
The XENON Collaboration Author List
Data Files A1 and A2

28 March 2015; accepted 25 June 2015
10.1126/science.aab2069

ECOLOGICAL THEORY

A general consumer-resource population model

Kevin D. Lafferty,[1]* Giulio DeLeo,[3] Cheryl J. Briggs,[2] Andrew P. Dobson,[4,5] Thilo Gross,[6] Armand M. Kuris[2]

Food-web dynamics arise from predator-prey, parasite-host, and herbivore-plant interactions. Models for such interactions include up to three consumer activity states (questing, attacking, consuming) and up to four resource response states (susceptible, exposed, ingested, resistant). Articulating these states into a general model allows for dissecting, comparing, and deriving consumer-resource models. We specify this general model for 11 generic consumer strategies that group mathematically into predators, parasites, and micropredators and then derive conditions for consumer success, including a universal saturating functional response. We further show how to use this framework to create simple models with a common mathematical lineage and transparent assumptions. Underlying assumptions, missing elements, and composite parameters are revealed when classic consumer-resource models are derived from the general model.

Malthus (*1*) first postulated that resource availability constrains consumer population growth in 1798. Since then, there have been about 1000 host-parasitoid, 3000 parasite-host, and 5000 predator-prey modeling studies, all describing interactions between consumers and their resources [summarized in (*2*, *3*)]. Here, we show how the seven state variables and associated transitions used in classic models can comprise a general consumer-resource model that underlies the structure of all ecological food webs (*4*). The general model describes population rates of change for searching, or questing, (Q); handling, or attacking, (A); and feeding or consuming (C) activity states of consumers and the

corresponding susceptible (S), exposed (E), ingested (I), and resistant (R) states for resources (Fig. 1; mathematical formulation summarized in Table 1 and further detailed in tables SB1 to SB3). Transitions among states are represented by generalized functions (*5*) (e.g., C_{aq}, the contact/attack generalized function) that are placeholders for potential formulas that describe biological details (e.g., the mass-action equation βQS). A general model solves several problems. First, its standard structure clarifies mathematical relationships among consumer strategies and ecological generalities, such as a universal saturating functional response. Second, the general model is a common framework for building simple models with transparent assumptions. Third, deriving classic models from a general model illustrates the extent to which past results have depended on simplifying assumptions about underlying biology.

The general model is not intended to describe any particular biological system; instead it must be first tailored to a generic consumer strategy. The full range of these strategies can be modeled with combinations of eight operationally defined criteria (table SC1). These criteria include the number of attacks per questing consumer (i.e., several for a lion, one for a juvenile hookworm), intimacy with the resource (e.g., consumers can die if their resource dies, a trait that correlates with the relative time spent consuming—such as for pathogens and macroparasites), and effects on the fitness of the resource (i.e., eventually fatal for a parasitoid wasp, blocked reproduction for a rhizocephalan barnacle, intensity-dependent morbidity for the human roundworm) (*6*). We also distinguish consumers, such as vultures or plants, that feed on living resources from those that feed on nonliving resources. These taxon-neutral strategies differ from other familiar consumer categorizations such as carnivore and herbivore in that they do not consider the taxonomy of the consumer or of the resource.

Using these criteria, we specify the general model to four familiar consumer-resource model types (predators, pathogens, parasitoids, and macroparasites) and seven additional distinct consumer strategies that are not often modeled, but for which there is a distinct model structure (parasitic castrator, autotroph, decomposer, detritivore, scavenger, social predator, and micropredator) (*6*). We illustrate relationships in model structure with a consumer-resource model "phylogeny" (Fig. 2A) and a principle-component analysis (fig. SC1 and tables SC1 to SC4). The major graphical separation among generic models corresponds to multiple or single attacks by the questing state (e.g., predators versus parasites; Fig. 2A). Specifically, predators can survive a failed attack and return to questing after a meal, whereas parasite questing stages die if they fail to infect a host. Consumer-resource models can be further differentiated by life-history characteristics. For example, parasite models cluster according to a single intimate (i.e., consumer lives with its resource) attack on a resource, whereas predator models cluster around multiple nonintimate attacks. Micropredator models (including mosquitoes, some leeches, and many herbivores that eat parts of plants) differ because they make repeated nonlethal attacks on their resources. That is, the "micro" in micropredator refers to the size of the meal relative to the size of the resource, not to the size of the consumer. As a result, micropredators act like predators but affect their resources like parasites. In both the parasite and predator clusters, generic models vary according to whether more than one consumer can attack an exposed resource and whether the resource is living or nonliving. The general model thus makes it possible to compare and contrast generic consumer strategies.

The general model reveals new insights into consumer-resource dynamics. One measure of dynamics is the expected number of offspring produced by an individual consumer encountering an unexploited resource population, otherwise known as R_0 (*7*). R_0 defines the conditions under which a consumer can invade a resource population. For the 11 consumer strategies, R_0 increases with resource contact, attack success, handling rate, resource conversion rate, and consumer life span (table SD1). It has long been known that constraints on resource handling (functional responses) (*8*) destabilize predator-prey dynamics by allowing prey to be released from their predators (*3*). Correspondingly, R_0 for all consumers, including parasites, saturates with resource density because contact rates asymptote (table SD2 and Fig. 2B). A saturating functional response prevents consumers from persisting on resources of low nutritional value even as those resources approach infinitely high densities. The universal half-saturation resource density of D_q/β (death rate of questing stages divided by per-capita contact rate; supplementary text D) implies that such constraints are greatest for consumers with durable and efficient questing states (characteristics more likely to describe a predator than a parasite). Regardless, an asymptotic contact rate means that all parasites are along a continuum from density-dependent to frequency-dependent transmission (*9*). Furthermore, the structure of R_0 differs among predators, micropredators, and parasites (boxes in Fig. 2; table SD1), indicating how different consumer strategies should be favored by longevity and body size (*6*).

Consumers have five distinct types of ontogenetic diet shifts that require composites of the general model (Fig. 3). Specifically, parasites with complex life cycles can have three types of ontogenetic diet shifts among life stages: (i) sequential host (schistosome), (ii) trophically transmitted (fish tapeworm), and (iii) vector transmitted (malaria). Such host shifts can correspond to different consumer strategies (e.g., for schistosomes, a parasitic castrator followed by a macroparasite). Most predators (e.g., dragonflies, amphibians, ant lions) have niche shifts related to metamorphoses that lead to nonoverlapping diets. In some cases, an ontogenetic diet shift accompanies a change between predation and

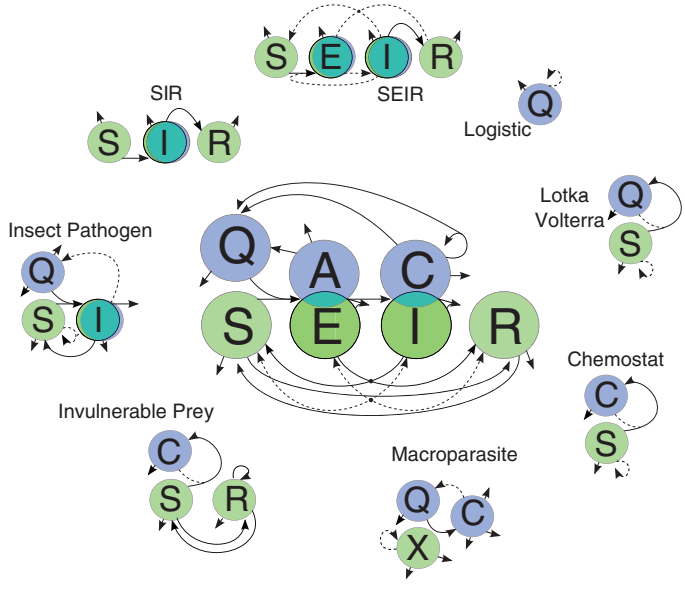

Fig. 1. Diagram of the general consumer-resource model and its relationship to classic consumer-resource models. Circles are state variables for questing (Q), attacking (A), and consuming (C) consumers (Y in blue/dark shading), under which are susceptible (S), exposed (E), ingested (I), and resistant (R) resources (X in green/light shading). Overlapping circles indicate that the values of the corresponding variables might be identical under some circumstances. Arrows represent transitions (of individuals or biomass) among states. A dashed line represents production or conversion (e.g., births), whereas a solid line is a transition from one state to another (implying no change in numbers from one state to the next). A solid node at intersecting arrows indicates consumer states might give birth to consumers in each state.

[1]Western Ecological Research Center, U.S. Geological Survey, Marine Science Institute, University of California–Santa Barbara, Santa Barbara, CA, USA. [2]Ecology, Evolution and Marine Biology, University of California–Santa Barbara, Santa Barbara, CA, USA. [3]Hopkins Marine Station Woods Institute for the Environment, Stanford University, Stanford, CA, USA. [4]Ecology and Evolutionary Biology, Princeton University, Princeton, NJ, USA. [5]Santa Fe Institute, Hyde Park Road, Santa Fe, NM, USA. [6]Department of Engineering Mathematics, University of Bristol, Bristol, UK.
*Corresponding author. E-mail: klafferty@usgs.gov

parasitism. In particular, the predatory (or sometimes nonfeeding) adult lays its eggs on its offspring's food. These "protelean" consumers include some macroparasites (e.g., bot flies, leaf miners), decomposers (e.g., blow flies) and many parasitoids (e.g., ichneumonid wasps, tachinid flies). Furthermore, although predators rarely engage in facultative parasitism, predators can be part-time micropredators (e.g., some leeches), scavengers (e.g., crows), or social predators (e.g., coyotes). In contrast, parasites almost always adhere to a single consumer strategy within a life stage. Other relevant complexity can be incorporated into models by subdividing states into classes (e.g., sex, size, genotype) and modifying the transitions among states to model other interspecific interactions (e.g., pollination by nectar feeders, phoresy). Ultimately, coupling consumer-resource models for multiple species leads to food-web models.

The general model is a common starting point for building simple models that have the desired balance of tractability, elegance, and analytical solutions versus a more explicit embrace of ecological mechanisms, fit to data, and accurate predictions (fig. SE1). To simplify the general model (*4*), the first step (as above) is to specify a generic consumer life-history strategy (table SC1; in supplementary text E we use an autotroph as an example). The next step is to delete state variables when, for instance, there is not a resistant resource state; or, for most pathogens and predators, the ingested resource is redundant; or, as for some infectious disease models, human population size is assumed constant. Then, the generalized functions need to be formulated with meaningful parameters. Once functions are formulated, time-scale separation can be used to subsume state variables by substituting an ephemeral state with its quasi-equilibrium (*8*). For example, a pathogen's microscopic infective stages (Q and A) can be assumed to quickly reach an equilibrium that can be absorbed into the C equation in Table 1. However, a consequence of assuming that states quickly reach equilibria is to increase the likelihood of local asymptotic stability (i.e., by reducing the dimensions of the system that can vary). This overestimate of stability increases with the time spent in the ignored state. Further assuming that some rates are fast relative to others can help simplify model structure (at the risk of simplifying dynamics), whereas composite parameters can be used to reduce the number of terms for presentation (at the risk of obscuring their meaning). Finally, there is the matter of which states to track. For instance, the abundance of subsumed states might or might not be counted as part of a consumer population (but failing to track them will underestimate the consumer population). Once these steps are complete, the resulting simplified model contains the legacy of the simplifying steps, thereby giving explicit meaning to composite parameters and derived functions.

When reducing the general model to the classic models that inspired our work, we find that they often subsume ephemeral states (e.g., the attacking and consuming states in the Lotka-Volterra model or the free-living stages in host-pathogen models) or exclude them, or both. For instance, the Lotka-Volterra predator-prey equations, the foundation of most dynamic food-web

Table 1. Model notation summary (supplementary text B). Dual subscripts indicate transitions between, or production to and from, states (e.g., H_{qc} is the transition rate from the consuming state to the questing state); an x or y subscript is for all states within a resource or consumer species, respectively (e.g., R_{sx} is the transition rate into the susceptible state from all resource states combined); single subscripts indicate state-specific nontransition (e.g., mortality) rates.

The general model in words
Consumer (Y)
d(Questing)/d*t* = Birth − Death + Handling I + Killing + Failure − Contact
d(Attacking)/d*t* = Contact − Death − Handling E − Resource Death − Failure
d(Consuming)/d*t* = Birth − Death + Handling E − Resource Death − Killing − Handling
Resource (X)
d(Susceptible)/d*t* = Birth − Death + Recovery + Vulnerability − Invulnerability − Contact
d(Exposed)/d*t* = Birth − Death − Recovery − Handling E + Contact
d(Ingested)/d*t* = Birth − Death − Recovery + Handling E − Killing
d(Resistant)/d*t* = Birth − Death + Recovery − Vulnerability + Invulnerability
With general function abbreviations
$dY_q/dt = B_{qc} - D_q + m(1\text{-}f)H_{qc} + mfA_iK_iY_c/X_i + mF_a - C_{aq}$
$dY_a/dt = C_{aq} - D_a - H_{ca} - j_aD_eY_a/X_e - F_a$
$dY_c/dt = B_{cc} - D_c + H_{ca} - j_cD_iY_c/X_i - A_iK_iY_c/X_i - m(1\text{-}f)H_{qc}$
$dX_s/dt = B_{sx} - D_s + R_{sx} + V_{sr} - I_{rs} - C_{aq}$
$dX_e/dt = B_{ex} - D_e - R_{xe} - H_{ca} + C_{aq}$
$dX_i/dt = B_{ix} - D_i - R_{xi} + H_{ca} - K_i$
$dX_r/dt = B_{rx} - D_r + R_{rx} - V_{sr} + I_{rs}$
State variables
$X = \sum X$ total resource population size
X_s = Susceptible (and unattacked) resources
X_e = Exposed resources
X_i = Ingested (i.e., infected) resources
X_r = Resistant resources
$Y = \sum Y$ total consumer population size
Y_q = Questing consumers
Y_a = Attacking consumers
Y_c = Consuming consumers
Generalized functions
A_i = aggregation of consumers per resource
B_{cc} = vertical transmission of a consumer
B_{qc} = birth (production) of new questing individuals
B_{xi} = birth of ingested resource (e.g., B_{ii} relates to vertical transmission above)
$B_{ex} = (B_{es} + B_{ee} + B_{ei} + B_{er})$
$B_{ix} = (B_{is} + B_{ie} + B_{ii} + B_{ir})$
$B_{rx} = (B_{rs} + B_{re} + B_{ri} + B_{rr})$
$B_{sx} = (B_{ss} + B_{se} + B_{si} + B_{sr})$, or = $f(X_0)$ for consumers that feed on resources that do not reproduce (carcasses, nutrients)
C_{aq} = contact/attack between questing consumers and susceptible hosts
D = background death
F_a = attacking failure
H_{ca} = handling by the attacking state
H_{qa} = return to questing after attacking (see supplementary text E)
H_{qc} = handling by the consuming state
I_{rs} = resistance
K_i = mortality/removal rate of an ingested resource
R = recovery of ingested resources
V_{sr} = susceptibility to consumers
Auxiliary parameters (1 = yes, 0 = no)
f = consumer kills the host as part of feeding
j = joint death (i.e., intimacy) between consumer and resource
m = multiple attacks by questing state

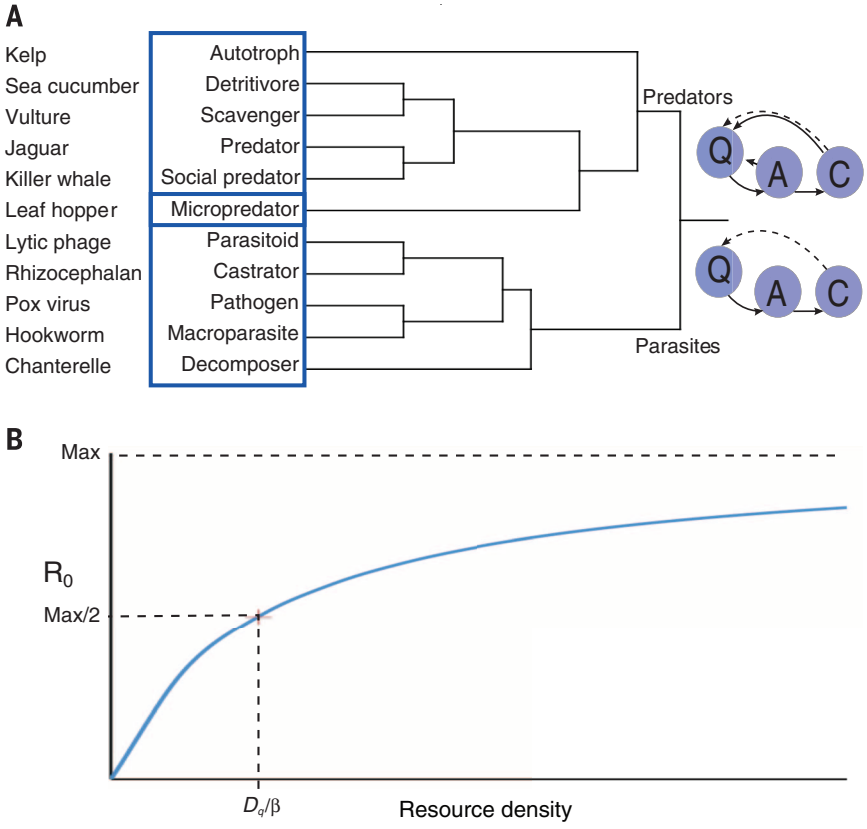

Fig. 2. Ten consumer strategies clustered according to similarities in model structure (supplementary text C). (**A**) Dendrogram using average clustering, including example, general consumer strategy, R_0 category (blue squares), and model diagram. (**B**) Despite differences in structure, R_0 saturates with resource density for all consumer strategies (supplementary text D) with a universal half-saturation resource density of D_q/β, or the ratio of deaths per contact for the questing state.

Fig. 3. Consumer-resource models with complex life histories. Many species change diet from one life stage to the other. This results in at least five distinct model structures, each of which has, at its core, a general model (fig. 3). For instance, protelean life histories add a new transition; specifically, the questing state returns to questing after an attack (H_{qa}). Furthermore, some protelean consumers have a free-living consumer stage (others do not).

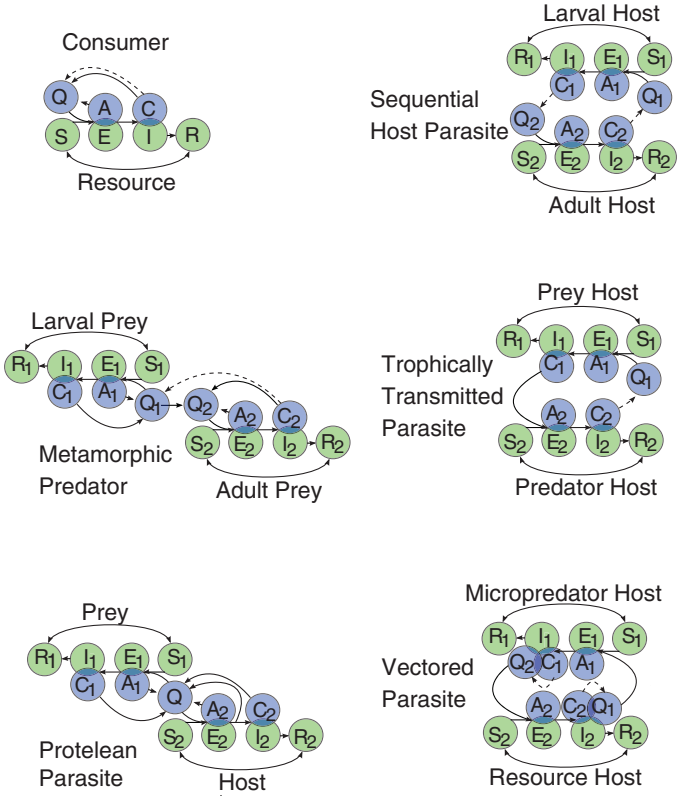

models, track only questing consumers and susceptible resources. Moreover, although the importance of a saturating functional response has been recognized in prey-predator models, classic models often assume that handling or contact is fast, or both, giving the impression that such consumers have unlimited potential to control their resources. Deriving classic models from a general-consumer resource model highlights these assumptions, specifies each model's relationship to all other consumer-resource models, and identifies the meaning of their composite parameters (table SF1).

The general consumer-resource model allows systematic mapping across consumer-resource population models. Having a common model structure exposes simplifying assumptions in classic consumer-resource models and allows us to contrast the structure of different consumer-resource relationships, specifying the conditions that favor one strategy over another. Consumer-resource interactions drive ecosystem functions, and ecosystem functions are the underlying mechanisms that govern all ecosystem services. The general model provides a useful foundation for understanding and constructing food-web models central to understanding ecological complexity.

REFERENCES AND NOTES

1. T. R. Malthus, *An Essay on the Principle of Population or a View of Its Past and Present Effects on Human Happiness, an Inquiry into Our Prospects Respecting the Future Removal or Mitigation of the Evils Which It Occasions (Reeves and Turner, London, 1872).*
2. R. M. Anderson, R. M. May, *Infectious Diseases of Humans: Dynamics and Control* (Oxford Univ. Press, Oxford, 1991).
3. W. W. Murdoch, C. J. Briggs, R. M. Nisbet, *Consumer-Resource Dynamics* (Princeton Univ. Press, Princeton, NJ, 2003).
4. Materials and methods are available as supplementary materials on *Science* Online.
5. T. Gross, U. Feudel, *Phys. Rev. E Stat. Nonlin. Soft Matter Phys.* **73**, 016205 (2006).
6. K. D. Lafferty, A. M. Kuris, *Trends Ecol. Evol.* **17**, 507–513 (2002).
7. O. Diekmann, J. A. P. Heesterbeek, M. G. Roberts, *J. R. Soc. Interface* **7**, 873–885 (2010).
8. J. H. P. Dawes, M. O. Souza, *J. Theor. Biol.* **327**, 11–22 (2013).
9. H. McCallum, N. Barlow, J. Hone, *Trends Ecol. Evol.* **16**, 295–300 (2001).

ACKNOWLEDGMENTS

This work was conducted as a part of the Parasites and Food Webs Working Group supported by the National Center for Ecological Analysis and Synthesis, a Center funded by NSF (grant DEB-0553768), the University of California–Santa Barbara, and the State of California, and by NSF Ecology of Infectious Diseases (grant OCE-1115965). A.P.D. was also sponsored by a Complexity Grant from the MacDonnel Foundation. Any use of trade, product, or firm names in this publication is for descriptive purposes only and does not imply endorsement by the U.S. government. We thank H. McCallum, M. Pascual, M. Wilber, R. Hechinger, J. McLaughlin, R. Warner, and S. Weinstein.

SUPPLEMENTARY MATERIALS

www.sciencemag.org/content/349/6250/854/suppl/DC1
Materials and Methods
Supplementary Text B to F
Figs. SC1 and SE1
Tables SB1 to SB3, SC1 to SC4, SD1 to SD3, and SF1
References (*10–21*)
CDF Program File

7 January 2015; accepted 23 July 2015
10.1126/science.aaa6224

HUMAN IMPACTS

The unique ecology of human predators

Chris T. Darimont,[1,2,3]* Caroline H. Fox,[1,2] Heather M. Bryan,[1,2,3] Thomas E. Reimchen[4]

Paradigms of sustainable exploitation focus on population dynamics of prey and yields to humanity but ignore the behavior of humans as predators. We compared patterns of predation by contemporary hunters and fishers with those of other predators that compete over shared prey (terrestrial mammals and marine fishes). Our global survey (2125 estimates of annual finite exploitation rate) revealed that humans kill adult prey, the reproductive capital of populations, at much higher median rates than other predators (up to 14 times higher), with particularly intense exploitation of terrestrial carnivores and fishes. Given this competitive dominance, impacts on predators, and other unique predatory behavior, we suggest that humans function as an unsustainable "super predator," which—unless additionally constrained by managers—will continue to alter ecological and evolutionary processes globally.

Humans have diverged from other predators in behavior and influence. Geographic expansion, exploitation of naïve prey, killing technology, symbioses with dogs, and rapid population growth, among other factors, have long imposed profound impacts—including widespread extinction and restructuring of food webs and ecosystems—in terrestrial and marine systems (*1*–*3*). Despite contributions from the "sustainable exploitation" paradigm (*4*), contemporary humans can rapidly drive prey declines (*5*–*7*), degrade ecosystems (*8*, *9*), and impose evolutionary change in prey (*10*, *11*). Owing to long-term coevolutionary relationships that generally limit exploitation rates, especially on adult prey, these are extreme outcomes that nonhuman predators seldom impose. Meanwhile, whether present and future exploitation can be considered sustainable is hotly contested, especially in fisheries. Debate has been largely restricted to elements of the sustainable exploitation model, namely, a model of prey abundance and yields to humanity (e.g., *12*, *13*).

Here, we approach the notion of sustainable exploitation differently by asking whether humans—extreme in their impacts—are extreme in their predatory behavior (*14*, *15*). Previous work has variously estimated exploitation by humans, nonhuman predators, or both, but systematic comparisons have focused on specific taxa or regions, have lumped all predators together, have been reconstructed indirectly, and/or did not include age classes (e.g., *14*, *16*, *17*). We address these limitations with data spanning wildlife, tropical wild meat, and fisheries systems (data files S1 and S2). We examine variation in annual finite exploitation rates of marine fishes from every ocean (n = 1494 estimates, 282 species from 110 communities) and terrestrial mammals from every continent except Antarctica (631 estimates, 117 species from 179 communities) (fig. S1 and tables S1 and S2) by predator type (humans versus nonhuman), ecosystem (marine versus terrestrial), region, and trophic level. We focus on adult prey because hunters and fishers overwhelmingly target adults (*18*). We complement this quantitative assessment by identifying additionally unique predatory behaviors by humans that (i) facilitate the large differences in exploitation rates we detect and (ii) elicit the manifold consequences of humanity's predatory hegemony.

Differences in exploitation rates between hunters and terrestrial predators varied among comparisons. Globally and pooled across trophic levels, exploitation rates by hunters (median = 0.06) did not differ from those of carnivores [median = 0.05; Wilcoxon test W = 46076, $P_{adj(2)}$ = 0.11] (Fig. 1A and figs. S2A and S3A). A paired comparison over shared prey within the same community, however, revealed that hunters exploit at higher rates than the highest-exploiting terrestrial predator [paired Wilcoxon test V = 929, $P_{adj(2)}$ = 0.03] (fig. S3B). Additionally, a similar paired comparison showed that the median proportion of mortality (an independent metric) caused by hunters (0.35) was 1.9 times that (0.19) caused by all other predators combined (paired Wilcoxon test V = 1605, P = 0.004) (Fig. 1B).

Trophic level and regional analyses (across taxa and areas with abundant data) revealed additional patterns. Although globally pooled comparisons showed that hunters and terrestrial predators exploited herbivores (artiodactyls) at similar rates [W = 14751, $P_{adj(9)}$ = 1.00] (Fig. 1C), hunters in North America and Europe exploited herbivores at median rates 7.2 and 12.5 times those of hunters in Africa [both $P_{adj(9)}$ < 0.04]; rates did not differ statistically between hunters and terrestrial predators within any of the regions (fig. S4A). Globally, hunters exploited mesocarnivores [W = 248, $P_{adj(9)}$ = 0.03] and large carnivores [W = 181, $P_{adj(9)}$ < 0.001] at higher rates than nonhuman predators by factors of 4.3 and 9.2, respectively (Fig. 1C). Remarkably, hunters exploited large carnivores at 3.7 times the rate that they killed herbivores [W = 2697, $P_{adj(9)}$ < 0.001] (Fig. 1C).

Fisheries exploited adult prey at higher rates than any other of the planet's predators (Fig. 1A and fig. S2B). Among nonhuman predators across all oceans, 50% of exploitation rates were less than 1% of annual adult biomass. In contrast, fisheries exploited more than 10% of adult biomass in 62% of cases. Overall, the median fishing rate (0.14) was 14.1 times the take (0.01) by marine predators [W = 83614, $P_{adj(2)}$ < 0.001] (fig. S3A). In paired comparisons, median fisheries exploitation (0.17) was 3.1 times the median rate (0.06) by the highest exploiting marine predator of the same prey [V = 382, $P_{adj(2)}$ = 0.02] (fig. S3B). At all trophic levels, humans killed fishes at higher rates than marine predators [all $P_{adj(9)}$ < 0.04] (Fig. 1D), but there were no differences in take by each predator across trophic levels [all $P_{adj(9)}$ ≥ 0.5]. Pooling all trophic levels, the median rate of Atlantic fisheries exploitation (0.20) was 2.9 times that of Pacific fisheries [median = 0.07, W = 6633, $P_{adj(4)}$ < 0.001] (fig. S4B).

Although our varied data set could impose biases in both directions (supplementary text), we reveal striking differences in exploitation rates between nonhuman predators and contemporary humans, particularly fishers and carnivore hunters. Interactions between human and natural systems likely underlie patterns. For example, global seafood markets, industrial processing, relatively high fecundity among fishes, and schooling behavior could, in part, explain the particularly high fisheries take, whereas gape limitation by piscivores and a generally species-rich marine environment might explain why marine predator rates are comparatively low. Higher human densities and reduced fish biomass (from longer exploitation) likely explain higher fishing rates in the Atlantic versus Pacific oceans. Moreover, motivations to kill typically inedible carnivores for trophy and competitive reasons [intraguild predation; (*7*)] are evidently powerful and drive acutely high rates. Although, in terms of numbers, it is easy to exploit high proportions of (less abundant) carnivore populations, the implications remain profound (below). In addition, whereas declines in tropical wild meat (*5*) might predict an opposite pattern, lower hunting rates of African herbivores could relate to simpler technology, less reporting, and/or longer adaptation to human predation.

Whereas sociopolitical factors can explain why humans repeatedly overexploit (*19*), cultural and technological dimensions can explain how. Human predatory behavior evolved much faster than competing predators and the defensive adaptations of prey (*20*). Indeed, division of labor, global trade systems, and dedicated

[1]Department of Geography, University of Victoria, Post Office Box 1700, Station CSC, Victoria, British Columbia V8W 2Y2, Canada. [2]Raincoast Conservation Foundation, Post Office Box 2429, Sidney, British Columbia V8L 3Y3, Canada. [3]Hakai Institute, Post Office Box 309, Heriot Bay, British Columbia V0P 1H0, Canada. [4]Department of Biology, University of Victoria, Post Office Box 3060, Station CSC, Victoria, British Columbia V8W 2Y2, Canada.
*Corresponding author. E-mail: darimont@uvic.ca

recreational pursuit have equipped highly specialized individuals with advanced killing technology and fossil fuel subsidy that essentially obviate energetically expensive and formerly dangerous search, pursuit, and capture. Moreover, agri- and aquaculture, as well as an ever-increasing taxonomic and geographic niche, leave an enormous and rapidly growing human population demographically decoupled from dwindling prey. In fact, low prey abundance can drive aggressive exploitation, because of the increased economic value of rare resources (*21*).

Emerging evidence suggests that the consequences of dominating adult prey are considerable. For example, human preference for large ornaments and/or large body size has fundamentally altered the selective landscape for many vertebrates. Not only can this rapidly alter morphological and life-history phenotypes (*11*), the resulting changes can modify the reproductive potential of populations (*22*) and ecological interactions within food webs [e.g., (*23*)]. In addition, owing to different behavior (e.g., age-class preferences and seasonality of exploitation), hunters likely cannot substitute for carnivores as providers of ecological services [e.g., regulation of disease and wildfire (*7*, *9*), as well as mesopredator control (*8*, *24*)]. Finally, less explored is the potentially substantial impact of prey biomass removal from ecosystems; global trade and sanitation systems shunt energy and nutrients from food webs of provenance to distant landfills and sewers.

These implications, the high exploitation rates that drive them, and the broadest taxonomic niche of any consumer uniquely define humans as a global "super predator." Clearly, nonhuman predators influence prey availability to humans [e.g., (*25*)]. But overwhelmingly these consumers target juveniles (*18*), the reproductive "interest" of populations. In contrast, humans—released from limits other predators encounter—exploit the "capital" (adults) at exceptionally high rates. The implications that can result are now increasingly costly to humanity (*26*) and add new urgency to reconsidering the concept of sustainable exploitation.

Transformation requires imposing limits of humanity's own design: cultural, economic, and institutional changes as pronounced and widespread as those that provided the advantages humans developed over prey and competitors. This includes, for example, cultivating tolerance for carnivores (*7*), designing catch-share programs (*27*), and supporting community leadership in fisheries (*28*). Also key could be a new definition of sustainable exploitation that focuses not on yields to humanity but rather emulates the behavior of other predators (*14*). Cultural, economic, and technological factors would make targeting juvenile prey challenging in many cases. Aligning exploitation rates on adults with those of competing predators, however, would provide management options between status quo exploitation and moratoria. Recent approaches to resolve controversies among fisheries scientists reveal how distant such predator-inspired management prescriptions are now. For example, although the mean "conservative" fishing rate estimated to rebuild multispecies fisheries across 10 ecosystems (0.04) is one-fourth their maximum sustainable yield rates (0.16) (*13*), it remains 4 times the median value we estimated among marine predators globally (0.01). Consequently, more aggressive reductions in exploitation are required to mimic nonhuman predators, which represent long-term models of sustainability (*14*).

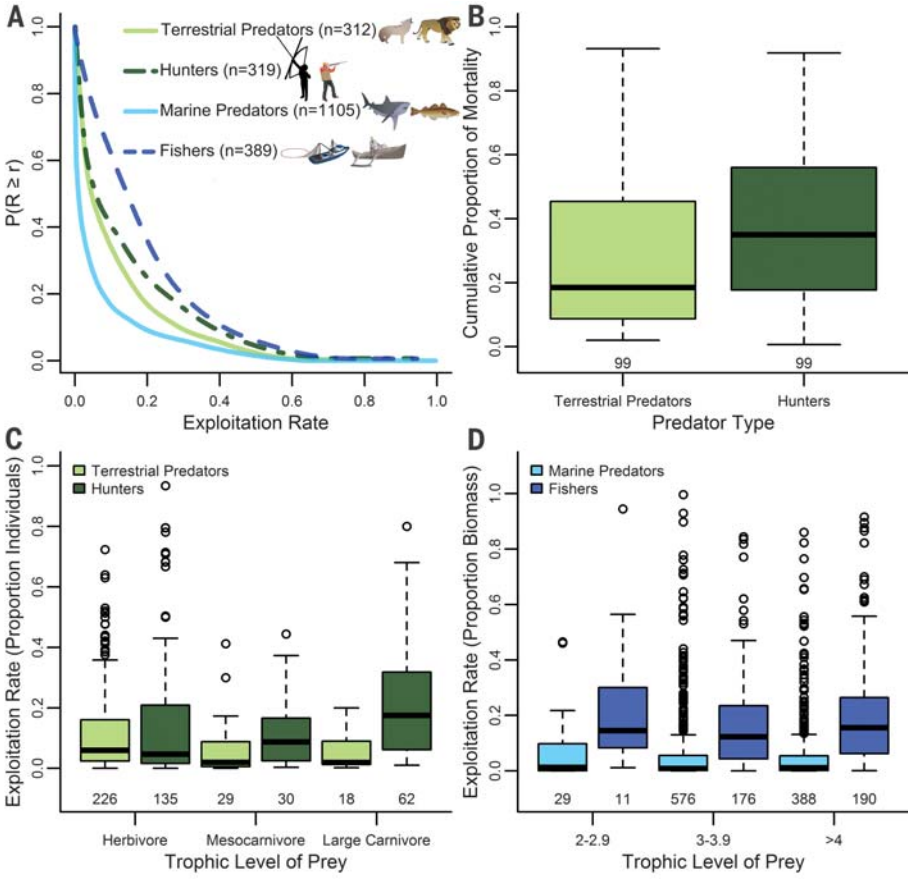

Fig. 1. Patterns of exploitation by human and nonhuman predators on adult prey. (**A**) Complementary cumulative distribution functions showing the probability of predators exploiting prey at a rate (*R*) greater than or equal to a given annual finite exploitation rate (*r*), on the basis of the number of available individuals in populations (terrestrial mammals) or biomass (marine fishes). (**B**) Proportion of annual mortality caused by hunters and all other (i.e., aggregated) terrestrial predators consuming the same prey population. (**C** and **D**) Exploitation rates of human and nonhuman predators across trophic levels in (C) terrestrial and (D) marine systems. Whiskers represent distance from upper and lower quartiles to largest and smallest nonoutliers. [Art by T. Saxby, K. Kraeer, L. Van Essen-Fishman/ian.umces.edu/imagelibrary/ and K. Eberlins/123rf.com]

REFERENCES AND NOTES

1. A. D. Barnosky, P. L. Koch, R. S. Feranec, S. L. Wing, A. B. Shabel, *Science* **306**, 70–75 (2004).
2. W. J. Ripple, B. Van Valkenburgh, *Bioscience* **60**, 516–526 (2010).
3. J. B. Jackson *et al.*, *Science* **293**, 629–637 (2001).
4. R. Hilborn, C. J. Walters, D. Ludwig, *Annu. Rev. Ecol. Syst.* **26**, 45–67 (1995).
5. E. J. Milner-Gulland, E. L. Bennett, *Trends Ecol. Evol.* **18**, 351–357 (2003).
6. B. Worm *et al.*, *Science* **314**, 787–790 (2006).
7. W. J. Ripple *et al.*, *Science* **343**, 1241484 (2014).
8. J. K. Baum, B. Worm, *J. Anim. Ecol.* **78**, 699–714 (2009).
9. J. A. Estes *et al.*, *Science* **333**, 301–306 (2011).
10. S. R. Palumbi, *Science* **293**, 1786–1790 (2001).
11. C. T. Darimont *et al.*, *Proc. Natl. Acad. Sci. U.S.A.* **106**, 952–954 (2009).
12. T. A. Branch, *Mar. Policy* **32**, 38–39 (2008).
13. B. Worm *et al.*, *Science* **325**, 578–585 (2009).
14. C. W. Fowler, L. Hobbs, *Proc. Biol. Sci.* **270**, 2579–2583 (2003).
15. Materials and methods are available as supplementary materials on *Science* Online.
16. D. Pauly, V. Christensen, *Nature* **374**, 255–257 (1995).
17. C. Collins, R. Kays, *Anim. Conserv.* **14**, 474–483 (2011).
18. N. C. Stenseth, E. S. Dunlop, *Nature* **457**, 803–804 (2009).
19. D. Ludwig, R. Hilborn, C. Walters, *Science* **260**, 17–36 (1993).
20. G. J. Vermeij, *Evolution* **66**, 2007–2014 (2012).
21. F. Courchamp *et al.*, *PLOS Biol.* **4**, e415 (2006).
22. C. N. K. Anderson *et al.*, *Nature* **452**, 835–839 (2008).
23. N. L. Shackell, K. T. Frank, J. A. Fisher, B. Petrie, W. C. Leggett, *Proc. Biol. Sci.* **277**, 1353–1360 (2010).
24. L. R. Prugh *et al.*, *Bioscience* **59**, 779–791 (2009).
25. P. Yodzis, *Trends Ecol. Evol.* **16**, 78–84 (2001).
26. J. S. Brashares *et al.*, *Science* **345**, 376–378 (2014).

27. C. Costello, S. D. Gaines, J. Lynham, *Science* **321**, 1678–1681 (2008).
28. N. L. Gutiérrez, R. Hilborn, O. Defeo, *Nature* **470**, 386–389 (2011).

ACKNOWLEDGMENTS

We thank M. Arseneau, L. Grant, H. Kobluk, J. Nelson, and S. Leaver for data collection; L. Reshitnyk for creating fig. S1; and P. Ehlers and J. Ehlers for statistical assistance. S. Anderson, J. Baum, T. Branch, J. Brashares, A. Calestagne, S. Carlson, T. Davies, D. Kramer, T. Levi, J. Reynolds, and the "Ecology@UVic" discussion group offered insight on drafts. We thank the Raincoast Conservation, Tula, Wilburforce, and Willowgrove Foundations. C.T.D. and T.E.R. acknowledge Natural Sciences and Engineering Research Council of Canada Discovery Grant 435683 and National Research Council Canada Operating Grant 2354, respectively. Data and R code available in Dryad (doi:10.5061/dryad.238b2). T.E.R. conceived of the idea and created the preliminary data set. C.T.D., H.M.B., C.H.F., and T.E.R. designed the research. C.T.D. led data collection and project management. H.M.B., C.T.D., and C.H.F. conducted analyses. C.T.D., C.H.F., H.M.B., and T.E.R. wrote the manuscript.

SUPPLEMENTARY MATERIALS

www.sciencemag.org/content/349/6250/858/suppl/DC1
Materials and Methods
Supplementary Text
Figs. S1 to S6
Tables S1 to S2
References (*29*, *30*)

24 April 2015; accepted 13 July 2015
10.1126/science.aac4249

PLANT MICROBIOME

Salicylic acid modulates colonization of the root microbiome by specific bacterial taxa

Sarah L. Lebeis,[1,2]*† Sur Herrera Paredes,[2,3,4]† Derek S. Lundberg,[2,5]†‡ Natalie Breakfield,[2]§ Jase Gehring,[2]‖ Meredith McDonald,[2] Stephanie Malfatti,[6]¶ Tijana Glavina del Rio,[6] Corbin D. Jones,[2,4,5,7] Susannah G. Tringe,[6] Jeffery L. Dangl[2,3,4,5,7,8]*

Immune systems distinguish "self" from "nonself" to maintain homeostasis and must differentially gate access to allow colonization by potentially beneficial, nonpathogenic microbes. Plant roots grow within extremely diverse soil microbial communities but assemble a taxonomically limited root-associated microbiome. We grew isogenic *Arabidopsis thaliana* mutants with altered immune systems in a wild soil and also in recolonization experiments with a synthetic bacterial community. We established that biosynthesis of, and signaling dependent on, the foliar defense phytohormone salicylic acid is required to assemble a normal root microbiome. Salicylic acid modulates colonization of the root by specific bacterial families. Thus, plant immune signaling drives selection from the available microbial communities to sculpt the root microbiome.

Recognition of plant pathogens in leaves leads to dramatic changes in transcription, synthesis of defense phytohormones and antimicrobial compounds, and elaboration of physical barriers (*1*, *2*). Defense phytohormones are structurally diverse plant secondary metabolites that integrate plant immune system output responses while repressing cell growth and proliferation. Salicylic acid (SA), jasmonic acid (JA), and gaseous ethylene mediate localized and systemic plant immune responses (*3*, *4*). Nonspecific systemic acquired resistance is mediated by SA in leaves (*5*). In contrast, induced systemic resistance in leaves can be triggered by specific rhizobacteria colonizing roots and is mediated by JA and ethylene (*4*). SA and JA act antagonistically in responses to infection by biotrophs, at least in leaves (*6*). The defense phytohormones control a set of overlapping signaling sectors, each contributing to the regulation of plant defense via transcriptional and biosynthetic output in leaves (*7*).

Accessions of *Arabidopsis thaliana* show variation in defense phytohormone profiles after infection, even though they share similar root-associated bacterial microbiota (*8*–*10*). Previous studies examined the roles of defense phytohormones in shaping the wild-type root microbiome by using single mutant lines defective in their biosynthesis or perception, or exogenous defense hormone application in combination with bacterial culturing and/or lower-resolution profiling methods. No generalizable clarity has emerged to date (*11*, *12*). We therefore compared the bacterial root microbiome of wild-type *A. thaliana* accession Col-0 with a set of isogenic mutants lacking biosynthesis of, and/or signaling dependent on, at least one of the following: SA, JA, and ethylene. We focused on those with multiple mutations that eliminated overlapping defense-signaling sectors (Fig. 1A and table S1) (*13*). We anticipated that this experimental design would reveal the contributions of plant defense phytohormones to wild-type root microbiome composition.

Through sequencing the 16*S* rRNA gene, we profiled bacterial communities of rhizosphere (soil directly adjacent to the root) and endophytic compartment (EC) from roots grown in a previously characterized wild soil from the University of North Carolina Mason Farm biological preserve, as well as unplanted bulk soil (figs. S1 to S4, tables S2 to S4, and supplementary materials, materials and methods 1 to 3 and 6a to 6d) (*10*). Sample fraction (soil, rhizosphere, or endophytic compartment) and the differentiation of endophytic samples from bulk soil and rhizosphere explained the largest proportions of variance across the bacterial communities examined (table S5) (*8*, *10*). Endophytic bacterial communities were less diverse than bulk soil and rhizosphere communities (Fig. 1B and fig. S4), with reduced representation of Acidobacteria, Bacteroidetes, and Verrucomicrobia and enrichment of Actinobacteria and Firmicutes [analysis of variance (ANOVA), q value < 0.05]. Individual Proteobacteria families were either enriched or depleted in endophytic communities as compared with those of bulk soil and rhizosphere samples (fig. S5 and supplementary materials, materials and methods 6b). These results are consistent with distributions of bacterial phyla from *A. thaliana* roots grown in four wild soils (*8*, *10*).

Plant genotype affected phylum-level bacterial root endophytic community composition [4.3 to 5.0%, canonical analysis of principal coordinates (CAP)] (Fig. 1B and supplementary materials, materials and methods 4b and 6e) (*14*), with both hyperimmune *cpr5* and immunocompromised quadruple *dde1 ein2 pad4 sid2* mutant communities displaying lower α-diversity indices than that of the wild type (Fig. 1B, fig. S4B, and supplementary materials, materials and methods 1b). The relative abundance of Firmicutes was lower in immunocompromised *jar1 ein2 npr1*, *ein2 npr1*, and *npr1 jar1* mutants, which all lack response to SA (Fig. 1, A and B, and table S1). Actinobacteria were less abundant in *cpr5* and *pad4* endophytic samples, whereas Proteobacteria were more abundant in *cpr5* and *jar1 ein2 npr1* (Fig. 1, A and B; fig. S8; and supplementary materials, materials and methods 4a). Only mutants that lacked all

[1]Department of Microbiology, University of Tennessee, Knoxville, TN 37996-0845, USA. [2]Department of Biology, University of North Carolina, Chapel Hill, NC 27599-3280, USA. [3]Howard Hughes Medical Institute, University of North Carolina, Chapel Hill, NC 27599-3280, USA. [4]Curriculum in Bioinformatics and Computational Biology, University of North Carolina, Chapel Hill, NC 27599-3280, USA. [5]Curriculum in Genetics and Molecular Biology, University of North Carolina, Chapel Hill, NC 27599-3280, USA. [6]Joint Genome Institute, U.S. Department of Energy, Walnut Creek, CA, USA. [7]Carolina Center for Genome Sciences, University of North Carolina, Chapel Hill, NC 27599-3280, USA. [8]Department of Microbiology and Immunology, University of North Carolina, Chapel Hill, NC 27599-3280, USA.
***Corresponding author. E-mail: slebeis@utk.edu (S.L.L.); dangl@email.unc.edu (J.L.D.)** †These authors contributed equally to this work. ‡Present address: Department of Molecular Biology, Max Planck Institute for Developmental Biology, 72076 Tübingen, Germany. §Present address: NewLeaf Symbiotics, St. Louis, MO 63132, USA. ‖Present address: Department of Molecular and Cell Biology, University of California, Berkeley, Berkeley, CA 94720, USA. ¶Present address: Lawrence Livermore National Laboratory, Livermore, CA 94550-9234, USA.

three defense hormone signaling systems exhibited diminished survival that correlated with the presence of an unidentified oomycete in the root microbiota of survivors (fig. S2 and supplementary materials, materials and methods 3g).

We identified, using a zero inflated negative binomial (ZINB) model, bacterial families and operational taxonomic units (OTUs) in the root endophyte microbiome of each mutant plant line that were differentially abundant as compared with wild-type plants (tables S6 and S7, fig. S9, and supplementary materials, materials and methods 6b). Both the number of differentially abundant bacterial taxa and their identity differed in endophytic samples from mutants. Among 52 differentially abundant families in surviving *dde1 ein2 pad4 sid2* mutant endophytic samples, nearly all were depletions (Fig. 1C and fig. S6), which is consistent with this mutant's decreased α-diversity (Fig. 1B). Differentially abundant bacterial families were consistent with the significant relative phyla differences observed in specific defense hormone mutants (Fig. 1B and fig. S6A). In *cpr5*, for example, nine Actinobacteria families were identified with decreased relative abundance, and 12 Proteobacteria families were identified with increased relative abundance, in comparison with wild type (Fig. 1C, fig. S5, and table S6). These differences demonstrate that defense phytohormones modulate root microbiome composition at multiple taxonomic levels from phylum to family.

We then compared the enrichment and depletion profiles across the mutant genotypes in order to identify shared patterns (fig. S6C and supplementary materials, materials and methods 6d). Two striking genotype groups were observed (Fig. 1C). Group 1 mutants constitutively produce and accumulate SA, whereas group 2 mutants either accumulate less SA or cannot respond to it. These two genotype groups exhibited complementary patterns of differentially abundant Proteobacteria: In group 1, these were α- and β-Proteobacteria, whereas in group 2, they were γ-Proteobacteria (table S6 and fig. S6A). Within genotype group 2, nearly all of the differentially abundant bacterial families in *sid2* were shared with *pad4* and *dde1 ein2 pad4 sid2*, especially those families depleted as compared with the wild type. Half of the *dde1 ein2 pad4 sid2* depletions were apparently SA-independent (Fig. 1D and fig. S6B).

We reanalyzed the data to ask whether the differential family abundances observed in specific mutant groups remained consistent at higher taxonomic (OTU) resolution (table S4, tab B; table S7; and supplementary materials, materials and methods 6b). We largely recapitulated mutant groups 1 and 2 at OTU resolution (fig. S7B). If the plant selected bacteria at a low (genus or species) taxonomic level, we would expect that only one or a few abundant OTUs would drive, and thus correlate with, family-level analyses. However, we observed that a number of OTUs from across the abundance range matched family-level enrichment profiles (fig. S7, C to F, and supplementary materials, materials and methods 6b). These results suggest that defense phytohormones, particularly SA, modulate taxonomic groups of bacteria at the family level in the root, and not by altering the abundance of a small number of dominant strains within each differentially abundant family.

We next asked whether the bacterial families affected by the plant defense phytohormone mutants corresponded to taxa that were normally either enriched or depleted in wild-type roots compared with bulk soil. We resequenced two regions of the 16*S* gene across a subset of the samples using a different technology. This allowed us to eliminate sequencing and amplification biases. We identified 19 enriched and 23 depleted families in endophytic samples of wild-type roots compared with soil (table S8, fig. S11, and supplementary materials, materials and methods 6c). Consistent with phyla-level analyses (Fig. 1B), 79% of the bacterial families enriched in endophytic samples were Actinobacteria or Proteobacteria. Further, 55% of the endophytic-enriched families in SA mutants are Actinobacteria or Proteobacteria (tables S6 and S8). A similar pattern was observed in the OTU-level analysis, in which 42 and 48% of the endophytic-enriched bacterial families contained at least one OTU that is further enriched in the phytohormone mutants (tables S7 and S8).

Six of the 19 endophytic-enriched families (table S8) were depleted in the *cpr5* mutant that constitutively produces SA (table S6), suggesting that these six bacterial families are sensitive to SA or SA-dependent processes. Five different endophytic-enriched families (table S8) were further enriched in group 2 mutants that lack SA biosynthesis and signaling (table S6). Thus, these five bacterial families are candidates for taxa whose colonization is normally limited by wild-type levels of SA and/or SA-dependent processes. In contrast, 12 of the 23 endophytic-depleted families (table S8) were further depleted in group 2 mutants but not in group 1 mutants. Hence, these endophytic-depleted families may require SA-dependent processes to maintain even their very low abundance in the wild-type endophytic compartment (tables S6 and S8). Thus, SA is required to modulate the assembly of a normal root microbiome. In its absence, core root bacterial community composition is substantially

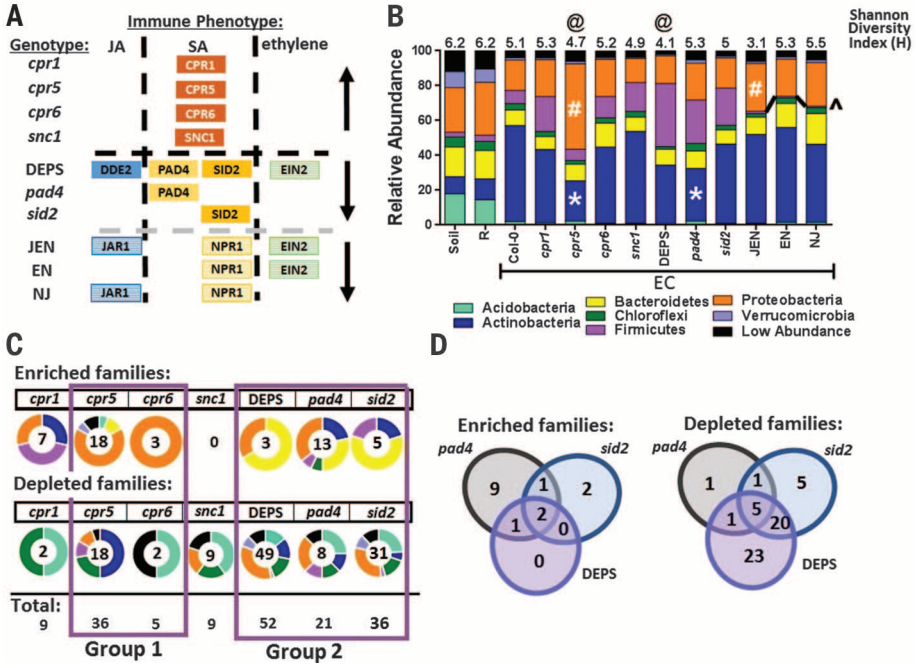

Fig. 1. Defense phytohormone mutants have altered root bacterial communities compared with those of wild-type plants. (**A**) JA, SA, and ethylene mutants (names at left) derived from wild-type Col-0. Upward and downward black arrows at right indicate hyper- and hypo-immune mutants, respectively. (**B**) Phyla distributions were separated into sample fractions [soil, Col-0 rhizosphere (R), or EC] and plant genotypes. Shannon diversity indices are listed above each bar. Asterisk indicates a phylum significantly lower than Col-0 EC at $P < 0.001$; pound sign indicates a phylum significantly higher than Col-0 EC at $P < 0.05$; and caret indicates that JEN, EN, and NJ Firmicutes relative abundances were significantly lower than Col-0 EC at $P < 0.04$; "@" indicates that the Shannon diversity index is significantly lower than Col-0 EC at $P < 0.001$ (all ANOVA with post hoc Tukey test). (**C**) The phyla distribution [circles color-coded as in (B)] of bacterial families identified as either enriched or depleted in ECs of each mutant compared with Col-0. The number of families in each category is noted inside each donut. Groups defined by means of Monte Carlo testing of Manhattan distances. (**D**) Venn diagrams showing the overlap of (left) enriched or (right) depleted group 2 families from (B).

altered. However, these changes to the bacterial microbiome are not sufficient to alter survival of these mutants in this particular wild soil.

We asked whether bacteria isolated from roots can colonize sterile roots in the context of a defined but complex synthetic bacterial community. We planted sterile seedlings (wild type and defense phytohormone mutants) in a calcined clay substrate inoculated with a synthetic community (SynCom) of bacteria (supplementary materials, materials and methods 5). Sixteen SynCom strains (table S9) were members of 10 families enriched in endophytic compartments of wild-type plants as compared with soil (table S8), and 18 strains matched family OTUs altered in plant defense hormone mutants (tables S6 and S9). Further, 21 of the 38 strains belonged to families that matched endophytic-enriched OTUs from a published census of plants grown in wild Mason Farm soil (*10*).

Both bulk soil and endophytic compartment microbiomes changed over 8 weeks after SynCom inoculation (Fig. 2A). Fourteen of the 38 SynCom strains were "robust colonizers" (fig. S13C, table S9, and supplementary materials, materials and methods 6h). Six of these 14 are from families predicted to be endophytic-enriched in roots from our Mason Farm soil census (Fig. 2B, overlapping black and orange circles, and table S9), corroborating their ability to colonize roots. We identified six "SynCom EC-enriched" isolates and eight "SynCom EC-depleted" isolates (Fig. 2C, table S4e, and supplementary materials, materials and methods 6f). Five of the six SynCom EC-enriched strains belong to families also predicted to be endophytic-enriched in roots from the Mason Farm soil census (Fig. 2B, overlapping orange and red circles, and table S9), supporting their categorization as endophytic compartment–enriched families (table S8). Thus, (i) some but not all SynCom isolates robustly colonized the endophytic compartment of host plants in these mesocosms, (ii) the soil and endophytic microbiomes still differed in this context, and (iii) there was considerable overlap in enrichments and depletions between the SynCom and wild soil colonization experimental platforms at the family level.

Seven bacterial isolates were differentially abundant between wild type and the defense phytohormone mutants in the SynCom experiments (Fig. 3 and supplementary materials, materials and methods 6f), including at least one representative from each of the four phyla present in the inoculum (table S9). Six of the seven isolates were either depleted (*Streptomyces* sp. 136, *Chryseobacterium* sp. 8, *Pseudomonas* sp. 50, and *Escherichia coli*) or were sporadic or non-colonizers (*Bacillus* sp. 125 and *Brevundimonas* sp. 374). Four of these six overlapped with families predicted to be differentially abundant across genotypes in our Mason Farm soil census (Fig. 3B and table S6), and six of seven (all except *Bacillus* sp. 125) were enriched in the defense phytohormone mutants (Fig. 3C). The profiles of differentially abundant isolates in *pad4* and *sid2* mutants overlapped (Fig. 3C). These data integrate our SynCom experiments with our wild soil census and demonstrate increased abundance in the SA-deficient mutants of isolates that were "sporadic or non-colonizers" across all wild soil endophytic samples. Thus, altering SA production and signaling in the host plant prevents it from fully excluding bacterial taxa that a wild-type plant shuns.

Exogenous SA application to our SynCom experiments also affected bacterial community composition in both bulk soil and endophytic compartment samples (CAP 0.3 to 1.5%) (fig. S14A, table S5, and supplementary materials, materials and methods 5b and 6e), which is consistent with rhizosphere changes in plants treated with SA or JA (*15*, *16*). Two isolates were enriched [*Flavobacterium* sp. 40 (Bacteroidetes) and *Terracoccus* sp. 273 (Actinobacteria)] and one depleted [*Mitsuaria* sp. 370 (β-Proteobacteria)] in the presence of exogenous SA (table S9; fig. S14, B and C; and supplementary materials, materials and methods 6f). *Terracoccus* sp. 273 abundance was higher in both SA-treated bulk soil and root endophytic samples (Fig. 4A), and its growth was enhanced by SA in liquid media (Fig. 4B and supplementary materials, materials and methods 5c), although its genome contains no obvious SA catabolism genes (taxon IDs in table S9). In contrast, *Mitsuaria* sp. 370 was depleted in endophytic

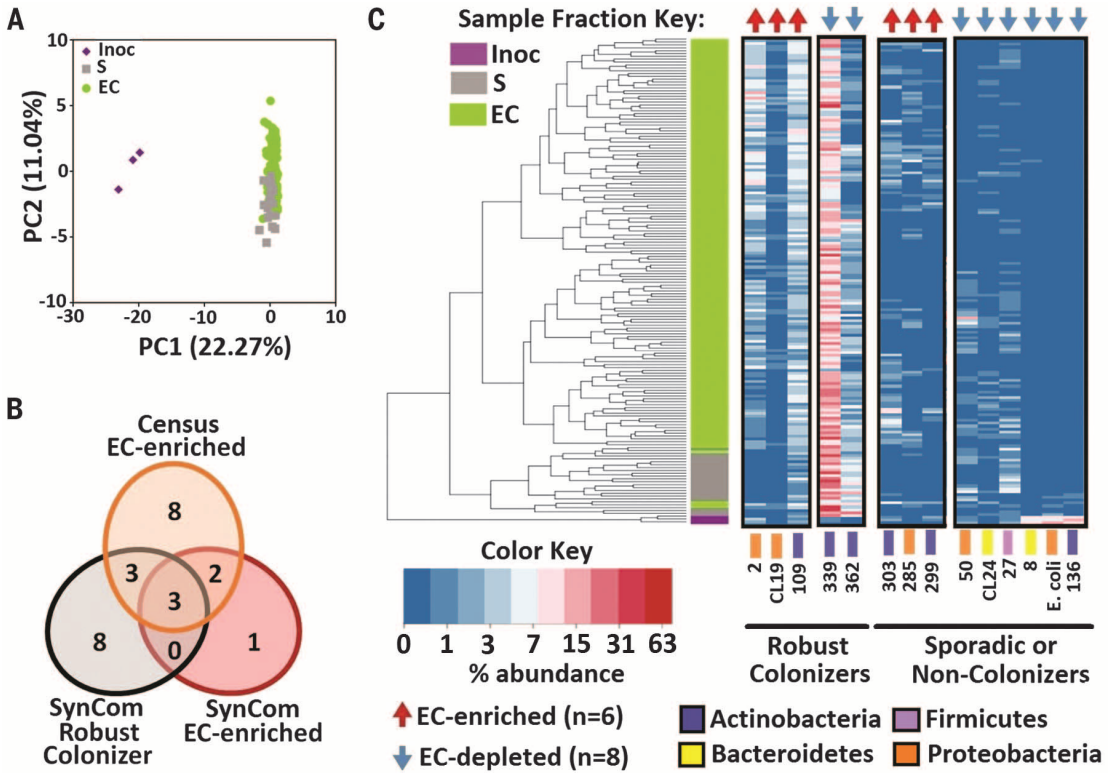

Fig. 2. A 38-member synthetic community recapitulates differentiated microbiome colonization. (**A**) Principal coordinates analysis showing the inoculum (purple diamonds), soil (gray squares), and EC (green circles) samples. (**B**) The overlap of SynCom members that were robust colonizers of Col-0 EC (black), EC-enriched (red), or matched EC-enriched families from the census of roots grown in wild Mason Farm soil (orange) (Fig. 1). (**C**) Hierarchical clustering and heat map showing percent abundance (log_2 scale) of selected isolates. Sample clustering splits by fraction (left) and EC samples grouping by biological replicate. Isolates are grouped by their presence in the majority of Col-0 EC samples (Robust colonizers) or absence in the majority of Col-0 EC samples (sporadic or non-colonizers). Isolates are color-coded to phyla as in Fig. 1. Isolates that were significantly more abundant (red arrows) or less abundant (blue arrows) in EC with respect to bulk soil are denoted along the top.

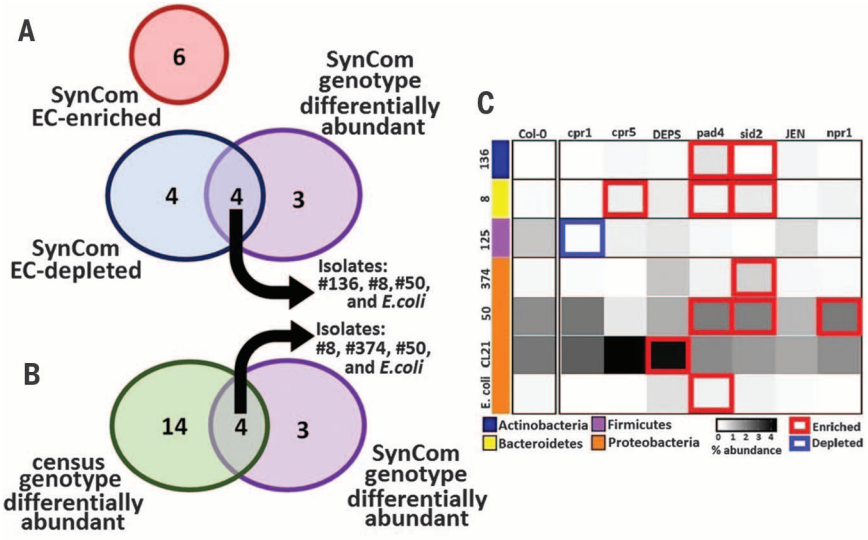

Fig. 3. Defense phytohormone mutants exhibit increased abundance of EC-depleted microbes. (**A**) Overlap of SynCom EC-depleted (Fig. 2C) and SynCom isolates differentially abundant in defense phytohormone mutants (SynCom genotype differentially abundant). No SynCom EC-enriched isolates (Fig. 2, B and C) were affected by plant genotype. (**B**) Overlap of the same SynCom genotype differentially abundant isolates from (A) compared with isolates present in the SynCom from families that were genotype differentially abundant in the wild soil census (green circle) (table S8). (**C**) Heat map of isolates (color-coded by phylum as in Fig. 1) differentially abundant between defense phytohormone mutants and Col-0. Grayscale shows the mean abundance of the corresponding isolate (rows) in the EC of a given genotype (columns). Genotype differentially abundant families predicted as enriched or depleted by the ZINB model are boxed in red or blue, respectively (supplementary materials, materials and methods 6f).

samples treated with SA and grew less well in its presence (Fig. 4, C and D). *Streptomyces* sp. 303 was weakly enriched in SA-treated samples (q value <0.07) (Fig. 4E), grew on minimal media with 0.5 mM SA as a sole carbon source (Fig. 4F), and contains orthologs to a previously characterized *Streptomyces* SA-degradation operon (fig. S14D and table S9). Thus, the broader effects of SA on microbiome composition consist of both direct and indirect effects on the physiologies of individual community members from limited, specific taxa.

We demonstrate that plant defense phytohormones sculpt the root microbiome in characteristic ways. Elimination of all three defense phytohormone signaling sectors results in abnormal microbial profiles in the root, which may be linked to lowered survival in a wild soil. SA, a key immune regulator in leaves, also modulates the composition of the root microbiome. Plants with altered SA signaling have root microbiomes that differ in the relative abundance of specific bacterial families as compared with those of wild type. It will be of interest to address whether and how the extra- and intracellular plant immune system receptor systems further condition root bacterial community composition. We demonstrated that different bacterial strains could make use of SA in different ways, whether as a growth signal or as a carbon source. Thus, SA influences the microbial community structure of the root. This may occur by gating bacterial taxa as a consequence of SA function in homeostatic control of immune system outputs, or via as-yet-undefined effects on microbe-microbe interactions and root physiology. Together, our results show that a

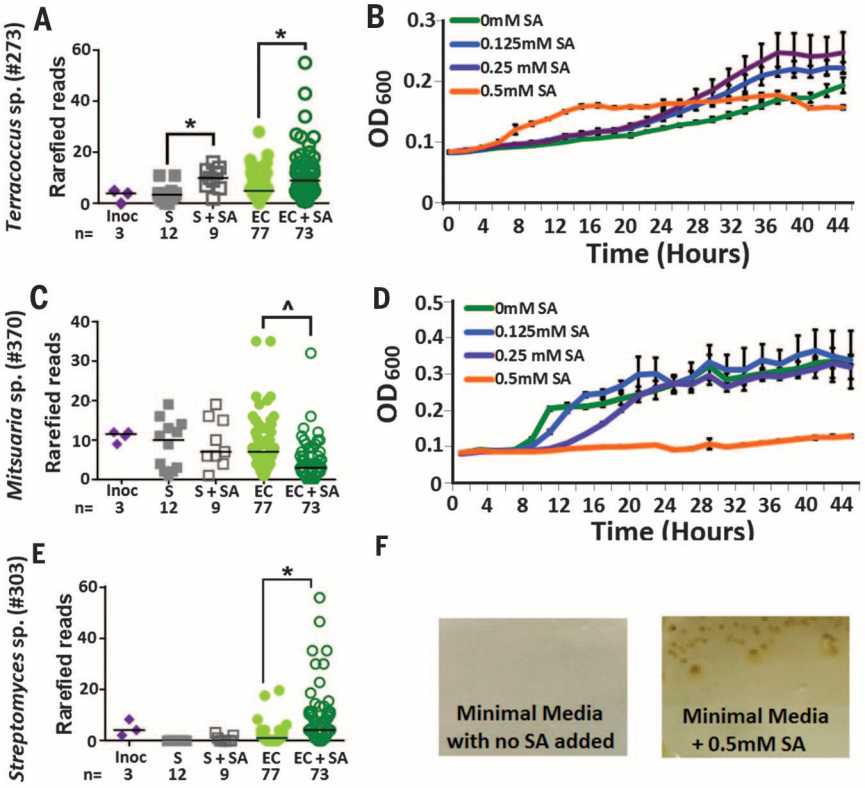

Fig. 4. SA directly affects synthetic community isolates. (**A**) *Terracoccus* sp. (273) reads from 400 rarefied consensus sequences for the synthetic community inoculum (purple diamonds), soil (gray squares), and EC samples (green circles) from SA-treated (open symbols) and -untreated (closed symbols) plants. Asterisk indicates significantly different between sample treatments at $P < 0.006$ by Mann-Whitney test. (**B**) Optical density of *Terracoccus* sp. (273) grown in buffered 1/10 LB with 0 (green), 0.125 (blue), 0.25 (purple), or 0.5 mM (orange) SA added. (**C**) *Mitsuaria* sp. (370) reads as in (A). Caret indicates significantly different between EC sample treatments at $P < 0.0001$ by means of Mann-Whitney test. (**D**) Optical density of *Mitsuaria* sp. (370) grown as in (B). (**E**) *Streptomyces* sp. (303) reads. Asterisk indicates significantly different between EC sample treatments at $P < 0.001$ by means of Mann-Whitney test. (**F**) *Streptomyces* sp. (303) aggregates in liquid cultures but grows on minimal media agar with 0.5 mM SA as the sole carbon source.

central regulator of the plant immune system, largely uncharacterized in the root, directly influences root microbiome composition. Our results could open new avenues for modulating the root microbiome to enhance crop production and sustainability.

Note added in proof: Figure 1 was revised since this paper's original publication in *Science* Express.

REFERENCES AND NOTES

1. P. N. Dodds, J. P. Rathjen, *Nat. Rev. Genet.* **11**, 539–548 (2010).
2. J. D. Jones, J. L. Dangl, *Nature* **444**, 323–329 (2006).
3. Y. Belkhadir, L. Yang, J. Hetzel, J. L. Dangl, J. Chory, *Trends Biochem. Sci.* **39**, 447–456 (2014).
4. C. M. Pieterse, D. Van der Does, C. Zamioudis, A. Leon-Reyes, S. C. Van Wees, *Annu. Rev. Cell Dev. Biol.* **28**, 489–521 (2012).
5. Z. Q. Fu, X. Dong, *Annu. Rev. Plant Biol.* **64**, 839–863 (2013).
6. B. Huot, J. Yao, B. L. Montgomery, S. Y. He, *Mol. Plant* **7**, 1267–1287 (2014).
7. Y. Kim *et al*., *Cell Host Microbe* **15**, 84–94 (2014).
8. D. Bulgarelli *et al*., *Nature* **488**, 91–95 (2012).
9. D. J. Kliebenstein, A. Figuth, T. Mitchell-Olds, *Genetics* **161**, 1685–1696 (2002).
10. D. S. Lundberg *et al*., *Nature* **488**, 86–90 (2012).
11. P. A. Bakker, R. L. Berendsen, R. F. Doornbos, P. C. Wintermans, C. M. Pieterse, *Front. Plant Sci.* **4**, 165 (2013).
12. R. Mendes, P. Garbeva, J. M. Raaijmakers, *FEMS Microbiol. Rev.* **37**, 634–663 (2013).
13. F. Katagiri, K. Tsuda, *Mol. Plant Microbe Interact.* **23**, 1531–1536 (2010).
14. M. J. Anderson, T. J. Willis, *Ecology* **84**, 511–525 (2003).
15. L. C. Carvalhais, P. G. Dennis, P. M. Schenk, *Appl. Soil Ecol.* **84**, 1–5 (2014).
16. R. F. Doornbos, B. P. Geraats, E. E. Kuramae, L. C. Van Loon, P. A. Bakker, *Mol. Plant Microbe Interact.* **24**, 395–407 (2011).

ACKNOWLEDGMENTS

This work was supported by NSF Microbial Systems Biology grant IOS-0958245 and NSF INSPIRE grant IOS-1343020 to J.L.D. S.H.P. was supported by NIH Training Grant T32 GM067553-06 and is a Howard Hughes Medical Institute (HHMI) International Student Research Fellow. D.S.L. was supported by NIH Training Grant T32 GM07092-34. J.L.D. is an Investigator of HHMI, supported by HHMI and the Gordon and Betty Moore Foundation (GBMF3030). S.L.L. was supported by the NIH Minority Opportunities in Research division of the National Institute of General Medical Sciences (NIGMS) grant K12GM000678. N.B. was supported by NIH Dr. Ruth L. Kirschstein National Research Service Award Fellowship F32-GM103156. The work conducted by the U.S. Department of Energy (DOE) Joint Genome Institute (JGI), a DOE Office of Science User Facility, is supported by the Office of Science of the DOE under contract DE-AC02-05CH11231. This work was also funded by the DOE–JGI Director's Discretionary Grand Challenge Program. We thank the Dangl laboratory microbiome group for useful discussions and S. Grant, S. Y. He, P. Hugenholtz, J. Kremer, and D. Weigel for critical comments on the manuscript. The supplementary materials contain additional data. J.L.D. is a cofounder, shareholder, and chair of the Scientific Advisory Board of AgBiome, a corporation whose goal is to use plant-associated microbes to improve plant productivity. Raw sequence data are available at the Short Read Archive accessions ERP010780 and ERP010863 and at the JGI portal http://genome.jgi.doe.gov/Immunesamples/Immunesamples.info.html, which requires registration to access.

SUPPLEMENTARY MATERIALS

www.sciencemag.org/content/349/6250/860/suppl/DC1
Materials and Methods
SupplementaryText
Figs. S1 to S14
References (*17*–*63*)
Tables S1 to S10
Databases S1 to S4

8 February 2015; accepted 26 June 2015
Published online 16 July 2015
10.1126/science.aaa8764

PARASITIC PLANTS

Probing strigolactone receptors in *Striga hermonthica* with fluorescence

Yuichiro Tsuchiya,[1,3]*† Masahiko Yoshimura,[1,2]† Yoshikatsu Sato,[1] Keiko Kuwata,[1] Shigeo Toh,[3] Duncan Holbrook-Smith,[3] Hua Zhang,[1] Peter McCourt,[3] Kenichiro Itami,[1,2,4] Toshinori Kinoshita,[1,2] Shinya Hagihara[1,2]*

Elucidating the signaling mechanism of strigolactones has been the key to controlling the devastating problem caused by the parasitic plant *Striga hermonthica*. To overcome the genetic intractability that has previously interfered with identification of the strigolactone receptor, we developed a fluorescence turn-on probe, Yoshimulactone Green (YLG), which activates strigolactone signaling and illuminates signal perception by the strigolactone receptors. Here we describe how strigolactones bind to and act via *ShHTL*s, the diverged family of α/β hydrolase-fold proteins in *Striga*. Live imaging using YLGs revealed that a dynamic wavelike propagation of strigolactone perception wakes up *Striga* seeds. We conclude that *ShHTL*s function as the strigolactone receptors mediating seed germination in *Striga*. Our findings enable access to strigolactone receptors and observation of the regulatory dynamics for strigolactone signal transduction in *Striga*.

Damages caused by the parasitic plant *Striga hermonthica* threaten food security in Africa. Infection of harvests by *Striga* leads to the loss of $10 billion U.S. dollars' worth of crops from the continent every year (*1*). Strigol and related strigolactones (*2*, *3*) derived from the host plants stimulate the germination of *Striga* by regulating the biosynthesis of plant hormones, including abscisic acid, gibberellins, and ethylene (*4*–*6*). So far, 17 strigolactones have been identified, which are unique according to the plant species (*7*–*9*). *Striga* recognizes host plants by sensing their particular strigolactone composition (*10*). However, the mechanism of how *Striga* senses minute amounts of structurally diverse strigolactones to identify their host targets remains unclear. Here we report the identification of the strigolactone receptor in *Striga*.

Strigolactones also function as plant hormones and as ecological signals for communicating with microbes (*11*–*13*). Genetic studies in model plants, including rice, *Arabidopsis*, and petunia, have led to identification of a group of α/β hydrolase-fold proteins as presumptive receptors for strigolactones (*14*–*17*). The unidentified strigolactone receptor in *Striga* may have a similar ligand selectivity to AtDWARF14 (AtD14), the strigolactone receptor in *Arabidopsis*, because AtD14 is also known to perceive natural and synthetic stimulants for *Striga* germination (*16*–*19*). However, *AtD14* regulates plant architecture, including shoot branching and root development, that has no obvious resemblance to *Striga* germination (*20*, *21*). In contrast, its homolog, *HYPOSENSITIVE TO LIGHT* (*AtHTL*)/*KARRIKIN INSENSITIVE2* (*KAI2*) is involved in seed germination stimulated by smoke-derived karrikins, a collection of imide-based agonists and non-natural stereoisomers of strigolactones in *Arabidopsis* (*16*, *22*, *23*). Therefore, the strigolactone receptors in *Striga* may have a comparable role to *AtHTL*, with ligand preferences similar to those of *AtD14* (fig. S1). On the other hand, the signaling processes of these homologs are highly related. Both AtD14 and AtHTL are considered to share an F-box protein, MORE AXILLARY GROWTH2 (AtMAX2), which directs their specific negative regulators to undergo ubiquitin-dependent proteasomal degradation (*24*, *25*). The ortholog of *AtMAX2* in *Striga* (*ShMAX2*) plays a role in regulating shoot branching and seed germination when expressed in *Arabidopsis*, thus suggesting that the signaling processes involving the F-box protein are conserved in *Striga* (*26*). Altogether, we hypothesized that *Striga* carries orthologs of either *AtD14* or *AtHTL* that have acquired new functions during the evolution of parasitism to respond to natural strigolactones and stimulate germination.

Here we report the use of small-molecule tools to probe the function of strigolactone receptors. AtD14 hydrolyzes strigolactones into the ABC-ring and D-ring fragments during the signaling process (fig. S2) (*15*). We applied this reaction to

[1]Institute of Transformative Bio-Molecules (WPI-ITbM), Nagoya University, Furo-cho, Chikusa-ku, Nagoya 464-8602, Japan. [2]Graduate School of Science, Nagoya University, Furo-cho, Chikusa-ku, Nagoya 464-8602, Japan. [3]Department of Cell and Systems Biology, University of Toronto, 25 Willcocks Street, Toronto, Ontario M5S 3B2, Canada. [4]Japan Science and Technology Agency–Exploratory Research for Advanced Technology, Itami Molecular Nanocarbon Project, Nagoya University, Furo-cho, Chikusa-ku, Nagoya 464-8602, Japan. ***Corresponding author. E-mail: yuichiro@itbm.nagoya-u.ac.jp (Y.T.); hagi@itbm.nagoya-u.ac.jp (S.H.)** †These authors contributed equally to this work.

develop a fluorogenic agonist for AtD14-type strigolactone receptors, Yoshimulactone Green (YLG). Fluorogenic substrates for hydrolyzing enzymes, such as protease, glycosidase, and phosphatase, have been widely used to track enzymatic activity (*27*). We designed YLG to be recognized by strigolactone receptors, with subsequent hydrolysis leading to the generation of fluorescent products (Fig. 1A and fig. S2). We proved this principle in several ways. Initially, we observed that recombinant AtD14 protein hydrolyzed YLG into fluorescein and the D-ring moiety in vitro. The increase in fluorescence with time and concentration showed a Michaelis constant (K_m^{YLG}) value at 0.63 μM and a catalytic cycle of 4.4 min per reaction (Fig. 1B and fig. S3). In contrast, YLG was poorly hydrolyzed by recombinant AtHTL protein, a characteristic shared with strigolactones, which selectively function through AtD14 (fig. S3) (*23*). YLG shares the binding pocket on AtD14 with physiologically active strigolactones, as indicated by the competition of hydrolysis of YLG alongside synthetic strigolactone, GR24, or natural strigolactones. Among the compounds investigated, (+)-5-deoxystrigol (5DS) displayed the strongest median inhibitory concentration (IC_{50}) value of 0.44 μM (Fig. 1C). This YLG competition assay reflects the binding specificity of the receptor, because the physiologically inactive analog, carba-GR24, failed to compete with YLG on hydrolysis by AtD14 (Fig. 1C) (*28*). We next found that treatment of YLG with wild-type *Arabidopsis* resulted in fluorescence in primary and lateral roots, where strigolactones have been reported to act on the growth or formation (Fig. 1D and fig. S4) (*21*); such fluorescence was absent in the *Atd14-1* loss-of-function mutant. As a third observation, we found that YLG restored shoot branching in the strigolactone biosynthetic mutant *max4-1* (Fig. 1E) (*29*). Together, these results led us to conclude that YLG works as an in vitro and in vivo fluorogenic agonist for *AtD14* in *Arabidopsis*.

YLG stimulated *Striga* germination, and subsequently 97% of germinating seeds emitted fluorescence (n = 229, Fig. 2A and fig. S5). Thus, YLG functions as a fluorogenic agonist in *Striga*, which cleaves the ligand as it is perceived. By searching a public *Striga* RNA-seq database, we

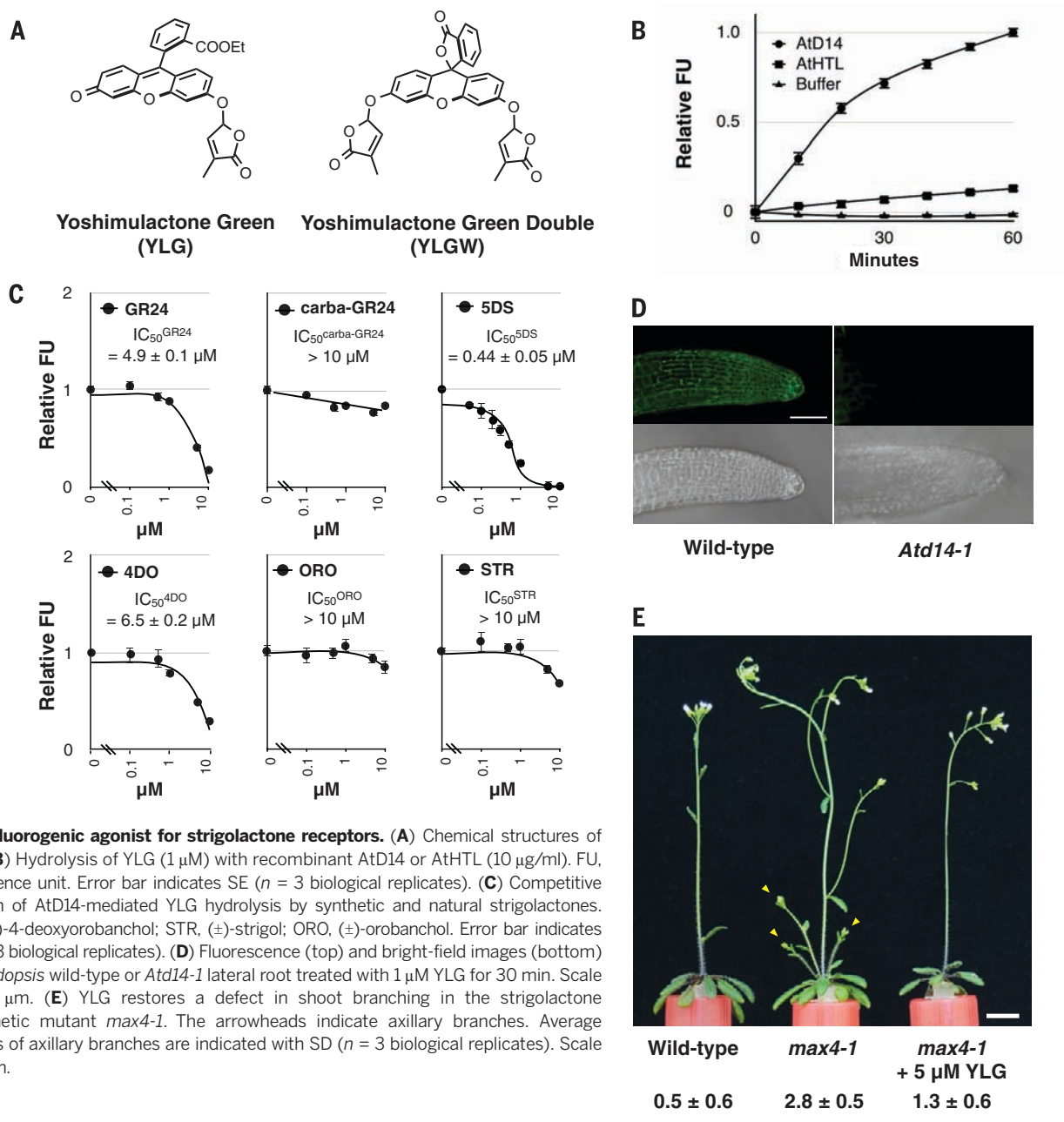

Fig. 1. Fluorogenic agonist for strigolactone receptors. (**A**) Chemical structures of YLGs. (**B**) Hydrolysis of YLG (1 μM) with recombinant AtD14 or AtHTL (10 μg/ml). FU, fluorescence unit. Error bar indicates SE (n = 3 biological replicates). (**C**) Competitive inhibition of AtD14-mediated YLG hydrolysis by synthetic and natural strigolactones. 4DO, (+)-4-deoxyorobanchol; STR, (±)-strigol; ORO, (±)-orobanchol. Error bar indicates SE (n = 3 biological replicates). (**D**) Fluorescence (top) and bright-field images (bottom) of *Arabidopsis* wild-type or *Atd14-1* lateral root treated with 1 μM YLG for 30 min. Scale bar, 50 μm. (**E**) YLG restores a defect in shoot branching in the strigolactone biosynthetic mutant *max4-1*. The arrowheads indicate axillary branches. Average numbers of axillary branches are indicated with SD (n = 3 biological replicates). Scale bar, 1 cm.

identified 12 genes as candidate receptors with sequences related to *AtD14* and *AtHTL: ShD14* and *ShHTL1* to *ShHTL11* (Fig. 2B and fig. S5). All 12 proteins have a conserved catalytic triad in α/β hydrolase, although only 10 recombinant proteins (*ShHTL2* to *-11*) hydrolyzed YLG and GR24 (Fig. 2C and figs. S5 and S6). To test the function of YLG in seed germination, we expressed *ShHTL7* in the *Arabidopsis Athtl-3* mutant, which is defective in germination (*16*). YLG and GR24 stimulated germination in the transgenic lines but not in the parental *Athtl-3*, indicating that *ShHTL7* is a functional strigolactone receptor that supports germination in *Arabidopsis* (Fig. 2D).

We next evaluated the relevance of hydrolysis in the evolution of parasitism (Fig. 2 and fig. S5). Phylogenetic analysis showed that the 10 genes in the YLG hydrolysis trait (*ShHTL2* to *-11*) coincide with a *Striga*-characteristic gene cluster extended from *AtHTL,* which suggests that these genes function in seed germination and subsequently acquire YLG hydrolytic activity (Fig. 2B). Figure 2C shows that a subgroup including *ShHTL4* to *-11* binds to natural strigolactones with moderate to high affinity. Moreover, the expression of this subgroup was induced by the potentiating treatment of seed conditioning, which may coordinate receptors to perceive strigolactones for germination (fig. S5). Of this subgroup, *ShHTL6* and *ShHTL7* showed indiscriminately high affinity to all of the strigolactones tested, whereas others favor particular strigolactones (Fig. 2C). Thus, from a few promiscuous receptors, multiple specialized receptors seem to have evolved to detect structurally diverse strigolactones more efficiently. This would have led to each different strigolactone being perceived by a different combination of receptors. Among the strigolactones that we tested, 5DS showed high-affinity binding (IC50 < 1 μM) to most of the receptors, which is consistent with its potency in stimulating the germination of *Striga* (fig. S7). This result may explain why 5DS-producing cultivars of some economically important crops such as sorghum, maize, and millet are susceptible to *Striga* (*10*, *30*). It is noteworthy that the strain we used was harvested from *Striga* growing on sorghum. It is possible that other strigolactones than 5DS may act as high-affinity ligands for the receptors in the locally propagated *Striga* population, which have adapted to different hosts.

The catalytically activated fluorescence in YLG allows us to track signal perception by the strigolactone receptors in intact *Striga* seeds.

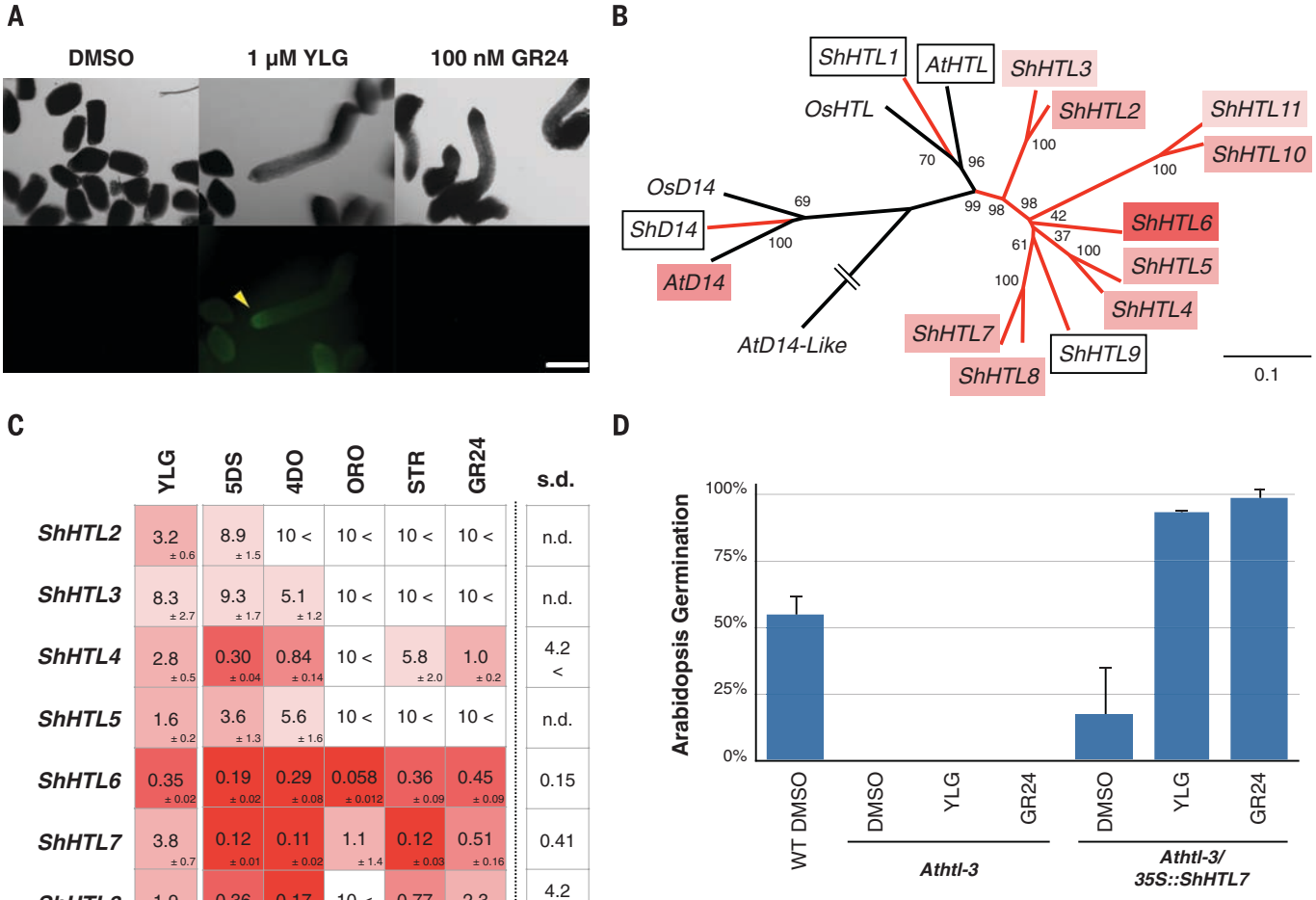

Fig. 2. Identification of strigolactone receptors in *Striga*. (**A**) YLG stimulates *Striga* seed germination with simultaneous release of the fluorophore. Top, bright-field image; bottom, fluorescence image. The arrowhead indicates the root tip. Scale bar, 300 μm. (**B**) Phylogenetic tree for strigolactone receptors in *Striga* (red line) as well as *Arabidopsis* and rice (black lines). The colors correspond to the heat map for the K_m^{YLG} values in (C). Bootstrap values of 1000 replicates are indicated by each node. (**C**) Biochemical parameters for the interactions of YLG, GR24, and natural strigolactones with *ShHTL*s. K_m^{YLG} and IC_{50} values for strigolactones are presented as a heat map with SD (n = 3 biological replicates). The variations among the IC_{50} values of strigolactones on each *ShHTL* are indicated in the right column as SD. (**D**) YLG and GR24 stimulate germination in *Arabidopsis Athtl-3* expressing *ShHTL7* under a 35S promoter. The error bar indicates SD (n = 3 independent lines).

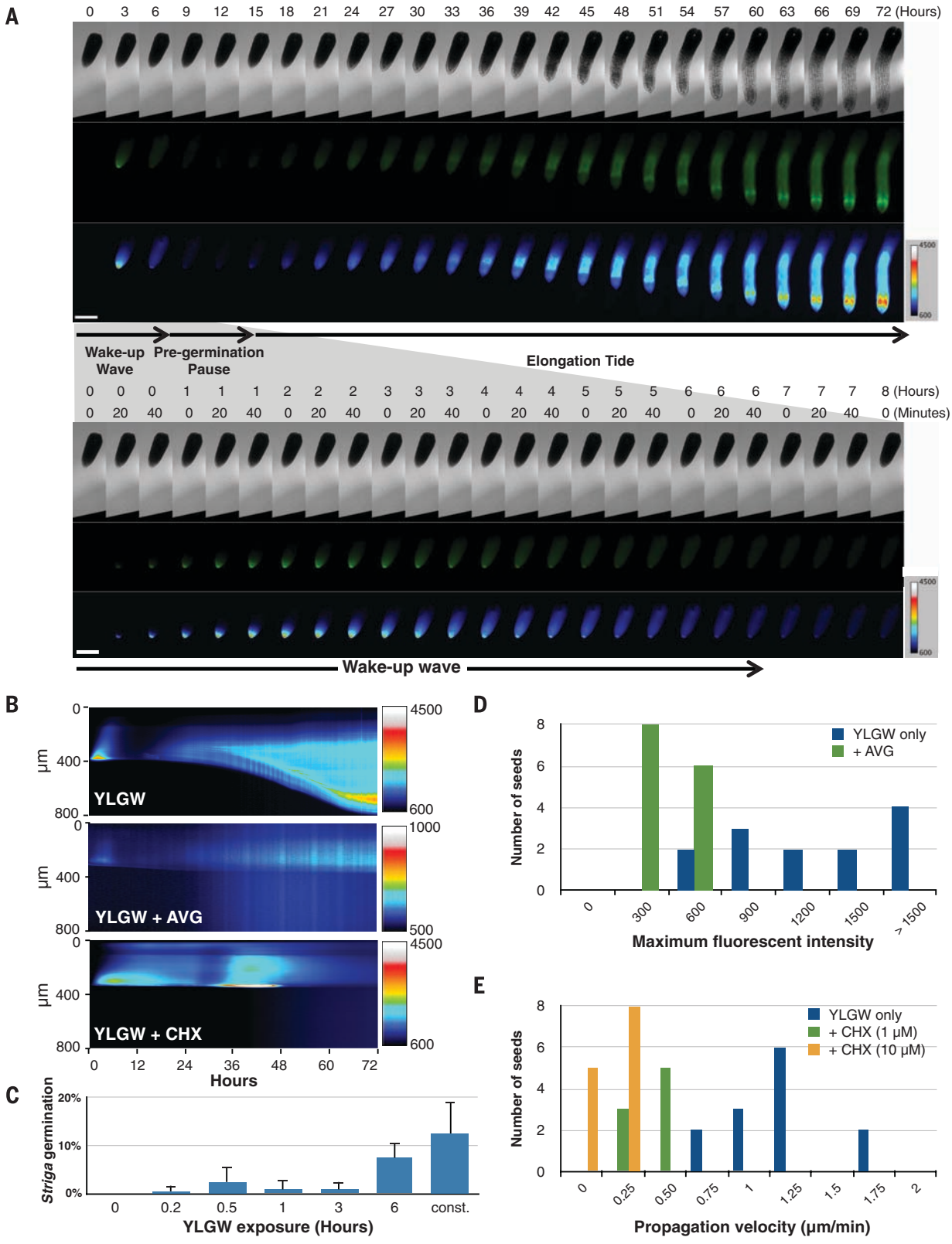

Fig. 3. Perception dynamics of strigolactone receptors during seed germination in *Striga*. (**A**) Time series of fluorescence images on the germinating *Striga* seed treated with YLGW (200 pmol) every 3 hours up to 72 hours or every 20 min up to 8 hours. Scale bar, 200 µm. (**B**) Kymographic analysis of YLGW-induced *Striga* germination in the presence of inhibitors. The detail of the kymograph is explained in the supplementary information. (**C**) Required period of YLGW exposure for *Striga* germination. *Striga* seeds were treated with YLGW for the indicated period (hours). Const., constantly exposed to YLGW. The error bar indicates SD (n = 3 biological replicates). (**D**) Statistical analysis for the effect of AVG on maximum fluorescent intensity (gray value) during germination. (**E**) Statistical analysis for the effect of CHX on the first wave. CHX slowed the propagation of the wake-up wave.

For this purpose, we improved the on/off ratio of YLG by attaching another D-ring to fluorescein (YLGW, Fig. 1A). This modification reduced the potency and selectivity toward strigolactone receptors but improved signal resolution and stability. We used YLGW to visualize their response at 5-min intervals over 3 days (Fig. 3A, movie S1, and figs. S8 and S9). Within 20 min of YLGW application, fluorescence appeared at the root tip of the *Striga* embryo. The fluorescence diffused toward the cotyledon over 6 hours (the wake-up wave) and then disappeared (the pregermination pause). The loss of fluorescence may arise from leakage of the fluorescent dye produced, and it indicates a reduction of hydrolytic activity within the cell. Morphological signs of germination (root elongation) accompanied the second fluorescence wave from the root tip (the elongation tide). All germinating embryos (n = 13) followed these three stages, although with varying kinetics (fig. S9). The fluorescence dynamics depended on the hydrolysis of YLGW, because GR24 treatment alone did not generate fluorescence (movie S2 and fig. S9). The dynamics are also linked to germination, because the nonconditioned embryo showed nonspecific fluorescence over the entire embryo (movie S3 and fig. S9). Neither *Arabidopsis* (nonparasitic) nor *Phtheirospermum japonicum* (hemiparasitic), which are known to germinate independently of strigolactone, showed wavelike propagation of fluorescence (movies S4 and S5). These data suggest that the perception dynamics are related to strigolactone-dependent germination. Pulse-feeding experiments showed that *Striga* seeds require at least 6 hours of exposure to YLGW for efficient germination, corresponding to the completion of the wake-up wave (Fig. 3C). This observation indicates that the wake-up wave is necessary for efficient germination. RT-PCR analysis after GR24 treatment showed only mild induction in several *ShHTL*s, which suggests that transcriptional regulation of these genes is of limited importance in the perception dynamics (fig. S5).

The addition of ethylene results in the strigolactone-independent germination of *Striga* seeds, and this approach has been used to extirpate *Striga* seeds from farmers' fields (*1*). To further explore the relationship of strigolactone and ethylene with germination, we inhibited germination using either the ethylene biosynthesis inhibitor aminoethoxyvinylglycine (AVG) or the protein translation inhibitor cycloheximide (CHX) (*5*). Both compounds inhibited *Striga* germination induced by GR24 or YLGW in a dose-dependent manner (fig. S10). However, the response differed for YLGW-dependent fluorescence (Fig. 3, B, D, and E, and movies S6 to S8). AVG caused a loss of fluorescence intensity, whereas CHX delayed the arrival of the wake-up wave. Thus, protein translation is required to produce the factors that wake up the entire embryo by spreading competence to respond to strigolactones from the root tip.

Ethylene, the biosynthesis of which is induced by strigolactone signaling, enhances strigolactone perception and thus forms an amplification loop (*5*). This signal amplification may explain how *Striga* recognizes minute amounts of strigolactones in the soil.

We envisage that the identification of strigolactone receptors and the establishment of a small-molecule reporter system will accelerate research to combat *Striga*.

REFERENCES AND NOTES

1. G. Ejeta, in *Integrating New Technologies for Striga Control* (World Scientific Publishing, Toh Tuck Link, Singapore, 2007), pp. 3–16.
2. C. E. Cook, L. P. Whichard, B. Turner, M. E. Wall, G. H. Egley, *Science* **154**, 1189–1190 (1966).
3. B. Zwanenburg, A. S. Mwakaboko, *Bioorg. Med. Chem.* **19**, 7394–7400 (2011).
4. S. Toh *et al.*, *Plant Cell Physiol.* **53**, 107–117 (2012).
5. Y. Sugimoto *et al.*, *Physiol. Plant.* **119**, 137–145 (2003).
6. Y. Tsuchiya, P. McCourt, *Mol. BioSyst.* **8**, 464–469 (2012).
7. X. Xie, K. Yoneyama, K. Yoneyama, *Annu. Rev. Phytopathol.* **48**, 93–117 (2010).
8. K. Ueno *et al.*, *Phytochemistry* **108**, 122–128 (2014).
9. H. I. Kim *et al.*, *Phytochemistry* **103**, 85–88 (2014).
10. K. Yoneyama *et al.*, *New Phytol.* **206**, 983–989 (2015)
11. V. Gomez-Roldan *et al.*, *Nature* **455**, 189–194 (2008).
12. M. Umehara *et al.*, *Nature* **455**, 195–200 (2008).
13. K. Akiyama, K. Matsuzaki, H. Hayashi, *Nature* **435**, 824–827 (2005).
14. T. Arite *et al.*, *Plant Cell Physiol.* **50**, 1416–1424 (2009).
15. C. Hamiaux *et al.*, *Curr. Biol.* **22**, 2032–2036 (2012).
16. S. Toh, D. Holbrook-Smith, M. E. Stokes, Y. Tsuchiya, P. McCourt, *Chem. Biol.* **21**, 988–998 (2014).
17. A. Scaffidi *et al.*, *Plant Physiol.* **165**, 1221–1232 (2014).
18. Y. Seto *et al.*, *Proc. Natl. Acad. Sci. U.S.A.* **111**, 1640–1645 (2014).
19. K. Fukui *et al.*, *Bioorg. Med. Chem. Lett.* **21**, 4905–4908 (2011).
20. F. Chevalier *et al.*, *Plant Cell* **26**, 1134–1150 (2014).
21. C. Ruyter-Spira *et al.*, *Plant Physiol.* **155**, 721–734 (2011).
22. Y. Tsuchiya *et al.*, *Nat. Chem. Biol.* **6**, 741–749 (2010).
23. M. T. Waters *et al.*, *Development* **139**, 1285–1295 (2012).
24. F. Zhou *et al.*, *Nature* **504**, 406–410 (2013).
25. L. Jiang *et al.*, *Nature* **504**, 401–405 (2013).
26. Q. Liu *et al.*, *New Phytol.* **202**, 531–541 (2014).
27. J. Han, K. Burgess, *Chem. Rev.* **110**, 2709–2728 (2010).
28. J. W. J. F. Thuring, G. H. L. Nefkens, B. Zwanenburg, *Agric. Food Chem.* **45**, 1409–1414 (1997).
29. K. Sorefan *et al.*, *Genes Dev.* **17**, 1469–1474 (2003).
30. A. A. Awad *et al.*, *Plant Growth Regul.* **3**, 221–227 (2006).
31. S. Nakamura *et al.*, *Biosci. Biotechnol. Biochem.* **74**, 1315–1319 (2010).

ACKNOWLEDGMENTS

We thank A. Babikier for providing the *Striga* seeds; S. Yoshida and K. Shirasu for providing *Phtheirospermum* seeds; T. Nakagawa for the pGWB611 binary vector (*31*); M. Okumura for instructions on MEGA; E. Nambara for critical reading; H. Hirukawa and H. Tsuchiya for the artwork; and A. Miyazaki for proofreading the manuscript. This work was supported by the Advanced Low Carbon Technology Research and Development Program of the Japan Science and Technology Agency (643 to T.K.) and by a Grant in Aid for Scientific Research from the Ministry of Education, Culture, Sports, Science, and Technology (22119005 to T.K.). Y.T., S.T., D.H.-S., and P.M. were funded by the Natural Sciences and Engineering Research Council of Canada. A part of this work was supported by the Japan Advanced Plant Science Network. ITbM is supported by the World Premier International Research Center Initiative, Japan. Nagoya U. has filed for a patent (patent application no. 2015-132707) regarding the following topic: "Fluorescent probes and screening methods for the small-molecule regulators of germination in *Striga hermonthica*." Inventors: S. Hagihara, M. Yoshimura, Y. Tsuchiya, K. Itami, and T. Kinoshita. Nucleotide and amino acid sequences corresponding to *ShD14* and *ShHTL*s have been deposited in GenBank under accession numbers KR013120 to KR013131. YLG and YLGW are available from M. Yoshimura at Nagoya U. We declare no financial conflicts of interest in relation to this work. The supplemental materials contain additional data.

SUPPLEMENTARY MATERIALS

www.sciencemag.org/content/349/6250/864/suppl/DC1
Materials and Methods
Figs. S1 to S10
Table S1
Movies S1 to S8

20 April 2015; accepted 22 July 2015
10.1126/science.aab3831

RNA SPLICING

An alternative splicing event amplifies evolutionary differences between vertebrates

Serge Gueroussov,[1,2] Thomas Gonatopoulos-Pournatzis,[1] Manuel Irimia,[1,3] Bushra Raj,[1,2] Zhen-Yuan Lin,[4] Anne-Claude Gingras,[2,4] Benjamin J. Blencowe[1,2]*

Alternative splicing (AS) generates extensive transcriptomic and proteomic complexity. However, the functions of species- and lineage-specific splice variants are largely unknown. Here we show that mammalian-specific skipping of polypyrimidine tract–binding protein 1 (PTBP1) exon 9 alters the splicing regulatory activities of PTBP1 and affects the inclusion levels of numerous exons. During neurogenesis, skipping of exon 9 reduces PTBP1 repressive activity so as to facilitate activation of a brain-specific AS program. Engineered skipping of the orthologous exon in chicken cells induces a large number of mammalian-like AS changes in PTBP1 target exons. These results thus reveal that a single exon-skipping event in an RNA binding regulator directs numerous AS changes between species. Our results further suggest that these changes contributed to evolutionary differences in the formation of vertebrate nervous systems.

A major challenge in evolutionary biology is to determine which gene regulatory changes contributed to species-specific phenotypes (*1*–*3*). Comparative transcriptomic analyses revealed that vertebrate organ alternative splicing (AS) patterns diverged more rapidly than gene expression differences (*4*–*6*). These AS differences were largely attributed to changes in the use of conserved cis-regulatory elements (*4*, *5*). However, a small number of lineage- and species-

dependent AS changes were detected in nucleic acid–binding proteins, suggesting that splicing differences in trans-acting regulators also contributed to the extensive diversity found among vertebrates (*4*). One such change involves mammalian-specific skipping of an exon (exon 9 in humans, exon 8 in mice) in the polypyrimidine tract–binding protein 1 (PTBP1)/hnRNPI (*4*). PTBP1 controls cell- and tissue-dependent AS, as well as other steps in gene expression (*7*). Exon 9 encodes an intrinsically disordered and conserved linker between RNA recognition motif 2 (RRM2) and RRM3, two of the four RRMs in PTBP1 (Fig. 1A and fig. S1A).

To investigate the role of mammalian-specific exon 9 skipping, we performed RNA sequencing (RNA-seq) to profile AS in 293 cells engineered to express 3xFLAG-tagged PTBP1 transgenes with exon 9 included (PTBP1+Ex9) or deleted (PTBP1ΔEx9) (Fig. 1B and fig. S1B). In these cells, endogenous PTBP1 and PTBP2 [a paralog with partially redundant activity (*8*)] were depleted using small interfering RNAs (siRNAs). The percentage of transcripts with a sequence spliced in [percent spliced in (PSI)] was estimated for cassette exons [including 3 to 27 nucleotide microexons (*9*)], alternative 5′/3′ splice sites, and more complex AS events. The percentage of transcripts with an intron retained (PIR) was estimated for intron-retention events (*10*). AS events displaying an absolute ΔPSI or ΔPIR of ≥15% upon knockdown of PTBP1 and PTBP2, as well as a "rescue" of ≥50% of the levels observed in the control siRNA treatment, were analyzed further (supplementary materials and methods).

Approximately 1500 AS events showed differential regulation upon knockdown and rescue of PTBP1 (fig. S1C). Comparable proportions of most classes of AS events displayed increased and decreased PSI changes. In contrast, 67 and 92% of retained introns and microexons, respectively, showed increased inclusion levels upon PTBP1 knockdown ($P < 1 \times 10^{-8}$, hypergeometric test), consistent with recent findings (*11*). Comparison of the distributions of cassette exon ΔPSI values after induction of each PTBP1 isoform reveals that exon 9 inclusion results in significantly greater restoration of PSI values for both repressed (Fig. 1C, top panel) ($P < 1 \times 10^{-12}$, two-sided Mann-Whitney U test) and stimulated exons (Fig. 1C, bottom panel) ($P < 2.2 \times 10^{-16}$, two-sided Mann-Whitney U test). Reverse transcriptase polymerase chain reaction (RT-PCR) assays validated 23 of 23 analyzed RNA-seq predictions (Fig. 1, D and E, and fig. S2, A to C). Moreover, titration experiments confirmed that PTBP1+Ex9 and PTBP1ΔEx9 impart their distinct regulatory activities due to the presence and absence of exon 9 rather than differences in relative expression (fig. S3).

Recombinant PTBP1+Ex9 and PTBP1ΔEx9 proteins displayed similar binding affinities for a variety of RNA substrates in gel mobility shift assays (fig. S4). Moreover, in vivo cross-linking followed by immunoprecipitation (CLIP-seq) analysis revealed that these isoforms have near identical binding profiles surrounding PTBP1-regulated exons in vivo (fig. S5). Sequences overlapping RRM2 and exon 9 in PTBP1 define a minimal splicing repressor domain (*12*). Confirming this finding, deletion of this region markedly reduces PTBP1 splicing regulatory activity (fig. S6, A to C). However, the presence of exon 9 without RRM2 partially restores activity for a subset of analyzed target exons (fig. S6D). Collectively, these results indicate that exon 9 possesses splicing regulatory activity that is partially separable from the repressive activity conferred by RRM2 and

[1]Donnelly Centre, University of Toronto, Toronto, Ontario M5S 3E1, Canada. [2]Department of Molecular Genetics, University of Toronto, Toronto, Ontario M5S 1A8, Canada. [3]EMBL/CRG Systems Biology Research Unit, Centre for Genomic Regulation (CRG), Dr. Aiguader 88, 08003 Barcelona, Spain. [4]Lunenfeld-Tanenbaum Research Institute, Mount Sinai Hospital, 600 University Avenue, Toronto, Ontario M5G 1X5, Canada.
***Corresponding author. E-mail: b.blencowe@utoronto.ca**

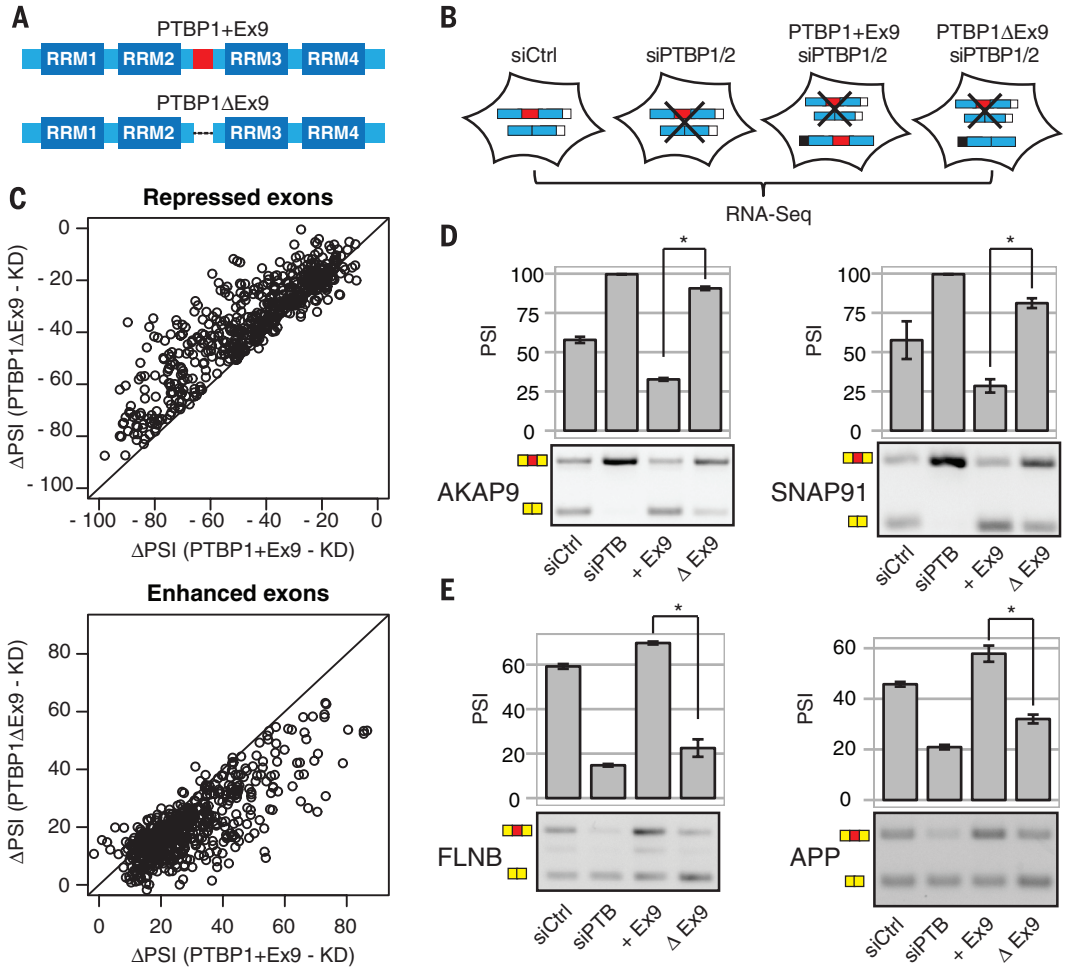

Fig. 1. A mammalian-specific AS event alters the global splicing regulatory activity of PTBP1. (**A**) Diagram showing the position of human PTBP1 exon 9. (**B**) Strategy for assessing the role of exon 9 in splicing regulation. Endogenous proteins were depleted with siRNAs. Knockdown was rescued with stably integrated, siRNA-resistant PTBP1+Ex9 or PTBP1ΔEx9. (**C**) Scatterplots showing changes in PSI relative to control for all cassette exons upon expression of PTBP1+Ex9 (x axis) or PTBP1ΔEx9 (y axis). (**D** and **E**) Representative RT-PCR validations of AS events, detected by RNA-seq, with inclusion (D) preferentially repressed by PTBP1+Ex9 or (E) preferentially enhanced by PTBP1+Ex9. Bar plots show mean PSIs from three independent RT-PCR experiments. Error bars denote SE. *$P < 0.05$, two-tailed t test.

that skipping of exon 9 reduces the negative and positive regulatory activities of PTBP1 without substantially affecting RNA binding activity.

To investigate whether exon 9 inclusion influences splicing of PTBP1 target exons in other cell types, we investigated whether its PSI correlates significantly with PSI values of isoform-dependent and -independent target exons (fig. S7A) across 64 diverse human cell and tissue types (fig. S7B). As a control, we examined correlations between exon 9 PSI and PSI values of alternative exons that are not regulated by PTBP1. We observed a significantly higher correlation of exon 9 PSI with PSI of isoform-dependent target exons versus PSI of isoform-independent target exons or exons not regulated by PTBP1 (Fig. 2A, left panel) ($P < 1 \times 10^{-7}$, two-sided Mann-Whitney *U* test). These differences in correlation are not a consequence of isoform-dependent exons having a greater sensitivity to overall PTBP1 levels, because both isoform-dependent and -independent exons display a similar correlation with total PTBP1 mRNA levels (Fig. 2A, right panel) ($P = 0.40$, two-sided Mann-Whitney *U* test). Moreover, exon 9 PSI values do not correlate significantly with PTBP1 mRNA levels (fig. S7C) ($P = 0.66$, Pearson's product-moment correlation). Exons with inclusion levels that significantly correlate with the PSI of exon 9 ($P < 0.05$, Pearson's product-moment correlation) are enriched in genes functionally associated with cytoskeleton (e.g., *FLNB* and *MYO18A*) and nervous system development (e.g., *APP* and *APBB2*) (Fig. 2B, fig. S7D, and table S1). Thus, mammalian-specific skipping of exon 9 modulates the splicing levels of a large number of functionally coherent PTBP1 target exons across diverse cell and tissue types.

PTBP1 represses a network of neural-specific alternative exons in non-neural cells and tissues (*8*, *13*, *14*). Activation of this network is required for neuronal differentiation and depends on PTBP1 silencing by miR-124 (*8*, *13*, *14*). Many PTBP1-repressed exons are activated by the neuronal-specific Ser/Arg (SR)–related protein of 100 kD (nSR100/SRRM4) (*15*, *16*). Given that skipping of PTBP1 exon 9 reduces its repressive activity, we considered that this change might have evolved to further silence PTBP1 and render target exons permissive to activation by nSR100. To investigate this, we employed an in vitro model in which mouse embryonic stem (mES) cells are differentiated into cortical glutamatergic neurons (fig. S8, A and B). During differentiation, we observed the expected reduction in Ptbp1 and increase in nSR100 expression (*16*) (fig. S8C).

Concomitant with reduction of Ptbp1 mRNA levels, skipping of Ptbp1 exon 8 (orthologous to human exon 9) progressively increases during neuronal differentiation of two independent mES cell lines (CGR8 and R1) (Fig. 3, A and B, and fig. S8D). The transition from skipping to inclusion of exons that are negatively regulated by Ptbp1 and positively regulated by nSR100 begins between neuroepithelial stem cells and radial glia (*16*). This stage is associated with appreciable Ptbp1 mRNA expression but also corresponds to Ptbp1ΔEx8 supplanting Ptbp1+Ex8 (Fig. 3, A and B, and fig. S8D). These results suggest that preferential expression of Ptbp1ΔEx8 further derepresses the Ptbp1 and nSR100 coregulated neural AS network. Consistent with this proposal, Ptbp1 isoform-dependent exons, relative to Ptbp1 isoform-independent exons, display significantly higher inclusion early in the differentiation process (Fig. 3C and fig. S8E) ($P = 0.010$, two-sided Mann-Whitney *U* test) but exhibit significantly lower inclusion at later stages [i.e., between days 1 and 7 (T4 in fig. S8D); $P = 8.3 \times 10^{-5}$, two-sided Mann-Whitney *U* test]. To confirm whether Ptbp1ΔEx8 is a weaker repressor than Ptbp1+Ex8, we used in vitro splicing assays to compare the ability of each isoform to compete with nSR100. Splicing reporters containing neural-specific exons from the *PTBP2* and *Daam1* genes (*15*) were incubated with comparable amounts of recombinant nSR100, PTBP1+Ex9, and PTBP1ΔEx9 proteins (Fig. 3D and fig. S8, F and G). Relative to PTBP1+Ex9, PTBP1ΔEx9 has a reduced ability to outcompete nSR100 and promote skipping of each alternative exon.

To confirm whether Ptbp1 exon 8 skipping affects the kinetics of activation of neural exons in vivo, we used the clustered regularly interspaced short palindromic repeats (CRISPR)–Cas9 system to create mES cell lines that constitutively and uniquely express Ptbp1+Ex8 or Ptbp1ΔEx8 (Fig. 3E and fig. S9A). We then monitored Ptbp1

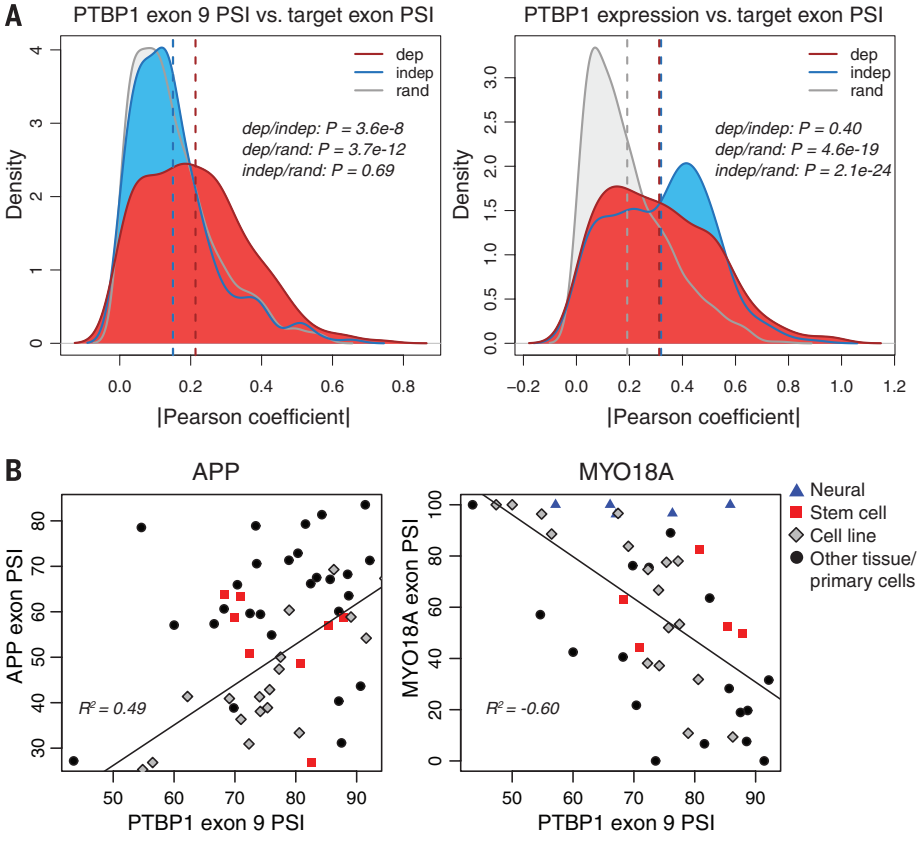

Fig. 2. PTBP1 exon 9 inclusion correlates with target exon inclusion across diverse human cells and tissues. (**A**) Analysis of Pearson correlation coefficients (PCCs) derived from RNA-seq comparisons of PTBP1 exon 9 PSI and PSIs of PTPB1 isoform-dependent target exons identified in Fig. 1. PCCs were computed from pairwise comparisons across 64 diverse human cell and tissue types (see supplementary materials). Plots show distributions of the absolute values of PCCs for different groups of target exons (dep, PTBP1-regulated and isoform-dependent; indep, PTBP1-regulated and isoform-independent; rand, not regulated by PTBP1). *P* values (two-sided Mann-Whitney *U* test) from comparing the indicated distributions are shown. (**B**) Scatter plots showing isoform-dependent PTBP1 targets whose PSI correlates significantly with PTBP1 exon 9 PSI across human cells and tissues (false discovery rate multiple testing correction; $P < 0.05$, Pearson's product-moment correlation).

target exon levels during differentiation of the lines into glutamatergic neurons. Expression of Ptbp1ΔEx8 resulted in earlier activation of target exons relative to that observed during differentiation of wild-type (WT) cells (Fig. 3F and fig. S9B). In contrast, constitutive expression of Ptbp1+Ex8 significantly delayed activation of the same targets (Fig. 3F and fig. S9B). Skipping of Ptbp1 exon 8 is therefore important for the activation of target exons during neuronal differentiation. Moreover, Ptbp1ΔEx8 expression led to earlier activation of key neural markers, whereas Ptbp1+Ex8 expression delayed their activation (Fig. 3G and fig. S10). These results demonstrate that a change in inclusion of a single alternative exon significantly affects the kinetics of regulatory transitions during mammalian neuronal differentiation.

Having established that skipping of exon 9 (or exon 8) reduces the regulatory activity of PTBP1 (or Ptbp1) in mammalian cells, we investigated

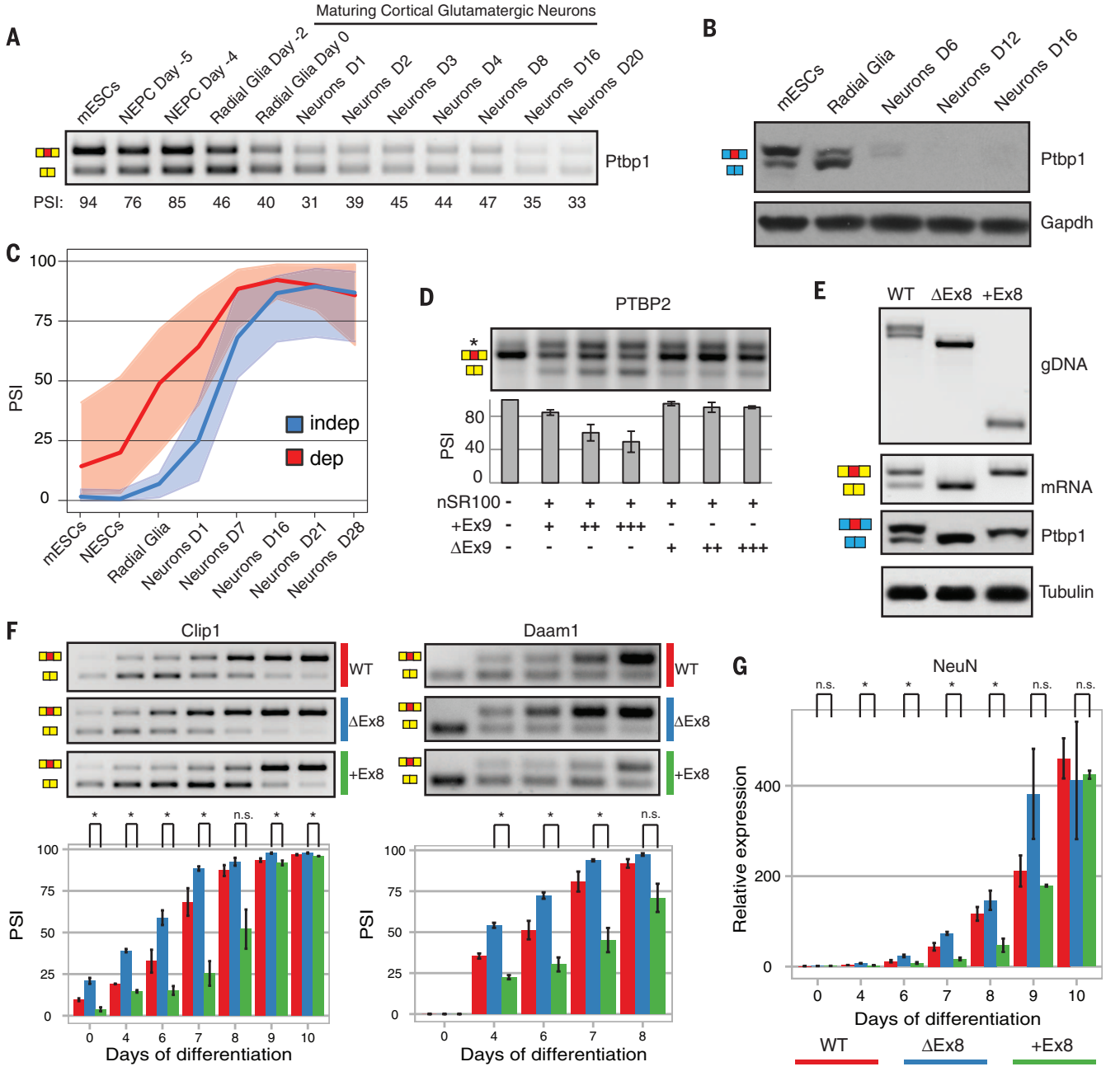

Fig. 3. Regulation and function of Ptbp1 isoforms during neuronal differentiation. (**A**) RT-PCR and (**B**) Western blot analysis of exon 8 inclusion during differentiation. mESCs, mouse embryonic stem cells; NEPC neuroepithelial stem cells; Gapdh, glyceraldehyde-3-phosphate dehydrogenase. (**C**) Plot of median Ptbp1 target exon PSIs during differentiation. Areas of lighter shading indicate the first and third quartiles. Red, mouse orthologs of human isoform-dependent events (dep); blue, isoform-independent events (indep). (**D**) In vitro splicing of PTBP2 exon 10 with varying combinations of purified nSR100, PTBP1+Ex9, and PTBP1ΔEx9. (**E**) Validation of CRISPR-Cas9–mediated deletion and knock-in of exon 8 at the level of genomic DNA (gDNA), RNA, and protein by PCR, RT-PCR, and Western blot, respectively. (**F**) Alternative splicing of Ptbp1-regulated exons was monitored by RT-PCR during differentiation in WT cells, cells with exon 8 deleted, or cells with exon 8 constitutively included. Quantification represents three independent differentiation experiments. Error bars indicate SE. *$P < 0.05$, two-tailed t test. n.s., not significant. (**G**) Expression of NeuN during differentiation was monitored by quantitative RT-PCR in the same lines. Quantification is as in (F).

whether introducing this mammalian-specific AS event in a nonmammalian context is sufficient to alter regulation of PTBP1 target exons. One or both copies of orthologous exon 8 were deleted in the chicken DT40 B cell line to generate cells that coexpress PTBP1+Ex8 and PTBP1ΔEx8 or that exclusively express PTBP1ΔEx8 (Fig. 4A). We performed RNA-seq analysis of the mutant and WT cell lines to assess the impact of exon deletion on the chicken transcriptome. Homozygous deletion of exon 8 resulted in splicing changes (PSI ≥ 15%) for 58 cassette exons, whereas heterozygous deletion resulted in intermediate changes in the same direction (Fig. 4B). Similar to the results in human cells, affected genes are enriched in gene ontology terms associated with the cytoskeleton (table S2). This set included exons in the *TPM1*, *MAGI3*, and *OSBPL9* genes whose human orthologs displayed isoform-dependent regulation in 293 cells. RT-PCR assays validated 24 of 31 (77%) analyzed events (Fig. 4C and fig. S11A). We further detected changes in exons of FLNB and PTBP2 (fig. S11B) that are isoform-dependent in 293 cells (Fig. 1E and fig. S2A) but had smaller predicted changes (PSI < 15%) in DT40 cells, possibly due to cell-type–specific contextual differences. In contrast, we did not detect significant changes in 12 of 12 exons not predicted to be affected by deletion of PTBP1 exon 8 (fig. S12). Affected exons probably comprise direct PTBP1 targets, because their flanking intronic sequences are significantly enriched in PTBP1 binding motifs (*17*), and the position of the enriched motifs is consistent with the expected direction of PTBP1-dependent regulation based on in vivo PTBP1 binding map data (fig. S5) (*18*, *19*) (Fig. 4D). Thus, expression of the PTBP1ΔEx8 isoform in chicken cells results in a weaker splicing regulator that leads to increased inclusion of PTBP1-repressed exons and reduced inclusion of PTBP1-stimulated exons. These results support the conclusion that an evolutionary change in PTBP1 exon 9 (or exon 8) inclusion is sufficient to alter the regulation of many exons, including those with important developmental functions.

Rapid evolutionary change in AS patterns has largely been driven by the gain and loss of

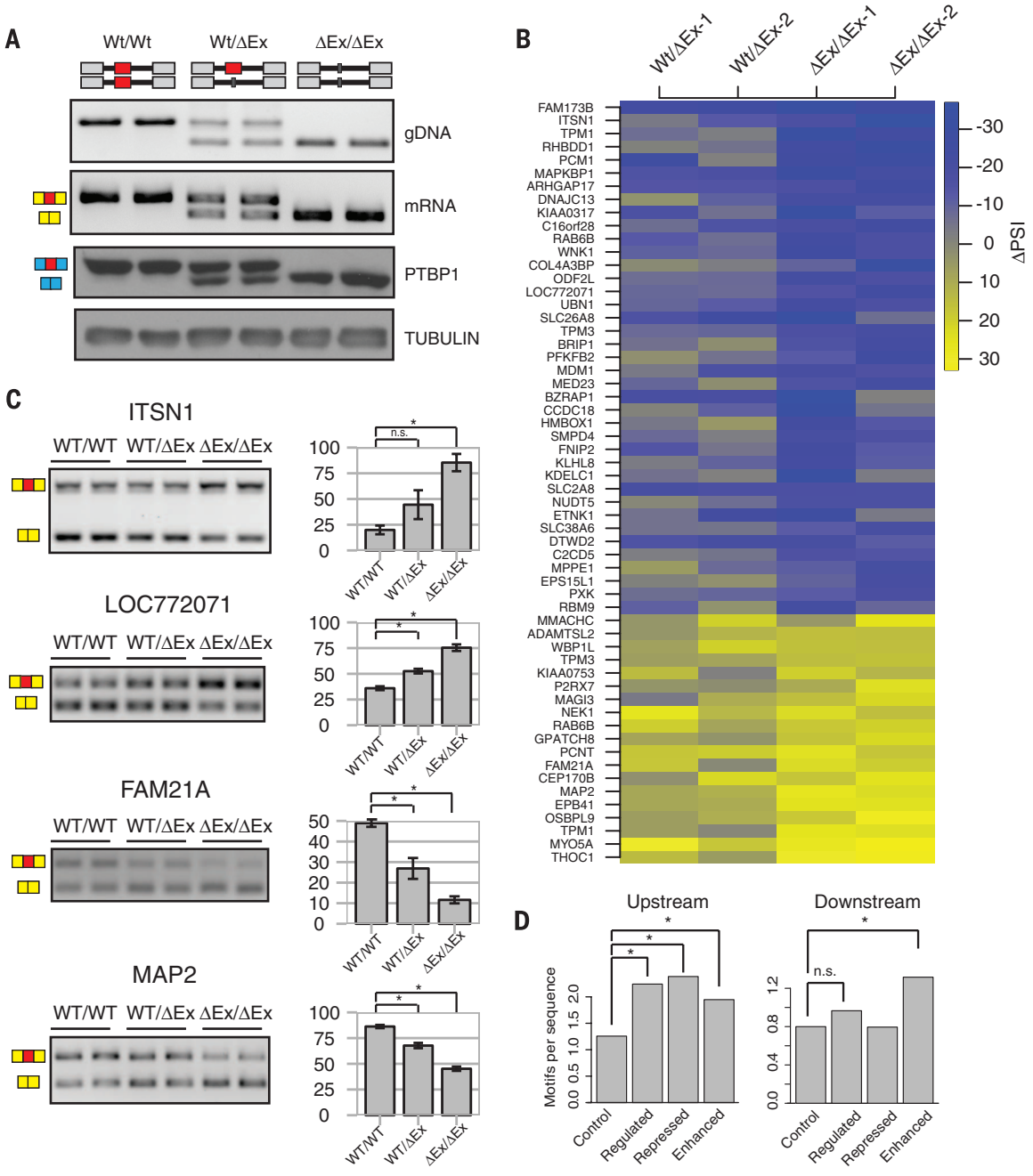

Fig. 4. Consequences of expressing a mammalian-like PTBP1 isoform in chicken cells. (**A**) Validation of heterozygous and homozygous deletions of PTBP1 exon 8 at the DNA, RNA, and protein levels by PCR, RT-PCR, and Western blot, respectively. (**B**) Heat map of average ΔPSI of exons affected by PTBP1 exon 8 deletion. Analyses were performed using two independent cell lines for each genotype. (**C**) Representative RT-PCR validations of AS events detected by RNA-seq. Bar plots show mean PSIs from six independent assays (three for each independent cell line). Error bars denote SE. *P < 0.05, two-tailed t test. n.s., not significant. (**D**) Number of PTBP1 motifs per 300 nucleotides of intronic sequence upstream (left) or downstream (right) of queried exons. *P < 0.05, exact binomial test.

cis-regulatory elements (*4*, *5*). It has been proposed that this change is partially a consequence of relaxed selection pressure acting on newly evolving splice isoforms, whereas the simultaneous expression of ancestral splice isoforms allows maintenance of core gene functions (*20*). However, the results of this study provide evidence that rapid change in AS can also be driven by splicing changes in trans-acting regulators. The mammalian-specific skipping of PTBP1 exon 9 (or exon 8), characterized here, simultaneously affects the levels of many additional AS events. Given that the affected target exons are concentrated in genes associated with cytoskeletal and neurobiological functions and that their regulatory kinetics are significantly affected by exon 8 inclusion levels during neuronal differentiation, this event may have evolved to modulate the timing of transitions in the production of neural progenitors and mature neurons so as to affect brain morphology and complexity. Thus, a single AS event has served to amplify the rate of evolutionary change in developmentally associated AS patterns.

REFERENCES AND NOTES

1. S. B. Carroll, *Cell* **134**, 25–36 (2008).
2. C. P. Ponting, *Nat. Rev. Genet.* **9**, 689–698 (2008).
3. A. Necsulea, H. Kaessmann, *Nat. Rev. Genet.* **15**, 734–748 (2014).
4. N. L. Barbosa-Morais *et al.*, *Science* **338**, 1587–1593 (2012).
5. J. Merkin, C. Russell, P. Chen, C. B. Burge, *Science* **338**, 1593–1599 (2012).
6. A. Reyes *et al.*, *Proc. Natl. Acad. Sci. U.S.A.* **110**, 15377–15382 (2013).
7. P. Kafasla *et al.*, *Biochem. Soc. Trans.* **40**, 815–820 (2012).
8. P. L. Boutz *et al.*, *Genes Dev.* **21**, 1636–1652 (2007).
9. M. Irimia *et al.*, *Cell* **159**, 1511–1523 (2014).
10. U. Braunschweig *et al.*, *Genome Res.* **24**, 1774–1786 (2014).
11. Y. I. Li, L. Sanchez-Pulido, W. Haerty, C. P. Ponting, *Genome Res.* **25**, 1–13 (2015).
12. F. Robinson, C. W. Smith, *J. Biol. Chem.* **281**, 800–806 (2006).
13. E. V. Makeyev, J. Zhang, M. A. Carrasco, T. Maniatis, *Mol. Cell* **27**, 435–448 (2007).
14. Y. Xue *et al.*, *Cell* **152**, 82–96 (2013).
15. J. A. Calarco *et al.*, *Cell* **138**, 898–910 (2009).
16. B. Raj *et al.*, *Mol. Cell* **56**, 90–103 (2014).
17. D. Ray *et al.*, *Nature* **499**, 172–177 (2013).
18. M. Llorian *et al.*, *Nat. Struct. Mol. Biol.* **17**, 1114–1123 (2010).
19. A. Han *et al.*, *PLOS Comput. Biol.* **10**, e1003442 (2014).
20. Y. Xing, C. Lee, *Nat. Rev. Genet.* **7**, 499–509 (2006).

ACKNOWLEDGMENTS

We thank A. Dziembowski for providing DT40-Cre1 cells, U. Braunschweig for assistance with CLIP-seq analyses, and N. Barbosa-Morais and T. Sterne-Weiler for advice on statistical testing. We also acknowledge D. Torti, D. Leung, and G. O'Hanlon in the Donnelly Sequencing Centre for generating RNA-seq data. S.G. is supported by a *Natural Sciences and Engineering Research Council* of Canada Alexander Graham Bell Studentship, T.G.-P. is supported by fellowships from European Molecular Biology Organization and Ontario Institute for Regenerative Medicine, and M.I. was supported by a Long-Term Fellowship from the Human Frontier Science Program. This research was supported by grants from the Canadian Institutes of Health Research to B.J.B. and A.-C.G. and by a Natural Sciences and Engineering Research Council of Canada John C. Polanyi Award to B.J.B. B.J.B. holds the Banbury Chair in Medical Research at the University of Toronto. Data presented in this manuscript are archived in the Gene Expression Omnibus under accession number GSE69656.

SUPPLEMENTARY MATERIALS

www.sciencemag.org/content/349/6250/868/suppl/DC1
Materials and Methods
Figs. S1 to S12
Tables S1 and S2
References (*21*–*25*)

4 February 2015; accepted 27 July 2015
10.1126/science.aaa8381

SIGNAL TRANSDUCTION

Membrane potential modulates plasma membrane phospholipid dynamics and K-Ras signaling

Yong Zhou,[1] Ching-On Wong,[1] Kwang-jin Cho,[1] Dharini van der Hoeven,[2] Hong Liang,[1] Dhananiay P. Thakur,[1] Jialie Luo,[1] Milos Babic,[3] Konrad E. Zinsmaier,[3] Michael X. Zhu,[1,4] Hongzhen Hu,[1,4] Kartik Venkatachalam,[1,4] John F. Hancock[1,4]*

Plasma membrane depolarization can trigger cell proliferation, but how membrane potential influences mitogenic signaling is uncertain. Here, we show that plasma membrane depolarization induces nanoscale reorganization of phosphatidylserine and phosphatidylinositol 4,5-bisphosphate but not other anionic phospholipids. K-Ras, which is targeted to the plasma membrane by electrostatic interactions with phosphatidylserine, in turn undergoes enhanced nanoclustering. Depolarization-induced changes in phosphatidylserine and K-Ras plasma membrane organization occur in fibroblasts, excitable neuroblastoma cells, and *Drosophila* neurons in vivo and robustly amplify K-Ras–dependent mitogen-activated protein kinase (MAPK) signaling. Conversely, plasma membrane repolarization disrupts K-Ras nanoclustering and inhibits MAPK signaling. By responding to voltage-induced changes in phosphatidylserine spatiotemporal dynamics, K-Ras nanoclusters set up the plasma membrane as a biological field-effect transistor, allowing membrane potential to control the gain in mitogenic signaling circuits.

Plasma membrane (PM) potential (V_m) has been linked to cell survival and proliferation (*1*, *2*). Dividing cells are more depolarized than quiescent cells, and oncogenically transformed cells are generally more depolarized than normal parental cells, indicating that V_m may be inversely coupled to pro-proliferative pathways (*2*). The mechanisms that might link V_m to cell proliferation are poorly characterized. Ras proteins are membrane-bound signaling proteins involved in cell differentiation, proliferation, and survival (*3*). The three ubiquitously expressed Ras isoforms—H-, N-, and K-Ras—assemble into spatially distinct nanoassemblies on the PM called nanoclusters (*4*). Nanocluster formation is essential for activation of mitogen-activated protein kinase (MAPK) signaling by Ras because activation of the protein kinase RAF on the PM is restricted to Ras.GTP (GTP, guanosine triphosphate) nanoclusters (*5*). Nanocluster assembly requires complex interactions between PM lipids and the Ras lipid anchors, C-terminal hypervariable regions, and G domains; with interactions between Ras basic residues and charged PM lipids being particularly relevant (*6*). The diffusion of lipids in model membranes and phase separation of multicomponent bilayers is responsive to electric fields (*7*, *8*). We therefore tested whether the lateral distribution of anionic lipids in the PM is responsive to V_m and the potential consequences on Ras spatial organization.

We manipulated the V_m of baby hamster kidney (BHK) cells, measured by whole-cell patch clamping, by changing extracellular K^+ concentration (Fig. 1A). Simultaneously we quantified the nanoscale distribution of various green fluorescent protein (GFP)–labeled lipid-binding probes on the inner PM by using electron microscopy (EM) and spatial mapping (*4*, *9*, *10*). The analyses show that nanoclustering of phosphatidylserine (PS) and phosphatidylinositol 4,5-bisphosphate (PIP_2) was enhanced on PM depolarization, whereas there was no detectable change in the lateral distribution of phosphatidic acid (PA) or phosphatidylinositol 3,4,5-trisphosphate (PIP_3) (Fig. 1, B and C, and fig. S1). The enhanced clustering of PS was fast, being 80% complete within 30 s (the shortest assay time allowed by the EM technique) (Fig. 1D). PIP_2 clustering increased at a slightly slower rate (Fig. 1D). On repolarization of the PM, by switching from 100 mM [K^+] back to 5mM [K^+], nanoclustering of PS and PIP_2 reverted to control values with near identical kinetics (Fig. 1E). The PS content of the PM was unaffected by changing V_m (fig. S2). Fluorescence recovery after photobleaching assays of lipid spatiotemporal dynamics showed that the mobile fraction of fluorescently labeled PS and PIP_2 decreased significantly upon PM depolarization (fig. S3), consistent with the EM data. The differential effect of V_m on anionic PM lipids is concordant with observations that charged lipids respond differently to applied electric fields (*7*, *8*, *11*).

[1]Department of Integrative Biology and Pharmacology, Medical School, University of Texas Health Science Center at Houston, Houston, TX 77030, USA. [2]Department of Diagnostic and Biomedical Sciences, Dental School, University of Texas Health Science Center at Houston, Houston, TX 77054, USA. [3]Department of Neuroscience, University of Arizona, Tucson, AZ 85721, USA. [4]Program in Cell and Regulatory Biology, University of Texas Graduate School of Biomedical Sciences, Houston, TX 77030, USA.
***Corresponding author. E-mail: john.f.hancock@uth.tmc.edu**

The localization and lateral distribution of K-Ras on the PM requires electrostatic interactions between a C-terminal polybasic domain and PS (*9*, *10*, *12*, *13*). The electrostatic potential of the inner PM leaflet is independent of V_m, and concordantly total internal reflection fluorescence and confocal microscopy showed that K-Ras PM localization was insensitive to PM depolarization (fig. S5). However, EM spatial mapping experiments of BHK cells expressing GFP–K-RasG12V (GFP-labeled, constitutively GTP-bound K-Ras) showed that K-RasG12V peak $L(r) - r$ (L_{max}, where L represents a K function and r is radius) values correlated strongly with V_m, indicating that PM depolarization enhances K-Ras nanoclustering (Fig. 1F). The temporal dynamics of V_m-induced changes in K-RasG12V nanoclustering matched those of PS rather than PIP_2 (Fig. 1, D and E). To visualize nanocluster changes in intact cells, we used fluorescence lifetime imaging microscopy combined with fluorescence resonance energy transfer (FLIM-FRET). The fluorescence lifetime of GFP–K-RasG12V in cells coexpressing the FRET acceptor red fluorescent protein (RFP)–K-RasG12V decreased as a function of V_m (Fig. 1, G and H), indicating increased FRET between GFP–K-RasG12V and RFP–K-RasG12V and hence increased K-Ras nanoclustering. Conversely, expression of the Kv2.1 channel, which hyperpolarizes the PM (*14*) (fig. S6C), largely eliminated FRET between GFP–K-RasG12V and RFP–K-RasG12V, consistent with disruption of K-Ras nanoclustering (fig. S6). Expression of a nonconducting channel mutant, Kv2.1W369CY384T (fig. S6C), had no effect on the lifetime of GFP–K-RasG12V in control FLIM experiments (fig. S6B). PM depolarization did not change concentrations of intracellular Ca^{2+} in BHK cells (fig. S7). Concordantly, we obtained identical EM and FLIM results in Ca^{2+}-free buffers containing the Ca^{2+} chelator EGTA (fig. S8). PM depolarization also enhanced the nanoclustering of GFP-tK but not GFP-tH (GFP coupled to the isolated membrane-anchoring domains of K-Ras and H-Ras, respectively) (Fig. 1, F to H, and fig. S8, D and E). Thus, K-Ras nanoclustering is sensitive to V_m through a mechanism that requires the C-terminal polybasic domain.

In excitable differentiated mouse Neuro2A (N2A) neuroblastoma cells (*15*), PM depolarization with high $[K^+]$ also caused a significant decrease in GFP fluorescence lifetime in GFP-tK and RFP-tK coexpressing cells (Fig. 2, A and B), indicating increased GFP-RFP FRET from increased GFP-tK clustering. Similar results were observed with full-length K-RasG12V (Fig. 2, A and B). Glutamate receptor–induced PM depolarization (*15*) also enhanced K-RasG12V clustering (Fig. 2C). This effect appeared unrelated to activation of phospholipase C (PLC), because pretreatment with the PLC inhibitor U73122 did not abrogate glutamate-stimulated K-Ras clustering but effectively blocked increases in intracellular concentrations of Ca^{2+} (fig. S9). Thus, glutamate-induced changes in K-Ras nanoclustering are also mediated through a change in PM voltage.

We evaluated the causality between V_m-induced changes in PS or PIP_2 distribution and K-Ras clustering by quantifying their colocalization using EM spatial mapping and integrated bivariate K functions (LBI values) (*9*). PM depolarization significantly and selectively enhanced the association of K-Ras with PS but not with PIP_2 (Fig. 3A and fig. S10), consistent with V_m-induced changes in the PM PS distribution being causally associated with increased K-Ras nanoclustering. We therefore evaluated K-Ras clustering in PS auxotroph (PSA-3) cells (*16*), which, when grown

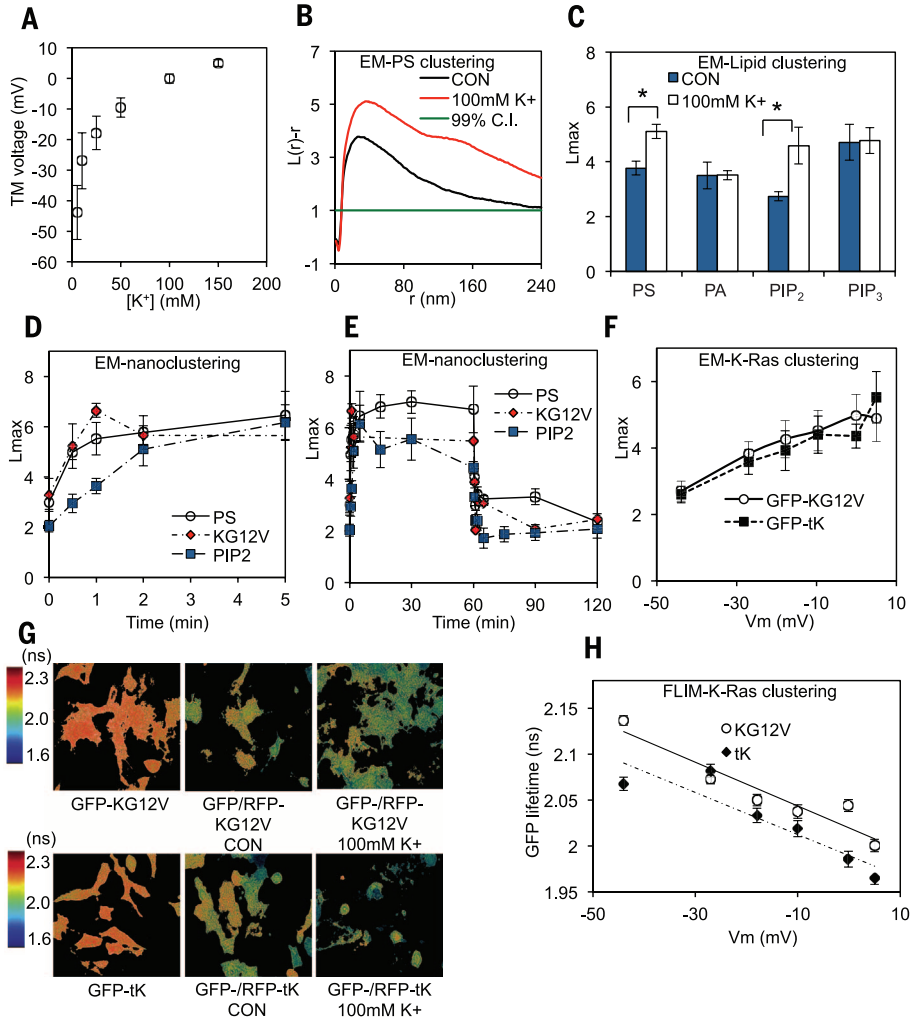

Fig. 1. PM depolarization enhances nanoclustering of lipids and K-Ras. (**A**) Whole-cell patch clamping of BHK cells to measure V_m in isotonic buffers containing different $[K^+]$. (**B**) Weighted mean K functions shown as $L(r) - r$ for a PS lipid probe ($n \geq 8$) in control (CON) and depolarized BHK cells. $L(r) - r$ values >99% confidence interval (C.I.) for a random pattern indicate clustering. Depolarization (100mM $[K^+]$) significantly increased PS clustering ($P < 0.001$, bootstrap test). (**C**) Peak $L(r) - r$ values, L_{max}, derived from curves as in (B), quantify the extent of nanoclustering of lipid probes for PS, PIP_2, PA, or PIP_3 in control and depolarized (100 mM $[K^+]$) BHK cells. (**D**) Short time course (<5 min) of changes in L_{max} values for PS, PIP_2, and GFP–K-RasG12V (KG12V) in BHK cells depolarized with 100 mM $[K^+]$ at $t = 0$ min. (**E**) Time course of depolarization (5 to 100 mM $[K^+]$ at $t = 0$ min) and repolarization (100 to 5 mM $[K^+]$ at $t = 60$ min), changes in L_{max} for PS, PIP2, and K-RasG12V. (**F**) Dependence of GFP–K-RasG12V or GFP-tK clustering, quantified as L_{max} values, on V_m varied as in (A). (**G**) FLIM images (GFP) of cells expressing GFP/RFP–K-RasG12V and GFP/RFP-tK FRET pairs. (**H**) Fluorescence lifetime of GFP–K-RasG12V or GFP-tK in cells expressing the cognate RFP-FRET pair plotted against V_m. Each point is the mean (±SEM) GFP lifetime measured in >60 individual cells. Significant differences (*$P < 0.001$) were evaluated by using one-way analysis of variance (ANOVA). Error bars in all panels represent SEM.

in the absence of ethanolamine, synthesize ~30% less total PS (*16*) and are depleted of PS in the inner PM leaflet (*9*, *16*). EM-spatial mapping and FLIM-FRET imaging of ethanolamine-starved PSA-3 cells showed that PS depletion rendered K-Ras nanoclustering insensitive to V_m (Fig. 3, B and C).

Enhancing K-Ras.GTP nanoclustering increases activation of the RAF-MAPK cascade (*5*). We therefore examined the effect of V_m on

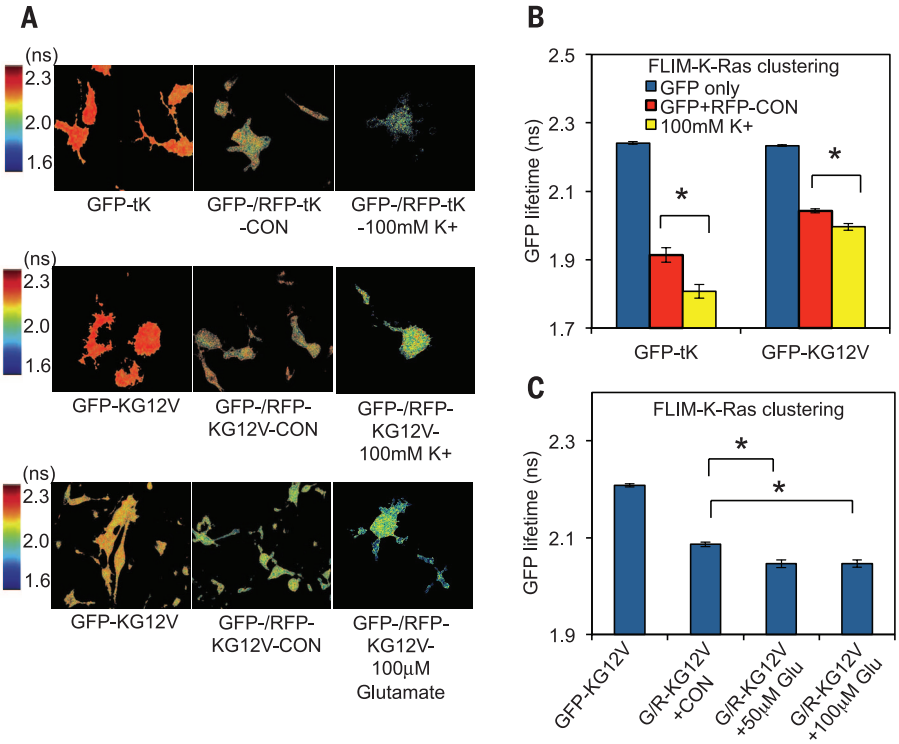

Fig. 2. Plasma membrane depolarization enhances K-Ras nanoclustering in mouse neuroblastoma cells. (**A**) FLIM images of differentiated N2A cells expressing the FRET pairs: RFP/GFP-tK or RFP/GFP–K-RasG12V (GFP-KG12V and depolarized with 100 mM [K^+] or 50 to 100 μM glutamate (Glu). (**B** and **C**) Quantification of fluorescence lifetime of GFP–K-RasG12V or GFP-tK in N2A cells expressing the cognate RFP-FRET pair treated as in (A). Each data point is the mean (±SEM) GFP lifetime measured in >60 individual cells. Significant differences (*P < 0.01) were evaluated by using one-way ANOVA.

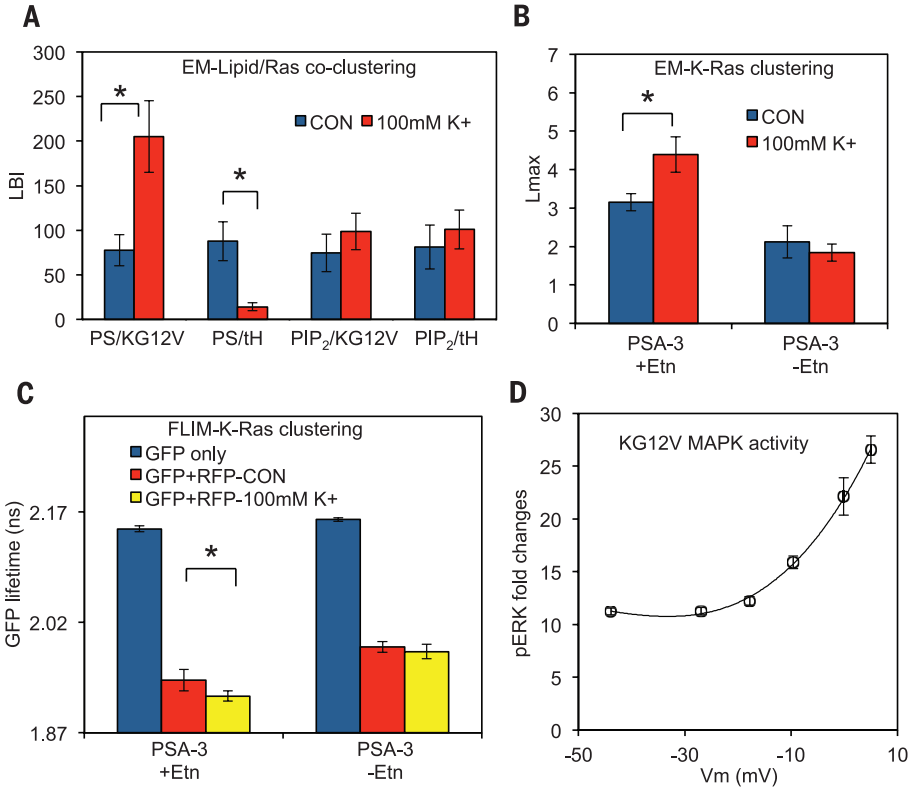

Fig. 3. PS mediates V_m-induced changes in K-Ras nanoclustering and signaling. (**A**) PM sheets from BHK cells expressing RFP–K-RasG12V, and a GFP-tagged lipid-binding probe for PS or PIP_2, were labeled with anti-GFP-6nm gold and anti-RFP-2nm gold and visualized by EM. Bivariate K functions (summarized as LBI values) were used to quantify the colocalization of PS or PIP_2 with GFP–K-RasG12V and GFP-tH nanoclusters. Statistical significance was evaluated in Mann-Whitney tests (*P < 0.05). Additional lipid reorganization results are shown in fig. S10E. (**B**) Univariate EM-spatial mapping of PM sheets prepared from PSA-3 cells expressing GFP–K-RasG12V and grown with or without ethanolamine (±Etn). (**C**) FLIM imaging of PSA-3 cells expressing GFP–K-RasG12V or coexpressing RFP–K-RasG12V and grown ±Etn. (**D**) MAPK activation in K-RasG12V–transformed BHK cells (and wild-type cells fig. S11) measured by quantitative immunoblotting for phosphorylated ERK (pERK) after PM depolarization as in Fig. 1A.

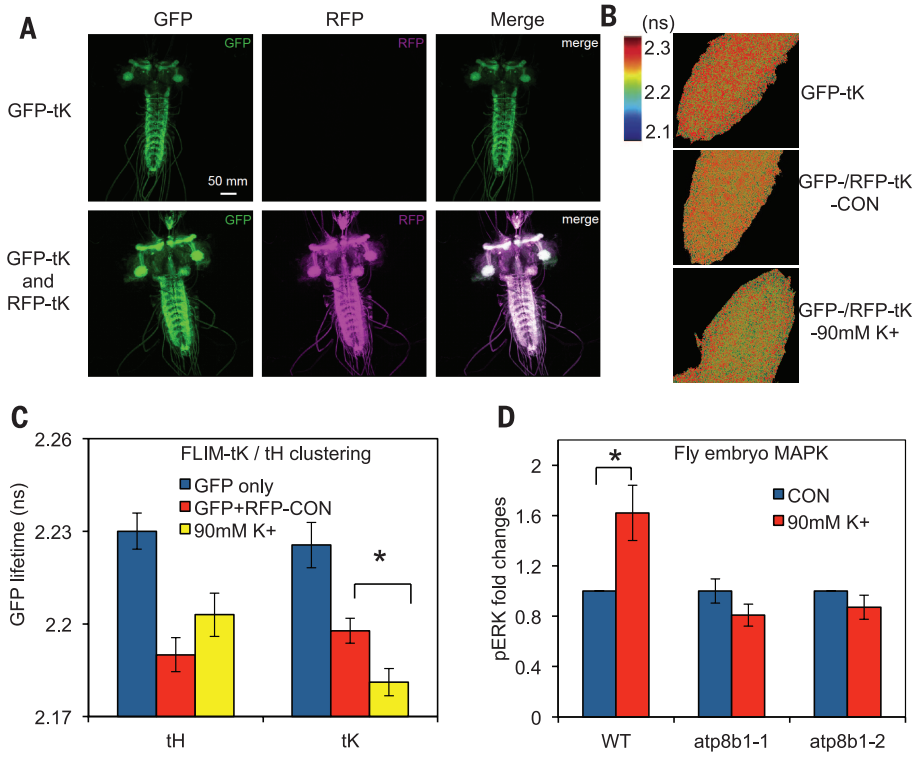

Fig. 4. Enhanced K-Ras clustering and MAPK signaling in intact fly embryo after PM depolarization. (**A**) Confocal images of flies expressing GFP-tK, or coexpressing GFP-tK and RFP-tK, from a neuronal-specific promoter. (**B**) FLIM imaging of brains from flies in (A) in control buffer and after depolarization with high [K^+]. (**C**) Quantification of fluorescence lifetime of GFP-tK in fly brains expressing the cognate RFP-FRET pair treated as in (B); results are mean (±SEM, n = 9). High [K^+] had no effect on the fluorescence lifetime of GFP-tH in fly brains expressing GFP-tH and RFP-tH. (**D**) Fly embryos from wild-type (WT) and mutant *atp8b* flies incubated in 5 or 90 mM K^+ for 15 min and then immunoblotted for pERK. Results are quantified as mean ± SEM (n = 3).

K-Ras–specific MAPK signaling. Progressively reducing V_m enhanced phosphorylation of extracellular signal–regulated kinase (ERK) in K-RasG12V–expressing cells (Fig. 3D and figs. S11 and S12), consistent with the EM and FLIM results. ERK activation was nonlinearly dependent on V_m (Fig. 3D) unlike L_{max} (Fig. 1F). This is expected because the K-Ras clustered fraction (ϕ), which determines MAPK signaling output (*5*), is a nonlinear function of L_{max} (*4*) (fig. S13). MAPK activation increased rapidly in response to PM depolarization (<30 s), concordant with the time scale of enhanced K-Ras clustering, and recovered within 30 min of PM repolarization (fig. S14). V_m-induced activation of MAPK signaling in K-RasG12V–expressing PSA-3 cells was abolished under conditions of PS depletion (fig. S11C). Thus, depleting cellular and PM PS levels effectively uncouples V_m from K-Ras clustering and signaling. Because the amounts of K-Ras.GTP are fixed in K-RasG12V cells, V_m regulates signal gain in the K-Ras signaling circuit by controlling the extent of K-Ras nanoclustering.

Last, we observed similar results in vivo in *Drosophila* (Fig. 4A) (*17*). Depolarization of intact fly brains expressing GFP-tK and RFP-tK resulted in increased GFP-RFP FRET (Fig. 4, B and C), indicating enhanced K-Ras clustering. Concordantly, depolarization of wild-type fly embryos significantly stimulated MAPK activation, whereas depolarization of *atp8b* mutant embryos (fig. S15) that lack a PM PS flippase (*18*, *19*) had no effect on MAPK activation (Fig. 4D and fig. S16L). Lack of *atp8b* diminishes the inner PM leaflet of PS (*18*, *19*) (fig. S16, A to K) and is thus a partial phenocopy of PS-deficient PSA-3 cells (fig. S11).

We show that PM depolarization induces rapid and substantial changes in the nanoscale organization of the anionic phospholipids, PS and PIP_2, on the inner leaflet of the PM. An important consequence of the PS reorganization is increased K-Ras nanoclustering, which enhances K-Ras–dependent MAPK signaling in nonexcitable and excitable cells, as well as intact fly embryo. Reduced PM V_m has long been associated with cell survival, proliferation, and differentiation (*1*, *2*). Yet, no compelling mechanism has been proposed to explain the input of electrical signal to cell signaling cascades. We suggest that K-Ras nanoclusters, by responding to V_m-induced changes in PS spatiotemporal dynamics, allow the PM to act as a field-effect transistor to control the gain in Ras signaling circuits. Neuronal development, including plasticity, long-term potentiation, and memory, is strongly associated with V_m and MAPK signaling (*20*, *21*); it is thus feasible that changes in PS-mediated K-Ras lateral segregation potentially play an important role these processes.

REFERENCES AND NOTES

1. S. Sundelacruz, M. Levin, D. L. Kaplan, *Stem Cell Rev.* **5**, 231–246 (2009).
2. D. J. Blackiston, K. A. McLaughlin, M. Levin, *Cell Cycle* **8**, 3527–3536 (2009).
3. J. F. Hancock, *Nat. Rev. Mol. Cell Biol.* **4**, 373–385 (2003).
4. S. J. Plowman, C. Muncke, R. G. Parton, J. F. Hancock, *Proc. Natl. Acad. Sci. U.S.A.* **102**, 15500–15505 (2005).
5. T. Tian *et al.*, *Nat. Cell Biol.* **9**, 905–914 (2007).
6. Y. Zhou, J. F. Hancock, *Biochim. Biophys. Acta* **1853**, 841–849 (2015).
7. P. S. O'Shea, S. Feuerstein-Thelen, A. Azzi, *Biochem. J.* **220**, 795–801 (1984).
8. J. T. Groves, S. G. Boxer, H. M. McConnell, *Proc. Natl. Acad. Sci. U.S.A.* **95**, 935–938 (1998).
9. Y. Zhou *et al.*, *Mol. Cell. Biol.* **34**, 862–876 (2014).
10. N. Ariotti *et al.*, *J. Cell Biol.* **204**, 777–792 (2014).
11. T. Starke-Peterkovic, R. J. Clarke, *Eur. Biophys. J.* **39**, 103–110 (2009).
12. T. Yeung *et al.*, *Science* **319**, 210–213 (2008).
13. K. J. Cho *et al.*, *J. Biol. Chem.* **287**, 43573–43584 (2012).
14. K. S. Park, D. P. Mohapatra, H. Misonou, J. S. Trimmer, *Science* **313**, 976–979 (2006).
15. J. B. Van der Valk, H. P. Vijverberg, *Eur. J. Pharmacol.* **185**, 99–102 (1990).
16. S. Lee *et al.*, *Genes Cells* **17**, 728–736 (2012).
17. A. H. Brand, N. Perrimon, *Development* **118**, 401–415 (1993).
18. T. S. Ha, R. Xia, H. Zhang, X. Jin, D. P. Smith, *Proc. Natl. Acad. Sci. U.S.A.* **111**, 7831–7836 (2014).
19. C. C. Paulusma *et al.*, *Hepatology* **47**, 268–278 (2008).
20. S. Impey, K. Obrietan, D. R. Storm, *Neuron* **23**, 11–14 (1999).
21. R. J. Kelleher 3rd, A. Govindarajan, H. Y. Jung, H. Kang, S. Tonegawa, *Cell* **116**, 467–479 (2004).

ACKNOWLEDGMENTS

This work was supported by grant RP130059 from the Cancer Prevention and Research Institute of Texas and grant R01NS081301 from NIH.

SUPPLEMENTARY MATERIALS

www.sciencemag.org/content/349/6250/873/suppl/DC1
Materials and Methods
Figs. S1 to S16

23 December 2014; accepted 2 July 2015
10.1126/science.aaa5619

TRANSCRIPTION

Allosteric transcriptional regulation via changes in the overall topology of the core promoter

Steven J. Philips,[1] Monica Canalizo-Hernandez,[2] Ilyas Yildirim,[2] George C. Schatz,[2] Alfonso Mondragón,[1]* Thomas V. O'Halloran[1,2,3]*

Many transcriptional activators act at a distance from core promoter elements and work by recruiting RNA polymerase through protein-protein interactions. We show here how the prokaryotic regulatory protein CueR both represses and activates transcription by differentially modulating local DNA structure within the promoter. Structural studies reveal that the repressor state slightly bends the promoter DNA, precluding optimal RNA polymerase-promoter recognition. Upon binding a metal ion in the allosteric site, CueR switches into an activator conformation. It maintains all protein-DNA contacts but introduces torsional stresses that kink and undertwist the promoter, stabilizing an A-form DNA–like conformation. These factors switch on and off transcription by exerting dynamic control of DNA stereochemistry, reshaping the core promoter and making it a better or worse substrate for polymerase.

Although transcription factors can introduce kinks, bends (*1*), or loops in DNA (*2*), the mechanistic roles of such distortions are not always clear. Factors in the prokaryotic MerR family alter DNA structure between the core promoter elements where they repress and activate transcription in response to many signals, including metal ion concentration changes (*3*, *4*). The activator conformation of MerR proteins introduces a DNA distortion at the center of the operator (*3*, *5*–*7*), and structural studies of the activator protein-DNA complexes reveal a kink at this site (*8*–*10*). This distortion is thought to stimulate transcription by realigning the suboptimally spaced –10 and –35 core promoter elements (fig. S1A); however, the mechanisms of allosteric conversion, repression, and activation remain unknown. To understand how a protein can switch transcription off and on while bound to a single site, we solved the structures of the DNA complexes of *Escherichia coli* CueR in the repressor and activator conformations.

CueR, a member of the metalloregulatory subfamily of MerR proteins, is a Cu^{I}- and Ag^{I}-sensing factor that controls expression of metal homeostasis genes *copA* and *cueO* (*11*–*15*). The metal-bound state, Ag^{I}-CueR (i.e., activator), cocrystallized with a 23–base pair (bp) DNA based on *E. coli copA* promoter, P_{copA} (table S1 and figs. S1 and S2). Given the extreme affinity of CueR for copper (K_d = 2 × 10^{-21} M) (*12*), crystallization of the metal-free (i.e., repressor) complex required mutation of metal-binding residues (C112S and C120S) and deletion of residues disordered in the DNA-free Ag^{I}-CueR structure (C129 to G135) (*12*). This variant is a repressor in the presence or absence of copper and cocrystallized with a 26-bp P_{copA} DNA (table S1 and figs. S1 and S2). Both structures were solved using molecular replacement and single-wavelength anomalous diffraction; the activator and repressor complexes were refined to 2.8 Å and 2.1 Å, with final models that include CueR residues 1 to 130 and 1 to 111, respectively (Fig. 1, A and B and table S2).

In both structures, the protein is a dimer, with each protomer contacting the duplex via an N-terminal DNA binding domain (DBD) composed of four α helices in a winged helix-turn-helix motif (Fig. 1A). A hinge loop connects the DBD to a long dimerization helix (DH). In the activator structure, the DH is followed by a metal-binding loop (MBL) and a two-turn C-terminal α helix (CTH) (Fig. 1A and fig. S3, A and B). These features, as well as the Ag^{I} coordination, are similar in the presence and absence of DNA (fig. S3, C to F) (*12*). As discussed below, the MBL and CTH are disordered in the repressor complex.

The most striking difference between these complexes is the DNA conformation. The stereochemistry of the central seven base pairs, which are B-form DNA (B-DNA) in the repressor complex, switches in the activator complex to an A-DNA–like structure known as TA-DNA, first described for the TBP/DNA complex (fig. S4, A to F, and table S3) (*16*). The two central bp steps ($T_{12}T_{13}$ and $T_{13}G_{14}$) in the repressor complex exhibit elevated roll angles (14° and 10°), consistent with a slight distortion at the center of the DNA. These become highly kinked (33° and 23°) as the minor groove becomes significantly wider than the major groove in the activator complex (Fig. 1, C and D) and alters the trajectory of the helical axis by ~36° relative to the repressor complex DNA (Fig. 1E). The repressor undertwists the DNA by ~50° and the activator further undertwists the DNA by ~22°, for a total of ~72° (fig. S5A). Other MerR-family activator/DNA complexes show similar distortions (table S3 and fig. S5B) (*8*, *10*). Molecular dynamics simulations reveal that the activator duplex structure rapidly relaxes to B-DNA upon removal of protein constraints, supporting the idea that the DNA distortions are energetically distinct states that are stabilized by two different protein conformations (fig. S6).

Remarkably, protein-DNA contacts in repressor and activator complexes are indistinguishable in the two structures. CueR interacts with phosphate groups at the distal edges of the pseudopalindrome through three Arg residues from α2 and the loop wing of the DBDs (Arg18, 31, and 37) that serve as clamps that "grip" the DNA backbone (i.e., R-clamps) (fig. S7, A and B). Mutagenesis and functional assays reveal that all three residues are required for transcription activation (fig. S7, C and D). We conclude that these conserved R-clamp residues (fig. S8) (*8*–*10*) play a key role as the activator conformation exerts the torque needed to distort the duplex into the A-DNA–like conformation.

In terms of DNA recognition, Tyr36 inserts into the minor groove and forms H bonds to N2 of $G_{22/23'}$ and O4′ of $T_{23/24'}$. Lys15 inserts into the major groove and forms H bonds to N7 and O6 of $G_{18/19'}$ and N7 of $G_{17/18'}$ (fig. S7B), and may confer DNA-binding site specificity (*10*). These interactions are not conserved among *E. coli* MerR proteins (fig. S8). A conserved feature among MerR proteins is the van der Waals (VDW) packing of an aromatic residue against a base in the major groove (*8*–*10*). In both CueR/DNA structures, the aromatic ring of Phe19 sits perpendicular to and forms VDW contacts with C_{15} and $G_{16'}$ (fig. S7B). This appears to contribute to the stability of the activator state (*10*); however, these interactions are unchanged in the repressor complex. Thus, the transcriptional switching event is not explained by changes in individual side-chain interactions with DNA.

The allosteric switch starts with metal binding to stabilize the MBL conformation. This triggers displacement of key residues in the hinge between DBD and DH (Fig. 2A). The hinge residue Arg75 provides a direct allosteric link between the MBL and the DBD. The backbone carbonyl oxygen of Ala118′ of the MBL forms an H bond with Arg75 Nε, displacing a water molecule and flipping the residue; Nη1 now H-bonds with the backbone carbonyl oxygen atoms of Asp72 and Phe70 on α4 of the DBD (Fig. 2A). Mutation of Arg75 to alanine decreases transcription activation at P_{copA} in vivo, consistent with the loss of the H-bond communication network (Fig. 2C and fig. S9A). The activator conformation is further stabilized when the CTH docks into the opened

[1]Department of Molecular Biosciences, Northwestern University, Evanston, IL 60208, USA. [2]Department of Chemistry, Northwestern University, Evanston, IL 60208, USA. [3]The Chemistry of Life Processes Institute, Northwestern University, Evanston, IL 60208, USA.
*Corresponding author. E-mail: t-ohalloran@northwestern.edu (T.V.O.); a-mondragon@northwestern.edu (A.M.)

hydrophobic cavity (Fig. 2B). Hydrophobic residues Ile122, Ile123, and Leu126 project into this cavity, displacing Phe70 but not disrupting the H bond with Arg75 (Fig. 2, A and B). This locks in a new orientation between the two protomers in the activator complex. These changes shift the DHs (α5 and α5′) in a small "scissors" movement (Fig. 3A) and decrease the distance between the two DBDs by ~6 Å (Fig. 3B). Because the DBDs move as rigid domains that tightly clamp onto the DNA, their rotation (Fig. 3C) and translation (Fig. 3D) readily force the kinking and undertwisting of the intervening DNA.

To test this mechanism, two types of allosteric-control (AC) CueR variants were made: a Cu^{I}-independent constitutive activator ($CueR^{CA}$) and a constitutive repressor ($CueR^{CR}$). Early phenotype screens (*17*, *18*) and studies of A89V/S131L MerR identified variants that activate transcription in the absence of the effector, Hg^{II} (*19*). We mutated homologous positions in CueR (T84V/N125L) (fig. S9B) and evaluated transcription in a *cueR* knockout *E. coli* strain (Δ*cueR*) using

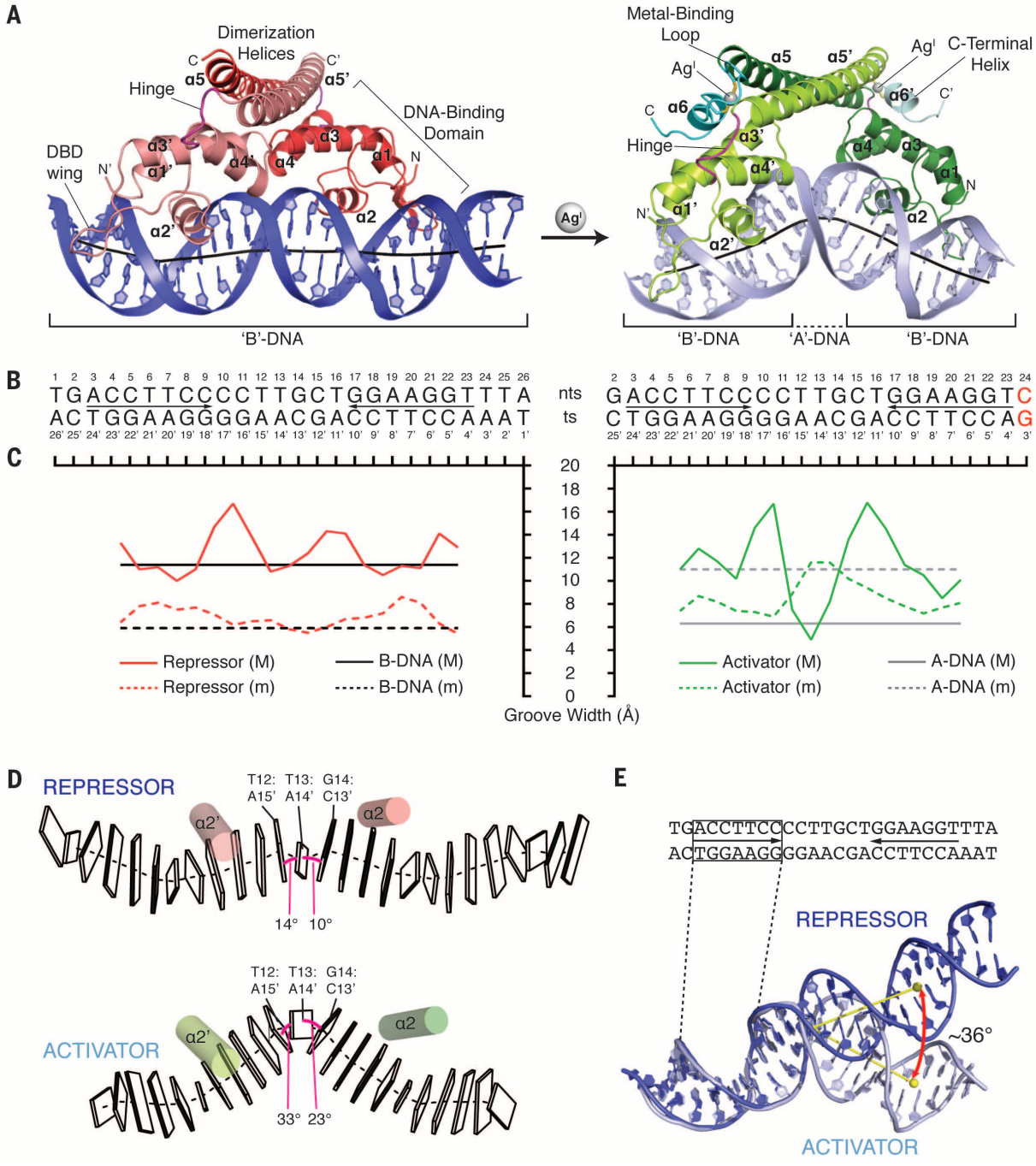

Fig. 1. Crystal structures of repressor and activator complexes with DNA. (**A**) Repressor and activator CueR/DNA structures. (**B**) Sequences of crystallized DNA duplexes. (**C**) DNA groove widths (M, major groove; m, minor groove). (**D**) Kinks at the central bp steps. The minor grooves are shaded black, and kinks are defined by the roll angles (pink lines) between the bp steps. (**E**) The activator introduces a ~36° angular change in the DNA.

in vivo β-galactosidase reporter assays. This variant exhibits clear Cu^{I}-independent transcription activation at all added copper concentrations (Fig. 2D), supporting its designation as a constitutive activator. To investigate whether the CTH communicates the allosteric signal to the DBD via docking into the hydrophobic cavity, we evaluated a mutant lacking the CTH (fig. S9C) and found that it was a constitutive repressor at all copper concentrations (Fig. 2E), providing additional support for the allosteric mechanism. Inspection of other MerR-family proteins suggests that the repression and activation mechanisms, including docking of the CTH, can be employed by proteins with similar C termini (e.g., SoxR) and by homologs with larger C termini (e.g., BmrR). These results reveal how the allosteric transition induces pronounced stereochemical reorganization of the structure and orientation of the core promoter elements with little or no change in protein-DNA contacts or affinity (*20*, *21*). To understand how these changes lead from repression to activation of transcription, we next considered the promoter geometry from the polymerase point of view.

MerR family proteins are thought to work by adjusting the phase angle and distance between the hexameric polymerase contact sites—namely, the –35 and –10 promoter elements (Fig. 4). In consensus *E. coli* promoters, there are 17 bp between these elements, but in MerR-type promoters, there are 19 to 20 bp (*22*). Assuming B-DNA, the –10 and –35 elements of the latter are 72° out of phase with respect to the productive conformation and have a longer separation between the two polymerase binding sites (Fig. 4A). In the repressor/DNA complex, the promoter is shortened by ~3 Å (Fig. 4B), consistent with hydrodynamic and biophysical studies of apo-MerR-family/DNA complexes (*20*, *23*, *24*). The repressor also undertwists the DNA, reducing the phase angle by 50° (to ~130°), a value approaching that of a 17-bp promoter (Fig. 4, B and D). Conversion to the activator structure induces further DNA undertwisting and kinking, which shortens the duplex by an additional ~6 Å relative to the repressor complex. This results in phasing and spacing parameters that are close to that of a 17-bp promoter (~108°) (Fig. 4, C and D), corroborating studies of other MerR-family/DNA complexes (*5*, *8*–*10*, *24*). Although this two-dimensional analysis provides a plausible account for transcription from the activator complex, it also suggests that the repressor, which also decreases the distance and the phase angle between the elements, should stimulate transcription. Clearly, it does not. The question of how the repressor exerts

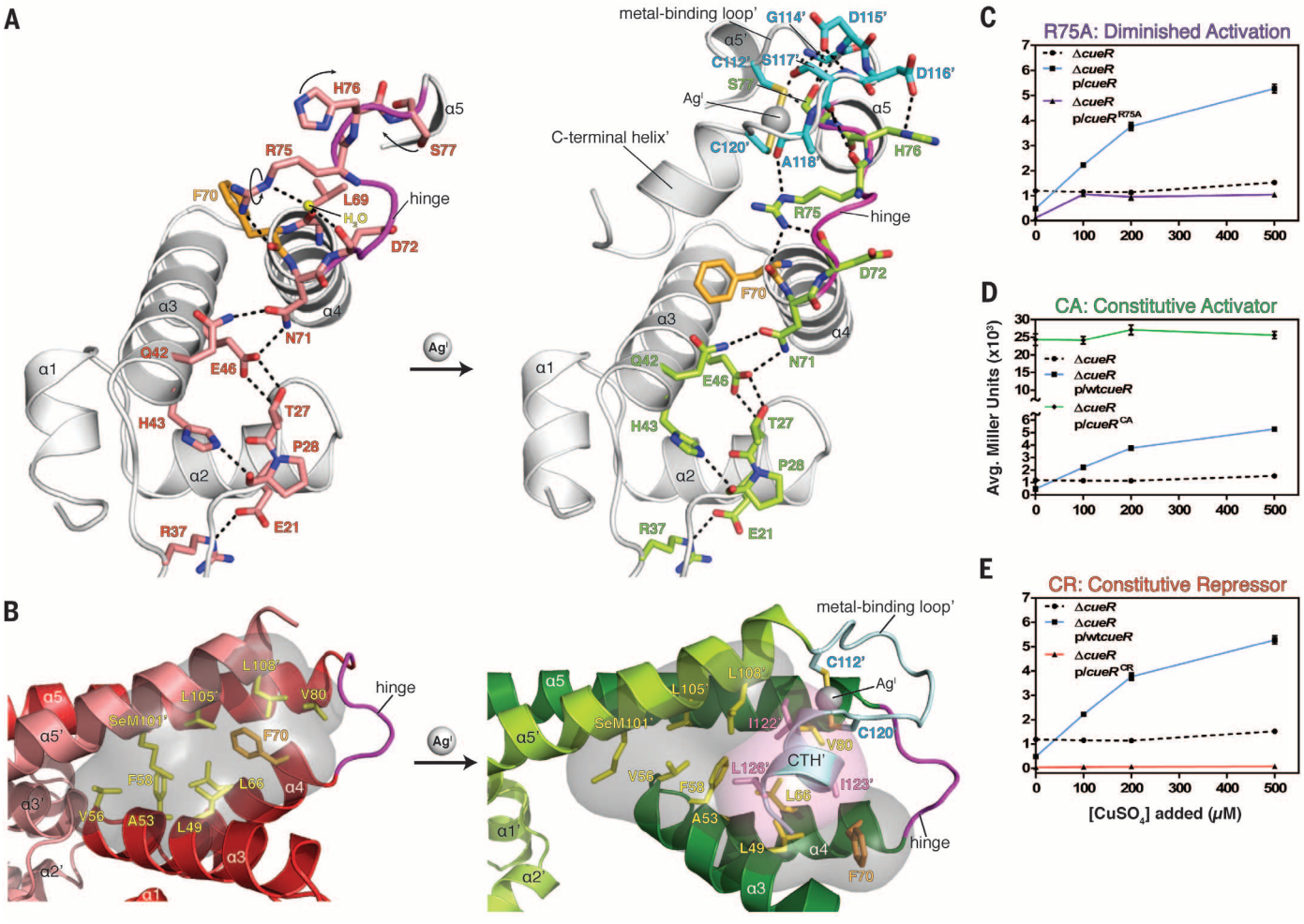

Fig. 2. The allosteric signal is propagated through the C-terminal loop-helix motif to the hinge. (**A**) Comparison of repressor (left) and activator (right) CueR depicting the transformations occurring at the CTH and hinge upon Ag^{I} binding: hinge residues R75, H76, and S77 are displaced (arrows) and form new H bonds (dashed lines) with CTH residues. (**B**) The hydrophobic cavity formed by DBD and DH residues (yellow), F70 (orange), and surfaces (gray) are shown in the repressor (left). The CTH′ residues and surfaces (pink) dock into the opened hydrophobic cavity in the activator (right). (**C** to **E**) β-galactosidase activity for AC mutants. Error bars (under symbols) correspond to SD. (C) The *cueR*^{R75A} variant exhibits full repression in the absence of copper and diminished activation upon addition of copper. (D) The *cueR*^{CA} variant exhibits greatly increased activation at all copper concentrations. (E) The *cueR*^{CR} variant exhibits full repression at all copper concentrations.

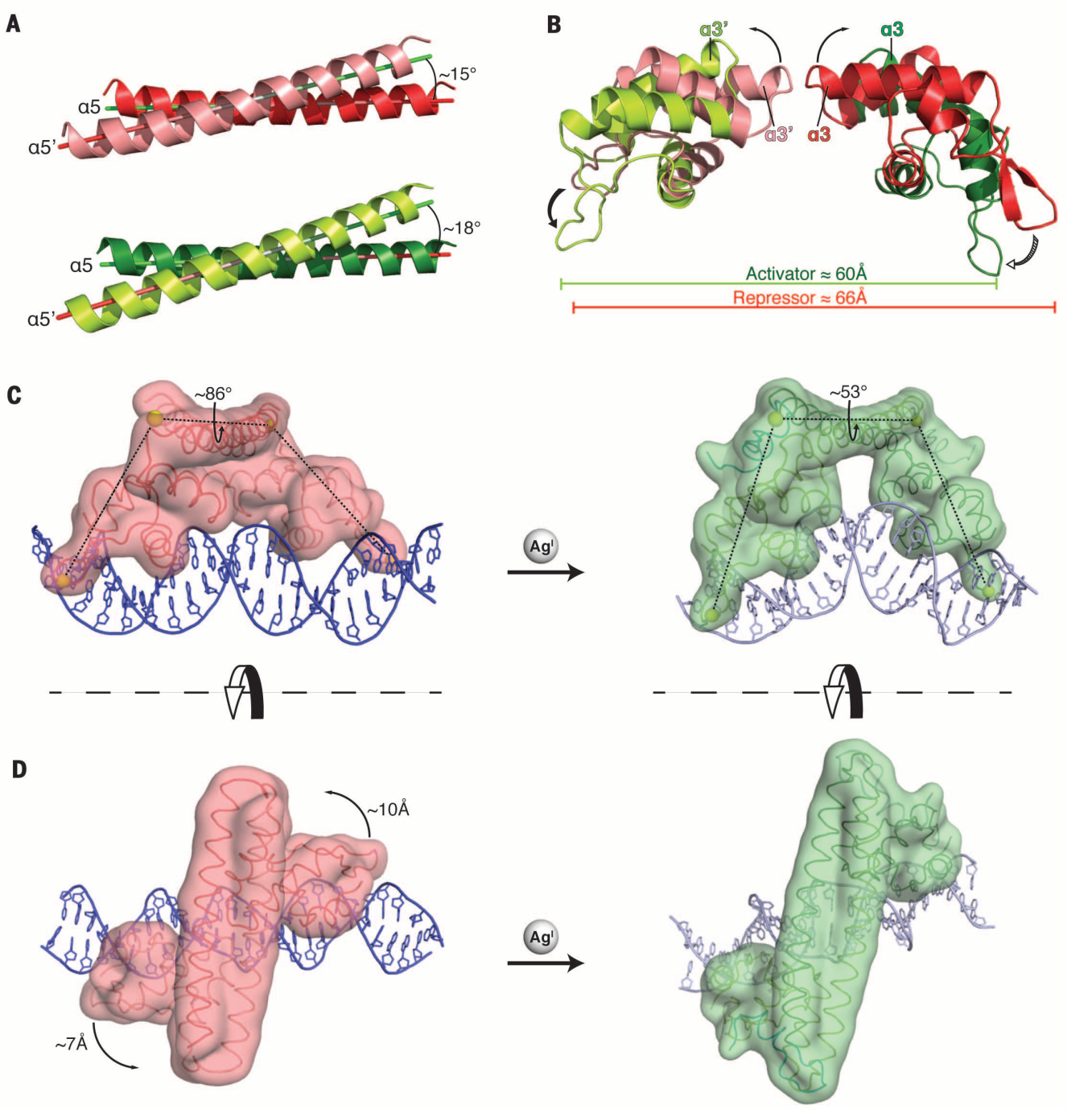

Fig. 3. The DBDs rotate and translate upon metal binding. (**A**) The slight "scissors" motion of the repressor (top) and activator (bottom) DHs (α5 and α5′) is shown. (**B**) The repressor DBDs rotate, bringing the wings closer by ~6 Å, and (**C**) decreasing the dihedral angle by ~33°, resulting in kinked/undertwisted DNA in the activator complex. (**D**) The complexes from (C) are viewed from the top. The DBDs translate by ~7 Å and ~10 Å, respectively. The DBDs move as rigid bodies: Superposition of the individual repressor and the activator DBDs reveals a root mean square deviation of ~0.5 Å for main chain atoms.

transcriptional silencing is best understood from a three-dimensional perspective.

By examining how these proteins alter the overall shape of the promoter with respect to the polymerase surface, we can account for repression as well as activation. Both structures were modeled onto structurally characterized RNA polymerase (RNAP)/DNA complexes (fig. S10 and Fig. 4E) (*25*). Consistent with results showing that MerR can form stable ternary complexes with the promoter and RNAP (*7*, *21*), we find that CueR and RNAP can bind on opposite faces of DNA without steric penalties (fig. S10, A and B). By overlaying CueR/DNA and RNAP complexes at the –35 element where the DNA interacts with the polymerase σ4 domain, we find that the repressor-imposed DNA conformation prevents contacts with the –10 element by forcing it ~40 Å away from the σ2 domain (fig. S10, A and B). This is accomplished by two bends that move the DNA toward the repressor and away

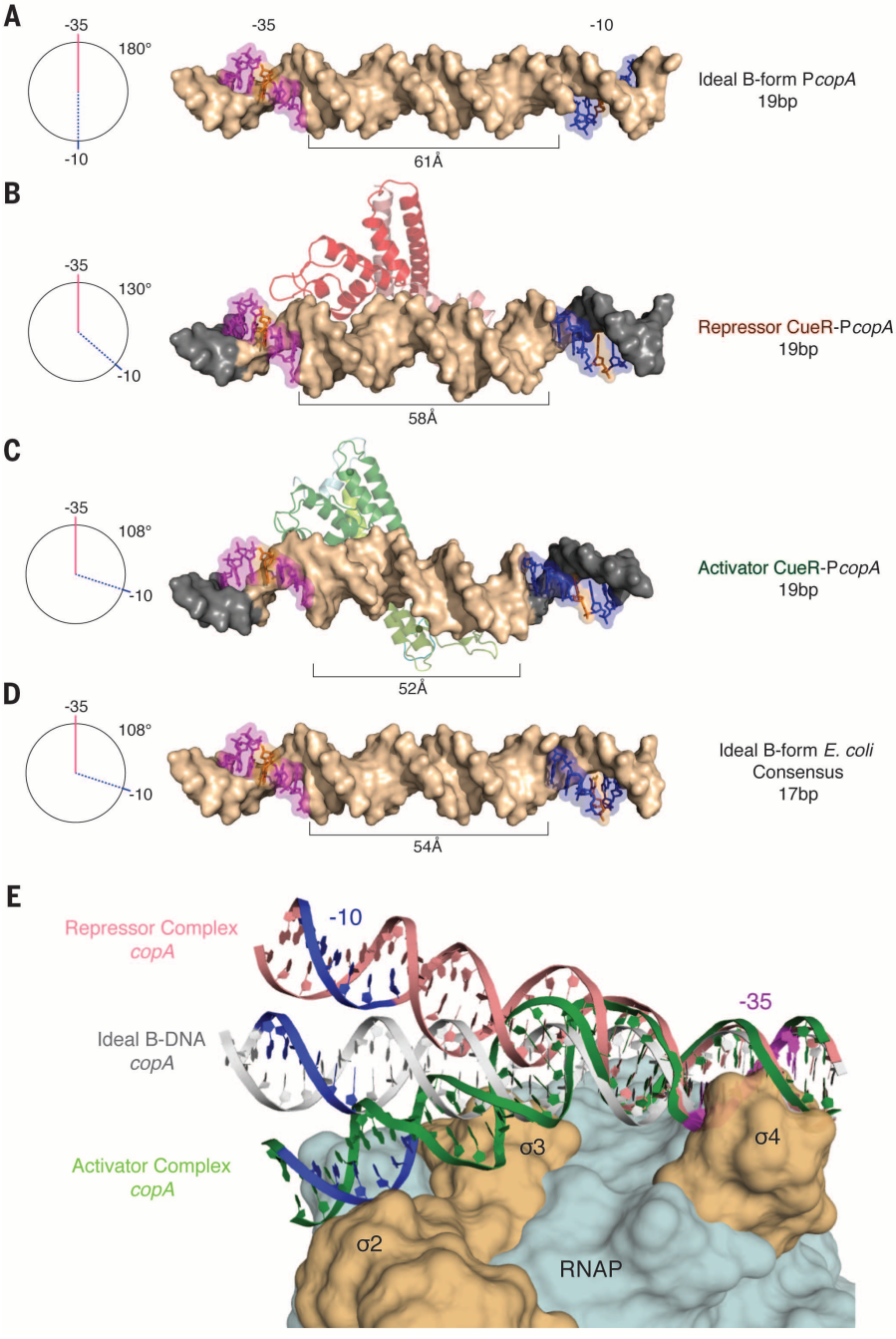

Fig. 4. CueR bends, undertwists, and kinks DNA for transcription control. (**A**) B-DNA model of P_{copA} (19 bp), (**B**) repressor CueR/DNA complex, (**C**) activator CueR/DNA complex, and (**D**) B-DNA model consensus *E. coli* promoter (17 bp). In (B) and (C), the crystallized DNA (tan) is extended with ideal B-DNA (gray) to include promoter elements. The radial plots (left) show relative positions of the two elements looking down the central axis, with –35 in front; the corresponding angle between –10 and –35 is given. (**E**) DNA from the repressor and activator complexes and the B-DNA model of P_{copA} were modeled onto RNAP (see fig. S10). The repressor complex DNA is bent away from σ2. The transition from repressor to activator kinks the DNA, positioning the –10 element in close proximity to σ2.

from the polymerase (fig. S10C). These bends map to DNaseI hypersensitivity sites in repressor MerR/DNA complexes, indicating that they persist in solution (*5*). We propose that this undertwisting and shortening of the promoter by the repressor poises the conformation of the DNA substrate but maintains a substantial energetic barrier to transcription activation. As it switches from the repressor to the activator conformation, CueR introduces a major kink in the central base pairs of the promoter, bringing the –10 element to the σ2 domain. The repressor and the activator forms modulate the overall shape of the core promoter in order to place the highly critical –10 element bases (*26*, *27*) away from or near the RNAP σ2 domain, respectively (Fig. 4E and fig. S10B). Thus, regulatory factors can reshape a core promoter via local changes in DNA stereochemistry and thereby stimulate facile switching between inactive and active transcription states.

REFERENCES AND NOTES

1. R. Rohs *et al.*, *Annu. Rev. Biochem.* **79**, 233–269 (2010).
2. R. Schleif, *FEMS Microbiol. Rev.* **34**, 779–796 (2010).
3. N. L. Brown, J. V. Stoyanov, S. P. Kidd, J. L. Hobman, *FEMS Microbiol. Rev.* **27**, 145–163 (2003).
4. Z. Ma, F. E. Jacobsen, D. P. Giedroc, *Chem. Rev.* **109**, 4644–4681 (2009).
5. A. Z. Ansari, J. E. Bradner, T. V. O'Halloran, *Nature* **374**, 370–375 (1995).
6. C. E. Outten, F. W. Outten, T. V. O'Halloran, *J. Biol. Chem.* **274**, 37517–37524 (1999).
7. B. Frantz, T. V. O'Halloran, *Biochemistry* **29**, 4747–4751 (1990).
8. E. E. Heldwein, R. G. Brennan, *Nature* **409**, 378–382 (2001).
9. K. J. Newberry, R. G. Brennan, *J. Biol. Chem.* **279**, 20356–20362 (2004).
10. S. Watanabe, A. Kita, K. Kobayashi, K. Miki, *Proc. Natl. Acad. Sci. U.S.A.* **105**, 4121–4126 (2008).
11. F. W. Outten, C. E. Outten, J. Hale, T. V. O'Halloran, *J. Biol. Chem.* **275**, 31024–31029 (2000).
12. A. Changela *et al.*, *Science* **301**, 1383–1387 (2003).
13. J. V. Stoyanov, J. L. Hobman, N. L. Brown, *Mol. Microbiol.* **39**, 502–512 (2001).
14. C. Petersen, L. B. Møller, *Gene* **261**, 289–298 (2000).
15. K. Yamamoto, A. Ishihama, *Mol. Microbiol.* **56**, 215–227 (2005).
16. G. Guzikevich-Guerstein, Z. Shakked, *Nat. Struct. Biol.* **3**, 32–37 (1996).
17. W. Ross, S. J. Park, A. O. Summers, *J. Bacteriol.* **171**, 4009–4018 (1989).
18. K. M. Comess, L. M. Shewchuk, K. Ivanetich, C. T. Walsh, *Biochemistry* **33**, 4175–4186 (1994).
19. J. Parkhill, A. Z. Ansari, J. G. Wright, N. L. Brown, T. V. O'Halloran, *EMBO J.* **12**, 413–421 (1993).
20. N. M. Andoy *et al.*, *Biophys. J.* **97**, 844–852 (2009).
21. T. V. O'Halloran, B. Frantz, M. K. Shin, D. M. Ralston, J. G. Wright, *Cell* **56**, 119–129 (1989).
22. A. O. Summers, *Curr. Opin. Microbiol.* **12**, 138–144 (2009).
23. C. Liu, E. Kim, B. Demple, N. C. Seeman, *Biochemistry* **51**, 937–943 (2012).
24. A. Z. Ansari, M. L. Chael, T. V. O'Halloran, *Nature* **355**, 87–89 (1992).
25. K. S. Murakami, S. Masuda, E. A. Campbell, O. Muzzin, S. A. Darst, *Science* **296**, 1285–1290 (2002).
26. Y. Zhang *et al.*, *Science* **338**, 1076–1080 (2012).
27. A. Feklistov, S. A. Darst, *Cell* **147**, 1257–1269 (2011).

ACKNOWLEDGMENTS

We acknowledge NIH grants R01GM038784 and U54CA143869, Life Sciences Collaborative Access Team staff assistance at the Advanced Photon Source, a U.S. Department of Energy (DOE) Office of Science User Facility operated for DOE Office of Science by Argonne National Laboratory (contract DE-AC02-06CH11357), and the Structural Biology Facility, Northwestern Lurie Cancer Center. Coordinates and structure factors (accession numbers 4WLS and 4WLW) are deposited in the Protein Data Bank.

SUPPLEMENTARY MATERIALS

www.sciencemag.org/content/349/6250/877/suppl/DC1
Materials and Methods
Figs. S1 to S10
Tables S1 to S3
References (*28*–*69*)

25 February 2015; accepted 21 July 2015
10.1126/science.aaa9809

TRANSCRIPTION

Structures of the RNA polymerase-σ^{54} reveal new and conserved regulatory strategies

Yun Yang,[1,4]* Vidya C. Darbari,[1,2]* Nan Zhang,[3] Duo Lu,[1,2]† Robert Glyde,[1,2] Yi-Ping Wang,[4] Jared T. Winkelman,[5] Richard L. Gourse,[5] Katsuhiko S. Murakami,[6] Martin Buck,[3] Xiaodong Zhang[1,2]‡

Transcription by RNA polymerase (RNAP) in bacteria requires specific promoter recognition by σ factors. The major variant σ factor (σ^{54}) initially forms a transcriptionally silent complex requiring specialized adenosine triphosphate–dependent activators for initiation. Our crystal structure of the 450-kilodalton RNAP-σ^{54} holoenzyme at 3.8 angstroms reveals molecular details of σ^{54} and its interactions with RNAP. The structure explains how σ^{54} targets different regions in RNAP to exert its inhibitory function. Although σ^{54} and the major σ factor, σ^{70}, have similar functional domains and contact similar regions of RNAP, unanticipated differences are observed in their domain arrangement and interactions with RNAP, explaining their distinct properties. Furthermore, we observe evolutionarily conserved regulatory hotspots in RNAPs that can be targeted by a diverse range of mechanisms to fine tune transcription.

Gene transcription is a tightly regulated event. A range of factors are required to maintain RNAP in a signal-responsive, but inhibited, state and to target it to specific genes (*1*). Bacterial sigma (σ) factors, eukaryotic TFIIB, and other general transcription factors, are the primary promoter recruitment factors. The major variant σ^{54} (also called σ^{N}) is used in transcribing genes for numerous stress responses (*2*). Unlike the major σ^{70} class, which recognizes the –35 and –10 promoter DNA elements, the σ^{54} class directs RNAP to promoter sites through the –24 and –12 DNA elements and forms a stable closed promoter complex that is unable to spontaneously melt DNA and initiate transcripts (*3*). Instead, the initiation process requires adenosine triphosphate (ATP)–dependent activator proteins bound to upstream enhancer sites to actively remodel the RNAP-σ^{54}–DNA complex (*4*).

Our crystal structure of RNAP-σ^{54} reveals that σ^{54} contains four structural domains connected by long coils and loops that span a large area of the RNAP core enzyme, which consists of two α and β, β′, and ω subunits (*5*, *6*) (Fig. 1, A to C; fig. S1, A and B; and table S1). σ^{54} Region I (RI, residues 1–56) forms a hook composed of two α helices. Region II (RII, residues 57–120) also contains two α helices (residues 57–85) in addition to loops that are buried inside the RNAP (Fig. 1, A and C). The RNAP core-binding domain (CBD) of σ^{54} extends as a structural fold to residue 250 and consists of two α-helical subdomains. Following on from the CBD, the backbone extends back to connect to a loop region; before an extra-long α helix (residues 315–353, hereafter called ELH, spanning 50 Å); followed by the HTH domain (residues 365–385), involved in interaction with the –12 promoter elements (*3*). The domain containing the RpoN box (RpoN domain), which is responsible for recognizing the –24 promoter elements, consists of a three-helical bundle (residues 415–477) (Fig. 1A) (*3*). The σ^{54} polypeptide chain snakes back and forth through its loop regions embedded in the RNAP. We carried out cross-linking experiments between σ^{54} and RNAP in solution using a *p*-benzoyl-L-phenylalanine–incorporated RNAP library. The amino acids that are cross-linked to σ^{54} agree well with the RNAP-σ^{54} crystal structure (Fig. 1D, yellow, and fig. S1C).

We crystallized RNAP-σ^{54} in complex with a 28–base pair (bp) DNA containing the –24 and –12 promoter elements. The crystals diffracted to 8 Å resolution, the electron density for DNA was unambiguous (Fig. 1E), and the molecular envelope for the holoenzyme was clear. We thus constructed a structural model of RNAP-σ^{54}–DNA (Fig. 1E and fig. S1D).

All σ factors contain a major RNAP CBD and a major DNA binding domain, which recognize either the –35 or –24 elements. The CBD of σ^{54} (Fig. 1A) binds toward the upstream face of the RNAP (Fig. 1C) (on the basis of the promoter DNA binding orientation), which interacts extensively with many functional modules within the RNAP, including the β flap (residues 835–937), the C terminus of the β subunit (residues 1267–1320), the β′ zipper/Zn-binding domain (residues 35–100), and the β′ dock domain (residues 370–420), as well as the α-subunit carboxyl-terminal domain (α-CTD) (Fig. 2A). Using FeBABE cleavage assays, we have previously mapped residue 198 of σ^{54} (within the CBD) to a region within the β flap (*7*).

The RpoN domain of σ^{54} is the most conserved domain among σ^{54} from different organisms (fig. S2). This domain extends from the main body of RNAP and does not contact other parts of σ^{54} or core enzyme (Fig. 1, A and C). Instead, it interacts with an adjacent RNAP molecule in the crystal, which suggests that its location is flexible in solution. In the RNAP-σ^{54}–DNA complex model, the RpoN domain is indeed moved relative to the RNAP-σ^{54} structure (fig. S1D). Unlike the flexible RpoN domain, the RIII-HTH domain of σ^{54}, which binds to the –12 promoter region, stably associates with the RNAP core through RI–RIII (Fig. 1E and fig. S1D) (*8*–*10*). Our data thus suggest that –12 binding is a major functional determinant for the σ^{54} holoenzyme promoter recognition, as well as a stable closed complex formation.

The σ^{54} RI plays an inhibitory role and contains contact sites for its cognate activator proteins (*11*, *12*). RI interacts with RIII, forming a structural module that lies along the cleft between β and β′ (Figs. 1C and 2B), where template strand DNA enters the active-site cleft (*13*). Our structure clearly suggests that the entry of promoter DNA into RNAP is blocked by RI and RIII of σ^{54}. The way the RNAP-σ^{54} crystal structure fits into the cryoelectron microscopy map of activator-bound RNAP-σ^{54} holoenzyme (*14*) positions the RI helices inside the connecting density leading to the activator protein, which indicates that RI in the RNAP-σ^{54} structure is presented favorably to contact the activator (fig. S3A).

RII penetrates deeply into the DNA binding channel (Fig. 1 and Fig. 2, C and D). RII can be divided into three subregions based on their locations in the holoenzyme. RII.1 (residues 57–85) occupies the downstream DNA binding cleft of RNAP, just above the bridge helix, and thus plays an inhibitory role (Fig. 1 and Fig. 2, C and D, and fig. S3A, right). RII.2 (residues 86–105) occupies the space of the DNA template strand (Fig. 2, C and D), which indicates that RII.2 has to relocate to permit template-strand DNA access into the RNAP active site and for transcription initiation. RII.3 (residues 105–120) extends along the path that is occupied by RNA in the transcribing complex (Fig. 2, C and D), which suggests that it will also need to relocate upon RNA synthesis.

Comparisons between σ^{54} and σ^{70} holoenzyme structures reveal that, overall, they contact similar regions of the RNAP core enzyme (Fig. 3, A and B), in agreement with the idea that specific factors unrelated by structure and sequence can be functionally similar (*15*). However, the relative

[1]Centre for Structural Biology, Imperial College London, South Kensington SW7 2AZ, UK. [2]Department of Medicine, Imperial College London, South Kensington SW7 2AZ, UK. [3]Department of Life Sciences, Imperial College London, South Kensington SW7 2AZ, UK. [4]State Key Laboratory of Protein and Plant Gene Research, College of Life Sciences, Peking University, China. [5]Department of Bacteriology, University of Wisconsin, Madison, WI 53706, USA. [6]Department of Biochemistry and Molecular Biology, Center for RNA Molecular Biology, Pennsylvania State University, University Park, PA 16802, USA.
*These authors contributed equally to this work. †Present address: State Key Laboratory of Bioactive Substance and Function of Natural Medicine, Institute of Materia Medica, Chinese Academy of Medical Sciences and Peking Union Medical College, China.
‡Corresponding author. E-mail: xiaodong.zhang@imperial.ac.uk

location of functional domains is completely different. For example, the σ^{54} CBD is located upstream, which blocks the RNA exit tunnel (Fig. 3C), whereas σ_2, the major CBD of σ^{70}, contacts the downstream β′ region (Fig. 3, A and B). The structural differences suggest that σ^{54} CBD, and hence σ^{54}, will have to dissociate or relocate to allow progression from transcription initiation to elongation, whereas σ^{70} can loosely associate with the RNAP core even during transcript elongation, in agreement with earlier biochemical data (*16*, *17*). σ^{70} region 4 (σ_4), which recognizes the −35 promoter element, occupies the upstream surface blocking the RNA exit channel instead (Fig. 3B).

The inhibitory RI of σ^{54} interacts with RIII across the RNAP cleft and blocks the template strand from entering. On the other hand, $\sigma_{1.1}$ of σ^{70}, which also has an inhibitory role (*18*), is located in the downstream DNA channel,

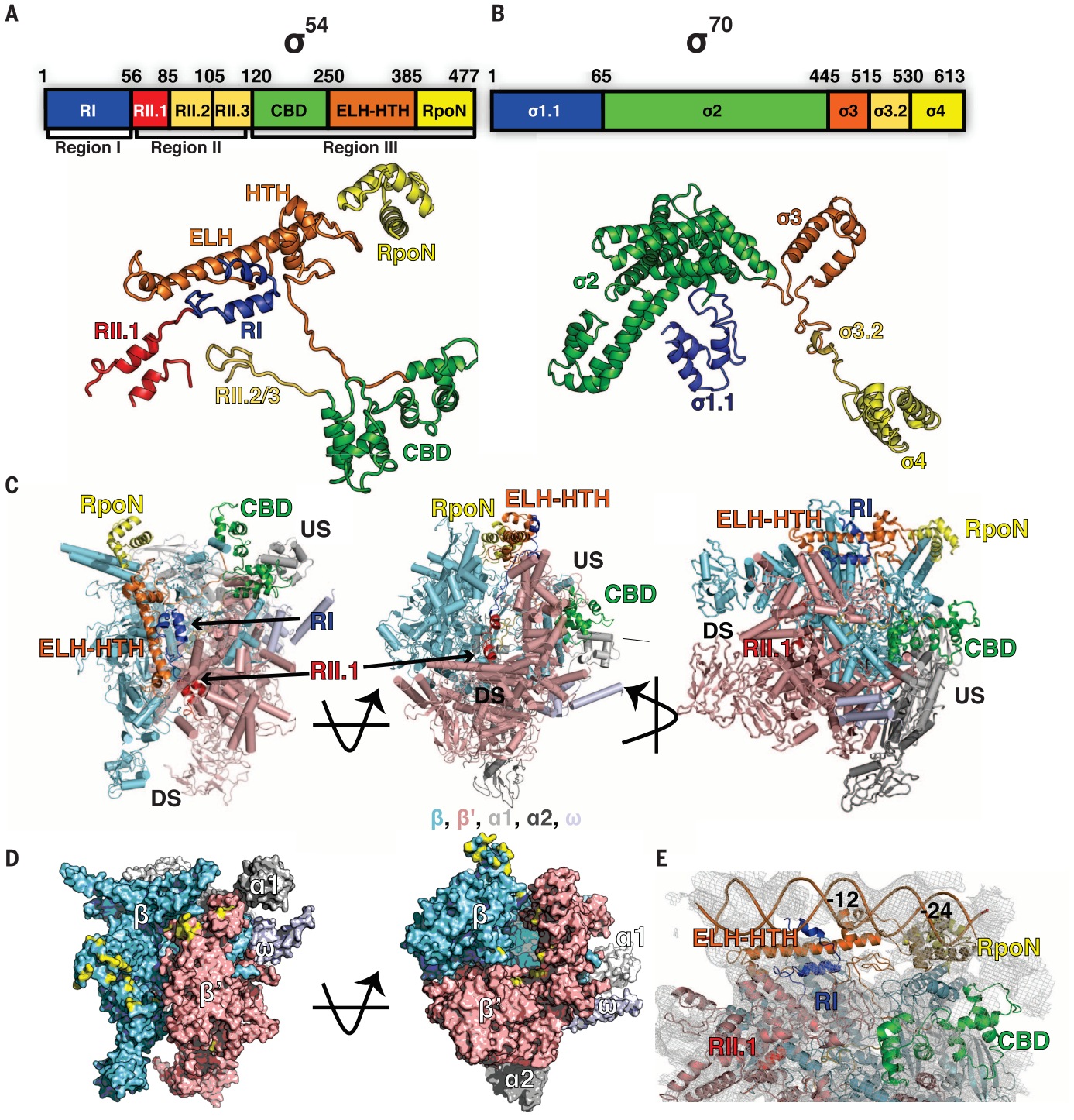

Fig. 1. Structure of complete RNAP-σ^{54}. (**A**) Structure and schematic diagram of σ^{54}. (**B**) Structure of σ^{70} (PDB 4YG2) with similar functional domains colored accordingly. (**C**) Holoenzyme in different orientations, RNAP core in cylinders. β, cyan; β′, salmon pink; α, gray; ω, pale blue; σ^{54} in ribbon and colored as in (A); DS, downstream; US, upstream. (**D**) Residues of β and β′ subunits that are cross-linked to σ^{54} are mapped onto the structure and colored in yellow. (**E**) Electron density map and structural model of RNAP-σ^{54}–DNA.

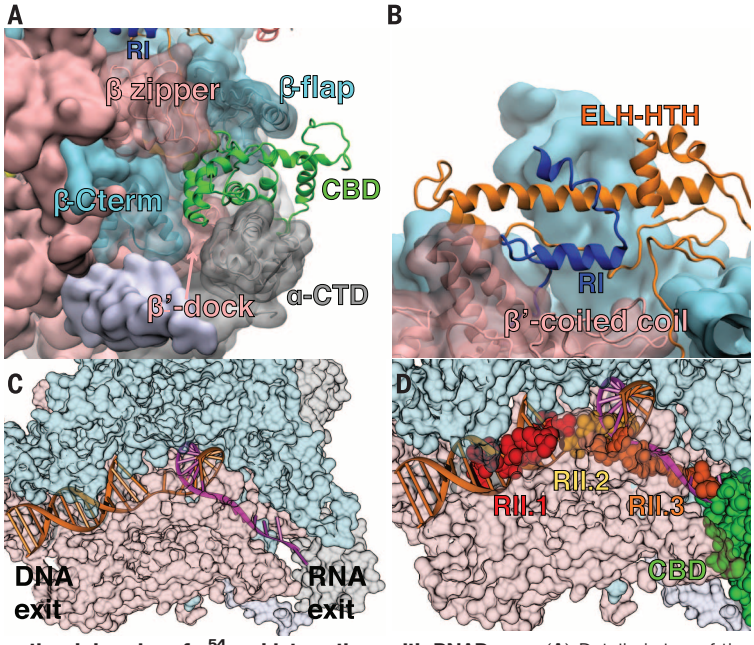

Fig. 2. Functional domains of σ^{54} and interactions with RNAP core. (**A**) Detailed view of the CBD and RNAP interactions. (**B**) RI and RIII. (**C**) DNA-RNA channels, with DNA, orange, and RNA, magenta. (**D**) Overlay with RII.1, RII.2, and RII.3.

overlapping with the region occupied by σ^{54} RII.1 (Fig. 3), which suggests that $\sigma_{1.1}$ and RII.1 might play related roles in transcription regulation. However, $\sigma_{1.1}$ connects with σ_2 by only a single flexible linker, which allows the $\sigma_{1.1}$ to move readily from the RNAP cleft (Fig. 1B, Fig. 3B). σ^{54} RII.1 is connected to the RI and CBD. RI interacts with RIII-ELH, whereas the linker that connects RII.1 with the CBD is embedded in the DNA/RNA channel of RNAP (Fig. 2, C and D). Because of its topological restraint, σ^{54} RII.1 cannot relocate easily without affecting the conformation of other parts of σ^{54}; RII.1 will thus block downstream DNA entry.

Notable conformational differences exist between the σ^{70} and σ^{54} holoenzymes in many key modules within the RNAP when superposed on the bridge helix, chosen because the catalytic center must be conserved (fig. S3B). The β′ coiled coil, with the whole β′ subunit, is rotated, which narrows the downstream DNA channel by as much as 5 Å (fig. S3B). However, the clamp, which consists of β and β′ domains forming the walls of the downstream DNA channel, was shown to adopt multiple conformations in solution (*19*). The β′ coiled coil forms helical bundles with σ_2 of σ^{70} and helps

Fig. 3. Comparisons of σ^{54} and σ^{70} holoenzymes. (**A**) RNAP-σ^{54} with RNAP displayed as spheres and σ^{54} as surface. (**B**) RNAP-σ^{70}, same view as in (A). (**C**) Elongation complex (PDB code 2O5J).

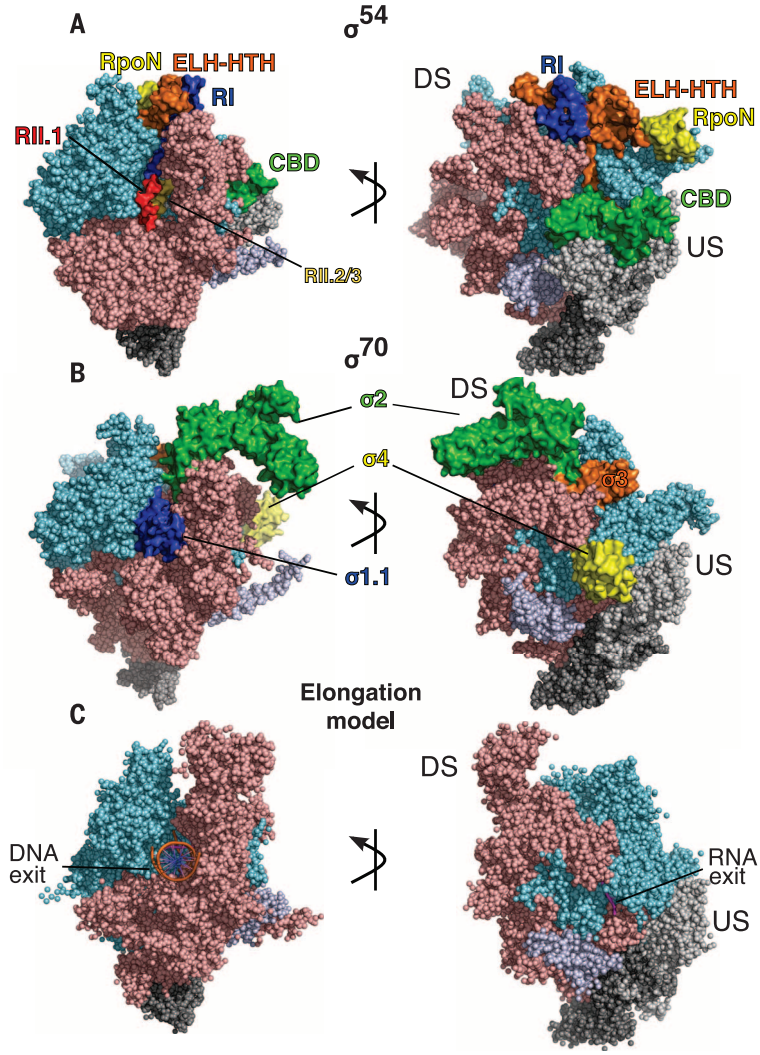

to stabilize the unpaired nontemplate DNA strand and, hence, the transcription bubble (*20*) (fig. S4A). The B linker of TFIIB also interacts with the β′ coiled coil (fig. S4B). In the σ^{54} holoenzyme structure, the β′ coiled coil does not form a helical bundle with σ^{54} (fig. S4C). However, it is possible that enroute to transcription initiation, this interaction is established, in agreement with our biochemical data (fig. S4D).

σ^{54} occupies multiple locations along the DNA and RNA path within the RNAP core. These locations are also targeted by other regulatory factors and in other RNAPs. For example, RI and RIII sit across the RNAP cleft, blocking the DNA template strand entry (Fig. 4A). At similar locations, domains 2 and 3 (σ_2 and σ_3) of σ^{70} form a V-shaped wedge that acts as a gate to allow the template strand to enter the active cleft (Fig. 4B) (*13*, *21*). TFIIB also uses two subdomains, the B core and the B linker, to occupy similar areas in Pol II (Fig. 4C). This area is thus occupied by σ^{54} to inhibit, while guiding the template strand delivery by σ^{70} and TFIIB. Furthermore, σ_2 of σ^{70} contains a number of aromatic residues that are shown to interact with the nontemplate strand and therefore facilitate DNA melting and transcription bubble formation (*20*). In σ^{54}, there are few aromatic residues in this region (RI and RIII–ELH) that could facilitate DNA melting, in agreement with data showing that although deletion of σ^{54} RI can bypass the requirement of activator proteins, it fails on double-stranded DNA (*11*). Activator proteins may therefore be directly required for transcription bubble opening. The downstream DNA channel is occupied by both RII.1 of σ^{54} and $\sigma_{1.1}$ of σ^{70} (Fig. 4D). A negatively charged region of TFIIF is also located in the downstream DNA channel of Pol II (*22*). RII.2 of σ^{54} is located in the channel that is occupied by the template strand DNA in the transcribing RNAP (Fig. 2D). Both σ^{70} and TFIIB lack equivalent structural features. This area, however, is occupied in Pol I by part of the expander (Fig. 4E), a unique insertion in Pol I compared with Pol II and shown to stabilize an expanded active center cleft (*23*, *24*) (Fig. 4E). Similar to RII.3, both region 3.2 in σ^{70} (the σ finger) and the B reader in TFIIB are shown to overlap with the space that would be occupied by RNA (Fig. 4, D and F) (*25*). Indeed, RII.3 shares sequence homology with the σ finger, especially the highly conserved DDE motif (fig. S2). Acidic residues in these elements are proposed to facilitate template DNA loading and RNA separation from DNA and to guide it toward the exit channel (*25*–*28*). It is possible that RII.3 also performs similar roles.

Our structure uncovers a diverse range of regulatory strategies used by σ^{54} in tightly controlling transcription initiation. These include blocking the template strand from entering the RNAP active cleft by RI and RIII, occupying the downstream DNA channel by RII.1, and interfering with the template strand and synthesized RNA by RII.2–RII.3. The position of RI and RIII plays a vital role in these regulatory functions. Activator proteins interact with RI and could relocate RI, RIII–ELH, and RII and release the inhibition posed by some of these structural elements (fig. S3A) (*29*, *30*). Precisely how activators overcome these multiple modes of inhibition, as well as the role of ATP in this process, remains to be determined. Furthermore, we show that although σ^{54}, σ^{70}, TFIIB, TFIIF, and Pol I subunits have no sequence or structural similarities, they target the same elements within their respective RNAPs. Our structure and comparisons thus provide clear evidence that regulatory hotspots within RNAPs are functionally conserved. Different transcription factors, irrespective of their structures and sequences, are used to target these hotspots in order to exert a fine-tuned transcription regulation strategy (fig. S5). It will be interesting to see the extent to which additional multisubunit RNAPs use these regulatory strategies.

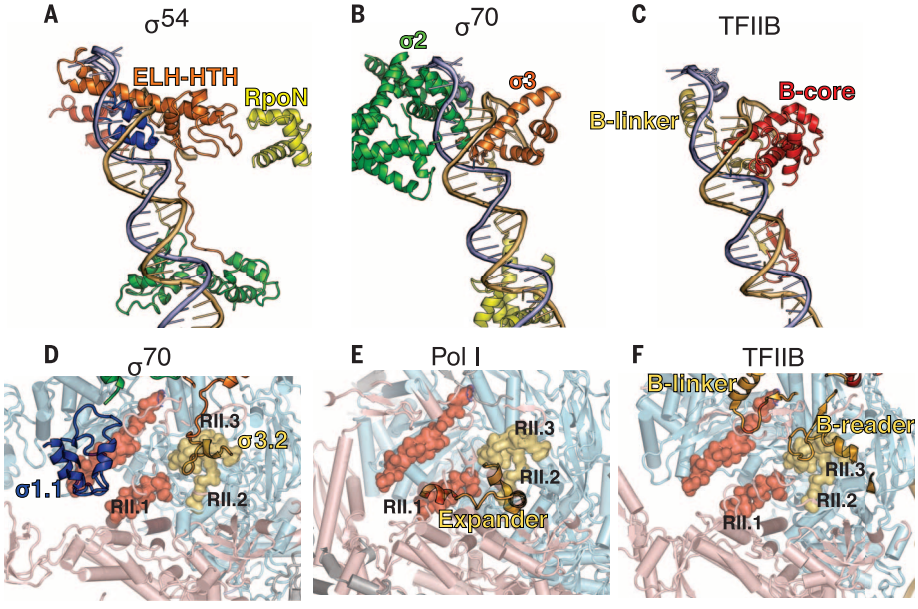

Fig. 4. Regulatory elements of σ^{54} and comparison with σ^{70}, TFIIB, and Pol I. (**A**) σ^{54}, (**B**) σ^{70}, and (**C**) TFIIB in relation to template strand (gold), as defined in the complex with a full transcription bubble (4YLN). (**D** to **F**) Comparison of σ^{54} with σ^{70}, Pol I (4C2M), and TFIIB (4BBS) in the RNAP DNA-RNA channel; structures are superposed on the bridge helix. σ^{54} represented as spheres; σ^{70}, TFIIB, and Pol I expander are shown as ribbons; and RNAP as cylinders.

REFERENCES AND NOTES

1. R. A. Mooney, S. A. Darst, R. Landick, *Mol. Cell* **20**, 335–345 (2005).
2. A. Feklístov, B. D. Sharon, S. A. Darst, C. A. Gross, *Annu. Rev. Microbiol.* **68**, 357–376 (2014).
3. M. Buck, M. T. Gallegos, D. J. Studholme, Y. Guo, J. D. Gralla, *J. Bacteriol.* **182**, 4129–4136 (2000).
4. M. Rappas, D. Bose, X. Zhang, *Curr. Opin. Struct. Biol.* **17**, 110–116 (2007).
5. P. Cramer, *Curr. Opin. Struct. Biol.* **12**, 89–97 (2002).
6. F. Werner, D. Grohmann, *Nat. Rev. Microbiol.* **9**, 85–98 (2011).
7. S. R. Wigneshweraraj *et al.*, *EMBO J.* **23**, 4264–4274 (2004).
8. Y. Guo, J. D. Gralla, *Proc. Natl. Acad. Sci. U.S.A.* **95**, 11655–11660 (1998).
9. Y. Guo, C. M. Lew, J. D. Gralla, *Genes Dev.* **14**, 2242–2255 (2000).
10. P. C. Burrows, S. R. Wigneshweraraj, M. Buck, *J. Mol. Biol.* **375**, 43–58 (2008).
11. J. T. Wang, A. Syed, J. D. Gralla, *Proc. Natl. Acad. Sci. U.S.A.* **94**, 9538–9543 (1997).
12. M. Chaney, M. Buck, *Mol. Microbiol.* **33**, 1200–1209 (1999).
13. Y. Zuo, T. A. Steitz, *Mol. Cell* **58**, 534–540 (2015).
14. D. Bose *et al.*, *Mol. Cell* **32**, 337–346 (2008).
15. K. B. Decker, D. M. Hinton, *Annu. Rev. Microbiol.* **67**, 113–139 (2013).
16. G. Bar-Nahum, E. Nudler, *Cell* **106**, 443–451 (2001).
17. J. Mukhopadhyay *et al.*, *Cell* **106**, 453–463 (2001).
18. B. Bae *et al.*, *Proc. Natl. Acad. Sci. U.S.A.* **110**, 19772–19777 (2013).
19. A. Chakraborty *et al.*, *Science* **337**, 591–595 (2012).
20. A. Feklistov, S. A. Darst, *Cell* **147**, 1257–1269 (2011).
21. K. S. Murakami, S. Masuda, E. A. Campbell, O. Muzzin, S. A. Darst, *Science* **296**, 1285–1290 (2002).
22. Z. A. Chen *et al.*, *EMBO J.* **29**, 717–726 (2010).
23. C. Engel, S. Sainsbury, A. C. Cheung, D. Kostrewa, P. Cramer, *Nature* **502**, 650–655 (2013).
24. C. Fernández-Tornero *et al.*, *Nature* **502**, 644–649 (2013).
25. D. Kostrewa *et al.*, *Nature* **462**, 323–330 (2009).
26. S. Sainsbury, J. Niesser, P. Cramer, *Nature* **493**, 437–440 (2013).
27. X. Liu, D. A. Bushnell, D. Wang, G. Calero, R. D. Kornberg, *Science* **327**, 206–209 (2010).
28. R. S. Basu *et al.*, *J. Biol. Chem.* **289**, 24549–24559 (2014).
29. A. Sharma *et al.*, *Nucleic Acids Res.* **42**, 5177–5190 (2014).
30. L. J. Friedman, J. Gelles, *Cell* **148**, 679–689 (2012).

ACKNOWLEDGMENTS

We thank M. Michael and D. Bose for their earlier contributions to this project; A. Forster, J. Liu, and beamline scientists at the Diamond Light Source for their help with data collection; and members of X.Z.'s and M.B.'s labs for helpful discussion. We thank D. Wigley, R. Dixon, R. Weinzierl, C. Fernández-Tornero, and R. Wigneshweraraj for critically reading the manuscript. Y.Y. was funded by the Chinese National Science Foundation and the China Scholarship Council. The majority of this work was funded by the UK Biotechnology and Biological Sciences Research Council to X.Z. and M.B. K.S.M. is supported by NIH grant GM087350. Y.-P.W. is funded by 973 National Key Basic Research Programme (2015CB755700) in China. J.T.W. and R.L.G. were supported by NIH grant R37 GM37048 (to R.L.G.). The atomic coordinate has been deposited in the Protein Data Bank with accession code 5BYH.

SUPPLEMENTARY MATERIALS

www.sciencemag.org/content/349/6250/882/suppl/DC1
Materials and Methods
Figs. S1 to S5
Tables S1
References (*31*–*43*)

20 March 2015; accepted 15 July 2015
10.1126/science.aab1478

NEW ENGLAND BioLabs® Inc.

Count on it.

Introducing the NEBNext® Library Quant Kit for Illumina®

Accurate quantitation of next generation sequencing libraries is essential for maximizing sequencing data output and quality. The NEBNext Library Quant Kit for Illumina is a qPCR-based method that delivers higher consistency and reproducibility of quantitation than other currently available methods. With optimized kit components and a more convenient protocol, you can count on your quantitation values, every time.

To learn more and request a sample, visit **www.neb.com/E7630**

With the NEBNext Library Quant Kit, optimal cluster density is achieved from quantitated libraries with a broad range of library size and GC content.

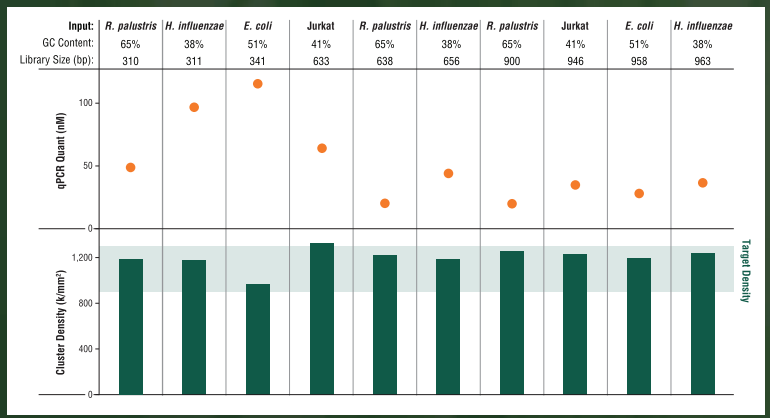

Libraries of 310–963 bp from the indicated sources were quantitated using the NEBNext Library Quant Kit, then diluted to 8 pM and loaded onto a MiSeq® (v2 chemistry; MCS v2.4.1.3). Library concentrations ranged from 7–120 nM, and resulting raw cluster density for all libraries was 965–1300 k/mm2 (ave. =1199). Optimal cluster density was achieved using concentrations determined by the NEBNext Library Quant Kit for all library sizes.

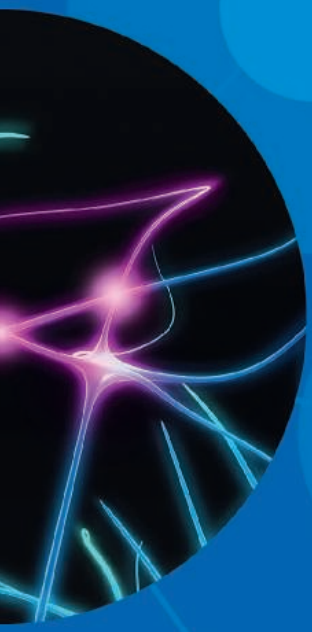

LILIANE BETTENCOURT PRIZE FOR LIFE SCIENCES

The 18th Liliane Bettencourt Prize for Life Sciences was awarded to **Scott Waddell**, Professor of Neurobiology and Wellcome Trust Senior Research Fellow in the Centre for Neural Circuits and Behaviour at the University of Oxford. Scott leads a team studying memory, motivation and neural transposition. He is also a Senior Research Fellow of Pembroke College, Oxford, and Co-Director of the Oxford Martin School Programme on Mind and Machine.

The Liliane Bettencourt Prize for Life Sciences, worth € 250,000, has been awarded every year since 1997 to a European researcher under the age of 45, who is recognised within the scientific community for the quality of their international publications. In addition to their status as an author and leader in their own scientific field, the candidate must be leading a particularly promising research project and have the personal qualities for mobilising an entire team.

Established in 1987 as a public interest foundation, the Bettencourt Schueller Foundation was set up by Liliane, André Bettencourt and their daughter Françoise Bettencourt Meyers, in memory of Eugène Schueller, a renowned researcher and chemist. Its mission is to "take talent to the top", in order to contribute to a stronger French society and boost France's influence on the international stage. This mission is focused on three main areas: life sciences, the arts and the promotion of an inclusive society. Driven by strong convictions, the Foundation's approach and actions serve the common good, thus demonstrating a firm commitment to social responsibility.

Bettencourt Schueller Foundation
27-29 rue des Poissonniers • 92200 Neuilly-sur-Seine • France
www.fondationbs.org • Contact: sciences@fondationbs.org

PRIZE WINNER

Scott Waddell

Scott Waddell is Professor of Neurobiology and Wellcome Trust Senior Research Fellow in the Centre for Neural Circuits and Behaviour at the University of Oxford. He is also a Senior Research Fellow at Pembroke College, Oxford, and co-director of the Oxford Martin School Programme on Mind and Machine.

He leads a team studying memory, motivation and neural transposition. Scott returned to the United Kingdom in 2011, after 5 years as a post doctoral fellow at Massachusetts Institute of Technology and 10 years leading a research group in the Department of Neurobiology at the University of Massachusetts Medical School (USA). His post doctoral discovery in the fruit fly mushroom bodies of DPM neurons, two large cells required for memory consolidation, revealed that fly learning mechanisms could be investigated at cellular resolution. Lately, his team has demonstrated that distinct subsets of dopaminergic neurons play different roles in controlling motivated behaviour and reward learning in the fly. These neurons, that also innervate the mushroom bodies, indicate a previously unforeseen similarity between fly and mammalian reinforcement systems. In addition, the Waddell team's surprising discovery of jumping genes in the fly's mushroom bodies has provided a means of understanding molecular mechanisms that contribute to making each brain unique.

BETTENCOURT SCHUELLER FOUNDATION

The Keystone Symposia 2015–2016 Conference Series

Human Nutrition, Environment and Health (T1)
Organizers: Martin Kussmann, Hannelore Daniel & Jacqueline Pontes Monteiro
Oct 14–18, 2015 | China World Hotel | Beijing | China
Deadlines: Discounted Registration: Sep 10, '15

Diabetes: New Insights into Molecular Mechanisms and Therapeutic Strategies (T2)
Organizers: Takashi Kadowaki, Juleen R. Zierath, Nobuya Inagaki & Barbara B. Kahn
Oct 25–29, 2015 | Westin Miyako Kyoto | Kyoto | Japan
Deadlines: Discounted Registration: Aug 25, '15

Systems Immunology: From Molecular Networks to Human Biology (A1)
Organizers: Ronald N. Germain, Aviv Regev, Nir Hacohen & Dana Pe'er
Jan 10–14, 2016 | Big Sky Resort | Big Sky, Montana | USA
Deadlines: Discounted Abstract/Scholarship: Sep 21, '15; Abstract: Oct 20, '15; Discounted Registration: Nov 10, '15

Cytokine JAK-STAT Signaling in Immunity and Disease (A2)
Organizers: Curt M. Horvath, John J. O'Shea & Stephanie S. Watowich
Jan 10–14, 2016 | Sheraton Steamboat Resort | Steamboat Springs, Colorado | USA
Deadlines: Discounted Abstract/Scholarship: Sep 21, '15; Abstract: Oct 20, '15; Discounted Registration: Nov 10, '15

Molecular and Cellular Basis of Growth and Regeneration (A3)
Organizers: Alejandro Sánchez Alvarado, Duojia D.J. Pan & Valentina Greco
Jan 10–14, 2016 | Beaver Run Resort | Breckenridge, Colorado | USA
Deadlines: Discounted Abstract/Scholarship: Sep 22, '15; Abstract: Oct 21, '15; Discounted Registration: Nov 10, '15

Nuclear Receptors: Full Throttle (J1)
Organizers: Carol A. Lange, Jennifer K. Richer & Karen E. Knudsen
joint with **Metabolism, Transcription and Disease (J2)**
Organizers: Peter Verrijzer, Katherine A. Jones & Paolo Sassone-Corsi
Jan 10–14, 2016 | Snowbird Resort | Snowbird, Utah | USA
Deadlines: Discounted Abstract/Scholarship: Sep 23, '15; Abstract: Oct 22, '15; Discounted Registration: Nov 12, '15

Biology of Down Syndrome: Impacts Across the Biomedical Spectrum (A4)
Organizers: Victor Tybulewicz, Elizabeth Fisher, Thomas Blumenthal & Jeanne Lawrence
Jan 24–27, 2016 | Hilton Santa Fe Historic Plaza Hotel | Santa Fe, New Mexico | USA
Deadlines: Discounted Abstract/Scholarship: Sep 24, '15; Abstract: Oct 26, '15; Discounted Registration: Nov 20, '15

Traumatic Brain Injury: Clinical, Pathological and Translational Mechanisms (J3)
Organizers: Ann C. McKee, Ramon Diaz-Arrastia & Lee E. Goldstein
joint with **Axons: From Cell Biology to Pathology (J4)**
Organizers: Giampietro Schiavo, Bruce D. Carter and Rejji Kuruvilla
Jan 24–27, 2016 | Eldorado Hotel & Spa | Santa Fe, New Mexico | USA
Deadlines: Discounted Abstract/Scholarship: Sep 24, '15; Abstract: Oct 27, '15; Discounted Registration: Nov 23, '15

Drug Discovery for Parasitic Diseases (A5)
Organizers: Leann M. Tilley, Philip J. Rosenthal & Kelly Chibale
Jan 24–28, 2016 | Granlibakken Resort | Tahoe City, California | USA
Deadlines: Discounted Abstract/Scholarship: Sep 28, '15; Abstract: Oct 28, '15; Discounted Registration: Nov 23, '15

Small RNA Silencing: Little Guides, Big Biology (A6)
Organizers: Phillip D. Zamore, Yukihide Tomari & Mihaela Zavolan
Jan 24–28, 2016 | Keystone Resort | Keystone, Colorado | USA
Deadlines: Discounted Abstract/Scholarship: Sep 28, '15; Abstract: Oct 28, '15; Discounted Registration: Nov 23, '15

Purinergic Signaling (J5)
Organizers: Joel Linden, Mark J. Smyth, Simon C. Robson & Kenneth A. Jacobson
joint with **Cancer Immunotherapy: Immunity and Immunosuppression Meet Targeted Therapies (J6)**
Organizers: Barbara Seliger, Jerome Galon & Francesco M. Marincola
Jan 24–28, 2016 | Fairmont Hotel Vancouver | Vancouver, British Columbia | Canada
Deadlines: Discounted Abstract/Scholarship: Sep 29, '15; Abstract: Oct 29, '15; Discounted Registration: Nov 24, '15

Neurological Disorders of Intracellular Trafficking (A7)
Organizers: Dennis Drayna & Bettina Winckler
Jan 31–Feb 4, 2016 | Keystone Resort | Keystone, Colorado | USA
Deadlines: Discounted Abstract/Scholarship: Sep 30, '15; Abstract: Nov 2, '15; Discounted Registration: Dec 1, '15

Cell Biology and Immunology of Persistent Infection (A8)
Organizers: Herbert (Skip) W. Virgin, E. John Wherry, Anne O'Garra & Andrea Lynn Cox
Jan 31–Feb 4, 2016 | Fairmont Banff Springs | Banff, Alberta | Canada
Deadlines: Discounted Abstract/Scholarship: Oct 1, '15; Abstract: Nov 3, '15; Discounted Registration: Dec 1, '15

The Cancer Genome (Q1)
Organizers: Elaine R. Mardis, Sohrab Shah & Ben J. Raphael
joint with **Genomics and Personalized Medicine (Q2)**
Organizers: Michael Snyder, Leroy E. Hood & Heidi L. Rehm
Feb 7–11, 2016 | Fairmont Banff Springs | Banff, Alberta | Canada
Deadlines: Discounted Abstract/Scholarship: Oct 7, '15; Abstract: Nov 9, '15; Discounted Registration: Dec 7, '15

Fibrosis: From Basic Mechanisms to Targeted Therapies (Q3)
Organizers: Robert Lafyatis, Paolo G.V. Martini, Dean Sheppard & Lucie Peduto
joint with **Stromal Cells in Immunity (Q4)**
Organizers: Shannon J. Turley, Burkhard Ludewig & Melody A. Swartz
Feb 7–11, 2016 | Keystone Resort | Keystone, Colorado | USA
Deadlines: Discounted Abstract/Scholarship: Oct 8, '15; Abstract: Nov 10, '15; Discounted Registration: Dec 8, '15

Plant Epigenetics: From Genotype to Phenotype (B1)
Organizers: Scott D. Michaels, Doris Wagner & Nathan M. Springer
Feb 15–19, 2016 | Sagebrush Inn & Suites | Taos, New Mexico | USA
Deadlines: Discounted Abstract/Scholarship: Oct 14, '15; Abstract: Nov 16, '15; Discounted Registration: Dec 15, '15

Obesity and Adipose Tissue Biology (B2)
Organizers: Yu-Hua Tseng, Philipp E. Scherer & Deborah Clegg
Feb 15–19, 2016 | Fairmont Banff Springs | Banff, Alberta | Canada
Deadlines: Discounted Abstract/Scholarship: Oct 15, '15; Abstract: Nov 17, '15; Discounted Registration: Dec 15, '15

Noncoding RNAs in Health and Disease (Q5)
Organizers: Ramin Shiekhattar & Roberto Bonasio
joint with **Enhancer Malfunction in Cancer (Q6)**
Organizers: Ali Shilatifard & Dale Dorsett
Feb 21–24, 2016 | Santa Fe Community Convention Center | Santa Fe, New Mexico | USA
Deadlines: Discounted Abstract/Scholarship: Oct 20, '15; Abstract: Nov 18, '15; Discounted Registration: Dec 18, '15

G Protein-Coupled Receptors: Structure, Signaling and Drug Discovery (B3)
Organizers: Arthur Christopoulos, Laura M. Bohn & Dominic P. Behan
Feb 21–25, 2016 | Keystone Resort | Keystone, Colorado | USA
Deadlines: Discounted Abstract/Scholarship: Oct 21, '15; Abstract: Nov 19, '15; Discounted Registration: Dec 21, '15

New Frontiers in Understanding Tumor Metabolism (Q7)
Organizers: Chi Van Dang, Katharine Yen & Navdeep S. Chandel
joint with **Immunometabolism in Immune Function and Inflammatory Disease (Q8)**
Organizers: Jeffrey C. Rathmell, Jonathan D. Powell & Amira Klip
Feb 21–25, 2016 | Fairmont Banff Springs | Banff, Alberta | Canada
Deadlines: Discounted Abstract/Scholarship: Oct 22, '15; Abstract: Nov 23, '15; Discounted Registration: Dec 21, '15

T Follicular Helper Cells and Germinal Centers (B4)
Organizers: Shane Crotty & Carola G. Vinuesa
Feb 26–Mar 1, 2016 | Hyatt Regency Monterey | Monterey, California | USA
Deadlines: Discounted Abstract/Scholarship: Oct 27, '15; Abstract: Nov 30, '15; Discounted Registration: Jan 5, '16

Immunity in Skin Development, Homeostasis and Disease (B5)
Organizers: Frank O. Nestle, Richard L. Gallo, Fiona M. Watt & Paul A. Khavari
Feb 28–Mar 2, 2016 | Granlibakken Resort | Tahoe City, California | USA
Deadlines: Discounted Abstract/Scholarship: Oct 28, '15; Abstract: Dec 1, '15; Discounted Registration: Jan 5, '16

Tuberculosis Co-Morbidities and Immunopathogenesis (B6)
Organizers: Hardy Kornfeld, Sarah M. Fortune & Thomas R. Hawn
Feb 28–Mar 3, 2016 | Keystone Resort | Keystone, Colorado | USA
Deadlines: Discounted Abstract/Scholarship: Oct 29, '15; Abstract: Dec 1, '15; Discounted Registration: Jan 5, '16

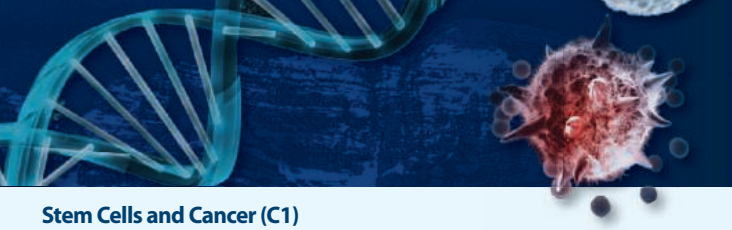

LIFE SCIENCE RESEARCH CONFERENCES AROUND THE GLOBE

www.keystonesymposia.org/2016meetings

Stem Cells and Cancer (C1)
Organizers: Austin Gurney, Connie J. Eaves & Jane E. Visvader
Mar 6–10, 2016 | Beaver Run Resort | Breckenridge, Colorado | USA
Deadlines: Discounted Abstract/Scholarship: Nov 4, '15; Abstract: Dec 7, '15; Discounted Registration: Jan 6, '16

Cancer Vaccines: Targeting Cancer Genes for Immunotherapy (X1)
Organizers: A. Karolina Palucka, Hyam I. Levitsky & Laurence Zitvogel
joint with **Antibodies as Drugs (X2)**
Organizers: Peter D. Senter, Anna M. Wu, Alan J. Korman & Karl Dane Wittrup
Mar 6–10, 2016 | Fairmont Chateau Whistler | Whistler, British Columbia | Canada
Deadlines: Discounted Abstract/Scholarship: Nov 5, '15; Abstract: Dec 8, '15; Discounted Registration: Jan 7, '16

Ubiquitin Signaling (X3)
Organizers: Philip Cohen, Michael Rape & Titia K. Sixma
joint with
NF-κB and MAP Kinase Signaling in Inflammation (X4)
Organizers: Steven C. Ley, Zhijian 'James' Chen & Jenny P.Y. Ting
Mar 13–17, 2016 | Whistler Conference Centre | Whistler, British Columbia | Canada
Deadlines: Discounted Abstract/Scholarship: Nov 11, '15; Abstract: Dec 14, '15; Discounted Registration: Jan 13, '16

Islet Biology: From Cell Birth to Death (X5)
Organizers: Klaus H. Kaestner, Christopher J. Rhodes & Yuval Dor
joint with
Stem Cells and Regeneration in the Digestive Organs (X6)
Organizers: Linheng Li, Martín G. Martín, James M. Wells & Markus Grompe
Mar 13–17, 2016 | Keystone Resort | Keystone, Colorado | USA
Deadlines: Discounted Abstract/Scholarship: Nov 12, '15; Abstract: Dec 15, '15; Discounted Registration: Jan 14, '16

Chromatin and Epigenetics (C2)
Organizers: Luciano Di Croce & Yang Shi
Mar 20–24, 2016 | Whistler Conference Centre | Whistler, British Columbia | Canada
Deadlines: Discounted Abstract/Scholarship: Nov 18, '15; Abstract: Dec 16, '15; Discounted Registration: Jan 20, '16

HIV Persistence: Pathogenesis and Eradication (X7)
Organizers: David M. Margolis, Satya Dandekar & Susana T. Valente
joint with **HIV Vaccines (X8)**
Organizers: David C. Montefiori & Mario Roederer
Mar 20–24, 2016 | Resort at Squaw Creek | Olympic Valley, California | USA
Deadlines: Discounted Abstract/Scholarship: Nov 19, '15; Abstract: Dec 17, '15; Discounted Registration: Jan 21, '16

Cancer Pathophysiology: Integrating the Host and Tumor Environments (C3)
Organizers: Sheila A. Stewart, Sandra S. McAllister & Lisa M. Coussens
Mar 28–Apr 1, 2016 | Beaver Run Resort | Breckenridge, Colorado | USA
Deadlines: Discounted Abstract/Scholarship: Dec 1, '15; Abstract: Jan 4, '16; Discounted Registration: Jan 28, '16

Modern Phenotypic Drug Discovery: Defining the Path Forward (D1)
Organizers: Jonathan A. Lee, Ellen L. Berg & Eugene C. Butcher
Apr 2–6, 2016 | Big Sky Resort | Big Sky, Montana | USA
Deadlines: Discounted Abstract/Scholarship: Dec 2, '15; Abstract: Jan 5, '16; Discounted Registration: Feb 2, '16

Mitochondrial Dynamics (D2)
Organizers: Richard J. Youle & Gia K. Voeltz
Apr 3–7, 2016 | Sheraton Steamboat Resort | Steamboat Springs, Colorado | USA
Deadlines: Discounted Abstract/Scholarship: Dec 2, '15; Abstract: Jan 6, '16; Discounted Registration: Feb 3, '16

Heart Failure: Genetics, Genomics and Epigenetics (Z1)
Organizers: Stuart A. Cook, Christine E. Seidman & Yigal M. Pinto
joint with **Cardiac Development, Regeneration and Repair (Z2)**
Organizers: Christine L. Mummery, Joseph C. Wu & Jonathan A. Epstein
Apr 3–7, 2016 | Snowbird Resort | Snowbird, Utah | USA
Deadlines: Discounted Abstract/Scholarship: Dec 3, '15; Abstract: Jan 7, '16; Discounted Registration: Feb 4, '16

Myeloid Cells (D3)
Organizers: Arturo Zychlinsky, Judith E. Allen, Eicke Latz & Kate A. Fitzgerald
Apr 10–14, 2016 | INEC – Ireland's National Events & Conference Centre | Killarney, County Kerry | Ireland
Deadlines: Discounted Abstract/Scholarship: Dec 10, '15; Abstract: Jan 11, '16; Discounted Registration: Feb 10, '16

New Therapeutics for Diabetes and Obesity (G1)
Organizers: Richard D. DiMarchi, Matthias H. Tschöp & Nancy A. Thornberry
April 17–20, 2016 | Estancia La Jolla Hotel & Spa | La Jolla, California | USA
Deadlines: Discounted Abstract/Scholarship: Dec 16, '15; Abstract: Jan 19, '16; Discounted Registration: Feb 16, '16

Gut Microbiota, Metabolic Disorders and Beyond (D4)
Organizers: Rémy G. Burcelin, Sven Pettersson & Tak W. Mak
Apr 17–21, 2016 | Hyatt Regency Newport | Newport, Rhode Island | USA
Deadlines: Discounted Abstract/Scholarship: Dec 17, '15; Abstract: Jan 20, '16; Discounted Registration: Feb 17, '16

Epigenetic and Metabolic Regulation of Aging and Aging-Related Diseases (E1)
Organizers: Anne Brunet, David M. Sabatini & Shelley L. Berger
May 1–5, 2016 | Hilton Santa Fe Historic Plaza Hotel | Santa Fe, New Mexico | USA
Deadlines: Discounted Abstract/Scholarship: Jan 5, '16; Abstract: Feb 2, '16; Discounted Registration: Mar 1, '16

Positive-Strand RNA Viruses (N1)
Organizers: Raul Andino & Peter D. Nagy
May 1–5, 2016 | Hyatt Regency Austin | Austin, Texas | USA
Deadlines: Discounted Abstract/Scholarship: Jan 6, '16; Abstract: Feb 3, '16; Discounted Registration: Mar 2, '16

Nucleic Acid Sensing Pathways: Innate Immunity, Immunobiology and Therapeutics (E2)
Organizers: Thomas Tuschl, Veit Hornung & Karl-Peter Hopfner
May 8–12, 2016 | Maritim Hotel & Conference Center | Dresden | Germany
Deadlines: Discounted Abstract/Scholarship: Jan 7, '16; Abstract: Feb 9, '16; Discounted Registration: Mar 8, '16

State of the Brain 2016 (R1)
Organizers: Terrence J. Sejnowski & Sten Grillner
May 22–26, 2016 | Alpbach Congress Centrum | Alpbach | Austria
Deadlines: Discounted Abstract/Scholarship: Jan 21, '16; Abstract: Feb 23, '16; Discounted Registration: Mar 22, '16

New Approaches to Vaccines for Human and Veterinary Tropical Diseases (M1)
Organizers: Vish Nene, Vishva M. Dixit, Rafi Ahmed & Yasmine Belkaid
May 22–26, 2016 | Southern Sun Cape Sun | Cape Town | South Africa
Deadlines: Discounted Abstract/Scholarship: Jan 21, '16; Abstract: Feb 23, '16; Discounted Registration: Mar 22, '16

B Cells at the Intersection of Innate and Adaptive Immunity (E3)
Organizers: Mikael C. I. Karlsson, Claudia Mauri, Eric Meffre & Andrea Cerutti
May 29–Jun 2, 2016 | Clarion Hotel Sign | Stockholm | Sweden
Deadlines: Discounted Abstract/Scholarship: Jan 28, '16; Abstract: Feb 29, '16; Discounted Registration: Mar 29, '16

Understanding the Function of Human Genetic Variation (K1)
Organizers: Kerstin Lindblad-Toh & Xavier Estivill
May 31–Jun 4, 2016 | Uppsala Konsert & Kongress | Uppsala | Sweden
Deadlines: Discounted Abstract/Scholarship: Feb 1, '16; Abstract: Mar 1, '16; Discounted Registration: Mar 31, '16

Autophagy: Molecular and Physiological Mechanisms (V1)
Organizers: Sharon A. Tooze, Ana Maria Cuervo & Noboru Mizushima
Jun 5–9, 2016 | Whistler Conference Centre | Whistler, British Columbia | Canada
Deadlines: Discounted Abstract/Scholarship: Feb 4, '16; Abstract: Mar 8, '16; Discounted Registration: Apr 5, '16

Common Mechanisms of Neurodegeneration (Z3)
Organizers: Bradley T. Hyman, Adriano M. Aguzzi & Ricardo E. Dolmetsch
joint with **Microglia in the Brain (Z4)**
Organizers: Beth Stevens & Richard M. Ransohoff
Jun 12–16, 2016 | Keystone Resort | Keystone, Colorado | USA
Deadlines: Discounted Abstract/Scholarship: Feb 11, '16; Abstract: Mar 10, '16; Discounted Registration: Apr 12, '16

Exosomes/Microvesicles: Novel Mechanisms of Cell-Cell Communication (E4)
Organizers: Richard A. Cerione & Xandra O. Breakefield
Jun 19–22, 2016 | Keystone Resort | Keystone, Colorado | USA
Deadlines: Discounted Abstract/Scholarship: Feb 18, '16; Abstract: Mar 17, '16; Discounted Registration: Apr 19, '16

KEYSTONE SYMPOSIA™
on Molecular and Cellular Biology
Accelerating Life Science Discovery

Abstracts submitted by the abstract deadline will be considered for short talks. Scholarships are for students/postdoctoral fellows. 2015-2016 conferences typically begin with afternoon registration and an evening welcome mixer on the first advertised day and conclude with an evening plenary session followed by food and entertainment on the last advertised day. However, some program formats vary. Please view up-to-date program details for each conference at **www.keystonesymposia.org** and then **/** and the alpha-numeric **program code** (e.g., **www.keystonesymposia/16A1**).

"What I do with my Octet HTX time? Climb."

Shave weeks off your lead selection programs.

Broader antibody cross-competition ups your odds of finding the best candidates, but larger epitope binning studies take time. The Octet HTX system lets you use any binning assay format, any size matrix, start a run and get analyzed results the same day or the next day for larger studies. You can also combine multiple experiments into one dataset to easily visualize and cluster antibodies in similar bins or binding groups.

Lucy gets out of the lab more often now to climb. What will you do with your extra time?

fortéBIO®
A Division of **Pall Life Sciences**

PALL Life Sciences

fortebio.com | 888-OCTET-75

Fast. Accurate. EASY.

AAAS 2016 ANNUAL MEETING | WASHINGTON, DC FEBRUARY 11–15

Global Science Engagement

The 2016 meeting focuses on how the scientific enterprise can meet global challenges in need of innovation and international collaboration.

aaas.org/meetings

Advance Registration Now Open

Register for the meeting and reserve a room now to receive lower rates. Join thousands of leading scientists, educators, policymakers, and journalists in Washington, DC to discuss recent developments in science and technology.

Advance registration is available online: aaas.org/meetings

Two Faculty Career Features

THERE'S A SCIENCE TO REACHING SCIENTISTS.

September 18, 2015
Reserve ads by September 1
Ads accepted until September 14

October 9, 2015
Reserve ads by September 22
Ads accepted until October 5

For recruitment in science, there's only one Science

Hiring faculty? Whatever your timing, we've got two special features for your **Faculty ads** this fall! The September 18 feature covers strategies and resources to build teaching skills. The October 9 feature offers strategies for moving into academia from other industries.

What makes *Science* the best choice for recruiting?

- Read and respected by 570,400 readers around the globe
- 60% of our weekly readers work in academia and 67% are Ph.D.s. *Science* connects you with more scientists in academia than any other publication
- Your ad dollars support AAAS and its programs, which strengthens the global scientific community.

Special packages available when you advertise in both features

Why choose these faculty features for your advertisement?

- Relevant ads lead off the career section with special Faculty banner
- September 18 issue will be distributed at the Biotechnica Meeting in Hanover, Germany, 6–8 October.

Expand your exposure. Post your print ad online to benefit from:

- Link on the job board homepage directly to Faculty jobs
- Dedicated landing page for faculty positions
- Additional marketing driving relevant job seekers to the job board.

SCIENCECAREERS.ORG

ScienceCareers
FROM THE JOURNAL SCIENCE AAAS

To book your ad: **advertise@sciencecareers.org**

The Americas
202-326-6582

Europe/RoW
+44(0)1223-326500

Japan
+81-3-3219-5777

China/Korea/Singapore/Taiwan
+86-186-0082-9345

NMR Spectrometer Series

The new JNM-ECZS series NMR is a next generation NMR spectrometer that incorporates ultra-high accuracy RF circuitry utilizing the latest digital high-frequency technology. The compact spectrometer design features unprecedented levels of performance and expandability to support the most advanced NMR experiments. The 43% reduction in size of the JNM-ECZS series compared to previous models simplifies NMR spectrometer placement in modern laboratories. Performance features critical to NMR data collection such as RF phase, frequency, and amplitude control, NMR pulse shape waveform data table size, and digital receiver performance have been improved by several orders of magnitude. These features collectively support the most advanced NMR experiments that combine a wide variety of NMR pulses in complicated NMR pulse sequences. A complete set of high-performance NMR probes are available for the JNM-ECZS spectrometer to support many NMR applications, including a new high-sensitivity liquid-nitrogen probe capable of variable temperature experiments from -40°C to 150°C.

Jeol
For info: 978-535-5900
www.jeolusa.com

pH Meters

New pH electrodes, the IoLine electrodes, have a unique iodine/iodide reference system with a patented three-chamber reservoir system. IoLine electrodes offer unbeatable stability, fast response times, and high accuracy at a higher speed compared to traditional Ag/AgCl reference systems. It is a 100% metal ion-free reference system, ideal for Tris buffer solutions in complex biotech applications, or precision processes within immunoassay production. In addition to the unique IoLine electrodes, the TruLine and ScienceLine pH and mV electrodes are also available. TruLine electrodes are compact in design, available as glass or plastic probe bodies, and can be ordered with or without temperature sensors and with a refillable option. The TruLine electrodes are proven, highly versatile laboratory electrodes for the most demanding measurements. The ScienceLine electrodes include the temperature sensor and can be ordered with a platinum or ground junction.

Xylem Analytics
For info: 978-778-1010
www.xylemanalytics.com

Solvent Recovery System

The SolventTrap SVOC Solvent Recovery System can recover solvents evaporated during the concentration step prior to injection into a GC or HPLC. The SolventTrap SVOC comes coupled with the DryVap In-line Drying and Evaporation System for a complete dry-evaporate-trap solvent system, consistent with the workflow and environmentally friendly. The system can recover 95% dichloromethane (DCM) evaporated from six 180 mL samples simultaneously, using vacuum and an auxiliary chiller. Recent enforcement of environmental air regulations has shown laboratories that compliance is a must and anything that can reduce the solvent emitted into the air is a valuable laboratory addition. Additionally, there is less chance of operator exposure to solvent vapors making the workplace safer.

Horizon Technology
For info: 603-386-3654
www.horizontectinc.com

SLE Synthetic Sorbent Line

The Novum Simplified Liquid Extraction (SLE) sorbent line has been extended to include tube formats, in addition to the original 96-well plate formats. Novum is a synthetic alternative to traditional diatomaceous earth SLE (also known as supported liquid extraction) products and provides a simplified approach to traditional liquid-liquid extraction (LLE). Novum is now available in 1, 3, 6, and 12 cc tubes. Novum tubes can be automated using a liquid handler and can also be run using a cost-effective vacuum manifold to run 12 or 24 samples at once for increased throughput over traditional LLE. Extraction techniques used prior to LC and GC can improve results and reduce wear and tear on the instrument. As the first of its kind, the synthetic Novum SLE sorbent can be used with the same solvents as traditional SLE sorbents while delivering improved lot-to-lot reproducibility.

Phenomenex
For info: 310-212-0555
www.phenomenex.com/novum

Live Cell Imaging

The CytoSMART System is an easy-to-use and affordable live cell imaging system that enables researchers to take time-lapse videos and images of their cell culture without needing to manually inspect their cells. The images taken with the CytoSMART Device are transmitted into the CytoSMART Cloud, enabling researchers to view their cell culture outside of the lab at any time through a web browser, whether via a computer, tablet, or smartphone. The system combines 24 hour peace of mind with a number of advanced functions. Among others, these include a graphical readout that reports ongoing cell confluency and automatic email alerts that can be configured to inform the user when certain milestones are reached (e.g., based on confluency). CytoSMART System is ideal for a number of applications, such as cell culture monitoring and documentation, migration and scratch assays, and cell culture standardization.

Lonza
For info: 301-898-7025
www.lonza.com

Electronically submit your new product description or product literature information! Go to www.sciencemag.org/products/newproducts.dtl for more information.

Newly offered instrumentation, apparatus, and laboratory materials of interest to researchers in all disciplines in academic, industrial, and governmental organizations are featured in this space. Emphasis is given to purpose, chief characteristics, and availability of products and materials. Endorsement by *Science* or AAAS of any products or materials mentioned is not implied. Additional information may be obtained from the manufacturer or supplier.

want new technologies?

antibodies
apoptosis
biomarkers
cancer
cytometry
data
diseases
DNA
epigenetics
genomics
immunotherapies
medicine
microbiomics
microfluidics
microscopy
neuroscience
proteomics
sequencing
toxicology
transcriptomics

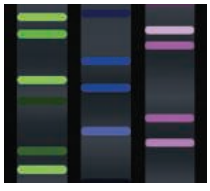

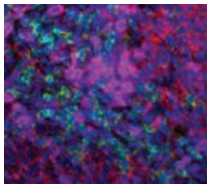

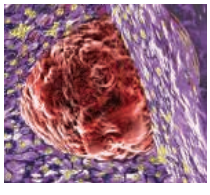

watch our webinars

Learn about the latest breakthroughs, new technologies, and ground-breaking research in a variety of fields. Our expert speakers explain their quality research to you and answer questions submitted by live viewers.

VIEW NOW!
webinar.sciencemag.org

Science
AAAS

Brought to you by the *Science*/AAAS Custom Publishing Office

@SciMagWebinars

CELL SIGNALING TECHNOLOGY

EPIGENETICS:
DISCOVERY THROUGH VALIDATION

692 CST antibodies for epigenetic-related targets, including histone modifications, epigenetic regulators, and general transcription factors.

226 CST antibodies validated for ChIP according to ENCODE* Consortium guidelines.

Validated Tools for Discovery:

» SimpleChIP® Kits to facilitate Chromatin IP from cells and tissue.

» PTMScan® Kits and Services to enable MS-based discovery of methylated and acetylated proteins.

» Most ChIP-validated antibodies approved for additional applications like IHC, Flow, IF and WB.

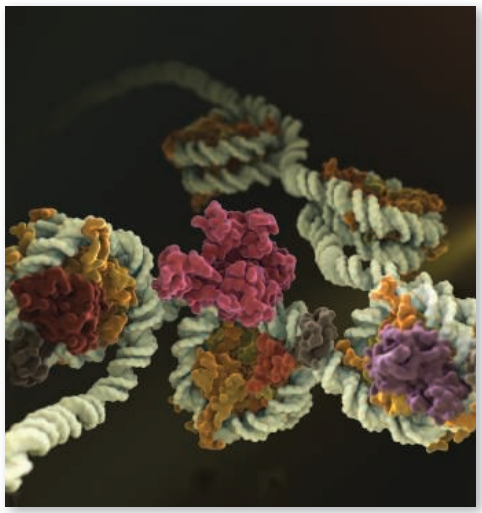

Molecular model of chromatin.

Learn more at: www.cellsignal.com/epigeneticdiscovery

*Landt S.G. et al. (2012) *Genome Res.* 22, 1813–1831.

15PADEPIGNONE0079ENG_00

Cell Signaling TECHNOLOGY®

There's only one Science

Science Careers Advertising

For full advertising details, go to ScienceCareers.org and click For Employers, or call one of our representatives.

Tracy Holmes
Worldwide Associate Director
Science Careers
Phone: +44 (0) 1223 326525

THE AMERICAS

E-mail: advertise@sciencecareers.org

Fax: +1 (202) 289 6742

Tina Burks
Phone: +1 (202) 326 6577

Nancy Toema
Phone: +1 (202) 326 6578

Online Job Posting Questions
Phone: +1 (202) 312 6375

EUROPE / INDIA / AUSTRALIA / NEW ZEALAND / REST OF WORLD

E-mail: ads@science-int.co.uk

Fax: +44 (0) 1223 326532

Sarah Lelarge
Phone: +44 (0) 1223 326527

Kelly Grace
Phone: +44 (0) 1223 326528

Online Job Posting Questions
Phone: +44 (0) 1223 326528

JAPAN

Katsuyoshi Fukamizu (Tokyo)
E-mail: kfukamizu@aaas.org
Phone: +81 3 3219 5777

Hiroyuki Mashiki (Kyoto)
E-mail: hmashiki@aaas.org
Phone: +81 75 823 1109

CHINA / KOREA / SINGAPORE / TAIWAN / THAILAND

Ruolei Wu
Phone: +86 186 0082 9345
E-mail: rwu@aaas.org

ScienceCareers
FROM THE JOURNAL SCIENCE AAAS

ScienceCareers.org

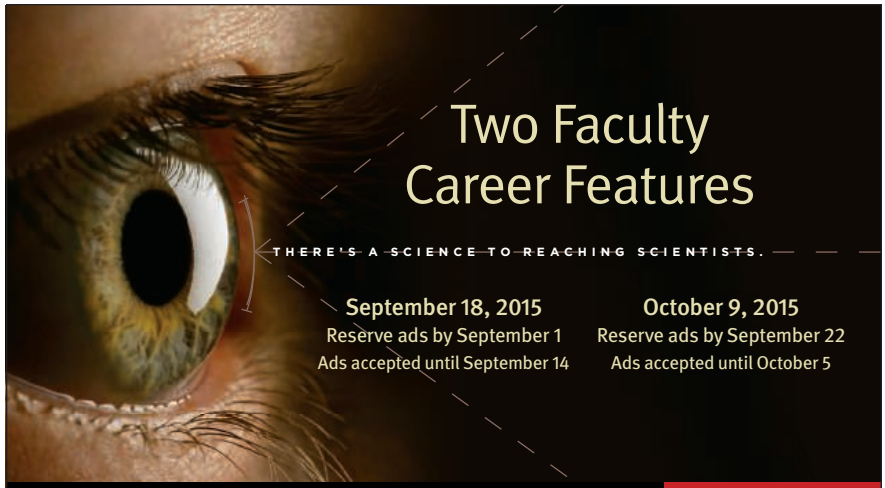

For recruitment in science, there's only one Science

What makes *Science* the best choice for recruiting?

- Read and respected by 570,400 readers around the globe
- 60% of our weekly readers work in academia and 67% are Ph.D.s. *Science* connects you with more scientists in academia than any other publication
- Your ad dollars support AAAS and its programs, which strengthens the global scientific community.

Why choose these faculty features for your advertisement?

- Relevant ads lead off the career section with special Faculty banner
- September 18 issue will be distributed at the Biotechnica Meeting in Hanover, Germany, 6–8 October.

Expand your exposure. Post your print ad online to benefit from:

- Link on the job board homepage directly to Faculty jobs
- Dedicated landing page for faculty positions
- Additional marketing driving relevant job seekers to the job board.

Special packages available when you advertise in both features

SCIENCECAREERS.ORG

Science Careers
AAAS

To book your ad: **advertise@sciencecareers.org**

The Americas
202-326-6582

Japan
+81-3-3219-5777

Europe/RoW
+44(0)1223-326500

China/Korea/Singapore/Taiwan
+86-186-0082-9345

C | A | U Kiel University
Christian-Albrechts-Universität zu Kiel

Kiel University intends to attract more qualified women for professorships.

The Institute of Anatomy at the Kiel University Medical Faculty invites applications for a lifetime professorship following the retirement of its current holder:

W3-Professorship in Anatomy
(Successor to Prof. Dr. med. Jobst Sievers)

We are looking for a candidate with an excellent international reputation in his or her main research area who will provide dedicated, high-quality teaching and research in the field of anatomy.

The successful candidate will be expected to play an active role in the faculty's research focus on "age-related mechanisms in the manifestation of disease" in the profile areas of inflammation, oncology and the neurosciences.

Scientific qualification should be demonstrated through a clearly structured, independent research profile with relevant publications in internationally recognized journals as well as successful acquisition of third-party funding. The successful applicant will be expected to participate actively and constructively in existing and planned research collaborations of the Medical Faculty and Kiel University.

Excellent basic and applied research in the field of anatomy / cell biology as well as in fields involving advanced microscopic or biophysical imaging methods are welcome. A degree in Medicine or the Natural Sciences with experience in anatomy is desirable. The candidate must possess excellent teaching skills and have a university teaching qualification. Ideas and concepts for teaching design and development are very welcome.

The successful candidate will be a member of the Institute's Board of Directors and therefore expected to play an active role in the administration of the Institute and the Medical Faculty. Pedagogical aptitude and a willingness to participate in academic self-administration are required.

The requirements for appointment provided under Article 61 apply, and a limited contract according to Article 63 (1) of the Higher Education Act (Hochschulgesetz) of the State of Schleswig-Holstein is possible. Further information is available at **www.berufungen.uni-kiel.de/de (German only).**

Kiel University seeks to increase the proportion of female scientists in teaching and research and urges qualified female candidates to apply. Women with equal qualifications, competence and professional performance will be given priority.

The University is committed to employing individuals with disabilities. For this reason, disabled applicants with equal qualifications, competence and professional performance will be given priority.

We explicitly encourage candidates with a migration background to apply.

Candidates are not required to submit a photograph with their application and are requested not to do so.

The Higher Education Act requires the Kiel University Medical Faculty and University of Lübeck Department of Medicine to work closely together as well as in close cooperation with the University Medical Center Schleswig-Holstein to determine and coordinate focus areas. The state further expects the clinics and institutes to cooperate with each other accordingly.

Applications should include the usual documents (curriculum vitae, publication list, list of lectures, copies of academic certificates), private and business addresses, telephone number and e-mail address should be submitted by **18.09.2015** to:

Dekan der Medizinischen Fakultät der Christian-Albrechts-Universität zu Kiel, Olshausenstr. 40, 24098 Kiel

For more information on structuring the application, see **www.medizin.uni-kiel.de > Fakultaet > Berufungsverfahren (German only).**

University of Nebraska Lincoln

Director
School of Biological Sciences

We are seeking an extraordinary individual to serve as Director of the School of Biological Sciences at the University of Nebraska-Lincoln (UNL), a public land grant research university and member of the Big 10/Committee on Institutional Cooperation, with a total enrollment of over 25,000 students. The School of Biological Sciences (SBS) is part of the College of Arts and Sciences, and plays a central role in undergraduate and graduate education and research at UNL. SBS faculty attract $12 million annually in competitive extramural research support, primarily from NIH and NSF. SBS has over 500 undergraduate majors and nearly 80 graduate students. Our 44 faculty members pursue research across the full spectrum of biology from molecules to ecosystems, and theory to empiricism. Research by SBS faculty members is highly collaborative, and benefits from strong linkages with other campus units.

We seek a Director who will promote integration and collaboration across levels of biological organization – from genes, cells, and physiology through organisms to populations, communities, and ecosystems – and between biology and other STEM and non-STEM disciplines. The Director will provide strategic leadership and vision to promote SBS excellence in research, education, and outreach; will effectively manage the School's resources; will be instrumental in fund raising and alumni relations; and will play a key role in developing strong relationships between SBS and other units across the campus and the university system.

UNL is committed to achieving academic excellence and continued growth and development within the Life Sciences. The successful candidate will be a dynamic individual with outstanding scientific credentials, a commitment to quality education, and the desire, ability, and vision to lead the School. Candidates for this position must have a PhD; an outstanding record, including accomplishments as a scientist, educator, and in service to their institution; an understanding of the strengths and opportunities offered by a School encompassing the breadth of biology; and demonstrated commitment to excellence. Candidates must qualify for the rank of Professor with tenure. Candidates with research interests in any recognized biological discipline will be considered. The successful candidate will receive a competitive salary and start-up package.

Additional qualifications include: proven success in academic leadership in the context of shared governance and transparent decision-making; excellent communication skills; an understanding of opportunities and challenges in the current funding climate; an interest in working with the university foundation, donors, and alumni to support fund raising; an appreciation of the SBS teaching mission and an awareness of the importance of innovation in instruction; a commitment to diversity; and experience managing financial and human resources.

Information about the department can be found at **http://www.biosci.unl.edu**.

For consideration, applicants must complete the on-line Faculty/Administrative form and submit application materials at **http://employment.unl.edu**, requisition **F_150108**. Application materials should include a cover letter, a curriculum vitae with a full list of publications, a summary of past, current, and pending research support, the names of three references, and brief statements of research, educational, service, and administrative interests. Inquiries regarding the position or the application process should be directed to: **BioSciDirectorSearch@unl.edu**, or **SBS Search Committee Chair, College of Arts and Sciences, University of Nebraska-Lincoln, 1223 Oldfather Hall, Lincoln, NE 68588-0312 (Fax: 402-472-1123)**.

Review of applications will begin **November 16, 2015** and continue until the position is filled.

The University of Nebraska is committed to a pluralistic campus community through affirmative action, equal opportunity, work-life balance, and dual careers.

WASHINGTON STATE UNIVERSITY

The School of the Environment at Washington State University is searching for two tenure-track faculty members.

Assistant Professor, Aquatic toxicology (Position #122147). The successful applicant will develop a nationally-recognized, regionally-relevant research program in aquatic toxicology using both traditional and molecular approaches and will also develop and teach undergraduate and graduate courses relevant to aquatic toxicology. Additional responsibilities include outreach programming to meet the needs of the Puget Sound and beyond, integrating aquatic toxicology research and extension at the Puyallup Research and Extension Center with other disciplines such as aquatic ecology, biology, entomology, hydrology, plant pathology, nutrient management, horticulture/crop production, and engineering. The successful applicant will work closely with the Washington Stormwater Center on stormwater effects on aquatic organism health. Position is located in Puyallup, WA.

Required: Earned doctorate in aquatic toxicology, or closely related field, at the time of hire; Evidence of research productivity commensurate with career level; evidence of ability to develop an original research program addressing needs of the Puget Sound and beyond; evidence of ability to develop effective outreach and academic programs; and evidence of excellent oral, written, and electronic communication skills.

Screening begins **October 15, 2015**. The position is available as early as January 1, 2016.

Assistant Professor, Forest Biometrics, emphasis on Quantitative Spatial Ecology (Position # 122149). The successful candidate will be expected to develop a dynamic, extramurally funded, internationally recognized research program focused on the Spatial Ecology dimensions of Forest Biometry and consistent with the missions of the WSU Agricultural Research Center. The successful candidate will develop and teach undergraduate and graduate courses to advance the School's re-emerging forestry program by introducing students to modern statistical, geospatial and computational tools. The person hired will successfully mentor M.S. and Ph.D. graduate students. Additional responsibilities include service to school, college and research community, and outreach to relevant stakeholders. Position is located at WSU Pullman.

Required: Earned doctorate in a discipline related to forest biometrics with an emphasis on Quantitative Spatial Ecology at time of hire.

Screening begins **November 15, 2015**. The position is available beginning August 16, 2016.

To see full description and/or apply for either of the positions visit: **https://www.wsujobs.com**. Application materials must include a letter describing how your experience and training meet qualifications for the position, a research plan, a statement of teaching philosophy, current vitae, and names and contact information for three professional references. *EEO/AA/ADA*

RADCLIFFE INSTITUTE
FOR ADVANCED STUDY
HARVARD UNIVERSITY

Academic Fellowships

The Radcliffe Institute Fellowship Program at Harvard University welcomes fellowship applications in natural sciences and mathematics. The Radcliffe Institute for Advanced Study provides scientists the time and space to pursue their career's best work. At Radcliffe you will have the opportunity to challenge yourself. Meet and explore the work of colleagues in other fields. Take advantage of Harvard's many resources, including the extensive library system. Radcliffe Institute Fellowship Program invites applications from people of all genders, and from all countries. We seek to build a diverse fellowship program.

Scientists in any field who have a doctorate in the area of the proposed project (by December 2014) and at least two published articles or monographs are eligible to apply for a Radcliffe Institute fellowship. The stipend amount of $75,000 is meant to complement sabbatical leave salaries of faculty members. Residence in the Boston area and participation in the Institute community are required during the fellowship year.

Applications for 2016-2017 are due by October 15, 2015.

For more information, please visit www.radcliffe.harvard.edu or email sciencefellowships@radcliffe.harvard.edu.

University of Minnesota
Diabetes and Endocrinology Metabolism Physician-Scientist / Ph.D. (Associate Professor - Tenured / Tenure Track)

The Division of Endocrinology and Diabetes Metabolism in the Department of Medicine at the University of Minnesota is seeking an outstanding scientist in the field of diabetes and obesity to participate in building a nationally-recognized research division within a growing department. The ideal candidate will have a proven track record in extramural funding, a history of collaborative research, and experience in teaching and mentoring. Responsibilities include maintaining an active research program, participating in educational activities of the division, and leading activities to build collaborative research in diabetes and obesity. Qualifications include an advanced scientific degree (PhD, MD, DO, or any combination), academic experiences that will allow appointment at the level of associate professor, or higher (dependent on qualifications), tenured or tenure track. Physician scientists are urged to apply, but will have limited responsibilities in the clinical aspects of the division.

The Division of Endocrinology and Diabetes Metabolism in the Department of Medicine at the University of Minnesota consists of 14 University-based faculty, 6 faculty based at the Minneapolis Veterans Administration Medical Center, and 3 faculty at Hennepin County Medical Center. Faculty are involved in all aspects of endocrinology practice and investigation, with particular strengths in diabetes and obesity. Training efforts are supported by a NIH T32 in Diabetes, Endocrinology, and Metabolism, as well as an AFGME-certified endocrinology training program. Opportunities exist for joint appointments in basic science departments for candidates interested in graduate education.

Qualified applicants are invited to apply online at: **https://www.myu.umn.edu/employment** and submit their CVs to Elizabeth Seaquist, M.D., DEM Director, at **seaqu001@umn.edu**.

The University of Minnesota is an Equal Opportunity Employer and Educator.

Niigata University

Tenure-track faculty positions in Solar Thermal Energy Utilization and Neuroscience of Disease

The Center for Transdisciplinary Research, Niigata University has established the Frontier Research Base for Global Young Researchers. We would like to invite worldwide applications for three tenure-track positions at the designation of **Associate or Assistant Professor** in the specified fields. The positions are supported by the Ministry of Education, Culture, Sports, Science and Technology (MEXT), Japan. The Center for Transdisciplinary Research would like to recruit talented, highly qualified young researchers who are distinguished within the international research community and create new scientific fields. The competitive applicants will have the potential to become leaders of future generations, hold a strong publication record, demonstrate the ability to obtain extramural funding, and be expected to build a vigorous research program. The Niigata area has a mild climate that adds to the quality of life.

Research fields and positions Solar Thermal Energy Utilization (Mechanical/ Chemical Engineering): one position for Associate Professor or Assistant Professor
Neuroscience of disease (Mechanisms of neurological disease, neurodevelopmental disorder, or mental disease): one position for Associate Professor and one position for Assistant Professor (Pair applications are preferred)

Promotion to a tenured position This position is offered up to March 31, 2020 as a faculty member in the Center for Transdisciplinary Research, with the consideration for tenure. Exceptionally outstanding researchers may be directly appointed with tenure as a Professor or Associate Professor in the Center for Transdisciplinary Research after April 1, 2020.

The deadline for applications is **October 12, 2015 (JST)**. Applicants should visit **http://www.niigata-u.ac.jp/tenure_track/english/** for application instructions.

Niigata University is an affirmative action/equal opportunity employer.

Research Promotion Division, Niigata University
tenure-t@adm.niigata-u.ac.jp

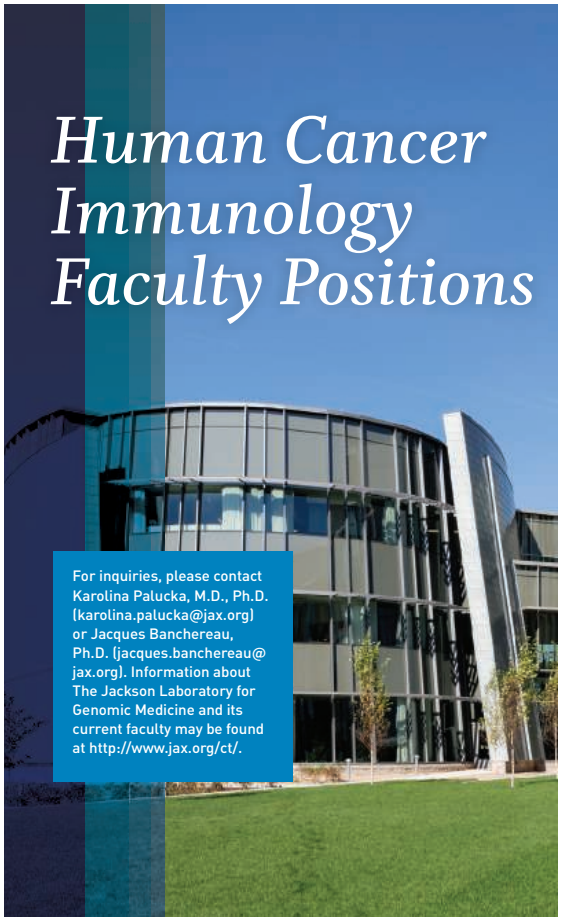

THE JACKSON LABORATORY FOR GENOMIC MEDICINE | Farmington, Conn.

The Jackson Laboratory for Genomic Medicine (JAX-GM) in Farmington, Conn., is seeking a top-level scientist to expand its research in human cancer immunology. The Jackson Laboratory is an NCI-designated Cancer Center, and the cancer immunology program works hand-in-hand with regional and national cancer centers. We are recruiting for a full, associate, or assistant professor to join a vibrant and expanding biomedical research institute with programs in human immunology, genomics, cancer biology, genetic engineering, epigenetics, bioinformatics and microbiomics.

We are looking for a researcher excited to join our collaborative effort to find novel solutions to cancer therapy and prevention by harnessing the exquisite power and specificity of the immune system. Candidates must have an M.D., Ph.D., or M.D./Ph.D., and the ideal candidate will have a significant publication and grant funding record in the fields of human immunology and human cancer immunology.

The Jackson Laboratory
Leading the search for tomorrow's cures

Applicants must apply online. Please submit a curriculum vitae and a concise statement of research interests as one document by selecting Faculty Positions on www.jax.org/careers position #4078. In addition, please have three letters of reference sent to: facultyjobs@jax.org.

We are an equal opportunity, affirmative action employer, considering all qualified applicants and employees for hiring, placement, and advancement, without regard to a person's race, color, religion, national origin, age, genetic information, military status, gender, sexual orientation, gender identity or expression, disability, or protected veteran status.

Faculty positions in Integrative Biosciences

IBio

Wayne State University (WSU) is recruiting 30 faculty (Open rank) for research and development programs in Integrative Biosciences. This initiative leverages a new 200,000 sq. ft. Integrative Biosciences Center (IBio) opening in 2015 that will house coordinated, multidisciplinary research teams and programmatic initiatives involving translational thrusts focused on pathophysiologies and accumulated stressors affecting health in evolving urban environments.

Phase 1 occupation of IBio includes a clinical research center as well as the WSU NIEHS-supported Center for Urban Responses to Environmental Stressors and established research teams at WSU in behavioral health, biomaterials and molecular imaging, diabetes and obesity.

Phase 1 recruitment (6-8 faculty) focuses on five primary areas: Brain & Behavioral Health; Bio & Systems Engineering; Interface of Genes, Ethnicity, Environment and Health; Metabolic Diseases (Diabetes and Obesity); and Urban Health Equity. Each theme includes basic discovery-driven research as well as translational, community and implementation sciences cutting across departments, programs, centers and colleges.

Faculty recruits (tenured, tenure-track or research-track) will integrate with, and be appointed in, department(s) and colleges or schools consistent with their area of training, expertise, and shared interests. Tenure-track and tenure appointments are expected to engage in all aspects of our academic mission including research, education and service. Wayne State University is an Equal Opportunity Employer committed to building a diverse faculty and educating a diverse student population.

Candidates must have a PhD, MD, PharmD. and/or related degree(s) in disciplines aligning with the focus areas and possess a demonstrated track record of and/or potential for exceptional science, creative discovery and/or knowledge translation and application. We would be pleased to receive applications from groups of faculty from one or several institutions who may wish to work together. Qualified candidates should submit (pdf) their *curriculum vitae* and a brief narrative describing their research and how it relates to the IBio initiative (http://www.IBio.wayne.edu) to Dr. Lanier at **IBio@wayne.edu**. Candidate packages will be reviewed by a search committee chaired by the University's Vice President for Research, Stephen M. Lanier, Ph.D. Competitive recruitment packages are available with salary and rank based on qualifications. Review of Phase 1 applications will begin immediately with applications accepted until **October 30, 2015**.

Founded in 1868, Wayne State University is a nationally recognized comprehensive, urban research university offering more than 370 academic programs through 13 schools and colleges to nearly 28,000 students. Wayne State's main campus in Midtown Detroit comprises 100 buildings over 200 acres including the School of Medicine, the Eugene Applebaum College of Pharmacy and Health Sciences and the College of Nursing. Wayne State University is one of three universities in Michigan with the Carnegie classification of institutions with "very high research activity." WSU is home to the Perinatology Research Branch of the National Institutes of Health and the Karmanos Cancer Institute, a National Cancer Institute-designated comprehensive cancer center. The IBio initiative also includes programmatic expertise and opportunities in the College of Liberal Arts and Sciences, the College of Engineering, the School of Law, the School of Social Work and the School of Business Administration as well as additional schools, colleges, centers and institutes.

The City of Detroit, with its storied history in innovation, is at an exciting point in its history with rapidly expanding development activities and true rebirth. Its vibrant downtown and cultural center envelop the WSU campus. With its large presence in the downtown area and its activities related to economic development, research and education, WSU plays a key role in the rapidly accelerating forward growth of the city. With immediate proximity to Canada and its location in the middle of the Great Lakes region along with professional sports, opera and symphony, Detroit and the metropolitan area (~5 million population) provide a rich culture with exceptional recreational and entertainment activities.

Research Position at ICYS, NIMS, Japan

The International Center for Young Scientists (ICYS) of the National Institute for Materials Science (NIMS) is now seeking a few researchers. Successful applicants are expected to pursue innovative research on broad aspects of materials science using most advanced facilities in NIMS (**http://www.nims.go.jp/eng/index.html**).

In the ICYS, we offer a special environment that enables young scientists to work independently based on their own idea and initiatives. All management and scientific discussions will be conducted in English. An annual salary approximately 5.35 million yen (level of 2014) will be offered depending on qualification and experience. Additional research grant of 2 million yen per year will be supplied to each ICYS researcher. The initial contract term is two years and may be extended by one more year depending on the person's performance.

All applicants must have obtained a PhD degree within the last ten years. Applicants should submit an application form, which can be downloaded from our web site, together with a resume (CV), a publication list, and a research proposal to be conducted during the ICYS tenure. All documents should reach the following address via e-mail by **SEPTEMBER 30, 2015 JST**. Please visit our website for more details (**http://www.nims.go.jp/icys/**).

ICYS Administrative Office,
National Institute for Materials Science
Sengen 1-2-1, Tsukuba, Ibaraki 305-0047, Japan
e-mail: icys-recruit@nims.go.jp

Los Alamos NATIONAL LABORATORY EST. 1943

Los Alamos National Laboratory (LANL), a multidisciplinary research institution engaged in strategic science on behalf of national security, has an opportunity to lead a group of approximately 75 staff members, postdocs and students.

SUB-ATOMIC PHYSICS GROUP LEADER

(R&D Manager 4) Job IRC40315

Provide overarching technical leadership and management for the Sub-atomic Physics Group (P-25) and its multiple scientific projects, and serve as a member of the Physics Division management team at Los Alamos National Laboratory. Report to the Physics Division Leader and contribute to the integrated management and technical leadership of the Division as a whole, working effectively and collaboratively with other groups and program management both within and outside the Division.

Minimum Job Requirements:

- PhD in physics or a closely related field
- Record of successful research in a scientific field relevant to at least one of the Group's core research areas or programs
- Strong record of effective written and verbal communication skills
- Demonstrated successful leadership of a line organization or a large project, of at least 5 staff or $5M per year or more, within a scientific research organization
- Demonstrated capability in program development and demonstrated scientific and organizational leadership
- Financial management skills and commitment to good business practices as demonstrated by performance and accomplishments in previous work assignments
- Demonstrated commitment to mentoring and professional development
- Demonstrated ability to successfully interact with regulatory and oversight agencies and personnel relevant to the Laboratory
- Record of commitment to safety, security, quality, diversity and AA/EEO
- Ability to obtain a Q clearance, which normally requires U.S. citizenship

To apply and learn more about the position, please see **Job IRC40315** at **careers.lanl.gov**.

EOE

ASSISTANT PROFESSOR EPIGENETICS

Division of Newborn Medicine
Boston Children's Hospital
and
Department of Genetics
Harvard Medical School

The Division of Newborn Medicine at Boston Children's Hospital and the Department of Genetics at Harvard Medical School seek a highly motivated individual with demonstrated potential for creativity and excellence for a laboratory-based joint faculty position at the Assistant or Associate Professor level. We are seeking advanced trainees and junior faculty who hold a Ph.D. and/or M.D., and whose scientific focus is on epigenetics broadly defined, with particular emphasis on developmental biology with connections to translational medicine. The successful applicant is expected to direct innovative and independent research, and to participate in the teaching of graduate and medical students. The successful candidate will receive an outstanding competitive start-up package, excellent space and facilities, and the benefits of a vibrant and interactive research community that offers opportunities for collaboration with both basic and translational investigators.

For further information about the Division of Newborn Medicine at Boston Children's Hospital, please see: **http://www.childrenshospital.org/research-and-innovation/rsearch/divisions/newborn-medicine**

For further information about the Department of Genetics at Harvard Medical School, please see: **http://genetics.med.harvard.edu**

Applicants should submit electronic copies of a curriculum vitae, a brief description of research accomplishments, and a description of future research interest (limit to 500 words); and should ask three referees to provide letters of recommendation. These materials should be sent by November 1, 2015, to: LaVondea.Elow@childrens.harvard.edu.

Applications from women and minority candidates are strongly encouraged. Harvard University and Boston Children's Hospital are Equal Opportunity/Affirmative Action Employers.

University Research Fellowship

These fellowships are for outstanding scientists in the UK, in the early stages of their research career, with the potential to become leaders in their field. Five years of funding is provided (with the opportunity to extend for three years), including a significant salary contribution and annual research expenses.

All areas of the life and physical sciences are covered, including engineering and mathematics, but excluding clinical medicine and research addressing a direct biomedical question. Awards are flexible: part-time working, sabbaticals and secondments can be accommodated and there is provision for maternity, paternity, adoptive or extended sick leave.

Royal Society – Science Foundation Ireland University Research Fellowships (funded by Science Foundation Ireland) are available for outstanding researchers in the Republic of Ireland.

royalsociety.org/grants/schemes/university-research

THE ROYAL SOCIETY

Do you apply innovative biodiversity science to global sustainability?

The California Academy of Sciences will fill several endowed positions with outstanding Ph.D. scientists focused on changing the world through cutting-edge biodiversity/ecological science, broader science communication, increasing diversity in science, and connecting their work to real-world sustainability outcomes.

The Academy offers a LEED platinum museum, aquarium, planetarium, extraordinary exhibits, and ~46 million specimens—a powerful setting for scientific research and engagement. Our new "cluster hires" will join ~100 scientists, students, and post docs.

We especially seek experts in coral reef biology, tropical rain forests, California biodiversity, and the impacts of global change on biodiversity, as well as in marine mammals and amphibian decline. Candidates with skills in "big data", modeling, GIS, visualization, genomics, and innovative field- and collections-based research, and who connect their work to larger sustainability challenges are especially compelling. Applicants must have a relevant doctorate and postdoctoral experience or equivalent training.

Applications will be reviewed until all positions are filled; for full consideration, apply by November 1, 2015 at http://calacademy.snaphire.com/jobdetails?ajid=vNXB8. Interviews will be held spring 2016; starting dates are negotiable.

Questions? Contact Dr. Meg Lowman (mlowman@calacademy.org), Chief of Science & Sustainability.

The California Academy of Sciences is an Equal Opportunity Employer and committed to ensuring that all employees and applicants receive equal consideration and treatment.

CALIFORNIA ACADEMY OF SCIENCES

55 Music Concourse Drive
San Francisco, CA 94118
www.calacademy.org

INDIANA UNIVERSITY
BLOOMINGTON

Tenure Track Faculty Position in Prokaryotic Biology

The Microbiology Program in the Indiana University Department of Biology (http://www.bio.indiana.edu) invites applications for a tenure-track faculty position in Prokaryotic Biology at the level of assistant professor. We are particularly interested in scientists exploring the systems biology, physiology, development, cell biology, environmental biology, and/or pathogenesis of prokaryotes, although all areas will be considered. This position is part of a significant, continuing expansion in the life sciences at IU Bloomington and represents an exceptional opportunity to join a strong Microbiology Program and new interdisciplinary initiatives. The successful candidate will be provided with a competitive startup package and salary, and will have access to outstanding research resources including state-of-the-art facilities for genomics and bioinformatics, light and electron microscopy, flow cytometry, protein analysis, analytical chemistry, biophysical instrumentation, and crystallography. Applicants must hold a Ph.D. and have relevant postdoctoral experience with a strong record of research accomplishments. Successful candidates will be expected to develop a vigorous externally funded research program, and to participate in teaching at the undergraduate and graduate levels.

Applications received by **October 15, 2015** will be assured of full consideration. Applicants should submit a cover letter, a CV, a research statement (5 pages emphasizing current and planned research), a statement of teaching interests (1 page), a list of three (or more) references, and up to 3 pdfs of published and/or submitted manuscripts using the submissions link at **http://indiana.peopleadmin.com/postings/1707**. For questions about the application procedure please contact **Jennifer Tarter (jenjones@indiana.edu)** or by mail at **1001 E. Third Street, Bloomington, IN 47405-7005** and for all other questions please contact **Yves Brun (ybrun@indiana.edu)**.

Indiana University is an Equal Employment and Affirmative Action Employer and a provider of ADA services. All qualified applicants will receive consideration for employment without regard to age, ethnicity, color, race, religion, sex, sexual orientation or identity, national origin, disability status or protected veteran status.

UC San Diego

Division of Biological Sciences

The Division of Biological Sciences (www.biology.ucsd.edu), Section of Ecology, Behavior and Evolution, invites applications for a faculty position at the tenure-track Assistant Professor level in Evolutionary Biology. We are broadly searching for an evolutionary biologist. Research topics could include, but are not limited to, vertebrate biology, evolutionary ecology, or comparative or population genomics.

All candidates must have earned a Ph.D. or equivalent degree, and be committed to teaching at the undergraduate and graduate levels. In addition to excellence and creativity in research and scholarship, successful candidates must also demonstrate a commitment to equity and inclusion in higher education. We are especially interested in candidates who have created or contributed to programs that aim to increase access and success of underrepresented students and/or faculty in the sciences, and/or have detailed plans to accomplish such goals.

Review of applications will commence by **October 1, 2015** and will continue until the position is filled. Interested applicants must submit a cover letter, curriculum vitae, statement of research, statement of teaching, a statement describing their past experience and leadership in fostering equity and diversity and/or their potential to make future contributions, 3-5 references, and 3-5 publications. Applications must be submitted through the University of California San Diego's Academic Personnel RECRUIT System at **https://apol-recruit.ucsd.edu/apply**.

The Division of Biological Sciences at UCSD is a vibrant center of scientific discovery, innovation, and collaboration. Our large research base spans many areas of biology and has one of the most celebrated graduate programs in the country. We are committed to academic excellence and diversity within the faculty, staff, and student body. This is where discovery comes to life.

UCSD is an Equal Opportunity/Affirmative Action Employer with a strong institutional commitment to excellence and diversity (http://diversity.ucsd.edu/).

By **Richard Krablin**

A risk worth taking

I was a newly minted Ph.D. atmospheric physicist living on the East Coast of the United States with a spouse and an 18-month-old daughter. One day, a job recruiter asked me if I wanted to move to Montana to work for a mining and smelting company. I hesitated. That sounded like a big risk. ¶ As a child growing up in northeastern Pennsylvania, I sought to understand the world around me. I wanted to be a scientist.

I aimed to do research, with expanding our understanding as my goal. But when I earned my science degree and it came time to look for a job, it was clear that academic positions were scarce. I expanded my options by looking for work in industry.

Given my training, jobs dealing with environmental issues seemed a natural focus. The year was 1970; Congress had just created the Environmental Protection Agency (EPA) and was working on new laws to reduce air and water pollution. I started interviewing with firms that had research centers. Then I received the urgent call from the headhunter (a role I hadn't known existed). A large minerals company had suddenly woken up to a world concerned about pollution—and had come to realize that it needed someone to help evaluate and manage the risks posed by its operations. I had never imagined myself in such a role, but I weighed the pros and cons and took the offer. We traveled cross-country. It was an adventure: the family's first trip west of Pittsburgh, Pennsylvania.

"I've gained an appreciation for the need to balance risks."

Early on, at a cocktail party, I met the senior vice president in charge of mining operations. His job, he told me, was "to dig," and my job was to help him avoid problems. It turned out there was plenty of science to do. Air pollution from mineral processing was an enormous issue; the search was on for ways to manage and reduce the associated risks. That meant identifying acceptable human exposures and effective, affordable controls. Getting the science right, however, was only a first step to achieving real-world results; I also had to persuade company executives. Luckily, that vice president became an ally: Not once did he turn down my requests to take action based on science.

Over the next 4 decades, my scientific background allowed me to expand my work. I moved eight times, helping firms manage health, safety, and environmental issues and the associated financial concerns. I gained unexpected influence: Who would have guessed that an atmospheric physicist would have the power to shut down one of the world's largest mining pits when ash falling from the 1980 eruption of Mount St. Helens, in Washington state, threatened both workers and expensive equipment? With one phone call, I stopped the mining for 2 days.

Over time, I learned that reducing risks meant we had to overcome big gaps in scientific understanding, both within industry and among the public. I studied business risks and discovered that science and technology often play an outsized role in finding solutions. And so does setting ambitious goals: Early on, I doubted industry could meet some of the aggressive targets that EPA set for reducing air pollution, but I ultimately saw these goals spur innovation and creative solutions that led to setting even higher standards.

My quest for scientific understanding has taken a form I never anticipated in graduate school. I still want to understand the world around me, but today I do so by using science to manage risk—a richer, broader, and more relevant role than I ever envisioned. I am now well past the old-fashioned retirement age, but there is much yet to explore, and I continue to apply my scientific skills as a consultant to industry. I've gained an appreciation for the need to balance risks—in our careers, in our impact on the environment, and in our uses of science. But I'm glad I took that first big risk, which opened a whole new world for me. ■

Richard Krablin is currently consulting on environment, health, and safety matters for industry through his firm Corporate Environmental Performance in Bethlehem, Pennsylvania. For more on life and careers, visit sciencecareers.org. Send your story to SciCareerEditor@aaas.org.